SEISMIC STUDIES IN THE REGION OF NORTHERN SKYE AND THE LITTLE MINCH

David Kenneth Smythe

Thesis submitted for the degree of
Doctor of Philosophy

Department of Geology
University of Glasgow
November 1987

ProQuest LLC.
789 East Eisenhower Parkway
P.O. Box 1346
Ann Arbor, MI 48106 – 1346

In memory of
Adam McLean
(1926-1983)

ACKNOWLEDGMENTS

Adam McLean was more than just the supervisor of this research; he imbued his students, including the author, with the spirit of scientific enquiry. He showed by his own example that clear reasoning and method is of equal value in the consideration of problems in the wider world as it is within the narrow domain of academic research.

T Neville George, as Professor of Geology, was a nominated co-supervisor. He communicated his genuine enthusiasm for geophysical techniques in the service of geology, astutely pointing out to the author that the research topic about to be undertaken was neither about a method, nor about an area, but was about a problem. This lesson has been well learned.

Jeremy Hall was a Lecturer in geophysics in the Geology Department during the period of full-time study. He passed on to the author his considerable expertise in both the theory and practice of seismic reflection, on innumerable occasions. He was, in effect, a second supervisor of the present research. In the field of reflection seismology the author is only following in his footsteps.

The author gratefully thanks the following individuals:

Bill Sowerbutts and Dave Howard, for being hard-working and selfless research assistants, without whom the field seasons of 1971 and 1972 would not have been possible.

Bob Cumberland, for his generous help (going well beyond his duties as a technician) in making the field work successful. He also took on the job of reducing and compiling the gravity data, and wrote FORTRAN graphics programs for the author's own data.

George Gordon (Glasgow University) and Tom Fitton (NERC Research Vessels Unit), for tirelessly building and repairing various items of equipment (especially hydrophones) until they worked.

Bob McQuillin and Mike Bacon of the Institute of Geological Sciences (IGS), for generously giving of their ideas and information, in what grew into a cooperative Glasgow-IGS project.

Bernard Raynaud, for sharing with the author both his ray tracing migration program and his theoretical understanding of that field. The author has learned a lot from studying and improving his FORTRAN programs.

Linda Pollock and Phil Bentley, for commenting upon and proof-reading drafts of the text.

The help of the following institutions and groups is gratefully acknowleged:

The Geology Department technicians and students who did the bulk of the field work.

The many tenants, crofters and other individuals in northern Skye, who were prepared to let a group of geophysicists drive all over their land, and even (accidentally) blow up a water main in the process.

ICI for supplying a variety of explosives in small quantities for academic experiments, together with a blaster for the marine work.

The masters and crew of the RRS John Murray and RV Calanus.

The Home Office (radio licensing department), for getting the BBC to issue an apology that the interference to TV sound in the Minch during the 1971 refraction surveys was "outside its control", when the high-pitched whistle was clearly emanating from the sonobuoys.

Merlin Geophysical Research Ltd, who have had the foresight to supply academic workers with affordable licences to use the SKS seismic reflection processing package.

The British Geological Survey (formerly IGS) for supply of its data in advance of publication, and for the use of its computer facilities in the preparation of this thesis.

The Natural Environment Research Council (NERC) for funding the research, both through a grant to the Geology Department, University of Glasgow, and by the award of a studentship to the author.

The Director of the Scottish Marine Biological Association for permitting his vessel, the RV Calanus, to be used at very short notice for purposes within the remit of NERC, but certainly of no use (or even detrimental) to marine biology.

The author has benefitted from innumerable discussions with many other individuals apart from those mentioned above. They include:

Ian Vann and other fellow research students in the Geology Department,

Mike Russell and Stuart Haszeldine (Strathclyde University),

Lindsay Parson, Pete Miles, Dave Roberts and Doug Masson (Institute of Oceanographic Sciences),

Phil Bentley and Roger Scrutton (Edinburgh University),

Jon Brewer, Sue McGeary and others in the BIRPS group,

Bob White and George Spence (Cambridge University),

John Chesher, Dan Evans, Andy Skuce and many other present and former colleagues in BGS.

CONTENTS

FIGURES

TABLES

SUMMARY

The northern Skye - Little Minch region is one of the most accessible regions on the continental shelf where the relationship between intra-continental extensional basins and passive margin formation might be investigated. Can the structure and infill of the presumed sedimentary basin here tell us something about the age of the nearby oceanic Rockall Trough?

A variety of geophysical tools are used to evaluate the structure and infill of the basin. Multichannel seismic reflection at six sites in northern Skye, and marine sonobuoy refraction lines in the Little Minch (both using dynamite sources) are supplemented by new and existing shallow seismic profiling (sparker) data. Gravity modelling elucidates the 3-dimensional structure.

The offshore geological map of the Little Minch is compiled from possibly the most comprehensive coverage of high resolution profiles of any area on the NW European shelf. The basin is bounded on the NW by the Minch Fault, which is shown to be the reactivated Outer Isles Thrust, and which now dips ESE or SE at about 20°. Offshore, the pre-Jurassic rift infill dips NW in several half-grabens bounded by the Minch Fault and by other eastward-dipping low-angle faults. The biggest of these, the Harris Fault, crops out some 8-10 km east of the Minch Fault, and brings steeply NW-dipping Carboniferous and Permo-Triassic sediments to the sea bed.

Torridonian sediments are inferred to comprise the basal rift infill, which is thickest below the Little Minch. The overlying 1.5 km of Permo-Triassic (and presumed late Carboniferous) is characterised by a regional velocity inversion. Interval velocities within the basin are corroborated by velocity measurements at outcrop (and in the laboratory) of sedimentary and igneous rocks from many localities in the north of Scotland.

Below northern Skye the pre-Jurassic Minch basin is bounded by NE-dipping low angle normal faults of NW-SE or NNW-SSE trend. The NW-SE gravity gradient here is due to rapid westward thickening of the rift infill, below a strong

sub-Jurassic unconformity. The Jurassic occupies an oval depression centred on NW Skye, and is probably a sag basin up to 1 km thick, developed during the phase of thermal subsidence following extension.

The late Palaeozoic rift basin lies at the right-angled intersection of two belts of basins; the Clyde Belt, trending NW-SE, and the Marginal Belt, trending NE-SW. The Marginal Belt is part of an intra-continental rift system extending from east Greenland to Porcupine Bight, which flanks the 'proto North Atlantic' rift zone. The northerly part of this deep-water rift may be intra-continental, but the Rockall Trough, which is the most southerly and widest part of it, is oceanic. Its age is controversial. It is shown that the arguments for a Cretaceous age relate not to the Rockall Trough itself, but to a newly postulated spreading phase of mid Cretaceous age which partially opened up the Hatton-Rockall Basin. The Rockall Trough predates this.

Stratigraphic evidence suggests that the Rockall Trough is pre-Cretaceous, and probably even pre-Jurassic, in age. The rival arguments which have been proposed for a late Palaeozoic age (rather than the currently accepted Cretaceous age) rely on the recognition of an important phase of rifting at that time; this phase includes the Sea of the Hebrides - Minches basin system, as shown by the detailed studies. However, the mechanism linking rifting to sea floor spreading is not yet well enough understood for the former to be used as a means of dating the latter.

A new link between intra-continental rifting and sea floor spreading is established by the demonstration that the Palaeocene flood basalts of northern Skye were extruded in an extensional-faulted environment. The Minch Fault was also a locus of basalt eruption at about the same time. The half-graben-controlled structural development of the Skye basalt pile is closely analogous to the growth of volcanic passive margins overlying stretched continental crust. The best-documented example of such a margin is the one west of the Rockall Plateau, where spreading began some 5 my after the eruption of the Skye lavas.

CHAPTER 1
INTRODUCTION

1.1 DEVELOPMENT OF SEDIMENTARY BASINS AT PASSIVE CONTINENTAL MARGINS

How does the widespread growth of sedimentary basins on the continental shelf adjacent to a rifted passive margin relate to the opening history of the newly formed ocean? This is a problem which has received considerable attention because of its relevance both to the dynamics of plate tectonic theory, and to the search for hydrocarbons. The two principal characteristics of such continental shelves are:

(1) They have subsided below sea level, so that if they have reached isostatic equilibrium, as can usually be assumed for older margins such as those bordering the Atlantic, they must have undergone crustal thinning and/or increased in overall density.

(2) They contain faulted sedimentary troughs trending generally parallel or sub-parallel to the margin, covered by wedges of sediment draped over the continental slope. The thickness of the later wedge determines whether the passive margin is defined as starved or mature. Mature passive margins have undergone more post-rift subsidence and sedimentation than starved margins.

The faulted sediments define the rift phase, whereas the overlying drape is known as the drift phase (Fig. 1.1). The breakup unconformity, separating the two sequences, is believed to postdate the onset of sea floor spreading by some time (see, for example, Curray 1980), since the overlying sequence laps onto the newly formed oceanic crust.

Mechanisms to explain the sedimentation and subsidence of passive margins are reviewed by Bott (1979). He points out that the only viable mechanism for the rift phase involves normal faulting of the brittle upper crust. Although his symmetrical grabens (after Vening Meinesz 1950), would now

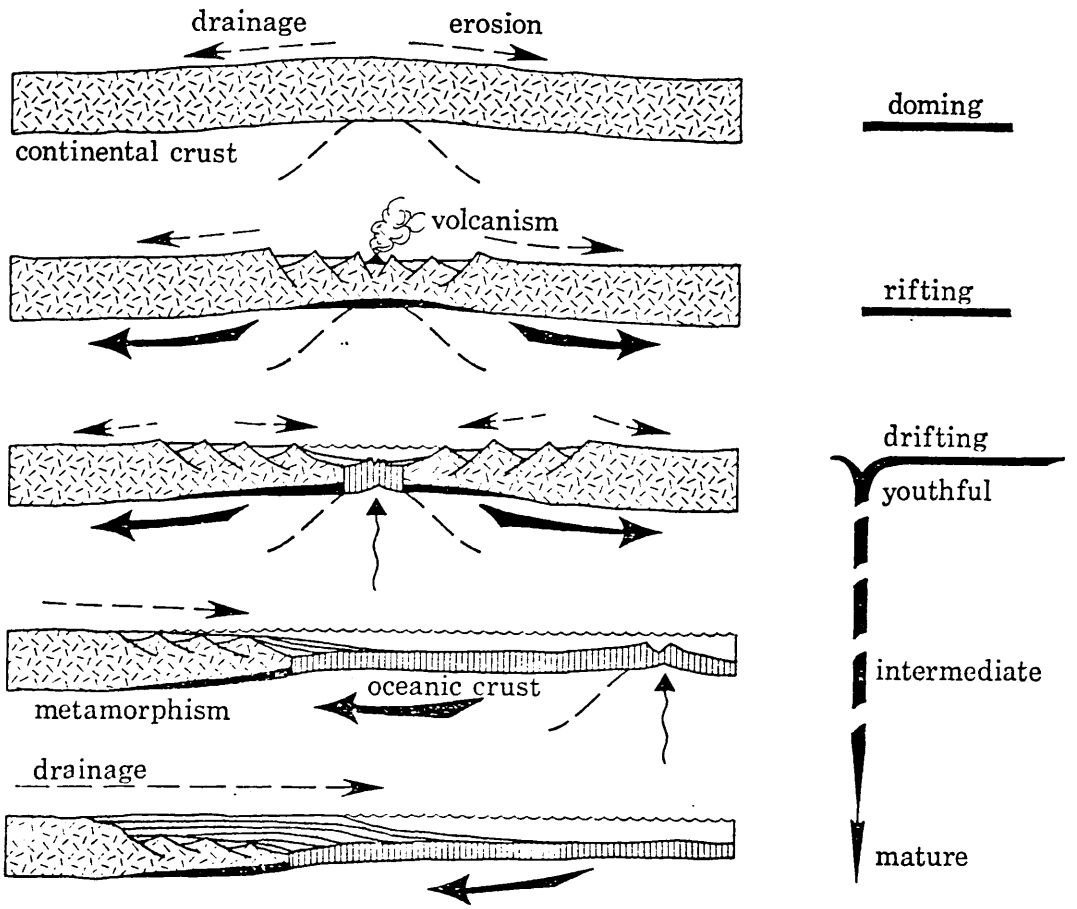

Fig. 1.1 Model of formation and evolution of rifted passive continental margin (reproduced from Curray 1980).

be replaced by asymmetrical half-grabens (e.g. Bally 1982), his main point, which is still valid, is that the rifting is due to regional horizontal tension in the lithosphere. This tension is, presumably, the same regional stress that goes on to break up the continental plate and permit the onset of sea floor spreading. The other mechanisms to account for the later phases of passive margin development discussed by Bott are not relevant here; what matters is the link between the rifting on a continental shelf near a passive margin, and the sea floor spreading which occurs (some time) later. Perhaps here we have a means of estimating the time of onset of spreading by studying the rift infill of the accessible adjacent margin.

The present study aims to explore this rifting/spreading relationship at the passive margins of the NE Atlantic, where the problem of the age of opening of the Rockall Trough remains to be solved. The bulk of this introductory chapter is devoted to a critical review of the evidence for the age of the Rockall Trough. This is followed by a resumé of the reasons for the choice of the northern Skye - Little Minch area as the region for detailed study.

1.2 THE NE ATLANTIC MARGIN

The late Cretaceous to recent opening history of the North Atlantic is well understood, being calibrated mainly by magnetic anomalies 34 and younger. Figure 1.2 shows a reconstruction to anomaly 13 time (35 Ma), just after spreading in the Labrador Sea had finished. The earlier phases are represented by the shaded strips between anomalies 34 (80 Ma) and 24 (55 Ma for anomaly 24B), and by the blank Y-shaped zone created by spreading at a triple junction between anomaly 24 and anomaly 13 time. Clearly the Rockall Trough and the Bay of Biscay are older than anomaly 34.

Only recently has a crucial experiment established that the Rockall Trough is, indeed, oceanic. A two-ship wide angle seismic profile, occupying essentially the same location in the centre of the Trough as the attempted refraction line of

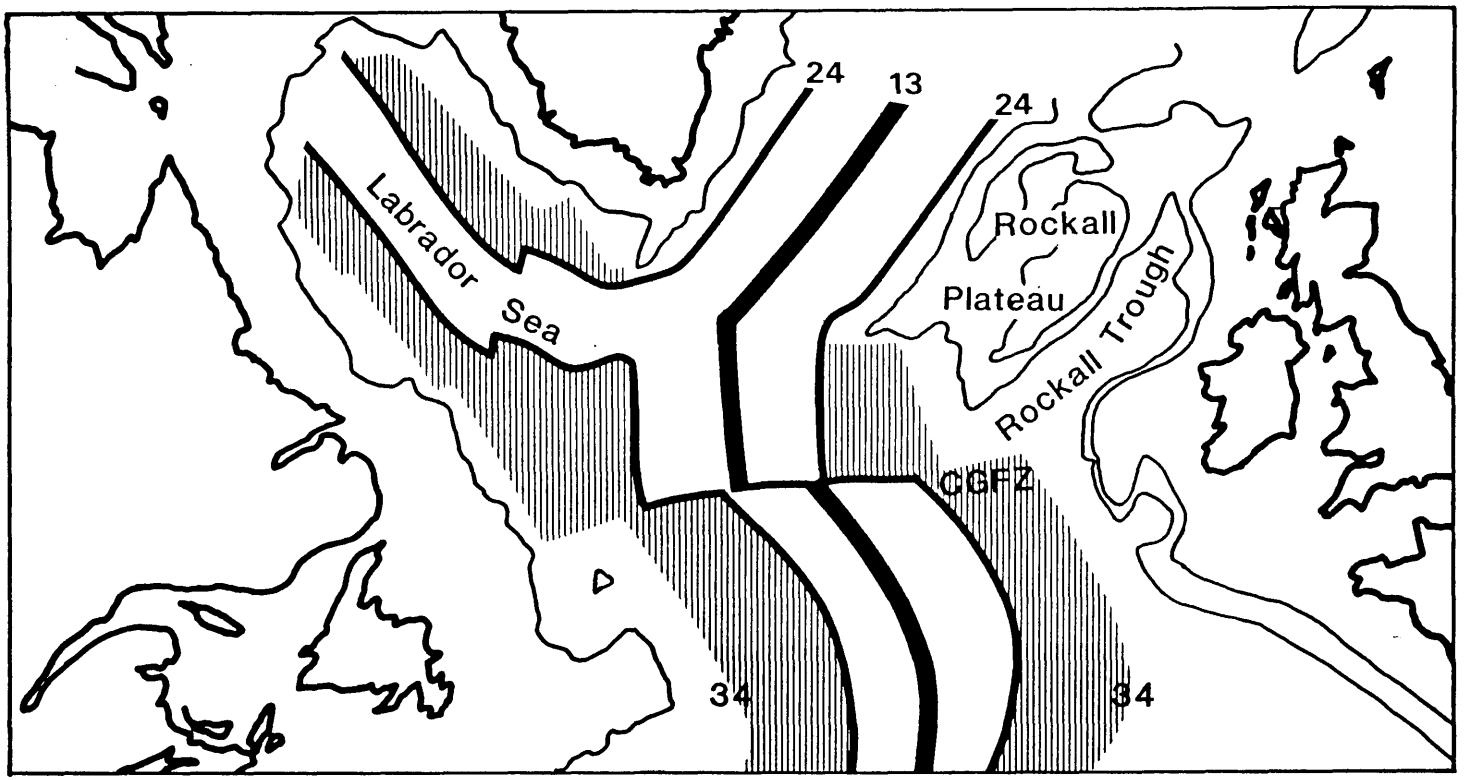

Fig. 1.2 North Atlantic reconstruction for anomaly 13 (c. 35 Ma). Shaded area is crust created between anomaly 24 and 34 time.
CGFZ - Charlie-Gibbs fracture zone.

Scrutton (1972), was observed by Cambridge and Durham Universities in 1985. The interpretation of the results, which is still in progress at the time of writing, shows that the crustal structure is typically oceanic (R S White and G D Spence, pers. comm. 1987). This result can be extended to the full 220 km or more width of the Trough, at least for the area clear of the masking effect of Tertiary basalts and intrusives south of 58°N, by the author's own complementary unpublished work, based mainly on commercial reflection data, which shows:

(1) Layer 2 can be mapped over the southern Trough as a characteristic seismic sequence, which is observed (at one location below either margin of the Trough) to pass laterally into

(2) apparent seaward dipping reflector sequences of the type now known to typify volcanic passive margins, formed by 'subaerial sea floor spreading' (Smythe 1980, 1983; Mutter et al. 1982).

The sea floor spreading origin of the Rockall Trough (south of 58°N) has, therefore, only recently been established. It is possibly even more surprising that the age of the opening is still uncertain and controversial. The discussion below is a critical review of the published evidence, which, despite coming to some novel conclusions regarding the pre-anomaly 34 spreading history of the NE Atlantic, demonstrates that the question is still far from solved.

1.3 DISCUSSION OF THE AGE OF OPENING OF THE ROCKALL TROUGH

1.3.1 INTRODUCTION

The Rockall Trough and Rockall Plateau played a part in the development of plate tectonic theory twenty years ago. The classic 'Bullard' fit of the North Atlantic continents at the 500 fathom contour (Bullard et al. 1965) required that Rockall Bank - comprising Rockall, Hatton, and George Bligh banks - be retained as microcontinental fragments to fill a large gap left in the fit between Europe and Greenland. The

refit suggested a number of predictions, two of which were that the Rockall Plateau should be continental, and that the Rockall Trough be oceanic. Although the plateau - at least the Rockall Bank part of it - was recognised within a few years to be continental (see, for example, Scrutton 1970, Roberts et al. 1973), the age of the 250 km wide Rockall Trough remains debatable. This continuing uncertainty affects the pre-Tertiary history of the whole North Atlantic, from Biscay to Svalbard. Figure 1.3 shows that the Rockall Trough is the most southerly segment of an essentially continuous strip of deeply buried crust bordering the NW European margin. This strip can be referred to as the proto North Atlantic, as it represents the first, abortive, attempt at opening of the North Atlantic ocean.

The aim of this discussion is to review, and where necessary, to refute the various hypotheses that have been postulated concerning the age of the Rockall Trough. This discussion might appear to be somewhat pedantic, but it is nevertheless necessary (cf. Ziolkowski 1972) to refresh and/or dispose of some of the arguments of the last twenty years or so, even though many of them would no longer be supported by their original authors. The ground is thereby prepared for a relatively straightforward summary of the problem as it appears at present.

In the last decade a great deal of commercial exploration has been carried out over the NW European margin, but practically all of this remains confidential. The problem of referring to and publishing confidential commercial data within a sound scientific methodology has been discussed before (Smythe et al. 1983, pp. 374-375). Fortunately, the main results of the stratigraphic test well 163/6-1A, drilled in the northern Rockall Trough, can now be quoted, although the full results remain confidential until 1990.

Why is the age of the Rockall Trough important? Clearly it is of some interest to the oil industry, as the region is a possible future hydrocarbon province, but it also has a wider significance. There are a number of questions whose solution hinges on the outcome of the age controversy. These questions will be reviewed in Section 1.3.4 below,

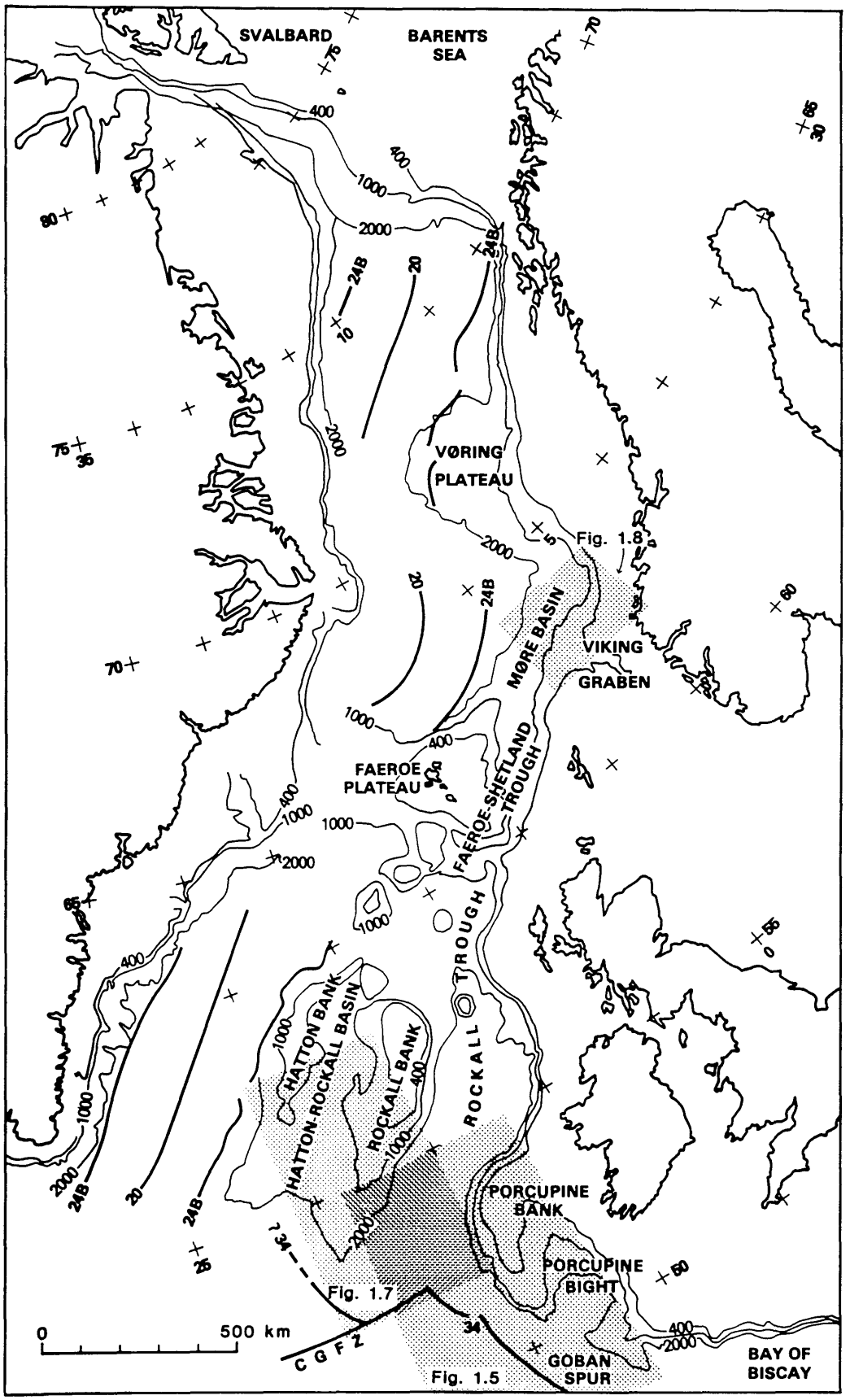

Fig. 1.3 North Atlantic reconstruction for anomaly 20 time (c. 45 Ma), showing oldest recognisable Tertiary anomaly 24B (c. 52 Ma). The 'proto North Atlantic' comprises the pre-Tertiary deep-water strip including the Rockall and Faeroe-Shetland Troughs, Møre Basin and inner Vøring Plateau. CGFZ - Charlie-Gibbs fracture zone. Stippling shows areas detailed in Figures 1.5, 1.7 and 1.8. This reconstruction is similar to that of Nunns (1983, fig. 5), but avoids the overlap of Greenland onto the Svalbard shelf evident in the latter. Transverse Mercator projection, central meridian 15°W.

after the examination of the age problem itself.

In summary, two principal ages, assuming a sea floor spreading origin have been most frequently quoted and discussed - Cretaceous and late Palaeozoic - of which the former is generally most favoured. The origin by sea floor spreading has been questioned, and a mechanism of development by intra-continental subsidence, starting in the late Palaeozoic, has been proposed instead (Talwani and Eldholm 1972). However, the question of the mechanism of origin is largely independent of the arguments for the age of development, and has, in any case, probably now been resolved beyond dispute. However, it is worth mentioning here that the main problem with the intra-continental subsidence hypothesis is one of scale. There is no currently understood mechanism whereby a pre-attenuation crustal thickness of 27-32 km (the thickness of the crust below the NW British shelf and the Rockall Plateau) could have been stretched out by a factor (ß) of around 5, to give the flat-lying 6 km-thick crust below the Trough, without producing tilted fault blocks in the stretched upper crust. It would be unusual for intra-continental stretching to exceed ß-factors of 2 or 3 without sea floor spreading taking over.

1.3.2 THE ARGUMENTS FOR CRETACEOUS SPREADING

The reasons for the widespread adoption in the early 1970s of a Cretaceous age for sea floor spreading in the proto North Atlantic, in preference to the previously assumed Permo-Triassic age (Bott and Watts 1971; discussed below), appear to have originated in the acceptance of a late Triassic - early Jurassic age for the start of opening in the Central Atlantic (i.e. between Africa and North America), combined with the reasonable assumption that Atlantic rifting advanced progressively northwards (e.g. Hallam 1971; Pitman and Talwani 1972). Thus the possibility of an earlier separation of Europe from Greenland, for example in the Permian or Triassic, seemed to be precluded.

1.3.2.1 Early Cretaceous Spreading

Given the above conclusion of a post-Triassic constraint on the age, the speculative suggestion of opening throughout the Cretaceous (Hallam 1971) was revised to an early Cretaceous episode by Roberts (1974), using the following reasons:

(1) Faunal provinciality. The provinciality of Jurassic ammonites in the northern hemisphere, with the Boreal fauna of east Greenland distinct from the Tethyan fauna of Europe (found as far north as the Hebrides) "implies a physical barrier" (Roberts 1974, p. 347) which would therefore preclude the existence of Jurassic or older ocean floor between these localities.

This view was shortly afterwards refuted by the discovery of a Middle Jurassic Boreal ammonite in a well core in the Viking Graben (Callomon 1975). But in any case the invocation of an actual physical barrier as an explanation for faunal provinciality was already outmoded, having been replaced by climatic considerations (cf. Casey and Rawson 1973).

(2) Orphan Knoll. DSDP hole 111 on Orphan Knoll encountered continental Bajocian sands containing derived anthracite fragments of South Wales coalfield affinities. This suggested that Orphan Knoll was attached to the European continent until at least post-Bajocian time.

This evidence, even if taken at face value, is only a constraint on the date of separation of Orphan Knoll itself from the Porcupine Bank area, and does not preclude an earlier opening of the Rockall Trough, if, for example, a transform-rift-transform geometry such as that used by Russell and Smythe (1978, fig. 1) is envisaged. In any case, the only sound conclusion which should be drawn from such evidence is that coal measures were being eroded within a few kilometres of the site during the middle Jurassic.

(3) Seaways. "The more complete geological history of the British Isles suggests a seaway, perhaps as early as the Valanginian" (Roberts 1974, p. 351).

Evidence of seaways is certainly suggestive of rift zones, but is not, of course, 'proof' of an oceanic floor. However, there is evidence for a seaway between east Greenland and the British Isles at various epochs back to the mid Permian, not merely back to the early Cretaceous (Callomon et al. 1972). More specifically, it has been inferred that a seaway existed to the NW of Scotland in the mid Permian, to connect the Bakevellia sea to the northern ocean (Pattison et al. 1973). Thus from this sort of evidence it can only be concluded that there may have been a rift zone (whether intra-continental or oceanic) in the region of the Rockall Trough in existence by mid Permian time.

(4) Sedimentation rates. Estimated sedimentation rates of the undated sedimentary pile in the Rockall Trough below a seismic reflector 'Y', dated as 76 Ma, and above supposed oceanic basement, suggested formation of the oceanic crust in early Cretaceous time.

Not only are such sedimentation rate estimates "notoriously unreliable" (Roberts 1975a, p.494), but Roberts et al. (1981) later substantially revised the age of reflector 'Y', to the late Palaeocene or early Eocene (52-55 Ma). Furthermore, the reflector originally identified by Roberts as top oceanic basement is 1-2 s of two-way reflection time (TWT) above the reflector now recognised to be the top of oceanic layer 2. This revision has been made by correlating commercial multichannel reflection profiles to crustal refraction profiles (unpublished work of the author), and is corroborated by the Cambridge/Durham wide-angle experiment referred to above. The discrepancy in identification of the top basement reflector can also be seen by comparison of the original time-to-basement map of Roberts (1975a, fig. 18) with the more recent version of Roberts et al. (1981, fig. 4), which was compiled from the better-quality multichannel reflection data available

to 1977. Clearly the extrapolation of sedimentation rates, particularly when the 'known' stratigraphy is subject to such drastic revision every few years, is a futile exercise.

(5) Magnetic anomalies. The last of Roberts's (1974) arguments cited a then-unpublished magnetic map, apparently showing that oceanic linear magnetic anomalies could be traced from west of Porcupine Bank into the Bay of Biscay, where, it was argued, the anomalies were of late Jurassic to early Cretaceous age.

The map was subsequently published (Roberts and Jones 1979), followed by a re-evaluation of the age of the anomalies (Roberts et al. 1981). This important evidence is discussed below.

1.3.2.2 More Arguments For Early Cretaceous Spreading

Two more arguments in support of early Cretaceous opening were put forward soon after Roberts's (1974) exposition:

(1) Wyville-Thomson Ridge. This trends NW-SE across the northern end of the Rockall Trough (Fig. 1.4). Bott (1975) suggested, from the results of a thesis by Himsworth (1973), that the ridge may be floored by oceanic crust contemporaneous with that of the Rockall Trough. The 'crust' underlies two sequences of sediment of which the uppermost is Oligocene and younger, separated by the widespread Eocene-Oligocene unconformity R4 (Roberts 1975a) from a thin lower sequence which may be "earliest Tertiary or Mesozoic". These inferences are "consistent with an early Cretaceous age for the Rockall Trough and Faeroe-Shetland Channel" (Bott 1975, p. 115), notwithstanding Himsworth's own conclusion that the reversely magnetised basaltic nature of the ridge complex suggested Permian sea floor spreading.

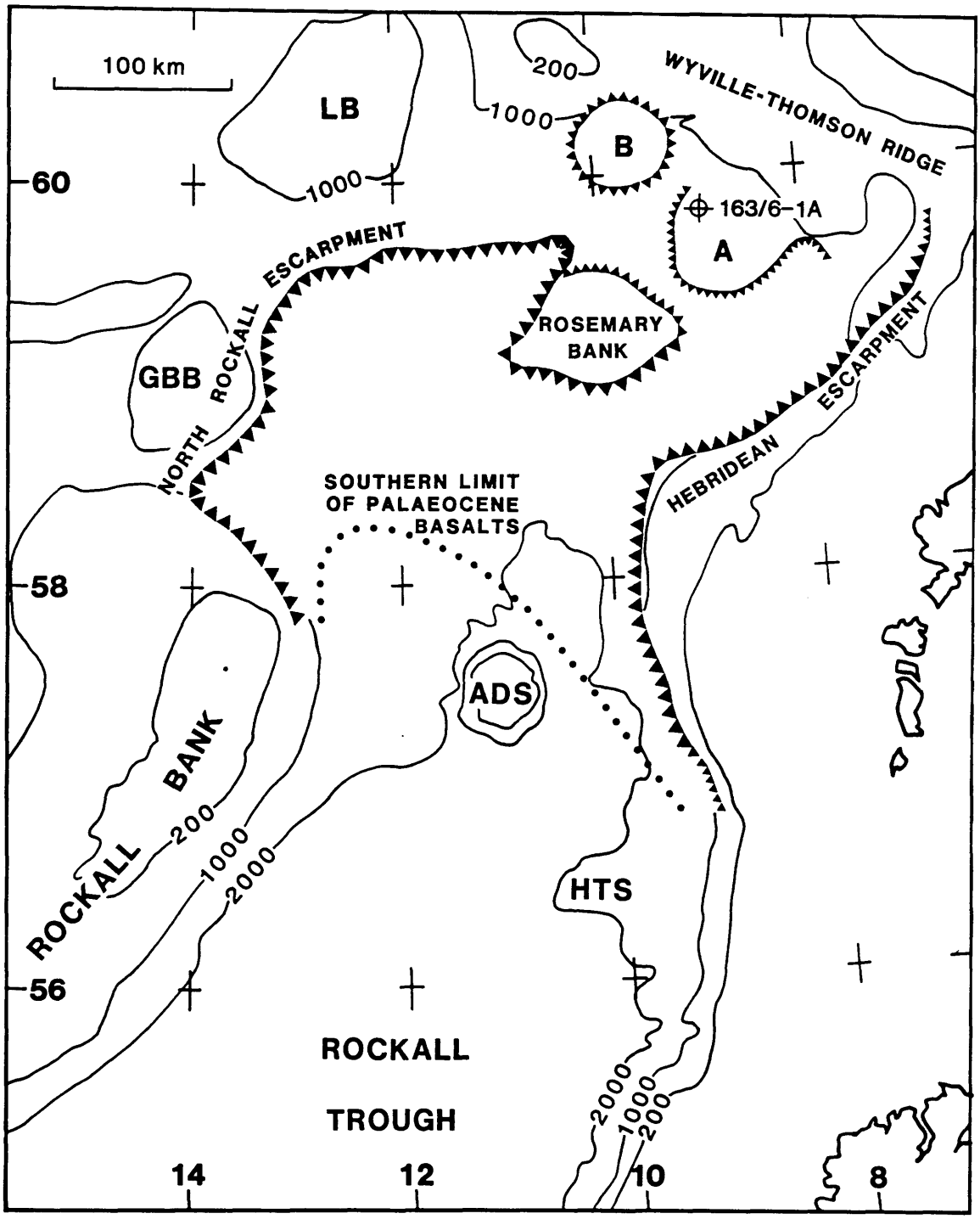

Fig. 1.4 Central and northern Rockall Trough region showing subcrop of buried basaltic escarpments (hachures) bounding thick sequences of Eocene age basalts covering the northern Rockall Bank, George Bligh Bank (GBB), Lousy Bank (LB) and Wyville-Thomson Ridge. Thinner underlying flows of late Palaeocene age underlie most of the northern Rockall Trough, ending in the region of the dotted line, south of which sills and intrusives of presumed Palaeogene age are common. Buried volcanic centres A and B (Roberts et al. 1983) are mainly escarpment-surrounded and form buried structural highs. ADS - Anton Dohrn seamount. HTS - Hebrides Terrace seamount. Bathymetry in metres.

The supposed oceanic basement here is now recognised (Roberts et al. 1983) to be the top of the Palaeocene-Eocene basalts underlying most of the northern Rockall Trough (Fig. 1.4), as proved by the stratigraphic test well 163/6-1A (Morton et al. in press), and as was originally suggested by Roberts (1970). It thus has no relevance to the age of the underlying crust.

(2) Cimmerian tectonism. The second supporting argument for early Cretaceous spreading related the mid Jurassic to early Cretaceous phase of extensional tectonism newly recognised on the continental shelf around the British Isles (cf. Ziegler 1975) to the initiation of spreading in the Rockall Trough (Roberts 1975b, p. 91), with the corollary that all such earlier phases back to late Palaeozoic times could be relegated to "post-Hercynian orogenic collapse" (Roberts 1974, p. 346) and/or a long period (c. 160 My) of rifting prior to sea floor spreading in the North Atlantic.

The importance of a late Palaeozoic rifting event in the North Atlantic is now widely acknowledged. For example, Ziegler portrays 'Rockall' and 'Faeroe' rifts on his Stephanian-Autunian palaeogeographic map (1982, enclosure 12), although he still favours Cretaceous sea floor spreading. Evidence of rifting, therefore, provides more support for late Palaeozoic spreading than for Cretaceous spreading.

1.3.2.3 Continental Reconstructions

Kristoffersen (1978) revised the identification of magnetic anomalies 31 and 32 in the North Atlantic to numbers 33 and 34 respectively. Anomaly 34 (c. 80 Ma) runs generally across the mouth of the Rockall Trough, and is offset by the Charlie-Gibbs fracture zone (Fig. 1.3). He also noted the contrast in the magnetic signature within different parts of the Rockall Trough; south of about 55°N it is "noisy" and correlatable with the oceanic crust further south, whereas

north of 55°N it is "very smooth", consistent with formation by spreading during a single geomagnetic polarity epoch, or with subsided continent (1978, p. 281). He inferred that if the crust north of 55°N formed by sea floor spreading, then it probably did so during the Cretaceous 'long normal' epoch (108-80 Ma); but his reconstructions implicitly reject this oceanic crust assumption, showing instead subsided continent (1978, fig. 11). He concluded that the continental subsidence of the central Rockall Trough took place simultaneously with the spreading that created the "noisy magnetic" crust in the southern Trough, during the late Cretaceous, between 90 or 95 Ma and anomaly 34 time, 80 Ma, (Kristoffersen 1978, p. 287).

Srivastava (1978) independently came to the similar conclusion of a late Cretaceous opening date for the Rockall Trough, although this was arrived at as a by-product of plate tectonic reconstructions for the North Atlantic, rather than by specific study of the trough itself. The absence of recognisable anomalies in the trough could be explained, he says, since "they would largely be formed during the Cretaceous normal polarity epoch" (1978, p. 351).

Kristoffersen's and Srivastava's conclusions regarding the Rockall Trough both rely on the long-recognised constraint that it is a quiet magnetic zone (Heirtzler and Hayes 1967), together with the assumption that spreading (if any) occurred just before the time of anomaly 34, and contemporaneous with spreading west of Porcupine Bank and in the Bay of Biscay. Both of their North Atlantic opening histories thus imply spreading in the Rockall Trough during the mid to late Cretaceous rather than during the early Cretaceous.

1.3.2.4 Revision Of Date To Mid-late Cretaceous

After the publication of the magnetic map of the Rockall Trough (Roberts and Jones 1979), Roberts et al. (1981) published a detailed argument in favour of a Cretaceous opening, but with the date now revised to late Cretaceous

time (100-70 Ma) rather than the early Cretaceous date (pre-120 Ma) previously postulated (Roberts 1974, 1975a, b). The four new lines of argument are discussed in turn.

(1) Seismic stratigraphy. Roberts et al. (1981) discuss seismostratigraphic units in the southern Rockall Trough (west of Porcupine Bank; Fig. 1.5) bounded by four reflectors R4, X, Y and Z above basement, referring back to the mapping and terminology described by Roberts (1975). Reflector Y is assigned a late Palaeocene - early Eocene age, instead of the previous late Cretaceous estimate. The lowest unit lies between reflector Z and the top basement. It contains strong reflectors which rest on basement "both within the Rockall Trough and beneath its margins and may thus, in part at least, post-date its formation, although they may be partly contemporaneous with rifting at the margins". The pre-Z unit is dated as post-Albian by tying in the seismic profiles to DSDP holes 400A and 402A in the Bay of Biscay. Since one of Roberts's co-authors (D G Masson) was a scientist aboard Deep Sea Drilling Project Leg 80, their stratigraphy was presumably also tied in to DSDP 550 (deGraciansky et al. 1981) drilled in June 1980 on the oceanic crust west of Goban Spur; however this additional link is not explicitly mentioned in the 1981 paper, which states that to the north of the mouth of the Rockall Trough the correlation of the sediments (implying post-Albian oceanic crust) "does become more tenuous in Rockall Trough itself".

A number of questions are raised by this sort of regional correlation exercise. Firstly, even a short-range stratigraphic extrapolation oceanward along seismic line CM-11 (Fig. 1.5), away from the basement high apparently sampled by DSDP 550, demonstrates that there are pockets of sediment up to 600-700 m thick lying in the lows between the block-faulted oceanic crust. These sediments are undoubtedly older than the late Albian sediments drilled on the top of the high; the question is, how much older? Clearly the ocean crust itself is older still. The resultant over-optimistically precise dating by Roberts et al. of the oceanic crust some 200 km further north still, in the mouth of the Rockall Trough, as 'post-Albian' leads to problems in assigning a suitable age to the magnetic

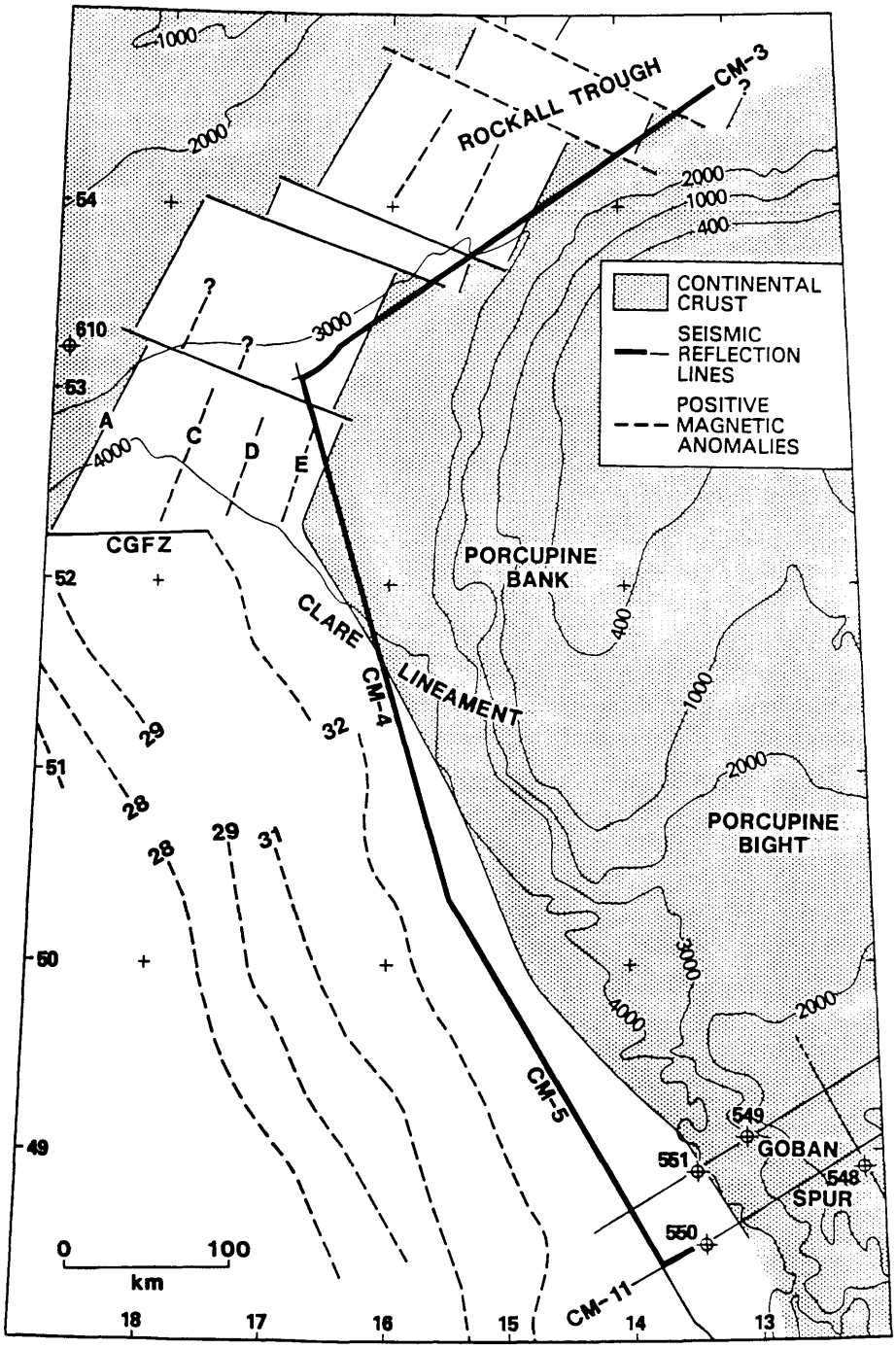

Fig. 1.5 Magnetic and stratigraphic correlations from Goban Spur region to Rockall Trough, according to Roberts et al. (1981). Area of map is located in Figure 1.3. A, C, D and E are modelled linear positive magnetic anomalies (see also Fig. 1.7). Anomaly 32 is now generally accepted as anomaly 34 (see Figs. 1.2 and 1.3). Bold portion of seismic reflection lines CM-3, CM-4, CM-5 and CM-11, tying seismic stratigraphy from Deep Sea Drilling Project (DSDP) well no. 550 to the Rockall Trough, is shown as a line drawing in Figure 1.6. CGFZ - Charlie-Gibbs fracture zone.

anomalies there. This is discussed below. Taking their seismostratigraphic correlations further north still, into the Rockall Trough proper, appears to be even more unsatisfactory as a way of dating the spreading in the Trough, since:

(a) Oceanic basement is significantly deeper in the Trough proper than west of Porcupine Bank, being buried by up to 2-3 km of pre-Z sediments,

(b) The mapping of reflectors X and Y by Roberts (1975) can be shown to be unsound, when transferred to the multichannel data available by 1977 (the locations of which are shown in Roberts et al. (1981). For example, a reflector on the multichannel data correlated as Y in the area of 56.3°N, 11.5 - 12°W becomes reflector X when tied to the old single channel data some 20 km further NE.

(c) No actual examples of the multichannel data in the Rockall Trough are presented by Roberts et al. (1981) - only line drawing interpretations of four unmigrated time sections (op. cit., fig. 2). While it is generally accepted that the only practicable method of publishing regional seismic data is to use line drawings (as is done here), some short samples of the data themselves should have been presented to try to demonstrate the authors' identifications of the reflectors and basement types. No justification is offered, for example, for interpreting the undulating basement on the drawing of one line (E-F) as oceanic, whereas on another, line G-H, with almost identical basement structure, it is labelled continental (Roberts et al. 1981, fig. 2).

(d) The correlation of reflectors along a solitary seismic profile some 900 km from DSDP 550 into the Rockall Trough (Fig. 1.5) - the only multichannel line available to date - is extremely difficult. It has been attempted by Bentley (1986, figs. 3.8 and 3.17) using a slightly simplified version of the line drawing used here. Figure 1.6 (in pocket inside rear cover) shows the line drawing of these data, made up from some

80,000 digitised coordinate pairs. Figure 1.6A shows the uninterpreted data; since almost every primary reflector has been digitised, subjective bias in choosing the 'important' ones has, it is hoped, been eliminated. Figures 1.6B and 1.6C show a progressive interpretation of the age of the sedimentary sequence, made using the character of the seismic sequences (which, of course, cannot be reproduced in a line drawing), and examination of interval velocities estimated from semblance plots at crucial localities along the line. The most important correlation is across the Clare lineament, where the sedimentary cover thickens considerably on the north side, and overlies deeper basement. It is interesting to note that corrected basement depth, after removal of a simple 1-dimensional loading effect of the sediments, is around 5.5 km on either side of the lineament.

The correlation across the lineament proposed here is similar to that obtained by D.G. Masson (pers. com. 1985) from a study of a reprocessed, time-migrated portion of the seismic section. The regional correlation differs from Bentley's (1986) interpretation in that his version ascribes the Albian (and older?) infill of Figure 1.6, between DSDP 550 and the Clare lineament, to younger Cretaceous rocks. This has the effect of dating the oldest infill at the northern end of the profile (in the Rockall Trough) as rather younger than proposed here. At higher levels the two independent interpretations are very similar. Notwithstanding these differences, Bentley has recognised that there is a major discontinuity across the Clare lineament, which he shows is the eastward prolongation of the Charlie-Gibbs fracture zone.

What the present correlation simply shows is that there are up to 2.5 - 3 km of pre-Upper Cretaceous sediment in the central part of the Rockall Trough. This thickness is typical of the whole trough across some 200 km of its width, and it is not just a local 'rifting' feature in the neighbourhood of the profile shown in Figure 1.6. It is most unlikely that the trough could have developed fully by presumed sea floor

spreading, and then have been covered by such a widespread blanket of sediment, all within the few million years of the late Albian. Although Bentley's (1986) stratigraphic correlations are somewhat different from those given here, he comes to a similar conclusion regarding the minimum age for spreading in the Rockall Trough.

(2) Magnetic modelling of basement. Prominent NNE-trending linear magnetic anomalies over the crust west of Porcupine Bank have been modelled by Roberts et al. (1981), partly in an attempt to refute the Permian spreading hypothesis of Russell and Smythe (1978). They conclude that the anomalies, which are labelled A, C, D and E in Figure 1.5, are from late Cretaceous oceanic crust, and that they can be recognised, traced across several fracture zones, in the Rockall Trough itself.

This modelling and interpretation has a number of weaknesses:

(a) Roberts et al. seem to have missed the important point that the mere presence of reversals within the oceanic crust here is sufficient to rule out the possibility of spreading during the late Carboniferous or Permian. Within the period 300-235 Ma (the Kiaman interval; McElhinny 1973) there are only two published normal events (or excursions), at around 260-265 Ma (Creer et al. 1971; Valencio and Vilas 1972; Turner and Vaughan 1977). These may both represent the same event, and it is very unlikely that this short event (or pair of events) could account for the observed anomalies, which occupy a zone some 120 km wide, and are up to several hundred nanoTeslas in amplitude.

(b) The geometry of opening of the Rockall Trough postulated by Russell and Smythe (1978, fig. 1) implies, in any case, that the area of crust west of Porcupine Bank studied by Roberts et al. is younger than the supposed Permian crust of the main trough.

(c) Their method of discriminating between 'Permian' and 'Upper Cretaceous' anomalies has little hope of

success, because both pairs of vectors (i.e. upward and downward-pointing) project onto the E-W 2-dimensional model profiles in similar directions, the projected Cretaceous vectors being somewhat larger than the Permian. There are no independent constraints on the positions of the magnetised blocks, nor on the magnetisations assumed within them. It is not surprising, therefore, that their 'Permian' model anomalies turn out simply to be a lower-amplitude version of their 'Cretaceous' anomalies (Roberts et al. 1981, fig. 5).

(d) Even accepting that the anomalies in the mouth of the Rockall Trough can be accounted for by reversals within ocean crust, "their northward change to a magnetic quiet zone remains problematic" (Roberts et al. 1981, p. 123). A simple rejection of the assumption that the anomalies continue north-eastwards removes this 'problem' of the change to a quiet magnetic zone; Figure 1.7 shows how the same anomalies can be correlated in an S-shaped pattern, running into the Hatton-Rockall Basin, and avoiding the main Rockall Trough altogether. The data in Figure 1.7 north of 54°N come from as yet unpublished high-quality aeromagnetic maps; however, examination of the older, published shipborne magnetic data (Roberts and Jones 1979), on which Roberts et al.'s interpretation is based, show that the anomalies do follow this S-bend trend, and that they cannot be convincingly traced north-eastwards into the Rockall Trough. The implications of this re-interpretation are discussed further below.

(e) As anomaly 32 west of Porcupine Bank (Roberts et al. 1981) is now accepted by at least two of the three co-authors as anomaly 34 (Masson and Miles 1984), this raises the problem of the origin of the post-late Albian, pre-34 anomalies. Although there are one or two documented reversals within the long Cretaceous normal polarity epoch (e.g. Pechersky and Khramov 1973; Van Hinte 1976), and a mixed polarity zone within the Albian has been sampled by drilling both at DSDP sites 263 and nearby 550, these occurrences do not seem

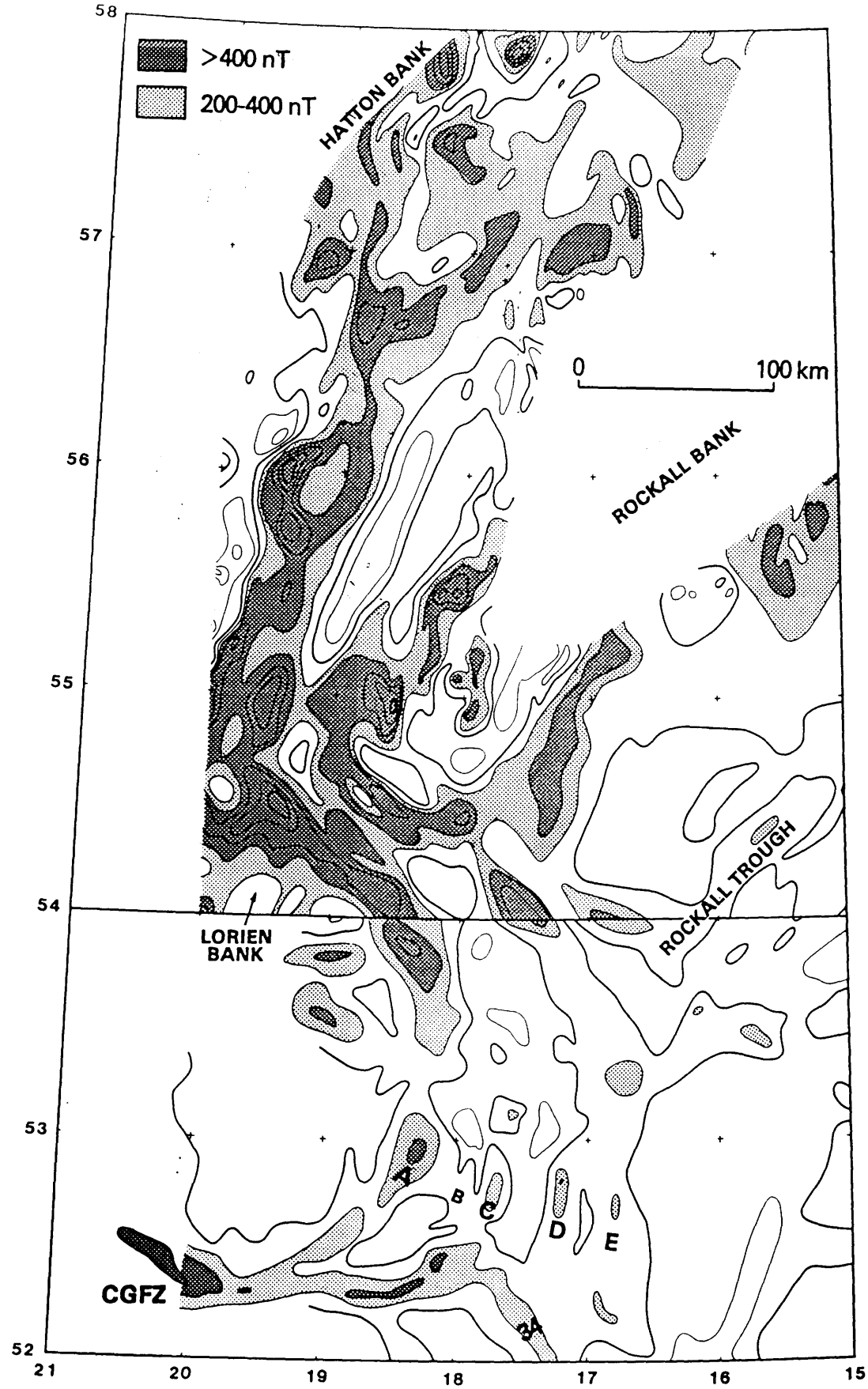

Fig. 1.7 Magnetic anomalies in the southern Rockall Trough and Hatton-Rockall Basin, at 200 nT contour interval. South of 54°N they are marine data redrawn from Roberts and Jones (1979), and as modelled by Roberts et al. (1981). North of 54°N they are based on unpublished aeromagnetic data held by BGS (flight height 300 m, E-W line spacing 15 km). Note the general continuity of the linear group of anomalies A - E in an S-shaped pattern running from the Charlie-Gibbs fracture zone (CGFZ) northwards into the southern Hatton-Rockall Basin, between Lorien and Rockall Banks. Whatever the origin of the anomalies, it is evident that they do not continue into the Rockall Trough. The same general S-shaped pattern can be seen on the published marine magnetic map.

to be sufficiently substantial reversals to account for the observed pre-anomaly 34 anomalies. P.R. Miles (pers. comm.) suggests the possibility that there are other reversals as well, still undocumented, within the long normal epoch, but this must be regarded as speculation. In view of the very weak 'post-late Albian' constraint on the age of the oceanic crust, derived from the seismic stratigraphy discussed above, one solution would be to regard this age as only very approximate, and permit the age of the crust in question to be somewhat older - early Cretaceous, for example. The anomalies could then represent two or three reversals within the M-sequence of the geomagnetic polarity reversal time-scale. This is preferable to the alternative of postulating major, but as yet undiscovered, anomalies within the late Cretaceous long normal epoch (100-70 Ma). However, with these caveats in mind, the tectonic event which produced these anomalies can be loosely referred to as the 'mid' Cretaceous sea floor spreading phase.

(3) Rosemary Bank. The magnetic anomaly over Rosemary Bank (Fig. 1.4) has been re-modelled by Miles and Roberts (1981), following a previous attempt by Scrutton (1971). After removal of the small positive anomaly over the crest of the seamount, the main negative anomaly has been modelled in three dimensions, leading to the conclusion that the causative body formed in high palaeolatitudes, appropriate to late Cretaceous or more recent time. Onlap of the mid Tertiary reflector R4 precludes a late Tertiary or younger age. Miles and Roberts conclude that their result is consistent with a mid-Cretaceous origin for the Rockall Trough, and rules out the tentative Permian age inferred by Scrutton, which was used as supporting evidence of early opening by Russell and Smythe (1978).

Miles and Roberts have therefore shown that Rosemary Bank cannot be cited as evidence for a Permian age for the Rockall Trough. However, the assertion by Roberts et al. (1983, p. 141) that the Tertiary lavas of the northern Rockall Trough have "no obvious relationship" to Rosemary Bank is untenable, because the North Rockall Escarpment, as mapped on commercial seismic reflection data, curls around

the bank as shown in Figure 1.4. It appears, therefore, that Miles and Roberts have merely succeeded in modelling the magnetic edge effect of the early Tertiary basalts, which have no direct bearing on the age of the Rockall Trough.

(4) 'Sills' in the Møre Basin. The most recently published argument for Cretaceous spreading in the Rockall Trough (Price and Rattey 1984) draws upon commercial seismic reflection data interpretation in the Møre Basin and eastern Norwegian Sea (Fig. 1.8). In the Møre Basin sill-like reflectors occur just below Price's and Rattey's base Upper Cretaceous horizon, which has been dated by correlation south to wells in the Viking Graben. Price and Rattey suggest that the intrusion of these sills may be an indication of a quasi-oceanic spreading event, followed by considerable subsidence here and in the Vøring Basin during the late Cretaceous.

From their observation of "strong discontinuous reflectors" in the southern Møre Basin, Price and Rattey make a series of increasingly speculative leaps in interpretation. Firstly, the events are interpreted as "apparent sills and lavas". Secondly, the 'sills' are "dated as pre-Cenomanian by seismic ties to wells in the North Sea". Thirdly, the 'volcanic events' are said to be "identical" to events seen in the southern Rockall Trough (Roberts et al. 1981) on "refraction seismic, gravity and magnetic profiles". Lastly, they are interpreted as "having formed by the accretion of oceanic crust in abnormally shallow water depths with contemporaneous, rapid clastic sedimentation. No single igneous basement surface would form in such circumstances".

Figure 1.8 summarises the published data in the Møre Basin, together with several interpretations. The location of the Faeroe-Shetland Escarpment is identical on the maps by Smythe (1983, fig. 2) and by Bøen et al. (1984, fig. 1). Similarly, the locations of the Palaeocene basalt feather edge (or lava front) are closely comparable, minor differences in the area of 63°N, 2°E being due to the latter authors interpreting some events as lavas rather than sills, as on the author's unpublished map. The versions by Hamar

Fig. 1.8 Summary map of published data on the Møre Basin (located in Fig. 1.3). Several versions of the Palaeocene basalt feather-edge subcrop are shown. Stippled area is interpreted as lava subcrop by Hamar and Hjelle (1984), but the interpretation of this area as early Tertiary sills is preferable (see text). Published seismic reflection sections or line drawings from sections are as follows: Profile 1 - Bøen et al. (1984, fig. 11); Geoprofile 3A - Bukovics et al. (1984, fig. 3A); V2803 - Talwani (1974), Smythe et al. (1983, figs. 10, 11). BP 75-39 - Smythe et al. (1983, fig. 6); B-3-74 (A) - Price and Rattey (1984, fig. 5); B-3-74 (B) and (C) - Hamar and Hjelle (1984, plates 12 and 11, respectively); MCS-160A - Mutter (1984, fig. 23); 2-75A - Rønnevik and Navrestad (1976, fig. 6). Unidentified line in area of 4-5°E, 62-62.5°N - Rønnevik et al. (1975, fig. 8, line CC'). Isochrons on base Cretaceous are redrawn from Bøen et al. (1984, fig. 10); if their interpreted age of this horizon is correct, then the Møre Basin is presumably pre-Cretaceous in age.

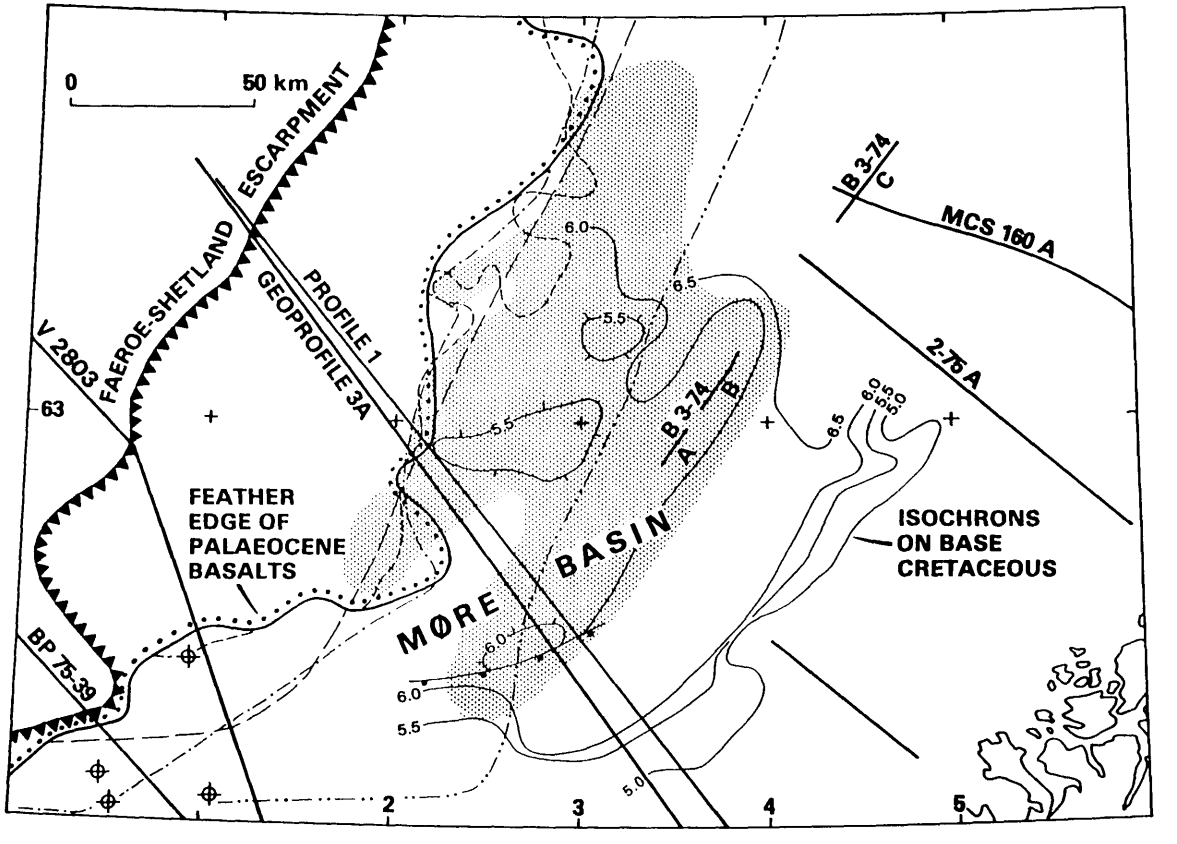

Feather edge of Palaeocene basalts:

Smythe (1983)

Other versions are:

Bøen et al. (1984)

Hamar & Hjelle (1984)

Bukovics et al. (1984)

Price & Rattey (1984)

Subcrop of 'eastern lavas' (Hamar & Hjelle 1984)

Published seismic reflection lines and profiles

Exploration wells

and Hjelle (1984) and Bukovics et al. (1984) of the lava front are also similar, but that by Price and Rattey (1984, fig. 3) is 50 km further south than the other four versions. As their sample of seismic data (Price and Rattey, fig. 5) is also apparently mislocated some 25 km south of its proper position, cartographic error is suggested. The unexplained oval region, some 130 km long by 70 km wide, on Price's and Rattey's map is described (in a provisional preprint of the paper) as an "area where pre-Cenomanian volcanic beds are inferred in the Møre Basin". This area approximates to the more complex zone of 'eastern lavas' mapped by Hamar and Hjelle (1984, fig. 6; stippled area in Fig. 1.8 herein), if Price's and Rattey's outline is moved northwards by 25-50 km to place it in the position its authors presumably intended.

There are two ill-founded arguments in Price's and Rattey's interpretation of the reflectors in question as representing mid Cretaceous oceanic crust:

Firstly, no independent evidence for an origin by eruption has been presented, but, in contrast, some of the events in the region cross-cut the sedimentary pile (e.g. Bøen et al. 1984, fig. 16). There is, therefore, no justification for interpreting them as lavas rather than as sills. Concordancy with bedding is not sufficient reason to prefer an eruptive over an intrusive origin. Francis (1982) has described the mechanisms of emplacement of sills, with particular reference to the Stephanian (c. 295 Ma) sill complexes of northern Britain. It is clear that on a regional scale such sills are essentially 'smooth', and concordant with bedding over areas on the order of 100 x 100 km^2 . They were intruded some 0.5 - 2 km below the contemporary land surface. At the depths at which the sill-like reflectors in the Møre Basin are observed, seismic reflection cannot resolve the small-scale structure, such as the step-and-stair transgressions seen in the field.

Hamar and Hjelle have, however, assumed that the features are all volcanic in origin, erupted at "as many as four stratigraphic levels". In their example (Hamar and Hjelle 1984, plate 12; line B-3-74 part B on Fig. 1.8), which is adjacent to the portion of the same line reproduced by Price

and Rattey (see Fig. 1.8; line B-3-74 part A), the lowest of these 'lava' events appears to be a water-column peg-leg multiple of the uppermost one. The observations that:

(1) They are 'thin' events (i.e. with the top and bottom not resolved as separate reflectors anywhere, and with good transmission of energy through each of them), and

(2) they occur at various stratigraphic levels (multiples omitted) throughout the upper, mid and lower Cretaceous,

strongly implies that even the concordant events are intrusive rather than eruptive. A basalt field subcropping over such a large region would be expected to show some thickness variations and, in places, features such as escarpments, internal bedding, and signs of intrusive centres (cf. Gatliff et al. 1984). It is highly unlikely that several such sub-provinces would occur without any of these features, one above the other, over an interval of 20-50 Ma, as Hamar and Hjelle's 'lava' interpretation implies.

Given that the case for at least some of the events as originating from lavas rather than sills has not been made, there is then no justification for dating the events as pre- or intra-Cenomanian. There is no reason to alter the conclusion of Hinz et al. (1982) that the events are simply Tertiary in age and are related to the late Palaeocene - early Eocene basalts to the west (Fig. 1.8). Bøen et al. (1984, p. 262) reached the same conclusion on regional grounds. The close age and spatial relationship of the early Tertiary volcanics and intrusives has been demonstrated further SW in the Faeroe-Shetland Trough (Smythe et al. 1983, fig. 6), where sills as well as lavas have been drilled (Gatliff et al. 1984). Limited occurrences of late Cretaceous intrusions are also likely (cf. Ridd 1983).

In the Møre Basin the sill events are 0.5 - 4 km below the top Palaeocene. Assuming probable shallow water depths at that time, this range of depth, as an estimate of

contemporary intrusion depth, is quite reasonable for sill intrusion during the late Cretaceous and Palaeocene.

Secondly, Price and Rattey have dated the reflector "immediately above the 'volcanic events'" as intra-Cenomanian, by tying to wells in the Viking Graben to the south. This is not as well established as Price and Rattey imply. If it were, then presumably the Norwegian Petroleum Directorate interpreters (Bøen et al. 1984), using a larger regional data base than available to Price and Rattey, would not have dated the same horizon as base Cretaceous. Isochrons on this horizon are shown in Figure 1.8, redrawn from Bøen et al. (1984, fig. 10). Similarly, the mapping by Norske Shell (Bukovics et al. 1984) shows a 'near base Cretaceous marker' (labelled horizon T30) subcropping over the Møre Basin and tied to wells at the NE end of the Viking Graben. Bukovics et al. (op. cit., fig 3A) attempt to illustrate the well-ties, in contrast to Price and Rattey, by reproducing a 'geoseismic section'. The location of this is shown in Figure 1.8 (Geoprofile 3A). Furthermore, the "firm stratigraphic control for the regional profiles" supposedly provided by drilling on the mid Norwegian margin at Haltenbanken (Price and Rattey 1984, p. 985) simply does not exist, as regional ties from that area to the Møre Basin are made by jump-correlating over major fault zones (e.g. Price and Rattey, op. cit. fig. 3).

Clearly it is premature, given our present limited understanding of the deeper stratigraphy and structure of the Møre Basin, to try to draw any firm conclusions about the age of spreading in the Rockall Trough, and about whether or not spreading extended as far north as the Møre Basin itself (or even further north still). Four wildcat wells have recently been completed in the UK sector of the SW Møre Basin (Fig. 1.8). When the results of these are made available, they should help to determine whether the cautious prediction of "at least 2-3 km of pre-Turonian sediments" in the Møre Basin (Smythe et al. 1983, p. 395) is correct.

1.3.2.5 Discussion Of Cretaceous Spreading

It is generally agreed that there was a phase of mid Cretaceous spreading represented by the strip of oceanic crust landward of anomaly 34, and seaward of southern Porcupine Bank and Goban Spur. The strip is shown in Figure 1.5 south of the Clare lineament where, however, anomaly 34 is labelled in its former guise as 32. The crust is reliably dated as late Albian (or possibly just older) by DSDP 550 (Figs. 1.5 and 1.6), and, in common with ocean crust of that age, it lacks magnetic reversals (R.A. Scrutton, pers. com.). This date also fits neatly into the geometric opening history south of 52°N, involving Iberia, Europe and North America, as outlined by Masson and Miles (1984). However, two problems emerge if this crust is traced northwards. First, why does it develop large magnetic anomalies, which, if oceanic in origin, are inconsistent with a mid or late Cretaceous age prior to anomaly 34? Second, why is this 'magnetic' crust not traceable into the Rockall Trough proper?

As has been shown above, none of the arguments for Cretaceous spreading relating to the main part of the Rockall Trough (i.e. north of 54°N) can be sustained. Furthermore, if one extrapolates southwards from the Norwegian Sea through the Møre Basin and Faeroe-Shetland Trough - basins which are all supposedly (on geometric grounds) underlain by crust continuous with that in the Rockall Trough - all the presently available evidence suggests that most of the crust in these northerly regions is of pre-Cretaceous age. It is certainly older than the Albian age proved west of Goban Spur. On the other hand, there is evidence of a major change in tectonic regime north of 60°N, beginning at around the early-late Cretaceous boundary, as outlined by Price and Rattey (1984, p. 991), together with considerable subsidence and sedimentation in the Faeroe-Shetland Trough, Møre Basin and Vøring Basin (but not the Rockall Trough) during the late Cretaceous. This suggests that a phase of spreading (or intra-continental rifting) had only just finished. Figure 1.9 shows an outline attempt to answer some of these problems.

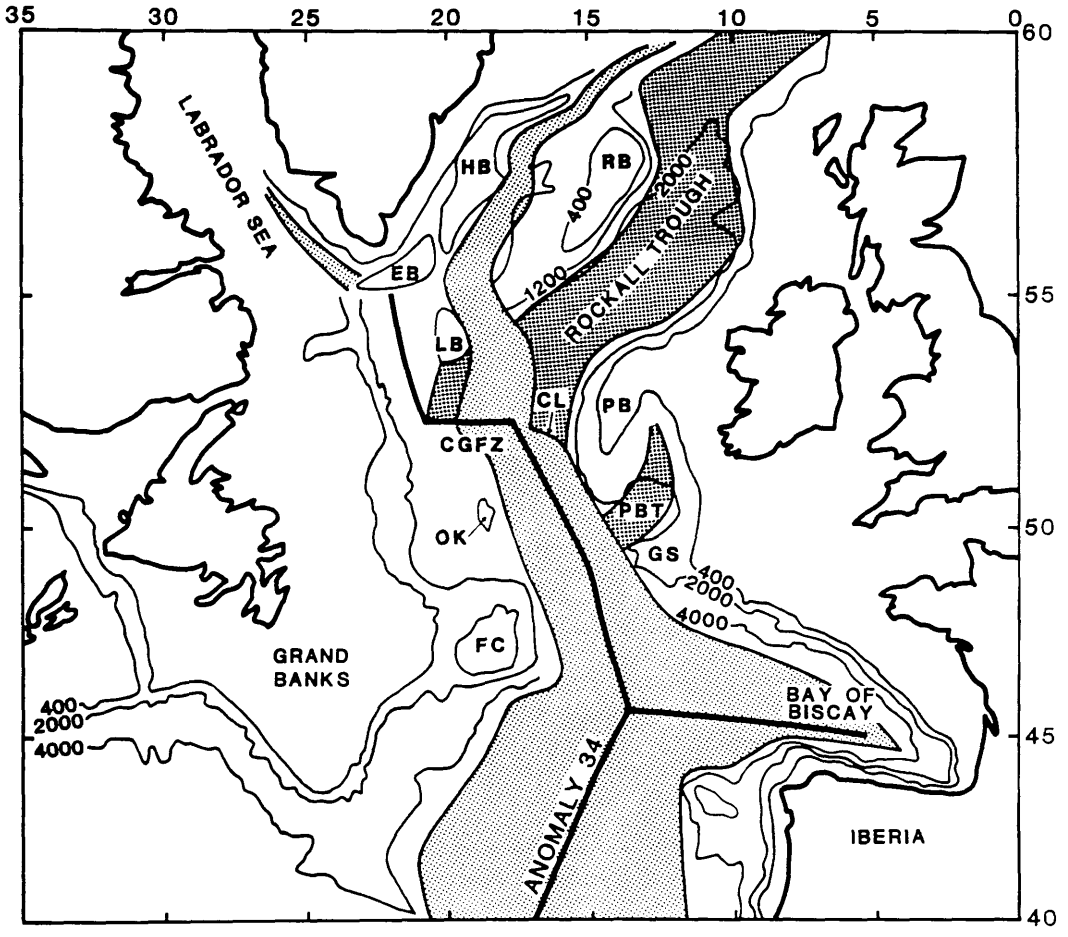

Fig. 1.9. North Atlantic reconstruction for anomaly 34 time (c. 80 Ma, early Campanian), redrawn from Kristoffersen (1978, fig. 6) with the fit of North America to Europe, and the location of anomaly 34 unchanged, but with Greenland some 100 km further south (see text). The 'mid' Cretaceous spreading phase (light stipple) corresponds to the partial opening of the Hatton-Rockall Basin, not the Rockall Trough as proposed by Roberts et al. (1981; see Fig. 1.5 above), the older oceanic crust of which is shown by the bold stipple. Note that this older strip terminates to the south at the Clare lineament, and is therefore inconsistent with the concept of a progressively northward-opening Atlantic. CGFZ - Charlie-Gibbs fracture zone; EB - Edoras Bank; FC - Flemish Cap; GS - Goban Spur; HB - Hatton Bank; LB - Lorien Bank; OK - Orphan Knoll; PB - Porcupine Bank; PBT - Porcupine Bight; RB - Rockall Bank.

Figure 1.9 is simply the anomaly 34 fit of North America to Europe of Kristoffersen (1978, fig. 6), with a shift in the position of Greenland (the justification for this alteration is discussed below). The figure shows that the pre- anomaly 34 'mid' Cretaceous crust which opened the Bay of Biscay and the area south of the Charlie-Gibbs fracture zone correlates satisfactorily with the spreading phase which produced the S-shaped pattern of magnetic anomalies (Fig. 1.7) and which partially opened the Hatton-Rockall Basin. There was an incipient triple junction complex developing at around 55°N, 20-23°W, incorporating minor motions of Edoras and Lorien Banks, as the Labrador Sea began to open, but spreading north of 52°N then shifted wholly west, to initiate the Charlie-Gibbs fracture zone, at anomaly 34 time. The prior spreading north of 57°N or so in the Hatton-Rockall Basin was probably very limited, as Figure 1.9 implies, and represented further north by a phase of intra-continental extension, the evidence for which has been mentioned above.

In summary, the 'mid' Cretaceous spreading phase by-passed the Rockall Trough, which was already in existence. The Clare lineament (Figs. 1.5, 1.6 and 1.9) represents a precursor of the Charlie-Gibbs fracture zone (Bentley 1986), and now juxtaposes the 'mid' Cretaceous crust with the older crust of the Rockall Trough proper. As we have already seen from the discussion above, if the Rockall Trough is indeed part of a continuous strip of 'proto North Atlantic' crust, then the seismo-stratigraphic evidence from the areas north of 60°N or so points to a pre-Cretaceous, and possibly even pre-Jurassic, age.

1.3.3 THE ARGUMENTS FOR LATE PALAEOZOIC SPREADING

The importance of the quiet magnetic zones bordering the North Atlantic continents was recognised early on (Heirtzler and Hayes 1967), and it was speculated that the sea floor beneath these zones could have developed during the Permian 'Kiaman interval' of reversed geomagnetic polarity. The quiet magnetic zone, extending northwards through the Rockall Trough (Roberts 1970) into the eastern Norwegian Sea (Avery et al. 1968), east of the magnetically striped

Tertiary sea floor (Fig. 1.3), is still an important constraint on the permissible ages of early sea floor spreading in the proto North Atlantic, although it also allows the alternative hypothesis of intra-continental subsidence (Talwani and Eldholm 1972).

1.3.3.1 Development Of The Arguments For Late Palaeozoic Spreading

Bott and Watts (1971) proposed that the Rockall and Faeroe-Shetland Troughs formed in "Triassic (or earlier) time", contemporaneous with the initiation of spreading between North America and Africa. They also mentioned several possible mechanisms whereby normal-faulted sedimentary basins could form on the shelf either "during the initial split" or later. They thus proposed a way of inferring the initiation of spreading from the effects of the relative horizontal tension on the adjacent shelf - in other words, what is nowadays referred to as the rift phase of plate separation and passive margin formation. However, there remains the practical difficulty of identifying the start of a rifting phase, and in a complex shelf area like NW Europe, of correctly associating it with the formation of a particular passive margin. Russell (1973) tried to relate changes in the tensional stress regime of northern Britain to the inception of spreading in the Rockall Trough at the end of the Carboniferous. He also introduced the idea of associating tholeiitic magma generation in the late Carboniferous with lithosphere separation - a concept which might seem to be readily acceptable in the British Isles, given the obvious analogous association of tholeiitic magmatism and the start of sea floor spreading in the early Tertiary.

Later, Russell (1976) developed a fuller analogy with the younger tectonic history of the Central Atlantic; he proposed that end-Carboniferous lithosphere separation, leading to spreading in the Rockall Trough during the early Permian, provided a more consistent analogous explanation of tectonic and magmatic events in the North Atlantic region than the Cretaceous opening history, which by then was the

orthodox view. A new feature of Russell's 1976 hypothesis was the inference that the late Permian (Zechstein) seaway between east Greenland and NW Europe (Callomon et al. 1972) implied the existence of an oceanic rift. In particular, the contemporaneous incursion of the distinct Bakevellia Sea into NW England from the Hebridean area (Pattison et al. 1973) implied that a seaway existed to the west of Scotland, as well as between east Greenland and Norway.

Russell and Smythe (1978) elaborated on the opening geometry of the supposed 'proto North Atlantic' rift suggested by Russell (1976), by plotting their reconstruction on an oblique Mercator projection (cf. Le Pichon 1968). This demonstrated graphically the feasibility of opening the North Atlantic before the Central Atlantic, using a transform-rift-transform geometry. They also suggested that the supposed Permian age of Rosemary Bank (Scrutton 1971) was a constraint on the minimum age of the Rockall Trough.

The conventional explanation (in contrast to Russell's 1973 hypothesis) of the late Carboniferous tholeiitic activity in northern Britain and the Oslo Graben had long been that it was a by-product of the Hercynian orogenic collision taking place at the same time some 500 km further south (see, for example, Francis 1978). Russell and Smythe (1983) postulated that this could indeed be the case, but only in an indirect way. They suggested that the proto North Atlantic rift could be viewed as a by-product of the diachronous Hercynian - Alleghenian collision forming Pangaea, while the tholeiitic magmatism of NW Europe, with its peculiar arcuate trend, was, in turn, a by-product of the rifting to the west and north. Their rifting history and explanation for the 90° swing in the trend of the intrusives has been tested quantitatively by finite element modelling of the stresses acting on the European plate during the rifting/intrusion phase (M J Russell, A G Skuce and the author, unpublished work).

In parallel with the development of the quantitative late Palaeozoic rift model discussed above, Haszeldine (1984) has undertaken a synthesis of regional palaeogeographic evidence for and against rifting in the North Atlantic region during the late Palaeozoic. He concludes that the evidence from

Upper Carboniferous rocks is consistent with a rift hypothesis, but not with the rival "megashear" or subduction hypotheses. He has tried to date the rifting/opening in the Rockall region by assuming that the dextral movement on the transform fault zone bounding the south end of the proto North Atlantic rift, presumed to run through the Biscay - Pyrenees area, was marked by similar displacements on the faults bounding the small 'fosse' basins in Cantabria, northern Spain. Movement on these ceased in latest Stephanian time. Haszeldine therefore postulates that the entire rifting/opening episode forming the Rockall Trough occurred during the late Carboniferous, and did not continue through the early Permian, as Russell and Smythe have assumed.

1.3.3.2 Discussion Of The Late Palaeozoic Hypothesis

There is no need to scrutinise each argument for late Palaeozoic spreading in detail, in contrast to their Cretaceous counterparts, because they all have the same overall weakness - simply, they all point (indirectly) to a major rifting episode in the late Carboniferous, but provide no direct evidence at all for the nature, width, or even the actual location of the rift. All the geological evidence presented in support of late Palaeozoic opening is equally consistent with a 'Rockall-Faeroe' rift zone, perhaps only 20-50 km wide, as with the supposed late Palaeozoic strip of oceanic crust more than 200 km across. Even the numerical modelling of the European plate, suggesting that its NW margin became completely decoupled from the Greenland plate (Russell et al. op. cit.) may only indicate that the continental lithosphere had been rifted to the stage where horizontal tensile stresses could not be transmitted across the rift. Whereas this inference may reasonably lead to the further inference that sea floor spreading might therefore be about to start, it does not necessarily follow that the full 200 km or more of spreading did occur immediately after the rifting phase.

Scrutton (1986) has argued that sea floor spreading normally follows the youngest identified rifting event, which in the

Rockall region he states is of late Jurassic - early Cretaceous age. He concludes that the Rockall Trough is therefore younger than early Cretaceous. Although his reasoning may well apply at passive margins where there was a single, well defined phase of opening, the problem in applying it here is that there have been several phases of spreading in and around the region, and several phases of rifting, from the late Palaeozoic to as recently as the Oligocene (the newly postulated Oligocene phase is discussed in Chapter 4). However, the argument highlights the assumption behind the 'early opening' views of Russell et al., that because the late Palaeozoic phase was the most important one, it is therefore the one most likely to have been the precursor of spreading. But with the removal of the Rosemary Bank constraint on the age of the Rockall Trough as being Permian or older (discussed above), the link between the well-documented late Palaeozoic rifting phase and the postulated late Palaeozoic spreading phase becomes rather more speculative than previously believed.

1.3.4 DISCUSSION

1.3.4.1 Outstanding Problems

In Section 1.3.1 it was pointed out that the age of the Rockall Trough was more than just a local problem in the evolution of the NE Atlantic. A number of important questions are, in fact, dependent on the age controversy. These questions can be summarised next under three loose headings - global, regional and local:

Global problems include:

(1) Do tholeiitic dyke swarms indicate the initiation of a spreading phase, or are they just evidence of local intra-continental tension, with no wider significance?

(2) Are the seaward-dipping reflector wedges seen at many passive margins underlain by thinned continent, or are they wholly or partly a product of sea floor

spreading?

(3) Did the Central and North Atlantic open progressively from south to north (in which case a post-early Cretaceous Rockall Trough fits the picture)?

(4) Do the loci of new mid-ocean ridges start by splitting apart some old continental lithosphere, rather than by occupying the site of an earlier, aborted spreading ridge?

(5) Do extension events on a continental shelf correlate in any systematic way with spreading phases nearby?

Regional problems include:

(6) How much of the proto North Atlantic rift zone (Fig. 1.3) is in fact oceanic? How, if at all, do phases of North Atlantic opening/rifting correlate with the rift phases of the basins west of the British Isles, and with those of the North Sea and east Greenland?

(7) Is North Atlantic rifting and opening a consequence of the diachronous collision episodes further south culminating in the Hercynian - Alleghenian orogeny?

(8) What is the age and subsidence history of the seamounts in the Rockall and Faeroe-Shetland Troughs? Do they sit on a relict mid ocean ridge? Have they been reactivated? Do their ages correlate with the intrusive episodes on the adjacent shelves?

Local problems include:

(9) What is the precise age of the 'mid' Cretaceous spreading phase which partially opened the Hatton-Rockall Basin? Is this phase truly oceanic, or is it in part intra-continental?

(10) What are the details of the spreading geometry of the area between SW Rockall Plateau, Goban Spur, and

the Grand Banks, with the numerous microcontinental fragments in between?

(11) How are the continent-ocean boundaries defined around the Rockall Trough region?

The origin of some of these questions can be found in the review above; the relevance of the others is discussed below.

1.3.4.2 Importance Of The Sequence Of Opening

The first opening between the Goban Spur (Europe) and the Grand Banks (Greenland - North America) is part of the same phase which began to open the Hatton-Rockall Basin (Fig. 1.9), according to the magnetic anomaly evidence discussed in detail above. The Rockall Trough (and Porcupine Bight) were both fully open before this phase started. It follows that the concept of the Atlantic splitting progressively northwards from the Central Atlantic is untenable, since there is no oceanic crust (nor extensively thinned continental crust) of the required age and width (c. 200 km) south of 52°N (Fig. 1.9) to correspond to that in the Rockall Trough. Bentley (1986) has also independently come to this conclusion.

The reconstruction shown in Figure 1.9 for anomaly 34 time is essentially the same as that calculated by Kristoffersen (1978) south of 52°N, and also corresponds to the opening geometry postulated more recently by Masson and Miles (1984). However, it is fundamentally different to the north, in that the Rockall Trough is shown as open, whereas Kristoffersen's reconstruction shows it closed. The reason for this difference is that in the revised version (Fig. 1.9), seaward dipping basalt reflector wedges now recognised at many passive margin localities around the Atlantic have been used as a new criterion for achieving a refit, according to the particular method of identifying the continent - ocean contact beneath them, described by Smythe (1983). The quality of fit, and the consistency or otherwise of the geometric opening history derived from it,

can therefore be regarded as a test of this particular interpretation of the seaward dipping reflectors. This explains the reference above to the Rockall Trough age problem as having a bearing on the global problem number (2) above, of whether the dipping reflector wedges are a product of sea floor spreading or of continental attenuation.

If the multi-stage opening history implied by Figure 1.9 is valid, the only feasible geometric solution for the abrupt southerly termination of the proto North Atlantic rift (the bolder stipple in Figure 1.9) is to accept something like the transform-ridge-transform geometry of Russell and Smythe (1978); this is irrespective of whether the Rockall Trough and its northerly continuation is underlain by truly oceanic, or by attenuated continental, crust. In either case, the 200 km or more of opening between the European plate and the Rockall Plateau (part of the Greenland - North America plate at the time) has to be transformed out to the SE and effectively lost in the poorly known plate geometry of the Tethys. Correlations of Precambrian outcrops across the closed Labrador Sea preclude the possibility of such a large transform motion being accommodated in that region, to the NW of the southern Rockall Trough. Acceptance of this kind of opening geometry implies:

(1) The proto North Atlantic rift developed first, and independently of, the other Mesozoic phases of spreading in the Central and North Atlantic, and

(2) It is therefore geometrically feasible for the rift to have opened at any prior time, right back to the formation of Pangaea in the late Palaeozoic.

1.3.5 SYNTHESIS AND CONCLUSIONS

The review of stratigraphic evidence necessarily introduced some previously unpublished data, but it has not been necessary to discuss the evidence for the origin of the thin, deeply buried crust of the Rockall Trough and other areas. The question of the age of the trough is largely independent of the problem of its origin. However,

reference to 'opening', although normally implying a sea floor spreading origin, can also be understood to include (considerable) continental attenuation, for example in the Vøring Basin or the Hatton-Rockall Basin. Now that large horizontal displacements of the continental lithosphere are believed to be necessary to form extensional basins (McKenzie 1978), it is quite permissible to talk, for example, about the 'opening' of the North Sea. Use of either meaning of the loose phrase 'opening' is possible in the following synthesis.

1.3.5.1 The Required Pre-drift Geometric Fit.

This is very tight, and takes us back to the classic Bullard et al. (1965) fit (which was also a tight reconstruction), in contrast to the various published refits of the 1970s, which were comparatively loose. That of Le Pichon et al. (1977) is probably the most frequently cited example of a loose fit. The synthesis outlined here depends very much on the use of a new, tight reconstruction to constrain the various opening phases. The justification for a tight fit is partly the use of seaward dipping basalt reflector wedges to identify continent-ocean boundaries (Smythe 1983), and partly the restoration of attenuated continental crust at passive margins to its presumed pre-rifting thickness and aerial extent. Details of the new reconstructions used here are, however, beyond the scope of this review.

1.3.5.2 Late Palaeozoic Rifting

Evidence for an important phase of late Carboniferous rifting is now good; it includes the systematic pattern of tholeiitic dykes and intrusions of the northern Britain - North Sea - Oslo Graben region (Russell 1976, Russell and Smythe 1978, 1983), the inferred tensile stresses from which have been quantitatively modelled in terms of a proto North Atlantic rift (Russell et al. unpublished work). There is also the recent exploratory drilling evidence of late Carboniferous freshwater and marine sediments west of

Britain and in the Porcupine Bight (Haszeldine 1984), in addition to the classic half-graben-controlled rift geology of onshore east Greenland. The importance of the rifting phase is now generally acknowledged, as signified, for example, by its prominence in the most recent synthesis of Ziegler (1982).

1.3.5.3 Opening Phase I

This comprises the contiguous strip of crust including the Rockall Trough, Faeroe-Shetland Trough, Møre Basin and inner Vøring Plateau (Fig. 1.3). Some 200-250 km wide in the south, it terminates abruptly at around 52°N, although the Porcupine Bight further south (Fig. 1.9) presumably developed at the same time. As discussed above, it is only an assumption - 'rift to drift' - that leads us to conclude, as a working hypothesis, that opening followed on from the rifting without a time gap.

The opening, in a NW-SE direction, in the southern part of this proto North Atlantic rift was presumably transformed out into the Tethys along a closed Bay of Biscay lineament - the 'proto Bay of Biscay' transform fault (Russell and Smythe 1978). Local stratigraphic evidence from northern Iberia suggests, indirectly, that this transform fault was active only until the Stephanian, which would put the entire rifting-opening episode into the late Carboniferous (Haszeldine 1984). However, if we look instead at the global picture of the formation of Pangaea, the transform fault may have also been the main lineament along which the early-to-mid Carboniferous Hercynian orogenic collision of western Europe was decoupled from the slightly younger Alleghenian orogeny to the SW, involving the collision of Africa into North America. Russell and Smythe (1983) suggest that the opening of the proto North Atlantic could have been a by-product of this diachronous collision, which terminated at the end of the early Permian. If this global view is correct, it would suggest that the opening phase spanned Stephanian to early Permian time.

These conjectures are all consistent with the important stratigraphic constraint discussed above, that the minimum age for the opening of the Rockall Trough is pre-Cretaceous, and probably pre-Jurassic.

1.3.5.4 Opening - Phase II

This phase, approximately mid Cretaceous in age, by-passed the Rockall Trough, but partially opened up the Hatton-Rockall Basin. The new crust formed is shown by the light stipple in Figure 1.9. In general terms it is contemporary with, or slightly younger than, the opening of the Bay of Biscay, and it also comprises the first opening between Goban Spur and Flemish Cap, i.e. between North America (south of the Labrador Sea) and Europe. Such stratigraphic evidence as has been cited in support of a Cretaceous age for the Rockall Trough, and which has not been completely invalidated, in general applies to this phase of spreading. For example, global interpretations of the North Atlantic such as those of Hanisch (1984) and Price and Rattey (1984), which draw, in particular, upon the evidence of Cretaceous rifting and subsidence in the Norwegian Sea, are equally consistent with this Phase II as with a supposed Cretaceous opening of the Rockall Trough.

1.3.5.5 Opening - Phase III

Just before anomaly 34 time (80 Ma), Phase II spreading was modified to begin opening the Labrador Sea, with the inception of the Charlie-Gibbs fracture zone (Fig. 1.9). Apart from the tighter pre-drift geometry, with a more southerly initial position of Greenland relative to North America, this phase is essentially as described by Srivastava (1978).

1.3.5.6 Opening - Phase IV

At around 54-55 Ma, just before anomaly 24B time, spreading began between Greenland and NW Europe again, but this time the location of the oceanic rift was west of the Faeroes and Hatton Bank. The early stages of this phase involved the completion of opening of the Hatton-Rockall Basin, along with small, but not insignificant, independent motions of the separate fragments between the Faeroe Plateau and Hatton Bank (see Fig. 1.3). An interesting feature of this initial fragmentation phase is that Lousy Bank (Fig. 1.4) may have moved NW with Greenland for some 50 km or more before being left behind. This implies that the crust around the bank, in the NW of the Rockall Trough, may be essentially oceanic, and of Eocene age, i.e. coeval with the eruption of the Tertiary basalts which now subcrop over the northern trough area (Fig. 1.4). Thus a small corner of the Rockall Trough is neither Palaeozoic nor Cretaceous in age, but is of early Eocene age.

There was a triple junction south of Greenland which persisted until the cessation of spreading in the Labrador Sea just after anomaly 13 time (35 Ma). Since then, spreading has continued between Greenland and Europe to open up the North Atlantic as we know it today.

1.4 SEDIMENTARY BASINS IN WESTERN BRITAIN

One of the outstanding global problems discussed above (Section 1.3.4.1) is the relationship between extensional events on a continental shelf and sea floor spreading nearby. The geology of the continental shelf west of Scotland (Fig. 1.10) ought to reflect in its structural history the stresses related to the opening of the Rockall Trough (opening Phase I above). The initiation of spreading west of the Rockall Plateau at about 55 Ma (Phase IV above), characterised by extensive 'volcanic' type passive margins probably related to a mantle plume beneath Iceland (White et al. 1987), is obviously related to the development of the Hebridean Tertiary igneous province, some 3-5 Ma previously. In the Palaeogene the new passive margin was several hundred

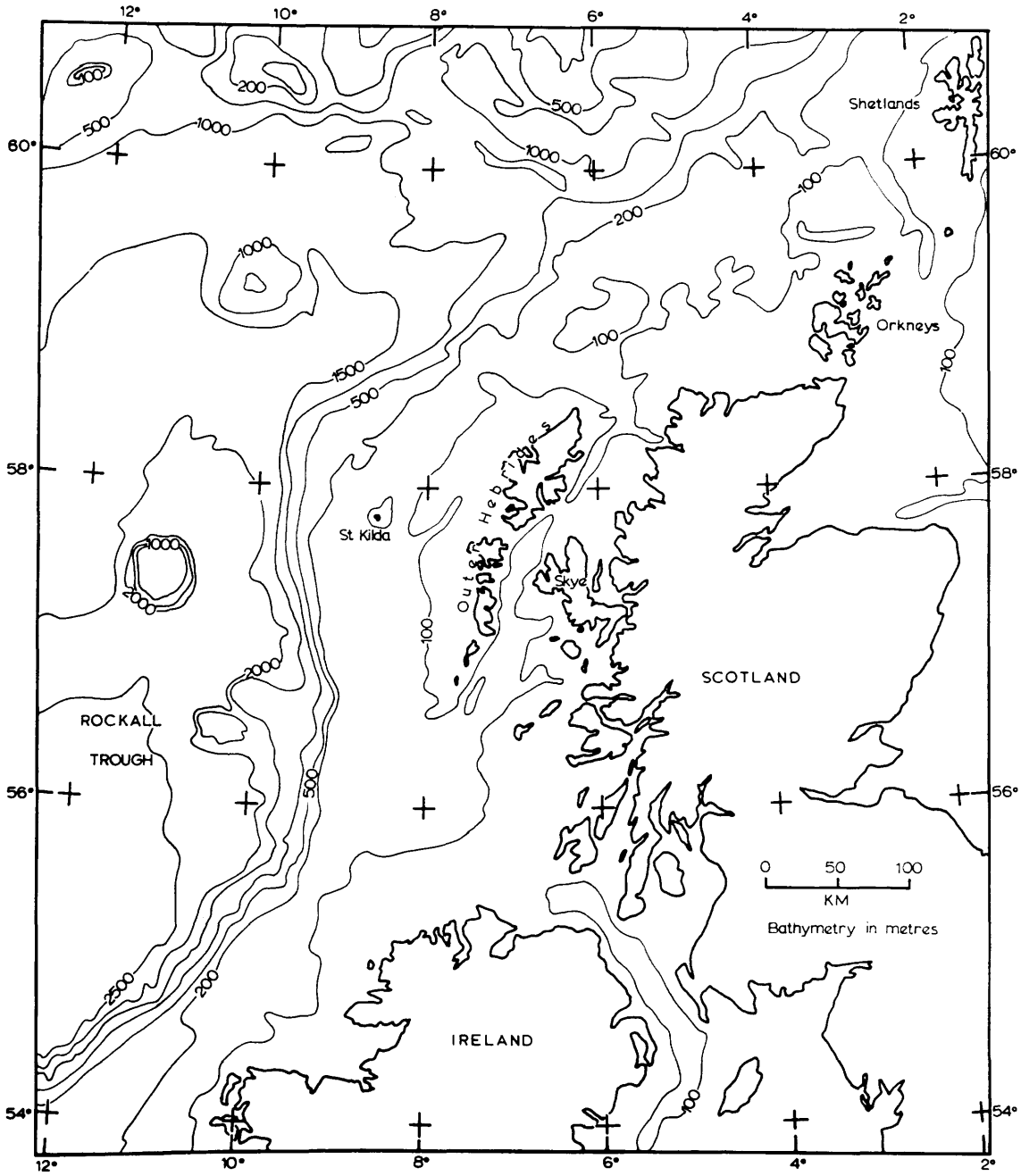

Fig. 1.10 Bathymetry of the continental shelf west of Scotland and of the NE part of the Rockall Trough. Contours in metres.

kilometres west of the Hebridean region, so it would be surprising if the earlier structural history of the Hebrides did not also reflect in some way the development of the much nearer passive margins of the Rockall Trough.

The existence of Mesozoic sedimentary basins in the offshore areas west of the British mainland has long been inferred from the onshore geology - see, for example, George's (1966) discussion of the Hebridean region - but confirmation has only come from geophysical exploration and geological sampling carried out since the mid-1960s. A summary of the evidence up to the early 1970s, at a time when little commercial exploration had been done (and none published) was given by Hall and Smythe (1973). Practically all of the basins known by then had been discovered and outlined by geophysical work carried out by Durham University researchers under Martin Bott.

McLean (1978) later synthesised the information, by then considerable, on the rifted basins of NW Britain, postulating that they fall into one or the other of two belts, which he called the Marginal Belt and the Clyde Belt (Fig. 1.11). He postulates that the north-westerly trending Clyde Belt, which may extend as far NW as the Little Minch, came into existence in late Carboniferous time (Namurian or Westphalian), but that the basins underwent most subsidence during the Permo-Triassic. The age of the Marginal Belt is less well determined, but it appears to have been in existence by the Permo-Triassic. He points out that if Bott's (1971) hypothesis of lower crustal ductile flow towards a passive margin, below a brittle, faulted upper crust, is a tenable mechanism of extension and subsidence on continental shelves at passive margins, then the continental margin of the Rockall Trough must have already been in existence by Permo-Triassic time. The alternative is to relegate the existence of the Marginal Belt to an ill-defined period of rifting, preceding sea floor spreading.

The basins west of Orkney and Shetland probably have a complicated relationship to the development of the Faeroe-Shetland Trough to the west, and there is little possibility here of elucidating the relationship (if any)

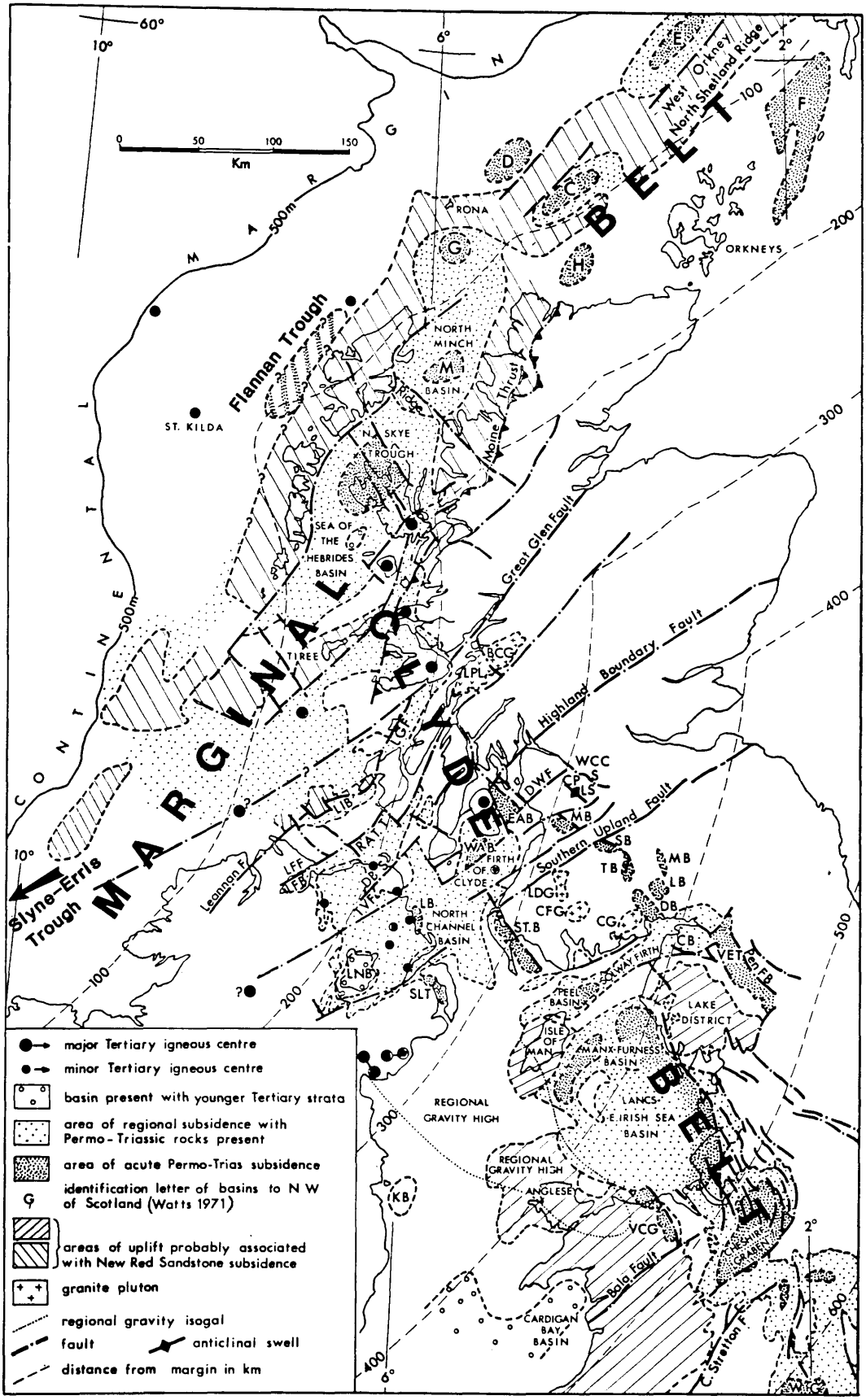

Fig. 1.11 Areas of subsidence where New Red Sandstone is preserved in NW Britain (reproduced from McLean 1978, fig. 1, with additions). McLean (1978) postulates the existence of a Marginal Belt, parallel to the NE Atlantic margin, and the Clyde Belt, trending NW-SE, possibly as far north as the Little Minch.

between the rift basins and passive margin formation. Indeed, the entire Faeroe-Shetland Trough, although continuous with the Rockall Trough, may be an intra-continental rift. Furthermore, the Shetland platform is bounded to the east by the Viking Graben system of the North Sea. The Slyne-Erris Trough NW of Donegal is little known (Fig. 1.11), with no onshore geology exposed. Likewise, the Flannan Trough west of the Hebrides (Jones 1981, Jones et al. 1986, Brewer and Smythe 1986) seems to be a minor, shallow basin about which little is known geologically. None of the basins in these regions therefore seems to be suitable for relating continental shelf rifting to passive margin formation. However, Skye and the Minches - Sea of the Hebrides region seems to be the only area of well-developed rift basin development near to the NW British continental margin with adequate geological control, and which permits the possibility of both onshore and offshore geophysical studies.

1.5 THE NORTHERN SKYE - LITTLE MINCH BASIN.

1.5.1 EVIDENCE FOR A DEEP SEDIMENTARY BASIN

The Minches have long been suspected of being the site of a Mesozoic sedimentary basin (e.g. Macculloch 1819, Mackinder 1907); Macculloch's geological cross-section from Trotternish to the Shiants, showing Jurassic below the Little Minch, could well be the earliest published geological interpretation of the structure of an offshore basin.

Until geophysical surveys were begun there was therefore no reason to believe that the basin might be anything other than a shallow NE-SW trending syncline containing up to 800 m of Jurassic in the centre, as proved in Skye, with a few pockets of Triassic rocks beneath.

Only a regional coverage of gravity stations had been obtained on land by Bullard and Jolly (1936) and at sea by Browne and Cooper (1949) when the first systematic gravity survey of the Tertiary volcanic districts was begun by

Martin Bott and his first research student, Jim Tuson, in 1955. The Bouguer anomaly map of northern Skye (Tuson 1959) shows a horseshoe-shaped low of about 15 mGal in amplitude opening NW into the Little Minch (Fig. 1.12A). The gradient on Trotternish was interpreted by Tuson as related to a faulted wedge of Triassic about 800 m thick, below a slightly thinner slab of Jurassic (Fig. 1.12B). He also interpreted the previous regional coverage in terms of linear belts of high and low gravity (Fig. 1.12C). Thus the trend of the low running through north Skye might be inferred to indicate the presence of a thick sedimentary infill extending southwestwards through the Sea of the Hebrides. The faulted margin of Tuson's Triassic basin in northern Skye trends NW into the Little Minch, whereas the regional trend of the suggested major basin is NE-SW. The published aeromagnetic maps of the Hebrides (sheets 10 and 12, Bullerwell 1968) also suggest that magnetic basement beneath the Sea of the Hebrides and Minches is several kilometres deep. Quantitative interpretation is complicated by lateral variations in magnetisation of the Lewisian (Powell 1970), and by Tertiary intrusions in the Skye - Little Minch area.

Northern Skye and its surrounding waters are a suitable area, therefore, for investigating by detailed geophysical surveys the age of the infill of basins, and the time relations of the differing fault trends. Stratigraphic proving of the age of the sediments could subsequently be made by means of a deep borehole on Skye, at a small fraction of the cost of a similar borehole offshore.

1.5.2 SUMMARY OF THE RELEVANT GEOLOGY

The sediments of NW Scotland, resting on the high-grade metamorphic Lewisian foreland belt, span many time intervals from the late Precambrian (990 Ma), to the present, and an important phase of volcanic activity in the early Tertiary is represented by the igneous rocks of Skye and its neighbouring islands. A regional geological guide (Richey 1961) is available, complemented and updated by sections in Craig (1983) and by several papers in the memoir edited by

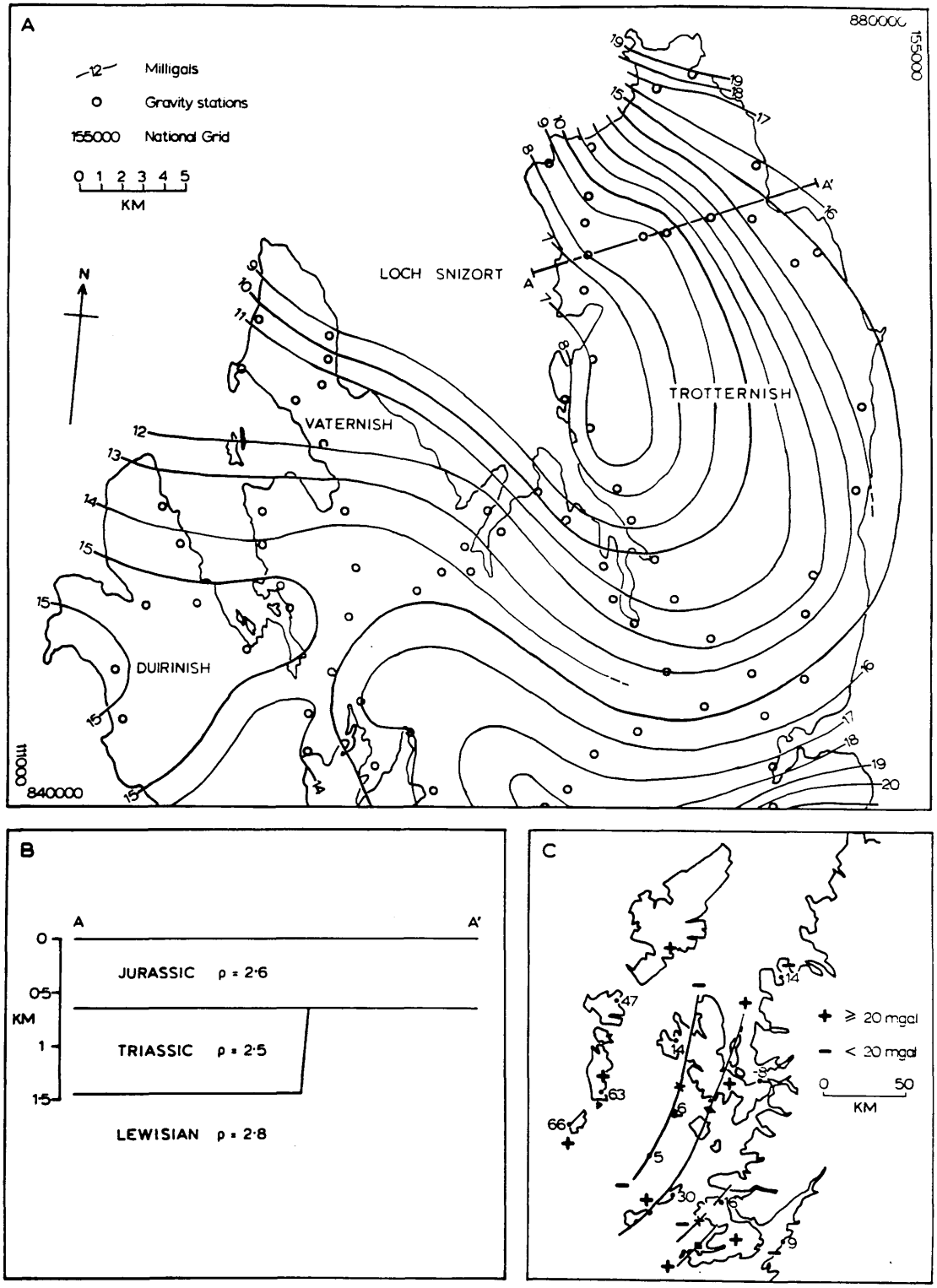

Fig. 1.12 Gravity interpretation of northern Skye, after Tuson (1959).
A. Bouguer anomaly map, with line of section A-A′ shown.
B. Tuson's 2-dimensional geological interpretation of the Bouguer anomaly along section AA′.
C. Tuson's interpretation of the regional gravity coverage in the Hebrides as published up to 1959.

Kay (1969).

Table 1.1 shows a generalised succession of the rocks cropping out on land in the NW of Scotland, with their approximate lithogies and thicknesses. Fig. 1.13, the solid geology map, is based on the published information (mainly by IGS) available at the start of the present work in 1970, and demonstrates how little was known of the offshore geology at that time.

The only offshore geological feature depicted, the transcurrent Minch Fault, is a speculative expanation of relations between the Lewisian of the NW mainland and the Outer Hebrides (Dearnley 1962), and its positioning is based purely on a supposed bathymetric lineament. The relevant features of the Lewisian are; its outcrop as two roughly linear belts flanking younger rocks, reflecting later structural controls; the prominence of NW-SE trending structures, e.g. shear zones, folds, and dyke swarms (Bowes 1969), which may have influenced structural trends in the much younger cover; and the variation of its physical properties with rock type, for example, the granulite belts are denser and more magnetic than the gneisses and schists (Powell 1970).

The thicknesses of Torridonian shown in Table 1.1 are stratigraphic (Stewart 1969), and probably not more than 4-5 km are structurally preserved at any one point on the NW mainland. Extrapolation westwards (i.e. downdip) from Raasay suggests that a similar thickness is likely to be preserved beneath northern Skye and the Minches (although this possibility seems not to have been considered by Tuson). Most of the Torridonian exposed on Skye, mainly in the SE, differs from the major outcrops of the NW mainland in lying within the marginal nappe zone of the Caledonides, and is slightly metamorphosed.

Up to 1600 m of Cambro-Ordovician rocks rest unconformably upon the Torridonian (Swett 1969), but the post-Caledonian tilt to the ESE of 5-20° makes it unlikely that any are preserved beneath the Minches. Much of the Torridonian as well was probably eroded from that area during the same period.

SYSTEM / ERA	STAGE / SERIES	LITHOLOGIES	MAXIMUM THICKNESS
TERTIARY	? Oligocene	? Clays	800 m
	Palaeocene	Dolerite sills	250 m
		Lavas	1600 m
JURASSIC	UPPER	Clays and shales	100 m
	MIDDLE Great Estuarine Series	Sandstones 50% Clays and shales 50%	210 m
	Bearreraig Sandstone Series	Sandstones 60% Clays and shales 40%	210 m
	LOWER	Shales 80%, sandstones 20%.	400 m
TRIASSIC	?	Breccias & conglomerates 50% Sandstones 25% Marls and clays 25%	300 m (Stornoway Formation 4000 m)
CAMBRO-ORDOVICIAN	?	Sandstones & siltstones 15% Carbonates 85%	? 1600 m
PRECAMBRIAN	Upper Torridonian (Torridon Group)	Arkosic sandstones 70% Sandstones & shales 25% Breccias 5%	7000 m
	Lower Torridonian (Stoer Group)	Gneiss breccia and conglomerate 20% Sandstone 80%	2300 m
	Lewisian	Granulite, gneiss, schist	-

Table 1.1 Generalised succession in NW Scotland, showing lithologies and thicknesses

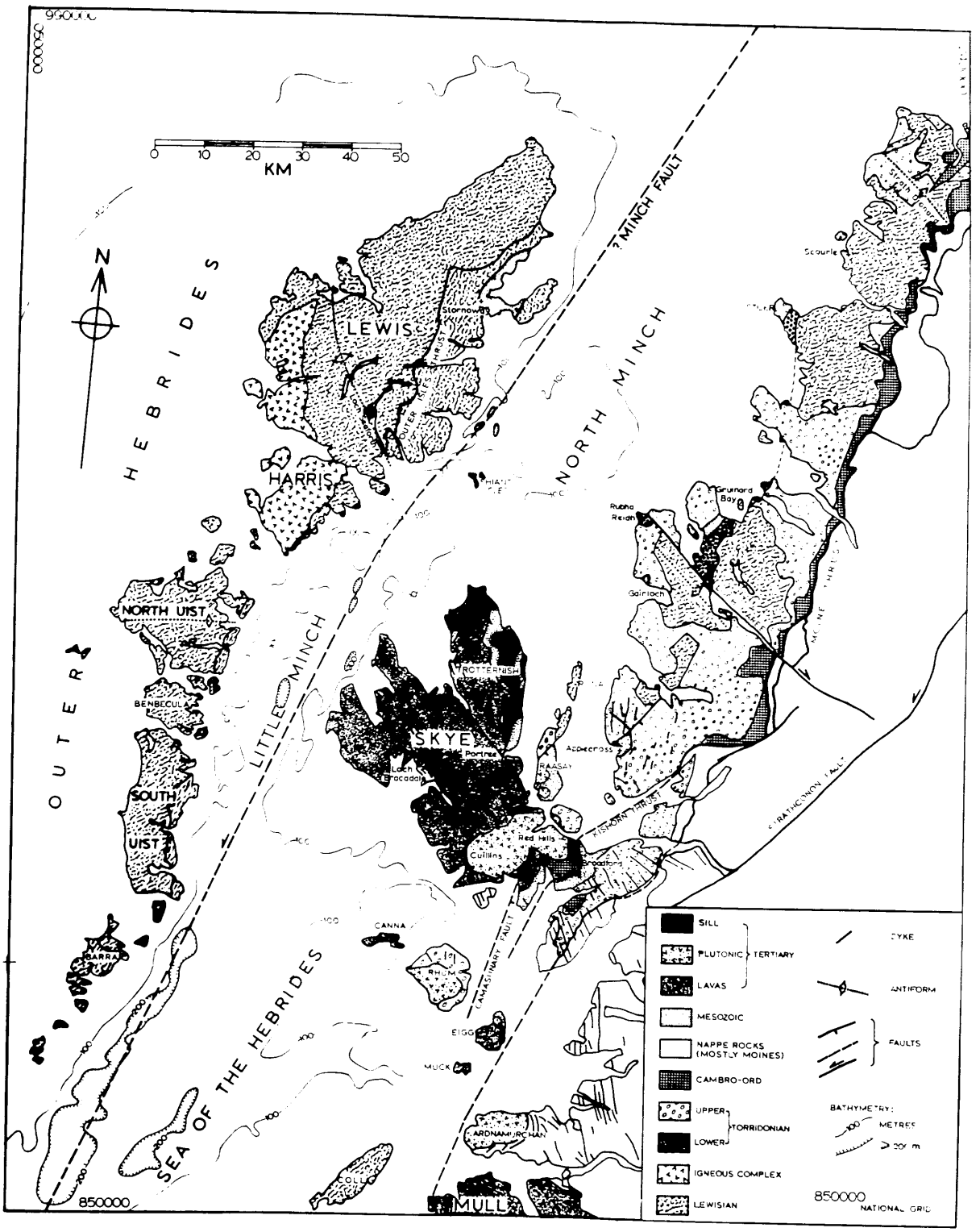

Fig. 1.13 Geology of NW Scotland compiled from published information (mostly IGS) available at the time that the present investigations were begun in 1970. Note the lack of offshore solid geological information.
National grid projection; bathymetry is from the OS topographic map of Great Britain, scale 1:625,000.

The most important recent advance relevant to the present work is the recognition from sedimentology that the Stornoway Formation is probably Triassic in age (Steel 1971, 1974; Steel and Wilson 1975), as originally suggested by Stevens (1914; see also Peach and Horne 1930, pp. 84-85), and not part of the Torridonian Formation or Old Red Sandstone (Steavenson 1928, Jehu and Craig 1934, Kursten 1957).

Palaeomagnetic pole vectors (Storetvedt and Steel 1977) also suggest a Triassic age, and do not support the older dates previously put forward. Furthermore, the discovery of mixed polarity appears to rule out deposition during the Kiaman interval of reversed geomagnetic polarity, which lasted from the Upper Carboniferous (Stephanian) until about the end of the Permian (about 300-235 Ma), with the exception of a short period of normal polarity at around 260-265 Ma (as discussed on p. 19 above).

The great thickness of 4 km quoted for this formation by Steel and Wilson is again stratigraphic, since modelling of the gravity map (McQuillin and Watson 1973) indicates that only 1 km is preserved by downthrow along the westerly bounding faults of the outcrop (R. McQuillin, pers. comm. 1976).

The discrepancy between these two thickness estimates can be accounted for by the strong diachronism of the sequence (see also Steel and Wilson 1975, fig. 5), as the locus of the fault-generated sedimentation shifted westwards with time. The Stornoway Formation displays the best evidence in the Minches of syn-depositional faulting in the Permo-Triassic, a process which is believed to control the infill of major basins both in the Minches and in other areas off western Scotland (Evans et al. 1981).

Elsewhere the Triassic outcrops comprise minor downfaulted outliers on the mainland (Richey 1961) or trivial pockets and patches in Skye (Steel et al. 1975) conformably underlying Lower Jurassic rocks, and preserved as infills of hollows in the pre-New Red Sandstone topography. Both these and the thicker Stornoway deposits are alluvial fan and flood-plain accumulations in a basin-and-range environment,

the basin deposits now largely hidden beneath the Minches, preserved by contemporaneous (and later) faulting and folding.

The cumulative maximum thickness of the Skye Jurassic rocks is over 900 m, but the general thickness preserved beneath Kimmeridgian outcrop or subcrop is probably more like 800 m (Fig. 1.14). The system is similarly developed throughout the Hebrides. The Lias, up to 400 m thick, is a dominantly marine facies of shales and calcarenites, deposited in a shallow sea, bordering a low-lying landmass in roughly the present position of Scotland (McCallum 1971, Hallam 1983). The overlying Bearreraig Sandstone Series (Morton and Hudson 1966), comprising massive cross-bedded sandstones with clays and shales, shows great variation in thickness and lithology in the south of Skye and Raasay, near to a contemporary shoreline (Morton 1965), whereas in northern Skye, further from the source of sediment, more uniform conditions prevailed.

The Great Estuarine Series of the Middle Jurassic is a mainly non-marine sequence of sandstones, shales and limestones, attaining its maximum thickness of 210 m in north Skye (Hudson 1962). Faunal and petrological studies (Hudson 1963, 1964) indicate an environment of deltas built into brackish water lagoons in what was probably an early Minch basin, since there appears to have been a small landmass to the west, in the area of the Outer Hebrides, as well as a larger one to the east. In fact, as Hudson (1964) states, the Middle Jurassic "palaeography looks remarkably like present-day Scotland without the Tertiary volcanics".

Upper Jurassic, mainly in the form of blue-grey clays and shales of Callovian - Kimmeridgian age, crops out on land only in northern Skye, and is up to 100 m thick. The general absence of Upper Jurassic and complete absence of Lower Cretaceous throughout the Hebrides is due to their erosion or non-deposition, prior to the Cenomanian transgression (Upper Cretaceous) which deposited greensands now found as small outliers throughout the Hebrides. Their maximum thickness is 20 m on Mull, but none are known in northern Skye.

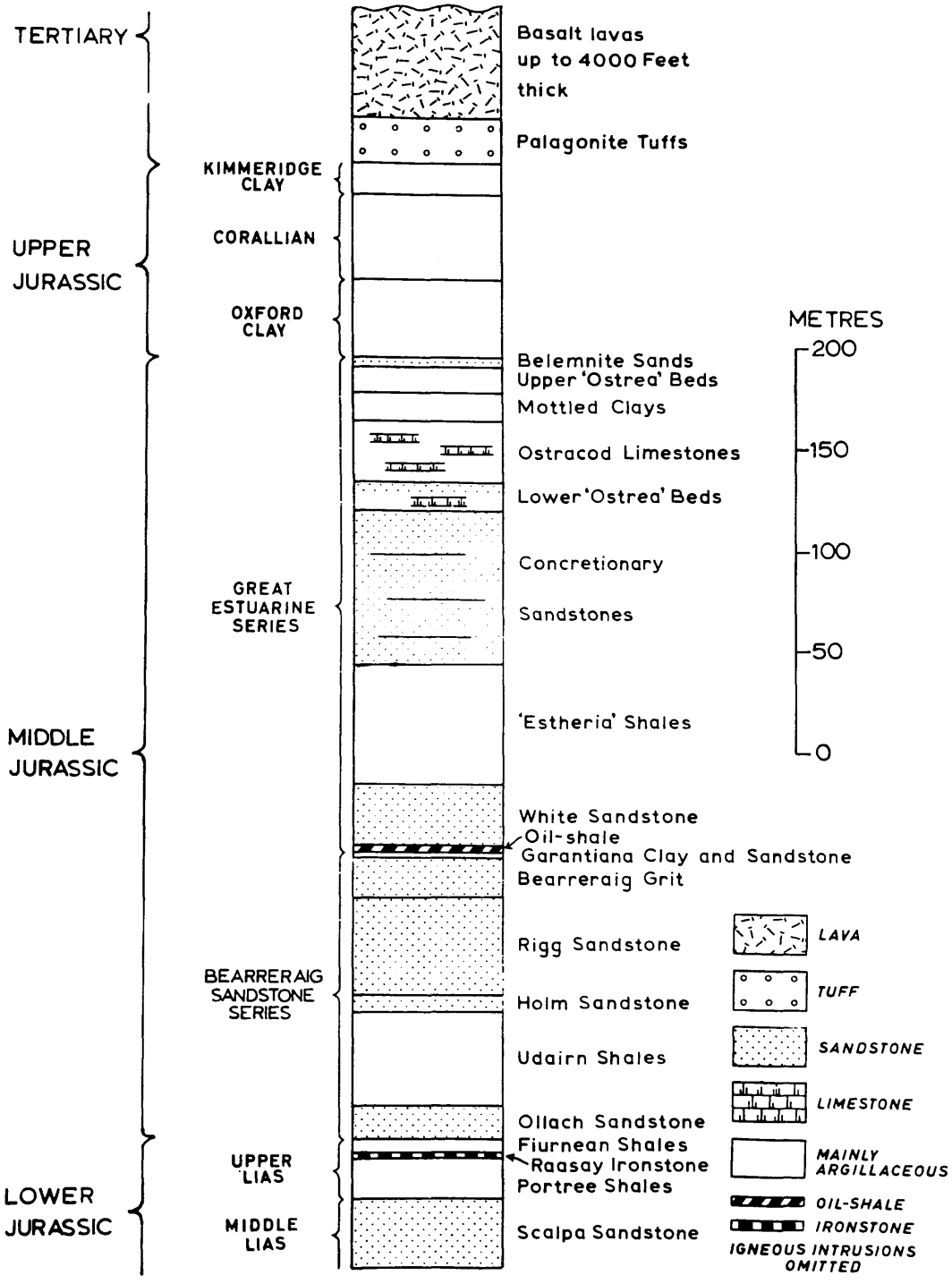

Fig. 1.14 Geological succession on northern Skye, based on Anderson and Dunham (1966, fig. 2).

Tectonic activity in the Skye-Minches area during the Mesozoic can be summarised as:

(1) Active faulting of NE-SW and NW-SE trends during the Permo-Triassic, defining depositional troughs deriving their infill locally.

(2) No significant faulting or folding during Jurassic times. Jurassic sediments overstep the Permo-Triassic fault-bounded prisms onto older rocks.

(3) Downthrow along major faults, particularly of NE-SW trend, during the Late Jurassic or early Cretaceous. The strongest evidence for this episode is found in south Skye, where pre-Albian downthrow to the SE of the order of 600-700 m on the Camasunary fault preceded the transgression of Cenomanian greensand (George 1966). The regional pattern of Mesozoic relict sediments in the Hebrides, preserved by downthrow to the SE along major faults (McQuillin and Binns 1973), probably came into existence at this time.

(4) Further downthrow along the same major faults, of end-Cretaceous or early Tertiary age; the Camasunary fault, for example, has a downthrow of 500 m dating from this period.

(5) Gentle en echelon folding of late Cretaceous or early Tertiary age, which on northern Skye trends NE-SW (Anderson and Dunham 1966, p. 174).

The Tertiary igneous activity mentioned above began in Skye with extrusion of palagonite tuffs, followed by plateau basalts, onto a mature base-levelled landscape. On north Skye five separate groups of lavas are recognised (Fig. 1.15), preserved by post-basalt faulting. Anderson and Dunham (1966) argue that the 1300 m thus preserved probably approaches the maximum thickness of the pile. It is also clear that the two lowest groups formerly extended much further than the present area of north Skye (see Fig. 1.15). The basalt outcrop has been confirmed by a preliminary geophysical and geological interpretation (McQuillin and Binns 1973) to extend 50 km to the SW,

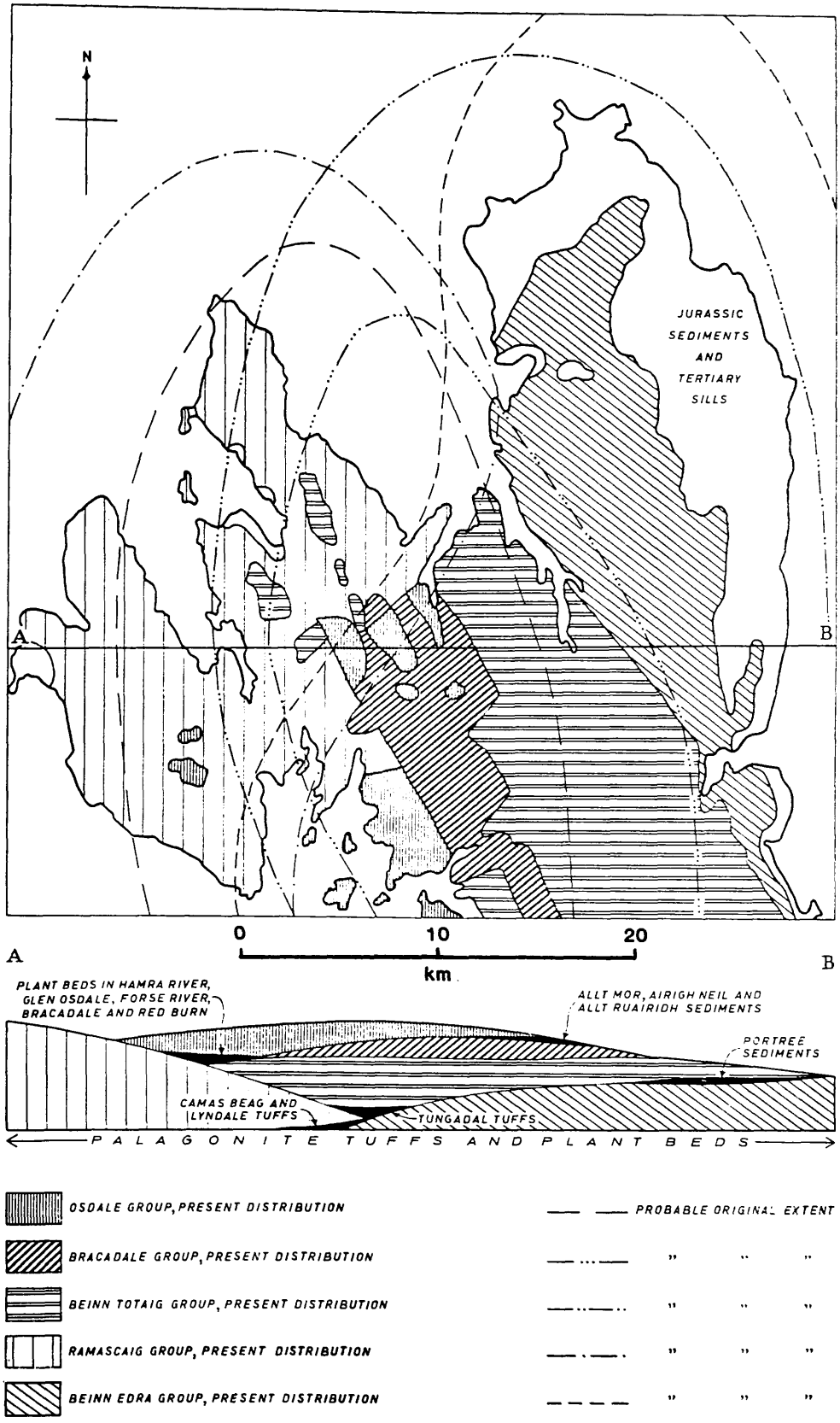

Fig. 1.15 Distribution of the five groups of lavas recognised in northern Skye (reproduced from Anderson and Dunham 1966, fig. 13).

through Canna, and isolated outliers occur even further SW near Barra (Fig. 1.16).

Age determinations of the basalts of Skye and Mull, summarised by MacIntyre et al. 1975, suggest that they were erupted in the mid-Palaeocene (61-62 Ma).

After the basalt eruption, but before most of the faulting or dyke intrusion, the Jurassic sediments of northern Skye were intruded by basic sills, which are probably all leaves of one major sill complex. Its main features are - intrusion at a constant level below the base of the lavas, with frequent transgressions, and a roughly constant aggregate vertical thickness of about 250 m. The aeromagnetic map suggests that the sill complex is even more extensive in the Little Minch north of Skye. All the small islands are composed of dolerite, intruding Jurassic sediments. Most of the NNW-SSE trending suite of dykes were intruded after the basalts and sills, and most of the plutonic rocks of the central complex came later still. However, this sequence, from a volcanic to a plutonic phase, as envisaged by Harker (1904), is now known to be over-simplified (Stewart 1965).

Large normal faults of NW or NNW trend have downthrown 1300 m of the lava pile in central north Skye (Anderson and Dunham 1966; see also Fig. 1.15), with a subsidiary set of faults at right angles. The faulting, together with gentle folding, may have been synchronous with deposition in several small basins of sediment, demonstrably of post-basalt age, and probably of Oligocene age, now found in the Sea of the Hebrides (Smythe and Kenolty 1975; see Figure 1.16). One such basin, the Canna Basin, between Canna and NW Skye, contains up to 800 m of late Oligocene terrestrial clays (Evans et al. 1979).

1.6 AIMS OF THE PRESENT INVESTIGATION

The aims of the present work were:

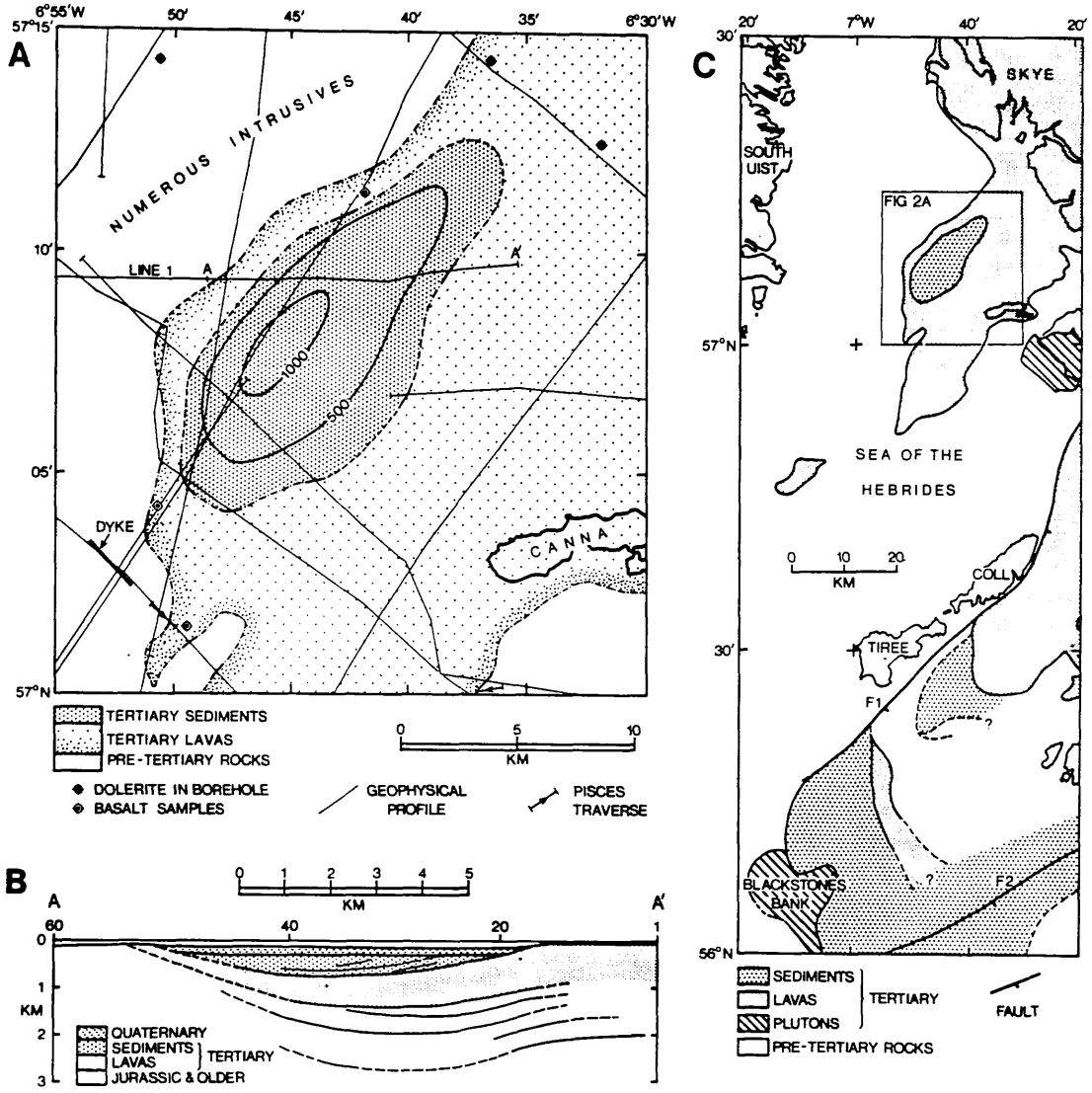

Fig. 1.16 Tertiary sediments in the Sea of the Hebrides (reproduced from Smythe and Kenolty 1975).
A. Map of the Canna Basin, since proved to contain Oligocene clays (Evans et al. 1979).
B. Depth-converted line drawing of multichannel seismic reflection profile AA' (located in Fig. 1.16A).
C. Regional map outlining areas of Tertiary sediments and igneous rocks.

(1) To confirm the existence of the suspected deep Mesozoic basin beneath northern Skye and the Little Minch.

(2) To infer the age and nature of the infill and of the bounding faults.

(3) To consider the relation of the structural development of the basin to others on the continental shelf, and to the age of opening of the Rockall Trough.

A refraction line on land in northern Skye would need to be about 10 km long to define layering in the Mesozoic down to depths of the order of 2-3 km. There is nowhere that a line of that length could be situated without encountering high-velocity lavas and intrusions at or near the surface, thus rendering first-arrival interpretations useless. Seismic reflection was therefore chosen as the main geophysical method on land.

The amount of reflection coverage that could be shot with the time and resources available was limited to between 15 km and 30 km of subsurface profile, with single-fold coverage and common depth point (CDP) spacing of 15 m. This corresponds to two seasons' fieldwork. This effort could be expended as:

(1) One or two continuous profiles across Tuson's basin below northern Skye, to yield the structure of the trough, or

(2) A set of isolated velocity surveys with multiple subsurface coverage and a variety of offsets, to give accurate velocity - depth information at each locality, but no structural information other than the local dip.

The latter alternative is chosen, because the structural information resulting from a continuous profile, but with poor velocity control (due to the necessarily small offsets which would have to be used), is less useful to the solution of the problem than observing between three and six localities scattered inside and outside the basin, each with good velocity-depth control - say V_{rms} accurate to within

0.1 km/s, down to depths of 2-3 km.

The velocity-depth information is more likely to help solve the main problem of the age and character of the infill of the basin, and structural information can be interpolated between the sites by gravity modelling, using the seismic reflection results as a control. A subsidiary programme of gravity fieldwork is therefore also desirable.

At sea in the Little Minch a refraction line of the necessary length would be feasible, since the lavas are absent, and the logistics of marine refraction are more simple. The prevalence of sills offshore, discussed in Section 1.5.2 above, might give rise to the same screening of Mesozoic lower velocity layers at depth, as the lavas would on land. Hence the positioning of the line is critical. Continuous profiling with shallow seismic profiling (sparker) and magnetics, run at night when refraction work is impracticable, provides information on shallow structures - of the order of 200-400 m below the sea-bed, and can be used to find the best place to shoot a refraction line.

A summary of the history of the research is as follows:

October 1970: research started; interpretation of available data, planning field work, etc.

June-July 1971: 3-week cruise on RRS John Murray in the Little Minch, refraction survey and continuous profiling.

July-September 1971: 10 weeks fieldwork in northern Skye; seismic reflection and gravity surveys.

October 1971 - June 1972: Preliminary interpretation and publication of results; planning further fieldwork.

June-July 1972: 2-week cruise on RV Calanus in Little Minch; refraction survey.

July-September 1972: 8 weeks in NW Skye; further seismic reflection work and gravity.

October 1972-October 1973: Interpretation of data.

November 1973 - March 1976: Further interpretation and compilation of all relevant Glasgow University and IGS data; this thesis was partially written up during this period.

From 1970 to 1973 the author held a NERC Research Studentship at Glasgow University, and since then has held various posts within the Marine Division of IGS (now BGS) in Edinburgh. Since 1976 the scope of the author's research has broadened to encompass North Atlantic plate tectonics, continental deep crustal reflection, and hydrocarbon assessment of sedimentary basins west of the British Isles. By 1985-86, the advances in understanding within these three fields, together with the feasibility of digital processing of the seismic reflection data, suggested that the original studies might be worth re-assessing, not least because the area is now of renewed interest to the oil exploration industry. Notwithstanding the commercial attention, the scientific aims of the work as understood in 1970 (and summarised above) are still pertinent and by no means entirely solved, as is demonstrated in the following chapters.

CHAPTER 2
EQUIPMENT AND FIELD TECHNIQUES

2.1 INTRODUCTION

The land seismic reflection surveys form the main effort of the investigations, and provide the most useful results. Orthodox commercial analogue exploration equipment is used, but the usual commercial techniques have been modified to suit the requirements and resources of academic research. The experience gained by the Glasgow University Geology Department in this field was extensive and probably novel for a university group. The work is described in some detail because the field techniques used are still valid in the present era of digital recording. On the other hand the marine surveys use standard equipment and techniques, and are therefore described briefly.

Units used normally are SI, with a few exceptions (in common geophysical use) such as milligals and gammas. Seismic velocities are normally given in km/s, but are sometimes quoted in the equivalent units of m/ms to reproduce the units of time and distance actually measured in the field. Field measurements of distance were all observed in metric units, with the exception of depth on the precision depth recorder (in fathoms) and ranges on the radar scanner (in nautical miles).

2.2 LAND SEISMIC REFLECTION

2.2.1 PREVIOUS WORK

Hall (1974) showed how the routine techniques of commercial seismic reflection exploration for oil can be scaled down to suit the limited resources of academic research. Although reducing the number of man-hours in the field compared with a commercial party naturally results in a proportionate decrease in the quantity of data gathered, there need not be any loss in the quality of individual seismic records. One

advantage, in fact, is that a small crew of, say, half a dozen men using one or two relatively light vehicles can work in places where a full-scale commercial party (employing perhaps two dozen people, with several large drilling, water and recording trucks) would be unable to gain access, perhaps because of difficult ground conditions or objections by landowners. Table 2.1 summarises the various field methods and developments tested during the five seasons 1968-1972 in which seismic reflection surveying was conducted by the Geology Department at Glasgow University. Successful results have been obtained both by continuous profiling with shallow penetration (as in north Ayrshire), and by the other extreme of obtaining much deeper penetration, on a few records only, to construct a short common depth point (CDP) profile, as in Skye in 1972. Other surveys have employed methods intermediate between these two. Thus the techniques, though modest by commercial standards, are extremely flexible and can be altered, if necessary, as a survey proceeds.

For the present study resources were available for an initial field season of 10 weeks in 1971, employing a party of 8 people. The possibility of a second field season the following year only arose after the first season's work had been completed. Experience on Mull in 1970 had shown that reflection profiling over a thin cover of lavas (100 m or less) gives poor results (or no results at all) using the techniques available. The same problems were expected to arise in similar areas in Skye.

Figures 2.1A and 2.1B show two records with different field geometry from Mull; these show little except 'ringing' of high frequency - mostly between 50 Hz and 100 Hz - inferentially because standing waves were set up in the lavas. No energy arrived from below the lavas, although it is probable that some reflectors exist a few hundred metres below the surface, so it must be assumed that little energy penetrated below the lavas. The records are fixed gain playbacks of fixed gain recordings, with approximately 30 Hz low-cut and 70 Hz high-cut filters used both on recording and on playback. Because of the shot-detector geometry the resonant energy must be travelling in a mainly vertical direction, and since the detectors respond only to the

Field season	1968-69	1970	1971	1972	1972	1972
Weeks duration	12	10	10	2	4	4
Place	North Ayrshire	SW Mull	Trotternish North Skye	Carsaig Bay SW Mull	Waterstein NW Skye	Edinbane NW Skye
Type of survey	Short continuous profiles, velocity surveys	Long continuous profiles over lavas	Velocity surveys & short continous profiles	Velocity survey	Velocity survey	Velocity survey
Maximum offset	495 m	825 m	1155 m	825 m	1155 m	1980 m
No. in crew	4	8	8	5	8	8
Percussion drilling	4cm diameter head sharp point	4cm diameter head sharp point	5cm diameter head blunt end	5cm diameter head blunt end	7cm diameter head blunt end & charge inserter	7cm diameter head blunt end & charge inserter
Charge size & weight	10cm x 3cm x 1/8kg	10cm x 3cm x 1/8kg	20cm x 3cm x 1/4kg	20cm x 3cm x 1/4kg	20cm x 3cm x 1/4kg OR 30cm x 4cm x 1/2kg	20cm x 3cm x 1/4kg OR 30cm x 4cm x 1/2kg
Usual number of sticks	2-4	4, later on 8	8	15	20 or 10	17 (usual) 25 (max)
Number of holes	2-4	4, later on 8	8	15-30	20	40 (usual) 50 (max)
Total weight per shot	1/4 - 1/2kg	1/2kg, later on 1kg	2kg	4kg	5kg	8kg (usual) 12kg (max)
Blaster	Unmodified HS-200	Unmodified HS-200	Double capacity HS-200 with delay system	Unmodified HS-200	Double capacity remote firing by radio	Double capacity remote firing by radio
Geophones	4 per channel unburied	4 per channel unburied, later on 7 per channel unburied	7 per channel unburied, later on 4 per channel buried in 1 hole	7 per channel individually buried	7 per channel individually buried	7 per channel individually buried
Recording	TI8000 records developed at base	TI8000 records developed at base	TI8000 & VAR camera. Records developed in the field	TI8000 & VAR camera. Records developed in the field	TI8000 & VAR camera. Records developed in the field	TI8000 & VAR camera. Records developed in the field
Records/day	4	6-8	4-8	2	2	1
Penetration	1 km	None (see text)	3 km	?0.3 km	3 km	7 km

Table 2.1 Development of seismic reflection field methods at Glasgow University between 1968 and 1972

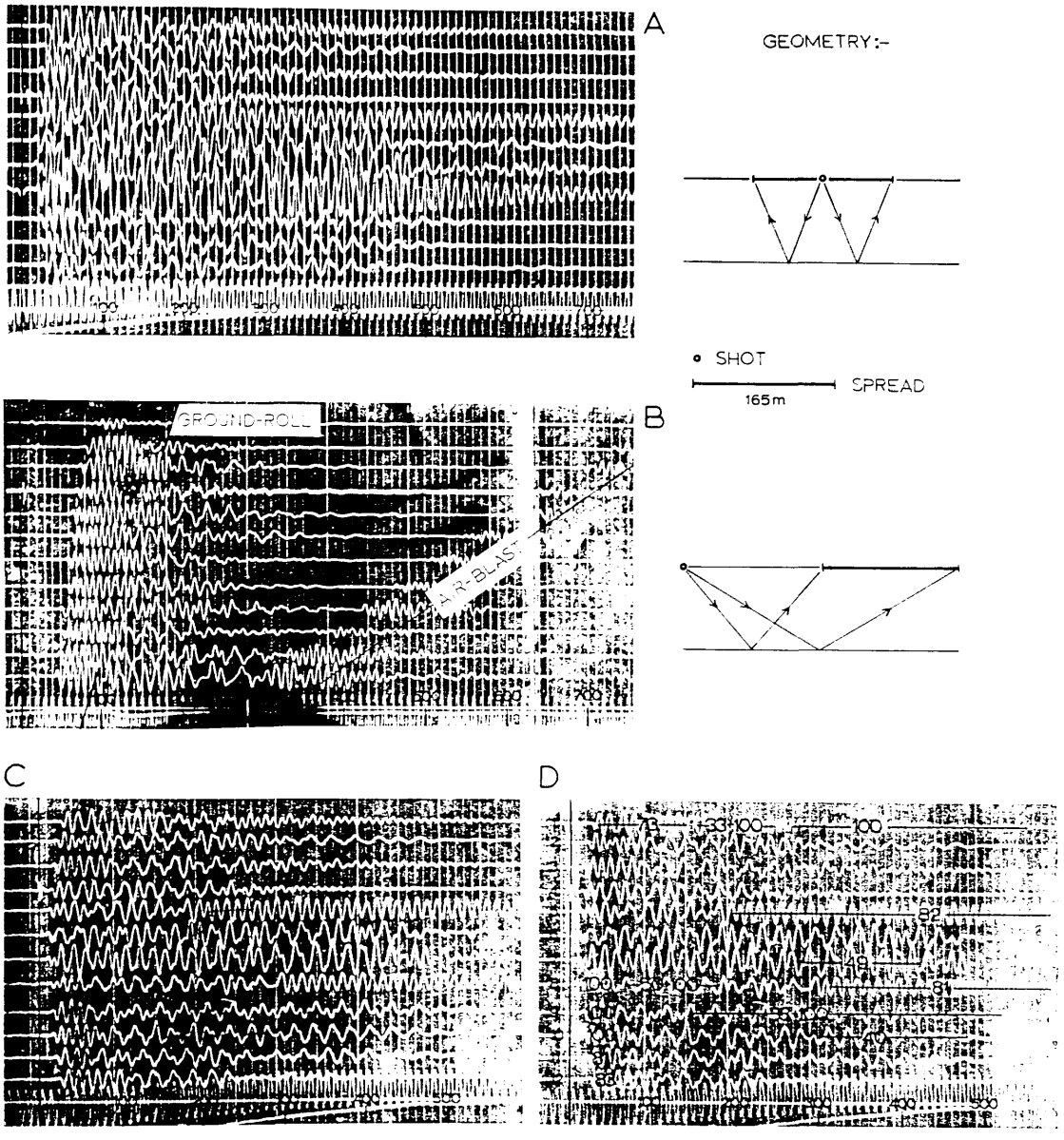

Fig. 2.1 Examples of seismic records from Mull. Fixed-gain playbacks of fixed-gain recordings. Time in ms marked along lower edge of each record.
A. Split-spread geometry.
B. Offset geometry.
C. Split-spread geometry.
D. Same record as C, with frequencies in Hz marked in.

vertical component of ground motion, the standing wave must be compressional. The P-wave velocity in the lavas, as shown by the first arrivals, is about 4.5 km/s, so the resonant wavelengths are of the order of 40 - 80 m. These would appear to be too large for any sort of phase reinforcement (Bragg reflection) by individual lava flows, which are 15 m or less in thickness (Fig. 2.2A). In Bragg reflection, the difference in path length CD between waves leaving a shot S and arriving at detectors D_1 and D_2 must be an integral multiple of the wavelength for the two signals at D_1 and D_2 to be in phase. For near-vertical incidence at a flow 15 m thick, the maximum wavelength that can be reinforced is thus 30 m.

A possible mechanism for the resonance is suggested by the record of Figures 2.1C and 2.1D (the latter having frequencies annotated), in which the 100 Hz resonance is superimposed upon a 33 Hz resonance, on channels 1 and 9 particularly. The resulting wave is of the form

$$\cos \Theta + A.\cos 3\Theta$$

Θ and 3Θ being the first two harmonics of a resonating layer (or other body) with a fixed (nodal) surface and a free (antinodal) surface (Fig. 2.2B). The wave shape of trace 9 (Fig. 2.1C) is simulated in Figure 2.2C for A = 0.8; the two components are in phase at $\Theta = 0$. The thickness H of the layer is

$$V_P/4f_1 \text{ or } 3V_P/4f_3$$

where f_1 and f_3 are the lower and higher frequencies, respectively. Using V_P = 4.5 km/s and f_1 = 33 Hz, we obtain H = 34 m, which is about equal to the total thickness of the lava pile at the locality. So the ringing may be a resonance of the whole lava pile, generated by a shot pulse which can be assumed to be minimum phase. However, after a dozen or more bounces off the top and bottom of the resonating layer of lavas, the phase and amplitude spectrum of what started out as a pulse have been substantially altered by a complex filtering process of the lava pile, setting up temporary resonances of the sort outlined above.

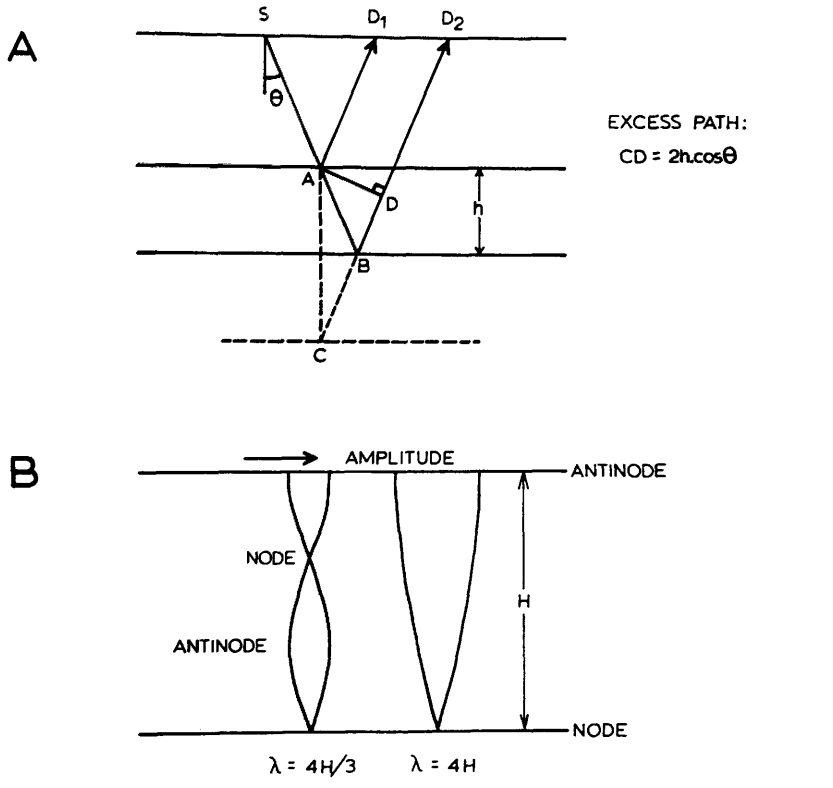

Fig. 2.2
A. Bragg reflection from multilayer.
B. Standing-wave amplitudes of first (fundamental) and third harmonics in layer of thickness H with free upper surface and fixed lower surface.
C. Harmonic simulation of part of the waveform of Fig. 2.1D, channel 9.

Since large areas of northern Skye are covered by thin lavas overlying Mesozoic sediments, the same problem of resonance may occur. The target reflectors in Skye, however, are much deeper than those expected in Mull, which would have had two-way travel times of only a few hundred milliseconds. So although the masking of shallow reflectors by resonant energy might be less important in Skye, little energy would actually penetrate the lavas to return from depths of the order of 1-3 km. Therefore extended continuous profiling over the postulated deep sedimentary basin below Skye (underlying the lavas) was considered to be impracticable. The north Ayrshire results (Hall 1974) suggested, in addition, that much bigger shots than those used in previous seasons would be required to ensure penetration to 2 km or so. The effort required to place large charges slows down the field party's progress, thereby ruling out the possibility of observing long continuous profiles.

2.2.2 AREAS CHOSEN FOR SEISMIC WORK

In place of extended profiling over the suspected basin, the alternative is to concentrate on isolated but detailed surveys inside and outside the area of the gravity low, in the hope that the velocity-depth information so obtained would establish the depth and character of the sedimentary infill, without outlining the basin structure in any detail. Tuson's gravity map (Fig. 1.12) delineates quite clearly the presumed NE margin of the basin below Trotternish, but leaves uncertain its continuation to the SW, because of the contribution to the Bouguer anomalies of the thick pile of lavas in the Vaternish area. The Trotternish peninsula is therefore the obvious area in which to concentrate the initial surveys, and if useful results were obtained there, further work would subsequently be carried out to the SW to provide regional information, and to link the land work with the marine surveys in the Little Minch.

Since accommodation for the field party had to be arranged six months in advance, and since daily round trips of more than 60 km or so over the poor roads to field localities would have wasted too much time, all the surveys in the 1971

field season (both seismic and gravity) were conducted in Trotternish.

To the NE of the Portree fault some 50% of the area of Trotternish consists of lava outcrop, the thickness of which in most of the ground adjacent to roads and tracks (i.e. accessible to the field party) is under 100 m (Fig. 2.3). A further 30% of the area has dolerite sill at outcrop, individual sheets of which are frequently 30 m or more in thickness. The same problems of resonance and poor energy transfer are as likely to be present when shooting over thick sills as over lavas. The area remaining is the 20% or so of Middle and Upper Jurassic clays, which generally occupy low ground, but which are extensively covered by landslipped lavas, especially to the east of the lava scarp. Jurassic outcrops not covered by landslip were therefore examined for suitability.

Some of the reflection surveys clearly had to be located within the area of the postulated trough, i.e. to the west of the approximate line of the Duntulm Fault in Figure 2.3, which had been suggested by Tuson to be the surface expression of the larger basin-margin fault at depth. Figure 2.3 shows that two localities might be suitable, depending upon access and terrain,

(1) The inlier of Glen Uig, and

(2) The area of Jurassic north of Uig Bay.

Leaves of the sill are likely to underlie these Jurassic rocks at depth, but as long as their thickness is only a fraction of seismic wavelengths (typically 60 m or more) they will be effectively transparent to seismic energy. To the north of Uig Bay the Jurassic outcropping between the NNE trending faults through Uig Bay and Glen Uig lies above a major leaf of the sill, which to the west of the former fault transgresses upwards to overlie the Jurassic outcrop. Accordingly, this locality is preferred to that east of the fault. No clues can be found from the near-surface geology about the sill complex below Glen Uig, but as the complex rarely cuts the lavas, and has an aggregate thickness of about 250 m (see Section 1.5.2 above), it is almost

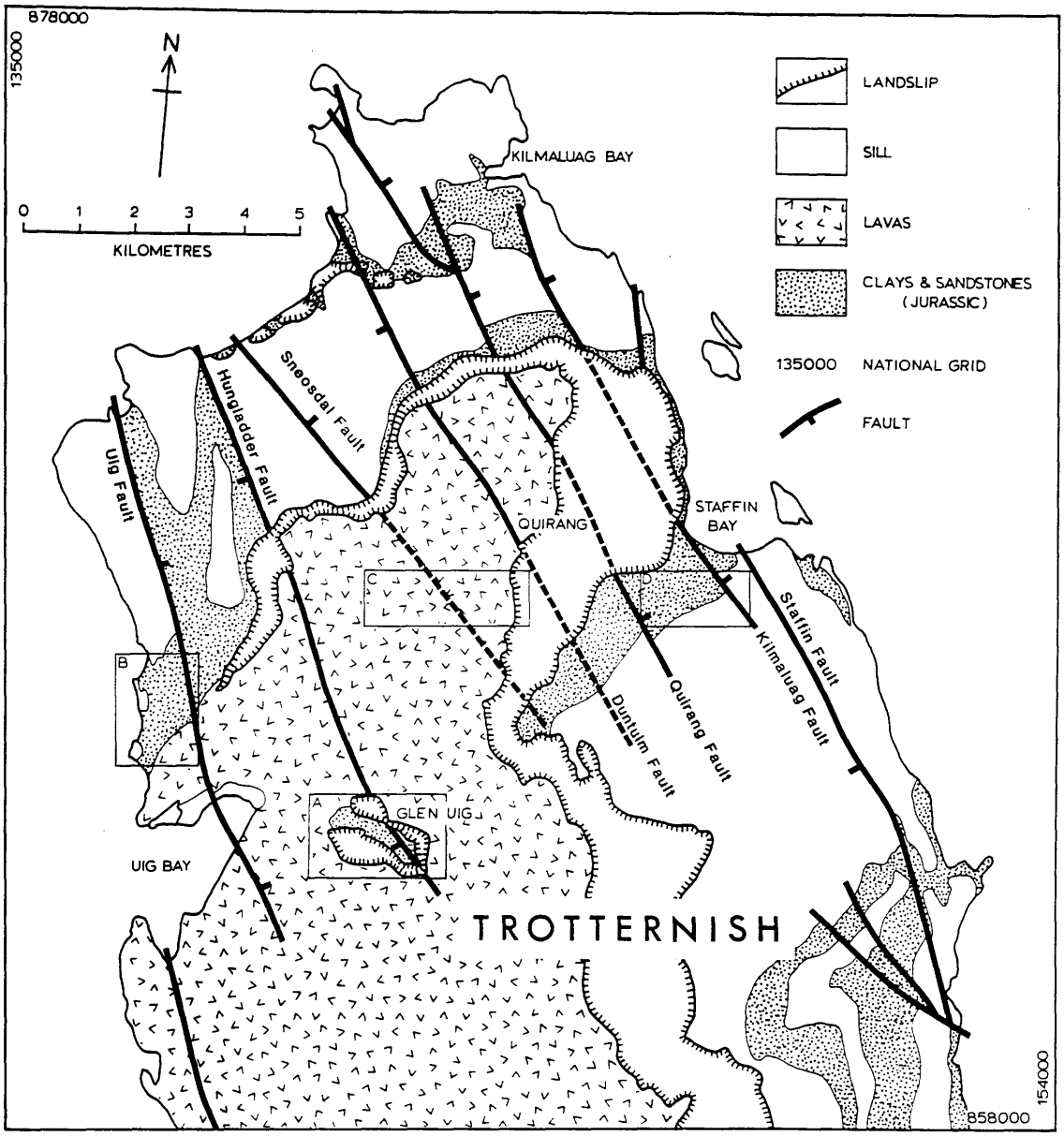

Fig. 2.3 Geology of north Trotternish, Skye (simplified from IGS North Skye sheet). Rectangles A-D are the areas shown in detail in Fig. 2.4A-D. Fault names are informal, supplied here to clarify the interpretation; dashed segments are likely subcrops below lavas and landslip. The Duntulm Fault is the possible surface expression of the fault bounding the NE margin of the deep sedimentary basin postulated by Tuson (see Figure 1.12).

certainly present at depth.

To the east of the basin region suitable areas exist at Kilmaluag Bay and at Staffin Bay. The possibility of observing a short continuous profile (2-3 km) over the lavas along the Uig - Staffin road near the Quirang was also borne in mind. Although the results here would probably be poorer than at other sites, this profile could potentially reveal the structure of the basin margin.

The preliminary considerations above had to be supplemented by inspection of the potential sites, to check on:

(1) Accessibility and site conditions. A velocity survey supplying useful information to depths of the order of 2 km requires shot - detector offsets of at least 1 km, and an even greater line length than this is desirable if the survey is to be combined with multiple subsurface coverage along a continuous profile (field geometry is discussed below). The line should be reasonably straight to minimise the dispersion of depth points. One end of the spread must always be within 300 m of the recording truck, due to the length of the extension cable available. For shifting gear manually, the line should preferably be on fairly flat, unfarmed or fallow ground, free of major obstacles like woods or rivers. It is essential, for safety during shot firing, that the shot points, which are every 165 m along the line, be at least 50 m from houses, and at least 20 m from overhead power lines and buried water or power supplies.

(2) Near surface conditions. Charges are placed at the base of the drift layer (usually boulder clay or peat), which must be a minimum of 1 m thick at all shot points, and preferably 2 m thick or more at most of them, in order to avoid surface damage and poor results.

(3) Ownership and tenancy of the land. The permission of the relevant farmers and landowners has to be obtained, and assurance given that damage and inconvenience will be negligible, and is covered by

insurance. In practice, if conditions 1 and 2 are fulfilled, then this assurance can be given with confidence.

(4) Other arrangements. The final choice of sites depends also upon their relative distance from the available accommodation, and the storage of explosives at a magazine may also influence the choice.

Surveys at sites 1-4, within the four areas A-D respectively (Figure 2.3) were carried out in 1971. Detailed site maps of the geology and line layouts of each of the six sites are given in Figure 2.4. Sites 5 and 6 were surveyed during an additional eight weeks of survey in summer 1972 in western Skye (Figs. 2.4, 2.5). The Jurassic inlier at Waterstein (site 5, in area E) was chosen to provide a link between the land surveys and the IGS marine refraction and reflection surveys some 10 km or so to the west, in spite of the problems that the three or more thick sills below the site would produce. The last survey, at Edinbane (site 6, in area F) was chosen in the hope that the base (at least) of the pile of lavas would be defined, where they are at their thickest. The site permits offsets of 2 km, and a thick cover of peat overlies bedrock. Details of the individual site conditions are given in Chapter 3.

2.2.3 INSTRUMENTATION

The Texas Instruments Inc TI 8000B 'Explorer' system, owned by the Geology Department at Glasgow University, is a 12-channel version of the last generation of analogue seismic equipment in common commercial use until the mid 1960s (see Sheriff and Geldart 1982, fig. 5.32). It is designed specifically for reflection work (see Appendix 1 for a description of the system). Input to each channel is fed to a high-gain amplifier which can be operated in fixed gain or time-varying gain modes. The output, having passed through a choice of high- and low-cut filters, is recorded on an AM tape recorder. At the same time an oscillograph provides a monitor record in real time. Playback displays from tape are limited to choosing different filtering and

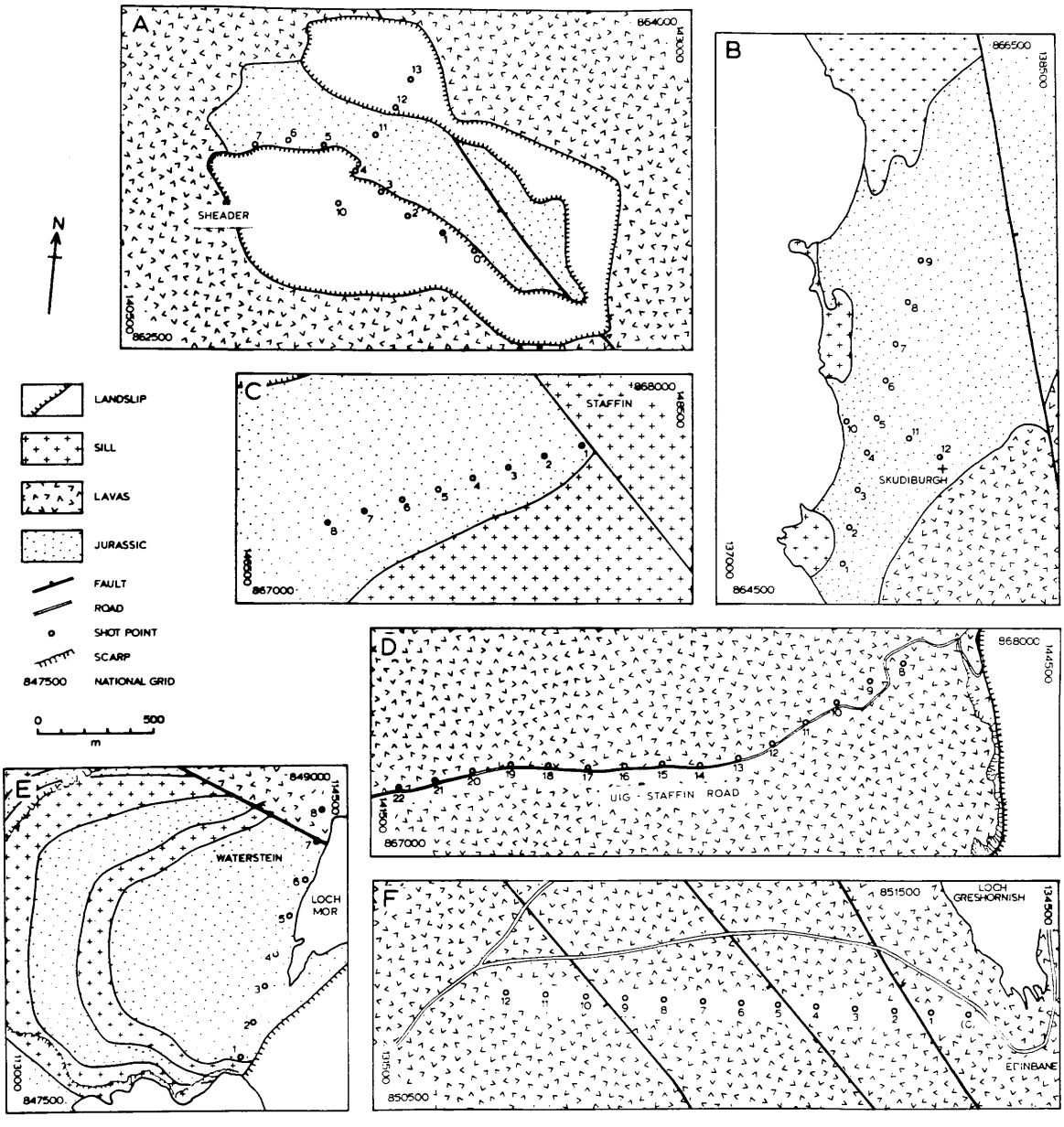

Fig. 2.4 Geology of the six seismic survey sites, showing positions of the lines. Shot points are all at 165 m intervals, defined to be a 'single' spread length.
A. Sheader: SK-1 (main line NW-SE), SK-1A (cross-line)
B. Skudiburgh: SK-2 (main line NNE-SSW), SK-2A (cross-line)
C. Staffin: SK-3
D. Quirang: SK-4
E. Waterstein: SK-5
F. Edinbane: SK-6
Locations of A-D are shown in Fig. 2.3, E and F in Fig. 2.5.

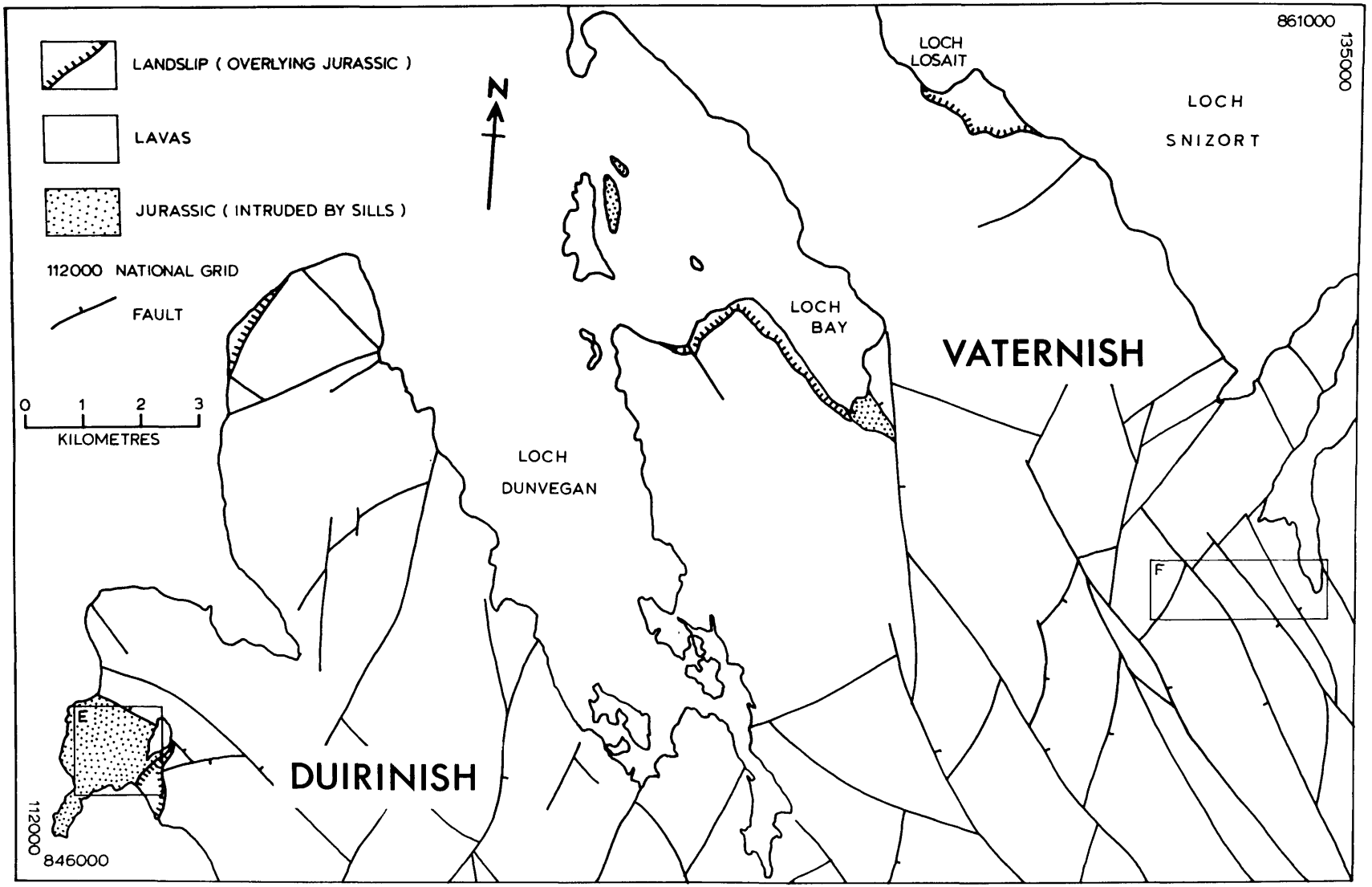

Fig. 2.5 Geology of Vaternish-Duirinish area, NW Skye (simplified from IGS North Skye sheet). Rectangles E and F - areas shown in detail in Fig. 2.4E, F.

gain settings (which are superimposed on the settings selected at the time of recording), and output display can be made either on a wiggle-trace or a variable area recording (VAR) oscillograph.

Analogue to digital conversion of the original field tapes has enabled digital processing of the data to be carried out.

Up to 7 geophones per channel are connected to a 'single spread' cable, giving a 15 m channel separation and a spread length of 11 x 15 = 165 m, or to alternate take-out points of two cables connected end to end, for a channel spacing of 30 m and 'double spread' length of 330 m. The 300 m long extension cable is connected to either end. A 150 V portable blaster, triggered manually or remotely (by the tape recorder) detonates the charges and supplies a simultaneous time break pulse to the recorder.

The recording equipment is installed in a long wheel base Land Rover, the windows of which are fitted with blinds so that the oscillograph paper records can be exposed and developed immediately (final rinsing and drying of the field records can be postponed to the end of each day's field work). The outdoor field equipment - explosives, cables, geophones, drills, protective clothing, etc. - is carried in a trailer. Although a field party of eight requires a separate vehicle, a small field party of up to six could if necessary be transported entirely by the Land Rover and trailer.

Additions and modifications to the basic equipment include

(1) A VAR camera (Fig. 2.6).

(2) Switch boxes controlling input and output signals and power supply.

(3) Re-wired compositing boards for the TI amplifier to make new trace-mixing patterns.

(4) Doubling of the blaster firing capacity, with a relative delay of detonation of two independent groups

A

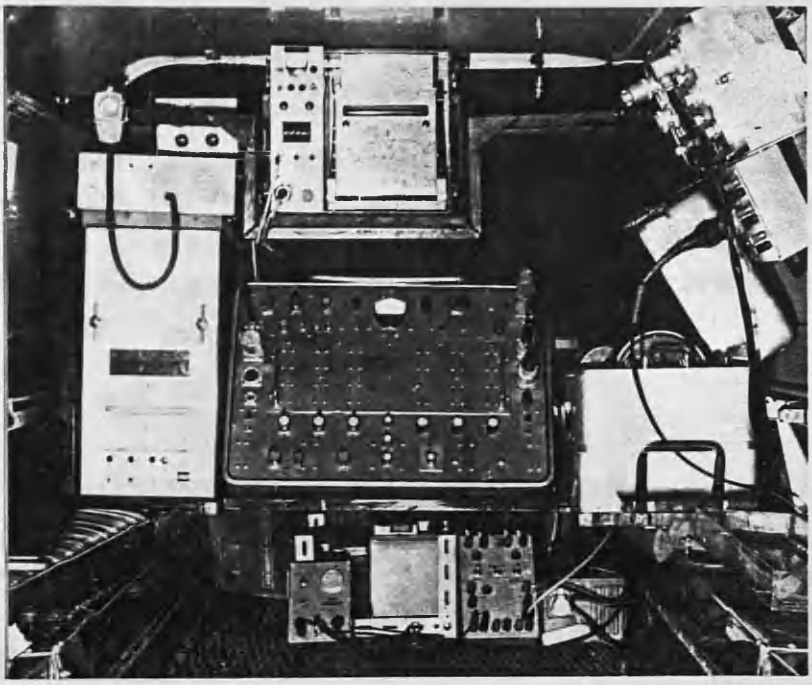

B

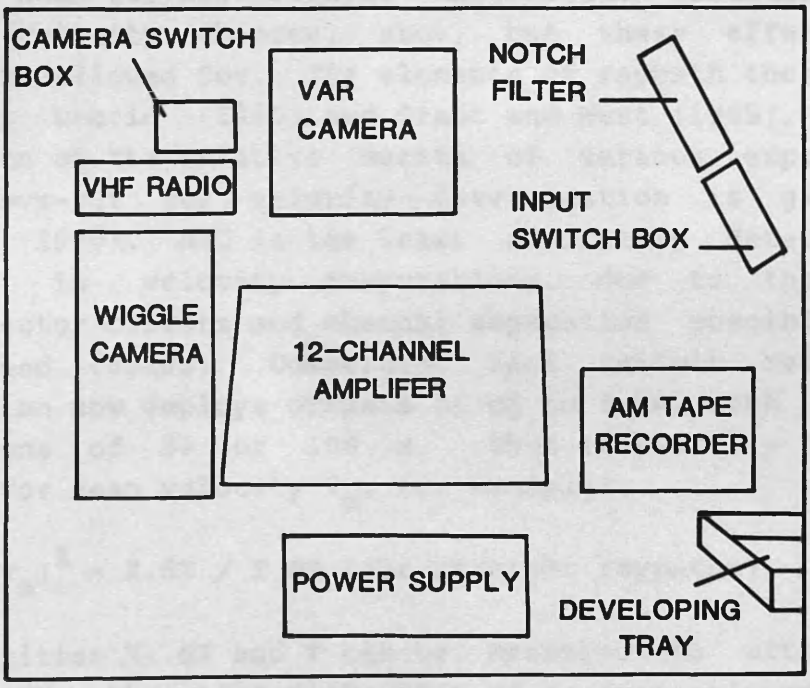

Fig. 2.6
A. TI 8000B 'Explorer' 12 channel seismic reflection recorder and ancillary equipment installed in 109" Land Rover.
B. Key to equipment shown in A.

of charges (1971 season only).

(5) Two-way VHF radios for communication between shot point and recording truck, with remote (radio) firing of shots (1972 season only).

The reasons for these changes, and their usefulness or otherwise, are discussed below. Technical details of the modifications designed and/or built by the author are given in Appendix 1, together with a summary specification of the TI 8000 system.

2.2.4 TIME-DISTANCE GRAPH CHARACTERISTICS

Velocity-depth information requires not only the identification of reflections from depth, but also of a normal move-out (NMO) - a measurable difference in the two-way travel time (TWT) of a pulse, produced by varying the shot-detector geometry. In practice the total move-out observed is a function also of the dip of the reflecting horizon, near-surface velocity and height irregularities, lateral velocity changes, etc., but these effects can usually be allowed for. The elements of raypath theory are given by Dobrin (1960) and Grant and West (1965), while a discussion of the relative merits of various expressions using move-out for velocity determination is given by Robinson (1970). NMO is the least accurately determinable quantity in velocity computations, due to the small shot-detector offsets and channel separation possible with the spread cables. Commercial land seismic reflection exploration now employs offsets of up to 3 km, with channel separations of 50 or 100 m. Thus in the 'T - delta-T' formula for mean velocity V_m, for example:

$$(V_m)^2 = X.dX \;/\; T.dT \text{ (for straight raypaths)}$$

The quantities X, dX and T can be measured to within 1%, whereas dT, the time difference of an event picked on two traces across a section, is usually less than 10 ms, but the event on each trace can only be picked to $\pm$ 1 ms. This 10% or larger error in dT thus leads to an approximate 5% error

in V_m. The addition of noise on top of the signal can shift the reflection peaks and troughs by a significant fraction of their period - i.e. several milliseconds either way - and this random error can only be overcome by averaging as many picks as possible. The modern digital methods of semblance plots (Taner and Koehler 1969), constant velocity plots, etc., as used on the data (see Chapter 3) are, in essence, merely sophisticated ways of using as much of the data as possible to achieve accurate velocities by statistical averaging.

For a given dX, the equation above shows that dT is roughly proportional to shot-receiver offset X, since T is very nearly constant over the range of X used in the present work. Larger offsets are clearly desirable to reduce the percentage error in dT. Examples of the T-X characteristics of theoretical representative reflections having vertical two-way times T_0 of 500, 1000 and 1500 ms are shown in Figure 2.7 for three typical velocities of 2.5, 3.0 and 3.5 km/s each. The depths corresponding to these velocities are given in Figure 2.7B, which shows that for dX's of one or two spread lengths, offsets X of at least half the depth to the reflector are needed for reasonable NMOs of 10-20 ms.

Since the 12 channels per shot can only be laid out over a distance of 330 m or less, a complete graph like Figure 2.7A is built up from a number of recordings. The largest offset of one shot gather is set equal to the smallest offset of the next, so that events can be correlated better from record to record. The two coincident channels (one on each shot record) should therefore be identical, other things being equal. This means that coverage in the present surveys is built up in multiples of 330 m (11 x 30 m) rather than 360 m, as would be the case if the end channels had not been duplicated.

Figure 2.7 also shows the bands of coherent noise generated by the shot. The first arrivals - the headwave along the top of the bedrock - are useful for static corrections (see Chapter 3), but result in a blind zone of up to 200 ms in width. This is not too crucial, since the aim of the work is not to detect shallow reflectors (say 400 m depth or less). However, the ground roll - the general term for

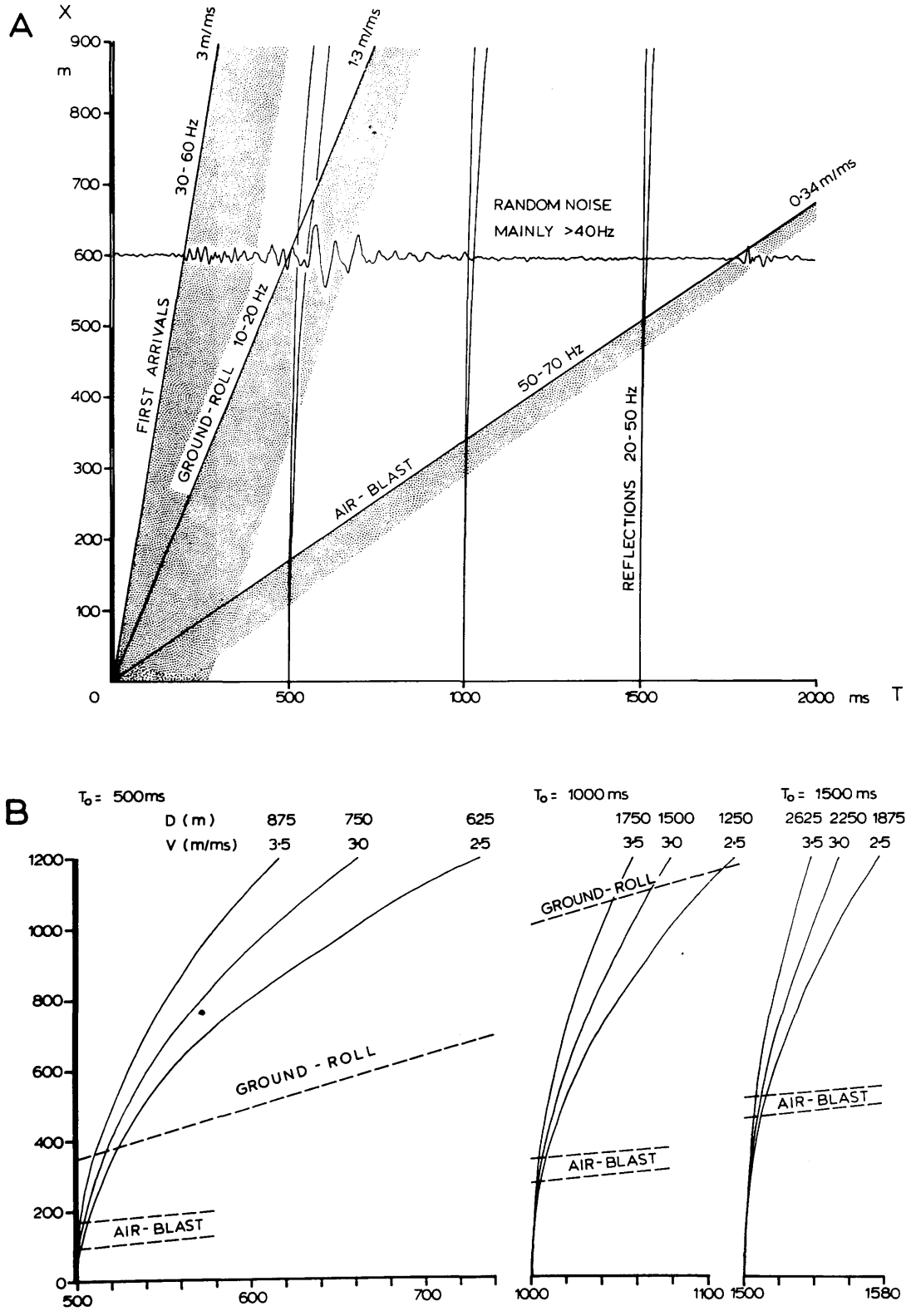

Fig. 2.7
A. Model time-distance graph showing three reflections with vertical two-way times of 500, 1000, and 1500 ms, respectively, their 'bandwidths' (the twin hyperbolae diverging at far offsets) covering the range of velocity 2.5-3.5 km/s.
B. Portions of A expanded in the T-direction to show moveout of the reflectors for velocities of 2.5, 3.0, and 3.5 km/s.

surface waves, of which the Rayleigh wave dominates - interferes with potential reflections having two-way times T_0 in the range 400-900 ms, but, being of significantly lower frequency (10-20 Hz) than the reflections (20-50 Hz), can be largely removed by low-cut filtering. The air blast, having a frequency spectrum of 50-80 Hz, can similarly be filtered out with a high-cut filter. In practice, though, even after bandpass filtering on recording, there is a band of some 150 ms in width within which reflections will be degraded or obscured. The single trace at 600 m offset in Figure 2.7A (drawn from a test field record) shows the relative amplitudes of these events, before appication of bandpass filtering or time-varying gain.

A T-X graph built up from a number of shot records is thus clear for the recording of potential reflections at times of greater than 800 ms or so, apart from the diagonal strip occupied by the air blast. But even within this area the signal may be obscured by random noise due to wind, rain, animals and people, etc. Noise is generally taken to include ground motions produced by the shot other than the identifiable effects like ground roll. Such non-random noise - i.e. unwanted signal - may be due to the mutual interference of multiple reflections, shallow refractions, point and edge diffractions, etc., which are likely to occur in seismically complex areas like Skye.

Increasing the charge size increases the signal to random noise ratio, but obviously leaves unaltered the ratio of useful signal (reflections) to unwanted signal (ground roll, obscure interference, etc.). Figure 2.8 illustrates this point with two records from Waterstein, which were shot under identical conditions of geometry, weather, instrument settings, etc., but with one of them using 11 times as much dynamite as the other. The two records are remarkably similar for the first second or so, showing that signal to noise ratio is good, even for the smaller shot (automatic gain control, AGC, has adjusted both records to the same overall level). Nevertheless, little of the seismic energy in this range can be interpreted in the form of reflections.

Figure 2.8 demonstrates also that the coincident channels of adjacent shot records should be very similar, if signal to

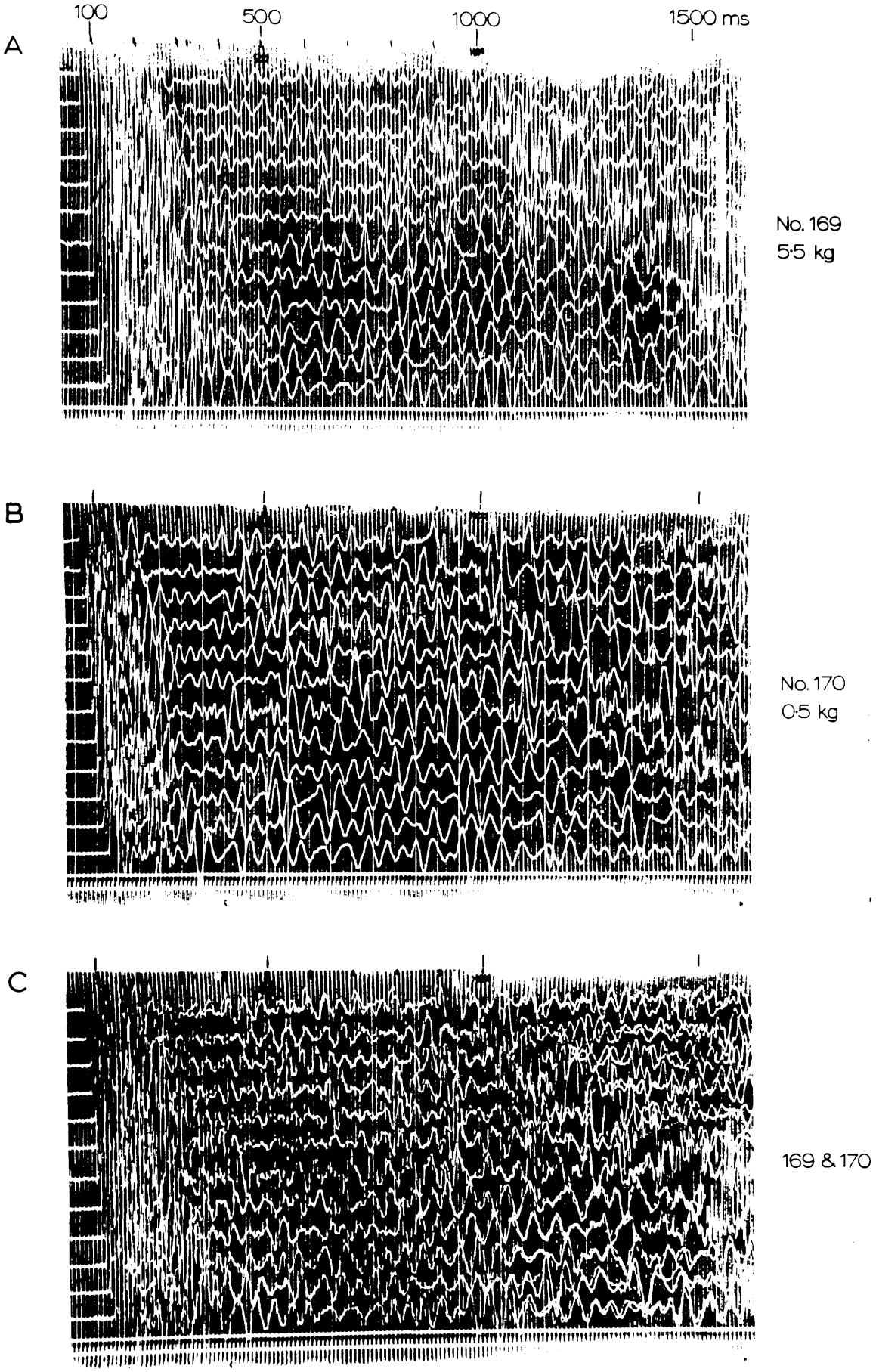

Fig. 2.8 Monitor records from Waterstein, NW Skye.
A. Main shot (no. 169), using 5.5 kg gelignite.
B. Experimental shot (no. 170) observed under identical conditions to A, but using only 0.5 kg gelignite.
C. Photographic superposition of record 169 on 170, showing their close similarity within the first second after detonation.

noise ratio is satisfactory. The extent to which they are alike provides a check on this ratio, and lack of correspondence after a couple of seconds or so, which turns out to be the case with the Skye results, indicates a deterioration in signal level.

2.2.5 FIELD GEOMETRY

One spread length is defined to be 165 m, and shot points are spaced at intervals of 165 m along a traverse line, although not all shot stations are necessarily used for shots. A 'single' spread is laid between two shot points, so that the two end channels are nominally at the shot points. Channel spacing is 15 m. However, 'double' spreads of 330 m, with a 30 m channel separation, are normally used. All spreads are thus multiples of 165 m away from a shot. Single spreads are only used:

(1) When trace-to-trace correlation seems to be poor,

(2) To complete tie-ins of subsurface coverage (explained below), and

(3) When there is no room for a double spread, for instance, at the end of a line.

The field geometries described below are designed for the manual picking of reflections on shot records, without any CDP gathering or other form of trace sorting. The field layouts are therefore designed to maximise continuity of subsurface coverage from the end of one shot gather (record) to the beginning of another. In the building up of a range of offsets, multiple subsurface coverage of the same depth points is produced, so that the data are also amenable (after digitisation) to the standard digital processing methods based around the CDP gather and stack.

A T-X graph for velocity determination is constructed in both the positive and negative X directions. Dix's methods (1955) is to start with a split spread (Fig. 2.9A) and increase the shot-spread offset X (using double spreads) by

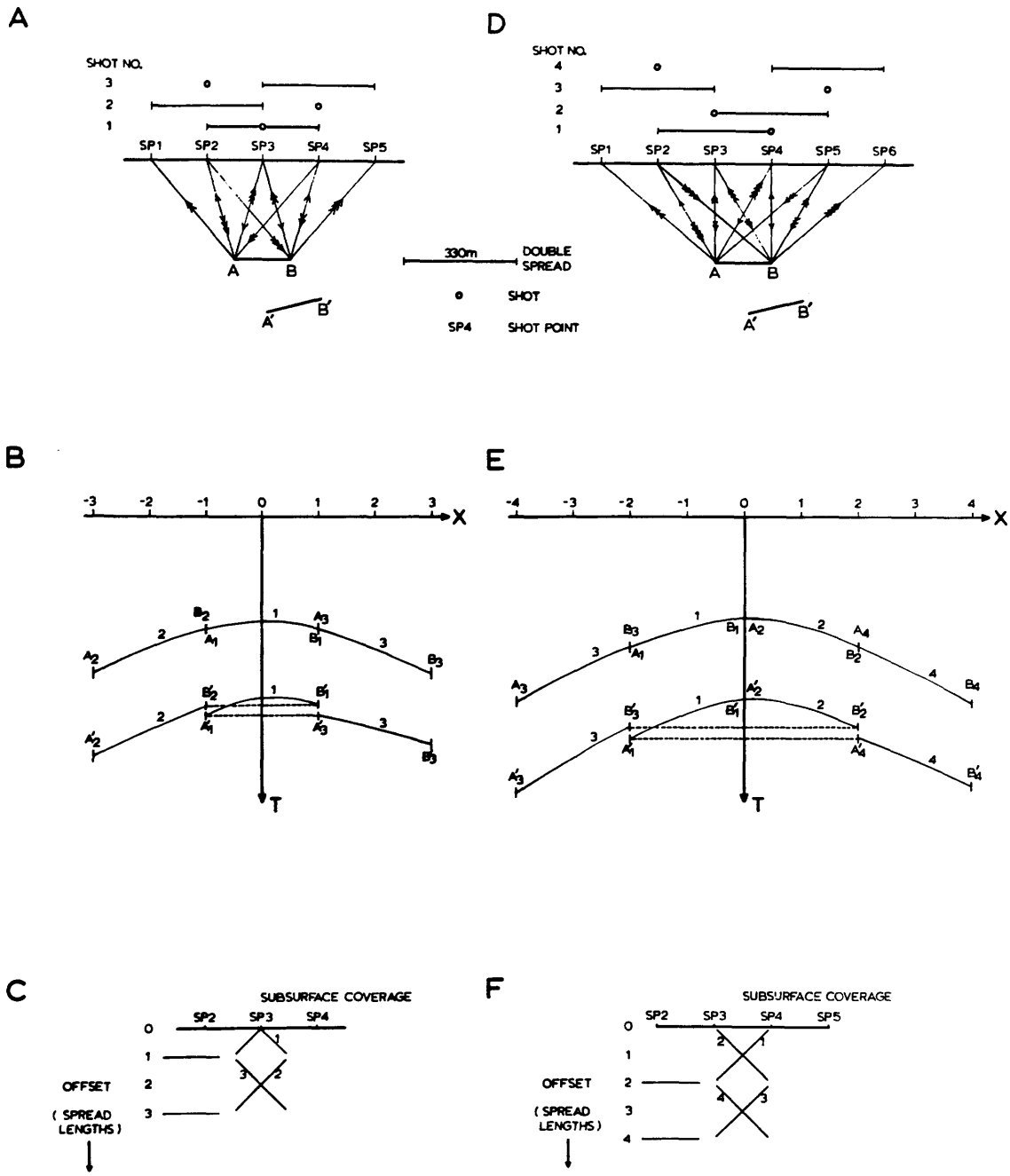

Fig. 2.9 Reflection shot-spread geometry for velocity survey. The left-hand figures A-C show Dix's method, whereas the right-hand figures D-F show an alternative method which avoids the use of a split spread.
A, D. Successive shot-spread layouts.
B, E. T-X graphs for reflectors AB and A'B'.
C, F. Subsurface-coverage - offset diagrams.

one spread length for successive shots in each direction. The resulting set of records comprises a 'velocity survey' or CDP survey. The same length of subsurface AB (horizontal) or A'B' (dipping) is thus observed each time, and comprises 12 CDPs. The nearest channel to the shot of any spread has a reflection raypath identical to that of the farthest channel from the previous spread from its shot. However, the offsets are of opposite sign. In the case of a dipping reflector A'B' (Fig. 2.9B), arrival B'_2 has the same time as B'_1. not A'_1. In practice the time difference between A'_1 and B'_2 is only a few milliseconds (for dips of less than about 30°), so that there is no trouble in correlating the reflection from one record to another.

Figure 2.9C is a plot of subsurface coverage against offset for the separate records. It shows that raypath reversals occur where the diagonal lines meet or cross, and is a more informative way of displaying coverage than direct shot-spread geometry, as in Figure 2.9A. An alternative to the Dix method is to start with an end-on shot (with zero shot-spread offset) as shown in Figures 2.9D-F. Essentially the only difference is that fold of coverage ends up as an even, rather than an odd, number. Available line length may determine whether an odd or even number of shots should be fired in total.

Digital processing can usefully use the above geometries. Let us assume that n shots were fired. There are therefore 12 CDPs each with an n-fold coverage. Semblance plots for velocity determination are normally made by averaging several CDPs, and in the present case the CDPs are only 15 m apart. It is therefore justifiable simply to bin all the data for the purpose of making a single 12n-fold semblance plot, and to display the n-fold stack as 12 traces to show up any hint of dip over the 165 m of coverage.

If only a velocity survey is required, as described above, the entire (double) spread has to be moved every shot by half its length, whichever alternative geometry is used (Fig. 2.10A). Since at most sites this survey is combined with some single-fold continuous profiling and rather wider subsurface coverage than just 12 CDPs, it is efficient to use the same spread for a number of shots without having to

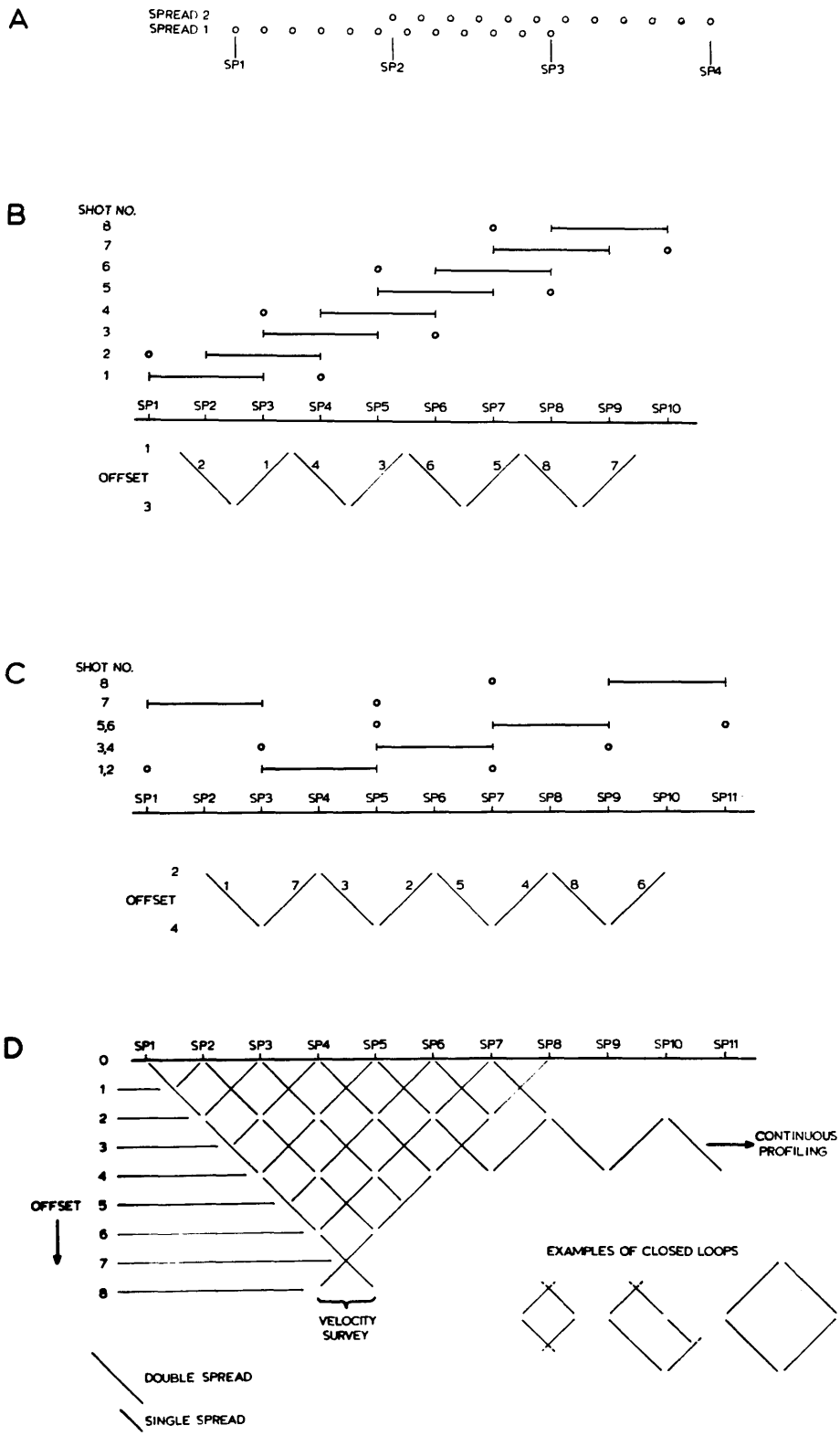

Fig. 2.10 Field geometry for continous profiling.
A. Successive geophone positions for double spread, moved one spread length.
B. Shot-spread positions and subsurface coverage diagram for offset of 1 spread length.
C. Shot-spread positions and subsurface coverage diagram for offset of 2 spread lengths.
D. Subsurface coverage diagram for combined velocity survey and continuous profiling, with multiple subsurface coverage.

shift it. The most suitable shot-spread offset range for the continuous single-fold profiling is decided from the T-X graph characteristics of the locality (see Section 2.2.4 above). If this is linked to a Dix-type of velocity survey, the shot-to-nearest-receiver offset has to be an odd number of single spread lengths, or else split spreads. Figure 2.10B illustrates the field and subsurface geometry for an offset of 1 spread length. The spread has to be lifted after each shot, as Figure 2.10A shows. But if split spreads are avoided both in the velocity survey and continuous profiling, an even-numbered offset (e.g. 2 in Figure 2.10C) enables us to use each spread twice, except for one at either end of the profile. The CDP coverage will thus be single-fold, except for every eleventh depth point, which will be 2-fold.

The combination of velocity and continuous profiling survey can be extended as shown schematically in Figure 2.10D. A trellis pattern of CDP coverage is built up, so that correlation of reflectors can be made around closed loops of 4 or more shot records. Most spreads are used for several shots, which is cost-effective, and if digital processing is used we get a fold of stack ranging from maximum in the centre to single-fold at either end of the trellis. Single spreads (15 m channel separation) are used to increase the number of loops, while avoiding the creation of loose ends in the trellis pattern. A useful by-product of the trellis pattern of coverage is an extensive T-X graph of first arrivals, which are required for the static corrections. This graph also provides shallow refraction information in place of shallow reflections for the uppermost 100-200 m of subsurface.

In addition to the main survey line, a few shots may be fired on a cross-line, at right angles to the main one. At most sites, however, lack of time and/or space prevented this from being done.

2.2.6 ENERGY SOURCES

A fundamental difference between the present, university-based, field crew and a commercial contractor is that the latter has the capability of drilling deep shot holes on a routine basis. The unusual near-surface geology of Skye - peat, overlying solid basalt - would, however, preclude the use of routine shot-hole drilling; a commercial operation would probably use Vibroseis instead of dynamite. However, Hall's surveys in Ayrshire (1971, 1974) have shown that the firing of a number of small charges of gelignite in the drift is an acceptable alternative to the usual commercial explosive-source procedure of detonating a larger charge (say 50 kg) 30 m or so down a hole drilled into bedrock. At least one problem is avoided by drift shooting - that of multiples or ghosts from the initial upward propagation of energy reflected back down at either the ground-air or bedrock-weathered layer interfaces (see, for example, Van Melle and Weatherburn 1953, Dix 1955, Dobrin 1960).

Two types of explosive source were considered;

(1) Sticks of polar ammon gelignite, and

(2) ICI Geoflex cord explosive.

The latter was rejected after limited experiment, as it requires to be ploughed in to be efficient. Use of a tractor-pulled plough would have severely curtailed the choice of sites for shot points, whereas manual digging in of the cord takes at least as long as drilling a set of holes for an equivalent amount of gelignite. During the 1971 season comparison recordings were made of 200 m of Geoflex in a 100 m long trench dug 0.3 m deep in the peat, and 8 sticks of gelignite (0.2 kg) as a 'point' source buried 3.2 m down. The two records are not significantly different, although the reflected energy from the Geoflex shot tends to be of slightly lower frequency. Contrary to what might be predicted from theory, the ground roll amplitude recorded (reduced by a 22 Hz low-cut filter) is not any lower for the linear source than for the point source.

The energy source used throughout the surveys was gelignite, sticks or part-sticks of which, about 3 cm in diameter, are placed individually in holes drilled to the base of the drift, which is anything from 0.8 to 2.1 m down.

At all the sites, the drift is either peat or boulder clay, usually water-saturated, overlying fresh (glaciated) bedrock varying in type from clay to basalt. The bedrock to weathered layer reflection coefficient R is thus as high as ~0.7 for the peat-lava interface at Quirang and Edinbane (lines 4 and 6 respectively), but negligibly small (~0.05) for the boulder clay - Jurassic clay interface at Sheader and Skudiburgh (lines SK-1, 1A and SK-2, 2A respectively).

2.2.7 FIELD METHODS

During the preliminary measuring out of a line (see 2.2.8 below) shot points are established and marked by ranging rods. The spread cables are then wound out between the desired shot points, with take-outs 1 and 12 at the two end rods. As the take-out separation is 50 ft (15.24 m) a slack length of 2.6 m would be left at the farther shot point if the cable were pulled taut. This is allowed for by laying the cable loosely, and by natural unevenness in the ground surface, so that the intervening take-outs end up within a few centimetres of the correct 15 m spacing. Geophones on a single spread are connected to each take-out of a single cable, whereas for the usual double spread they are connected to take-outs 1, 3...11 of the first cable and 2, 4...12 of the second. An extension cable is then laid, if required, to connect the spread to the recording vehicle.

The 7 geophones per channel normally used are connected in two groups of 4 and 3, each in series, and the two groups are then connected in parallel to the take-out, to give a total resistance of somewhat over twice that of an individual phone (300 ohms). Since n geophones in series have n-1 modes of oscillation which are poorly damped, whereas 2 in parallel have high electromagnetic damping for both modes (Seriff 1959), the series + parallel connection will preserve, as far as possible, the original damping

characteristics of the individual phones. The resulting low overall impedance of the group matches better the input impedance of the amplifiers, and, furthermore, if a geophone clip is accidentally pulled out just before a shot, only 3 or 4 of the phones will be open-circuited, and not all 7, as would happen if a series-only connection were used. The line resistance can be checked channel by channel before firing; it should be about 700 ohms at the near end of a double spread, rising to about 1 kohm at the far end.

Many papers on the use of geophone and shot patterns have been published, both empirical (e.g. McKay 1954, Lombardi 1955) and more theoretical (e.g. Jones 1945, Parr and Mayne 1955, Savit et al. 1958, White 1958). Some of these advocate the use of large numbers of geophones - as many as 36 per channel, for example - with weighted responses, but this is outside the scope of the equipment available. The aim of patterning the phones is to improve reflection quality by:

(1) Increasing signal to random noise ratio, the improvement being proportional to $(n)^{\frac{1}{2}}$, where n is the number of geophones,

(2) Improving the 'plant' (i.e. the effectiveness of the geophone response, varying with its position on or below the irregular ground surface) simply by laying as many as possible over an area (see Lombardi 1955),

(3) Enhancing events with low move-out and cancelling those with high move-out (see Savit et al. 1958).

The 7 geophones could be planted in line with the shot at a spacing of about 1 m to cancel out, or reduce to under 20%, the air blast, whose wavelength spectrum is of the order of 4-9 m (see Parr and Mayne 1955, fig. 3). However, it is found in practice that cancellation of random noise, reduction of side-on coherent noise, and better sampling of the ground to improve the 'plant', are all more valuable improvements produced if 6 of the phones are planted in a regular hexagon around the seventh, which is centrally positioned at the take-out. The spacing is up to the length of each geophone cable from the take-out, viz 3-4 m. The

much larger area taken up by the shot would, in any case, nullify any attempt at cancelling shot-generated noise by geophone patterning.

The predominant cause of poor record quality in Skye, bearing in mind the small charges used, is random noise due to wind and rain. The increase in noise due to a wind Force 5, say, relative to calm weather, can be as much as 20 dB. The first three sites of the 1971 season were observed during good weather, and the geophones were planted at the surface; but with the onset of high winds by mid September it was found necessary to bury the phones for the survey of Quirang. Tests during high wind show that 4 phones buried at the bottom corners of a 30 cm^3 hole in boulder clay immediately overlying lavas reduce noise by 20 dB, compared with 4 others planted on the surface in long grass. However, the reduction when they are planted in a similar hole in a thicker layer of peat is less dramatic - about 10 dB - since the peat appears to vibrate bodily under the effects of high wind. But even this reduction in noise enables shooting to go ahead in mediocre weather conditions, when it would otherwise be a waste of time. All shots in 1972 were recorded with 7 phones per channel in the hexagonal pattern, with each one buried in a separate hole about 30 cm deep. The intention was to obtain better-quality, if rather fewer, data.

The HS-200 blaster is designed to be operated beside the recorder, so that detonation and recording can be synchronised. Thus the 150 V firing pulse has to be conducted along a firing cable to the series-connected detonators. When the charges are more than 100 m away from the blaster a 500 m-long twin-core steel cable is used to complete the circuit. As the ICI 'Star' seismic detonators with 3 m wires have a resistance of about 4 ohms each, and require at least 1 A to fire them, the total resistance of the firing circuit must be less than 150 ohms. The firing cable has a resistance of about 0.1 ohm/m, making a total of about 100 ohms, so in practice no more than four or five detonators can be fired at once. This restricts the total weight of any shot to under 1 kg (e.g. four 20 cm-long sticks).

Immediately prior to the 1971 season the capacity of the blaster (and hence its charge-firing capability) was doubled by the addition of duplicate charging and relay-triggering circuits, to supply two independent outputs A and B (see Appendix 1). Output B has a variable detonation delay relative to A of 0-15 ms, calibrated to within 1 ms, so that an appropriate delay between two groups of charges a given distance apart will simultaneously tend to cancel the ground roll and beam the downgoing P-wave in a desired direction. Tests of the delay system showed, however, that it did not improve the results.

A few experimental shots in 1971, using larger charges, were fired by connecting up to 20 detonators to the blaster by short leads, thus overcoming the resistance limitation. The 500 m firing cable was used to transmit the time-break back to the recording vehicle stationed some distance away. Synchronisation of the blasting and recording was achieved by visual signalling.

A refinement of the method, incorporating portable VHF radios, was designed for the 1972 season. The blaster, now positioned near the charges, is remotely triggered by the cessation of a 1 kHz tone transmitted by radio from the recording van; the tone is cut off by the same micro-switch on the tape drum previously connected directly to the blaster. Safety devices ensure that the charges cannot be accidentally detonated by backgound whistle in the radios, and the firing sequence can be disabled at any time by the blaster operator. A dummy time-break is fed to the recorder from the tone generator, and is calibrated in the laboratory to coincide with actual detonation, thus obviating the need for a landline connection between blaster and recorder. However, under field conditions it is found that charge detonation is delayed, relative to the pseudo- shot break, by anything from 5 to 100 ms. This is thought to be due to poor signal to noise ratios in the radio sets, as the delay does not occur when there is a direct acoustic link.

Since an unpredictable shot detonation time is obviously unacceptable, one or two firing cables were used instead to relay the time break for the 1972 season, with the maximum available distance being 1500 m. Synchronisation of the

blast with the recording was achieved either by transmission of the tone, when signal level was reasonable, or by an oral count-down. A dummy run of the shot firing is carried out, to ensure that the time break will be recorded satisfactorily. The largest charge fired in this way is 20 kg, set off by 49 detonators, and took one day of field crew time (c. 50 man-hours) to prepare.

Hall (1971) has described the advantages of percussion drilling of shot holes in drift, compared with the more orthodox method of augering. A simple but effective percussion drill is rhythmically plunged to the base of the drift, or to the 2 m length of the drill shaft, by four labourers. The 7 cm diameter drill head makes a hole wide enough to take the 5 cm wide gelignite inserting device designed for the 1972 season. This comprises an open-bottomed sleeve to hold the stick, within which there is a plunger to push the stick out at the bottom of the shot hole.

The weight of charge placed in any particular hole depends upon the hole depth and the type of drift. Peat, although less efficient in transferring energy to bedrock than boulder clay, holds the charge down much better, due to its greater cohesiveness. A charge is most likely to blow out (i.e. break the surface and make a crater) in loose, dry boulder clay. This medium is also the most troublesome to drill through. Water is used during drilling as a lubricant, and to tamp the charges when in place. Table 2.2 (next page) shows the approximate weight of charge used for a given shot hole depth and drift type. The 'blow-out risk' column shows the weights with which blow-outs have occurred.

Clearly, there is more risk taken with shallow holes, but any damage is usually slight and can quickly be remedied. A useful precaution to prevent blow-outs of these shallow holes is to cover them before firing with a heap of boulders. The right-hand column shows theoretical cavity radii calculated from $R = B.W^{(1/3)}$, where W is the charge weight and B is a constant, equal to about 4 for soft clay (O'Brien 1967). This formula would appear to be inapplicable to charges exploded near the free (upper) and fixed (lower) surfaces of thin drift, as the cavities made

in practice are two to three times larger.

TABLE 2.2
CHARGE WEIGHTS PER SHOT HOLE

Depth (m)	Drift type	Usual weight of charge (g)	Weight for blowout risk (g)	Theoretical cavity radius (cm)
1.0	DBC	120	120	18
"	Peat	160	200	19
1.5	DBC	160	250	19
"	Peat	200	"	22
2.0	DBC; peat	250	500	24

(DBC: dry boulder clay)

Although drilling through wet peat is the simplest, holes must be loaded immediately before they collapse. Holes drilled in dry stiff clay, on the other hand, can be left for a day or two if need be. Peat is thus the most favoured drift encountered in Skye in which to drill shot holes, as its relative inefficiency in energy transfer is easily compensated for by drilling more holes, to achieve a greater total charge weight.

The minimum shot hole separation required to avoid the risk of coalescing cavities is 2 m. Usually, as many holes as are desired are drilled in the smallest possible area, which can normally be kept under 25 m^2. This is effectively a point charge. The actual shot position is as near as possible to the surveyed shot point as the local surface conditions will allow, the inline and crossline offsets of the shot in most cases being only a few metres. One patch of ground can only be used once for shots, due to the underground cavitation. The furthest that a shot has been from the nominal shot point is about 40 m, but as these are all at large shot-receiver offsets of 600-1000 m, the desired geometry is little affected. The digital processing makes due allowance for such shot offsets in the binning of

the traces into CDPs.

Other shot patterns used include shots with two groups separated by around 20 m, with relative delay of the nearer group to the spread, as described above. The many holes (up to 50) necessary for the large shots at Edinbane (line SK-6) permitted simulation of a linear charge, by drilling them in line as close together as possible. Such a linear charge, 70 to 80 m long, contains about 20 times more explosive than a similar length of doubled-up Geoflex. It both concentrates P-wave energy downward and tends to cancel in-line coherent noise. The results obtained with this pattern are very good, although only one shot a day can be fired.

The division of labour and time between the various tasks of a normal day's field work is given in Table 2.3.

TABLE 2.3
TIME SPENT DURING TYPICAL DAY (1972 SEASON)

Task	No. of people	Time (h) required	Comments
Laying spread	8	0.7 - 1.5	One or two spreads per day
Drilling	4		
Loading shot holes	2	3 - 4	30 - 50 holes per day;
Preparing charges and instruments	2		1 - 2 shots per day
Shooting	3-4	0.5	Longer if faults, or pause for weather
Clearing up shots and lifting spread	8	1 - 1.5	
Lunch and travel	8	2	
Length of average day		9 +/- 1 h	1 large shot less work than 2 smaller shots

Figure 2.11 shows a flow chart of the procedure prior to and during shooting. The two independent chains of action at the recording van and at the shot point are coordinated by radio instructions from the recorder operator. During the dummy run the firing line is replaced by a 100 ohm resistor, because if the line is left open-circuit no time break can occur. Shooting is postponed if the weather is bad, but prepared shots have to be detonated by the end of the day, whatever the weather. Buried geophones can be left overnight, but the spread cables are wound in at the end of the day, in case of damage. Any charges suspected of being undetonated by the shot are disposed of by inserting another small piece of gelignite together with a detonator down the hole. Suspect charges are never retrieved for examination.

Blowouts and cavities are filled in, so that the ground is returned as far as possible to its original state, and a visit some few weeks afterwards to check on ground collapse usually demonstrates that former shot points are all but unidentifiable.

2.2.8 SURVEYING

Errors in reflection time due to inaccurately corrected elevation will be kept to less than $\pm$ 0.3 ms if receiver station heights are known to within $\pm$ 0.5 m of their true height. Shot points are taped out and levelled, the latter being measured to $\pm$ 1 cm. Cumulative error along a line of several shot points may therefore add up to several centimetres, since closure is not carried out. A few geophone stations in between are also levelled, so that linear interpolation will give the elevations of the others to well within the required accuracy.

By straight raypath reflection geometry, and assuming a constant mean velocity V_m, the error dT in reflection time T is a function of the error dX in shot-receiver offset X, such that

$$dX = V_m^2 . \quad T \quad . \quad dT \; / \; X$$

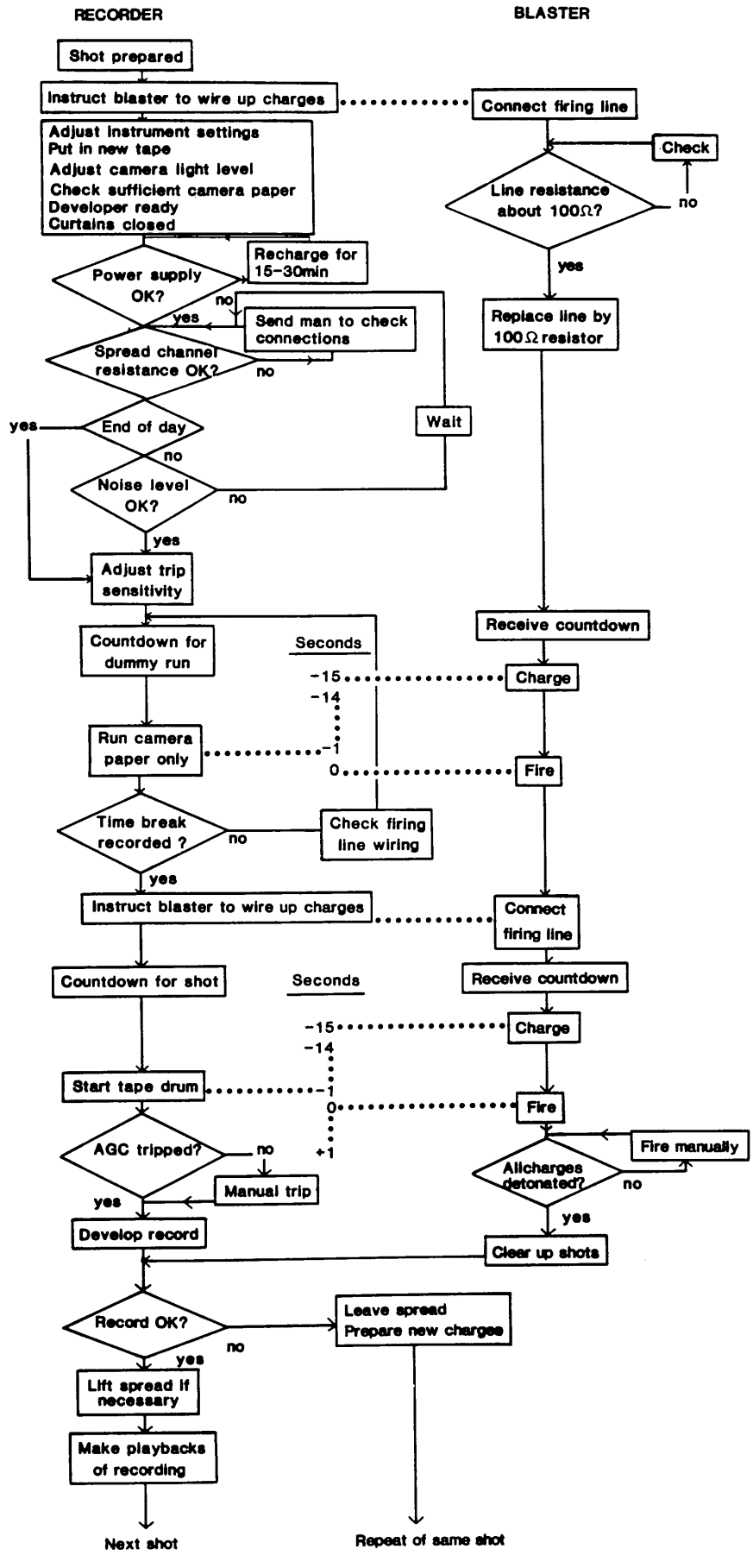

Fig. 2.11 Flow chart of field procedure for preparing and recording a shot.

If we wish to keep dT (due to dX) under 1 ms, then extreme values of the other variables, such as V_m = 2.5 km/s, T = 400 ms, X = 1000 m, result in dX = ± 2.5 m. At four of the six sites the lines are straight and the topography is subdued, so X is calculated (in the Merlin SKS line geometry processor) simply from the nominal straight-line station positions, with correction for inline and crossline shot offset. The shot position supplied to the processor is the centroid (i.e. weighted centre) of the shot pattern, whereas for the first arrival picking and T-X plots the offset X is from the nearest shot hole (of a shot pattern) to the receiver groups. For lines SK-1 (Sheader) and SK-4 (Quirang) the appreciable bends in the lines necessitate crooked-line geometry processing by SKS. The plotting of T-X graphs for the first arrivals uses offsets computed by some simple algorithms, approximating the dog-legs in the lines as measured from large-scale plans. Offsets calculated by the above methods are all estimated to be accurate to within ± 5 m, which is acceptable both for first break plots and for the digital reflection processing.

2.3 MARINE SEISMIC REFRACTION

2.3.1 AIMS OF THE SURVEY

The results of earlier, unpublished, geophysical surveys and geological sampling confirmed the existence of a sedimentary basin containing Mesozoic rocks in the Little Minch. A Bouguer anomaly map of northern Skye and the Little Minch (Fig. 2.12) was made available by IGS for consultation in 1970 to assist in planning the marine surveys. It suggests that the sedimentary basin is deepest below northern Skye. The steep gradient parallel to the eastern coastline of Harris indicates that the trough may be bounded on the NW by a large offshore fault a few kilometres from the coast.

Model refraction travel-time graphs were constructed, based on the gravity anomaly, and by converting plausible densities for basin infill and basement to seismic velocities using the Nafe-Drake curve (Ludwig et al. 1970). Such simple 1-dimensional models for a basin some 3-4 km

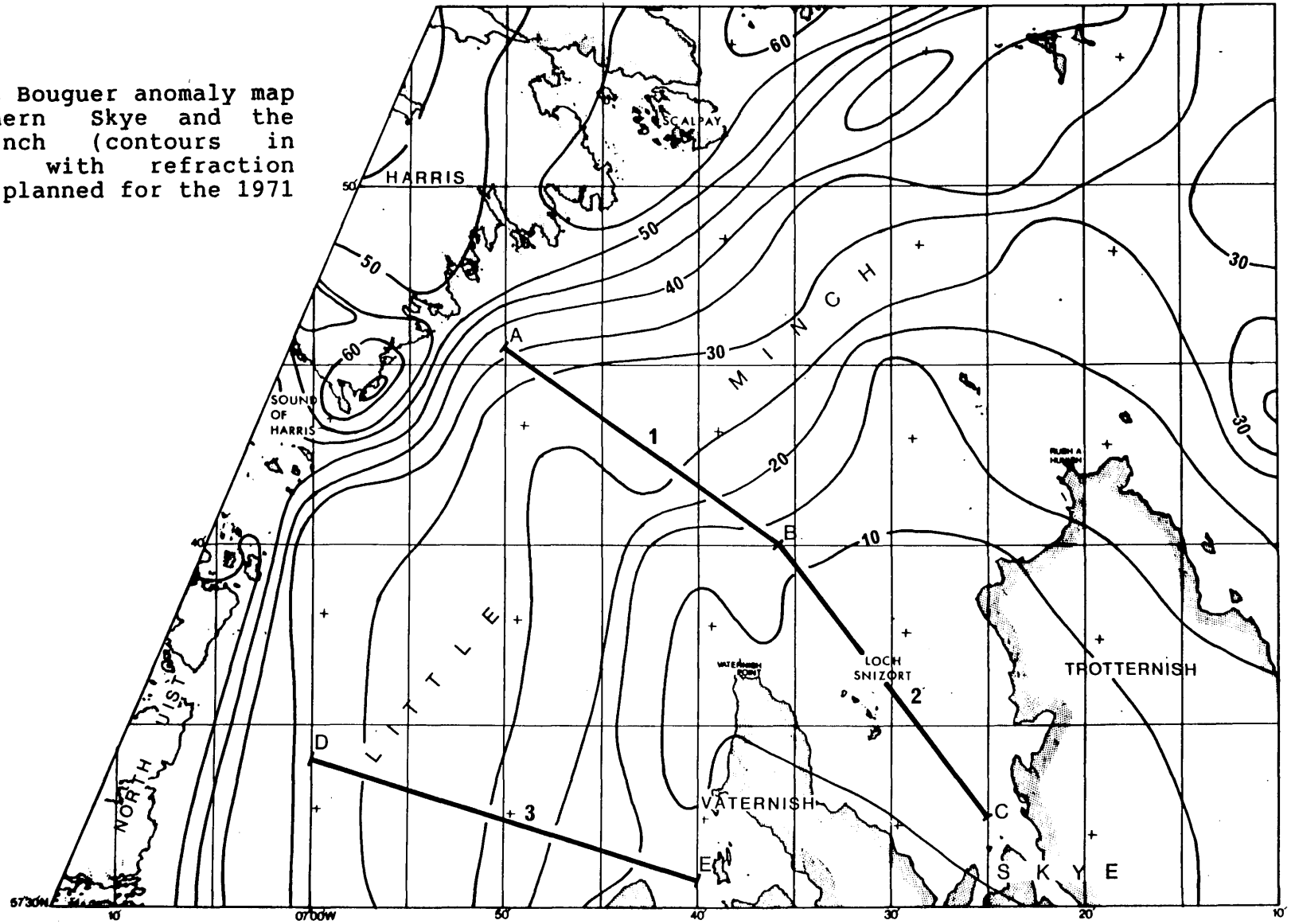

Fig. 2.12 Bouguer anomaly map of northern Skye and the Little Minch (contours in milligals) with refraction lines 1-3 planned for the 1971 cruise.

thick (satisfying the gravity anomaly) suggested that the critical distance for first arrivals from the sub-Mesozoic floor would be of the order of 12-15 km. A single NW-SE trending refraction line about 30 km long was therefore planned (Fig. 2.12). However, it was known from previous refraction work in the Firth of Clyde using the same equipment (Hall 1970a) that arrivals could not be expected at the full 30 km range, so the planned line was split into two 15 km long sections AB and BC. It was expected that full reversal would be obtained for each of these segments. Point A was sited close to the coast of Harris in the hope that the segment AB would intersect the NE-SW trending fault. A third line (DE in Figure 2.12) would also be attempted if the first two were observed successfully.

2.3.2 INSTRUMENTATION

Single-ship refraction shooting is a well-established technique. The particular equipment owned by the Glasgow University Geology Department has been described before by Hall (1971). It is a four-channel system, in which four Bradley sonobuoys transmit on 27 MHz to a Bradley receiver-demodulator rack, whose output is fed to the TI 8000 for recording on paper and magnetic tape (Fig. 2.13).

Hydrophones built in the Department and used in previous field seasons had proved somewhat unsatisfactory, because:

(1) Their heavy brass construction, although watertight, requires careful balancing with large cork floats in order to achieve mechanical decoupling of the hydrophone from the buoy, and

(2) It was thought that seawater eddies around the metal cage surrounding the transducer caused excessive noise.

So for these reasons, a set of lighter, cigar-shaped hydrophones, using the same transducer and pre-amplifier, was built in glass-fibre by Mr. G. Gordon, a departmental mechanic, in time for the 1971 survey.

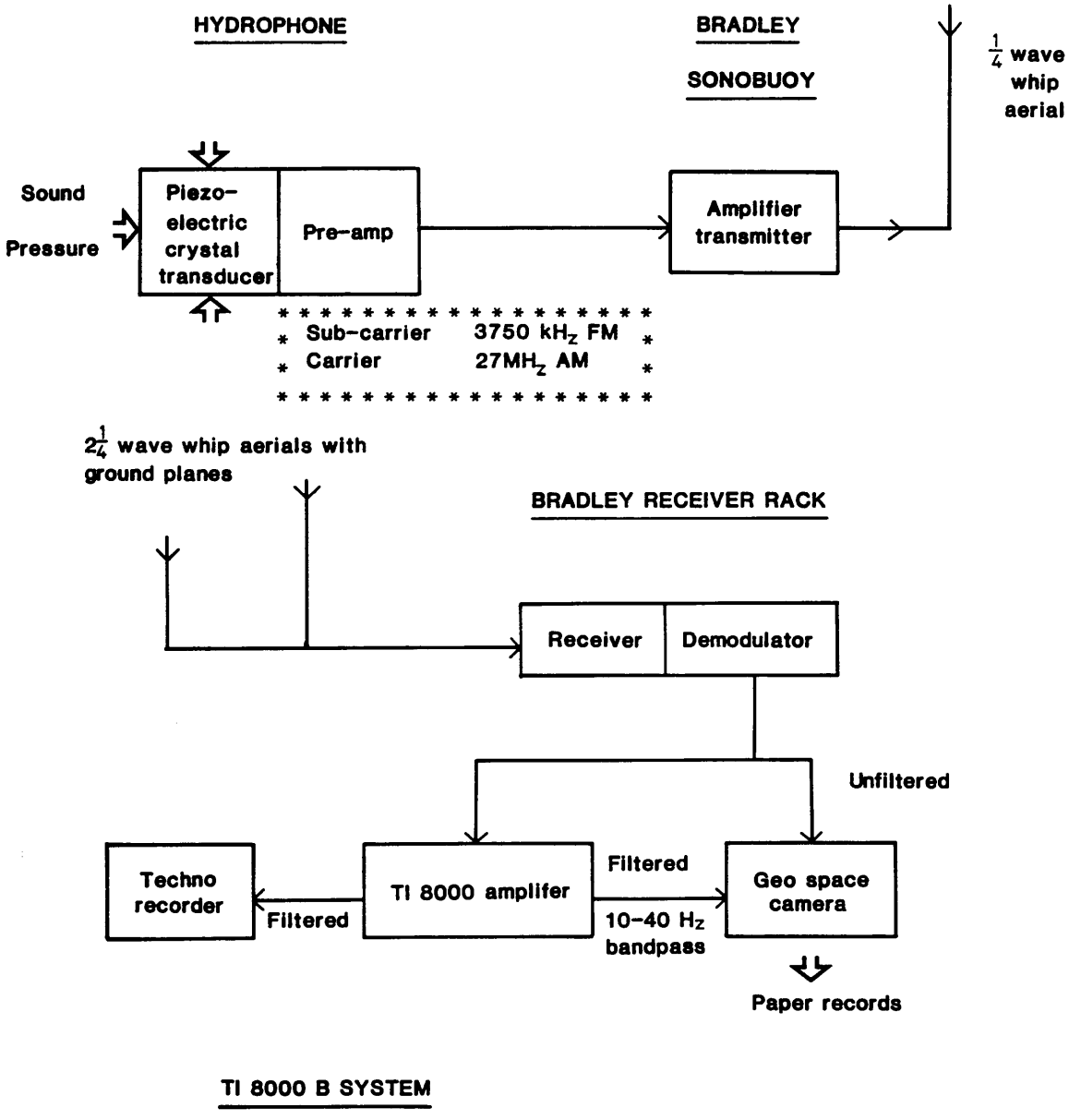

Fig. 2.13 Block diagram of signal path in Bradley/TI8000B seismic refraction system.

Difficulty had also been encountered in observing water-breaks on previous survey records, due to the low bandpass of the TI 8000 amplifiers (10 - 200 Hz). To solve this problem, outputs were taken from the Bradley demodulators direct to four galvanometers of the Geo Space camera (see Figure 2.13), so that the unfiltered signals could be recorded on the paper monitor record beside the filtered outputs from the TI 8000.

The duration of the recording time available with the above instrumentation is 6 s on magnetic tape. In theory, a monitor paper record could last for the time taken for a 45 m long roll to be used up at a rate of 13 cm/s - some 5.8 minutes. Thus an electronically detonated explosive source is clearly preferable to delay-fuse detonation, so that shooting and recording can be synchronised. Electrical detonation is also safer. The choice of explosive lay between ICI Marine Seismex, in cans of 37, 74 or 110 kg weight, and ICI Aquaflex - reels of explosive cord. The latter was chosen, as it is known to be more efficient and reliable.

2.3.3 THE 1971 SURVEY

The RRS John Murray cruise 71/8 for the Geology Department of Glasgow University covered the period 23 June to 14 July, about two weeks of which were spent in the Little Minch area. Refraction shooting was carried out by day and sparker/magnetic profiling (see Section 2.4 below) by night. Plans to use a sea-bottom gravimeter had to be abandoned after the NERC-owned instrument was found to be inoperable at the start of the cruise.

A Decca Hifix receiver was installed in the ship for this cruise, as the Hydrographic Office was running a Hifix chain in the Little Minch at the time. This receiver had to be re-calibrated each morning by lying the ship off Scalpay light or Vaternish light, whichever was the nearer. The chain's lane width in the survey area is about 150 m, so in theory, position can be read to a precision of 1.5 m (1/100th of a lane). In practice, of course, positioning is

subject to much larger errors, these being due to:

(1) Radar or sextant fixing of the vessel during each re-calibration - of the order of 30 m,

(2) The land paths over Vaternish and Trotternish from the slave stations on North Uist and Wester Ross, respectively, to Loch Snizort (see Figure 2.12), which introduce fixed but unknown errors, and

(3) Delay in taking readings when the ship is moving - 0.1 of a lane, or less, i.e. less than 15 m.

The fixed error due to land path propagation is unspecified by Decca, but if, like the Main Chain, it amounts to a few hundredths of a lane when the land path is only a small fraction of the total travel path, then it should be negligibly small. The overall error in Hifix positioning during the daytime surveys is thus probably less than 50 m.

Uncorrected Decca Main Chain 6C (North Scottish) was used as the working navigational tool throughout both the daytime and night-time surveys, rather than the more accurate Hifix, for the following reasons:

(1) Desired buoy and shot positions were pre-plotted on the bridge's Main Chain track plotter, to facilitate the seismic work,

(2) It made for easier communication with the bridge, and

(3) There would be internal consistency between the ship-board interpretation of the profiling survey and the refraction work.

Since the only Hifix receiver was situated in the laboratory, conversion of Hifix coordinates to Main Chain or geographical coordinates would otherwise have had to be made every time it was desired to give the bridge a navigational request. Furthermore, the Hifix lattice charts supplied by Decca are on the National Grid projection at 1:50,000, whereas the working plot sheets are:

(1) UTM projection at 1:100,000 with Main Chain lanes added (used in the laboratory), and

(2) Mercator navigational charts, at various scales, with Main Chain lanes (used on the bridge).

Obviously, accurate interconversion of the five coordinate systems - UTM, National Grid, geographical, and the two hyperbolic - is impracticable without automatic plotting and computing facilities.

The four buoys were initially launched free-floating, with a separation of about 700 m. Arrivals at the buoys from a series of shots can then be used to discriminate between horizontal and vertical velocity discontinuities (see Chapter 3), as well as providing redundancy (in case of failure), and helping in the recognition of arrivals.

Good first arrivals and water breaks were only observed from all four buoys for the first couple of shots of the survey. The buoys were at site A, off the coast of Harris (Fig. 2.12), and the ship was under way a few kilometres to the SE on line 1 (A-B), firing 30 m lengths of Aquaflex, towed at 2-3 knots from a 30 m long firing cable.

The various instrumental, logistical and geological difficulties which became apparent are, in roughly chronological order:

(1) Initially, unexplained misfires occurred. This was more or less cured by tying metal rings to the sea return wire of the detonator to reduce circuit resistance, and to help weigh down the Aquaflex connector, to counteract the buoyancy of the explosive cord. It is possible that the buoyancy was hindering the sliding of the connector down to the ball on the end of the shooting cable (some 15 - 20 m down) when the ship was sailing as slowly as 2-3 knots.

(2) Occasional premature firing due to a worn flash tube in the blaster; no spare was on board.

(3) Leaking hydrophones due to faulty design of the O-ring seal. These had to be taken apart, dried out internally, and a short-circuited transistor replaced. Electrical insulating tape wound tightly over the joint was found to make the hydrophones watertight.

(4) Mechanical coupling of hydrophone to buoy; this was cured by adjusting the floats on the hydrophone cable.

(5) Fast drift of the buoys - up to 2 knots - up and down the Little Minch in a NE-SW direction.

(6) Lack of arrivals other than water breaks (which were always good) at ranges of more than about 5 km, despite the doubling of charge length to 60 m, and deeper towing of the Aquaflex by using 40 m of shooting cable towed at only 1.5 knots.

Onboard interpretation of the profiling results during the cruise suggested that intrusives were at, or near, sea bed outcrop over about half of the area between northern Skye and Harris. These high-velocity, irregular, shallow layers were probably preventing penetration of energy. The pre-survey interpretation of the IGS sparker/magnetic data had not revealed the true extent of the intrusives below lines 1 and 2. Problems (5) and (6) above were thus tackled by shifting the work to a new line PQ (see Figure 2.14), some distance to the SW, where the intrusives appeared to be less widespread. By this time only one channel of the 4 channel system was still completely reliable, so deploying the others would probably have been a waste of time. The buoy was anchored in 140-160 m of water by 200 m of sisal to a light boat anchor. This method was very successful, since neither mechanical coupling to the hydrophone caused by the expected streaming out of the hydrophone cable, nor any significant anchor drag occurred, except once, when the sea-wave amplitude was more than 1 m.

The problem of lack of refracted energy remained, however, and was not solved by larger charge sizes. One shot, for example, used 100 m of Aquaflex, weighted down with about 4 kg of lead and steel rings. The ship's speed was 1.5 knots, and the explosive cord was in line with the buoy, which was

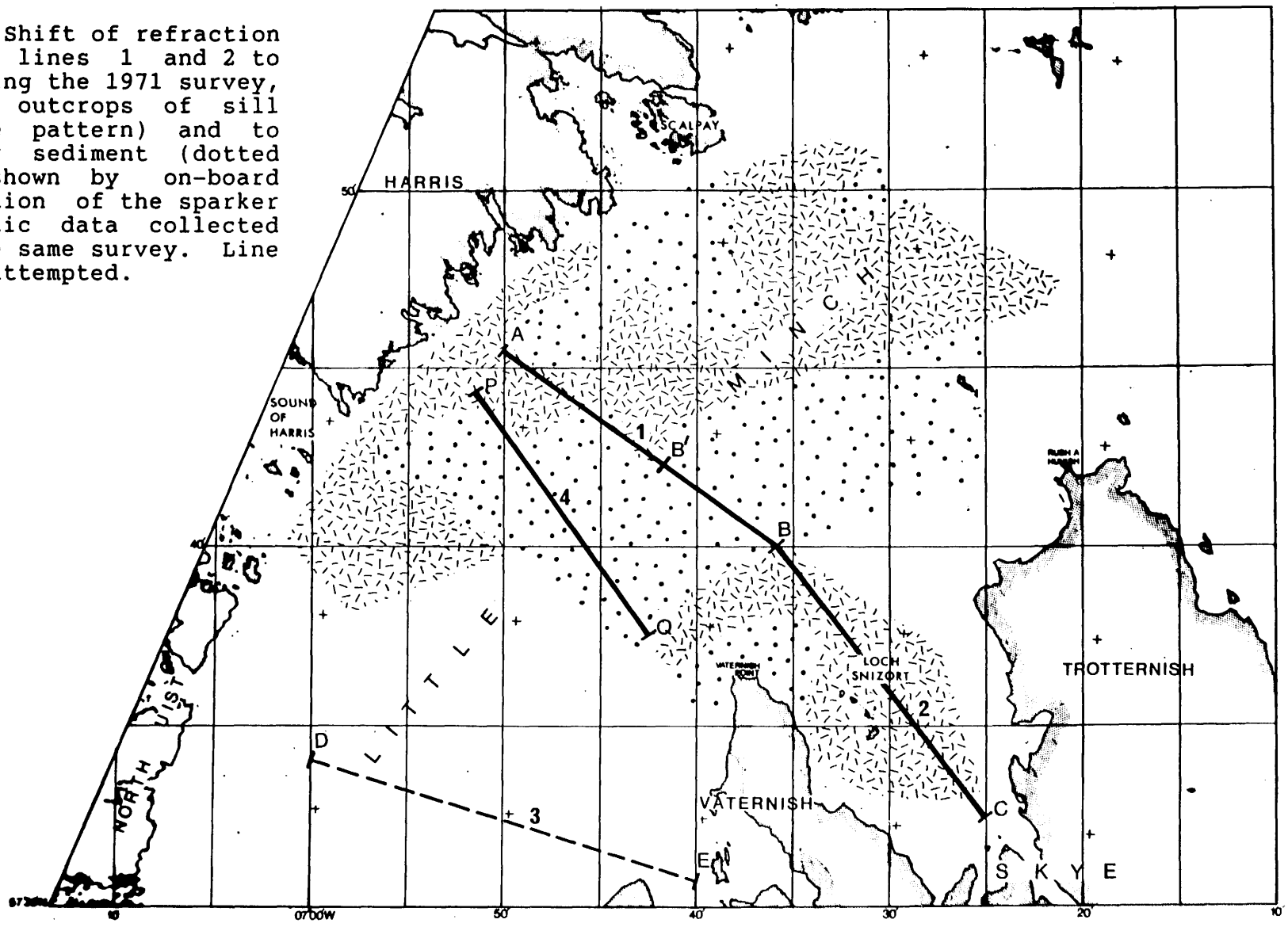

Fig. 2.14 Shift of refraction work from lines 1 and 2 to line 4 during the 1971 survey, to avoid outcrops of sill (short-line pattern) and to shoot over sediment (dotted pattern) shown by on-board interpretation of the sparker and magnetic data collected during the same survey. Line 3 was not attempted.

8 km away. Nevertheless only a good water-break was observed.

The last few days of the refraction survey were spent attempting to reverse the successful segment of line 1, by placing the one anchored buoy at B' (see Fig. 2.14) and firing shots along AB', a distance of about 10 km. Experiments to obtain wide-angle reflections at Q were also carried out by sailing past the anchored buoy while recording as many shots of 30 m lengths of Aquaflex as possible - about one every 400 m on average.

Measurements of sound velocity in water were made on most days before or during refraction work, using a meter suspended about 10 m below sea level. Velocities were found to be near constant.

2.3.4 MODIFICATIONS TO INSTRUMENTS

A set of newly designed hydrophones was built for a second cruise in 1972 (Fig. 2.15). The resulting instrument is small and light, to minimise drag and make neutral buoyancy balancing easier, and there is an external battery switch. Watertightness was proved by a submersion test of one hour at 30 m in Loch Lomond. Eight new pre-amp circuits were built and tested by the author, and the best-matched four of these chosen for use. The circuit is potted in silicone rubber compound so that accidental wetting will not cause damage. The new design proved to be successful.

In both refraction and reflection shooting, amplifier gain settings are usually adjusted before each shot so that the background noise level makes a very low-amplitude trace on the paper output (typically 1-3 mm in amplitude). If the instrument remains in 'fixed-gain' mode during recording, signals significantly above noise level will then be clearly and neatly recorded. The disadvantages of this are that large differences in signal amplitude between one trace and another may make comparison difficult - particularly in refraction shooting where the path length of arrivals from a common refractor and shot may be very different. Finally,

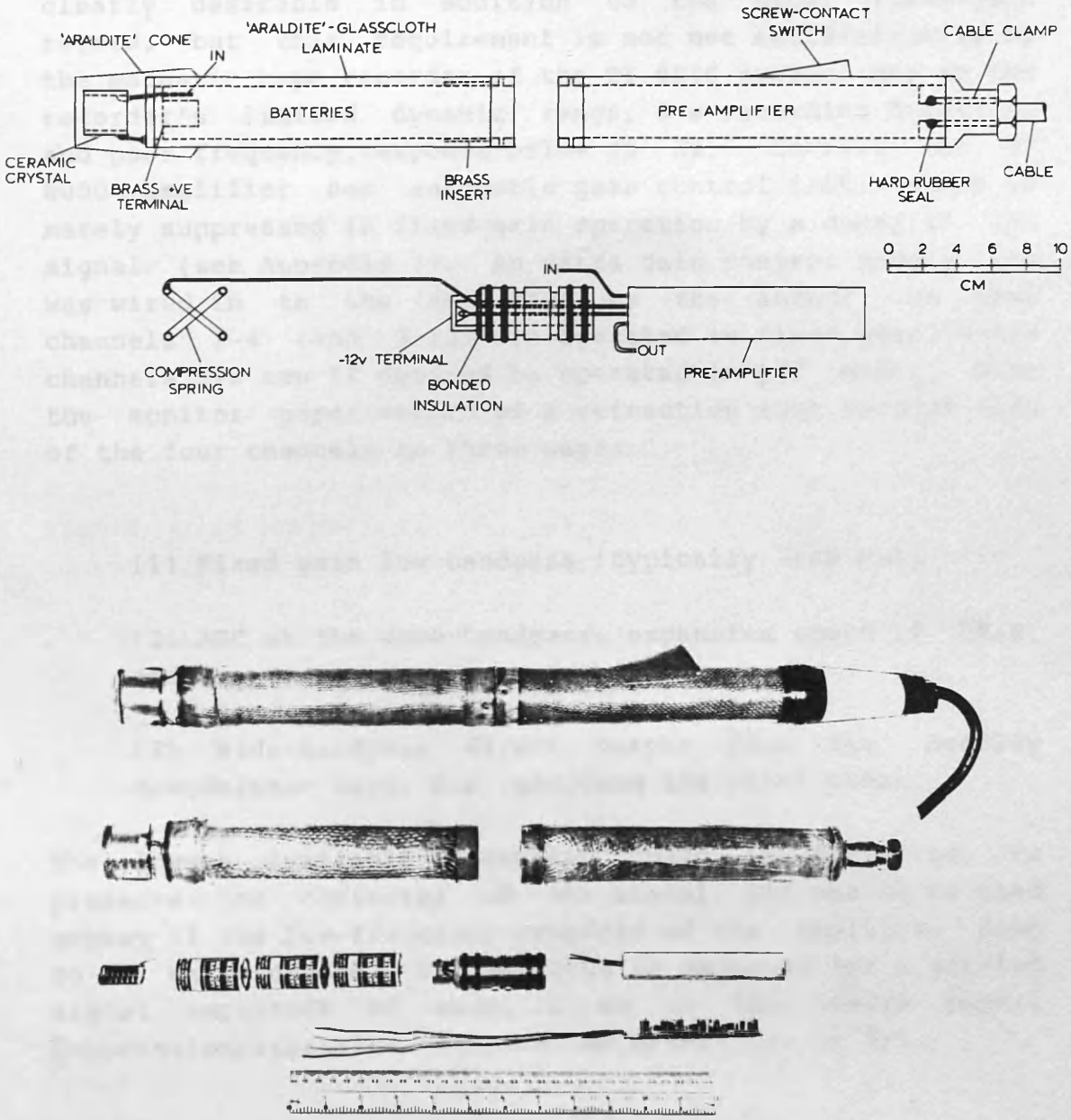

Fig. 2.15 Refraction hydrophone designed and built for the 1972 survey.
A. Diagrammatic cross-section showing main constructional details.
B. Photograph showing, from top to bottom:
(i) assembled hydrophone ready for use,
(ii) dismantled hydrophone shell,
(iii) internal components - spring, batteries, central O-ring sleeve, 'potted' pre-amplifier,
(iv) pre-amp before 'potting' in silicone rubber,
(v) 12" (30 cm) ruler for scale.

inspection of the character of the ambient noise will be difficult, since the amplitude of this has been reduced to a barely visible level. Some sort of time-varied gain is clearly desirable in addition to the usual fixed-gain record, but this requirement is not met satisfactorily by the magnetic tape recorder of the TI 8000 system, due to the recorder's limited dynamic range, 6 s recording duration, and poor frequency response below 20 Hz. However the TI 8000 amplifier has automatic gain control (AGC), which is merely suppressed in fixed-gain operation by a dummy 10 kHz signal (see Appendix 1). An extra gain control mode switch was wired in to the amplifier by the author, so that channels 1-4 (and 9-12) are operated in fixed gain, while channels 5-8 can if desired be operated in AGC mode. Thus the monitor paper record of a refraction shot records each of the four channels in three ways:

(1) Fixed gain low bandpass (typically 7-40 Hz),

(2) AGC at the same bandpass, expansion speed 20 dB/s, and

(3) Wide-bandpass direct output from the Bradley demodulator rack, for recording the water-break.

The lowest available expansion speed is preferred, to preserve the character of the signal, and has to be used anyway if the low-frequency response of the amplifier down to 7 Hz is needed. The AGC gain is adjusted for a written signal amplitude of about 1 cm on the camera paper. Compression/expansion ratio can be either 1/1 or 3/1.

2.3.5 THE 1972 SURVEY

Ship time on the NERC vessel RV Edward Forbes had been allocated for July 1972. The vessel could not be used, however, as re-fitting was behind schedule. At short notice the 18 m long RV Calanus, operated by the Scottish Marine Biological Association, was used instead, by kind permission of the Director of SMBA. Details of the cruise, which

lasted from 26 June to 8 July 1972, are given in the preliminary report issued by the Department of Geology, Glasgow University.

Refraction shooting was carried out during daytime, but the ship is unsuitable for 24 hour operation. A new attempt at a NW-SE refraction profile was made in the general area of the 1971 line PQ. Like the 1971 line A-B, this was to be shot in two parts, AC and CD (Fig. 2.16). The Calanus was able to sail right into the Sound of Harris, so that buoys anchored there (A in Fig. 2.16) would almost certainly be directly over Lewisian outcrop to the NW of the Minch fault. Interpretation of the 1971 and earlier Glasgow and IGS geophysical data (Smythe et al. 1972) suggested that this fault follows the steep bathymetric slope just off the eastern coast of the Outer Hebrides; a refraction line shot a few kilometers south-eastwards from within the Sound of Harris would therefore only need to record rockhead arrivals in order to confirm the postulated location of the fault.

The Decca Main Chain receiver on the ship was out of action for the whole cruise, so positioning is by radar range and bearing. Accuracy of this method (discussed in Section 3.3) is clearly a function of distance from land. At its worst, in the middle of the Little Minch about 12 km from the nearest landmark, relocated shotpoints are probably within 300 m of their true position. This error is probably no larger than that of corrected Main Chain fixes in the same area.

Double strength Aquaflex in 30 or 60 m lengths was used, and 74 shots gave satisfactory refracted arrivals and good water-breaks at ranges of up to 13 km. At least one channel of the four always worked well, but an unidentified fault in the ship-sonobuoy radio system (or possibly external interference) limited the range, rather than lack of seismic energy. Buoys which worked well in on-board tests often performed poorly in the water, probably for the same reason. Apart from this, the seismic system worked well throughout the cruise.

Because of the radio limit on the shot-buoy range, almost all the work was concentrated at the NW end of the line,

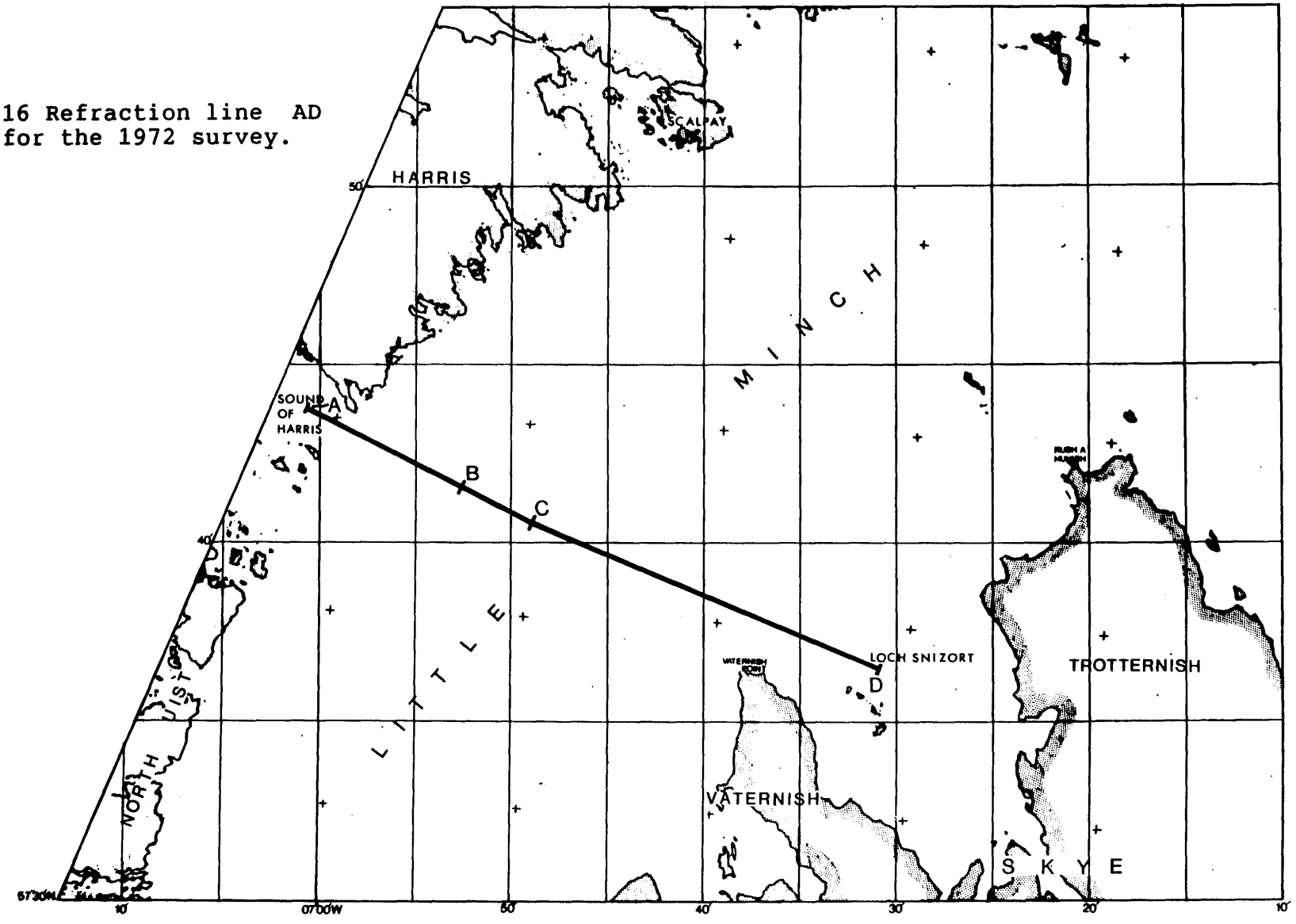

Fig. 2.16 Refraction line AD planned for the 1972 survey.

with buoys anchored at A, B, and C (Fig. 2.16). The AGC - mode channels (see Section 2.3.4 above) were found to give best results with a moderate expansion speed of 50 dB/s and a compression/expansion ratio of 3:1, i.e. a rather fast compression speed of 150 dB/s. The loss of the extended low frequency response of the amplifier (10 Hz instead of 7 Hz) using these settings did not appear to have an adverse effect on signal character.

2.4 MARINE SPARKER AND MAGNETIC SURVEY

2.4.1 PREVIOUS WORK AND AIMS OF THE SURVEY

In 1968 the Little Minch was surveyed from the RRS John Murray during the IGS reconnaissance of the continental shelf. 300 km of profile were observed with shallow seismic reflection (sparker), magnetometer, and gravity meter. In August 1970 an additional 284 km of sparker profiles were obtained during night-time operation of MV Vickers Venturer, which was carrying out geological sampling by day. Details of equipment used and operational notes for all the Little Minch profiling surveys to date are given in Table 2.4. The IGS survey tracks are shown in Fig. 2.17.

The IGS data described above were inspected in early 1971, and an independent preliminary interpretation of these was made by the author. The purpose of the Glasgow 1971 profiling survey was primarily to complement the marine refraction survey in the following ways:

(1) To define the limits of the sedimentary basin extending north and west from below northern Skye,

(2) To provide control on the shallow structure to aid interpretation of the refraction lines,

(3) To determine the influence of NE-SW and NW-SE trending faults and folds on the near-surface infill of the basin, and

DATE	OPERATOR	CONTRACTOR & VESSEL	LINE KM (N of 57 37')	METHOD	SOURCE	RECORDER	SETTINGS	NAVIGATION	COMMENTS
Sep-Oct 1968	IGS	NERC John Murray	303	Sparker	1 kJ EG&G	EG&G 254	1s firing 0.5s sweep 80-800 Hz pass	Decca Main Chain 6C	Routine reconnaissance survey of the continental shelf
				Magnetic	-	Varian	1000 nT scale		
				Gravity	-	Lacoste-Romberg	-		
				PDR	Ultrasonic				
August 1969	IGS	SSL	18	Deep seismic reflection	4-gun 'Seisprobe'	Leach 48-channel	-	Decca Hifix	Sections poor - not used in interpretation
August 1970	IGS	Wimpey Vickers Venturer	284	Sparker Pinger				Decca Main Chain 6C	Night profiling only. Geological sampling by day
Jun-Jul 1971	Glasgow Univ	NERC John Murray	957	Sparker	1 kJ EG&G	EG&G 254	1s firing 0.5s sweep 80-800 Hz pass	Decca Main Chain 6C +	Data obtained specifically
				Magnetic PDR	- Ultrasonic	Varian Muirhead	1000 nT scale 200 fathom scale	Decca Hifix	for this thesis
April 1972	Univ Coll London	NERC John Murray	120	Airgun				Decca Main Chain 6C	Results not used -sparker coverage in area adequate
1972-1973	Commercial companies		66	Deep seismic reflection					Results unavailable
1985	"		c.50	"					"
1985	BGS		c.30	Gravity		Lacoste-Romberg			Replaces the 1968 data
				Airgun					Not used here

Table 2.4. Equipment and operational notes of all geophysical profiling surveys in the Little Minch, 1968-85 inclusive. Glasgow University plus IGS total sparker coverage (used in this study) = 1544 km.

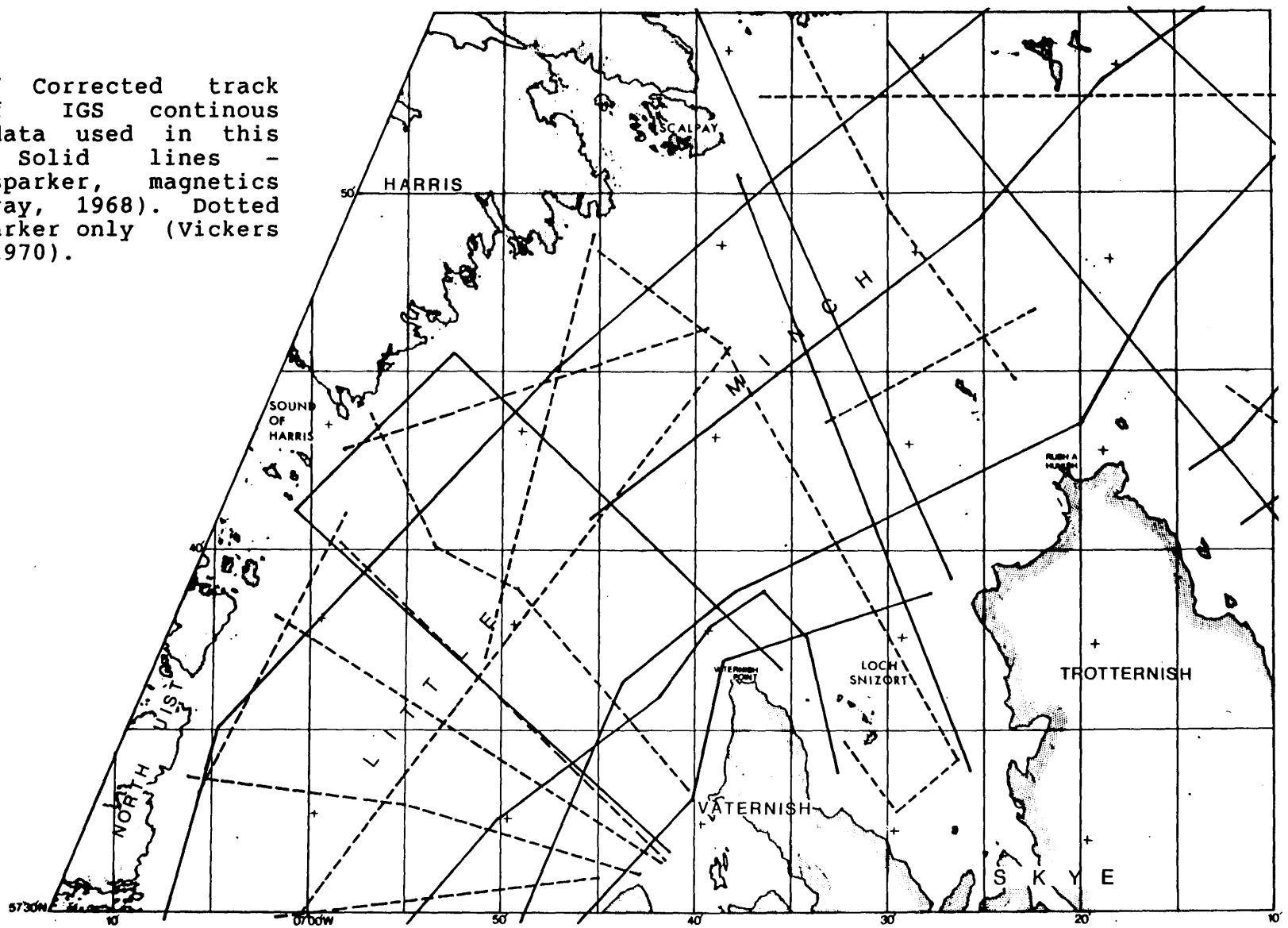

Fig. 2.17 Corrected track chart of IGS continous profiling data used in this thesis. Solid lines - gravity, sparker, magnetics (John Murray, 1968). Dotted lines - sparker only (Vickers Venturer, 1970).

(4) To estimate the extent and thickness of the offshore Jurassic, by extrapolation from northern Skye.

To achieve these aims in the time available it was decided to use a relatively close grid of lines within the immediate area of interest, rather than to extend the survey to the north or south. An ENE-trending set of profiles was chosen, for the following reasons:

(1) To intersect both the expected NE-SW and NW-SE structural trends,

(2) To complement rather than duplicate the existing IGS surveys, and

(3) Because this direction is parallel to the purple lanes of the best Decca Main Chain in the area (North Scottish, 6C). By running profiles along Decca Lanes, subsequent re-positioning of the observed fixes (discussed in Chapter 3) would be more reliable.

Some NW-SE lines were also planned, to tie between the ENE lines and to survey the proposed refraction lines.

2.4.2 INSTRUMENTATION AND SHIPBOARD OPERATION

The equipment and techniques employed during the profiling are standard aboard NERC research vessels, such as the John Murray, and need only be summarised here (see also Table 2.4):

(1) EG and G sparker. The 1 kJ sparker discharged once per second through a 9-candle array. The output from a multi-element hydrophone was fed to a Model 254 recorder operated with a sweep time of 0.5 s and a filter bandpass of 80-800 Hz. About 50 hours of potential profiling time were lost due to failure of the recorder and power supply generator, but otherwise the equipment functioned well.

(2) Varian magnetometer. This functioned satisfactorily, except for a 2 hour break, supplying paper records of 1000 gamma scale width.

(3) Muirhead precision depth recorder. This supplied, throughout the profiling, wet paper vertical depth profiles of 200 fathom scale width.

(4) Navigation. Two Decca Main Chain receivers (one each in the laboratory and the bridge) and a Decca Hifix receiver were used.

Shipboard operation comprised the usual rota of watchkeepers who marked up the records and logged data readings at every 10-minute fix. The uncorrected Main Chain fixes were plotted immediately on IGS 1:100,000 scale UTM Decca lattice charts as a guide to their reliability. The watchkeeper consulted the bridge when lane-jumps appeared to occur, whereupon the ship's officers supplied an independent check from the other Decca receiver or, if necessary, a radar position. Hifix readings were logged, but since this system is unreliable at night, when almost all the profiling was done, these results are only useful for cross-checking against Main Chain fixes when lane-jumps in the latter are suspected.

Fixes are numbered consecutively from 1-557, and not subdivided into separate lines. During the survey the refraction lines and the northern part of the area were profiled first, in case it would not be possible to complete the planned grid.

Distance made good and ship's heading were also logged at every fix. Average survey speed through the water was 5-6 knots, which is the best compromise between speed and relatively noise-free sparker records. As the John Murray can make 9-10 knots at full ahead, profiling was not necessarily begun at the point of breaking off from refraction work, but a little time was spent sailing to the most convenient point on the planned grid, which was more or less completely surveyed (Fig. 2.18) in the time available. Only a couple of NW-SE tie lines in the SW of the area were not profiled.

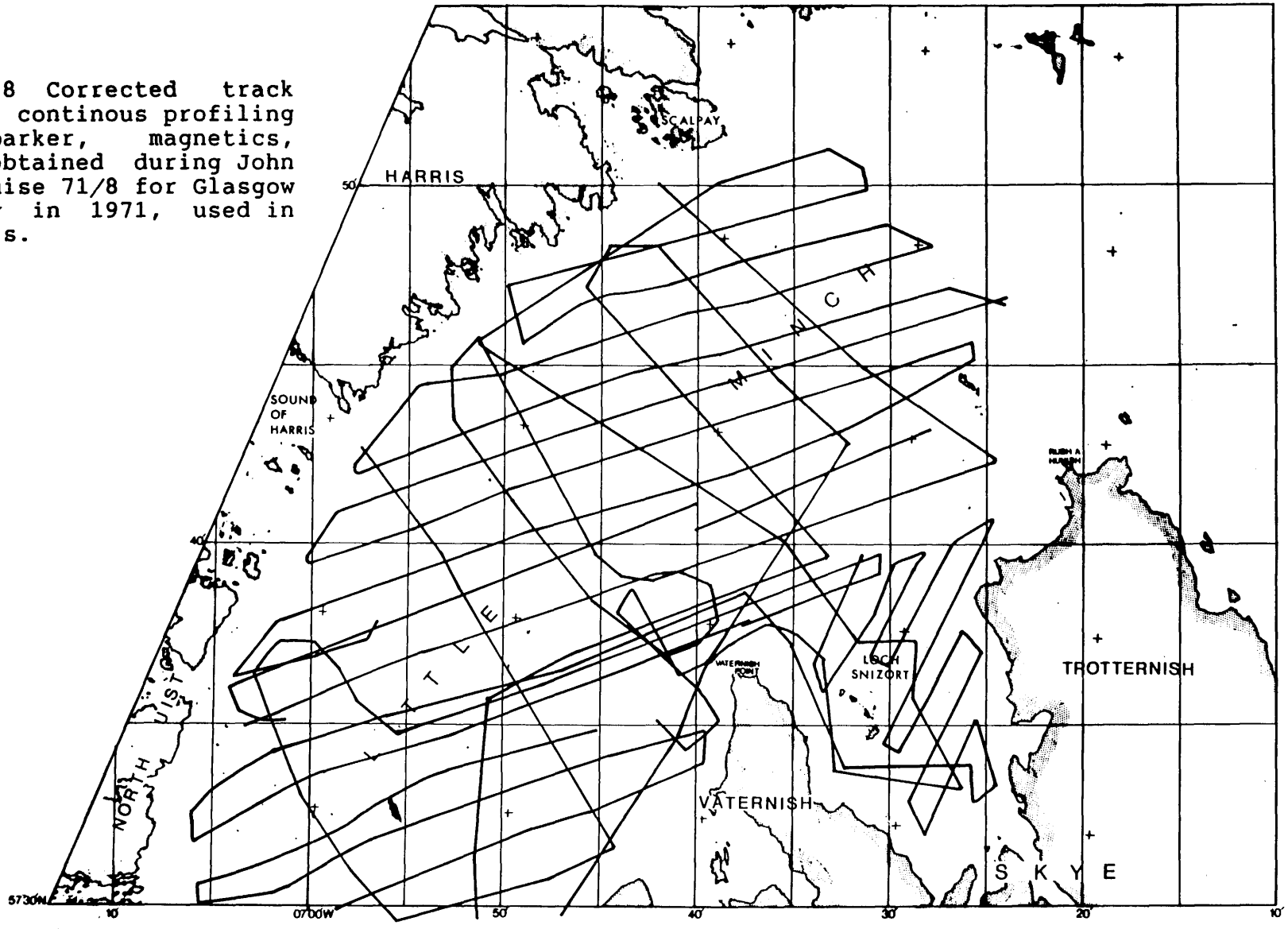

Fig. 2.18 Corrected track chart of continous profiling data (sparker, magnetics, P.D.R.) obtained during John Murray cruise 71/8 for Glasgow University in 1971, used in this thesis.

Weather during the profiling varied from wind Force 3 (with calm seas), to wind Force 5-6 (with high seas). The latter extreme just permitted profiling, within the constraints of operational safety and record quality, when refraction was not possible, for the same reasons.

No sparker or magnetic surveys were carried out during the 1972 RV Calanus cruise.

2.5 DETERMINATION OF PHYSICAL PROPERTIES

2.5.1 PURPOSE

The seismic investigations are used to obtain velocity-depth data, plus, if possible, a limited amount of structural information. At a more advanced stage of exploration the velocities and layer depths would be calibrated by the results of a deep borehole or well, of which there are none as yet in the Hebrides region. So for the present the velocities must be compared with those measured for known formations at or near the surface. Measurements of surface and near-surface (refraction or shallow interval) velocities are obtained as a by-product of the seismic reflection and refraction methods, e.g. from the first breaks on reflection records; but these results have to be supplemented by velocity measurements on formations of various ages and lithologies.

Rock densities are required for Bouguer corrections to gravity observations, and for subsequent interpretation of Bouguer anomaly maps and profiles. Density determinations can be made in the field by measuring gravity over a topographic feature (Nettleton 1939), but no sites suitable are present in northern Skye because of the relatively complex near-surface solid and drift geology; as a result the Bouguer anomaly field is spatially too variable.

Velocities were determined from field measurements on known formations at outcrop, especially of Mesozoic rocks, at various localities throughout the Hebrides during 1972 and 1973. Laboratory determinations of velocity and density

were also made on specimens collected at these and other localities. The results are presented in Section 3.2.

2.5.2 HAMMER SEISMIC VELOCITY

A Geophysical Specialties MD-1 single channel hammer seismograph (Mooney and Kaasa 1958) was used in Skye during the 1972 field season. It measures the elapsed time between a hammer blow and the arrival of a pulse at a nearby geophone, to a precision of 0.25 ms. A field trial in Skye suggested that the instrument was not functioning properly. One problem is that unless the threshold trigger amplitude is carefully adjusted at each hammer shot, the S-wave travel time may be measured, rather than P-wave, since the former wave, although slower, is generally of larger amplitude. Hall (1970b) has discussed the limitations of the instrument, the further use of which on Skye was abandoned in favour of measurements with hammer and TI 8000B recorder.

An apparent major drawback of using the multichannel recorder for small scale hammer-refraction work is that the times of events, displayed full-wave on paper, can normally only be read to an accuracy of about 1 ms. The technique described below has been found to compensate for this deficiency, which would otherwise lead to uncertainties in velocities of the order of 10%.

12 geophones are planted in line over bedrock at an interval of 2.5 m, parallel to the strike or to the true dip direction. Both should be measured if possible to estimate the anisotropy, if any, of the lithology. A 5 m interval was tried initially, but the effective range of sledgehammer blow giving a signal-to-noise ratio of at least 4 or 5, which is essential for accurate timing of the first breaks on the record, was found to be about 30 m. The bedrock to be measured should be as fresh (unweathered) as possible, and if the rock is porous it should be water-saturated, for realistic correlation with sub-surface velocities. A wave-cut platform at low tide or a wet quarry floor are suitable sites.

Paper monitor wiggle-trace records are made of hammer blows struck 1 m or so off the end of the spread. Three good records are obtained for three shots at either end of the spread. Oscillograph paper speed is the fastest possible - a nominal 30 cm/s - and wide-bandpass fixed-gain amplification is used. The position of the hammer blow need not be known accurately; it merely has to be in line with the geophones. Back in the laboratory the first breaks are examined under a low magnification (x ~10) binocular microscope with cross-wires and a stage adjustable in its own plane by a calibrated screw. Using this, the differences in time between the first break on the nearest trace to the shot and the other 11 traces can be found to an accuracy of about 0.3 ms, from a distance measurement (moving the stage with the record fixed to it) made to a precision of 0.1 mm. Averages of corresponding times on the three records are taken, and subsequent velocity computation is by least squares fitting to time-distance graphs using the 'minus' method (Hagedoorn 1959) for spreads shot from both ends. These computations, and the advantages of full-wave recording as opposed to simple transit-time measurement, are discussed in Section 3.2.

2.5.3 ULTRASONIC VELOCITY

Fresh rock specimens weighing 1-2 kg are cut into blocks having one, two, or three pairs of parallel faces, the three normals to the planes being roughly orthogonal. The PUNDIT (Portable Ultrasonic Non-destructive Indicating Tester) made by CNS Instruments Ltd, is a device which displays numerically, to a precision of 0.1 μs, the transit time of an ultrasonic pulse transmitted between two probes which are pressed onto opposite faces of the specimen. If porous, the rock is water-saturated by several days' immersion in an evacuated water-filled bell-jar, and if necessary a little grease is applied to the faces to improve the transducer contact. Minimum transit time observed under hand pressure is recorded, and the distance between the marked centres of the probes' disc shaped contact areas is measured to a precision of 0.01 mm using one of a set of large micrometer screw gauges. Several measurements can be made in different

positions on each block. The inaccuracy of the individual velocity (distance/time) determinations by the above procedure - of the order of 1% - is found to be much less than velocity variations between the different measurements on a single specimen, due to its anisotropy, which are frequently of the order of 10%.

2.5.4 DENSITY

The density of the same specimens used for ultrasonic velocity, plus some others, is determined by the usual method of weighing in air and weighing suspended in water. Porous specimens are fully water saturated. Several specimens from each locality are measured; like the ultrasonic method, the inaccuracy in density determination of individual samples, less than 0.01 g/cm^3, is much smaller than the variations of density due to compositional differences, which can easily be seen in the cut faces. In an extreme example, specimens of a dolerite sill vary from greyish, feldspar-rich, density ~2.8 g/cm^3, to a more greenish olivine-rich sample with a density ~3.1 g/cm^3.

Results are tabulated in Appendix 2.

CHAPTER 3
GEOPHYSICAL INTERPRETATION

3.1 SEISMIC REFLECTION

3.1.1 ANALOGUE SHOT RECORDS

As described in Chapter 2, the seismic reflection data were recorded on analogue Techno tapes, on which the traces had been filtered and gained in real time. The field survey layouts and tape recording parameters were not chosen with anything other than the existing analogue recording and playback system in mind. Had it been envisaged that digital processing might subsequently prove possible, some details of the surveys would have been designed differently.

During the period 1971-73, processing of the reflection records was limited to making further playback paper records with the following variables:

(1) Further application of bandpass filters and gain.

(2) Compositing (mixing) of adjacent traces, weighted 1:1 or 1:2:1 (see Appendix 1, Figure A3).

(3) Wiggle trace or VAR display.

(4) Vertical display scales of 13, 25 or 30 cm/s (wiggle) or 15 cm/s (VAR).

A number of permanent sets (i.e. photographically developed and fixed prints) of all the taped shot records were made, each with a variety of the choices and settings above. Geophysical interpretation was limited to correlating events from shot record to shot record, to identify reflections.

Static corrections for each trace of each shot are calculated from the field survey data, combined with first break times read from the monitor paper records. Figure 3.1 shows a typical form, partially filled in during the field surveys, used to calculate the trace statics. The

RECORD CORRECTIONS 104

STAFFIN (SK-3)

71/9/10/1140 ST 4/4-6

SEIS STN	X^2	X	XT	T	$\frac{X}{Vc}$	$t = T - \frac{X}{Vc}$	E	D-E	$Te = \frac{D-E}{Vc}$	Tw = Kt	Ts	CORRN. = Te+Tw+Ts	CHANN.
1		5		0	2	-						8	41
2		35		22	16	6	41.7	8.3	3.9	-1.2		8	43
3		65		38	30	8	41.9	8.1	3.8	-1.6		8	45
4		95		-		-						8	47
5		125		66	58	8	42.3	7.7	3.6	-1.6		7	49
6		155		80	72	8	42.5	7.5	3.5	-1.6		7	411
7		185		96	86	10	42.9	7.1	3.3	-2.0		7	52
8		215		108	100	8	43.7	6.3	2.9	-1.6		7	54
9		245		123	114	9	44.7	5.3	2.5	-1.8		6	56
10		275		137	128	9	45.7	4.3	2.0	-1.8		5	58
11		305		148	-	-						5	510
2		335		156	-	-						5	61
N	( )	( )	( )	( )									

$Vc = \frac{N(X^2) - (X)^2}{N(XT) - (T)(X)}$ = _____ = 2.15 m/msec

Vw = 1.5

$K = -\frac{(Vc-Vw)^{\frac{1}{2}}}{(Vc+Vw)}$ = -0.2

$Ts = \frac{D-Es+ds}{Vc}$ = 4.8

Es = 41.5

ds = 1.5

D = DATUM = 50m

All distances in meters, times in milliseconds.
Te = elevation correction
Tw = weathering correction
Ts = shot correction
X = distance of nearest seis to nearest shot hole

E = elevation
ds = depth of shot
Es = elevation of shot hole
Vc = velocity of first consolidated layer
Vw = weathering velocity

Fig. 3.1 Typical form used to calculate field statics.

weathering and subweathering (consolidated) velocities are derived from interpretation of first break picks plotted on T-X graphs, which were constructed after the end of the field work. The T-X first break results for all six sites are presented with the X-coordinate being the survey station position along the line. A useful additional plot can be made with the X-coordinate defined as offset (i.e. the data referred to a common origin). The sites, figure numbers, and a summary of the velocities derived from these graphs are shown in Table 3.1:

TABLE 3.1
SURFACE AND NEAR-SURFACE VELOCITIES FROM FIRST BREAKS

Fig. no.	Site	Line no.	X-coord of graph	Velocities (km/s) Weathered	Consolidated
3.2 3.3	Sheader	SK-1	Station Offset	2.0	2.0
3.4. 3.5	Skudiburgh	SK-2	Station Offset	2.0	2.2
3.6 3.7	Staffin	SK-3	Station Offset	1.5	2.1
3.8 3.9	Quirang	SK-4	Station Offset	1.5	4.5
3.10 3.11	Waterstein	SK-5	Station Offset	2.3	5.5
3.12 3.13	Edinbane	SK-6	Station Offset	1.5/3.0	4.8

At Sheader and Skudiburgh the near-surface layers comprise boulder clay on Upper Jurassic clay, whereas at Staffin there is peat overlying the Upper Jurassic clay. At the Quirang and Edinbane sites peat sits on top of basalt, which at the latter site has a weathering velocity of ~3.0 km/s. At Waterstein, thin Upper Jurassic clay overlies the gabbro of a sill.

Fig. 3.2 SK-1 first breaks

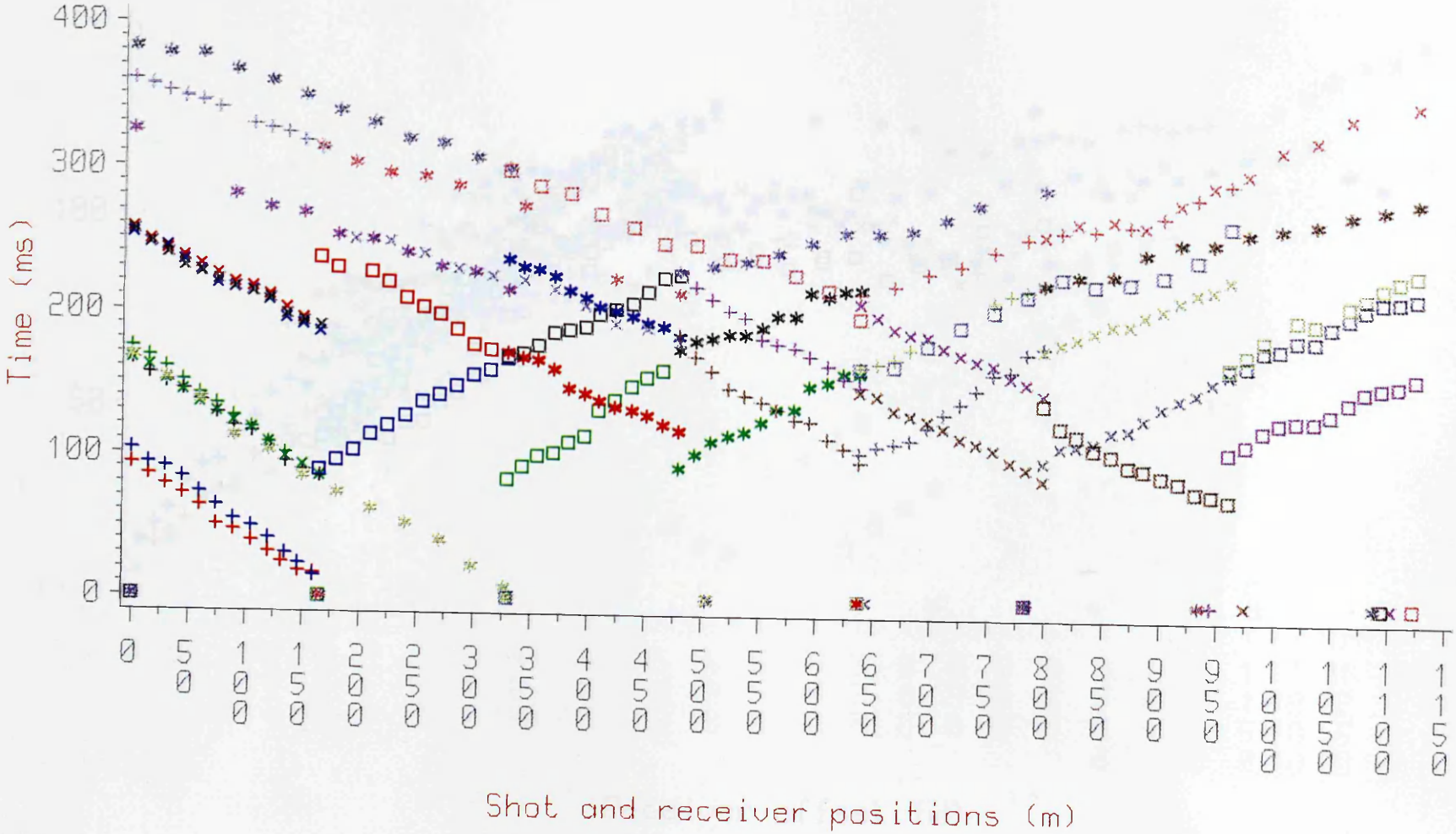

Fig. 3.3 SK-1 times reduced to 4.0 km/s vs.offset

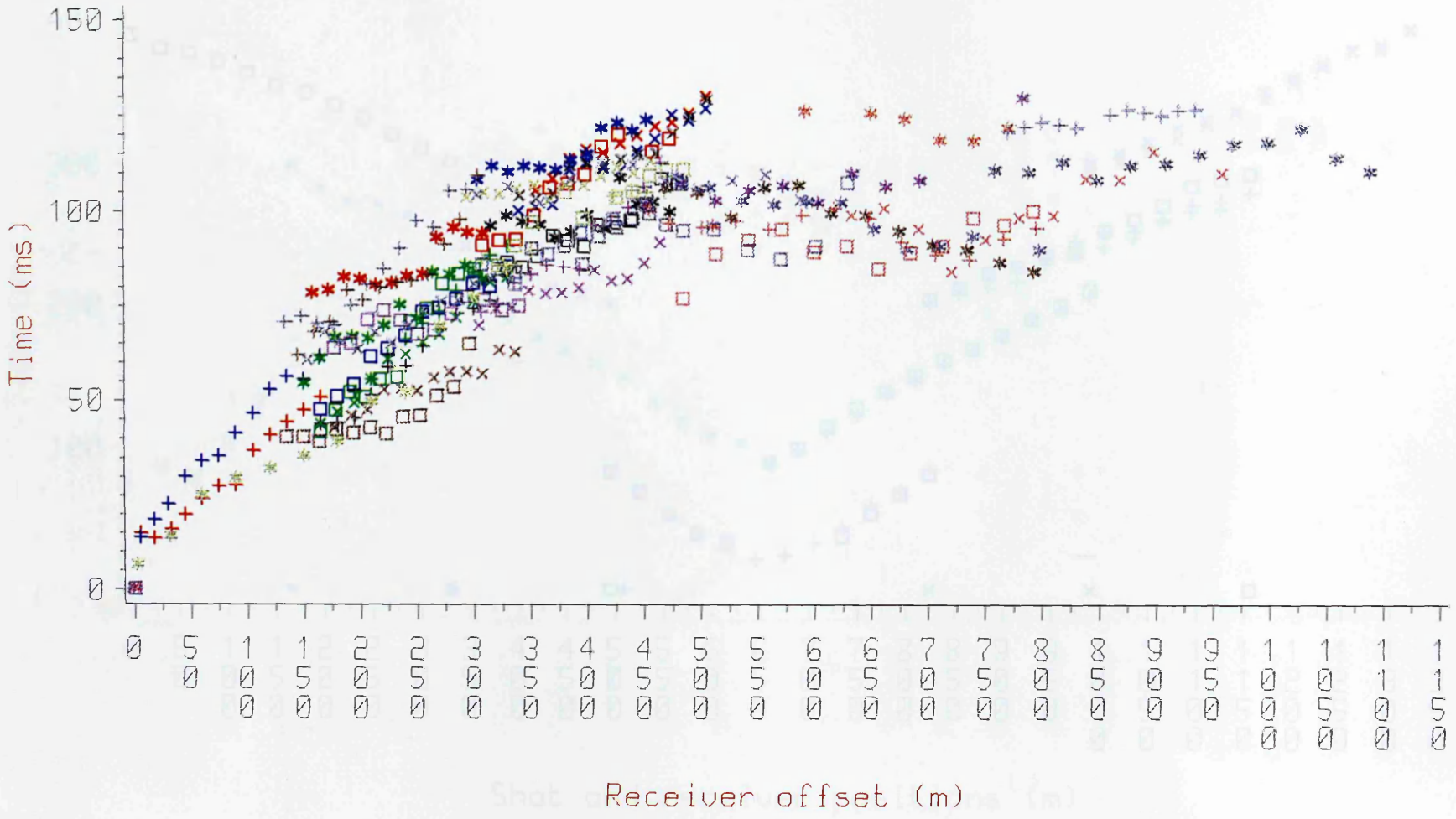

Fig. 3.4 SK-2 first breaks

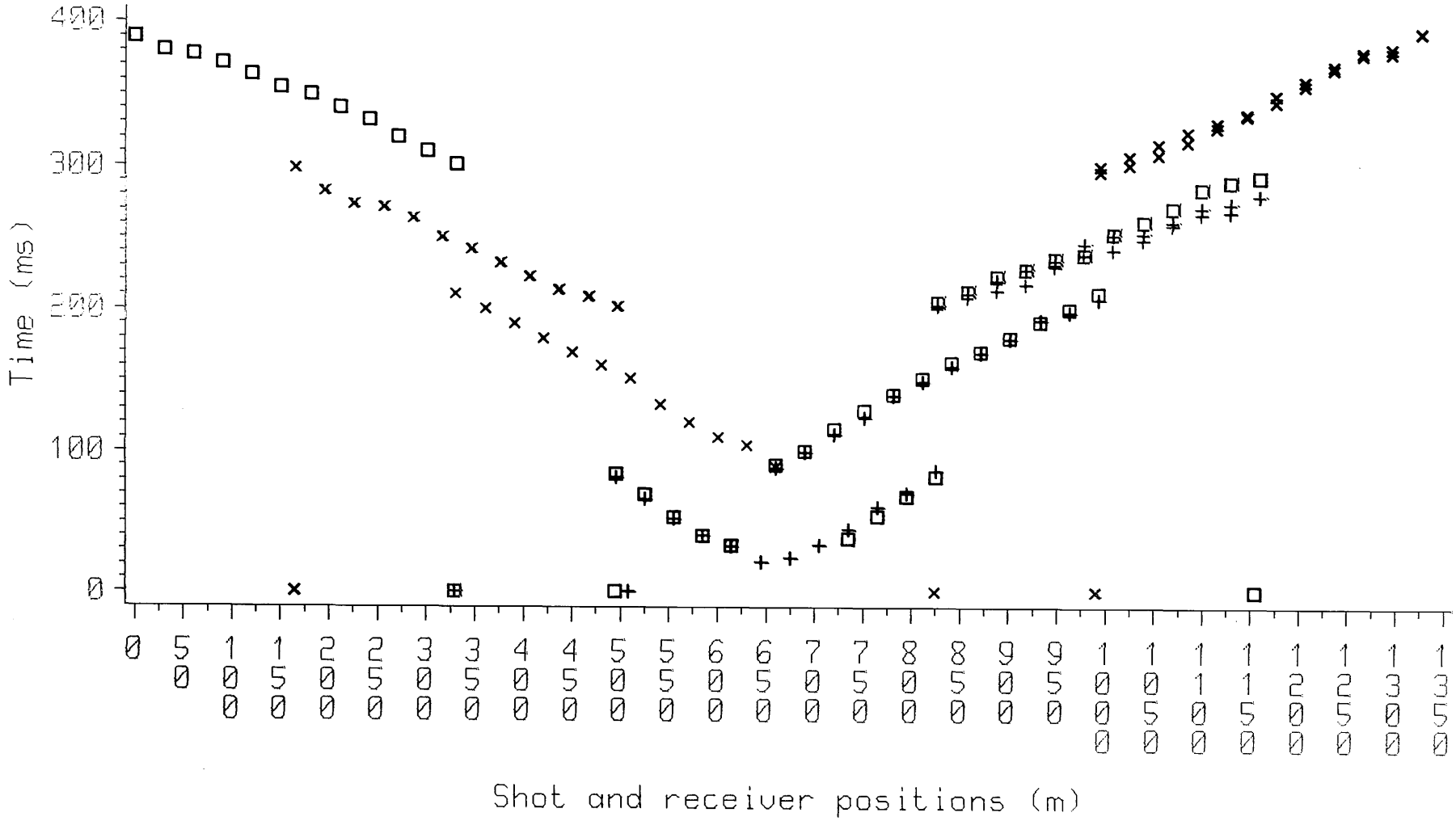

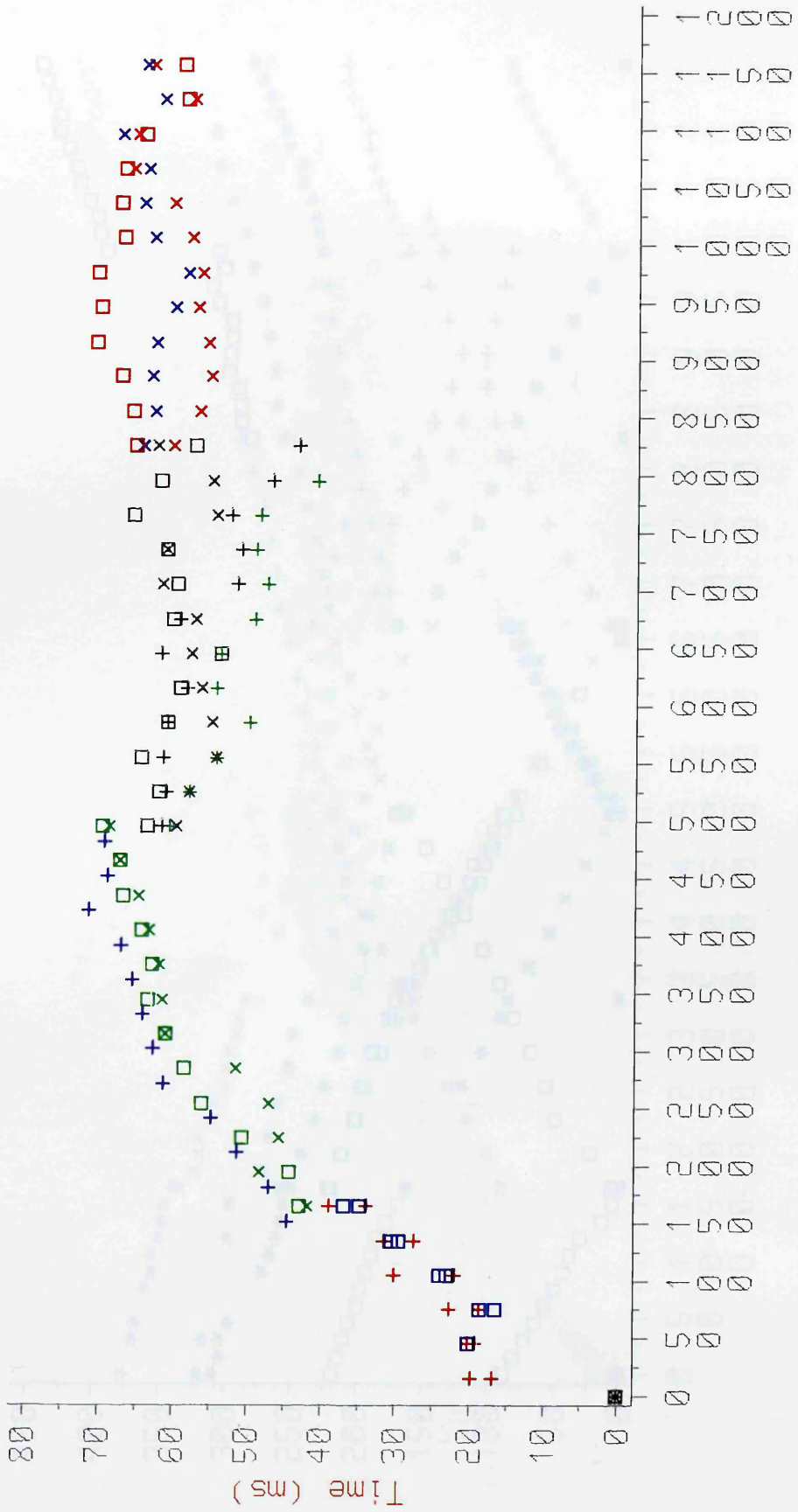

Fig. 3.5 SK−2 times reduced to 3.5 km/s vs. offset

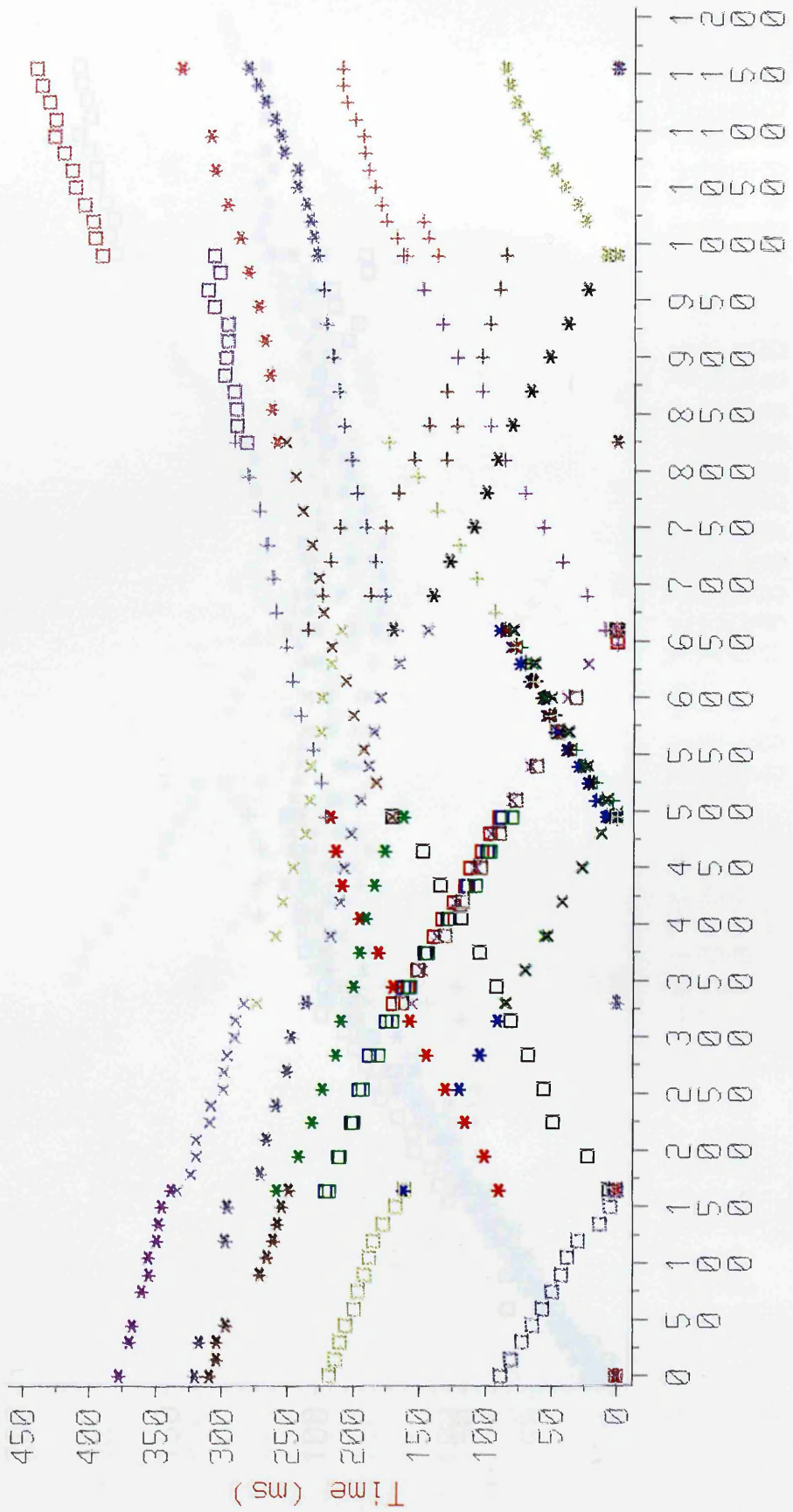

Fig. 3.6 SK-3 first breaks

Fig. 3.7 SK-3 times reduced to 4.5 km/s vs. offset

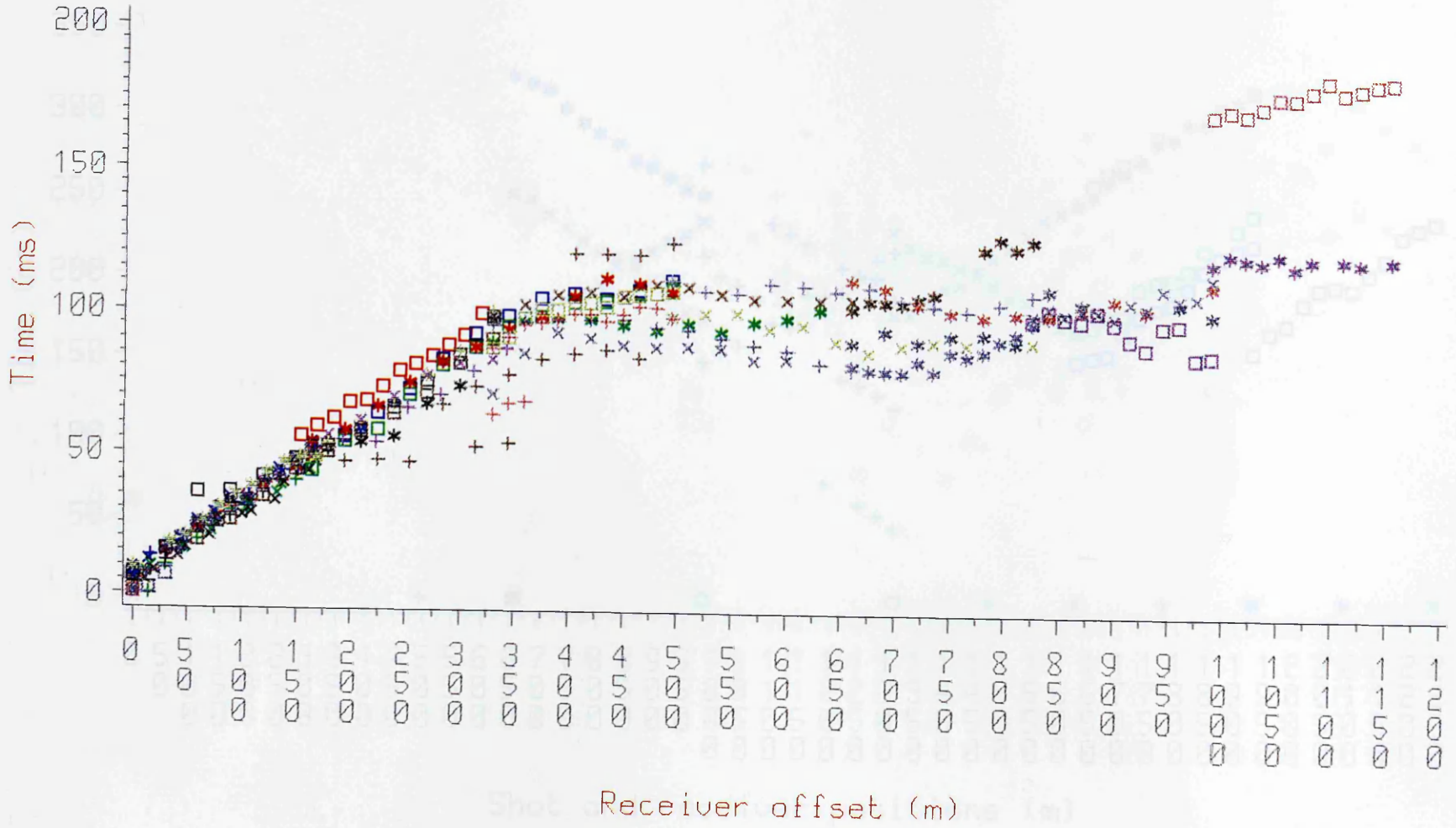

Fig. 3.8 SK-4 first breaks

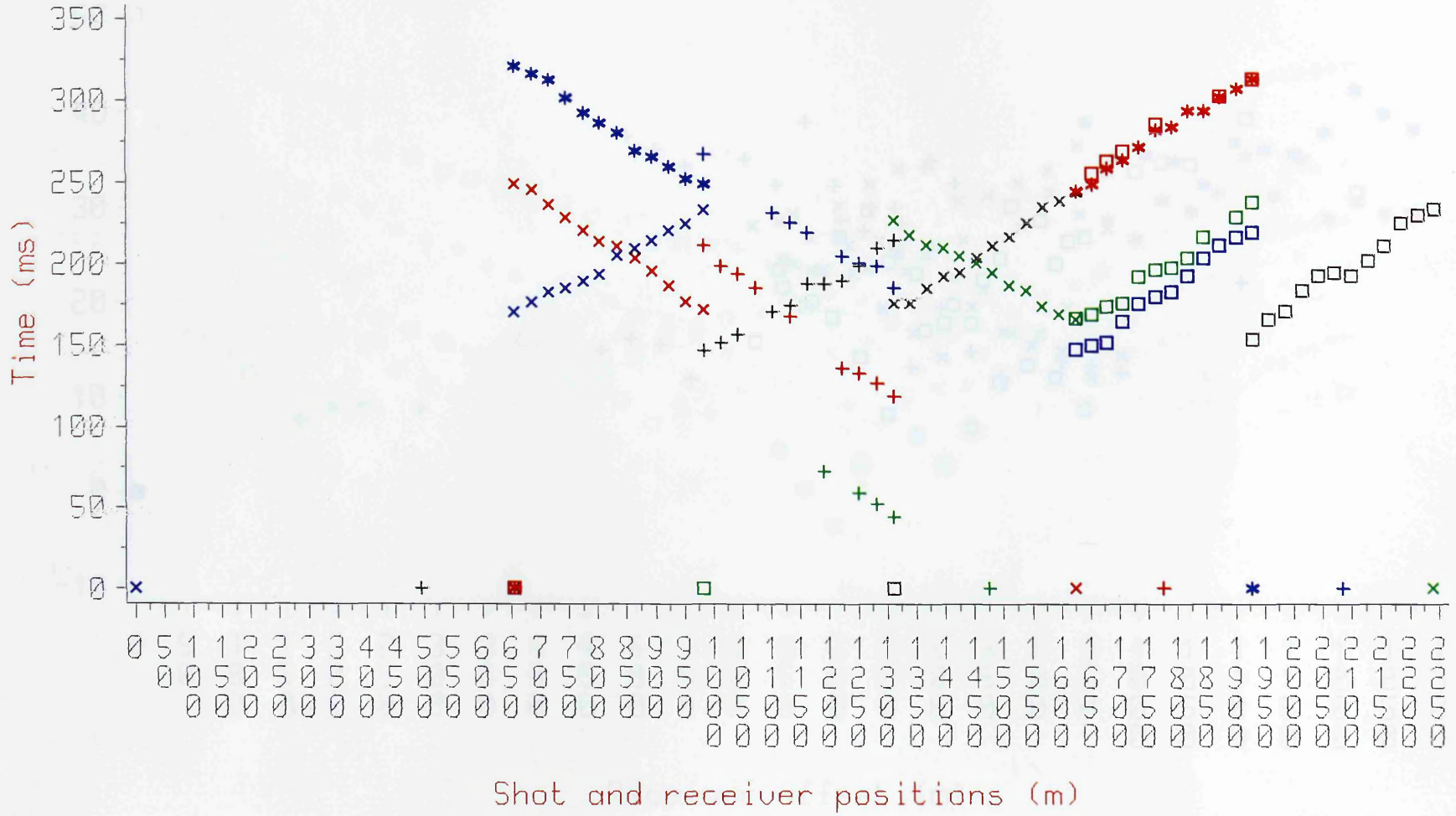

Fig. 3.9 SK–4 times reduced to 4.5 km/s vs. offset

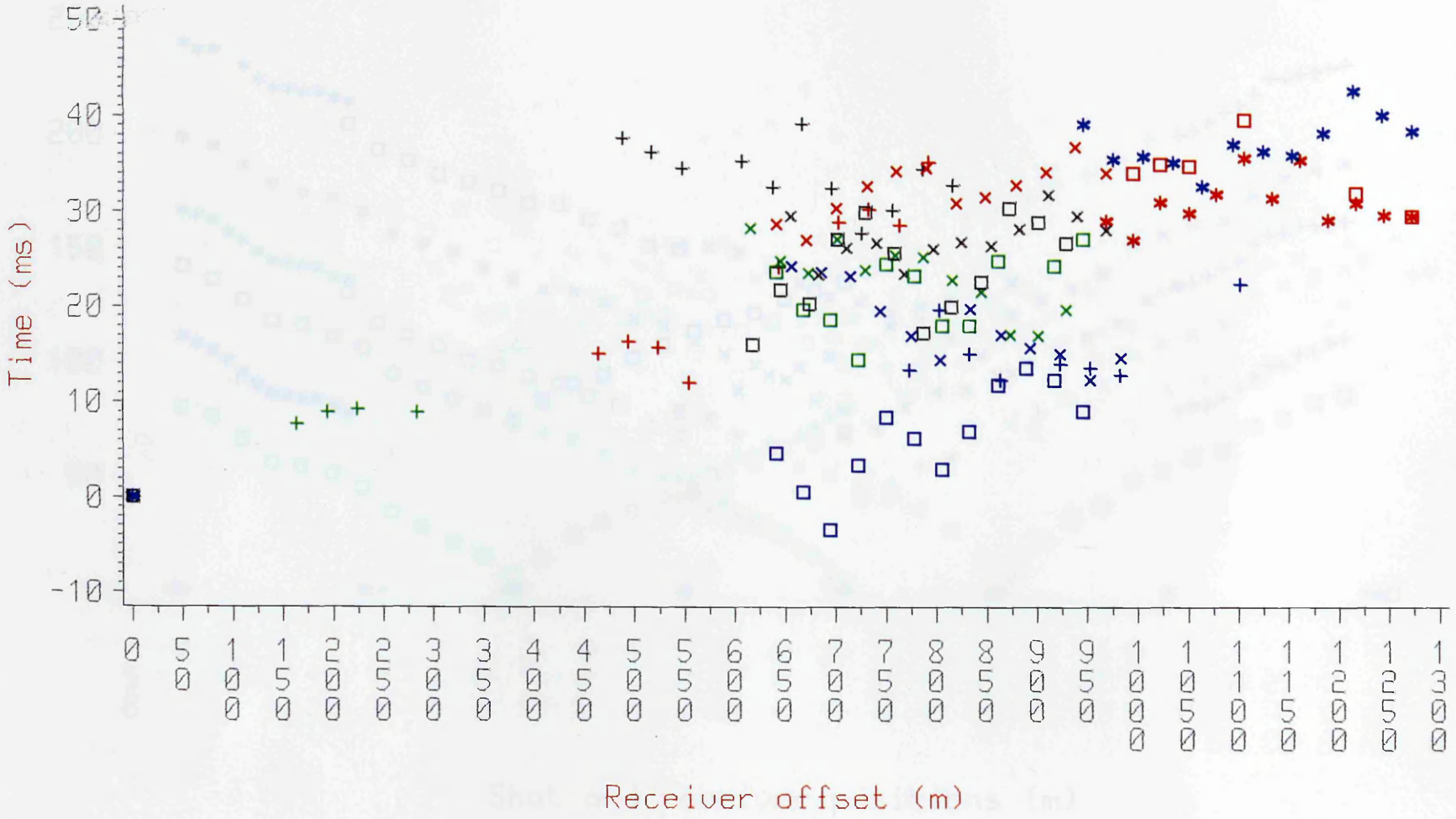

Fig. 3.10 SK–5 first breaks

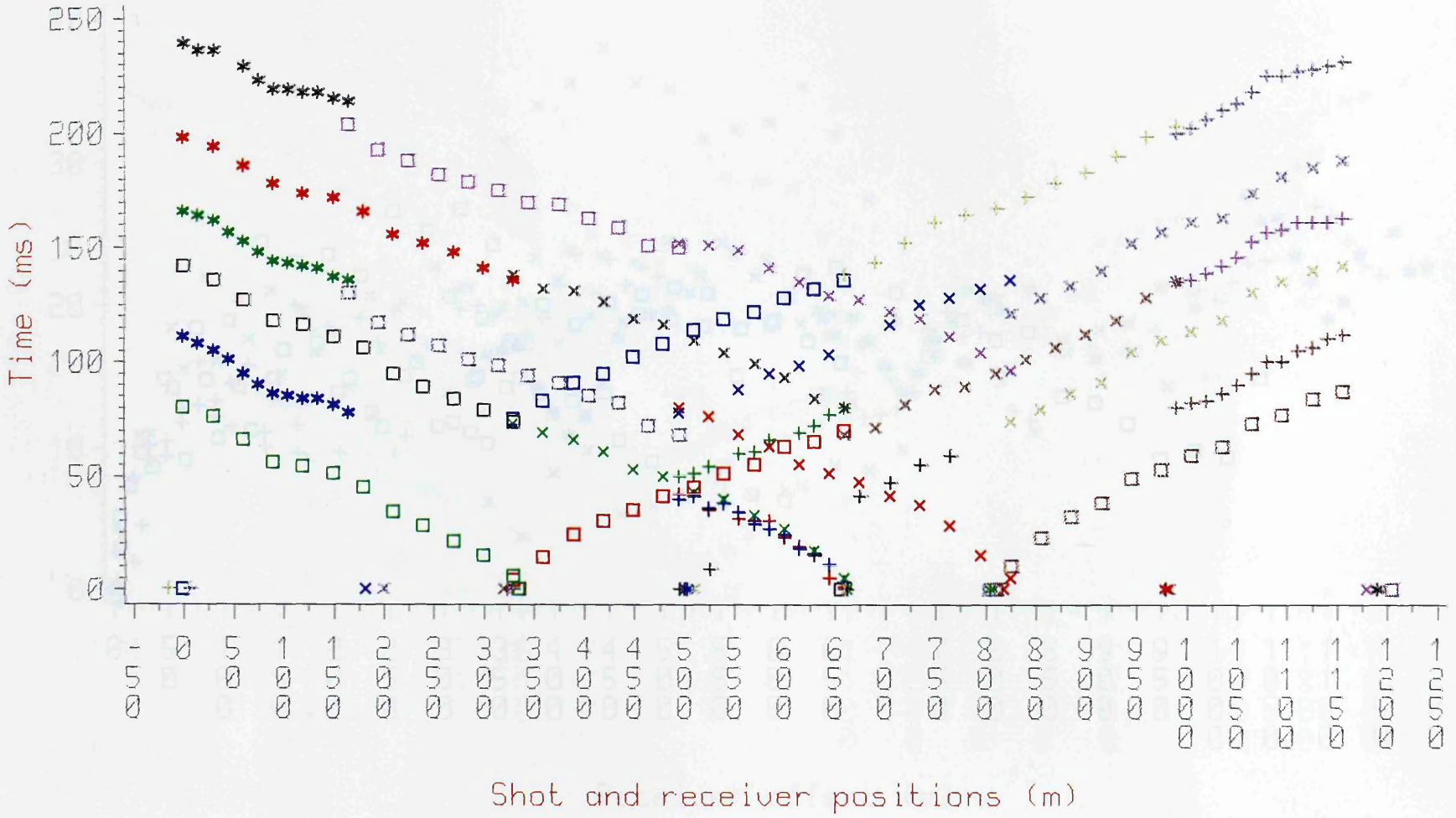

Fig. 3.11 SK-5 times reduced to 5.5 km/s vs. offset

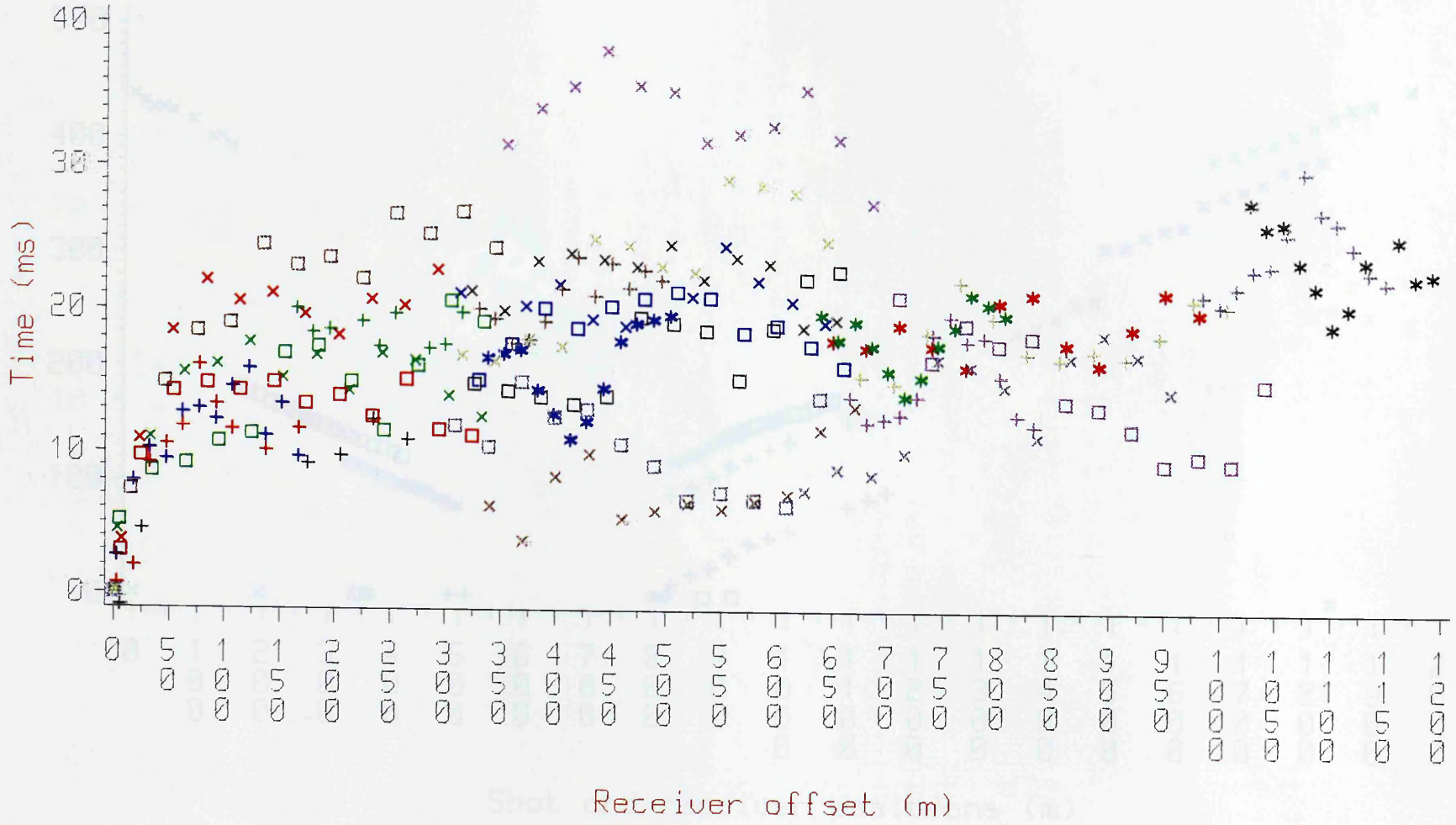

Fig. 3.12 SK–6 first breaks

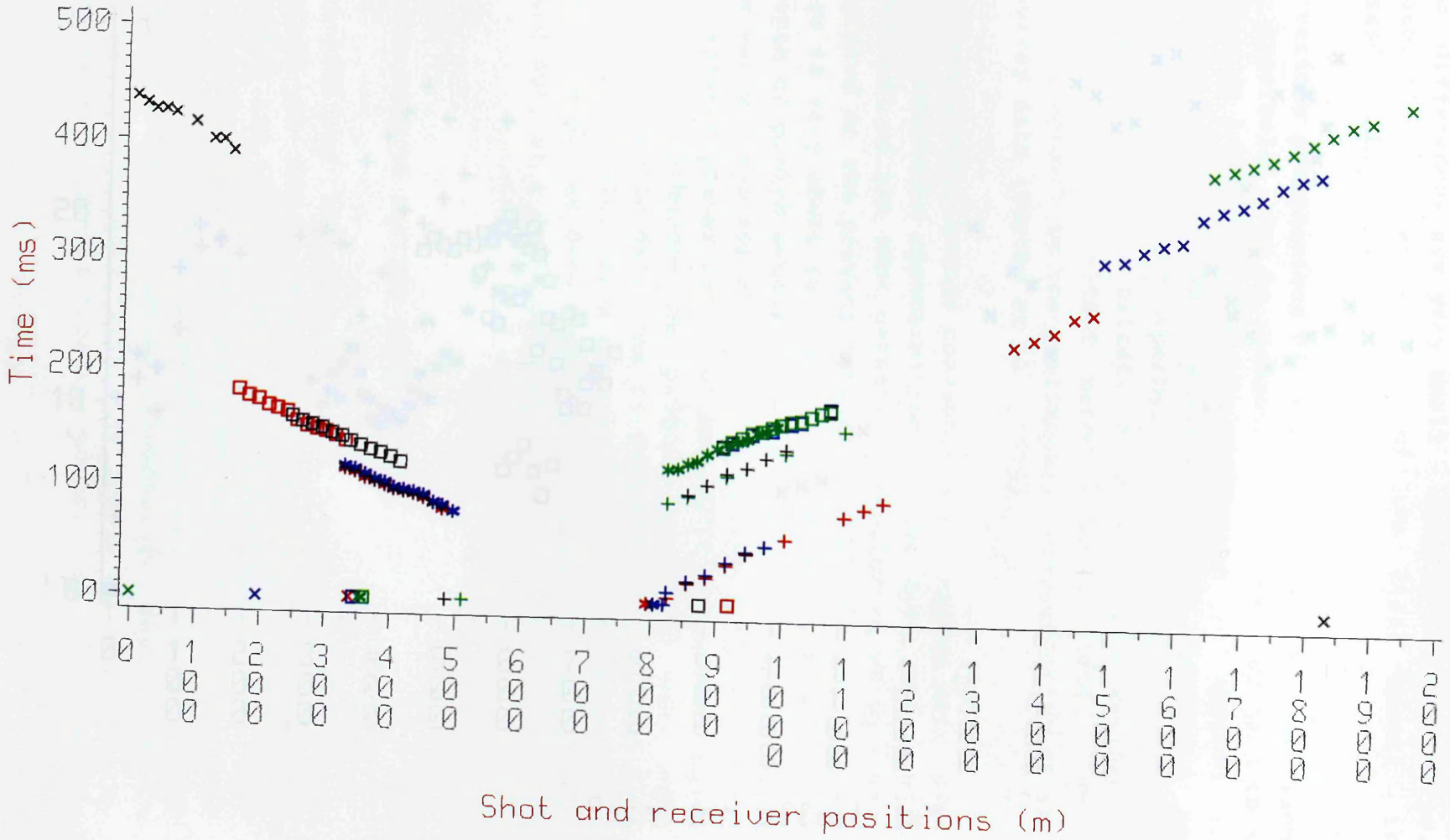

Fig. 3.13 SK-6 times reduced to 4.5 km/s vs. offset

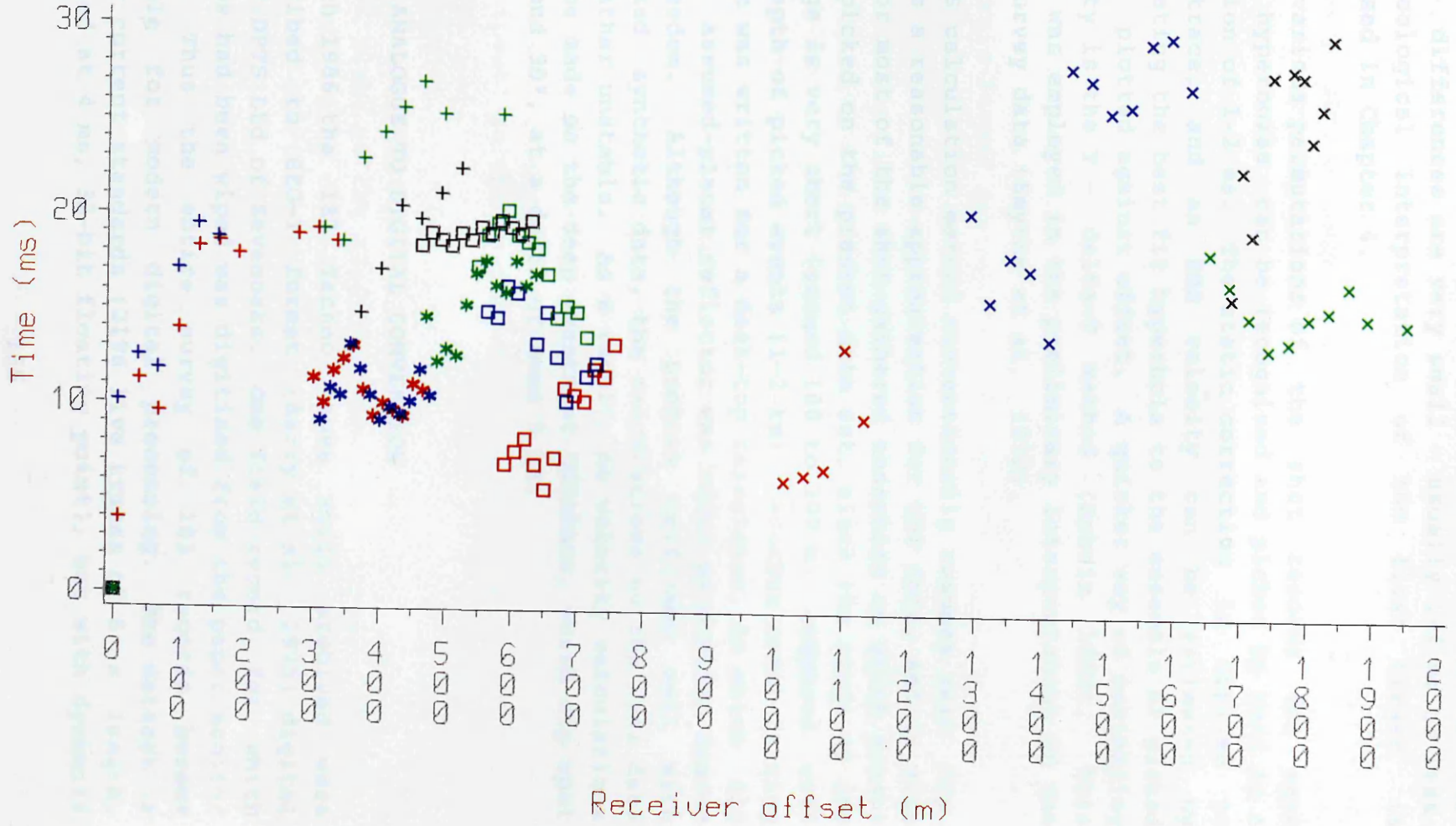

The static corrections computed by these methods are very small - typically 10-20 ms - and are made up mostly of the elevation correction to a local datum. Trace-to-trace static differences are very small - usually 1-2 ms or less. The geological interpretation of the first breaks is discussed in Chapter 4.

Using various permutations of the shot records for each site, hyperbolae can be recognised and picked by hand to a precision of 1-2 ms. The static correction is applied to each trace, and an RMS velocity can be estimated by calculating the best fit hyperbola to the ensemble of picked times, plotted against offset. A quicker way of estimating velocity is the T - delta-T method (Dobrin 1960). This method was employed in the preliminary interpretation of the 1971 survey data (Smythe et al. 1972).

The RMS calculation method conventionally assumes zero dip. This is a reasonable approximation for CDP data, and is also good for most of the shot-gathered ensembles on which events were picked on the present data set, since the range of CDP coverage is very short (around 100 to 200 m) compared with the depth of picked events (1-2 km). Another event-fitting program was written for a desk-top calculator, in which dip of an assumed-planar reflector was added as another degree of freedom. Although the program performed well with idealised synthetic data, the calculations on the real data were rather unstable. As a result, no velocity calculations could be made on the deep events at Edinbane, which dip west at around 30°, at a depth of some 5 km.

3.1.2 ANALOGUE TO DIGITAL CONVERSION

In March 1986 the 182 Techno tapes still archived were transcribed to SEG-Y format (Barry et al. 1975) digital tape by DPTS Ltd of Sevenoaks. One field record for which the tape had been wiped was digitised from the paper monitor record. Thus the entire survey of 183 records became available for modern digital processing. The dataset is tiny by current standards (2196 live traces of 6 s length, digitised at 4 ms, 32-bit floating point), but with dynamite

as its source, it is a useful addition to the commercial reflection data which has been recorded in recent years on north Skye under the exploration licence covering part of the present study area.

The SEG-Y tape was read onto disk on the Edinburgh University EMAS-A Amdahl machine, and Fortran routines written to sort and validate the data by display of the shot files on a Tektronix graphics terminal. A routine to edit the trace headers (most of which had been left blank at transcription stage) was also written.

3.1.3 PROCESSING UNDER MERLIN SKS

The Seismic Kernel System (SKS) of Merlin Geophysical Ltd was installed on the new VAX 8500 at BGS Edinburgh in February 1987. The Skye data provided a useful means of familiarisation with this extensive processing package, so processing of the data was started again from scratch - i.e. input from the SEG-Y tape. After sorting of the shot records into separate disk files, one for each line and cross-line, validation of every shot file was done by display of each, compared in turn with the original analogue monitors and playbacks, and with the analogue monitor made by DPTS during transcription.

Polarity is consistent throughout, but reversed - the upward kick on the geophones from the first breaks yields an upswing (peak) on the displayed trace. This has been left unchanged.

The shot break is picked from the DPTS analogue monitor, as it is not clear on the digitised auxiliary channel. Picking in this way can be done to $\pm$ 2 ms or so, and bypasses the problem of the delay introduced into the live traces by an anti-alias filter, but not into the two auxiliary traces, during transcription. Arrivals on the disk files are some 10 ms earlier than on analogue playbacks, but this mismatch is probably due to a delay introduced by the analogue filters, so has not been corrected for.

The timing channel, transcribed as the second auxiliary trace, showed excellent correlation with DPTS timing throughout every 6 s record.

3.1.4 PROCESSING STRATEGY

A substantial amount of information about the dataset is already available from the phase of analogue processing. As the subsurface coverage is of low fold, it is not expected that dramatically new reflection geometries will emerge from the digital processing. The main aims are simply:

(1) To display the data better than previously.

(2) To improve the 1-dimensional velocity-depth structure derived at each site.

On each shot record the residual ground roll and air blast not fully removed by the bandpass filter on recording can easily be recognised running diagonally across each file. Even though there are only 12 traces per shot gather, it is worth exploiting the apparent velocity of these unwanted effects by trying F-K domain filtering. However, there are problems in applying the process to CDP-binned land data. Further application of zero-phase bandpass filters, to remove everything outside the 15-60 Hz range, removes a lot of the coherent noise. The reflection energy peaks at around 30 Hz.

There is little merit in trying to preserve relative amplitudes, as the effect of the delay-tripped analogue AGC would be difficult to predict (retrospectively) and remove. Furthermore, the AM analogue recording obviously degraded the signal considerably, but in an unquantifiable way. A 'preprocessing' set of operations was therefore devised, to bring the data into a reasonably homogeneous and workable set of files (one for each line), on which the main processing would be carried out. Test shot records were also included in the dataset at this stage, even though they might be recognised subsequently to contain no useful data. This preliminary stage consists of:

(1) Reduction of shot record times to the shot break, read as described above.

(2) Removal of glitches and cross-channel interference, due to slight corruption of the analogue magnetic tapes, by 'surgical' muting.

(3) Discarding the auxiliary channels.

(4) Insertion of field geometry information into trace headers (this requires the building of a database for each line, which incorporates 'strategies' for binning into CDPs, etc).

(5) Muting of first breaks (mute windows designed by inspection of analogue data).

(6) Application of robust AGC to even out trace amplitudes.

(7) CDP gather.

(8) Bandpass filter (time-constant over the whole CDP gather).

Displays can be produced using:

(1) Hard copy screen dumps of ISAN (Interactive Seismic ANalysis) vector wiggle-trace displays on a Tektronix 4014 compatible terminal.

(2) Small bit-map (raster) plots on a DEC LN03 Plus laser-jet printer.

No large-scale raster display device was available during the period of data processing; however, to provide the small displays required, the laser-jet printer is adequate. Bit-map plots are displayed on it at its maximum resolution of 300 dots/inch, with one pixel (picture element) per dot. This gives very precise small-scale seismic plots, at the expense of having rather faint line and alphanumeric annotation. This causes the line-drawing plots (such as the semblance plots reproduced below) to be of patchy quality.

The solid fill of variable area plots is not reproduced very well at large scales (greater than 10 cm/s time scale) by this plotting device. Furthermore, the device driver has errors in it which lose continuity in the X direction (from one A4 sheet to the next in a plot file) and in the T direction (from one plot file to the next; multiple LN03 plot files are produced by the SKS job run from a single general plot file).

The screen-dump wiggle trace displays produced through ISAN are very useful for validating the correct order of shot files, etc., but of limited use in displaying test output panels from SKS, in which the variation from panel to panel is often very subtle.

During the period of use of SKS the following processing features were found to be unworkable on the system as installed at BGS (other bugs were cured as they were discovered):

(1) Land processing survey quality control maps.

(2) FK contour plots.

(3) Floating datum static correction.

(4) Time domain dip enhancement filter.

Apart from (1) above, these omissions are unimportant. A summary of the SKS processors used, together with a description of their function, and how to operate the package on the BGS machine, is given in a BGS internal report (Smythe 1987).

Processing of the lines is discussed in order of acquisition SK-1 to SK-6.

3.1.4.1 Line SK-1 (Sheader)

This site provides 41 useful shot records, after tests and faulty recordings are removed, of which 31 are single spread records (15 m receiver group interval) and 15 are double spreads (30 m receiver interval). The range of subsurface coverage and offsets is shown in an idealised way (i.e. assuming that the line is straight) in Figure 3.14. The line is rather bent, with some CDPs as much as 100 m south of the survey line. After 'crooked line' geometry processing, however, CDPs are ±70 m, at most, either side of the CDP bin line. Binning results in dropping of 5 traces out of 492, and double-binning of 5, to give 127 CDPs at a nominal 7.5 m CDP interval. Subsurface coverage is therefore about 940 m, with a fold of coverage of up to 11.

Figure 3.15 shows part of the CDP gather, produced as a check on static corrections, surgical muting, etc. The prominent bands running diagonally across the display, one of which is indicated by the pair of arrows, is the air blast. Its apparent velocity after CDP gather is half of the true velocity. Trace-to-trace correlation of potential reflections is good, indicating that there are no major problems with statics.

Fold of CDP coverage is too low for FK filtering methods to be attempted on CDP gathers. Due to the dropping and doubling of traces in the binning process, it is not possible to apply an FK dip filter to the shot gathers, as this processor requires complete shot gathers (i.e. traces 1-12 all present and in ascending order). It is not possible to apply the processor to the shot gathers and then subsequently apply the field geometry binning processes, as other processors then fail.

Figure 3.16A and B are 10 panels of constant velocity stacks, ranging from 2.0 to 4.0 km/s. Although signal-to-noise ratio is very low, a number of events can be seen (marked) between 0.4 and 2.1 s, stacking up in the range 2.2 - 3.2 km/s. The same range of constant velocity stack panels is shown in Figure 3.17, in a variable area mode of display. A 2-trace sum has been applied in an attempt to clean up the data.

Fig. 3.14

SK-1: Subsurface coverage and offset diagram

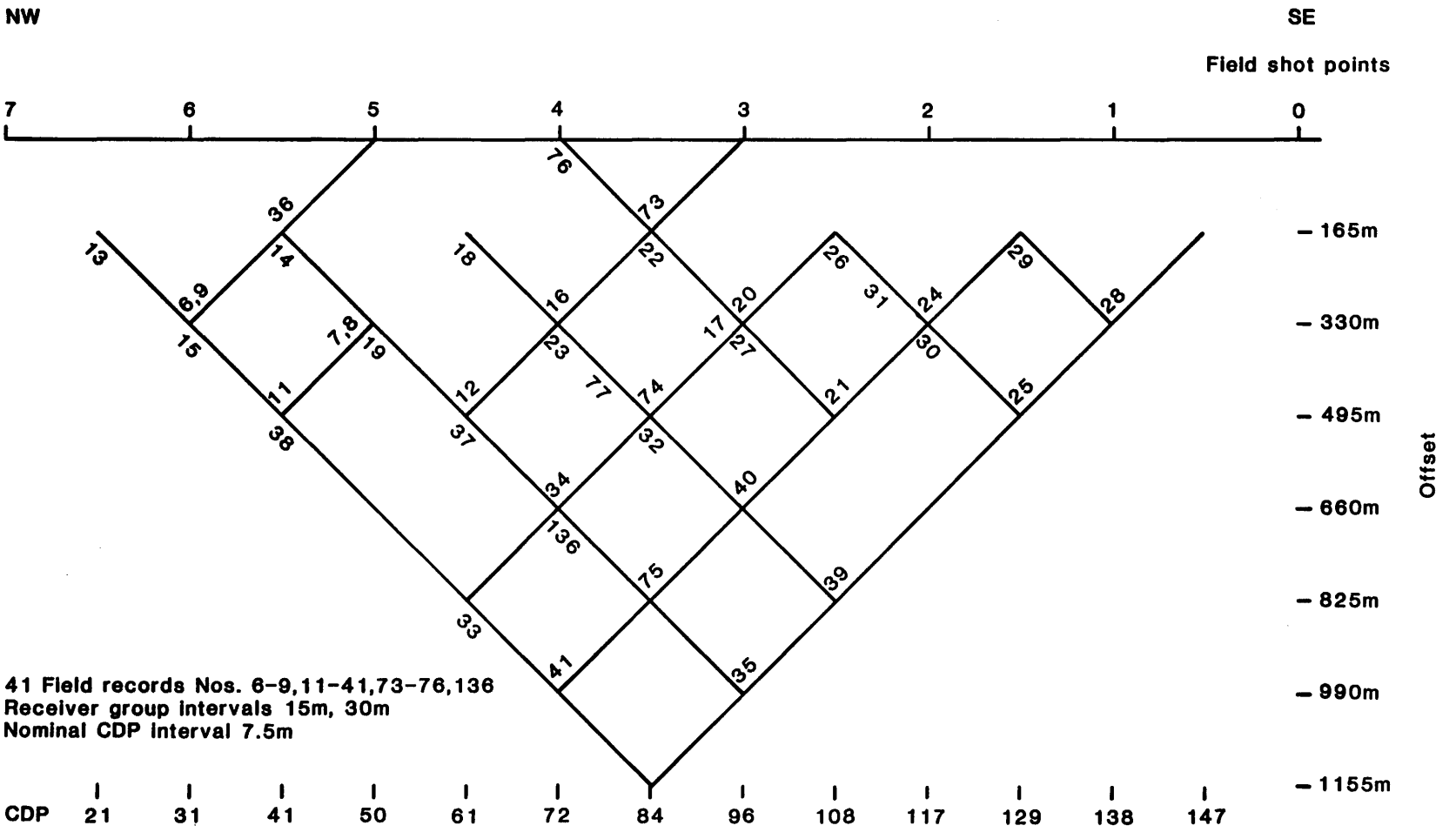

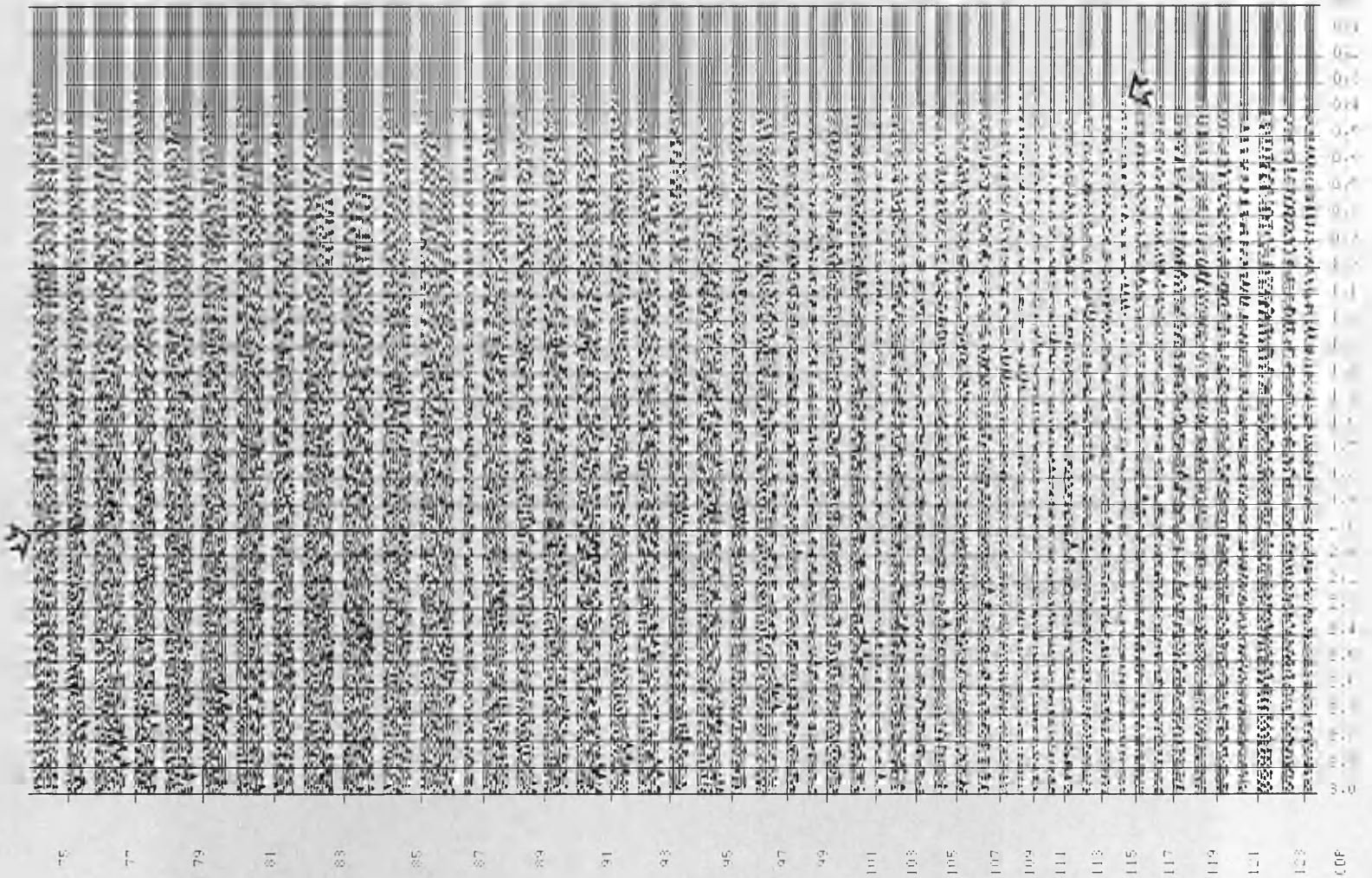

Fig. 3.15 SK-1 gathers, CDPs 74-123. CDPs 74-104 are used in the semblance plot (Fig. 3.18). Arrows show one example of air blast running diagonally across the display.

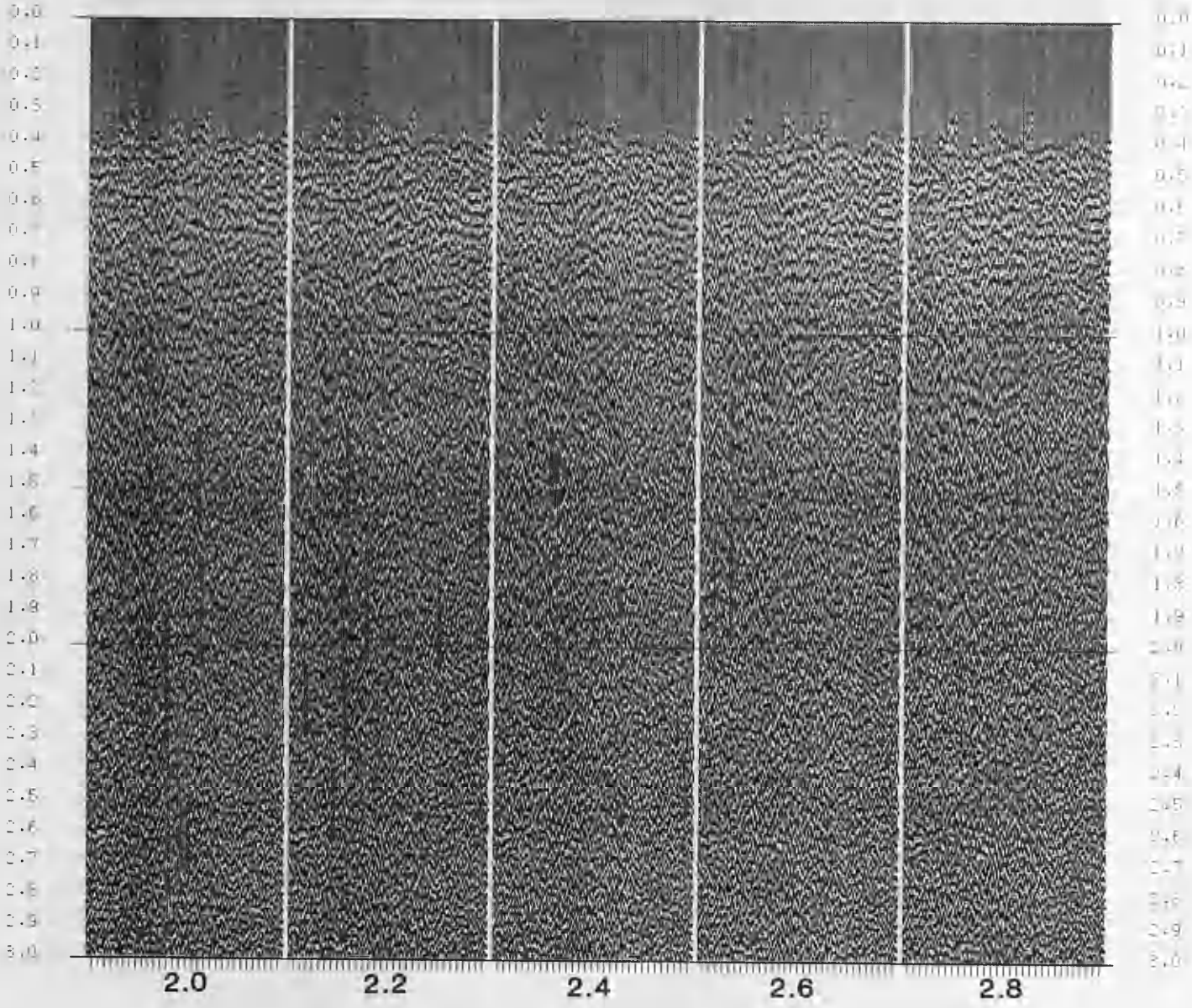

Fig. 3.16A SK-1 constant velocity stacks.

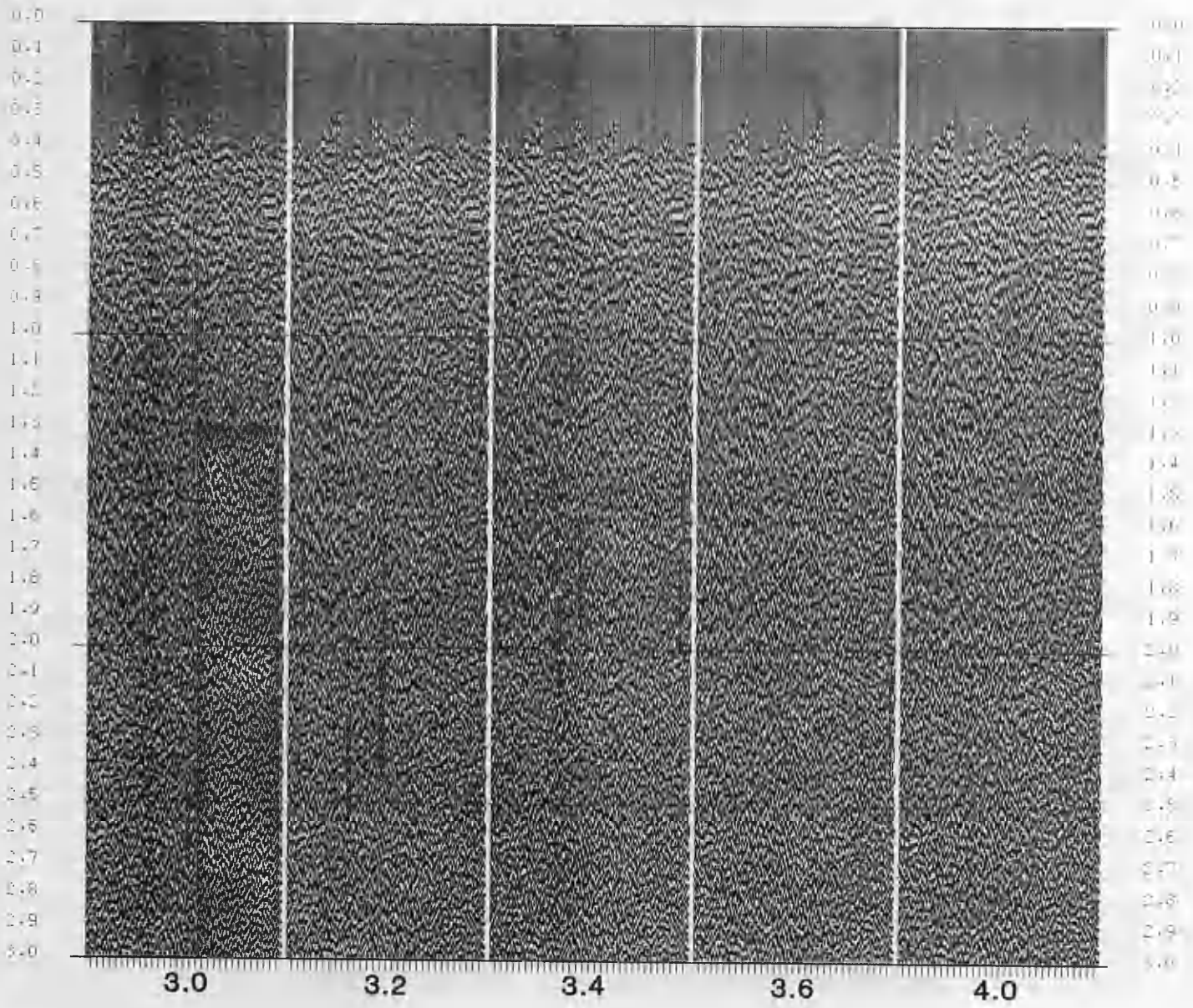

Fig. 3.16B SK-1 constant velocity stacks (continued).

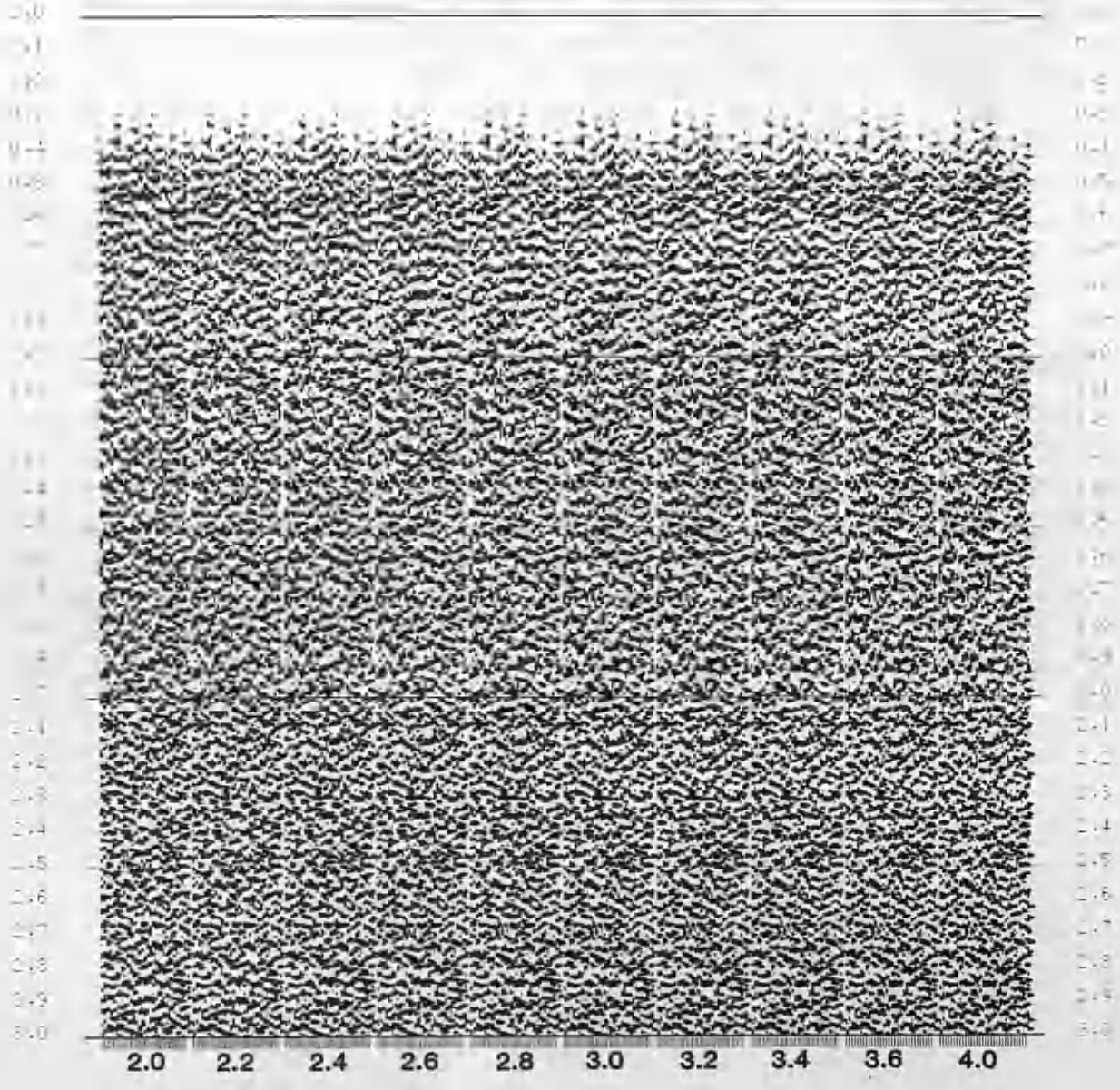

Fig. 3.17 SK-1 constant velocity stacks, 2-trace sum.

Although the dips of the stacked events are low (less than 10°), they are large enough to prevent the whole CDP gather being put into one semblance analysis for estimation of RMS velocities, as is done on some of the other lines. The central portion of CDP coverage, 74 - 104 (Fig. 3.15) is selected for semblance plotting, as this range covers all the reflector segments of interest, as seen on the constant velocity stacks; however, the range is not too great that destructive interference of the semblance scan will result from the dip of the reflectors. The semblance plot, made using 207 traces, is shown in Figure 3.18. Apart from the strong peak at 0.8 s, velocity 2.78 km/s, the plot is not very informative, as might have been predicted from the low amplitude of the events seen on the constant velocity stacks. Additional constant velocity displays, and another semblance plot using a longer trace window (80 ms instead of 50 ms as in the plot shown here) failed to produce any useful extra information. Finally, a compromise stacking velocity profile is deduced, based on both constant velocity and semblance plots. It results in the velocity-depth characteristics shown in Table 3.2:

TABLE 3.2
SK-1 VELOCITIES AND DEPTHS

Time (ms)	V(rms) (m/s)	V(int) (km/s)	Thickness (km)	Depth (km)
400	2100	2.10	0.42	0.42
800	2780	3.32	0.66	1.08
1500	2800	2.82	0.99	2.07
1780	2800	2.80	0.39	2.46
3000	3500			

The 1-dimensional velocity function tabulated above is used to stack the whole line. A series of such stacks using successively greater post-stack trace summation, is shown in Figure 3.19. It is interesting to note how the different degrees of summation bring out different aspects of the data, but with no one version being the best for all reflectors.

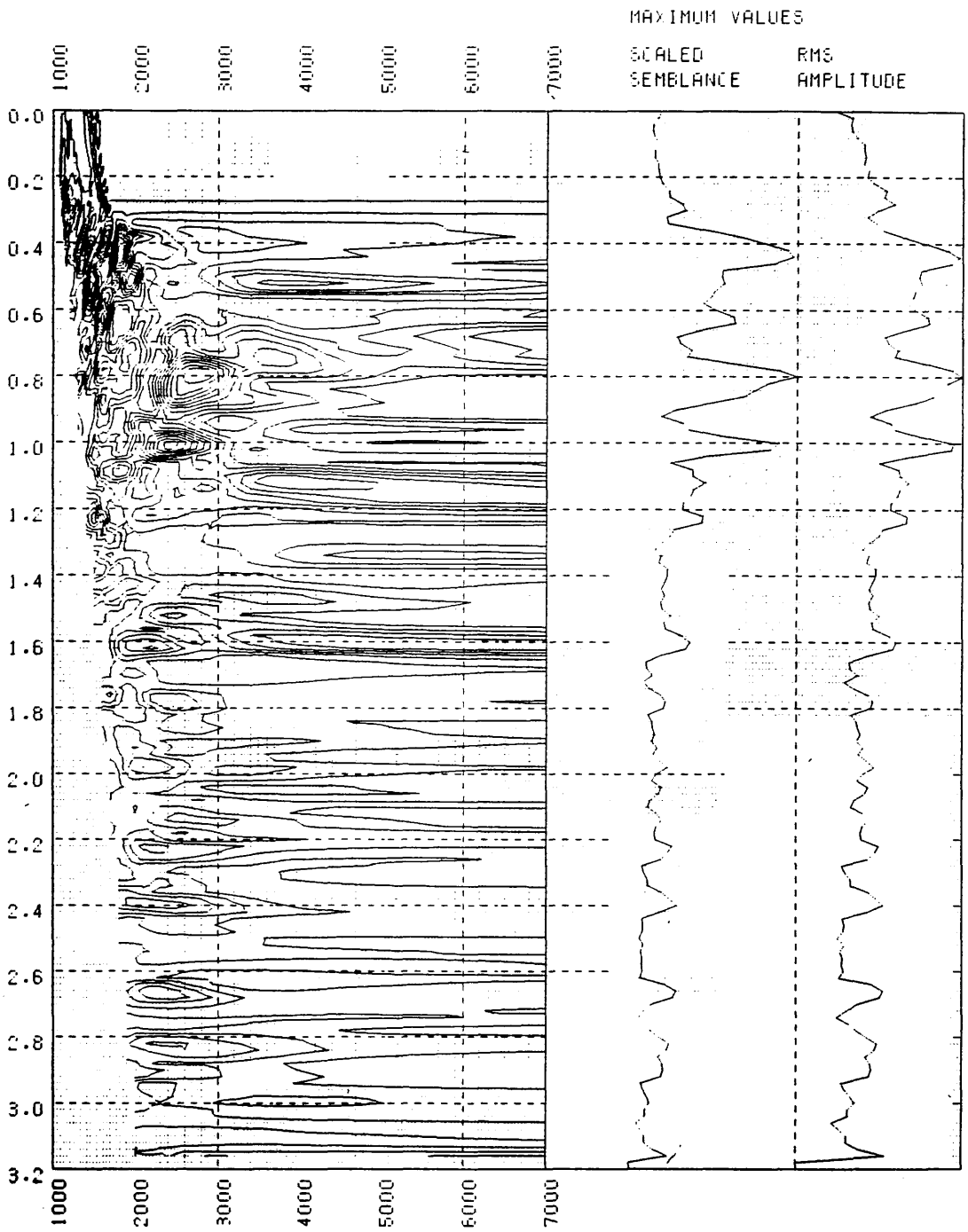

Fig. 3.18 SK-1 semblance plot, covering CDPs 74-104 (207 traces).

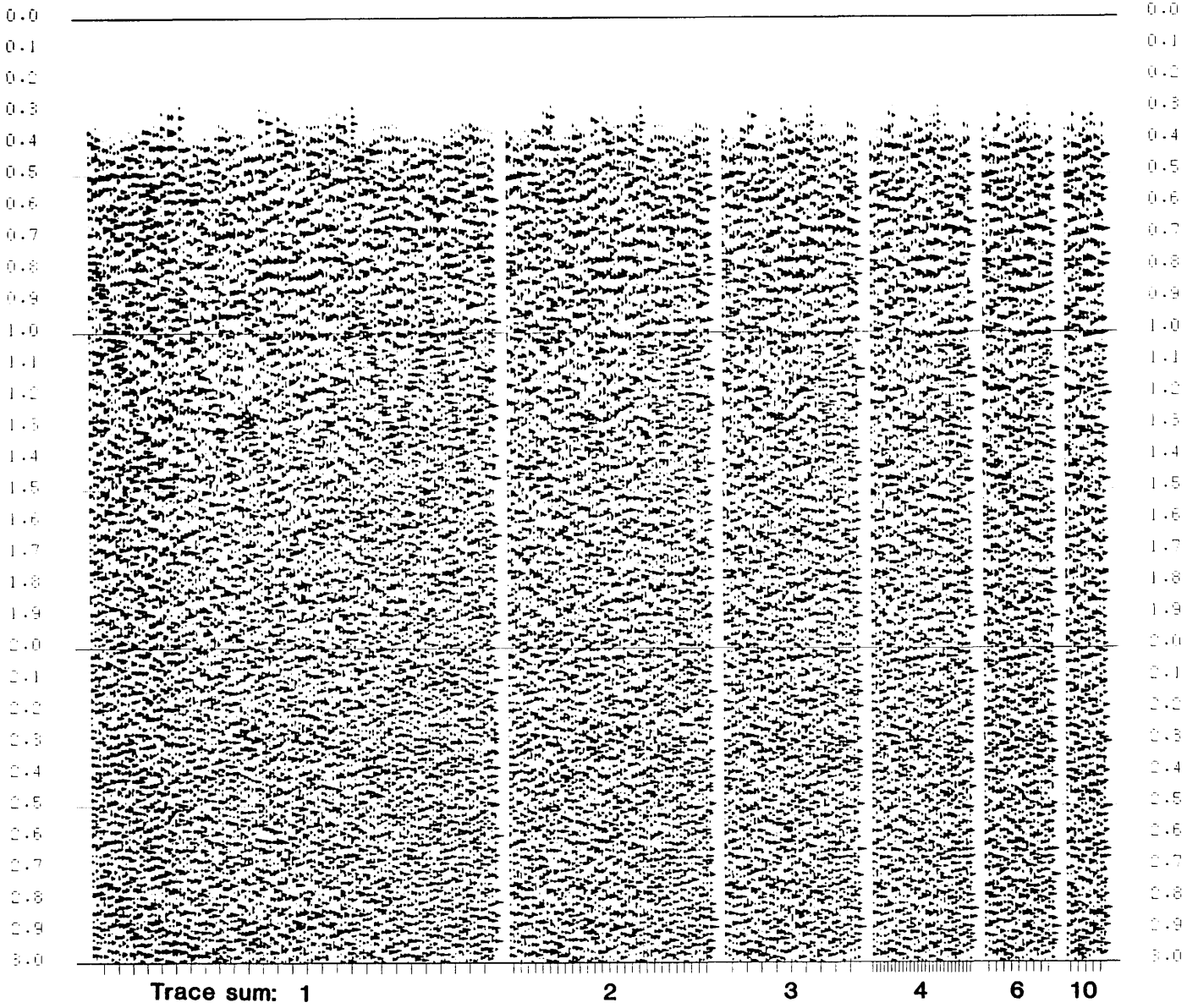

Fig. 3.19 SK-1 final stacks with progressively greater trace summation as indicated below each panel.

With such low amplitudes of reflectors, no deconvolution after stack is worth attempting. The final display of Figure 3.19 merely has a simple time-invariant bandpass filter (15-50 Hz), followed by robust automatic gain control, before plotting.

3.1.4.2 Line SK-2 (Skudiburgh)

This line comprises 12 shot records using a double spread (i.e. receiver group interval 30 m). None of the 12 records are test records, as field testing had been done on nearby line SK-2B. Figure 3.20 shows the subsurface coverage, which is 82.5 m to the NE and SW of shot point 5. The near-offset layout is a split spread, after which end-on shots use offsets of up to 1155 m in either direction.

The whole data set is used for testing the processing parameters. First, the 12 files (144 traces) are gathered into a common shot configuration - this is justified because the total CDP range is only 165 m. The field statics as calculated by hand in 1971 are not applied, as they only differ by up to 5 ms or so across all the traces. Instead, the traces are displayed as pseudo-CDP gathers on either side of an artificial common shot point. This fictitious geometry for the pupose of testing assumes that all the shots are at the same shot point, so that multiple traces at the same offsets (or CDPs) can be compared in what is, in effect, a common-offset gather; fold of coverage varies from 1 to 5 in this gather. After filtering and gaining as described above, it is seen that relative static shifts of up to 20 ms to some field records are required to make traces at the same CDP match up. Once this has been done, the data are then CDP stacked (i.e. trace summing at common offsets), producing the 78-trace gather shown in Figure 3.21.

This new gather has to be re-defined as a CDP gather for the purpose of subsequent processing. Such a 're-definition' is not as straightforward as it sounds - the SKS package does not easily permit alteration of data type in the middle of a processing run.

Fig. 3.20

SK-2: Subsurface coverage and offset diagram

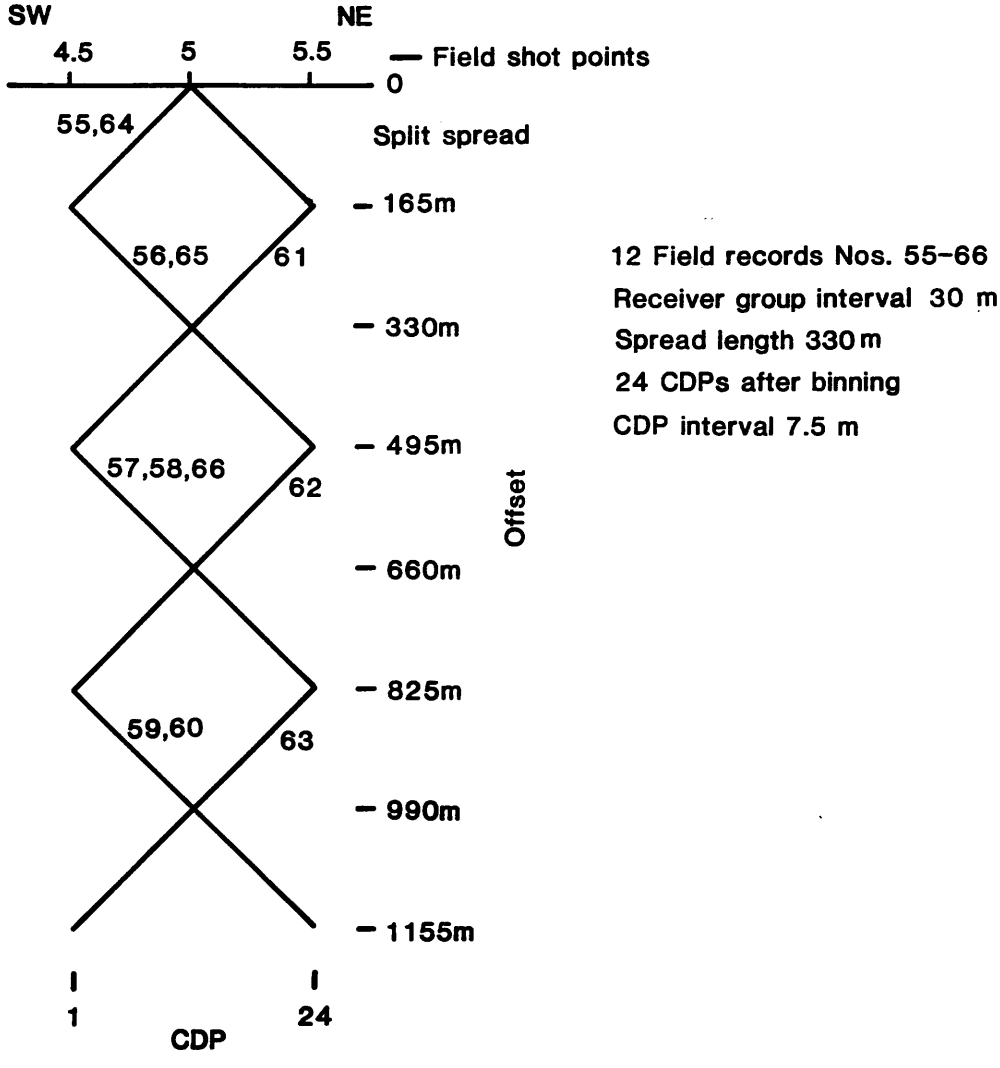

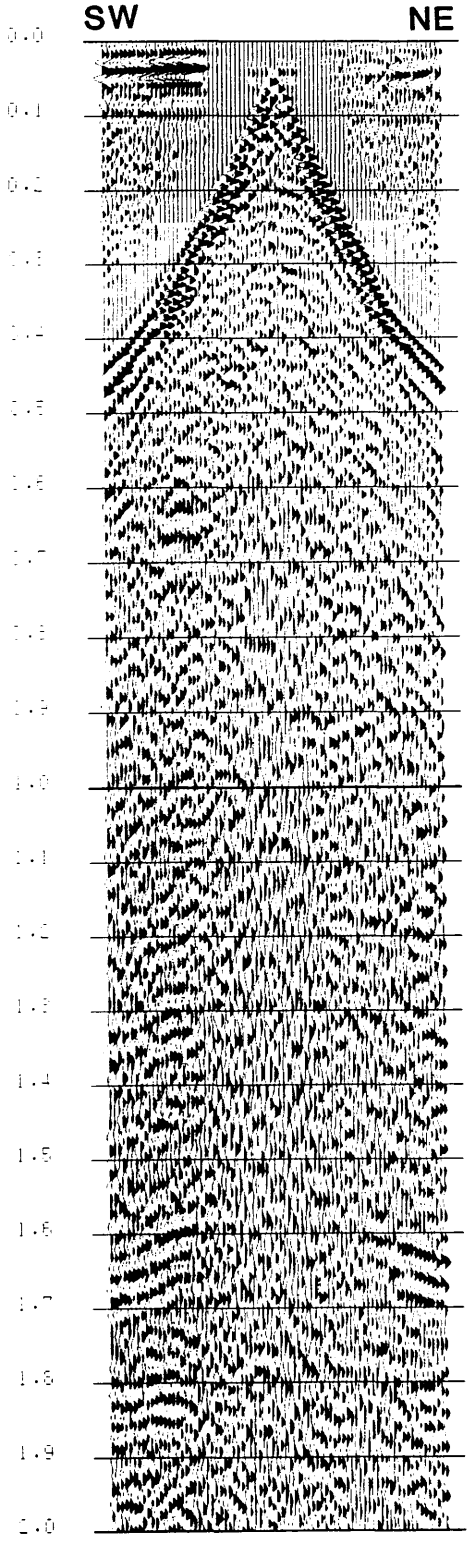

Fig. 3.21 SK-2 'test' geometry of 78 traces produced by common offset summing of all 144 traces. Note the good symmetry about the centre (zero offset) line.

Figure 3.21 shows excellent symmetry, thus justifying the earlier assumption that all data can be binned into one large CDP for the purpose of testing. This result is not obtainable if the static adjustments mentioned above are not made - the common offset sum across traces misaligned by up to 20 ms considerably degrades the data, which has a narrow-band frequency spectrum corresponding to a period of around 30 ms. The origin of the shot static differences is probably a combination of several factors:

(1) Elevation, shot depth and unconsolidated layer static corrections, viz. the manually calculated statics produced during the field work (see Figure 3.1). These, however, are only a few milliseconds.

(2) A static shift introduced in the analogue to digital conversion. This can be seen from the analogue monitors produced at this stage to be up to $\pm$7-8 ms.

(3) Differential shot statics, which are apparent on analogue field records using the same spread and (nominally) the same shot point. These can amount to 5 ms or so. It is somewhat surprising that two supposedly identical shots can produce slightly different timings of otherwise very similar records. These small, but not insignificant, corrections are not recognised in the original field static calculations in (1) above. Since these static differences appear to arise on playbacks, and are not present on the field monitor records, it is likely that they are due to differential delays introduced by the analogue bandpass filters. The TI 8000 amplifier manual shows that a step-function test input comes out, after filtering, as a wavelet, whose first peak and trough can have relative delays of about 5 ms from one filter bandpass setting to another.

Figure 3.22 illustrates the good symmetry of the CDP gather of Figure 3.21, before and after NMO. The strong reflector at 1.6 s is the one assigned to the base of the Mesozoic in the preliminary interpretation of the analogue data (Smythe et al. 1972). Even with this good event, there is a very poor signal to noise ratio at short offsets. Figure 3.23

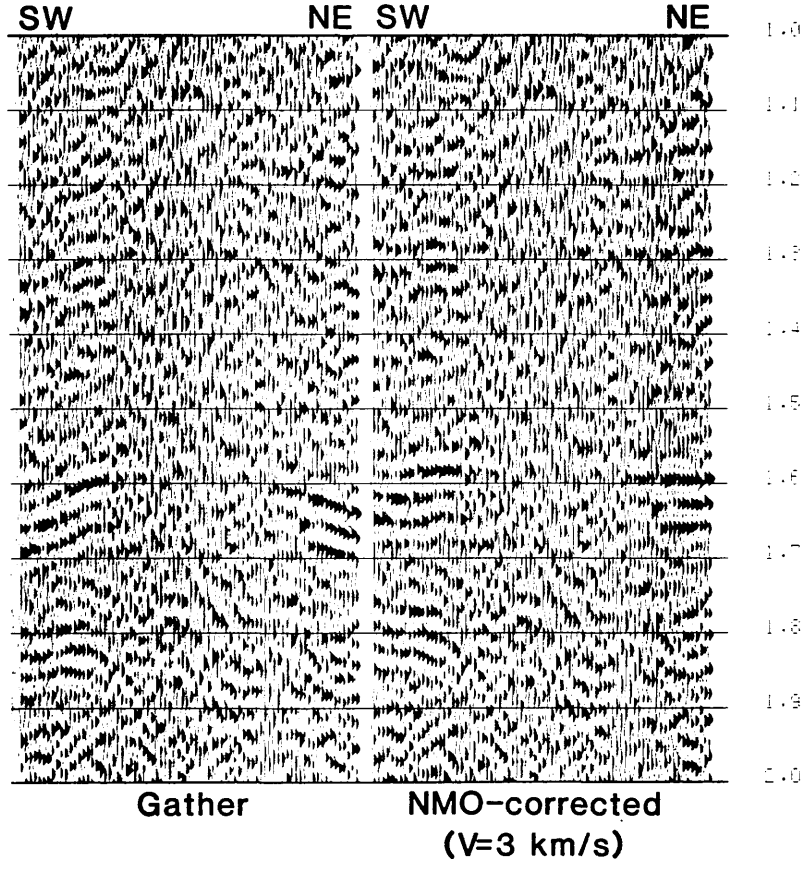

Fig. 3.22 SK-2 detail of 'test' geometry (Fig. 3.21) showing symmetry about the centre (zero offset) line both when gathered and after NMO. The strong reflector at 1.6 s is about 10 ms later at the right hand side, compared with the left hand side.

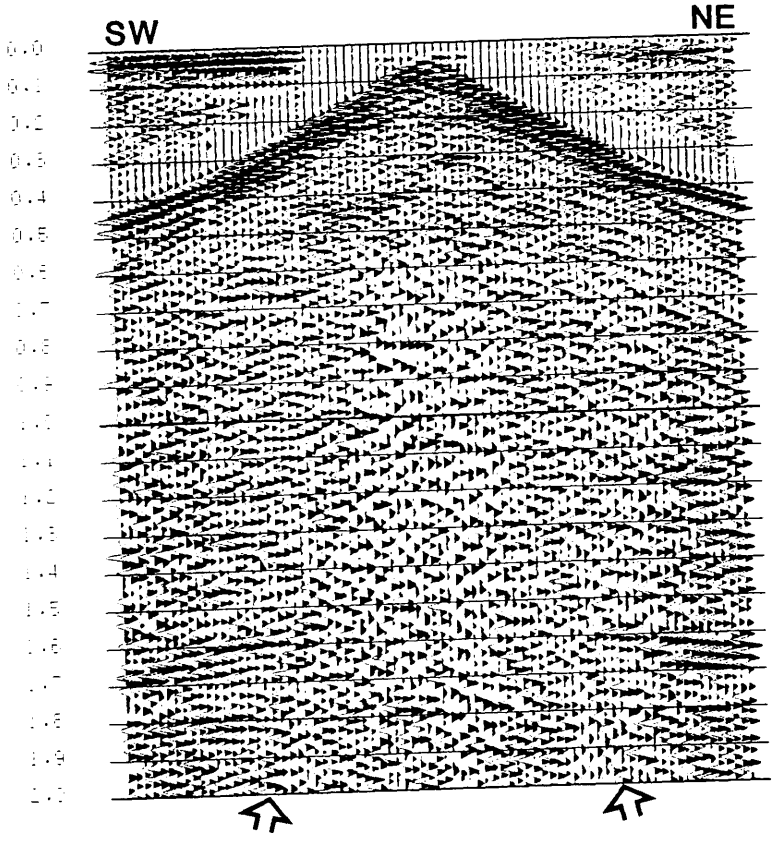

Fig. 3.23 SK-2 'test' geometry with expanded horizontal scale to show muting required: (1) on first arrivals, (2) surgical muting at offsets between the air blast lines (arrowed).

shows the same gather displayed at an expanded horizontal scale for the purpose of defining mute windows. It shows that at short offsets there is considerable low-frequency noise continuing after the air blast (arrowed). This unwanted signal could be ground-roll and/or reverberations set up by the air blast. Muting of the first breaks (down to 800 ms at the far offsets) is required, and experimental surgical muting of the low-offset central noise zone was also tried out. This is discussed below.

Figure 3.24 shows a suite of constant velocity, NMO-corrected panels after the front-end mute is applied. The 'base Mesozoic' reflector is nicely flattened at a constant velocity of 2.8 - 3.0 km/s, and there is a suggestion of reflectors at 1.1 - 1.3 s flattening at rather higher velocities.

Figure 3.25 shows two velocity spectra of the 78-trace CDP gather (produced from the previous common-offset sum of 144 traces). Figure 3.25A is the spectrum with only the front-end mute applied, and 3.25B also has the near-trace surgical mute, with the intention of seeing whether removing the noisy traces would improve the semblance. There is no significant difference, although the velocity resolution of the strong reflector at 1.6 s is marginally improved with the surgical mute. The surgical mute is not used further, on the basis that it is better to apply fewer processes rather than more, other things being equal.

The 12 field records of SK-2 are now binned into CDPs using their actual field geometry, not the artificial test geometry hitherto used. There are 24 CDPs, not 23 (as expected from the subsurface coverage diagram of Figure 3.20), due to offsets of some shots from the nominal shot point. The line is straight. The CDP gathers are NMO-corrected, using velocities derived from the semblance plot produced in the tests, and stacked. The velocities are given in Table 3.3:

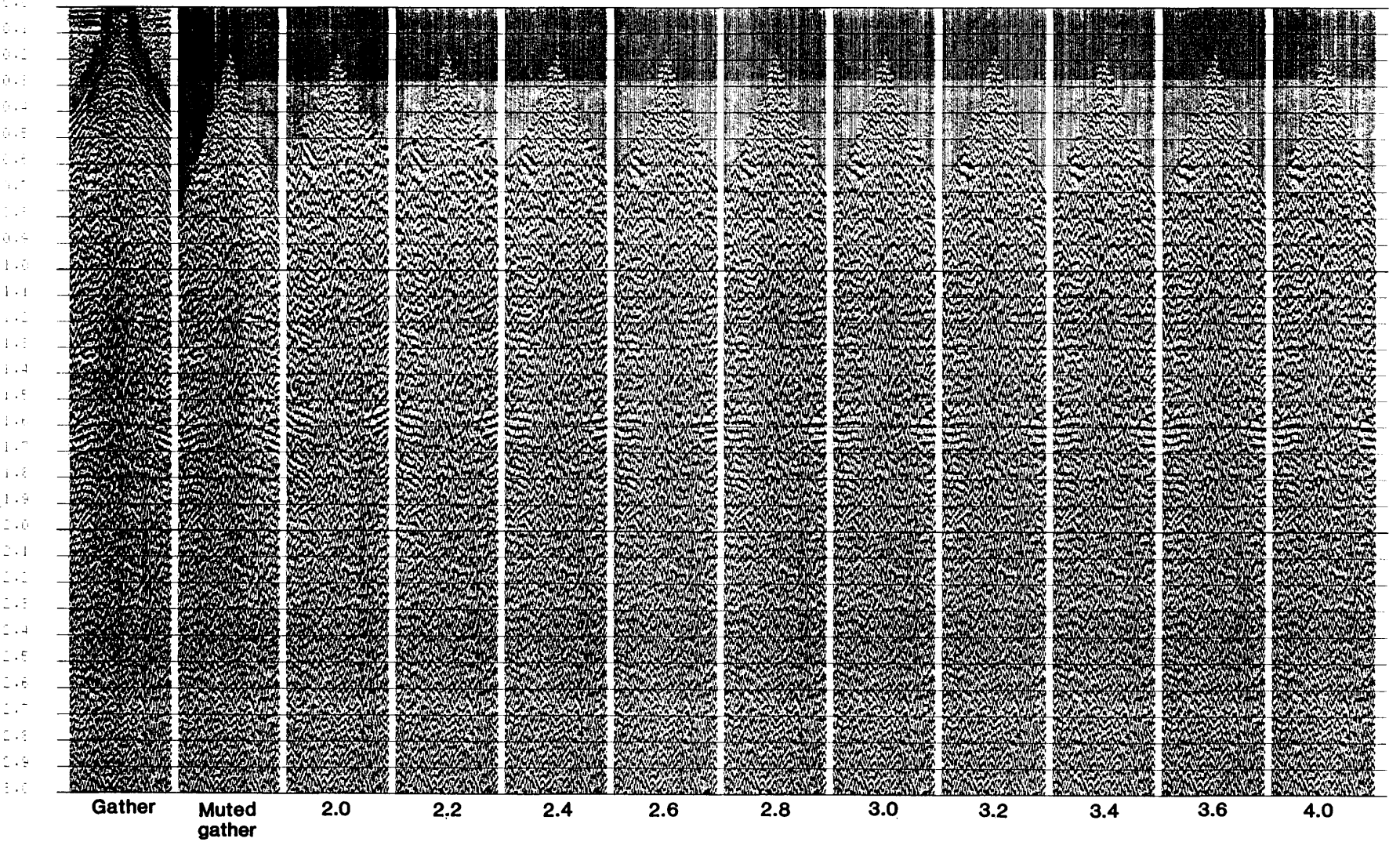

Fig. 3.24 SK-2 gather, muted gather, and NMO-corrected gathers for various constant velocities.

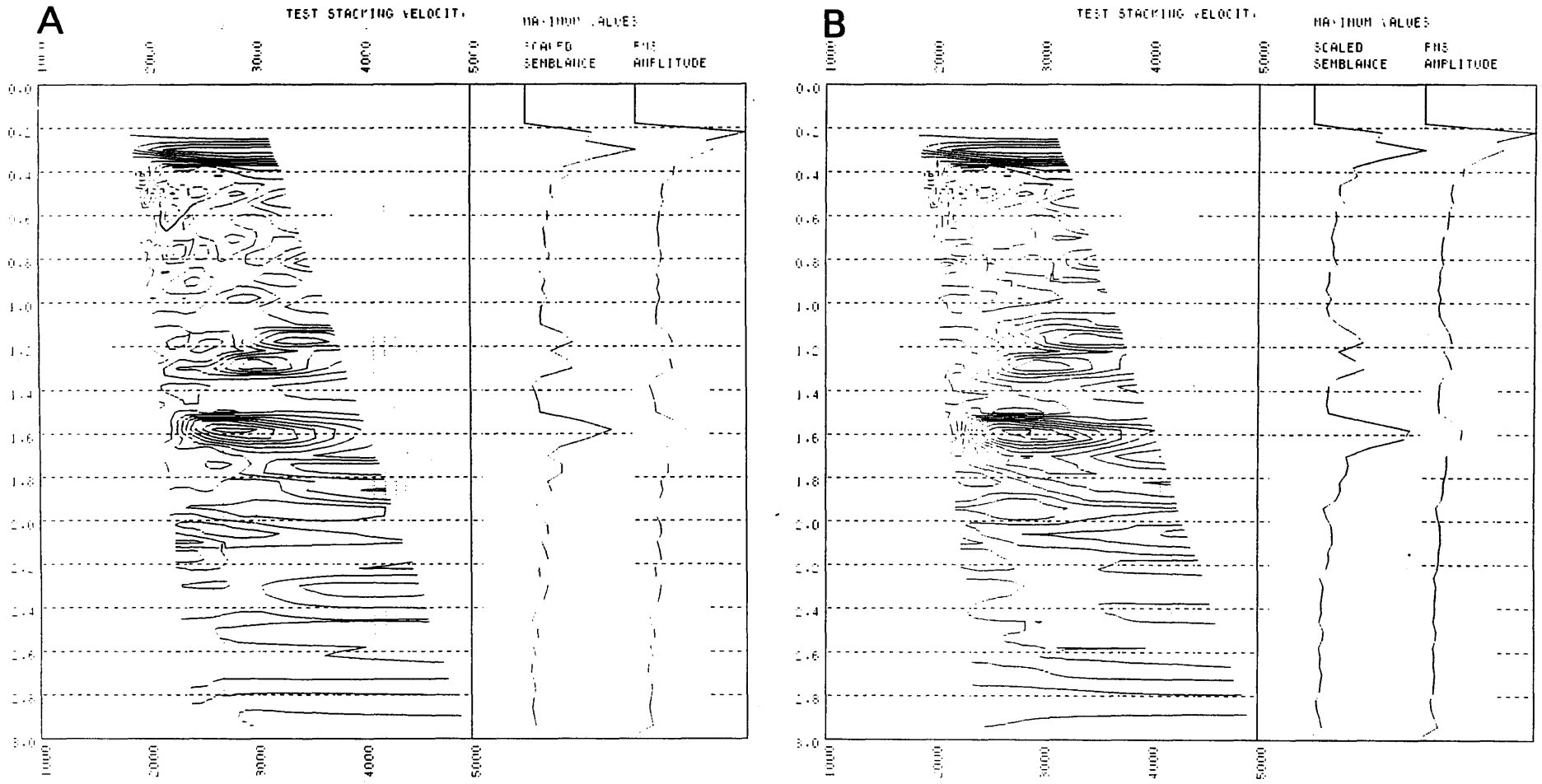

Fig. 3.25 SK-2 velocity spectra using the 78 traces of the 'test' geometry (Fig. 3.21).
A. Front-end muting (for first break removal) only.
B. Both front-end and surgical mute on low offset traces applied (see Fig. 3.23 for surgical mute zone).

TABLE 3.3
SK-2 VELOCITIES AND DEPTHS

Time (ms)	V(rms) (m/s)	V(int) (km/s)	Thickness (km)	Depth (km)
600	2100	2.10	0.63	0.63
1270	2900	3.46	1.16	1.79
1590	2800	2.36	0.38	2.17
2300	4000	5.85	2.08	4.25

Figure 3.26 shows panels of the stack with post-stack deconvolution operators (decon) applied. Panels labelled zero are the stack without decon. The first set of panels (Fig. 3.26A) shows decon designed around the strong reflector at 1.6 s, and applied over the whole trace. Panels 1 to 5 have increasing lags, from 4 ms (i.e. spiking decon) up to 72 ms. There is no improvement overall, although panel 3 (lag 24 ms) has successfully compressed the strong reflector wavelet. The panels of Figure 3.26B use an operator designed over the first 2 s of the trace, then applied to all the trace. Again, there is no significant improvement overall, and spiking-type short gaps clearly only degrade the data. The final stack, therefore, is considered to be that without decon. Post-stack filtering and scaling is unnecessary, as the traces have been sufficiently homogenised prior to stack by the narrow-bandpass, minimum-phase filtering and robust AGC.

No consistent structural dip is apparent from the 330 m width of stacked SK-2. However, the purpose of the line is to provide a spot-value, 1-dimensional velocity-depth profile. It is interesting to compare the interpretation of the velocity spectrum with the original calculations using the T - delta-T method. Figure 3.27A shows the pick of RMS (stacking) velocities. There is some evidence for an inversion between 1.1 and 1.6 s. The pick generally follows the semblance peaks, and allows for the inversion. Figure 3.27B shows the original (1971) average-velocity calculations, superimposed as dots on the 1987 semblance plot. There is a remarkable degree of correspondence between the old and the new results, particularly in the range 1.1 - 1.7 s. The solid line in the figure is the

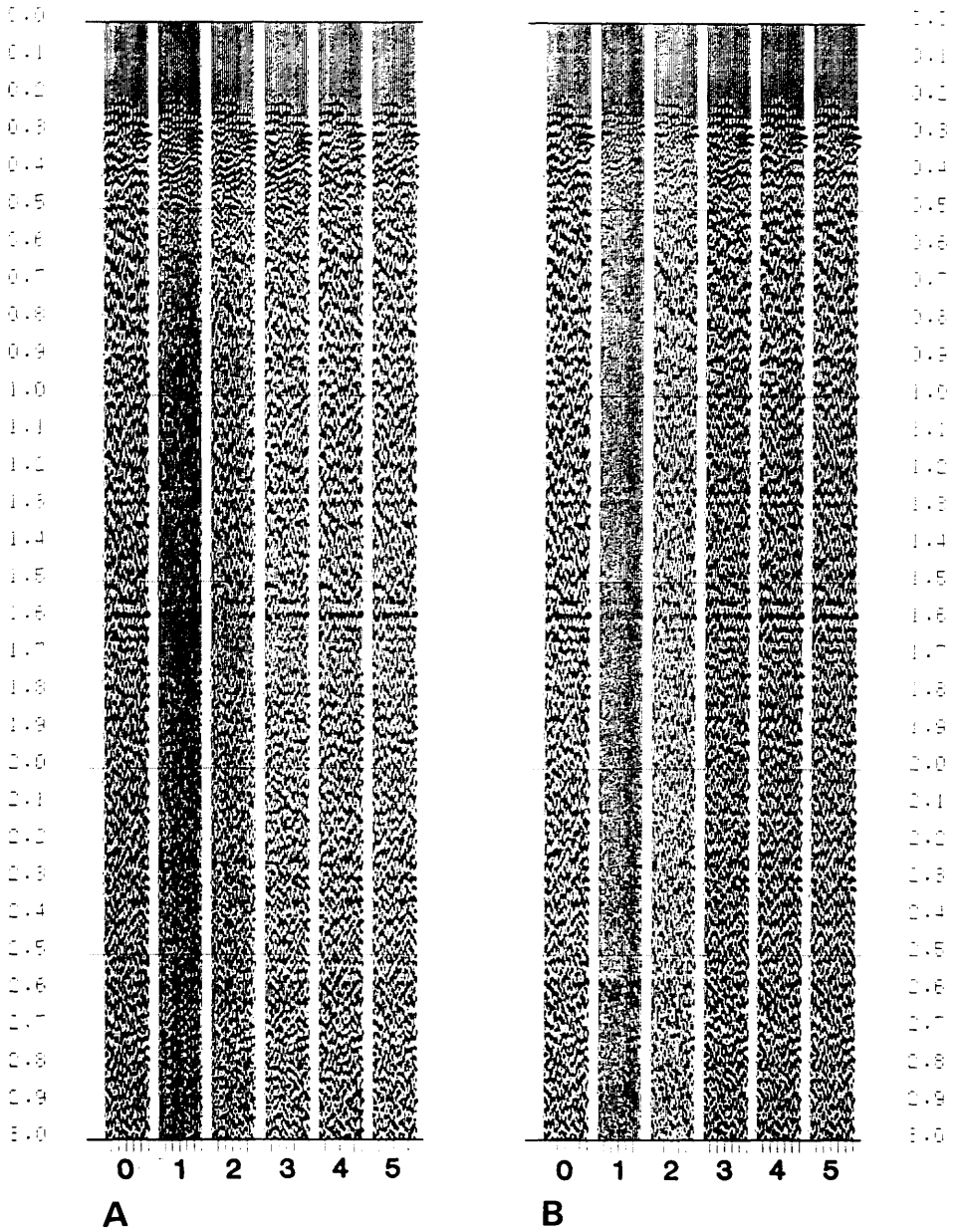

Fig. 3.26 SK-2 post-stack deconvolution test panels.
A. Operator design window of 240 ms around the strong reflector at 1.6 s.
B. Design window over whole trace from 0-2000 ms.
Panel number in each case is:

0 no deconvolution
1 4 ms lag (spiking operator)
2 12 ms lag
3 24 ms lag
4 48 ms lag
5 72 ms lag

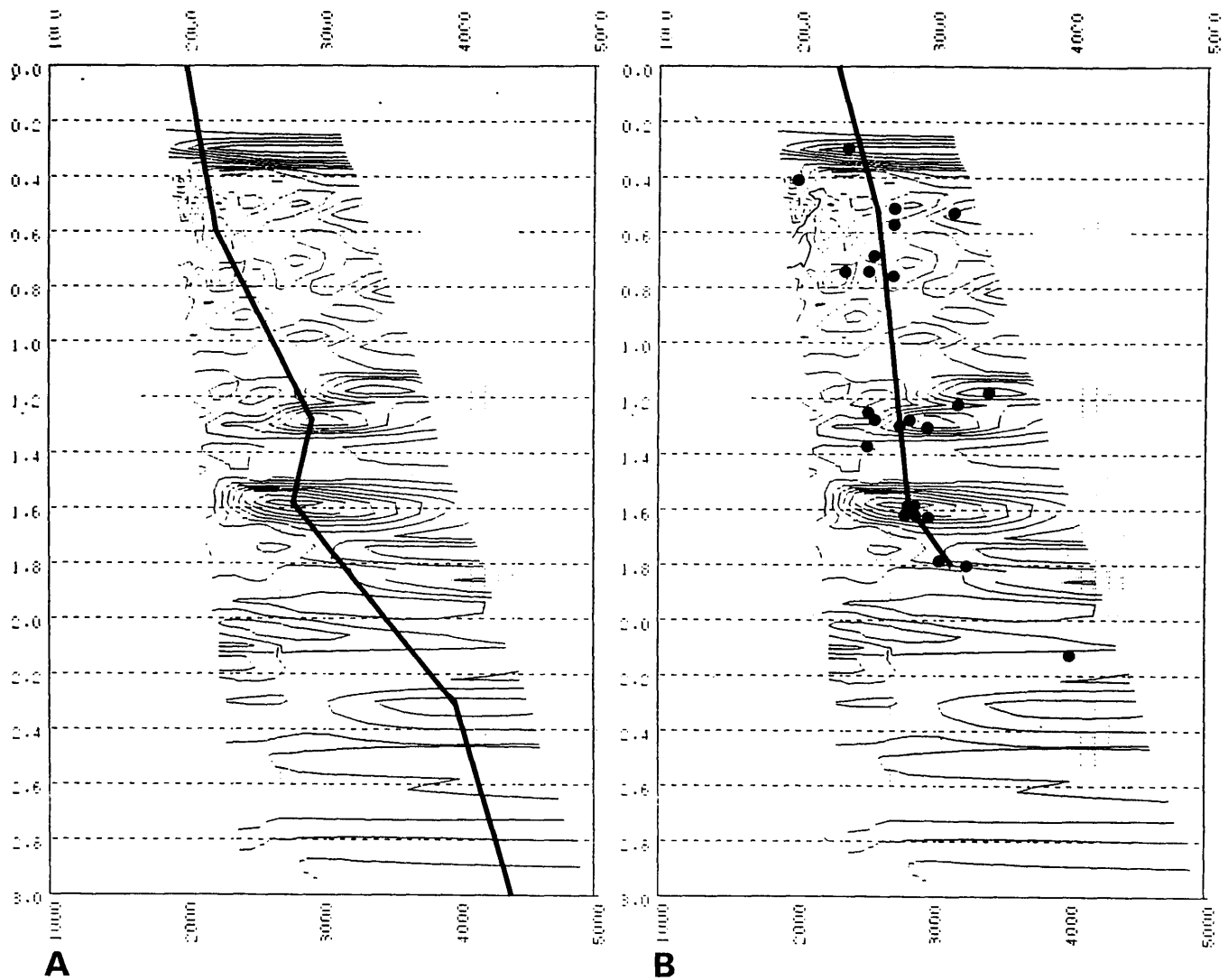

Fig. 3.27 SK-2 velocity spectrum.
A. Solid line shows velocities picked for stacking (1987).
B. Dots are the average velocities calculated by the T-ΔT method from the analogue records (1971), superimposed on the semblance plot. The solid line is the mean of these dots, as used in 1971 to derive interval velocities and depths (Smythe et al. 1972).

'RMS' curve chosen by inspection in 1971. Figure 3.28 summarises the 1971 and 1987 velocity results for SK-2. Whereas they differ in detail, the main result - that the low velocities attributable to the Mesozoic sediments extend to about 2.2 km - is unchanged. The tie-line drawn between the two columns in Figure 3.28 highlights this similarity. Below that depth, the poorly determined interval velocities are probably high (in excess of 4.5 km/s). It is not clear whether the more detailed interval velocity structure for the Mesozoic derived in the 1987 analysis is more realistic than the original, simpler layering, interpreted in 1971.

3.1.4.3 Line SK-2A (Skudiburgh Cross-line)

This comprises 3 records crossing the main line at right-angles at shot point 5 (Fig. 2.4B above). The tape of a fourth record was accidentally erased, and no monitor record was produced. A preliminary gather of the data, as in Section 3.1.4 above, shows no useful data.

3.1.4.4 Line SK-2B (Totscore)

This data set comprises 10 records, most of which are tests. This was the preliminary location of the line that was later moved to Skudiburgh. The data have not been processed.

3.1.4.5 Line SK-3 (Staffin)

This data set is made up of 8 test shots, followed by 28 production records. Figure 3.29 shows the subsurface coverage and offsets for the production records. The geometry forms 133 CDPs at 7.5 m spacing, giving 1000 m of coverage. There is a velocity survey in the centre of the line, made up of 8 field files with offsets in either direction of up to 1155 m.

Fig. 3.28

Comparison of manual and "automatic" velocity - depth calculations on SK-2 (Skudiburgh)

1971-T-ΔT method		1987- picks from velocity spectrum	
T_o (s)	$V_{average}$ (km/s)	T_o (s)	$V_{average}$ (km/s)
0.00	2.30	0.00	2.00
0.55	2.60	0.60	2.10
1.60	2.85	1.27	2.90
1.80	3.10	1.59	2.80
		2.30	4.00

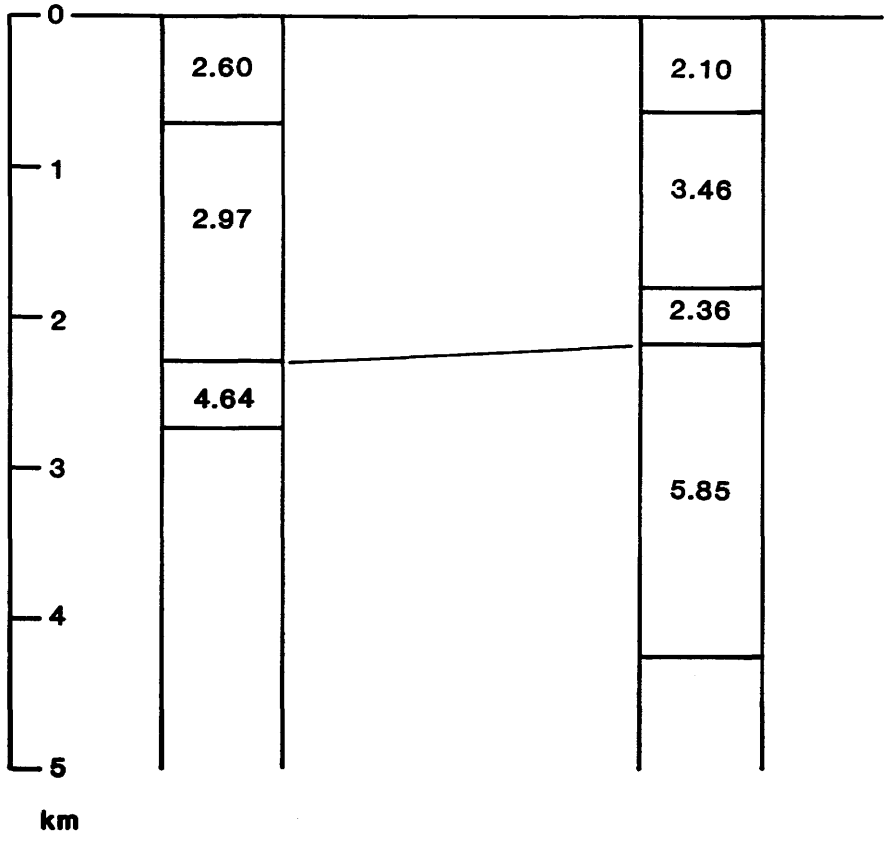

Fig. 3.29

SK-3: Subsurface coverage and offset diagram

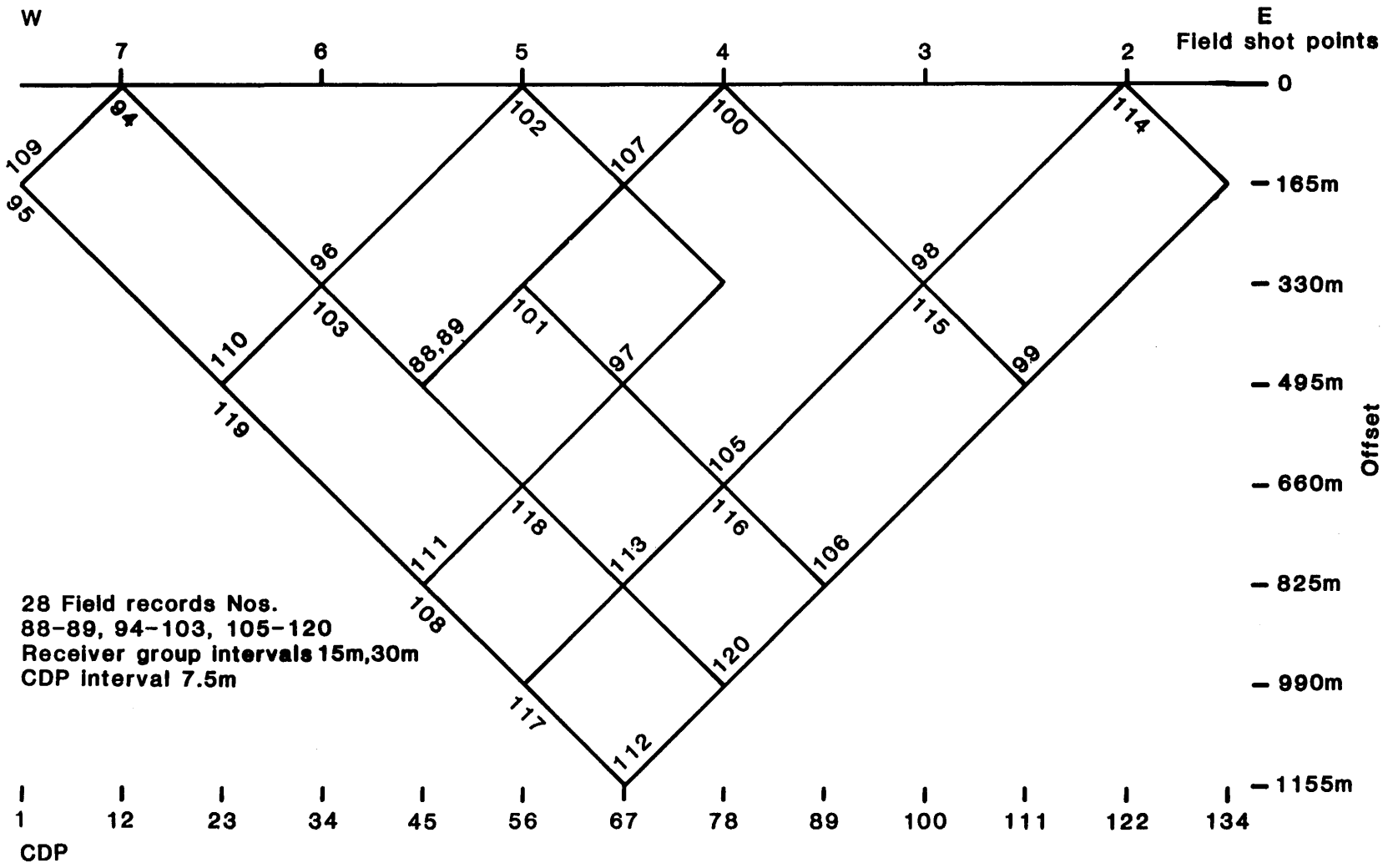

The first batch of tests, using all the data, reveal nothing. Trace-to-trace correlation, both in CDP gathers and in the common-offset domain, seems to be poor. The velocity survey subset of the data is therefore examined separately. A common-offset gather of these 96 live traces (Fig. 3.30) shows that record-to-record correlation (where there are two traces for a CDP) is good, and that shot statics are therefore not a problem. A CDP stack - in effect, a common-offset trace sum - can be performed, and judicious re-setting of trace header information carried out, to produce a single quasi-CDP gather of these data (Fig. 3.31). After muting out the first breaks (Fig. 3.31A), the resulting gather (Fig. 3.31B) shows very little potential reflection information. The only reflector is represented by the hyperbola at 0.3 - 0.4 s. This lack of information is confirmed by a velocity spectrum (semblance plot) of these data.

A third approach is therefore tried - to use all the production records. Figure 3.32A-C shows 15 constant velocity stacks, each comprising 133 stacked traces made from 336 live input traces - an average fold of stack of 250%. These suggest fairly high stacking velocities at shallow depth; the poor events which do have a maximum amplitude for a given velocity seem to be in the range 2.6 - 4.2 km/s at times shallower than 1 s, but no consistent trend is discernible. Although a velocity spectrum run for the complete data set (including test records) shows nothing, when velocity spectra are computed for the production data subset, divided into 5 CDP ranges each with about 85 traces, a consistent velocity-time trend is clear down to 1 s TWT (Fig. 3.33). This internal consistency is shown by plotting outlines of the main semblance peaks together on the same plot (Fig. 3.34). This enables a stacking velocity function to be picked in the range 500-1000 ms, summarised in Table 3.4:

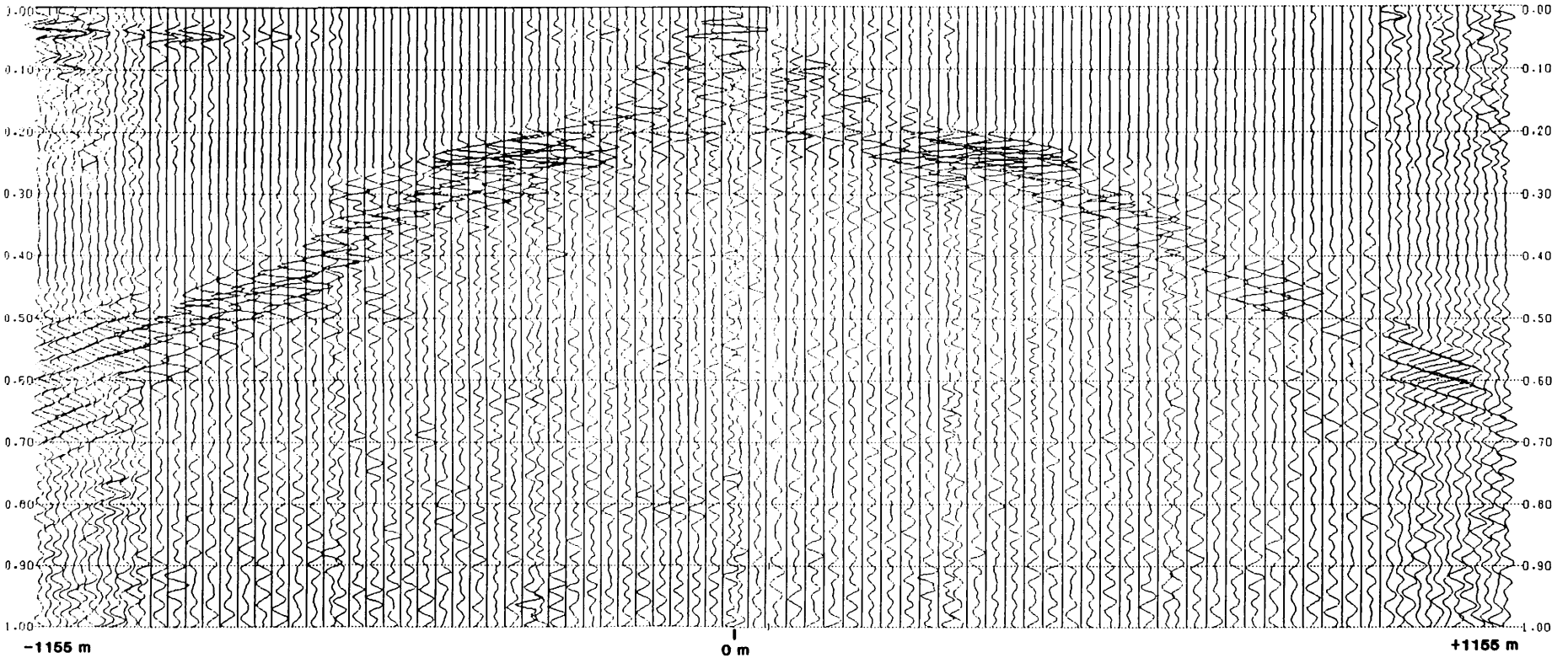

Fig. 3.30 SK-3 common receiver (common offset) gather of the 8 shot records comprising the 'velocity survey' between SPs 4 and 5 (Fig. 3.29). CDP spacing is 7.5 m, but dummy traces (vertical lines) fill many of these because of the use of 'double' spreads, which have a receiver group interval of 30 m. Minimum phase bandpass filtering of 20-60 Hz and robust AGC have been applied.

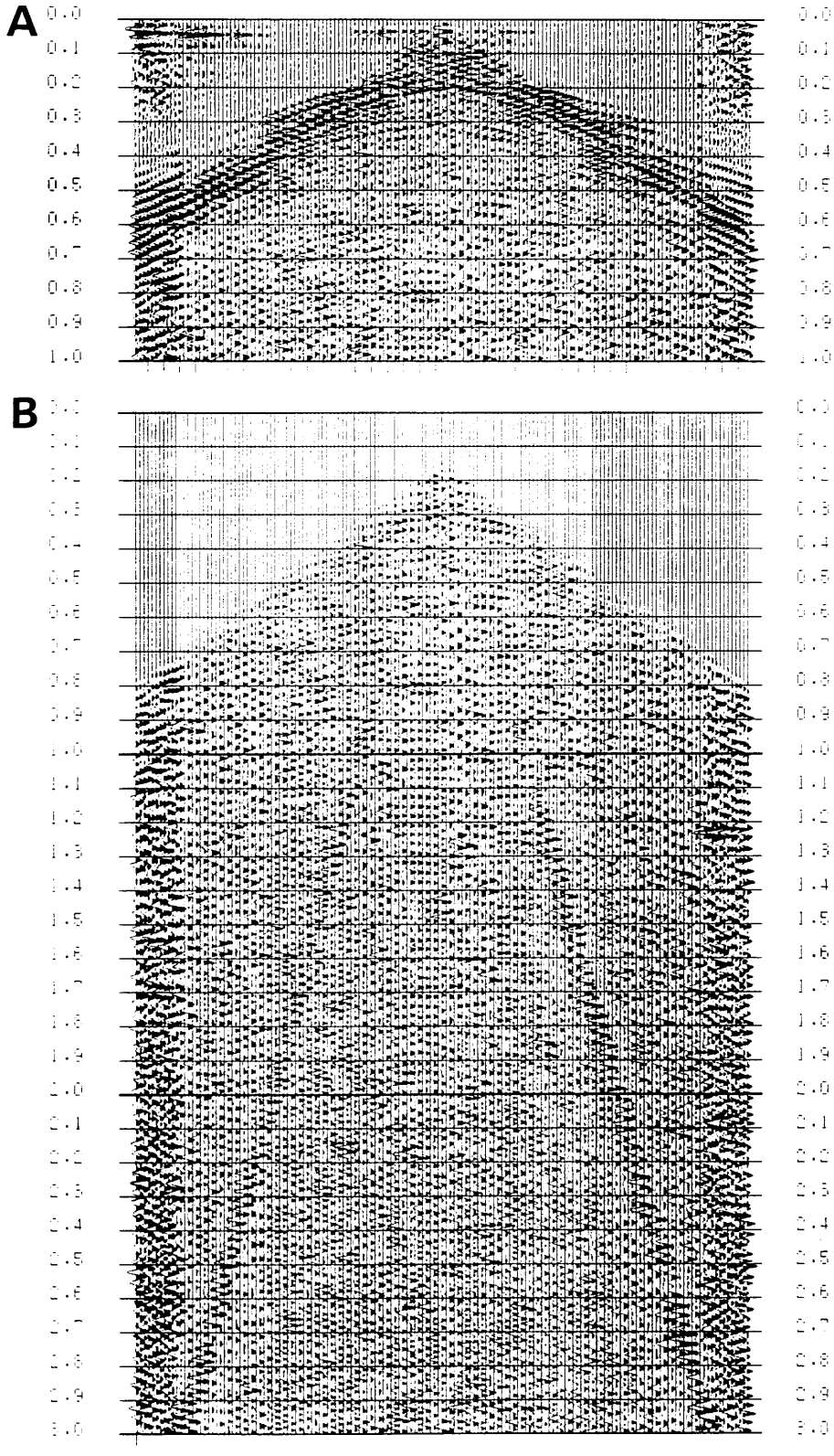

Fig. 3.31 SK-3: common offset sum of the data in Figure 3.30 produces this quasi-CDP gather. Vertical scale in seconds.
A. Top of section showing first arrivals.
B. First 3 s of data with front end mute applied. Note lack of reflectors, apart from the hyperbola at 0.3 - 0.4 s.

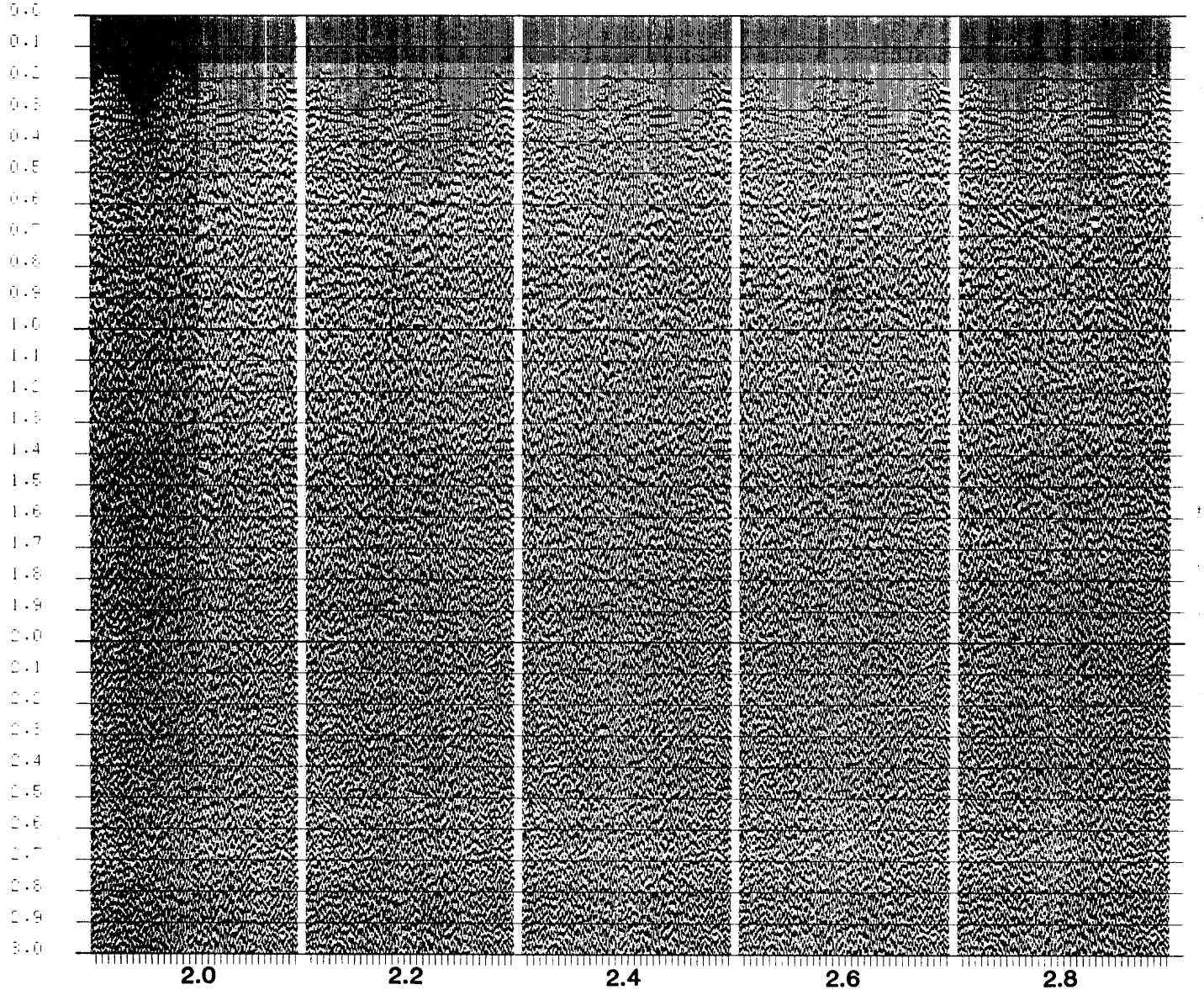

Fig. 3.32A SK-3 constant velocity stacks (velocity in km/s marked beneath each panel).

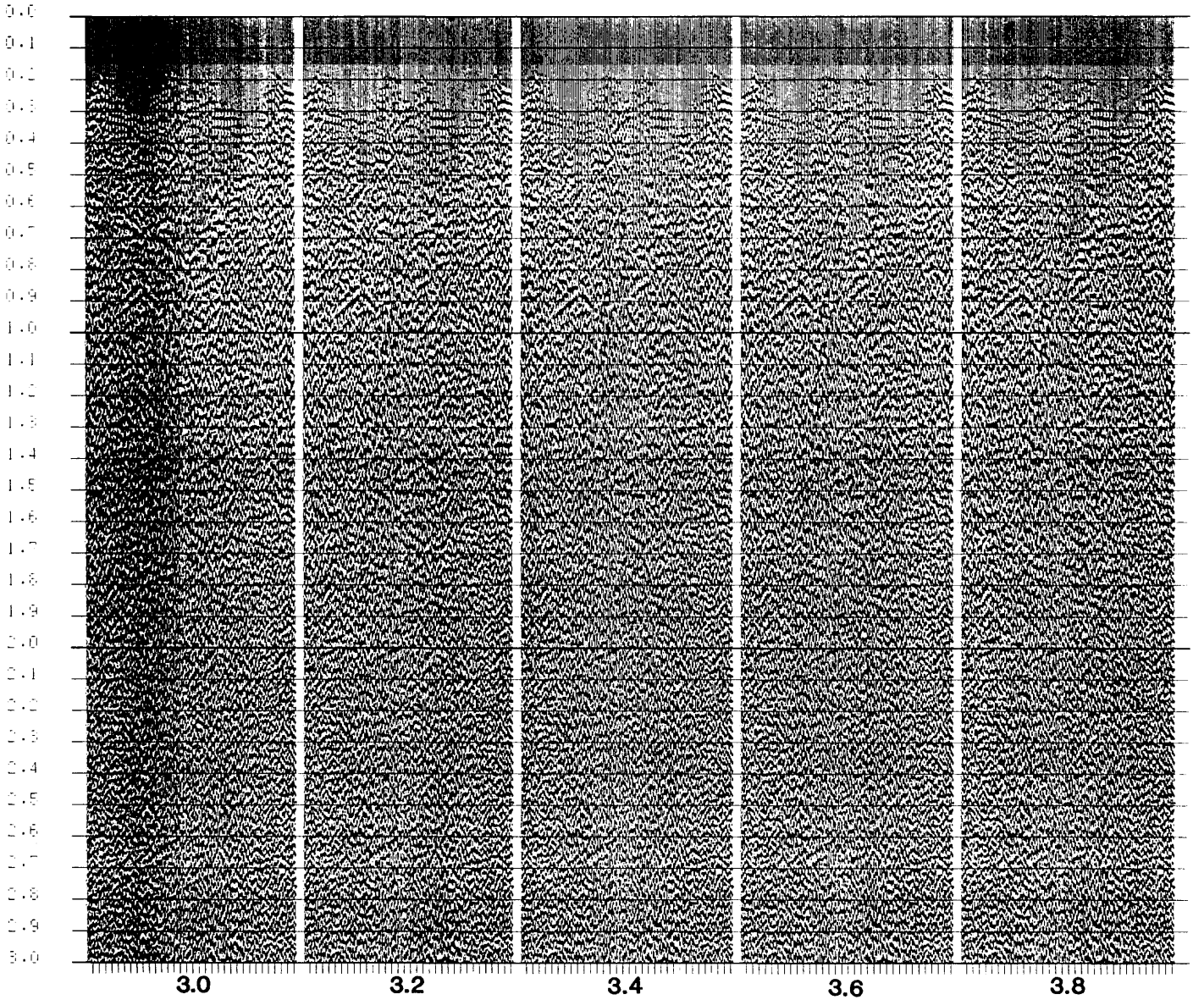

Fig. 3.32B SK-3 constant velocity stacks (velocity in km/s marked beneath each panel).

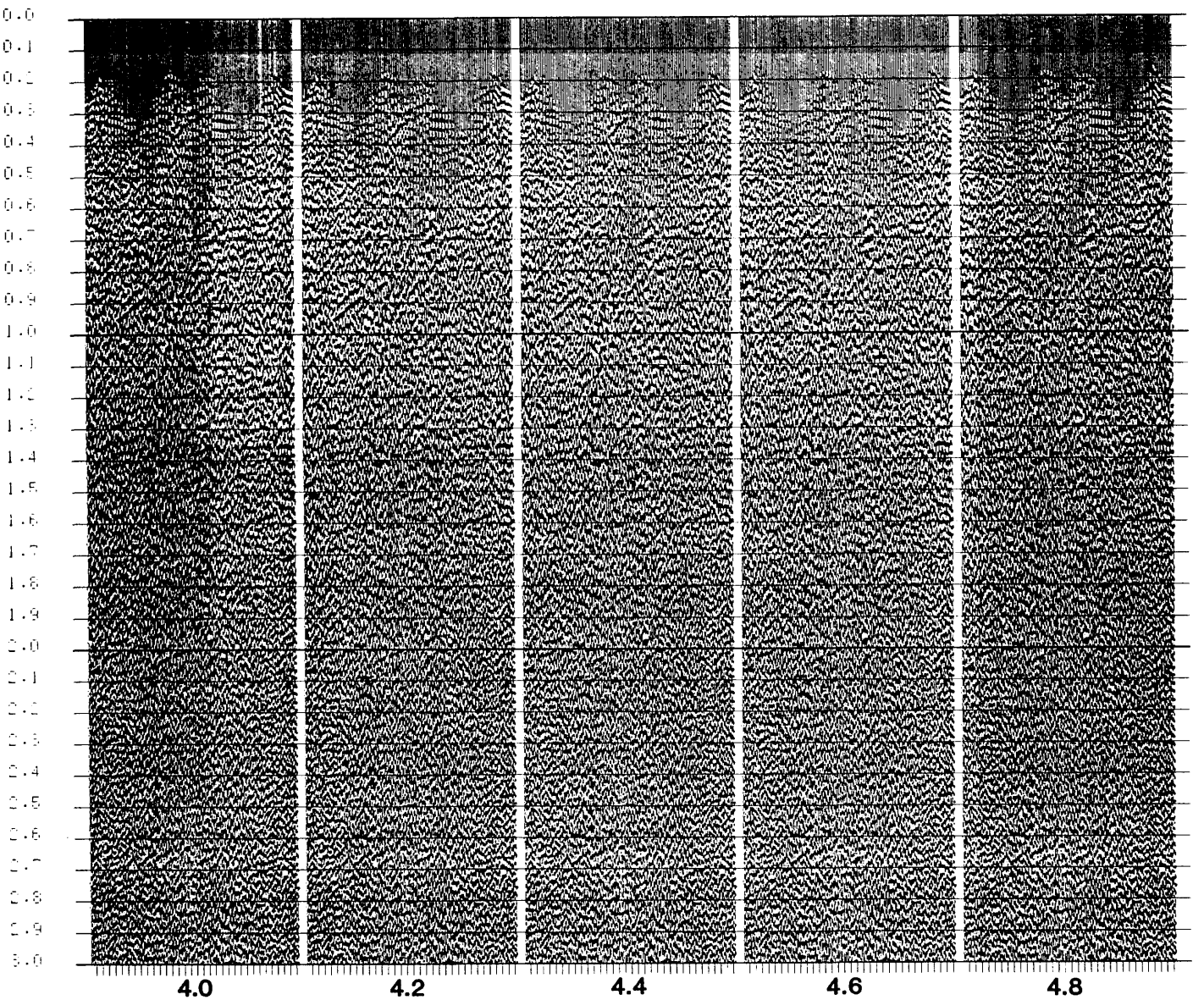

Fig. 3.32C SK-3 constant velocity stacks (velocity in km/s marked beneath each panel).

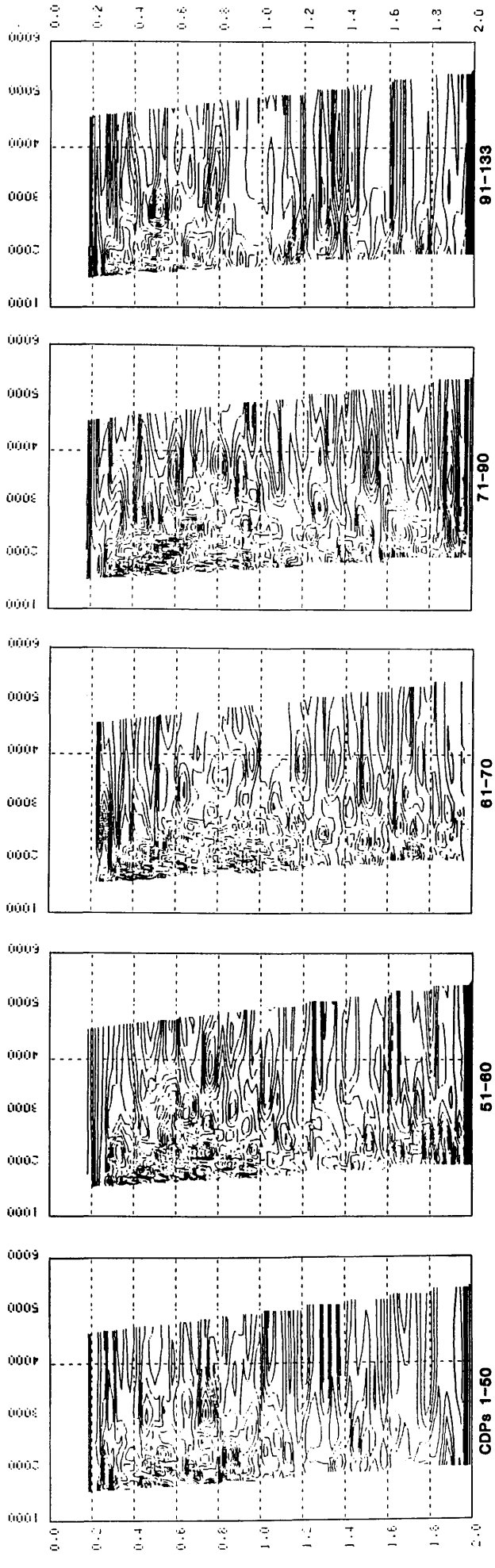

Fig. 3.33 SK-3 semblance plots for the five CDP ranges indicated.

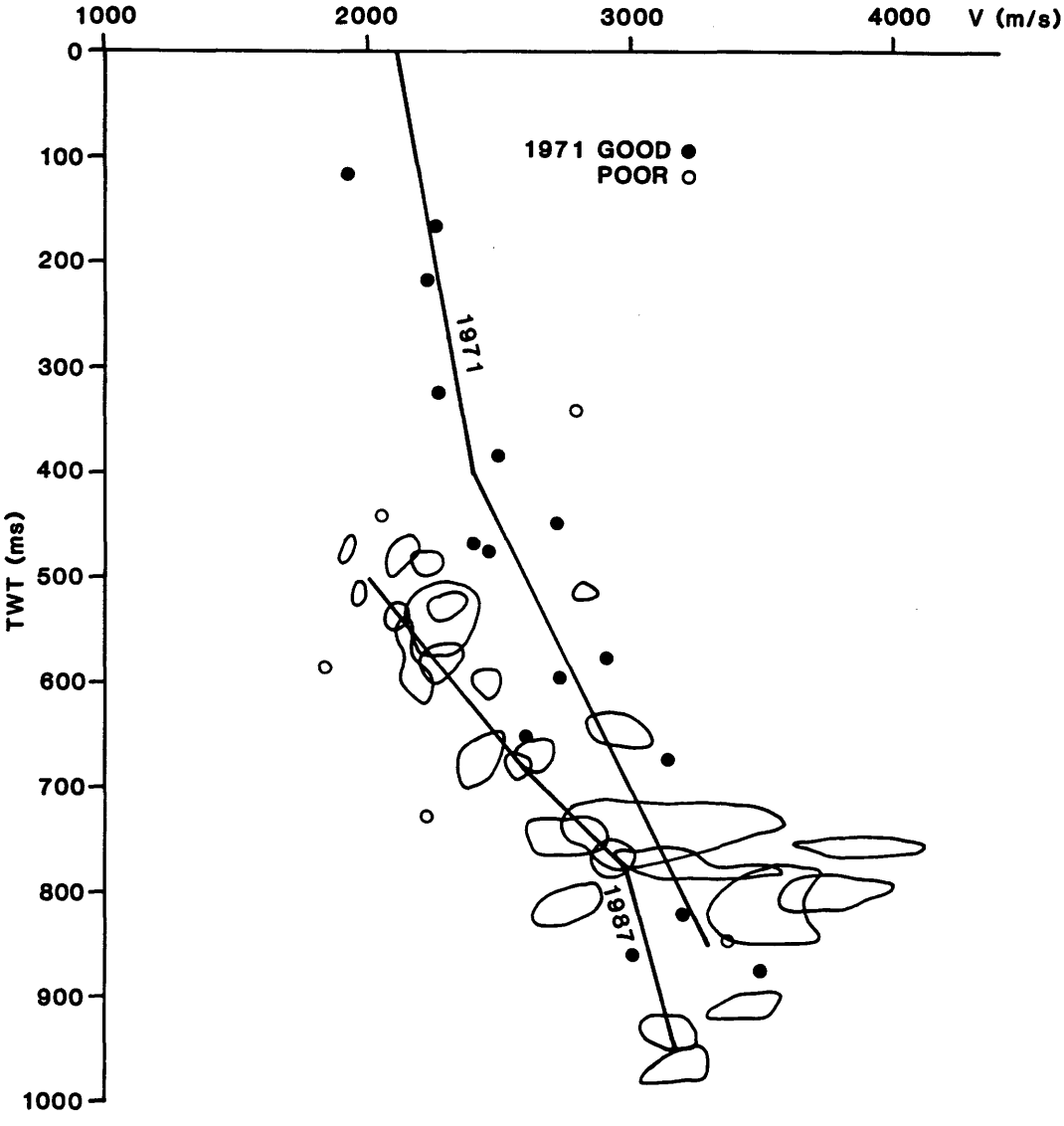

Fig. 3.34 SK-3 Significant peaks from the five semblance plots of Figure 3.33 plotted together. The '1987' line is the stacking velocity curve picked from these peaks. The solid and open circles are the individual mean velocities calculated in 1971 from analogue record sections. The '1971' solid line is the mean of these (chosen by inspection) used to calculate interval velocities and depths (Smythe et al. 1972).

TABLE 3.4
SK-3 VELOCITIES AND DEPTHS

Time (ms)	V(rms) (m/s)	V(int) (km/s)	Thickness (km)	Depth (km)
500	2000	2.00	0.50	0.50
680	2600	3.80	0.34	0.84
780	3000	4.92	0.25	1.09
950	3200	3.99	0.34	1.43
3000	5000			

As with the SK-2 data, it is interesting to compare the manually interpreted velocity function derived in 1971 from analogue shot records with the new result. Individual velocity-time picks using the T - delta-T method (in 1971) are also plotted on Figure 3.34, together with their accompanying velocity function line. The old line is published (in the form of interval velocities against depth) in Smythe et al. 1972.

The 1971 and 1987 versions of the interval velocity depth profile are compared in Figure 3.35. As with the SK-2 data, the two methods give comparable results, but with some greater detail in the newer method. Although both sets of interpretations are obviously based on poor data, they both indicate high velocities of 4 km/s or more at shallow depth below the low-velocity Jurassic of Staffin Bay.

The production data are stacked using the 1-dimensional velocity function given in Table 3.4. It is not worthwhile to try stacking with a spatially varying function (for example, by picking separate functions for each of the 5 panels of Figure 3.33), as the variation in each of these panels is unlikely to be statistically meaningful. The pre-stack data are passed through a slightly broader bandpass filter than before, and some post-stack filtering is then tested. Figure 3.36 shows 4 filter panels after stack. It is clear that the poor reflectors at less than 1 s are predominantly of low frequency - under 20 Hz - compared with the low-cut filter roll-off points of 18 - 27 Hz (and even 33 Hz occasionally) used in the field. A final stack using a simple time-variant bandpass filter is shown

Fig. 3.35
Comparison of manual and "automatic" velocity - depth calculations on SK-3 (Staffin)

1971-T-ΔT method		1987- picks from velocity spectrum	
T_o(s)	$V_{average}$(km/s)	T_o(s)	V_{rms}(km/s)
0.00	2.10	0.00	2.00
0.40	2.40	0.50	2.00
0.85	3.30	0.68	2.60
		0.78	3.00
		0.95	3.20

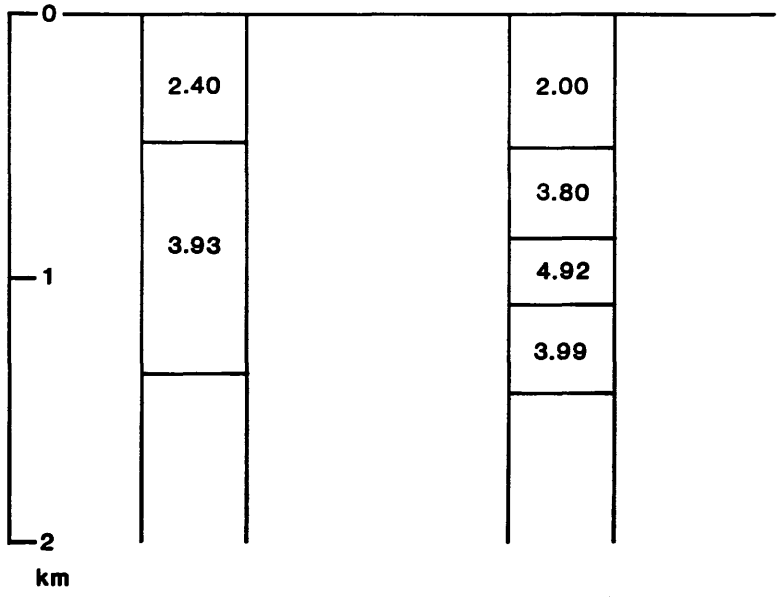

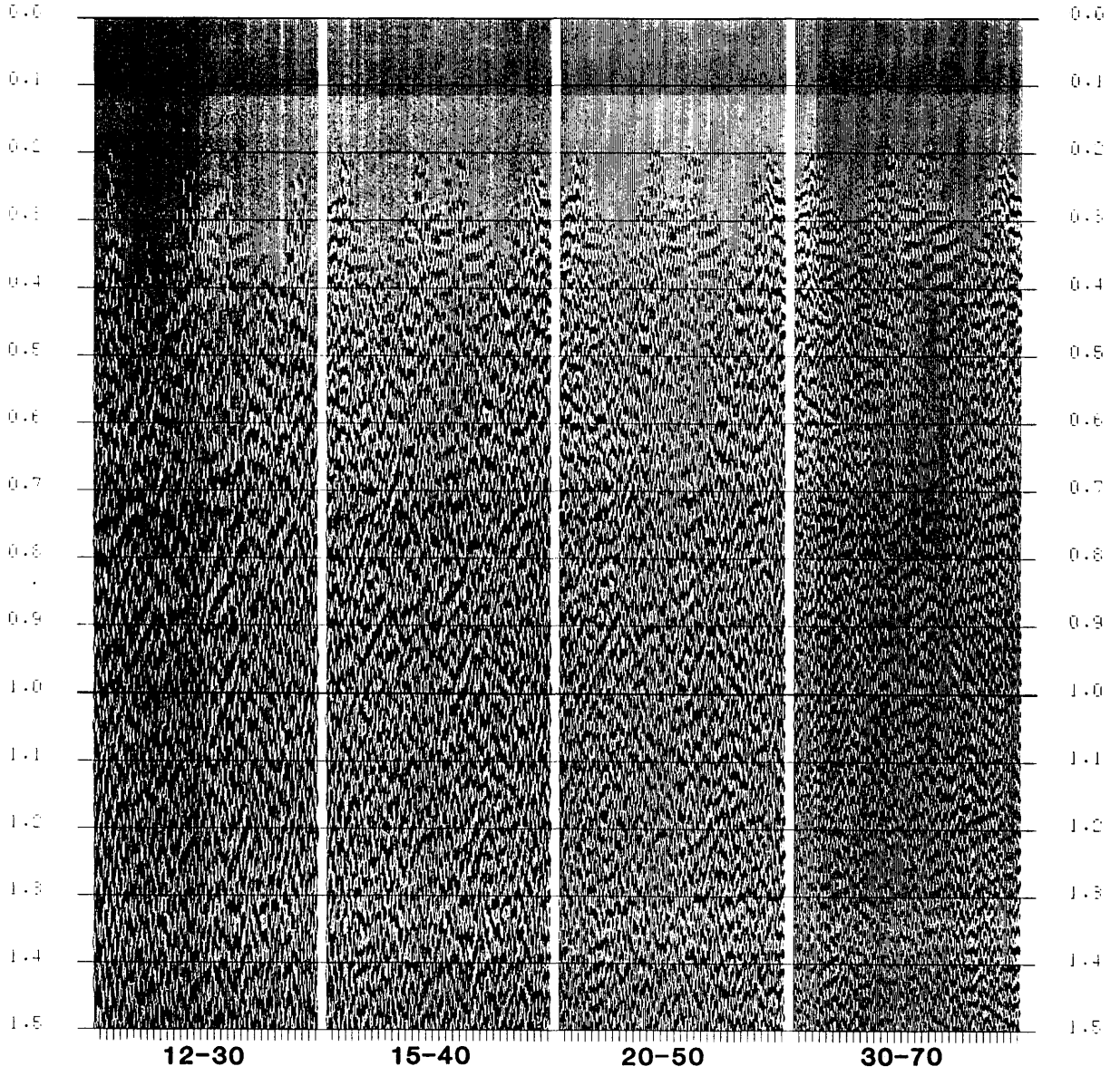

Fig. 3.36 SK-3 post-stack filter tests.
Time-invariant, zero phase bandpass filters are applied as indicated beneath each panel.

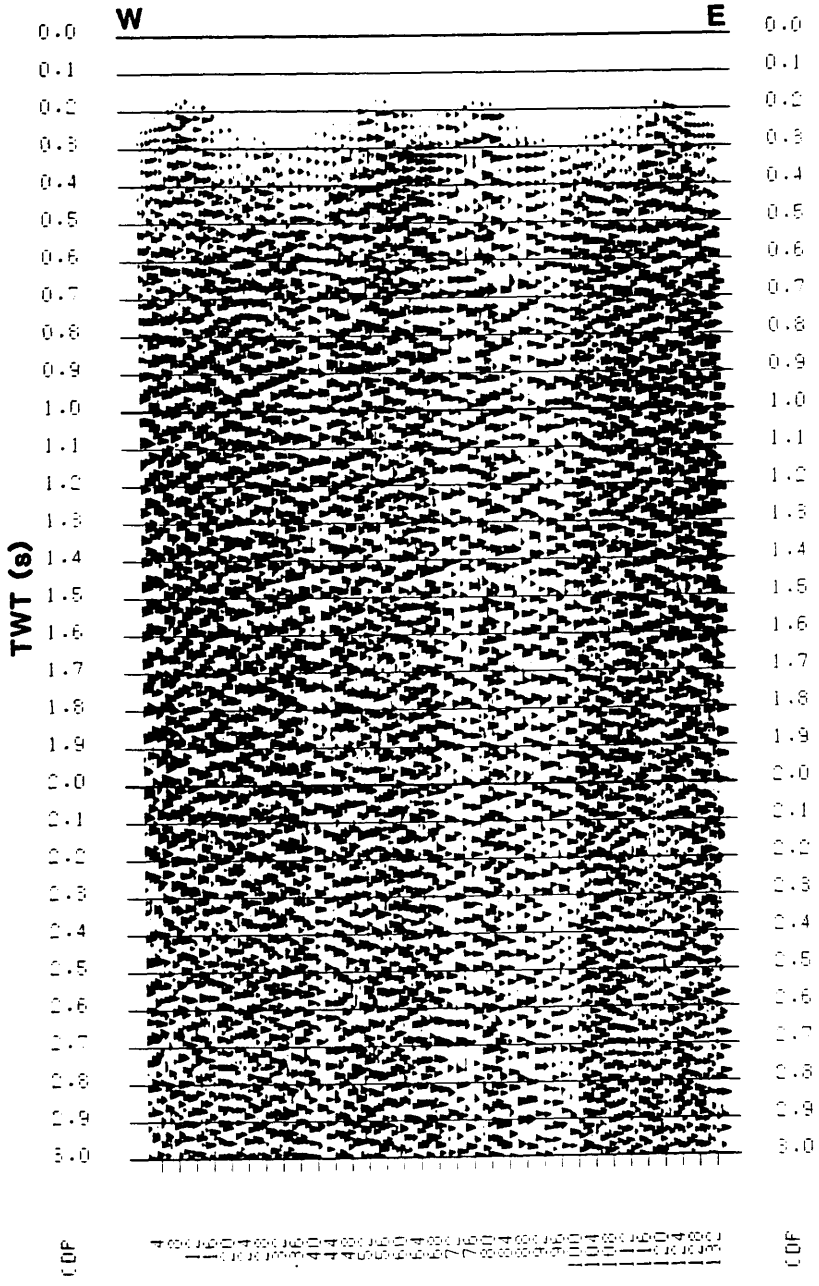

Fig. 3.37 SK-3 final stack. Time-variant bandpass filtering has been applied, followed by robust AGC. CDP interval is 7.5 m, and lighter panels down section (Variable area display) show zones where available CDP coverage is only at 15 m intervals.

in Figure 3.37. This new presentation reveals some westward-dipping structure, not resolvable from the previous work on the analogue shot records.

3.1.4.6 SK-4 (Quirang)

This short length of continuous profile was shot with 18 records, using double spreads (receiver group spacing 30 m). Figure 3.38 shows the subsurface coverage. The spread is offset 660 - 990 m from the shot for the continuous subsurface coverage, but extra shots at other offsets were fired to give a greater range of offsets at the CDPs between field shot points 13 and 15. The shot to near trace offset of 660 m is found to reduce ground roll to manageable amplitude, and the air blast comes in too late to interfere with the first 2 s of reflection time.

The traces from all 18 records are binned using the SKS 'crooked line' processing option. The binning process dropped 11 traces out of 216, but binned 4 traces twice and 1 trace 3 times; these results are a reasonable compromise between dropping too many and having bins that overlap too much. Figure 3.39 illustrates part of the binned CDP gather. At the left hand side there are dummy CDPs alternating with the traces from shot no. 128 (Fig. 3.38). The dummy traces result because the group interval of the spread is 30 m, whereas the processing bins (i.e. CDPs) are at a nominal 7.5 m interval. The thrice-binned trace can be seen at CDPs 144-146. This gather is made as a check for time consistency of the binned traces - below about 1 s of TWT the move-out (which has not been removed) is negligibly small, so that comparison of binned traces with differing offsets will not be greatly affected. Although the traces in each bin seem to be reasonably consistent, there are no definite reflectors against which the static shifts that have been applied can be calibrated. The statics applied include an elevation correction to reduce the data to sea level.

Three records (nos. 130, 131 and 133) were made at the same location using different sources. Some of the traces

Fig. 3.38
SK-4: Subsurface coverage and offset diagram

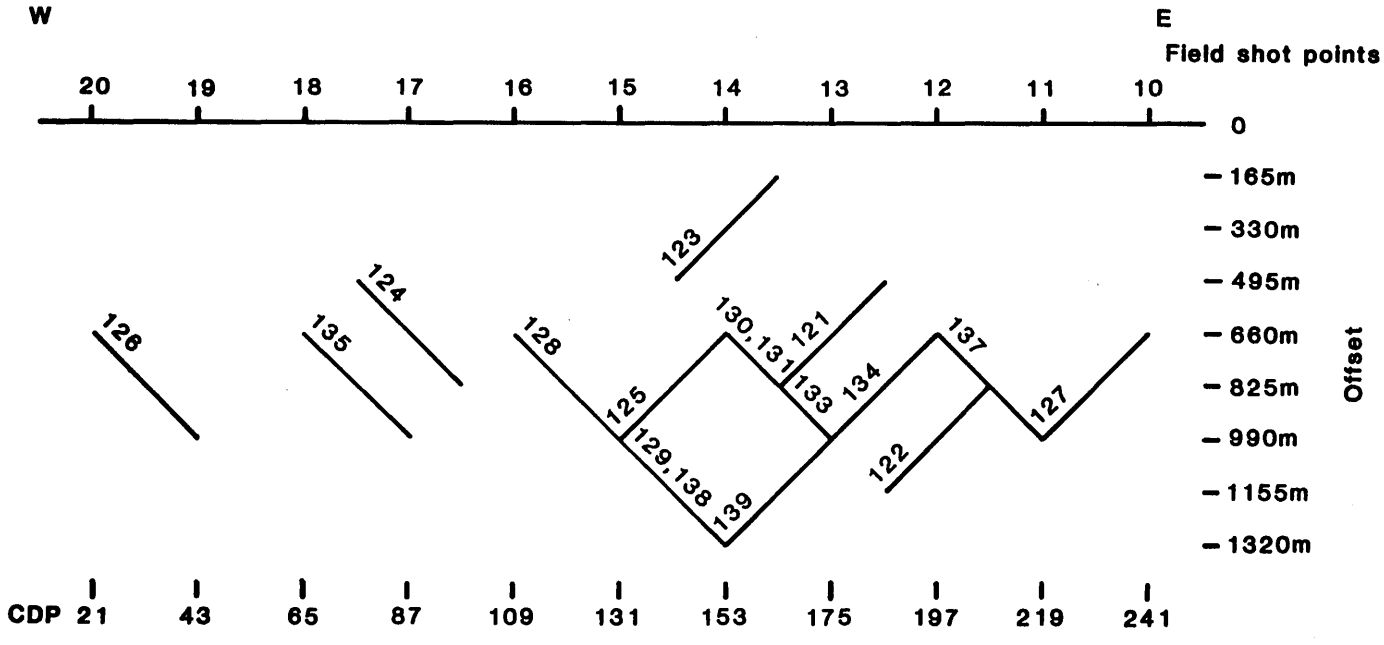

18 Field records Nos. 121–135, 137–139
Receiver group interval 30m, processed for CDP interval 7.5m

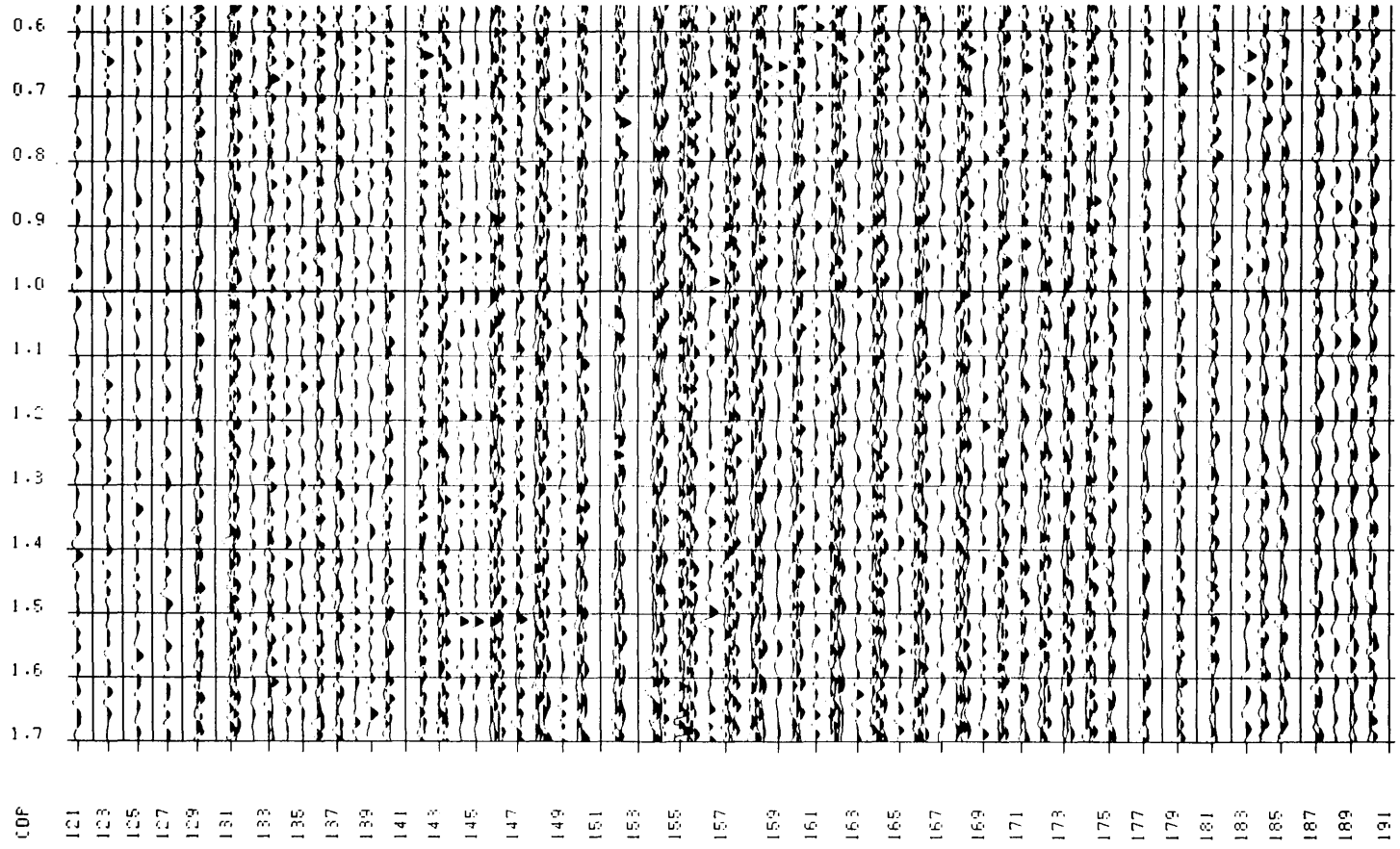

Fig. 3.39 SK-4 detail of CDP gather. CDPs are bins used in 'crooked line' processing, at an average spacing of 7.5 m. One dummy trace (vertical line) fills each empty bin. One trace has been binned three times (CDPs 144-146). Below 1 s or so the move-out should be negligibly small, so that static corrections can be checked; however there are no prominent reflectors with which to check the accuracy (or otherwise) of the static shifts.

corresponding to each can be seen in Figure 3.39 as the first three traces (in order 130, 131, 133 respectively) of even-numbered CDPs 158 to 174. Record no. 130 used 8 sticks of gelignite as a point source, whereas no. 131 used 8 sticks in two groups of four separated by 65 m, with a delay of 9 ms applied to detonation of the group nearer the spread. The aim of the latter configuration is to see whether ground roll is cancelled more effectively (see section 2.2.6 above). However, both records are similar.

Record no. 133 used 40 m of Geoflex buried in a shallow trench. Relative to the air blast, the amplitudes of both first breaks and ground roll seem to be lower than with shots 130 and 131, but in the absence of any strong characteristic reflector it is difficult to quantify whether the relative amplitude of reflections is greater with the line source than with the conventional point source. However, it is clear from the CDP gather display that stacking of these three records will add some events constructively and cancel some others.

The low fold of CDP coverage makes velocity analysis by semblance plots difficult. Although we can put a number of adjacent CDPs into the semblance analysis, the one- or two-fold coverage over much of the line means that we are effectively doing semblance plots on shot gathers, and that structure (especially dip) may substantially alter the results. As a compromise, 5 CDP ranges are chosen to use all the traces on the line (refer to Figure 3.38):

(1) CDPs 21-43 (i.e. simply a gather of shot 126),

(2) CDPs 64-97 (overlapping coverage of two shots),

(3) CDPs 108-157 (several shots over 375 m of subsurface),

(4) CDPs 158-197 (about 70 traces over 300 m of subsurface),

(5) CDPs 198-240 (30 traces over 323 m).

As expected the plots of (1), (2) and (5) simply give semblance maxima where correlations that can be seen by inspection across the traces have been flattened for a given, but not necessarily meaningful, NMO correction. The two plots of groupings (3) and (4) are shown in Figure 3.40. These show plausible semblance peaks down to 1.5 s or so, but no clear trend can be made out. There is merely a suggestion that RMS velocities increase from around 2.1 - 2.2 km/s at 0.5 - 0.6 s to greater tham 3 km/s at 1.5 - 1.6 s.

12 constant-velocity stacks are shown in Figure 3.41A-C. These show that the structure below 0.5 s is very steep, hence accounting for the poor quality of the semblance plots. Picking of well-stacked events on these constant-velocity plots concentrates on the areas of multiple subsurface coverage, since an event line-up on the areas of single-fold coverage remains lined up across all the plots - only its dip changes, and we have no a priori information on what the actual dip is. A 1-dimensional velocity function is chosen from the constant-velocity displays, to be used in the final stack. It is as follows:

TABLE 3.5
SK-4 VELOCITIES AND DEPTHS

Time (ms)	V(rms) (m/s)	V(int) (km/s)	Thickness (km)	Depth (km)
450	2600	2.60	0.58	0.58
650	2750	3.06	0.31	0.89
1100	3100	3.55	0.80	1.69
1600	3300	3.70	0.93	2.61
2500	3600	4.08		
6000	5000	5.80		

The final stack display, which incorporates some time-varying filtering, is shown in Figure 3.42. Its 'ringy' appearance is due to the very narrow bandpass of these filters. Although reflection quality is poor, a number of events, mostly of steep dip, can be seen as deep as 3 s. Their origin - whether or not they are primary real reflectors - is discussed in Chapter 4.

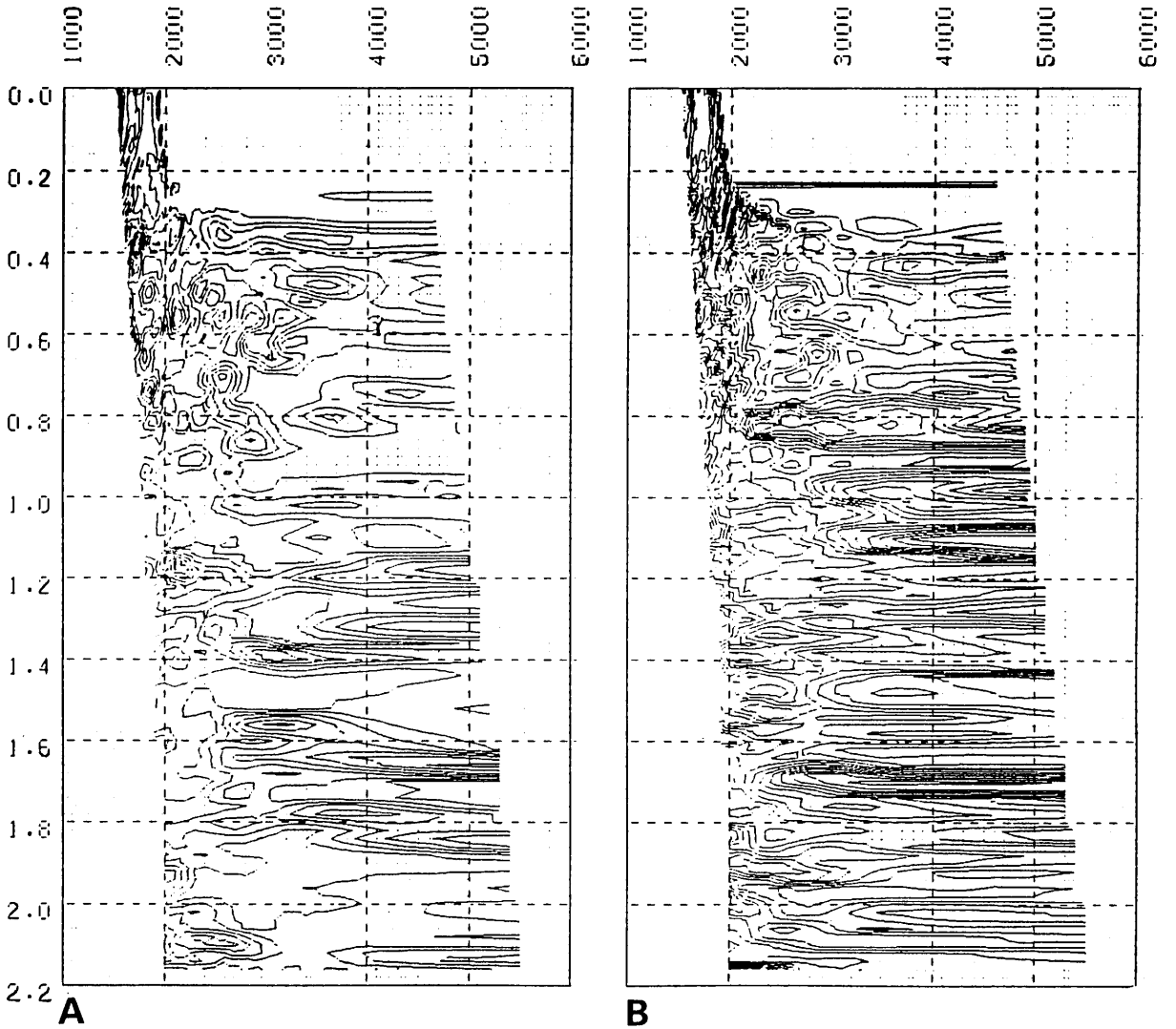

Fig. 3.40 SK-4 semblance plots.
A. CDPs 108-157 (several shots over 375 m subsurface).
B. CDPs 158-197 (about 70 traces over 300 m subsurface).
Other combinations of trace gathering attempted either have too few shots, or too much subsurface coverage; both of these result in semblance plots in which move-out is dominantly structural rather than hyperbolic (and thus diagnostic of rms velocity).

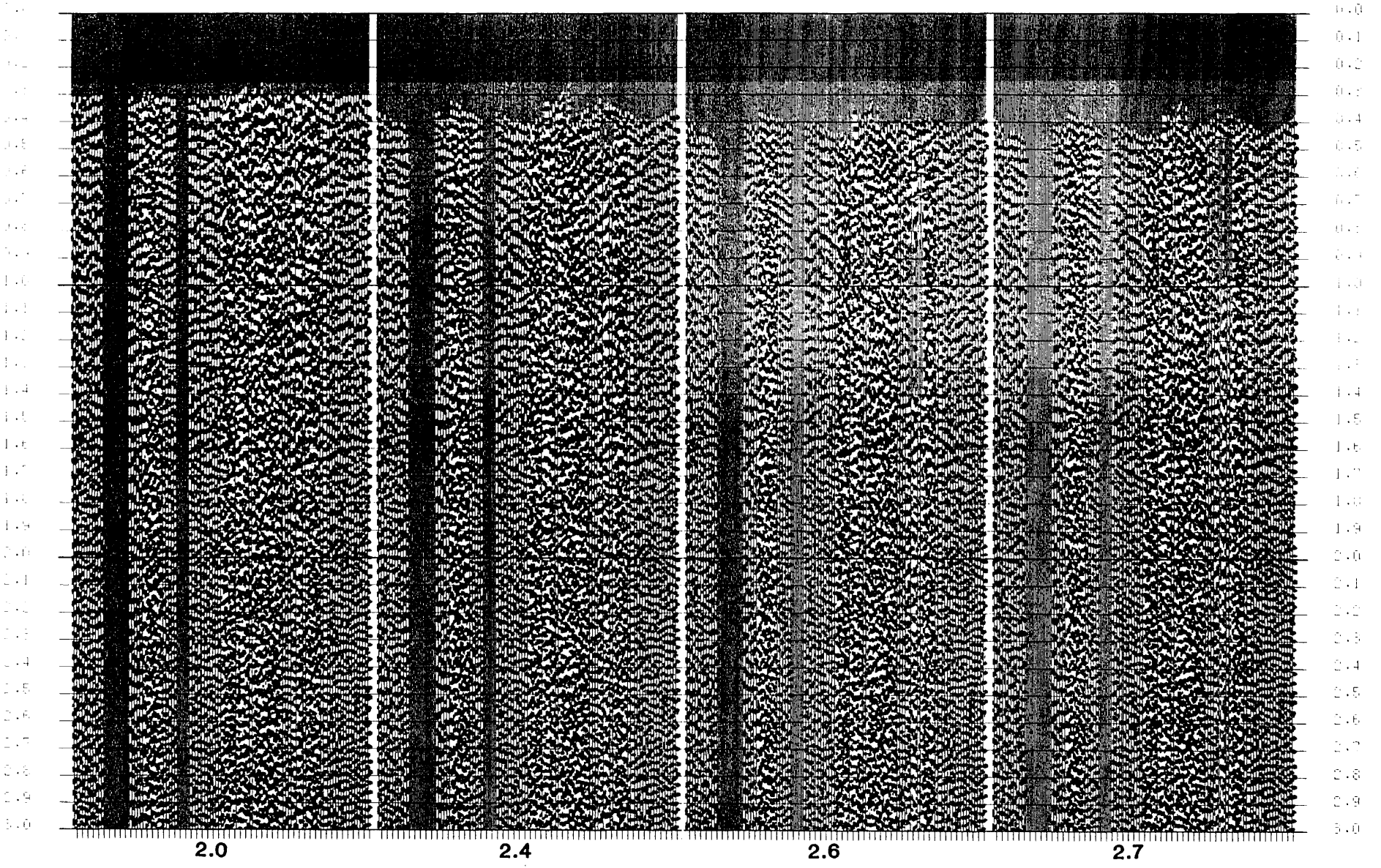

Fig. 3.41A SK-4 constant velocity stacks (velocity in km/s beneath each panel).

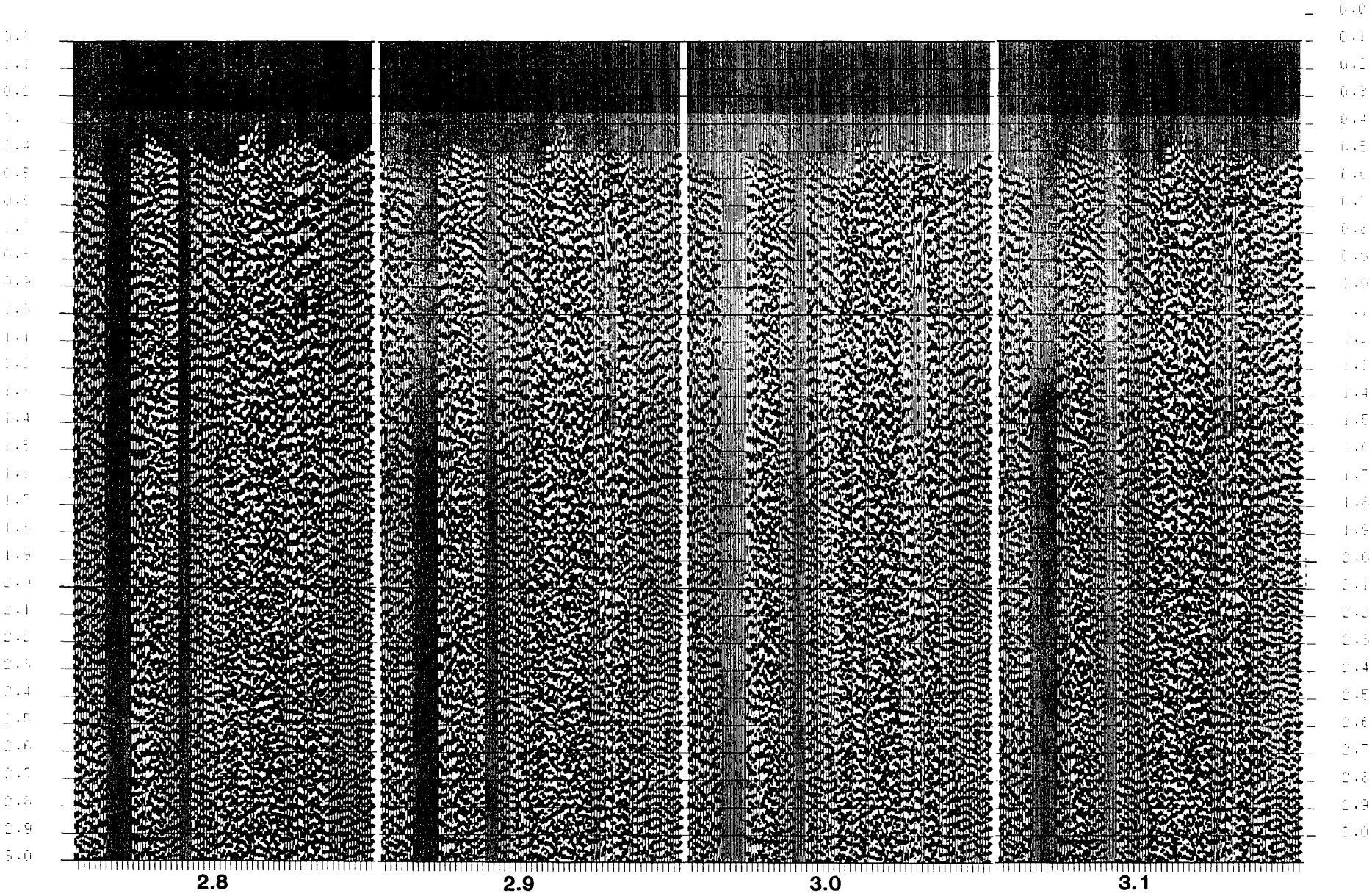

Fig. 3.41B SK-4 constant velocity stacks (velocity in km/s beneath each panel).

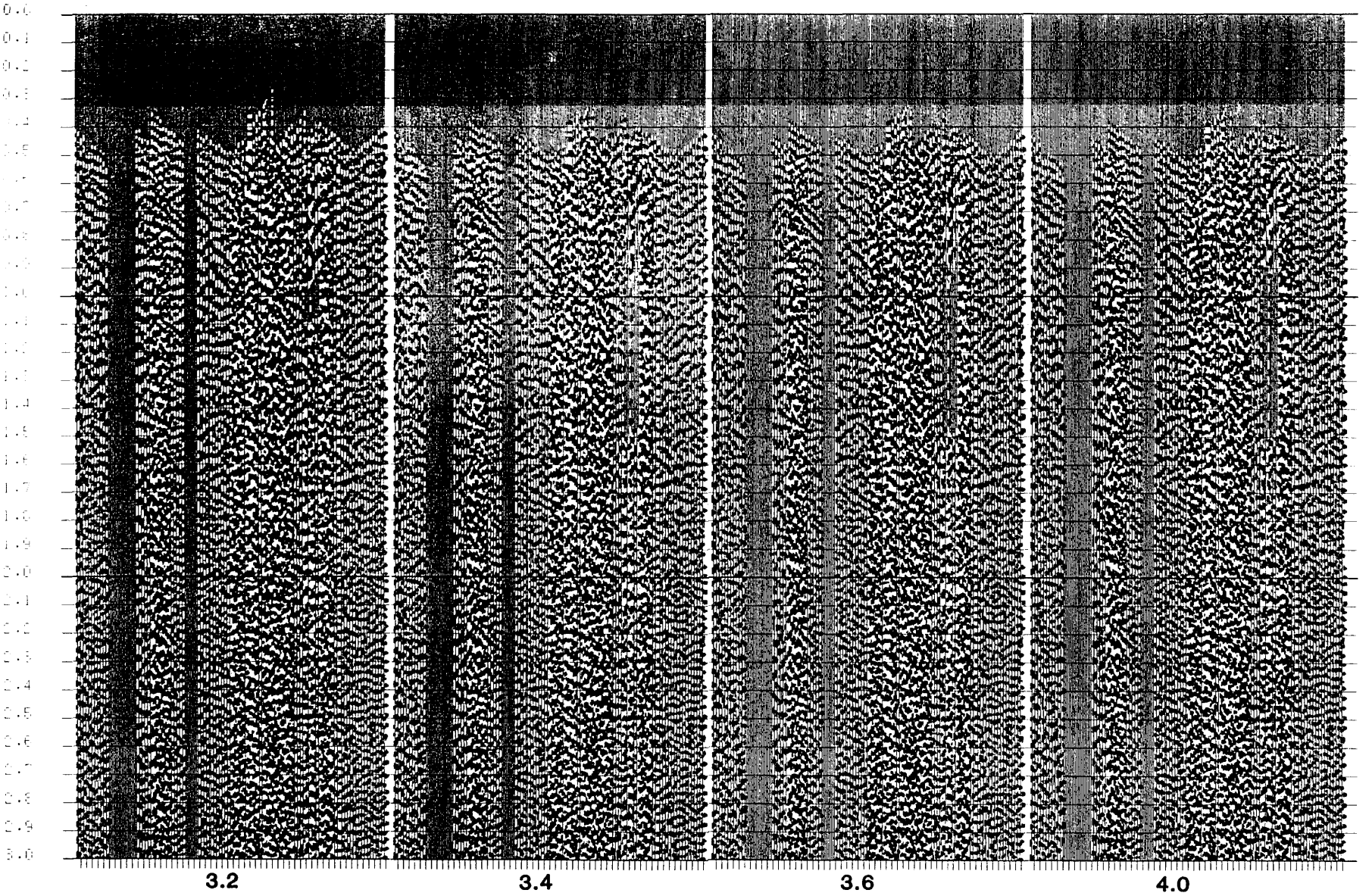

Fig. 3.41C SK-4 constant velocity stacks (velocity in km/s beneath each panel).

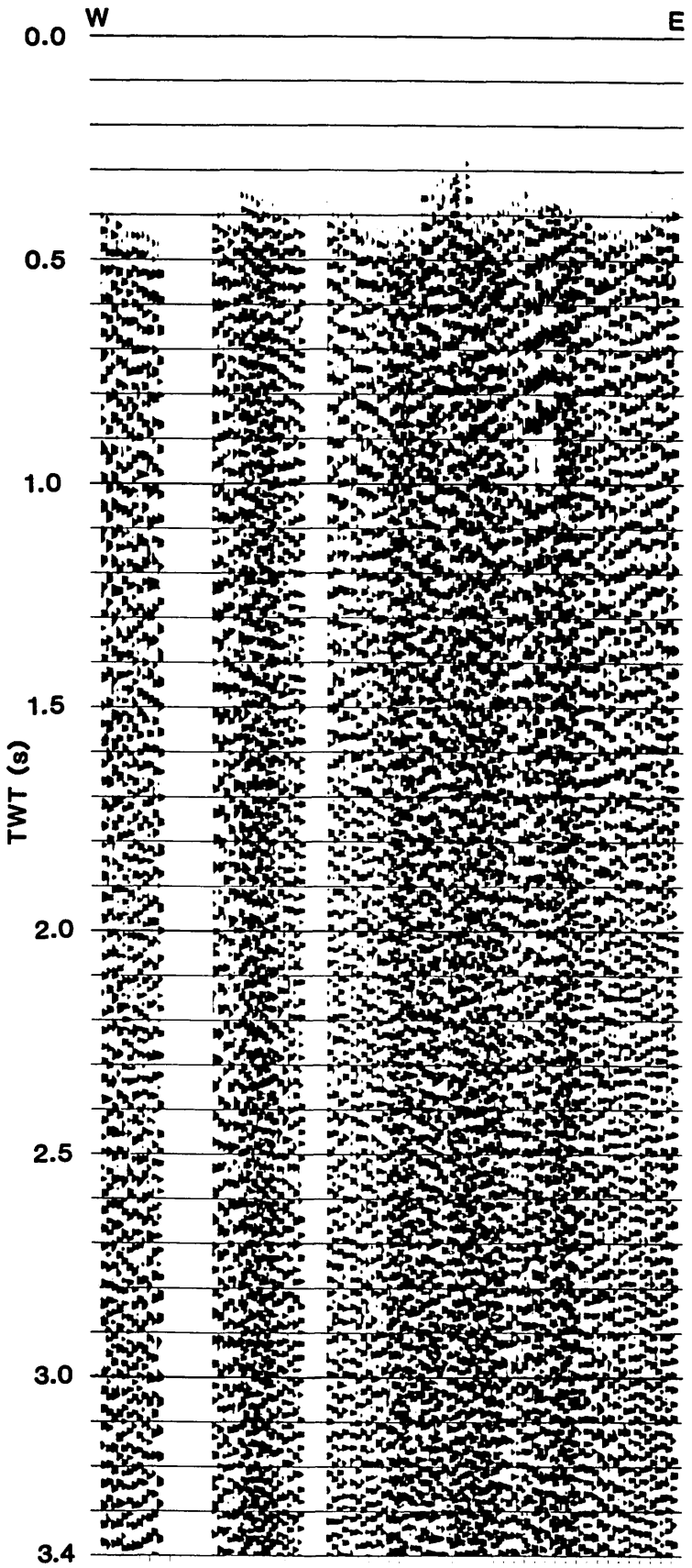

Fig. 3.42 SK-4 final stack, using velocities shown in Table 3.5. Zero phase bandpass of 15-45 Hz, followed by robust AGC, has been applied.

3.1.4.7 Line SK-5 (Waterstein)

The subsurface coverage of this velocity survey site is shown in Figure 3.43. Both single and double spreads were used (receiver group intervals of 15 and 30 m, respectively). Maximum offset is 1155 m, and the subsurface coverage spans a nominal 825 m, with a fold of up to 8. Crooked line geometry processing leads to all 300 traces of the 25 production shots being binned, with two traces binned twice. Six shot records were omitted from the processing; these comprise 5 test shots and 1 record for which the analogue tape appears to have been wiped.

The CDP gather (of which Figure 3.44 shows part) does not reveal any apparent problem with the static corrections that have been applied. Reflection energy, relative to other unwanted signal, is clearly low - presumably a consequence of shooting through thick sills - but some reflection-like events can be seen on some of the CDP gathers with a reasonable fold of cover; for example, CDPs 69 - 71, at 550 ms or so (Fig. 3.44).

A suite of 12 constant velocity stacks of the first 3 s of data is shown in Figure 3.45A and B. The reflections that can be discerned are weak, and obscured by coherent noise crossing the displays at 10-20 ms/trace. The events, which seem to be of low dip, stack best at the following velocities and times:

Velocity (km/s)	Two-way time (s)
2.7 - 3.0	0.6
2.8 - 2.9	0.9
2.9 - 3.2	1.5
?3.4 - 3.8	?2.0

The apparently low dips of the desired primary events permit some FK-domain filtering; this is done on shot gathers, removing dips of greater than 6 ms/trace in either direction. The processor used here does not permit double-binned or incomplete shot gathers, as it has been designed for regular (marine) geometries; fortunately this requirement only entails the removal of one trace from each pair of double-binned traces. A revised suite of constant

Fig. 3.43
SK-5: Subsurface coverage and offset diagram

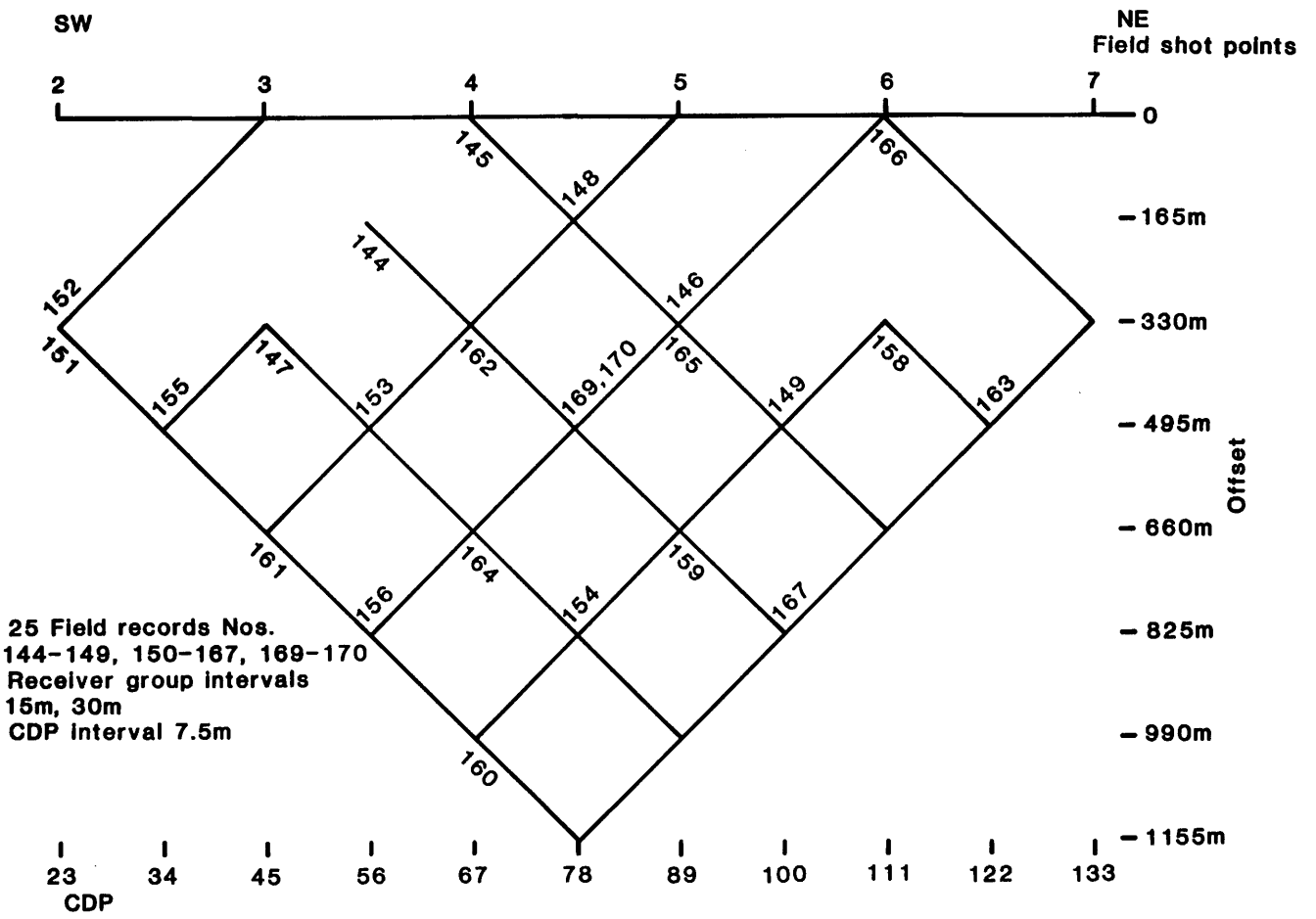

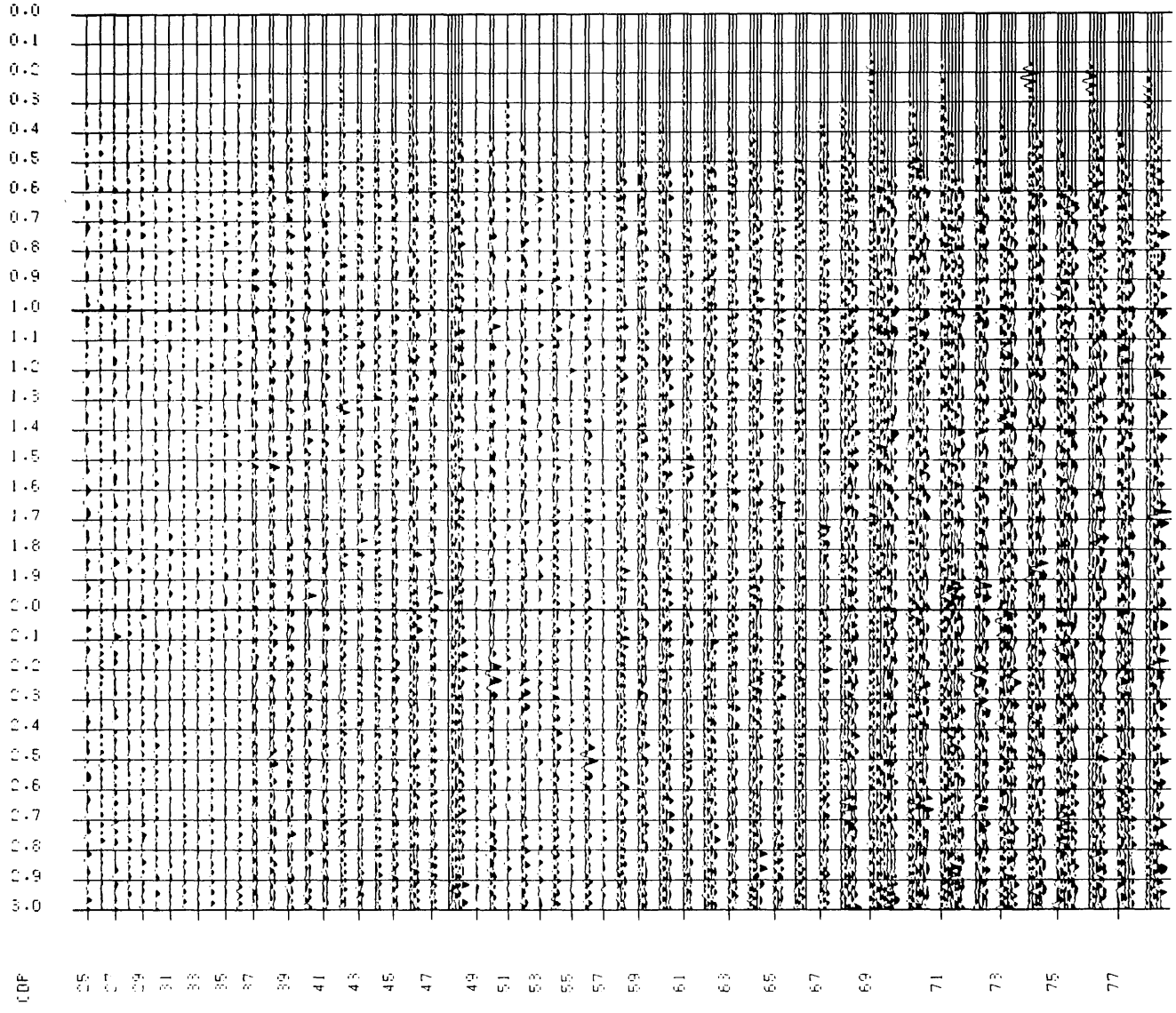

Fig 3.44 SK-5 CDP gather of southern part of line; fold of coverage varies from 1 (CDPs 25-36) to 8 (e.g. CDP 69). CDPs are bins at a mean 7.5 m spacing, designed by 'crooked line' field geometry processor. Note probable reflector at 0.55 s, CDPs 69-71, where the fold of cover is greatest.

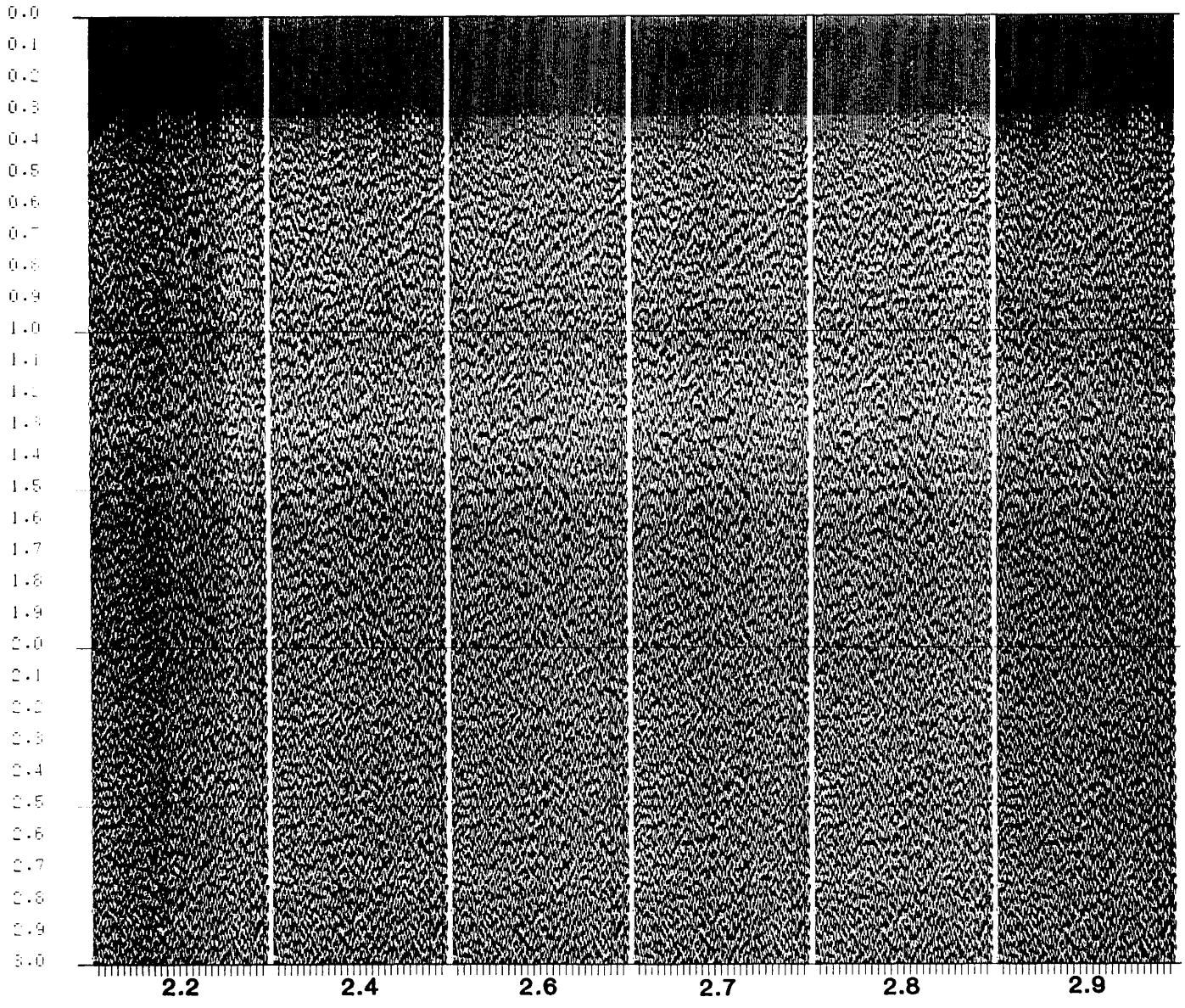

Fig. 3.45A SK-5 constant velocity stacks (velocity in km/s beneath each panel).

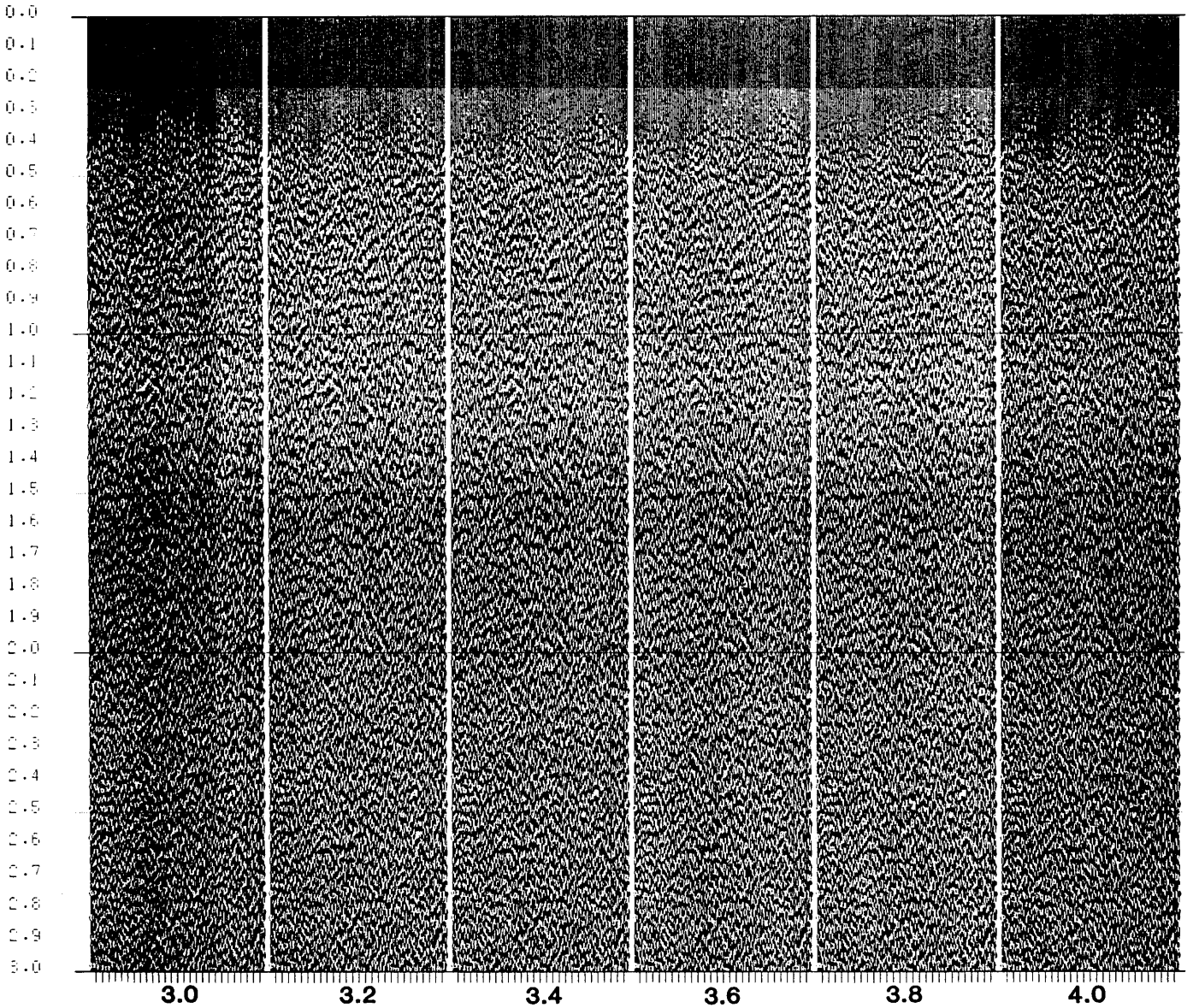

Fig. 3.45B SK-5 constant velocity stacks (velocity in km/s beneath each panel).

velocity gathers using this dip filtering is shown in Figure 3.46. Despite a chequerboard effect due, presumably, to aliased dipping events not having been removed by the dip filter, the displays are much cleaner.

A suite of 5 semblance plots, using all the traces, is shown in Figure 3.47. These do not have the dip filter applied. Although there is plenty of coherent energy stacking up on each of these gathers,there is very little consistency of semblance peaks from one gather to the next. The near-horizontal attitude of the presumed reflectors seen on the constant velocity stacks suggests that all traces can be binned to make one semblance plot, even though this will encompass some 825 m of subsurface coverage. Figure 3.48 shows three such plots. The first (Fig. 3.48A) is a semblance plot of the entire data set, without FK domain dip filtering. There are a number of plausible RMS peaks to choose from on this display, but it is not possible, for example, to decide that certain low-velocity events are multiples and can therefore be removed by the process of FK domain multiple attenuation. The corresponding semblance plot after the application of FK domain dip filtering on the shot gathers is shown in Figure 3.48B. This plot is somewhat cleaner than 3.48A, but no clear velocity trend emerges. An attempt to use a larger window of the trace over which semblance is calculated is shown in Figure 3.48C. The trace window here is 80 ms and 120 ms long, above and below 2000 ms, respectively. This does not result in a clearer display, compared with the standard 40 ms window; presumably the reflection wavelet is not much longer than 40 ms or so.

The semblance plot with FK dip filter and standard window length (Fig. 3.48B) is used to pick stacking velocities; these picks are shown in Figure 3.49. A choice of high velocity at shallow depth (shown by the two diamonds on Fig. 3.49) might seem plausible, comprising sills of P-wave velocity 5.5 km/s, heavily intruded into (baked) sediments of, say 2.5 - 3.0 km/s; however, this is rejected, because:

(1) There would be an impossible velocity inversion beneath the bottom of this high velocity interval, at about 0.55 s.

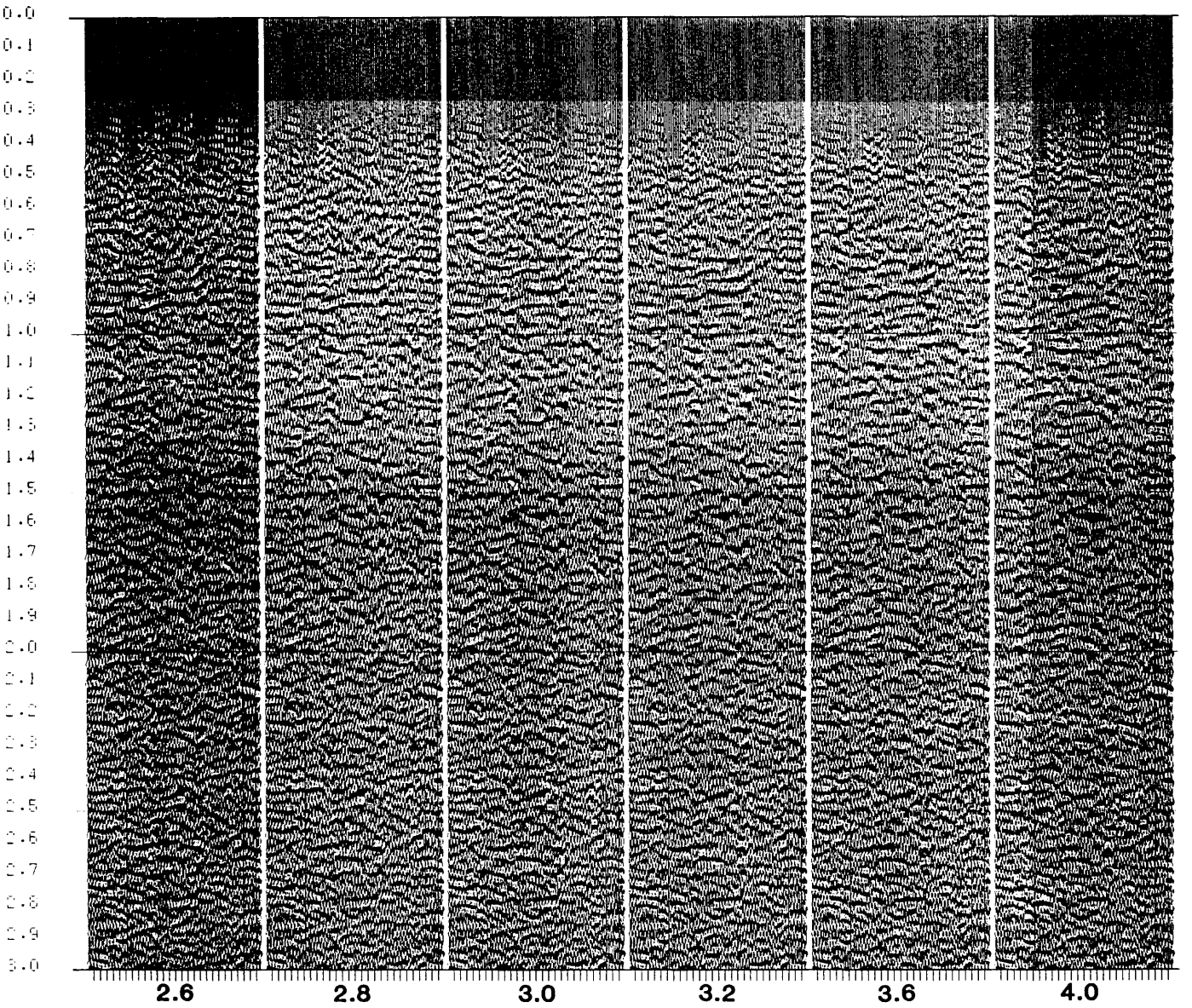

Fig. 3.46 SK-5 constant velocity stacks, after FK domain coherency filtering on each shot gather to remove steeply dipping events. Velocity is shown (in km/s) beneath each panel.

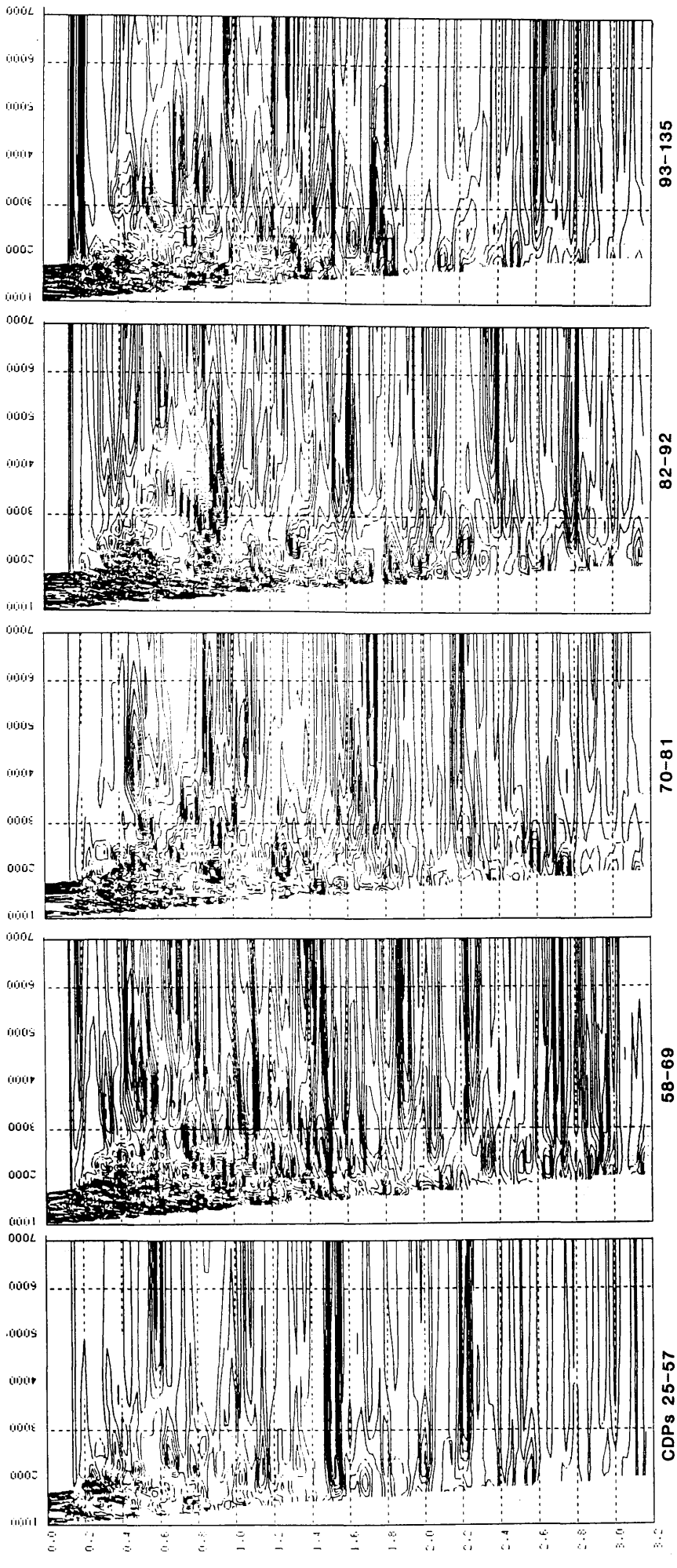

Fig. 3.47 SK-5 semblance plots of five ranges of CDP coverage; no dip filter on shot records applied.

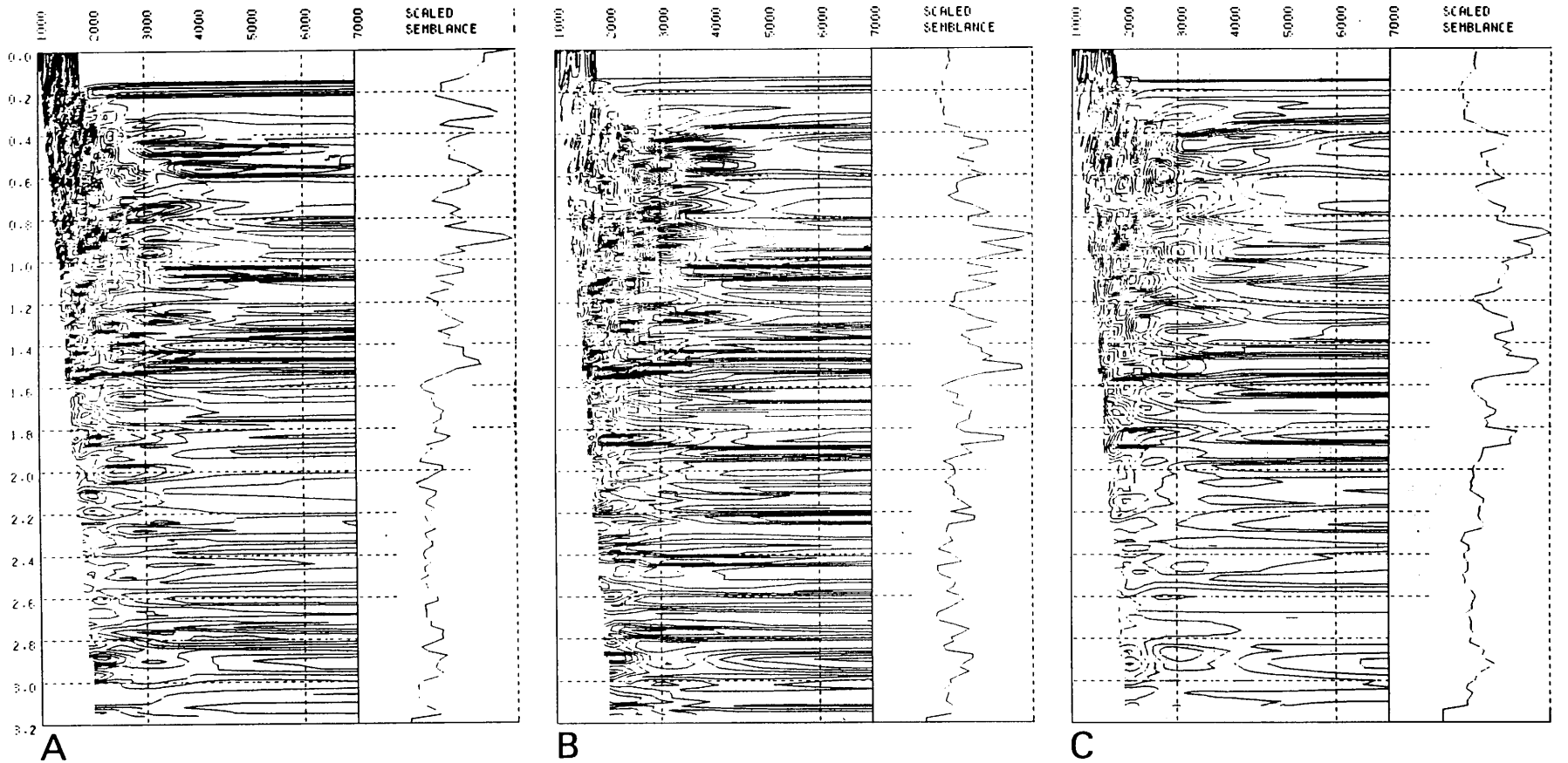

Fig. 3.48 SK-5 semblance plots using all available traces.
A. No FK domain dip filter applied. Standard window length of 40 ms used in semblance calculation
B. FK domain dip filter applied to shot gathers. Standard window for semblance calculation.
C. FK domain dip filter applied to shot gathers; trace windows for semblance calculation - 80 ms (0-2000 ms), 120 ms (below 2000 ms).

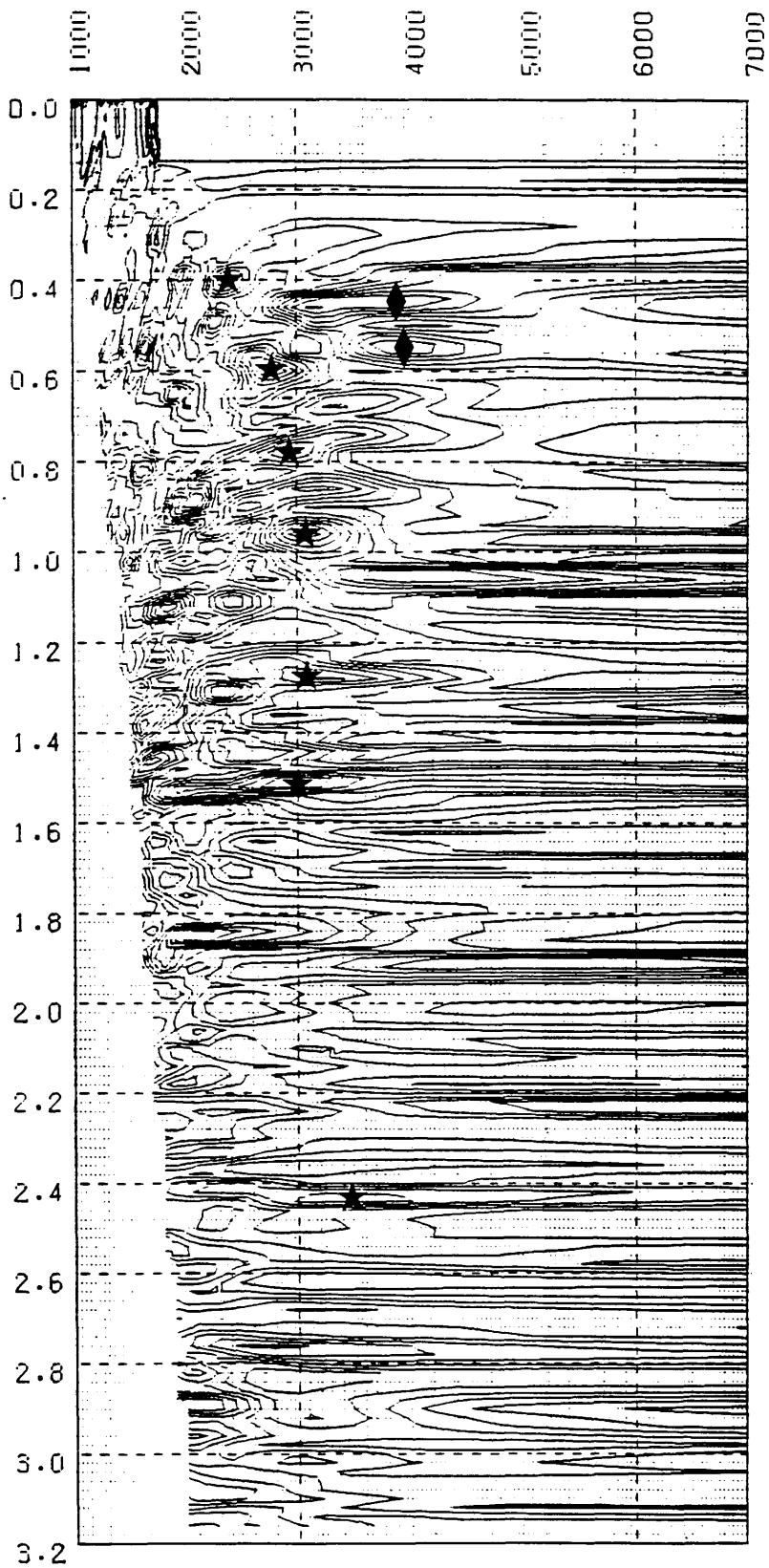

Fig. 3.49 SK-5 semblance plot after FK domain filtering on shot gathers; standard 40 ms window length used for semblance calculation (same display as Fig. 3.48B). Diamonds indicate high possible stacking velocities, but are rejected (see text) in favour of velocity curve shown by stars.

(2) The constant velocity stacks do not support the possibility of such high velocities within the first half second or so.

The stacking velocity curve chosen starts with a low interval velocity, and is shown by the stars on Figure 3.49. It gives the following interval velocities and depths:

TABLE 3.6
SK-5 VELOCITIES AND DEPTHS

Time (ms)	V(rms) (m/s)	V(int) (km/s)	Thickness (km)	Depth (km)
400	2400	2.40	0.48	0.48
600	2750	3.34	0.33	0.81
780	2950	3.54	0.32	1.13
950	3050	3.47	0.30	1.43
1280	3050	3.05	0.50	1.93
1530	3000	2.73	0.34	2.27
2420	3500	4.22	1.88	4.15

The data are stacked using the velocities in Table 3.6, and the result is shown in the panels in Figure 3.50. The leftmost panel shows the chequerboard effect of the FK filter, which can easily be removed by the simple expedient of summing adjacent pairs of traces. This is shown in the second panel. The narrower panels to the right show the effect of summing 3, 4, 6 and 10 traces respectively, but no additional improvement in the stack results from these. The final stack chosen therefore, is the one with the 2-trace sum, and thus covers 825 m of subsurface at a 15 m CDP interval.

Figure 3.51 compares the display with relatively broad-band filtering (10 - 60 Hz) on 3.51A, and narrow-bandpass filtering on 3.51B. As most of the shots were recorded using an analogue low-cut filter of 22 Hz, the high-cut of 40 Hz applied on 3.51B, in an attempt to remove higher frequency noise, tends only to degrade the whole display into a characterless 'ringing', or (literally) monotonous appearance. Nevertheless, there appear to be reflectors down to 2.4 - 2.5 s.

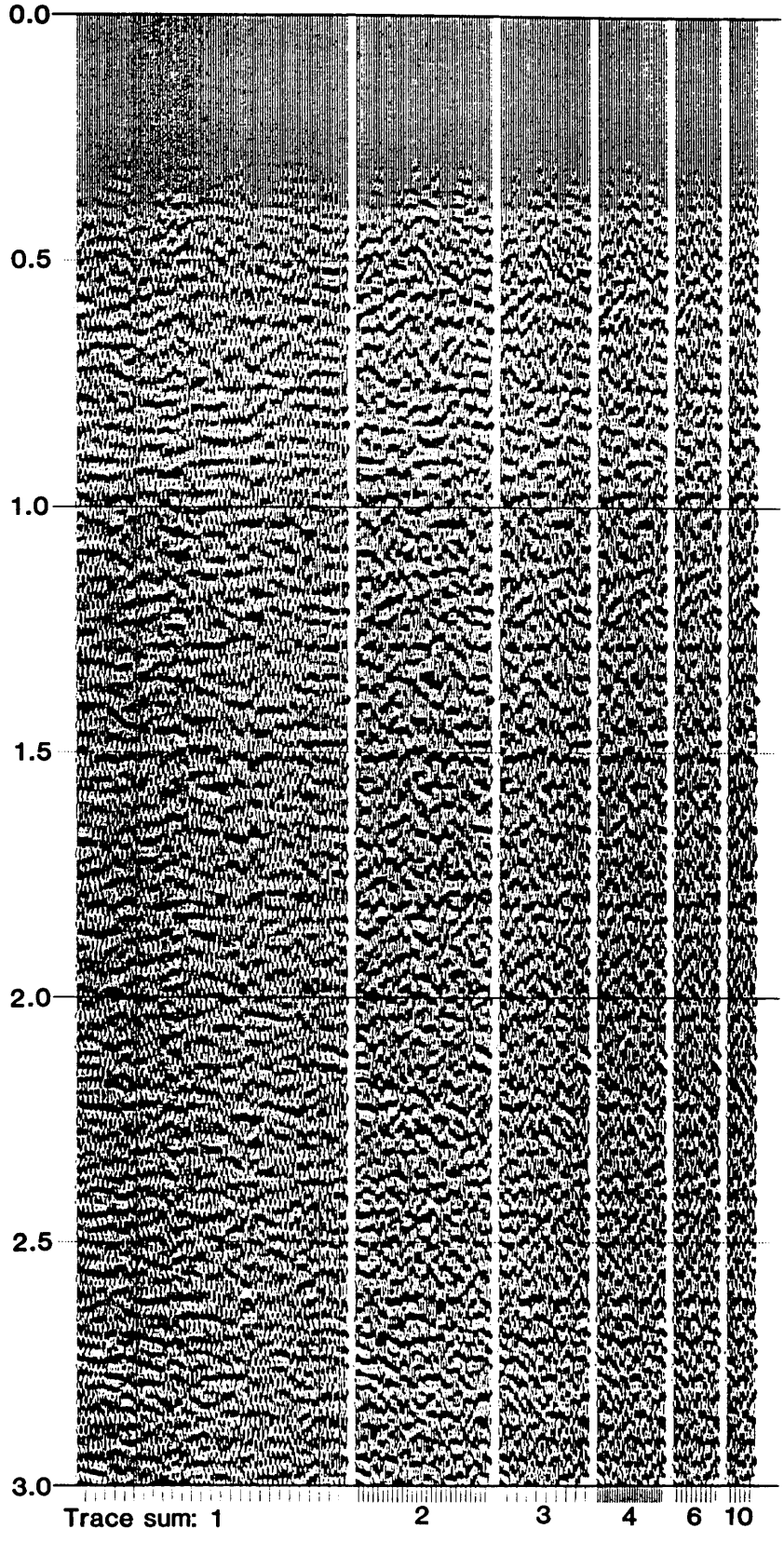

Fig. 3.50 SK-5 final stacks with progressively greater trace summation. Note the chequerboard effect on the leftmost display, due to the FK filter, which is removed by the 2-trace sum.

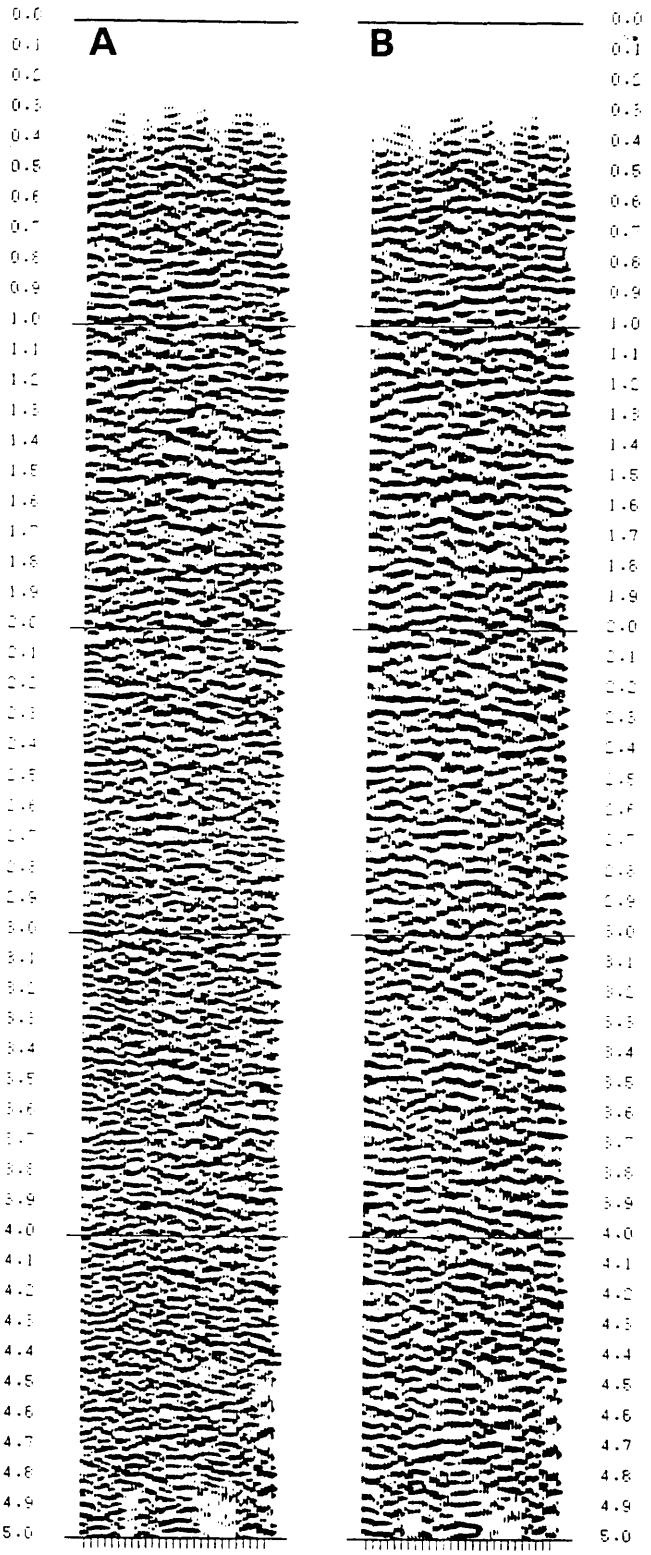

Fig. 3.51 SK-5 final stacks with different post-stack bandpass filtering. Most of the shot records making up the stack have an analogue low-cut filter of 22 Hz.
A. Broad bandpass filter, 10-60 Hz.
B. Narrow bandpass filter, 15-40 Hz.

3.1.4.8 Line SK-6 (Edinbane)

Edinbane is the only 'velocity survey' site on basalt. Very large charges were used here - up to 20 kg per shot, distributed in a line of 40 - 50 holes. Out of the 18 records made, only 10 are production shots, using the large source and offsets of up to 2 km. Figure 3.52 shows the subsurface coverage, which after straight line binning, taking into account mean shot positions of the linear shot arrays, results in a 510 m length of coverage from CDPs 22 to 80, at a CDP spacing of 7.5 m. There is a gap in the middle of this coverage, and fold is up to 5.

The large shots and offsets are designed to define the base of the basalts (at least), and if possible penetrate to the underlying sedimentary section.

The non-NMO corrected CDP gather (Fig. 3.53) shows good trace-to-trace correlation, with plenty of signal. The field statics applied are the elevation correction to shots and receivers, to reduce the terrain to a sea level datum, with a reduction velocity of 4.7 km/s.

Semblance plots of the two separate patches of CDP coverage (22-47 and 57-80, respectively) are disappointing, in that they show poor correlation between each other. However, they indicate stacking velocities in excess of 3 km/s throughout. A suite of constant velocity stacks, covering the range 3.2 - 5.2 km/s at an interval of 0.2 km/s, is shown in Figure 3.54. This set of tests is also disappointing, being dominated by a lot of stacked-in ground roll criss-crossing the displays at dips of about 4-5 ms/trace.

Figure 3.55A shows a semblance plot of the entire coverage of 120 traces. It shows a very well defined peak at 700 ms and a velocity of 4800 m/s, which may be the base of the basalts. Below that (coloured in red) there are a number of possible primary-reflector peaks, confused by many more peaks (coloured orange), which are probably from correlations of unwanted signals; some of these have a period of 700 ms, one below the other, and may, therefore, represent peg-leg multiple reflections within the

Fig. 3.52

SK-6: Subsurface coverage and offset diagram

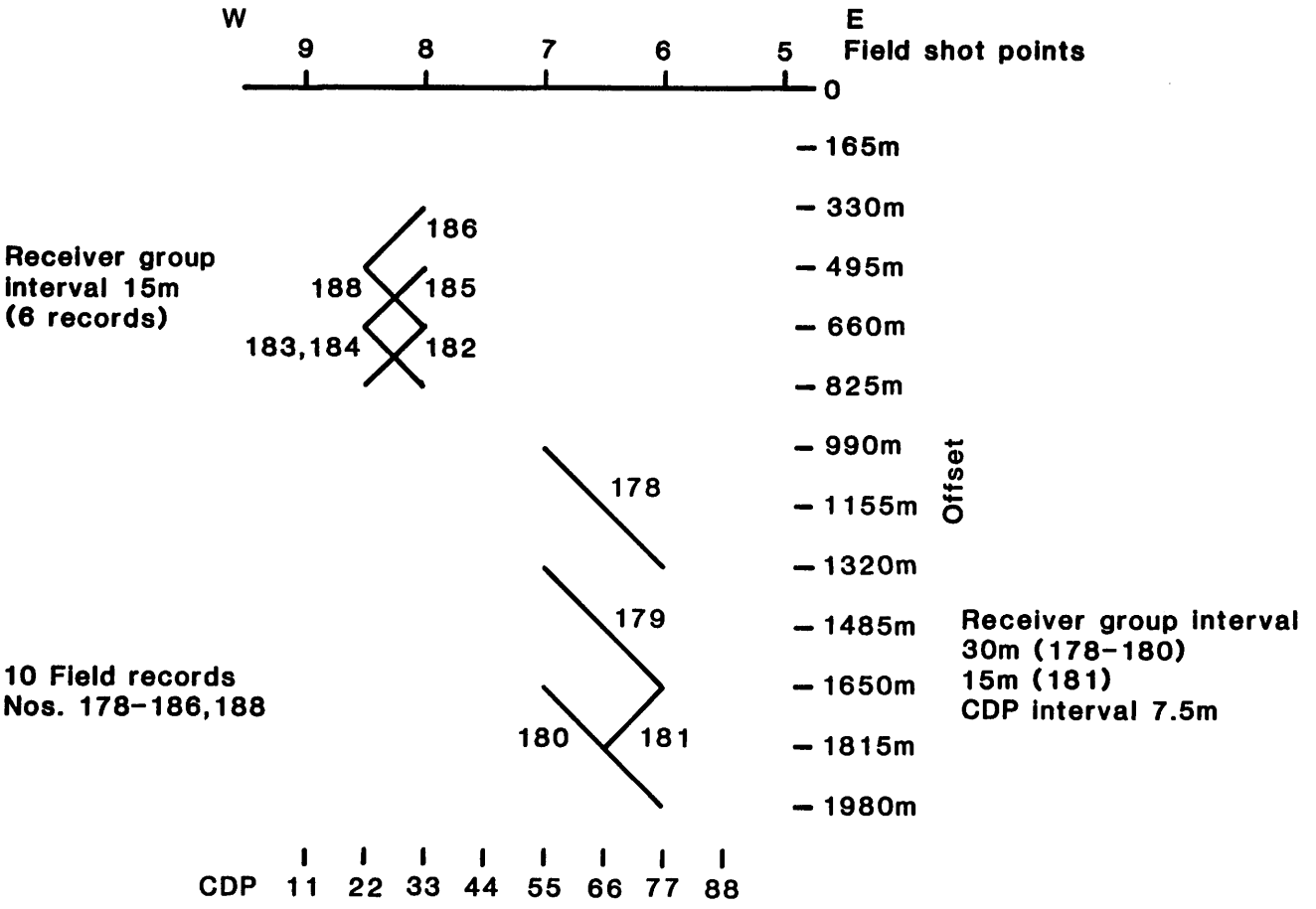

Fig. 3.53 SK-6 trace gather, CDPs 22-80 (whole data set). Field static corrections have been applied, but no NMO correction. Dummy traces are inserted for CDPs 48-56 inclusive.

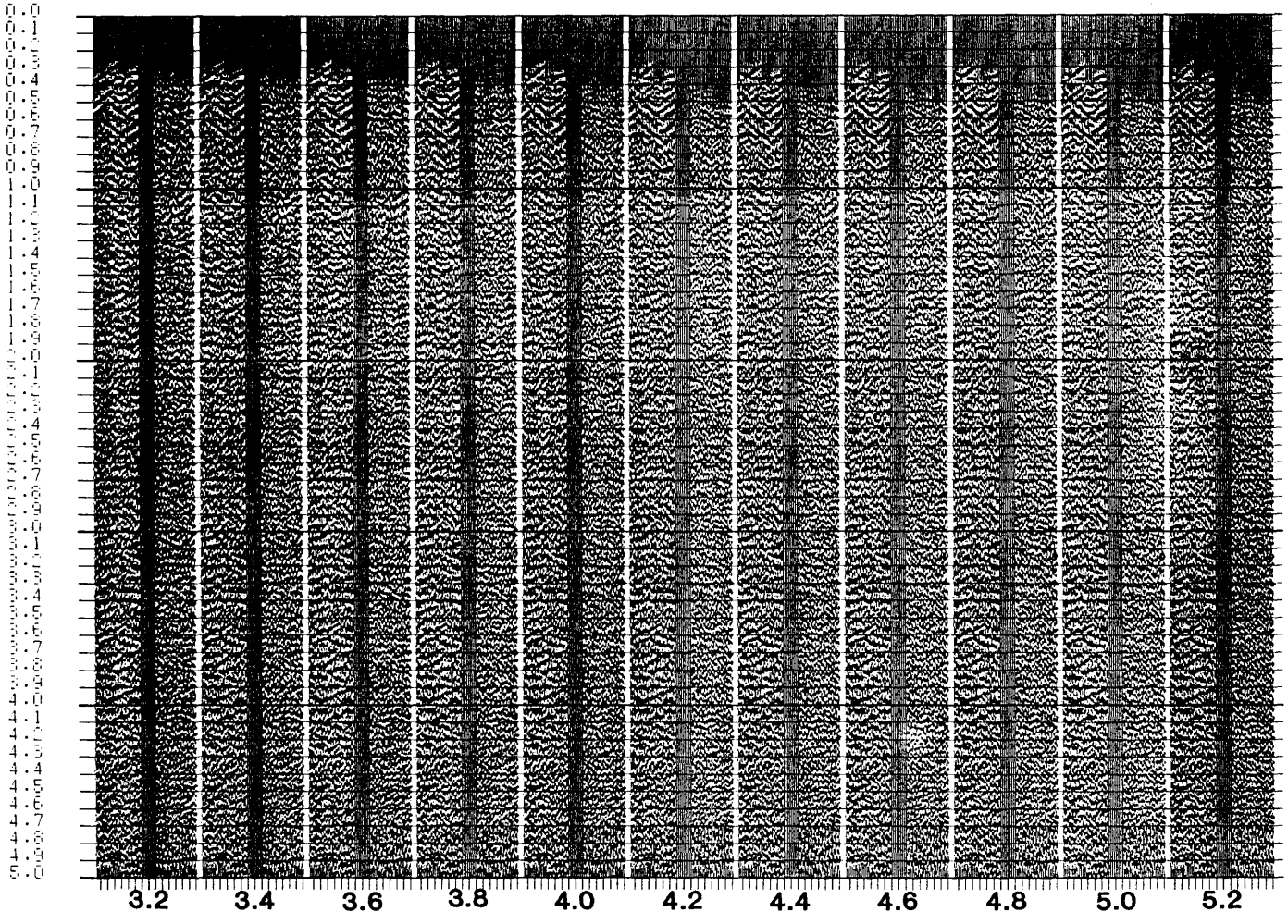

Fig. 3.54 SK-6 constant velocity stacks (velocity in km/s shown below each panel. The predominant criss-cross events present on all panels are due to ground roll.

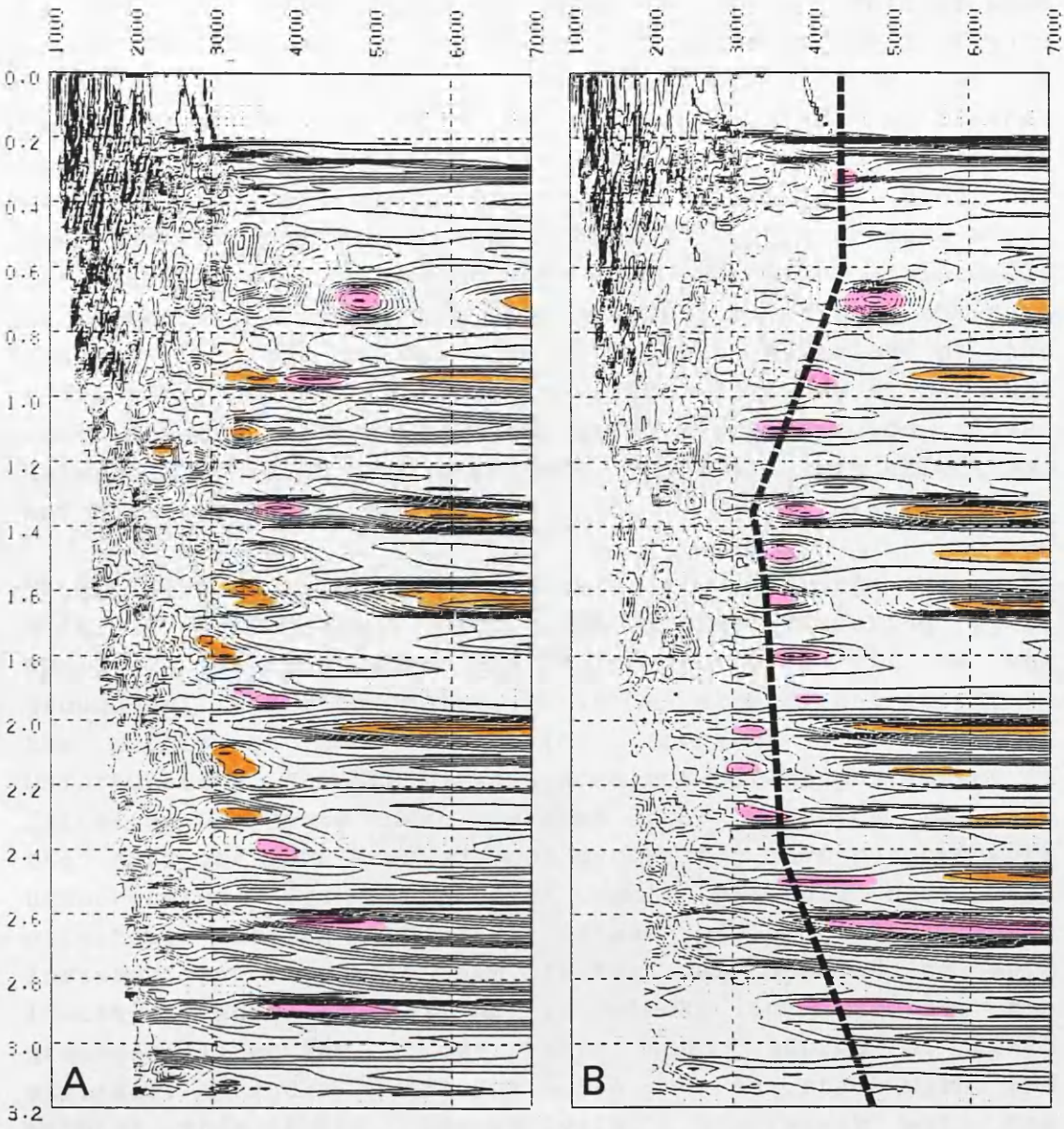

Fig. 3.55 SK-6 Semblance plots for the whole data set of 120 traces. Probable primary reflection peaks are shown in red, whereas multiples are shown in yellow.
A. Display without multiple attenuation. Note the strong peak at 4800 m/s, 0.7 s, probably from the base of the basalts.
B. Display after FK domain multiple attenuation carried out with the intermediate NMO correction curve shown by the dashed line. Events which are over-corrected at this NMO (i.e. they have stacking velocities to the left of the line) are removed by FK filtering.

high-velocity basalt layer at the surface.

Some of the lower (stacking) velocity energy can be removed by multiple attenuation in the FK domain. This is done using the intermediate NMO correction curve, shown in Figure 3.55B as the dashed line, superimposed on the spectrum resulting after this technique has been applied. A cleaner velocity spectrum is the result, from which a stacking velocity curve can now be picked. The semblance plot has the curious phenomenon that nearly every primary event (coloured in red) is paired with an event with essentially no moveout - i.e. very high stacking velocity - shown in orange. This may be due to a spatial aliasing of the reflectors, since the CDP coverage is empty at zero and small offsets. There is therefore no constraint on 'flat' hyperbolae having high semblance. However, this effect has not been studied in detail.

Figure 3.56 shows two final stacks, each with the same FK multiple attenuation and time-variant filtering (TVF) applied. TVF after stack has failed to remove all of the ground-roll and other noise, as it has significant energy in the middle of the reflection spectrum (15-50 Hz). Unfortunately, the SKS package does not permit post-stack FK filtering to remove these unwanted dips; attempts to turn the data set into a pseudo-CDP gather for this purpose were unsuccessful. Such a process would probably have been effective across the final stack of 51 live traces. Instead, an FK-domain fan filter was applied to each 12-trace shot gather before stack, to attenuate the ground-roll moving across these shot records at 10-15 ms/trace. Figure 3.56B and 3.56A show the stack with, and without, this filter, respectively. The stack with the filter shows better reflections at all depths, without having introduced spurious events, and is therefore to be preferred.

The final stack, with FK fan filtering, multiple attenuation, and post-stack TVF (Fig. 3.56B), is shown in Figure 3.57 alongside the semblance plot, so that correlation of reflectors and semblance peaks may be made. The stars on the latter indicate the position of the velocity curve used for stacking. It gives the following

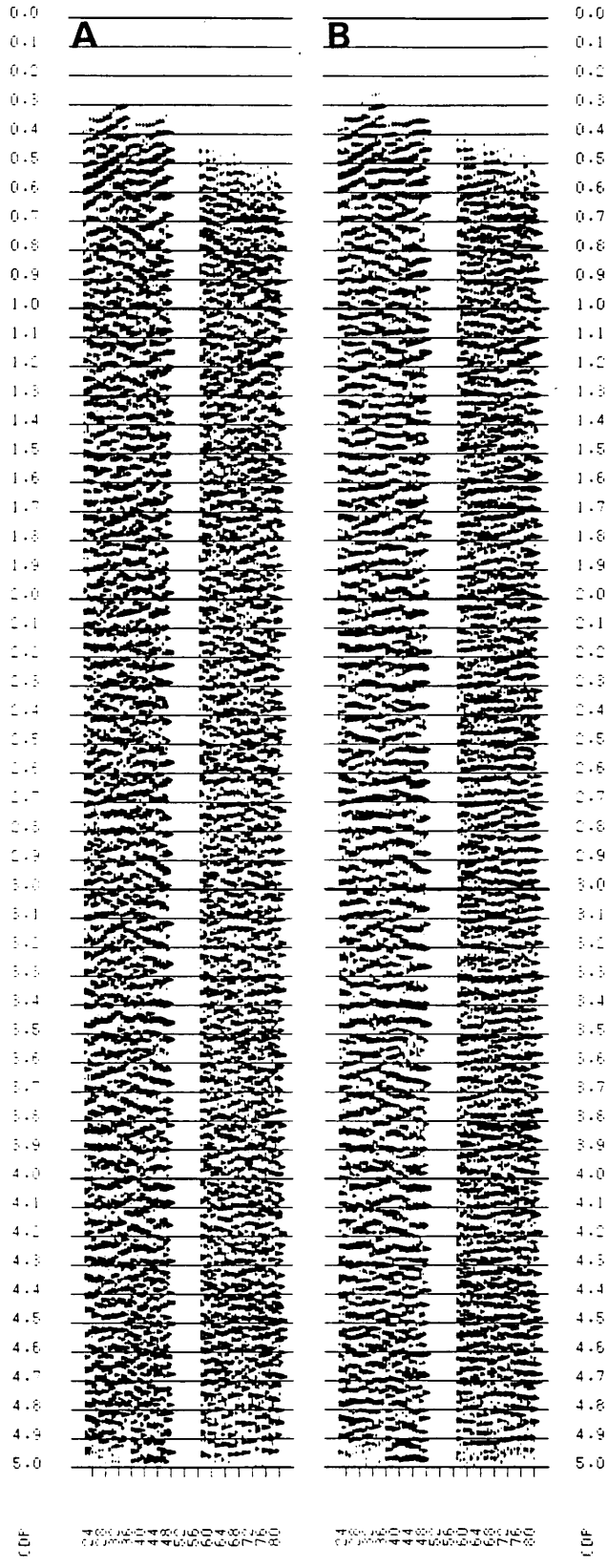

Fig. 3.56 SK-6 final stacks of 51 live traces; the variable area display is designed so that dummy traces and very low amplitude portions of traces are not displayed, hence the gap in the centre of each display.
A. Final stack without FK domain filter. FK multiple attenuation, post-stack bandpass filtering (15-50 Hz), and robust AGC have been applied.
B. Final stack as in A, but an FK domain fan filter has been applied to shot records in addition, to remove events moving across the records with low apparent velocity.

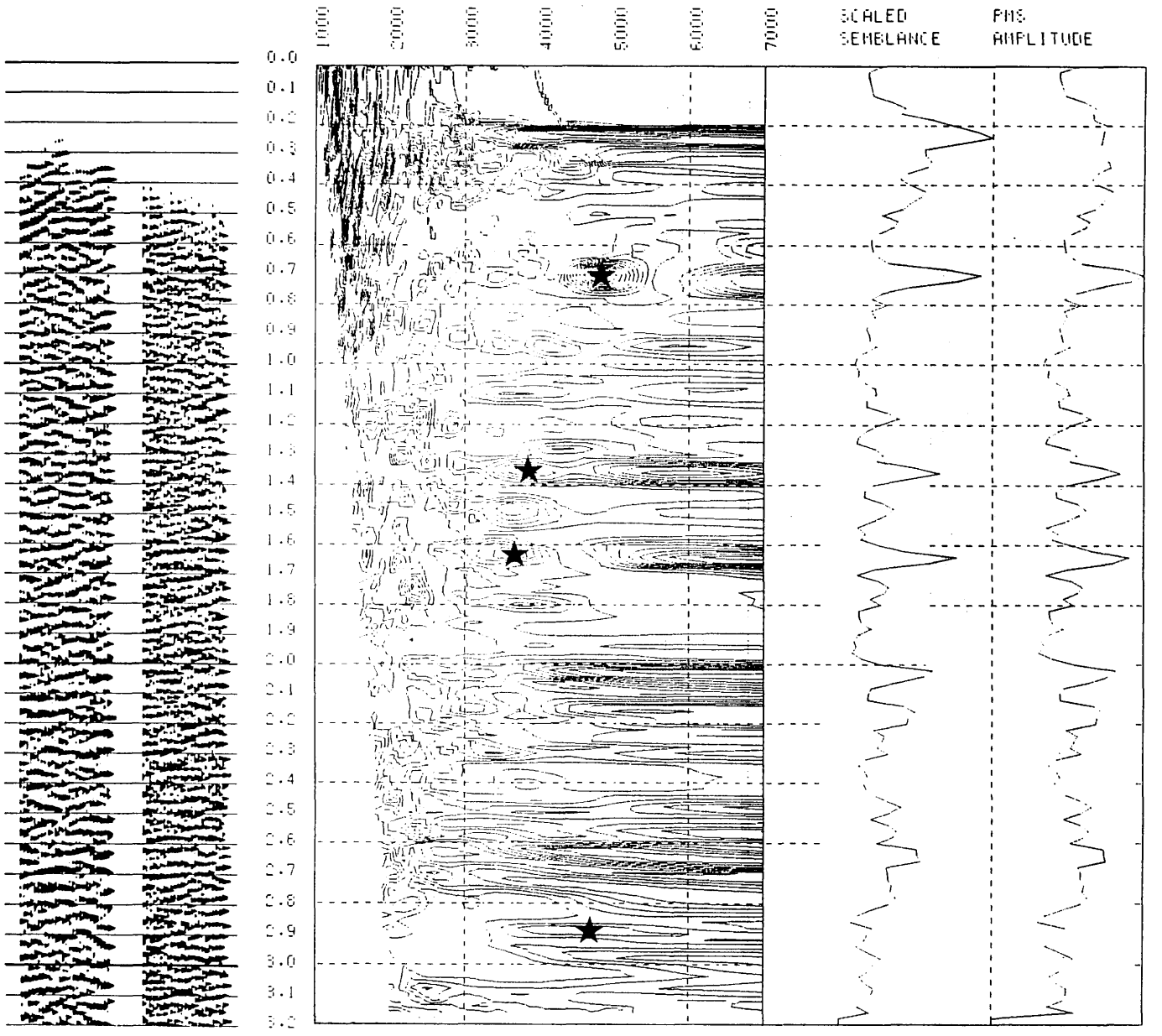

Fig. 3.57 SK-6 final stack (Fig. 3.56B) shown beside the semblance plot after FK domain multiple attenuation (Fig. 3.55B). Stars indicate peaks from which the stacking velocity curve was made up.

velocity-depth characteristics:

TABLE 3.7
SK-6 VELOCITIES AND DEPTHS

Time (ms)	V(rms) (m/s)	V(int) (km/s)	Thickness (km)	Depth (km)
700	4800	4.80	1.68	1.68
1350	3800	2.28	0.74	2.42
1630	3700	3.17	0.44	2.86
2900	4600	5.55	3.52	6.39

Below about 1.6 s events with move-outs rather different from the chosen curve are stacking up regardless. The results in the table above are probably reliable down to 1.63 s.

3.2 VELOCITY MEASUREMENTS

3.2.1 VELOCITIES FROM HAND SPECIMENS

The results of the laboratory measurements of velocity and density on hand specimens are tabulated in Appendix 2. They are summarised in Figure 3.58, which is a plot of velocity against density. The lithologies included are sandstone, cornstone, conglomerate, fine-grained arkose, gabbro and basalt.

The empirically-determined mean curves of P-wave and S-wave variation with density (Ludwig et al. 1970, fig. 11) have been added to the diagram as well. Although each of these curves is the mean of many points with a very wide scatter (typically ± 1 km/s for the P-wave curve, for example), it is, nevertheless, possible to draw a line separating all P-wave point values from all S-wave points - this is the dashed line in Figure 3.58.

It is clear that the results for the Triassic sandstones are all suspiciously low for a supposed P-wave, and it could be concluded that the S-wave has been observed instead,

Fig. 3.58 Ultrasonic velocity vs. density

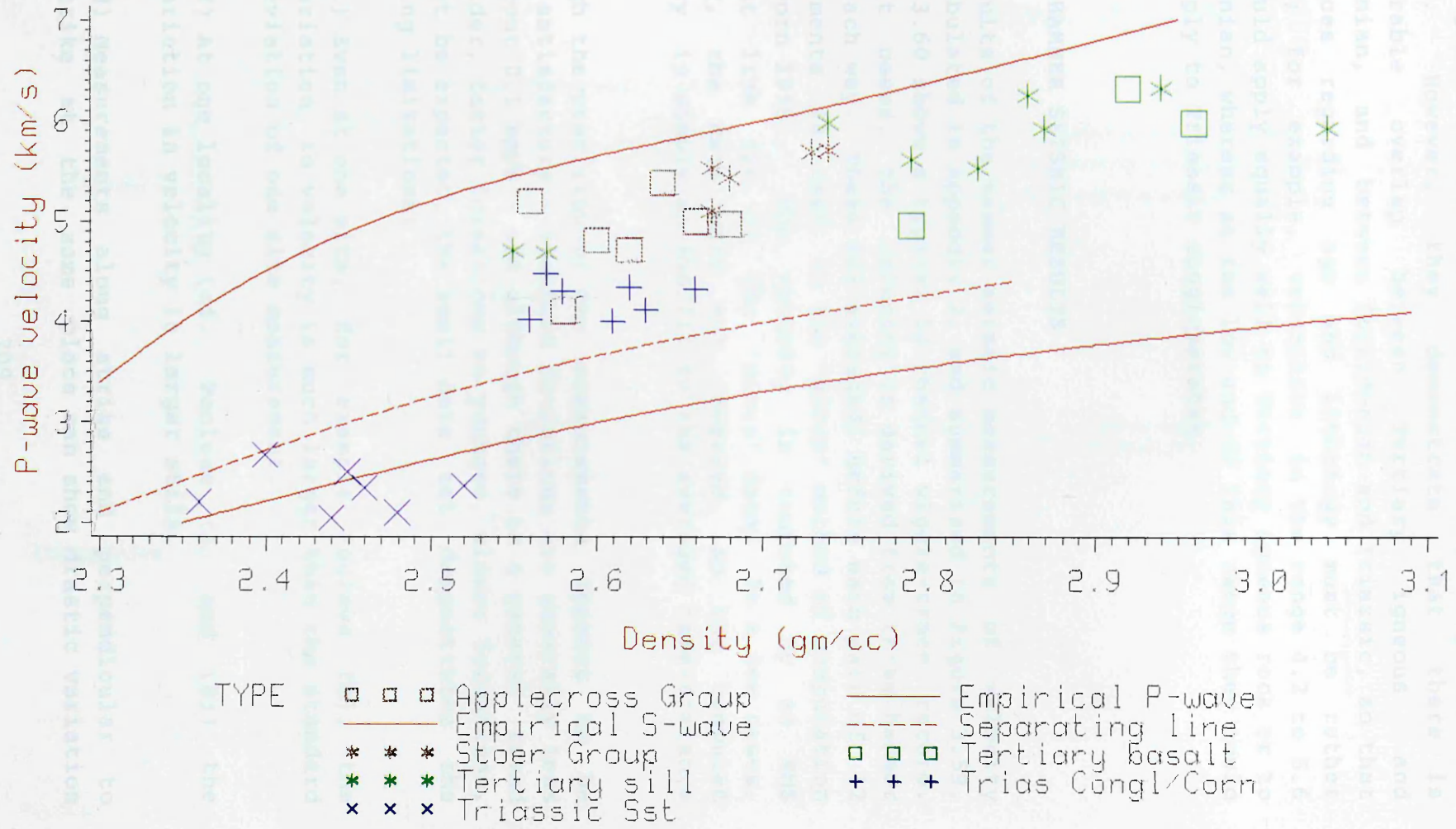

although why this should be the case is not clear. The remaining measurements fall within the range expected for P-waves. However, they demonstrate that there is considerable overlap between Tertiary igneous and Torridonian, and between Torridonian and Triassic, so that inferences regarding age and lithology must be rather limited; for example, velocities in the range 4.2 to 5.6 km/s could apply equally well to Tertiary igneous rock or to Torridonian, whereas at the low end of this range they could also apply to Triassic conglomerates.

3.2.2 HAMMER SEISMIC RESULTS

The results of the hammer seismic measurements of velocity are tabulated in Appendix 2, and summarised in Figure 3.59. Figure 3.60 shows a typical 12-channel wiggle-trace record. In most cases, the velocity is derived from three hammer blows each way. These are averaged, before each pair of 12 measurements is used in the 'minus' method of computation (Hagedoorn 1959). The velocity is computed by an RMS straight line fit to the 'minus' data. In a few cases, however, the data were not reversed, so the computed velocity is simply an RMS fit to the averaged time-distance data.

Although the precision of the measurements appears to be mainly satisfactory - standard deviations are generally less than about 0.1 km/s - and although there is a general trend from older, faster formations to younger, slower formations, as might be expected, the small data set demonstrates the following limitations:

(1) Even at one site, for example Poolewe (B), the variation in velocity is much larger than the standard deviation of one site measurement.

(2) At one locality (cf. Poolewe (A) and (B)) the variation in velocity is larger still.

(3) Measurements along strike and perpendicular to strike at the same place can show drastic variation

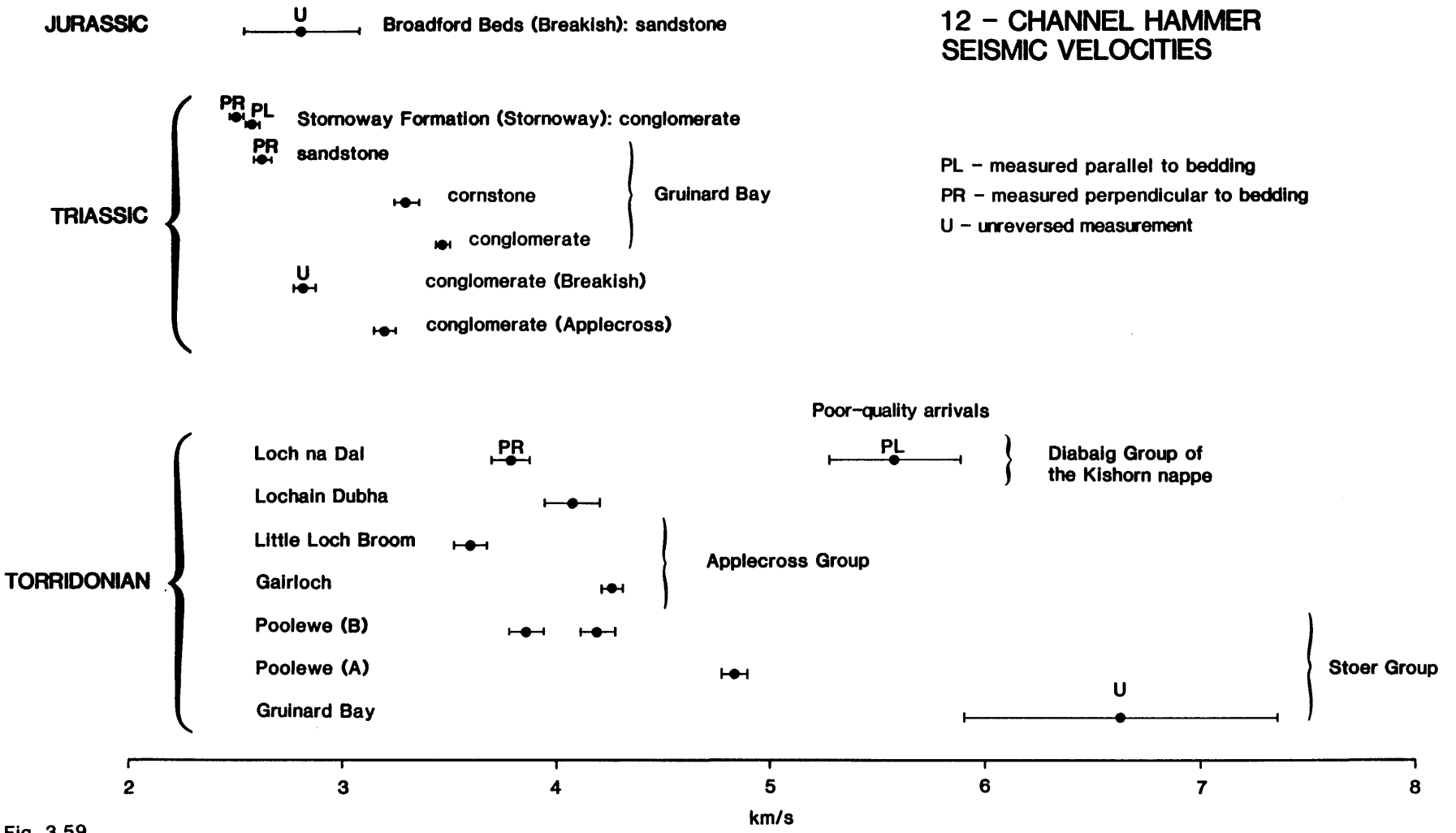
12 – CHANNEL HAMMER
SEISMIC VELOCITIES
PL – measured parallel to bedding
PR – measured perpendicular to bedding
U – unreversed measurement
JURASSIC
U
Broadford Beds (Breakish): sandstone
TRIASSIC
PR PL
Stornoway Formation (Stornoway): conglomerate
PR
sandstone
cornstone
conglomerate
Gruinard Bay
U
conglomerate (Breakish)
conglomerate (Applecross)
Poor-quality arrivals
TORRIDONIAN
Loch na Dal
PR
PL
Diabaig Group of
the Kishorn nappe
Lochain Dubha
Little Loch Broom
Gairloch
Applecross Group
Poolewe (B)
Poolewe (A)
Gruinard Bay
Stoer Group
U
2
3
4
5
6
7
8
km/s

Fig. 3.59

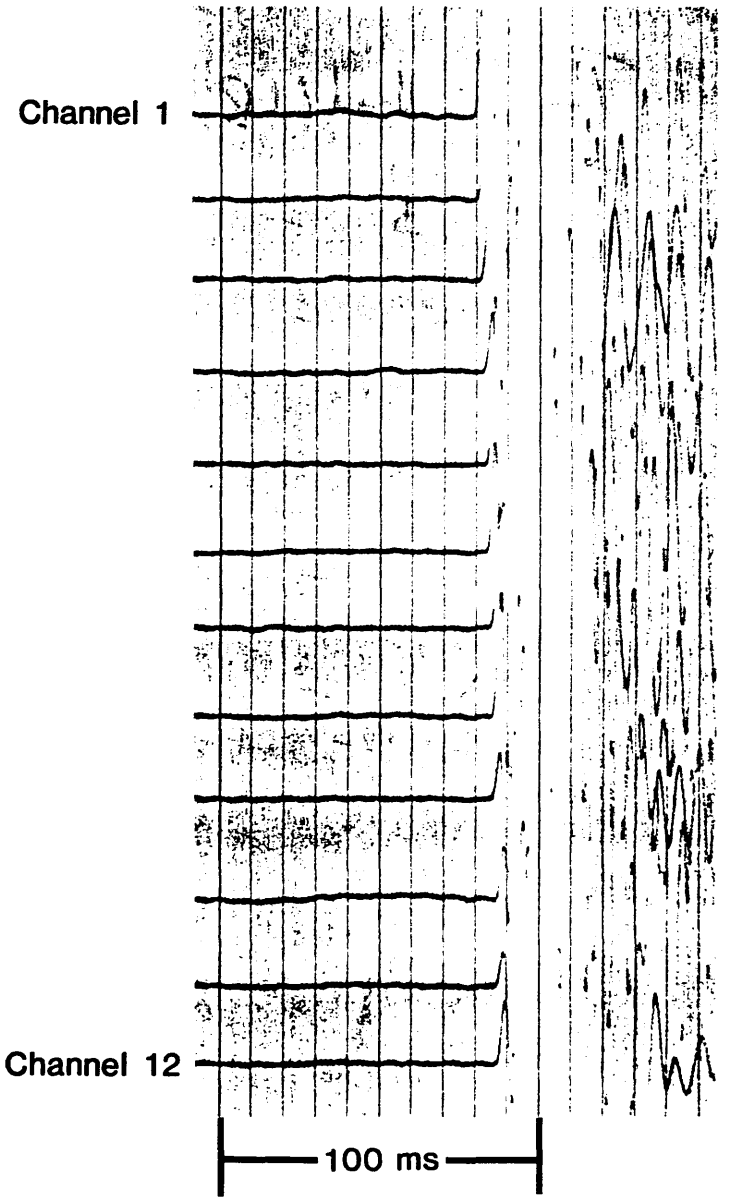

Fig. 3.60 Typical 12-channel hammer seismogram. The first breaks are picked by examination of the original records under a low magnification microscope.

(for example, Loch na Dal).

The full-wave oscillograph recording of all 12 traces (Fig.3.60) ensures that an accurate pick of the first arrival could be made even when it is clearly somewhat dispersive; automatic picking by a pre-set threshold amplitude setting would not take this into account, with the result that the apparent velocity computed could be slower than the true velocity. The full-wave recording also ensures that P-waves were actually being measured, and not S-wave arrivals.

3.2.3 DISCUSSION

The problems of interpretation of the velocity measurements discussed above are exemplified by a comparison of the ultrasonic with the hammer results at the five hammer seismic sites where hand-specimens were also successfully measured (failure of one or both of the methods at other sites prevented more of these paired observations from being available). Figure 3.61 shows the comparison; clearly, the two methods give rather different results, but the differences are not, at first sight, even systematic. However, the hammer seismic velocity at Gruinard Bay was derived from unreversed data, so we are probably justified in rejecting it altogether. It is then possible to conclude, tentatively, that the ultrasonic method gives velocities about 25% greater than by the hammer method, as suggested by the dashed line in Figure 3.61. Presumably this is due to the decelerating effect of open cracks at the surface where the hammer method is observed. Such cracks will have been 'filtered' out of the hand specimens for the ultrasonic measurements, by selection of solid chunks of rock suitable for the rock saw.

Fig. 3.61 ULTRASONIC VELOCITY VS. HAMMER SEISMIC VELOCITY

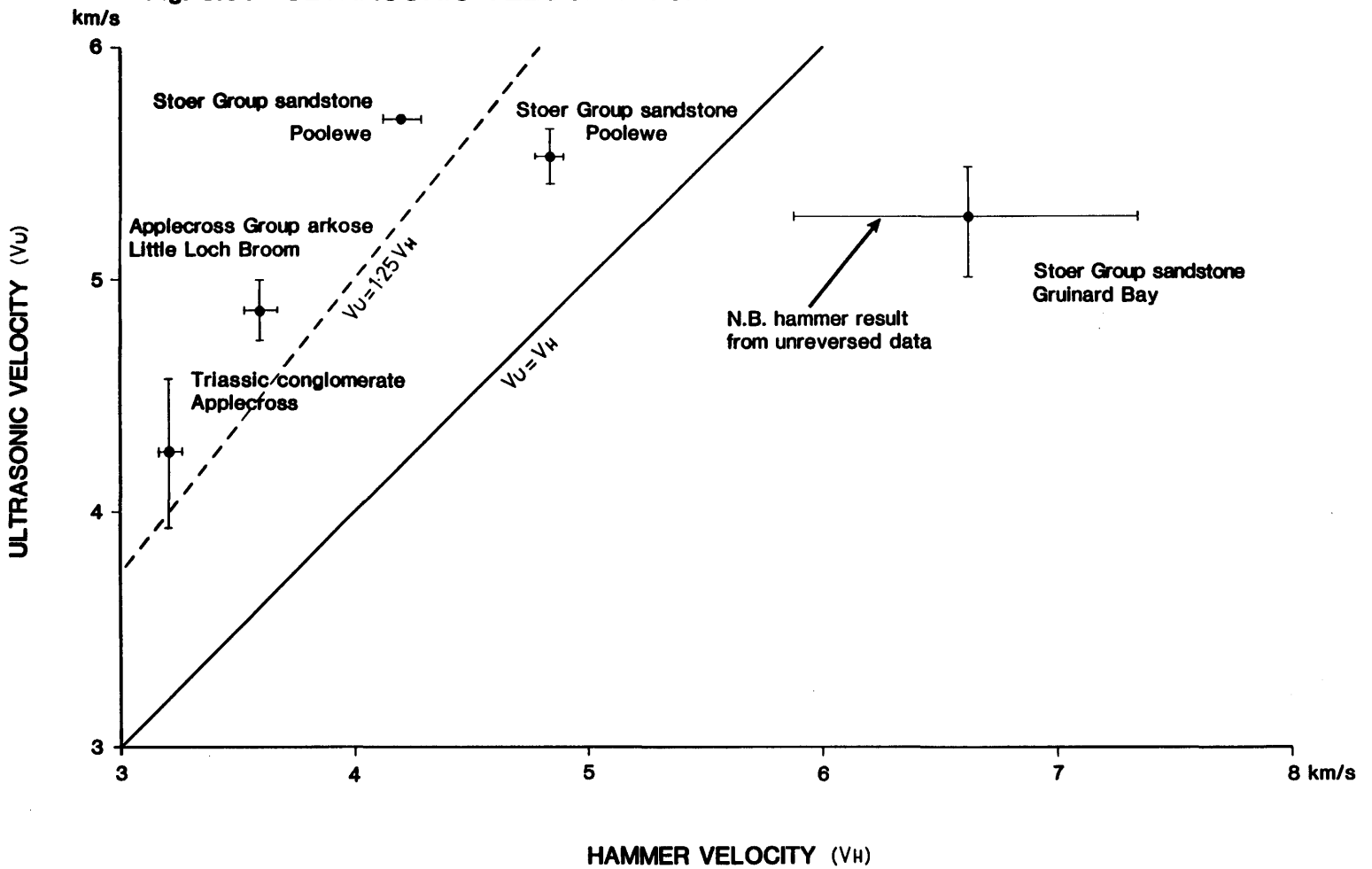

3.3 SEISMIC REFRACTION

3.3.1 THE 1971 SURVEY

Very few usable results emerged from the 1971 John Murray refraction survey, due to the technical problems described in Section 2.3.3. The location of the one short, unreversed segment of data (line AB) is shown in Figure 3.62, and a reduced travel time - distance plot of the first arrivals is shown in Figure 3.63. Distances are calculated from the water break (assuming a velocity of 1.49 km/s), which was easily observed as a late arrival on all records. The results are tabulated in Appendix 3.

Due to the large drift of the buoys, and the fact that the results are an amalgam of three attempts at shooting the line, the buoy locations are not consistent and not well located. This means that it is probably unwise to try to differentiate between velocities at the buoys (viz. the apparent velocity at the buoy 'array') and the velocities derived from the nominal buoy location (position A) and the shots. The results of Figure 3.63 can be most simply interpreted in terms of a 1-dimensional, three-layer model as shown in the Table 3.8 (in which sd indicates the standard deviation of the least squares fit):

TABLE 3.8
REFRACTION LINE A-B (1971) VELOCITIES AND DEPTHS

Velocity (km/s)	(sd)	Intercept (s)	(sd)	Layer thickness (km)	Depth to layer (km)
1.86	0.00	-0.001	0.003	0.55	0.55
2.58	0.24	0.411	0.075	0.34	0.89
3.60	0.40				

However, the errors are large; note that the intercept for the first layer goes nearly through the origin, even though the line is located in 140 m water depth. Furthermore, the 4 points defining the 3.6 km/s refractor imply that the apparent velocity at the buoys is much greater - around 4.5 km/s. Thus a 1-dimensional model is scarcely justifiable.

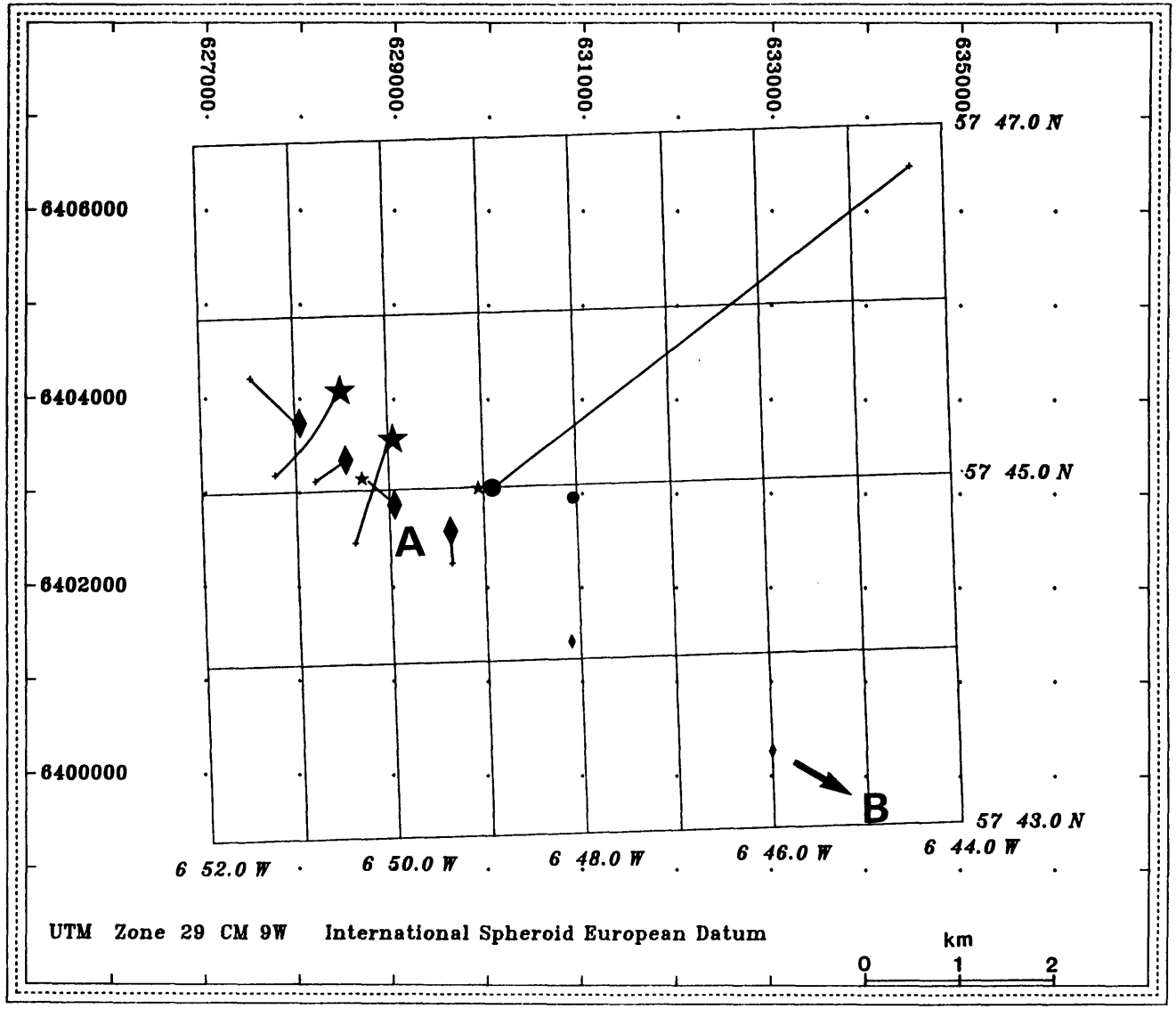

Fig. 3.62 Location map of refraction line A-B (1971). Large symbols are buoy launch positions, corresponding small symbols are shots received by these buoys. Straight lines join buoy launch to buoy recovery locations.

Fig. 3.63 Line A–B (1971): times reduced to 3.6 km/s

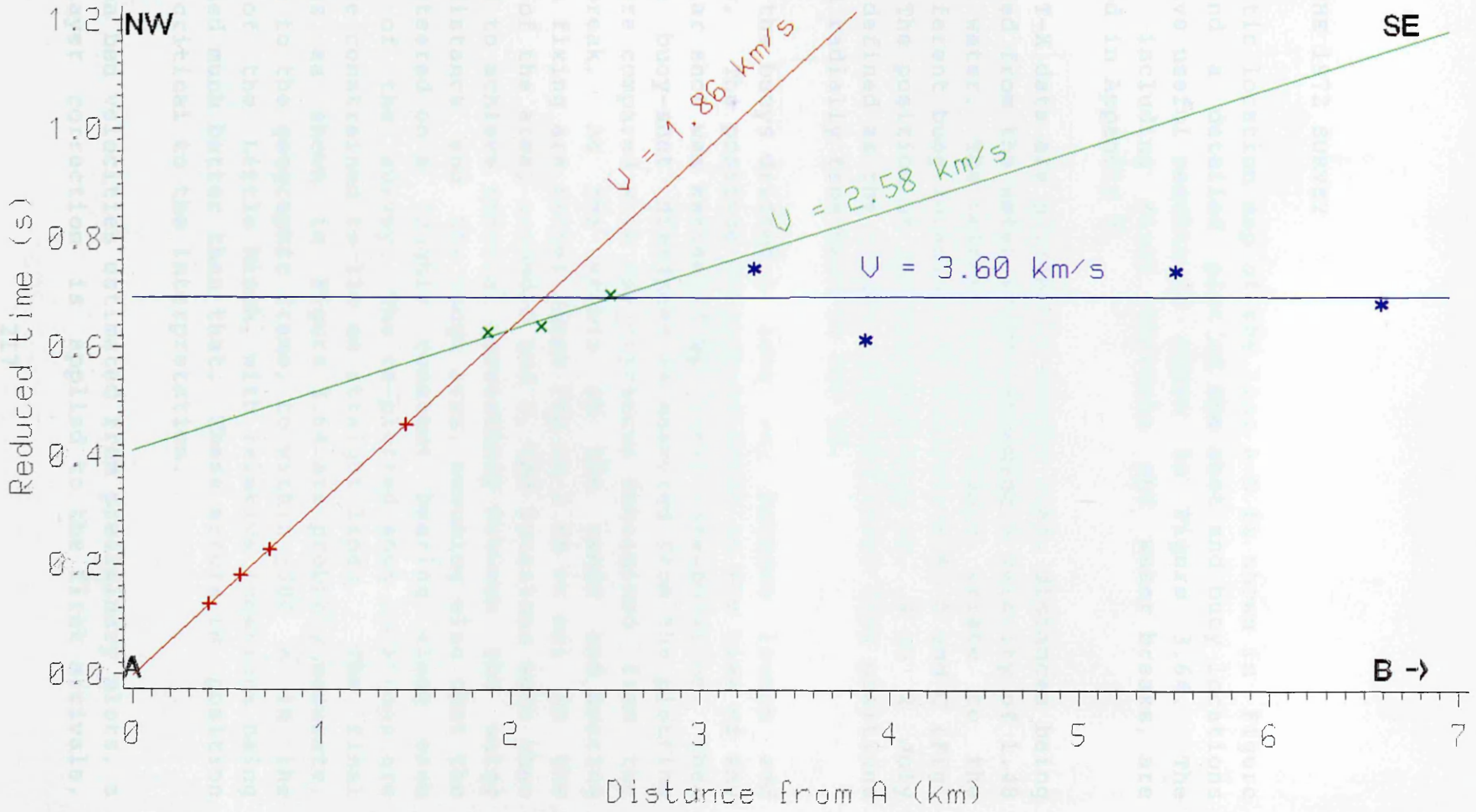

In conclusion, the 1971 results merely indicate velocities in the range 3-4 km/s at shallow depth (c. 1 km) in the area.

3.3.2 THE 1972 SURVEY

A schematic location map of the line A-D is shown in Figure 2.18, and a detailed plot of the shot and buoy locations which gave useful results is shown in Figure 3.64. The results, including first arrivals and water breaks, are tabulated in Appendix 3.

The raw T-X data are plotted in Figure 3.65, distances being calculated from the water breaks assuming a velocity of 1.48 km/s for water. The colours in this figure relate to the nine different buoy locations at localities A, B and C (Fig. 3.64). The position of the anchored buoy no. 4 on 2 July 1972 is defined as the origin, with the other buoy positions measured radially from here to the SE.

Some of the buoys drifted a long way between launch and recovery. The position of each of these at the time of any particular shot was estimated by linear interpolation, then all the buoy-shot distances as measured from the plotting sheet were compared with the distances determined from the water break. As the errors in the range and bearing position fixing are rather large (up to 1 km or so) in the centre of the area, around B and C, the locations were then adjusted to achieve internal consistency between the water break distance and the range arcs, assuming also that the vessel steered on a roughly constant bearing along each segment of the survey. The re-plotted shot locations are therefore constrained to lie on straight lines. The final locations as shown in Figure 3.64 are probably accurate, relative to the geographic frame, to within $\pm$300 m in the middle of the Little Minch, with relative locations being positioned much better than that. These errors in position are not critical to the interpretation.

Using sea bed velocities estimated from preliminary plots, a water layer correction is applied to the first arrivals,

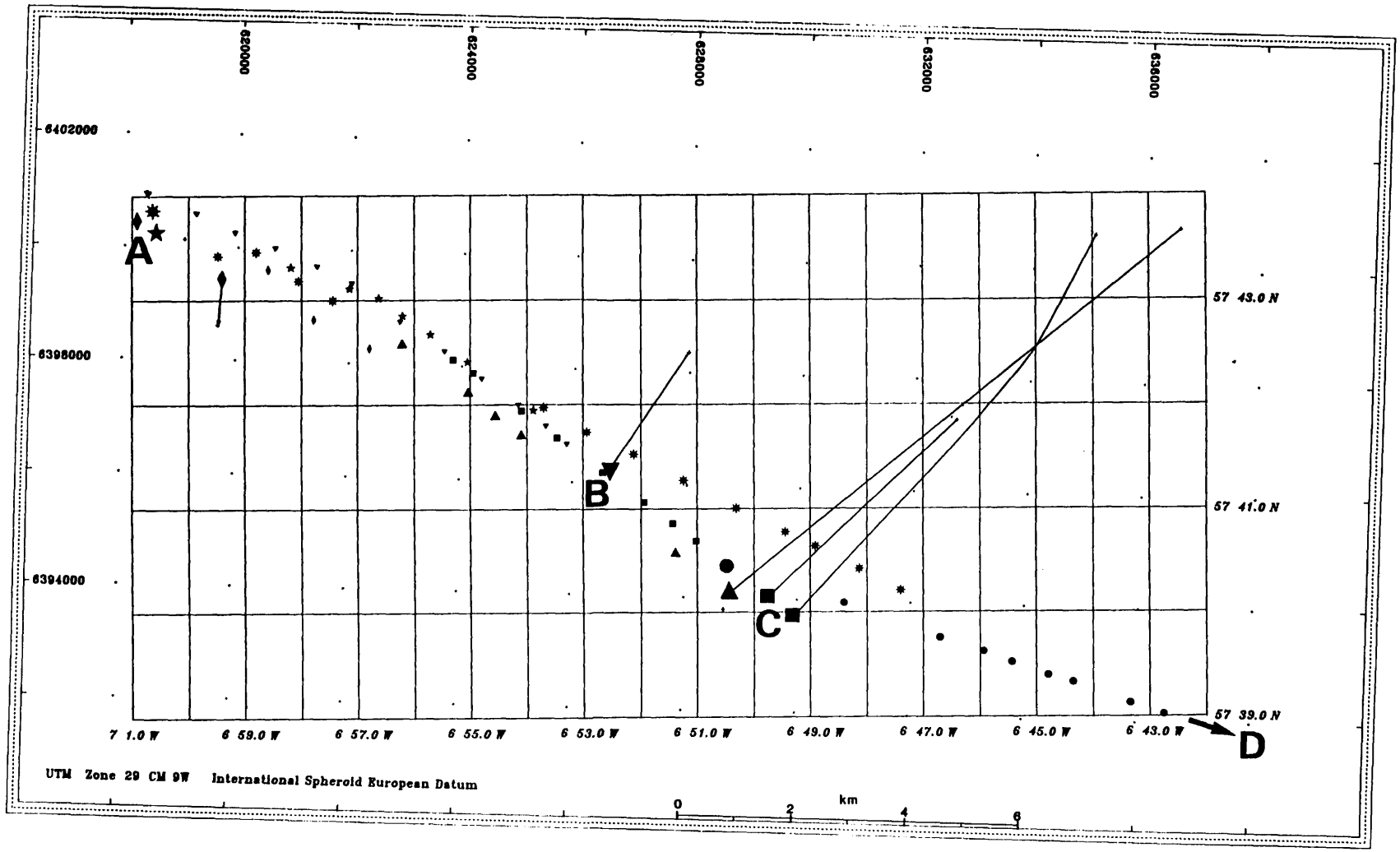

Fig. 3.64 Location map of refraction line A-D (1972). Large symbols are buoy launch positions, corresponding small symbols are shots received by these buoys. Straight lines join buoy launch to buoy recovery locations.

Fig. 3.65 Line A–D (1972): raw time–distance plot

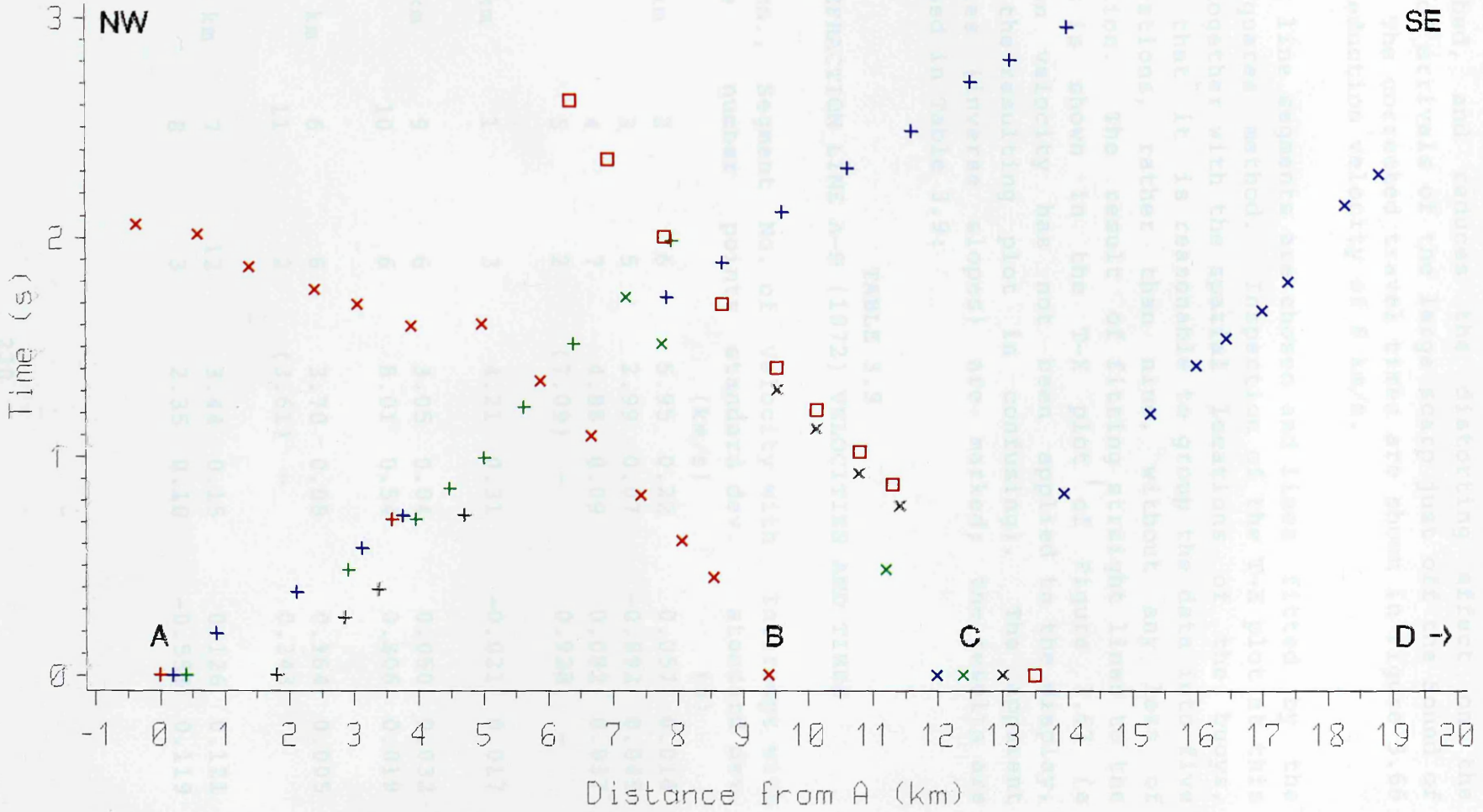

making due allowance for the hydrophone and shot depths. This has the effect of placing the shots and receivers on the sea bed, and reduces the distorting effect on the pattern of arrivals of the large scarp just off the Sound of Harris. The corrected travel times are shown in Figure 3.66 with a reduction velocity of 6 km/s.

Straight line segments are chosen and lines fitted by the least squares method. Inspection of the T-X plot at this stage, together with the spatial locations of the buoys, suggest that it is reasonable to group the data into five buoy locations, rather than nine, without any loss of information. The result of fitting straight lines to the segments is shown in the T-X plot of Figure 3.67 (a reduction velocity has not been applied to the display, because the resulting plot is confusing). The apparent velocities (inverse slopes) are marked; the results are summarised in Table 3.9:

TABLE 3.9
REFRACTION LINE A-D (1972) VELOCITIES AND TIMES

Buoy locn., distance	Segment number	No. of points	Velocity with standard dev. (km/s)		Intercept with standard dev. (s)	
A 0.0 km	2	6	5.95	0.22	0.057	0.018
	3	5	2.99	0.07	-0.592	0.045
	4	7	4.88	0.09	0.092	0.037
	5	2	(7.09)	-	0.928	-
A' 1.8 km	1	3	4.21	0.31	-0.021	0.017
B 9.4 km	9	6	3.05	0.04	0.050	0.032
	10	6	8.01	0.54	0.806	0.019
C' 12.0 km	6	6	3.70	0.08	0.164	0.005
	11	2	(3.61)	-	0.243	-
C 13.0 km	7	12	3.44	0.15	0.126	0.121
	8	3	2.35	0.10	-0.553	0.119

Fig. 3.66 Line A–D (1972): times reduced to 6 km/s
Water depth correction applied

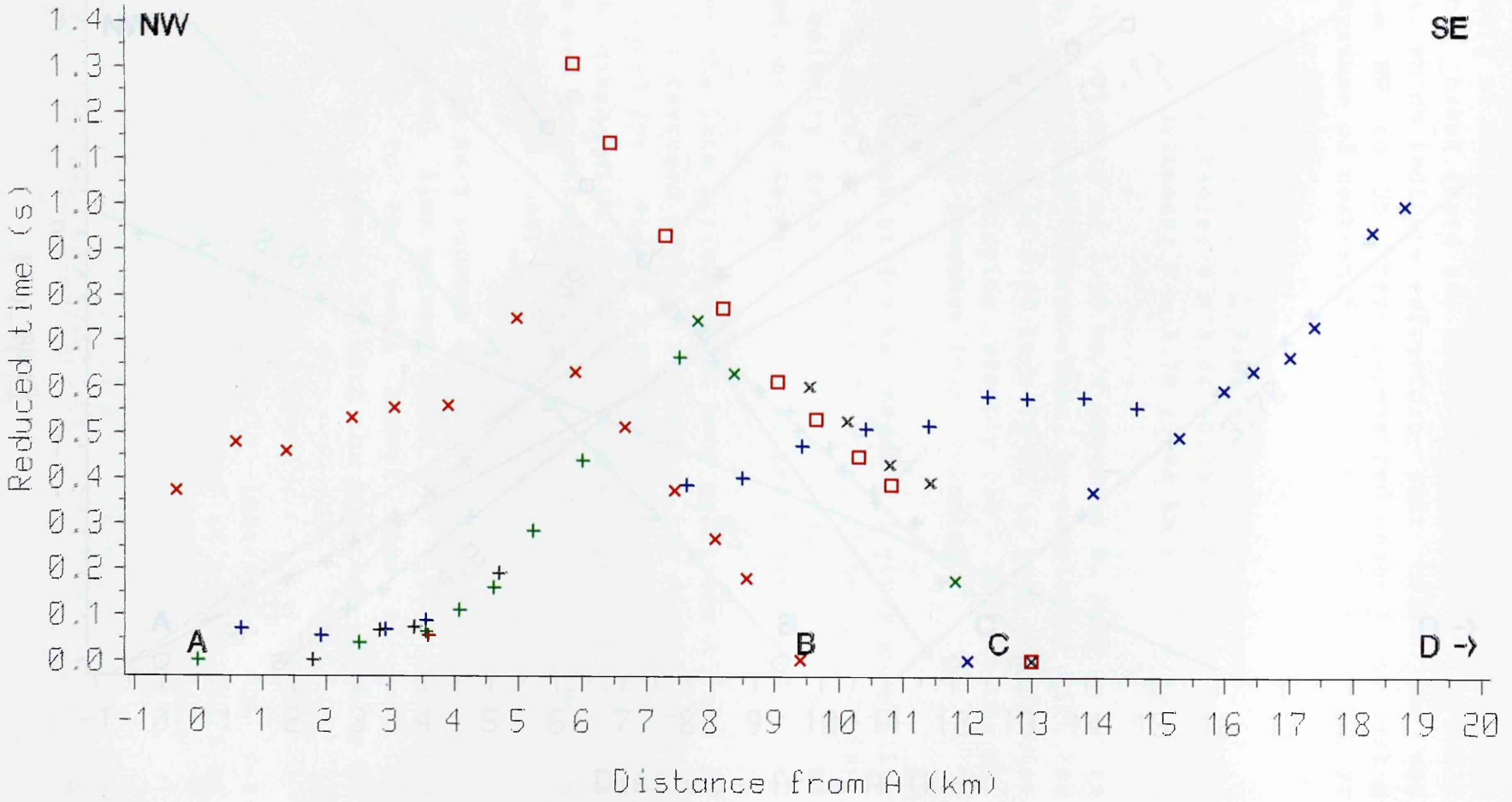

Fig. 3.67 Line A–D (1972): Time–distance plot

Water depth correction applied

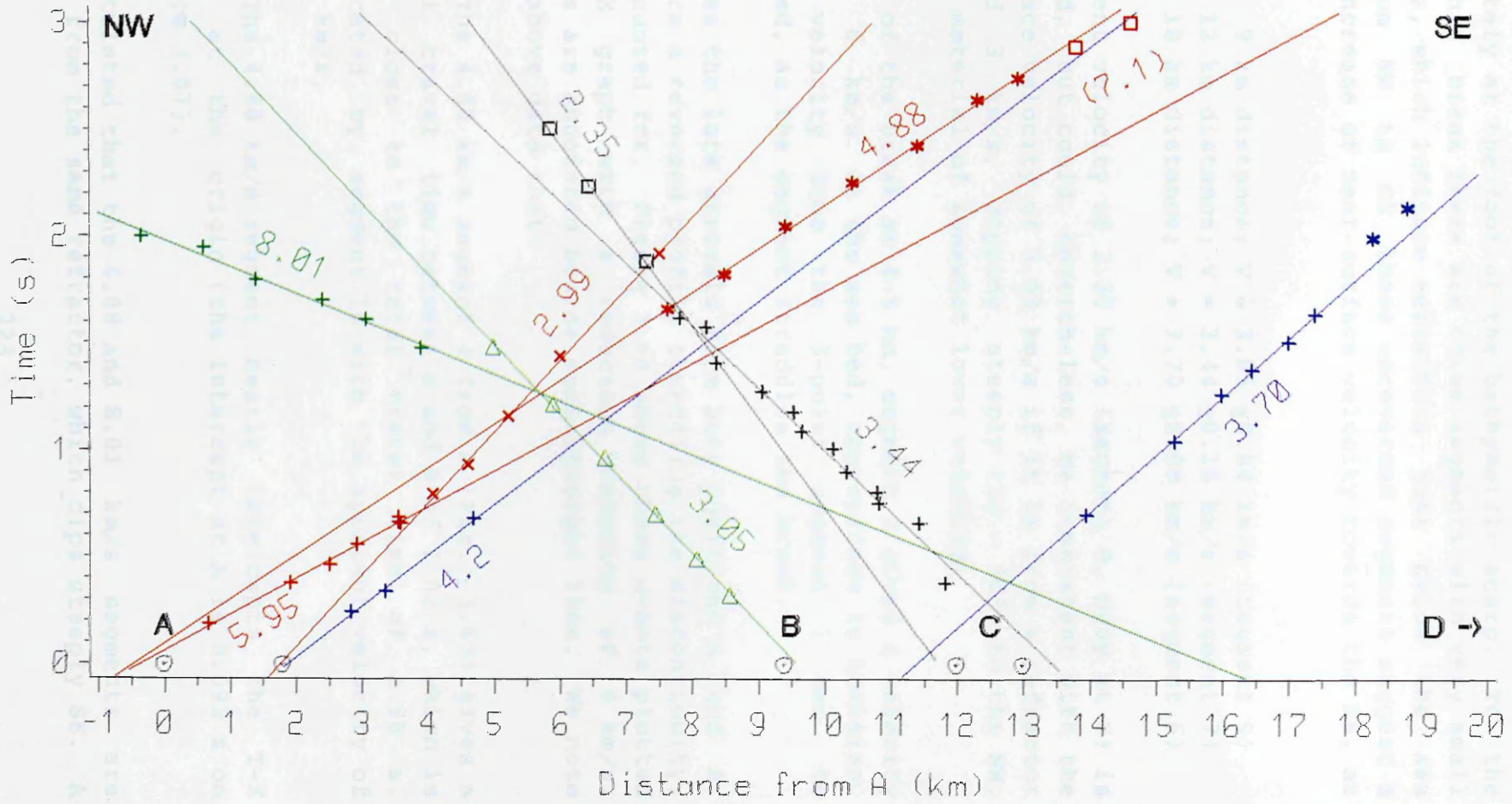

It is clear from these results that there is a large discontinuity in the data at 4 - 5 km distance, approximately at the foot of the bathymetric scarp. To the SE of this break there are three segments with very small intercepts, which indicate refractors just below the sea bed. From NW to SE these unreversed segments suggest a lateral increase of near-surface velocity towards the SE, as follows:

5 - 9 km distance; V = 3.05 $\pm$0.04 km/s (segment 9)
8 - 12 km distance; V = 3.44 $\pm$0.15 km/s (segment 7)
14 - 18 km distance; V = 3.70 $\pm$0.08 km/s (segment 6)

The apparent velocity of 2.35 km/s (segment 8, buoy at C) is unreversed, but could, nevertheless, be consistent with the near-surface velocity of 3.05 km/s if it is from a refractor of around 3 km/s, dipping steeply (20 - 30°) to the NW, overlying material of somewhat lower velocity.

To the NW of the break at 4-5 km, segment 2 gives a velocity of about 6 km/s at the sea bed, appropriate to Lewisian. The low velocity from the 3-point segment 1 can be disregarded, as the segment straddles the break.

This leaves the late arrivals from buoy positions A and B, which form a reversed profile straddling the discontinuity, to be accounted for. Figure 3.68 shows these events plotted on a T-X graph with a reduction velocity of 6 km/s; velocities are annotated beside each straight line. We note from the above data that:

(1) The 4.88 km/s segment 4 from A (Fig. 3.67) gives a total travel time between A and B of 2.02 s, which is very close to the total travel time of 1.98 s, indicated by segment 10 with the apparent velocity of 8.01 km/s,

(2) The 4.88 km/s segment nearly intercepts the T-X plot at the origin (the intercept at A is 0.092 s on Figure 3.67).

It is postulated that the 4.88 and 8.01 km/s segments are therefore from the same refractor, which dips steeply SE. A

Fig. 3.68 Line A–B (1972): times reduced to 6 km/s
Water depth correction applied

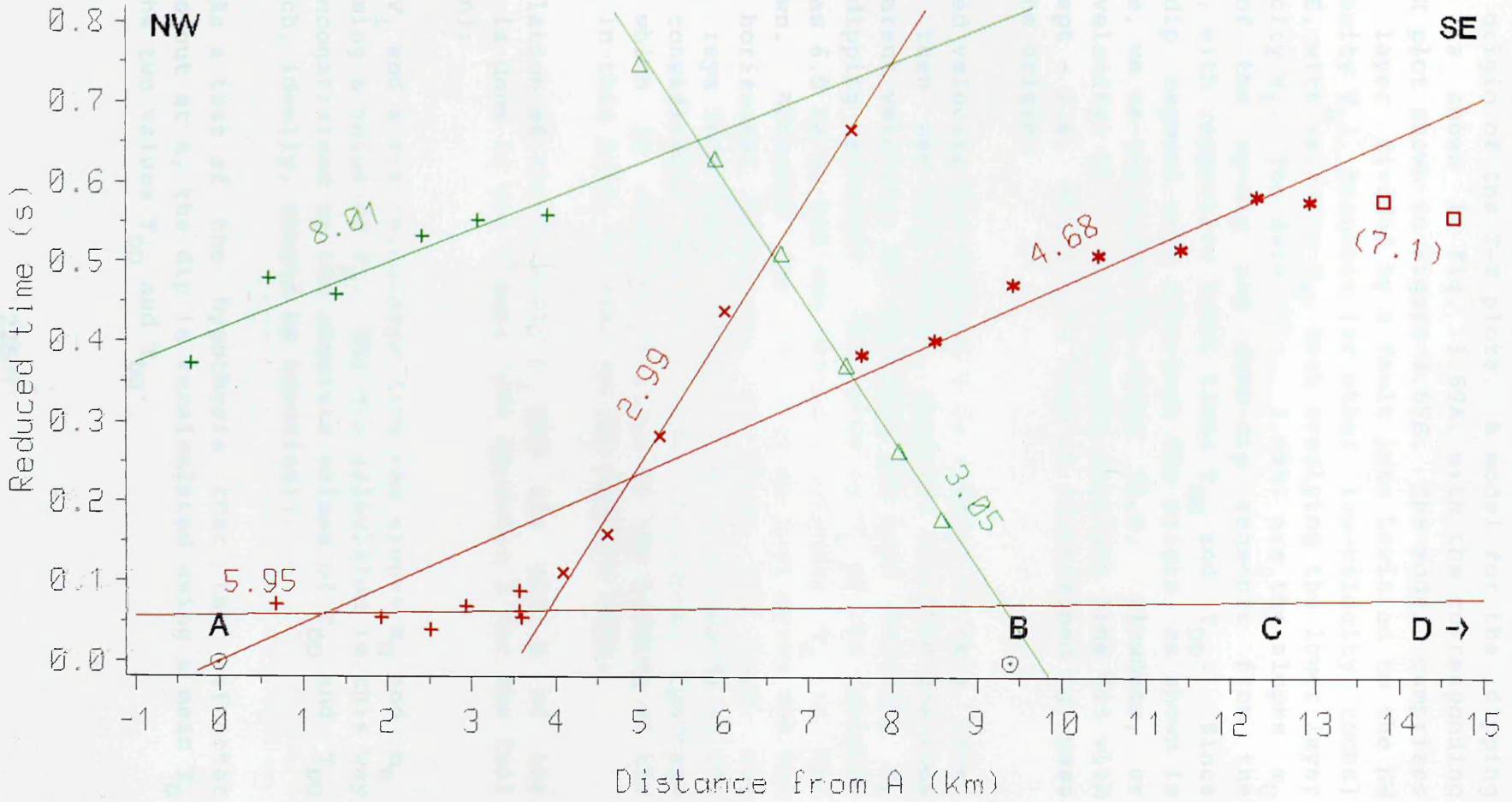

clear candidate for such a refractor is the Outer Isles Thrust, which crops out on the sea bed in the neighbourhood of A, the origin of the T-X plots. A model for the dipping refractor is shown in Fig. 3.69A, with the corresponding sketch T-X plot shown in Figure 3.69B. The model comprises an upper layer divided by a fault into Lewisian to the NW (with velocity V_L), Mesozoic (or other low-velocity rocks) to the SE, with velocity V_M, both overlying the lower layer with velocity V_1. The data (Fig. 3.69B) are the slopes m_U and m_D of the up-dip and down-dip segments from the refractor, with respective total times T_{DU} and T_{DD}. Since the downdip segment must intercept the origin, as shown in the figure, we re-calculate the slope (i.e. slowness, or inverse velocity) by a least-squares straight line fit with no intercept - i.e. the fitted line is constrained to pass through the origin.

The revised velocity for segment 4 is 4.68 $\pm$0.02 km/s (Fig. 3.68) We then use this result, together with the previous updip apparent velocity, to calculate the true velocity V_1 of the dipping refractor. The velocity V_L of the Lewisian is taken as 6.0 km/s, but the Mesozoic velocity V_M is not well known. Although the velocity at just below the sea bed, in a horizontal direction, is about 3.0 km/s, the refracted rays from depth will be travelling upwards to the SE at a considerable angle to the horizontal (perhaps 30-40°), which is roughly parallel to the bedding of the sediments in this area, as seen on the sparker data.

The calculation of the velocity V_1 and the dip a of the refractor is done in two stages (see Appendix 3 for the full derivation):

(1) V_1 and a are calculated from the slopes m_U and m_D assuming a value of V_M. The dip calculated in this way is unconstrained by the absolute values of T_{DD} and T_{DU} (which, ideally, should be identical),

(2) As a test of the hypothesis that the refractor crops out at A, the dip is recalculated using a mean T_D of the two values T_{DD} and T_{DU}.

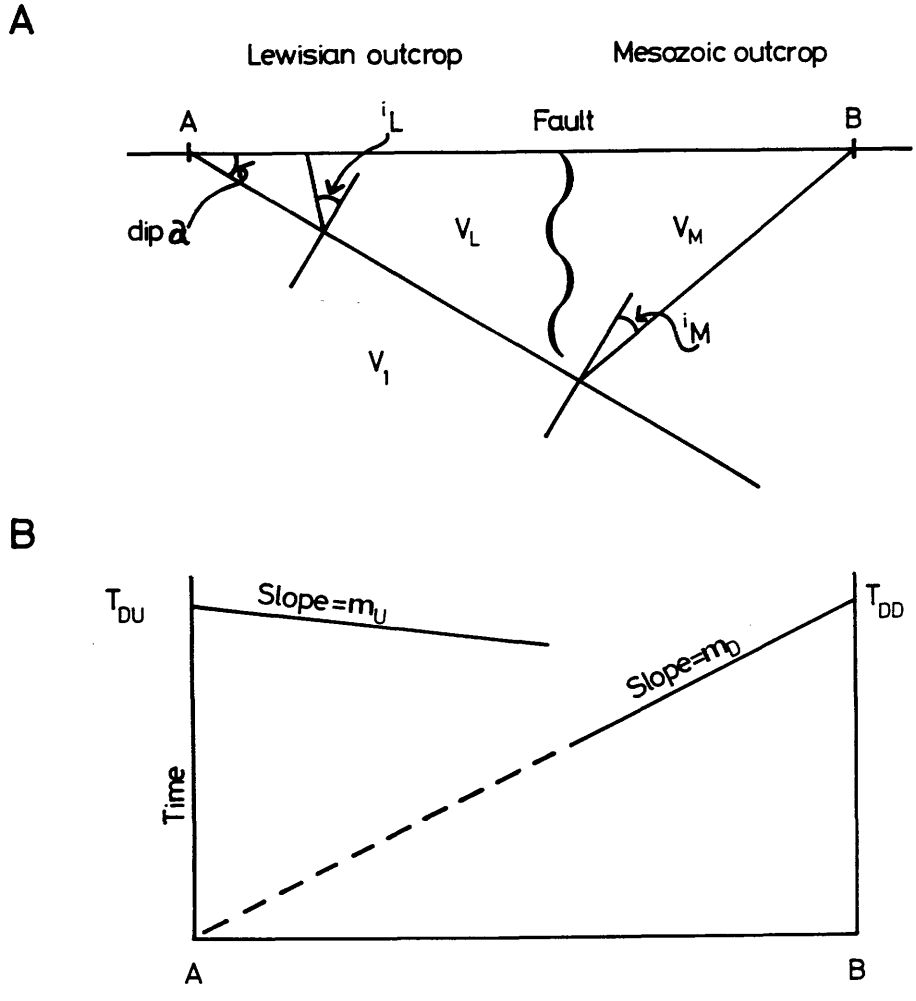

Fig. 3.69
A. Model for interpretation of refraction arrivals from dipping reflector (Outer Isles Thrust). The fault zone separating Lewisian and Mesozoic is the Minch Fault, which coalesces at depth with the Outer Isles Thrust.
B. Constraints on the travel times for the dipping refractor shown in Fig. 3.69A. The down-dip segment passes through A, the point where the refractor crops out. The total travel times T_{DD} and T_{DU} of the down-dip and up-dip segments, respectively, are identical.

The largest uncertainty is probably in the velocity V_M. Values above 4.6 km/s do not produce real roots to the quadratic equation used to recalculate the dip; this means that the wavefront refracting into the Mesozoic from the headwave travelling down the refractor is itself propagating downwards. One of the solutions produces very steep dips, and can be rejected on geometric grounds (see Appendix 3) as well as on geological grounds.

The results show that the 'unconstrained' and the recalculated dips correspond to within 0.5°, corroborating the hypothesis that the refractor is indeed the Outer Isles Thrust. Varying V_M gives the range of results shown in Table 3.10:

TABLE 3.10
DIP OF THE OUTER ISLES THRUST

V_M (km/s)	3.0	3.5	4.0	4.5	4.6	4.7
V_1 (km/s)	6.8	6.6	6.4	6.2	6.1	-
Unconstrained dip	13.6	16.5	20.3	27.3	30.5	-
Recalculated dip	13.7	16.5	20.4	27.5	30.8	-

The significance of these results for the interpretation of the Minch Fault and Outer Isles Thrust is discussed in Chapter 4.

3.4 SPARKER AND MAGNETIC SURVEYS

3.4.1 RELOCATING THE DATA

A plot of the raw Decca Main Chain position fixes on a UTM basemap shows a number of erratic features. Sparker and bathymetric data at line crossovers using these positions frequently do not correspond, and there is a further mismatch between the John Murray 1971 data and the earlier IGS data. However, a detailed bathymetric map of the Little Minch was compiled for IGS in 1974 (published in simplified form in Chesher et al. 1983, fig. 2); this shows unusually pronounced submarine features. Using a photographic

enlargement of this map to 1:50,000 scale as a base, it is possible to relocate the combined IGS/Glasgow data set by adjusting fix positions using the following criteria:

(1) The vessel maintains a nearly constant heading and speed along line segments; variations in heading and speed are smooth.

(2) The topography as seen on the sparker lines must match that of the bathymetric map, which was compiled from Decca Hifix positioning, and is therefore taken as accurate.

(3) The sub-bottom reflector geometry seen on pairs of crossing lines should tie.

The resulting fix map, combined with the bathymetry data, is then used for geological interpretation at 1:50,000 scale. The location data are digitised from this relocated map. Figure 3.70 is a plot of these digital data at 1:100,000 scale (in pocket of rear cover). Apart from localised site surveys, the resulting shallow seismic reflection data coverage is the most dense of any place on the UK continental shelf. Even so, the coverage is not quite detailed enough in some places to resolve the complex solid geology.

3.4.2 PRELIMINARY INTERPRETATION

The limitations of the analogue paper sparker records available include:

(1) They are original and unique; no playbacks or other copies can be made.

(2) Their horizontal scale in time (i.e. constant distance on the record between 10 minute fix marks) means that their true horizontal scale varies with ship speed.

(3) They are printed from left to right, irrespective of ship bearing.

(4) Their compressed horizontal scale can sometimes obscure, rather than elucidate, some geological features.

A digitising scheme was set up to try to circumvent these limitations, and some 5% of the sparker records were digitised as a pilot study. A sample test plot is shown in Figure 3.71. The two-way time (TWT) line drawing is scaled horizontally by merging the TWT and location files (Fig. 3.71A). The sea bed and other digitised reflector segments are labelled numerically. The TWT data are then stretched to depth (Fig. 2.71B) by applying mean velocities for each class of reflector. The depth-converted section can, of course, be displayed in a conventional azimuth (west and south at the left). The scheme was also able to incorporate the more precise bathymetry from the precision depth recorder records, to apply a correction to the sparker record water bottom. However, the digitising scheme was abandoned after the test phase, as it was not worth the considerable effort of digitising all of the sparker data.

A less ambitious procedure was adopted instead, of photographically reducing the sparker records and printing some of them reversed, so that lines have a consistent orientation. The reduced-scale prints are at an approximate 1:50,000 horizontal scale, which matches that of both the working map and the analogue magnetic records. The latter are used in conjunction with the sparker records (and the IGS sea bed samples and shallow boreholes) in a qualitative way to interpret the presence of magnetic rocks; this essentially geological interpretation is described in Chapter 4, which also includes samples of the data.

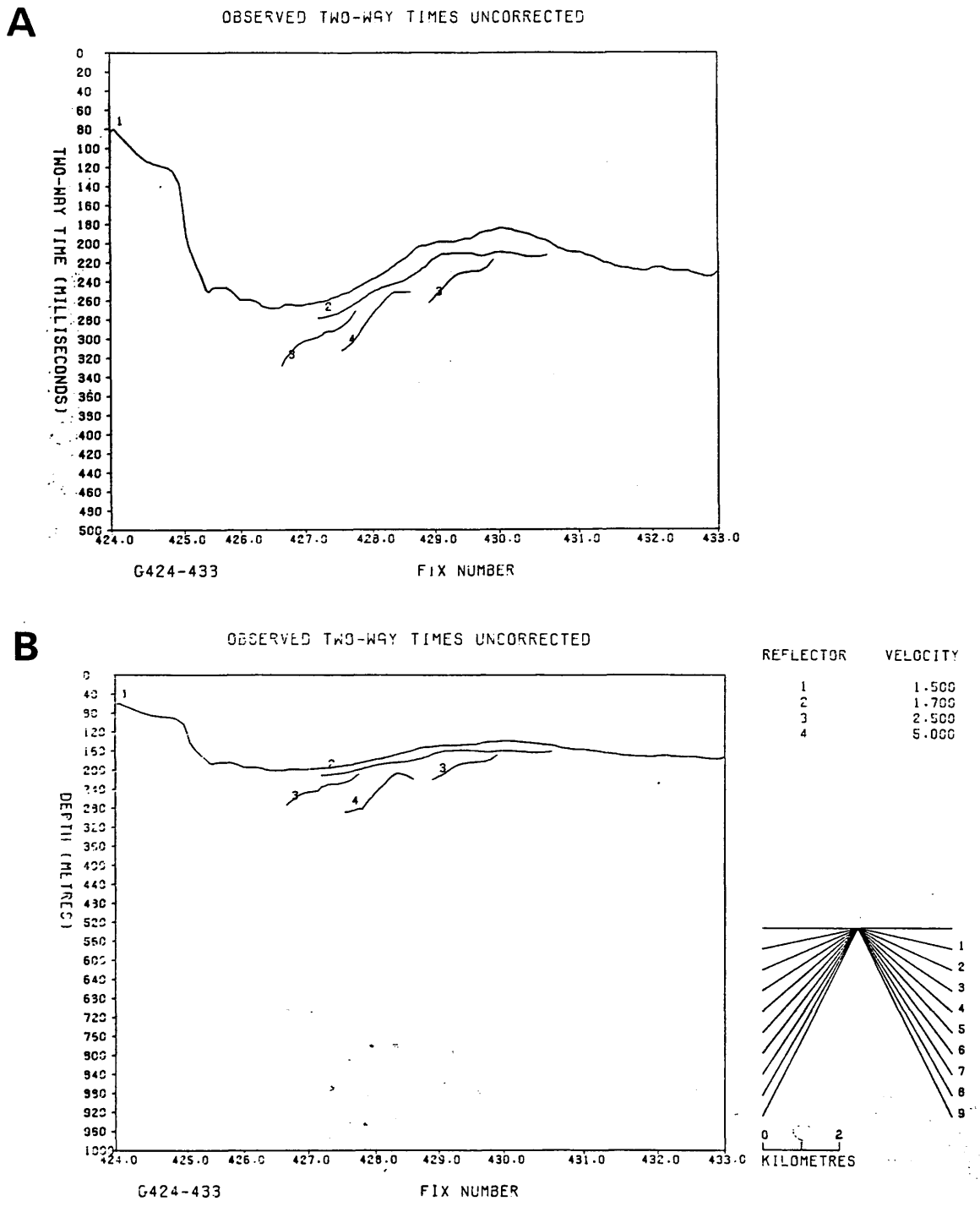

Fig. 3.71 Sample test plots from a sparker record digitising scheme.
A. Digitised line drawing of sparker record, after horizontal scaling to correct for variation in ship's speed, with the result that the 10-minute fixes along the bottom are not evenly spaced in horizontal distance. Re-scaling is done by merging the digitised sparker data with digitised location data (the map made from this data set is enclosed in the pocket as Figure 3.70).
B. Sparker line drawing of Figure 3.71A after a locally 1-dimensional depth conversion, using assumed mean velocities for each class of reflector, as shown in the table on the right. True dips in degrees are indicated in the fan diagram at bottom right.

CHAPTER 4
GEOLOGICAL INTERPRETATION

4.1 SHALLOW GEOLOGY OF NORTHERN SKYE AND THE LITTLE MINCH

4.1.1 INTRODUCTION

Two colour-printed maps of the solid geology of the Little Minch have now been published, both based on a simplified version of the author's interpretation of the data discussed in Section 3.4 above. The first of these (Chesher et al. 1983, fig. 3) is at 1:500,000 scale, and is included herein as Figure 4.1. It shows the prevalence of intrusives at the sea bed in the area between 57°N and 58°N, in contrast to the Sea of the Hebrides and the North Minch, to the south and north, respectively. This is not an artefact of the greater density of survey coverage within the present study area.

The second published map (British Geological Survey 1987) is included here as Figure 4.2 (in pocket inside back cover). At the larger scale of 1: 250,000, it shows the same simplified interpretation, but with the important modification of an outcrop of Oligocene adjacent to the Minch Fault, postulated from the discovery in 1980 of Oligocene in an offshore borehole. This is discussed below, following a discussion and re-interpretation of the geology of northern Skye itself.

4.1.2 STRUCTURE OF THE PALAEOCENE BASALTS OF NORTHERN SKYE

4.1.2.1 Limitations Of The Published Information

Northern Skye geology is clearly dominated by the influence of NW trending normal faults cutting both the basalts and the Jurassic; this trend is apparent both offshore, as is shown below, and in the gravity work of Tuson (see Fig. 1.12 above). It is desirable to elucidate the shallow structure, to find out:

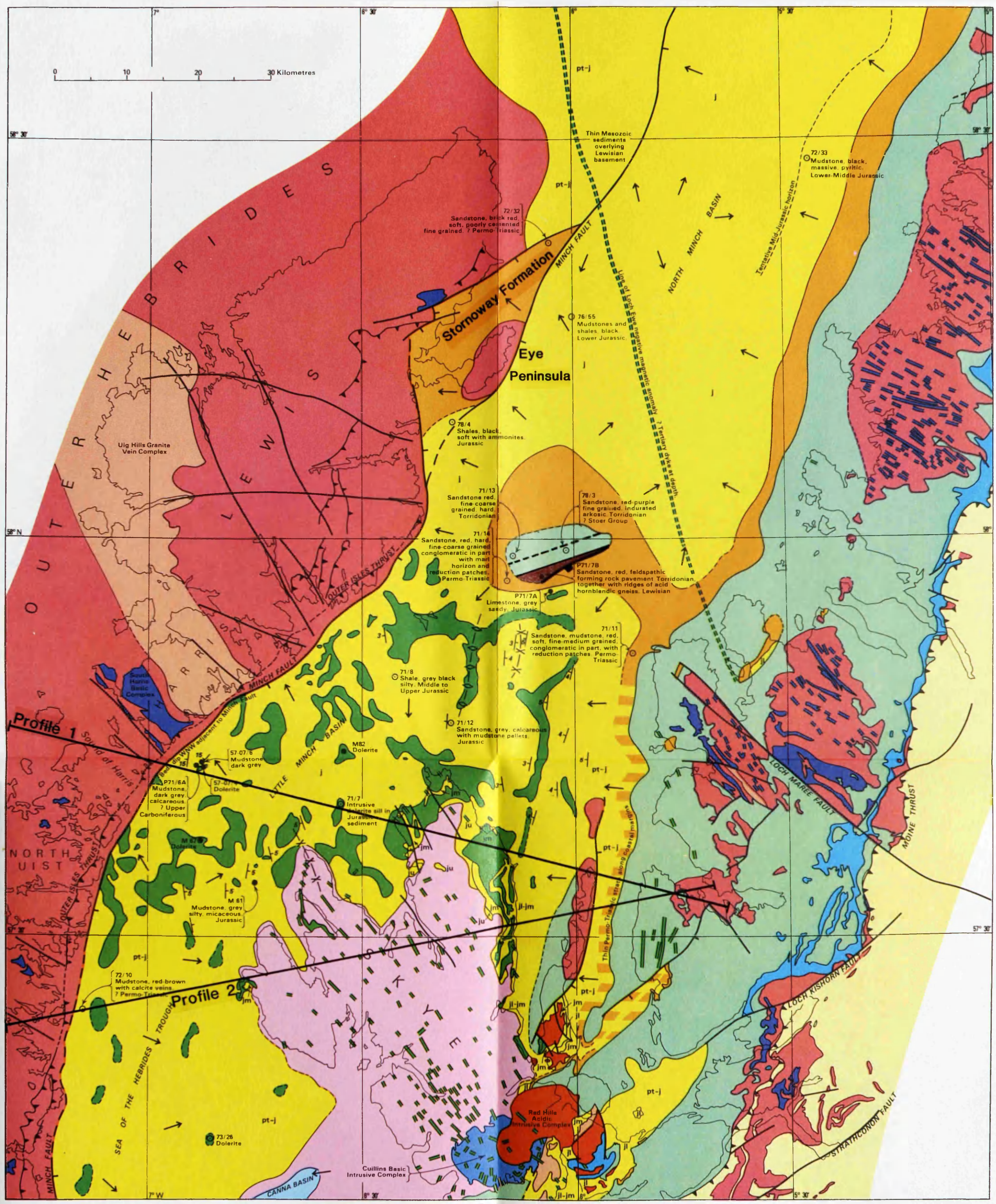

SEDIMENTARY ROCKS

- Tertiary
- Jurassic (j) — ju Upper, jm Middle, jl Lower. 'N.B. There are thin Cretaceous sediments on Skye'
- Permo-Triassic (pt)
- Cambro-Ordovician
- Torridonian
- Lewisian
- Moinian

IGNEOUS ROCKS

- Tertiary basaltic lavas
- Tertiary basaltic and doleritic, sills, dykes and minor intrusions
- Tertiary acidic intrusive complexes
- Tertiary basic and ultrabasic intrusive complexes
- Lewisian basic complexes
- Lewisian granitic complexes

STRUCTURES

- Geological boundary, broken line denotes uncertainty
- Fault and crush belt
- Thrust fault
- Axial trace of anticline
- Axial trace of syncline
- Bedding, dip in degrees
- Regional dip
- IGS Borehole
- IGS Sample Station solid outcrop

Fig. 4.1

Geology of the Minches (1983)

(1) What are the chief features (e.g. major faults), which will be important at depth?

(2) Whether the faulting is a reactivation of older, deeper features.

(3) The age of the faulting and folding.

The Geological Survey memoir on northern Skye (Anderson and Dunham 1966) refers to three major normal faults or fault complexes; the Portree Fault and Loch Greshornish Faults downthrow the basalts to the SW by about 300 m and 400 m, respectively; and the Loch Bay Faults further west downthrow the basalts to the NE by about 450 m (in fact, the throw, as portrayed on the cross-section of the Northern Skye 1" sheet [Institute of Geological Sciences 1964], is rather larger, at about 600 m). These three fault complexes are responsible for the outcrop pattern of the five groups of basalts (Anderson and Dunham, op. cit., fig. 13, reproduced above as Figure 1.15).

The map and memoir together indicate that the faults are post-basalt in age, and are essentially vertical. Each of the five groups of lava is presumed to be lensoid in cross-section, with an original depositional dimension of the order of 20-50 km in the E-W direction, and about twice as large in the N-S direction. Structural detail is said to be almost impossible to elucidate, because the dips recorded by the lava flows are depositional and not tectonic (op. cit., p.176). By way of example, the basalts in Trotternish are quoted as having westerly dips of 10-15°, but they rest on a surface dipping west at only ¼°. These figures are incorrect; the base of the basalts dips west at about 1½°, and the dips in the basalts themselves are usually under 10°. However, the disparity in dip remains to be accounted for - taken at face value, it would imply a source for the basalts to the east of Skye, which is inconsistent with the presumed source area below northern Skye itself.

The published solid geology map of northern Skye is not considered reliable because, for example, supposedly horizontal surfaces are mapped as crossing topographical contours. A large part of the problem is that the survey

was carried out in the 1930s using c.1900 6" to 1 mile Ordnance Survey base maps, which had no contours. These field sheets were only interpreted and drawn onto a reference set (still lacking National Grid and contours) much later, and from these the 1" solid map was compiled. It is apparent from inspection of both the field slips and the 6" reference sheets that exposure is generally very poor, and that the OS base maps are inadequate. Most faults are interpreted on the basis of vague topographic lineaments, and only the very large ones, such as the Loch Bay Fault, are mapped from more definite features like crush zones along linear eroded-out gullies. Presumably, many of the smaller faults are postulated to account for local changes in structural level, as inferred from stratigraphy. In short, whereas the major structure is probably accurate, local details should be viewed cautiously.

The interbasaltic sediments do not correspond to a clear pattern, either in the memoir account (Anderson and Dunham 1966, p. 77), or in the schematic cross-section (see Fig. 1.15 above). They are generally presumed to occur between lava groups, and where one or more of these groups is at pinch-out. The description is confused both by the use of nomenclature that occurs nowhere else in the memoir (nor in earlier works such as the Summaries of Progress (1935-1939), or Harker's (1904) classic memoir), and by some obvious errors both in the use of the basalt group names and in compass directions.

The problems outlined here can be largely resolved by a re-interpretation of the structural history of the lava pile, using some very simple quantitative ideas.

4.1.2.2 Revised Stratigraphy And Structure

The five lava groups used in the new model are as defined by Anderson and Dunham (1966, p. 81):

	Approx. thickness
5. Osdale Group (alternating basalt and mugearite flows)	500 m
4. Bracadale Group (alternating basalt and trachyte flows)	150 m
3. Beinn Totaig Group (porphyritic basalt at top, alternating basalt and mugearite flows below)	600 m
2. Ramasaig Group (mugearite flow at top, alternating porphyritic and non-porphyritic basalts below)	800 m
1. Beinn Edra Group (mugearite flow at top, mainly non-porphyritic basalts below)	300 m
Total thickness	2350 m

It is assumed that the Beinn Edra Group is older than the Ramasaig Group, although this is not known for certain.

It is postulated that each group of lavas is fault-bounded, and deposited in a shallow half-graben on one side or other of one of the three major normal faults mentioned above. This new model has a number of simple assumptions:

(1) Each group is wedge-shaped (Figure 4.3), with its maximum thickness at the bounding fault.

(2) The active extensional fault is the main source of the flows, and 'instantaneous' compensatory downthrow occurs as each flow is extruded, to bring the new ground surface to the horizontal.

(4) There is no (significant) erosion.

(5) There has been negligible further throw on the major faults since eruption of the lavas.

In the schematic diagram of stratigraphic thicknesses (Fig. 4.3), the Bracadale Group has been put in as box-shaped rather than wedge-shaped, as it is not clear which of the two bounding faults was the dominant. A small wedge to the west of the Loch Bay fault has been added to the top of the Ben Totaig Group, to account for the major outlier of Bheinn

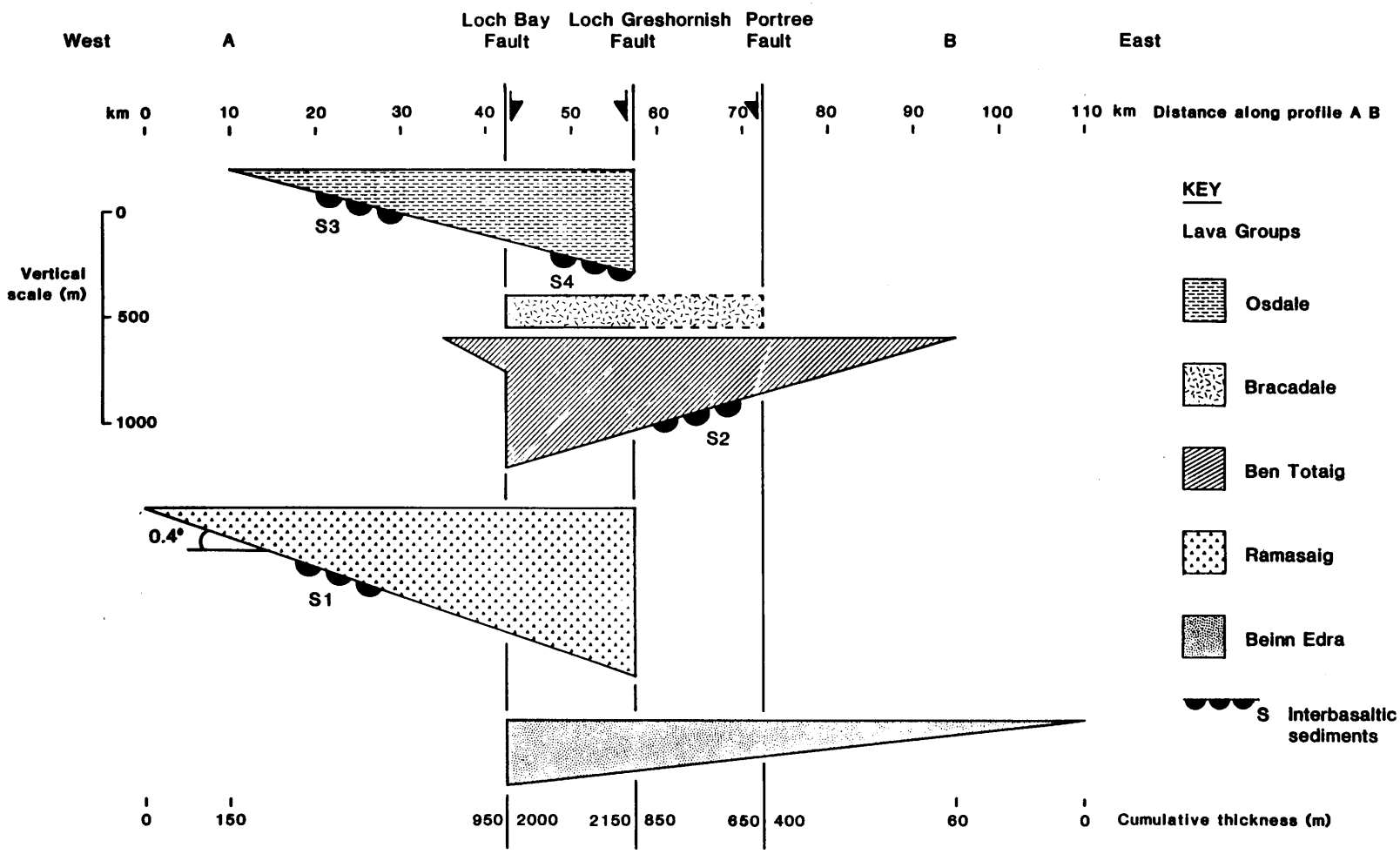

Fig. 4.3 Stratigraphic thicknesses of the five groups of northern Skye lavas along the profile A-B of Figure 4.4. In this new model it is postulated that each group is erupted along, and controlled by, one of the three low-angle normal faults named at the top. The interbasaltic sediments can be classified into groups S1-S4, which are presumed to just pre-date the eruption of the overlying lavas.

Bhreac. The stratigraphy of the interbasaltic sediments is discussed below. Figure 4.4 shows the areal distribution of the five groups, in relation to the three major faults. In general, the feather-edge of each group is placed in the same area as in the old lensoid interpretation (Fig. 1.15), but the opposite margin is now bounded by one of the three faults.

Adding up the five polygons of Figure 4.3 results in the cross-section of Figure 4.5, in which the maximum thickness of lavas deposited is 2000-2100 m between the Loch Bay and Loch Greshornish fault systems. The cross-section A-B is the same as that shown in Figure 1.15, and is approximately along the line of the detailed cross-section accompanying the 1" Northern Skye solid geology map. A schematic topography and sea level have been added, showing that about 400 m have been eroded from the top of the pile since its deposition. In the east, in Trotternish, some 200-300 m have been removed, and in the far west only 150-200 m have been eroded; this suggests that there has been a regional tilt to the west during or since this erosional period.

The simple model outlined here accounts for all the major present-day outcrops of the five groups. The maximum thickness of basalts preserved is about 1550-1600 m (below sea level datum), between the Loch Greshornish and Loch Bay Faults. Reflection line SK-6 is located near to the profile, and the strong reflector presumed to be from the base of the basaltic pile (see Figs. 3.55 and 3.56A) is at a depth of 1680 m, which is in good agreement with the model.

The locations of the interbasaltic sediments have been revised somewhat from the memoir account (Anderson and Dunham 1966, pp. 77, 82; see also Summ. Prog. Geol. Surv. 1937, p. 77, 1939, p. 75). The 12 localities fall into four clear groups labelled S1 - S4 on Figure 4.3. Although these varied small occurrences of lignite, sandstones, shales, conglomerates and agglomerate could, in principle, have been deposited at any time between the underlying and overlying lava groups, it is logical to presume that they avoided erosion by being dated just prior to the overlying lavas. This is why the schematic lenses

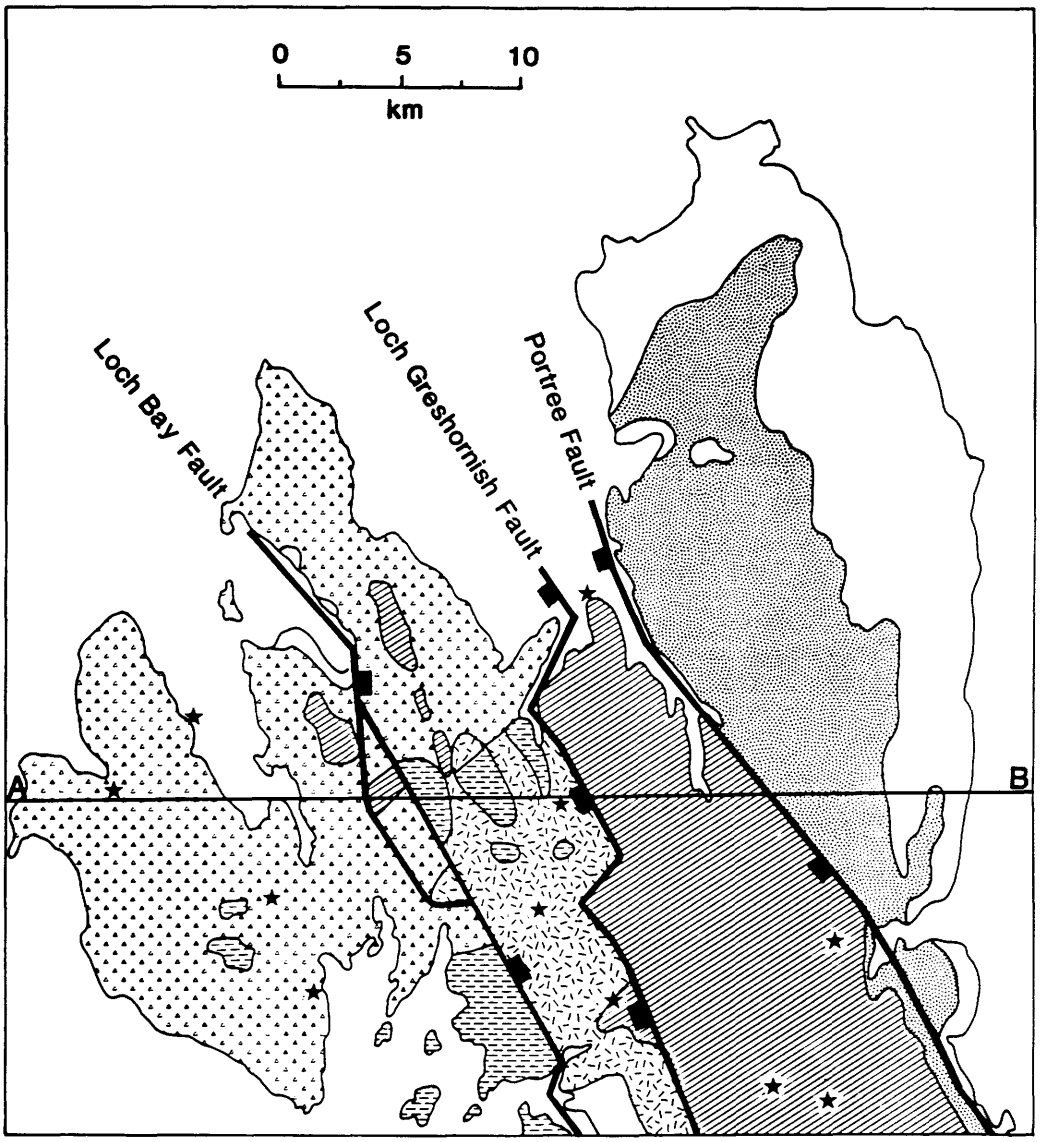

Fig. 4.4 The five groups of Palaeocene lavas in northern Skye (key to patterns in Figure 4.3), showing the three main fault systems postulated to control their deposition and preservation. Stars show sites where interbasaltic sediments occur. Section A-B is illustrated in Figure 4.5. The outcrop pattern follows Anderson and Dunham (1966, fig. 13, which has been reproduced above as Figure 1.15).

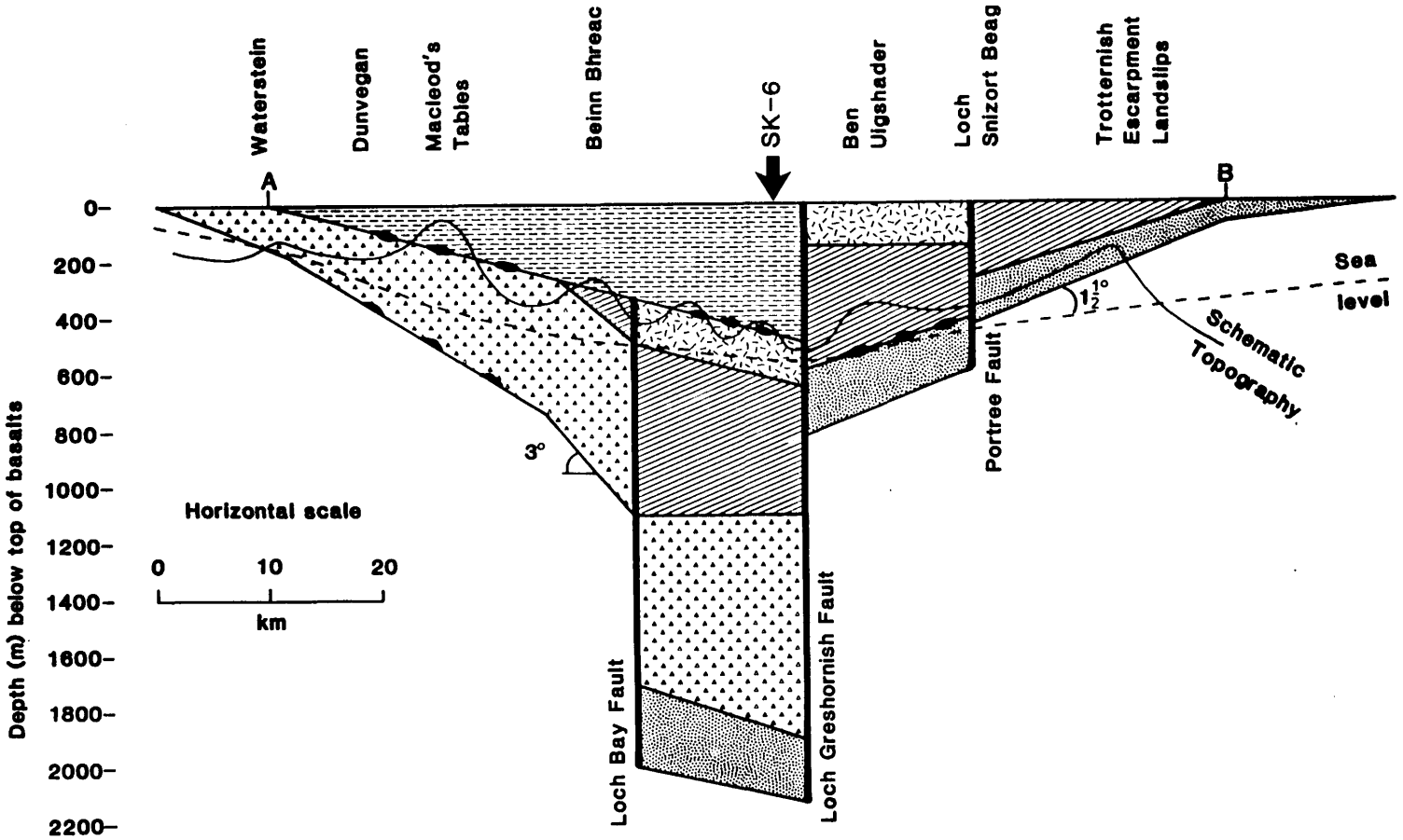

Fig. 4.5 Cross-section A-B (located in Figure 4.4) through the northern Skye basalts. The pile has been obtained by adding up the polygons of Figure 4.3, and the present-day outcrop pattern (Fig.4.4) results from erosion down to the topography shown schematically. Seismic reflection profile SK-6 indicates a thickness of 1680 m of basalt below sea level (see Table 3.7). The model above predicts 1600 m. Interbasaltic sediments are indicated by the black lenses.

shown in Figure 4.3 are attached to the underneath of a group. The implication is that they represent the earliest phase of subsidence of a particular half-graben, just before being buried by basalt flows.

The three localities constituting sedimentary group S3 in western Skye reveal dreikänter of sandstone pebbles "probably derived from the Torridonian Sandstone" (Summ. Prog. Geol. Surv. 1939, p. 75). Modern sedimentological evidence would suggest, however, that such wind-blown material is more likely to have been derived from the semi-arid Permo-Triassic, rather than the Torridonian.

An interesting feature of this model is that half-graben subsidence alternated in sense between down-to-the-east and down-to-the-west (Figs. 4.3, 4.5). This is the sort of behaviour to be expected from subsidence on a set of synthetic and antithetic faults. Although the three major faults have been shown schematically as vertical, it is demonstrated below that they are low-angle. The Loch Bay Fault is the synthetic, and the two other fault sets are antithetic to it.

Lastly, the concept of low-angle normal faults (whether listric or straight in cross-section) can account, in principle, for the disparity in dip of basalt bedding with the regional basal surface to the basalts, as mentioned above. The wedge model of intra-half-graben eruption implies that the steepest dip of the base of any flow, after it has been extruded and 'immediately' downthrown, is under ½° (see Fig. 4.3). Therefore the regional base ought to be more or less parallel to the flows above it. The fact that it is not the case suggests that small block rotations on many small low-angle normal faults may have occurred, but have not been recognised. Thus the Beinn Edra Group of Trotternish may show a predominant dip of 5-10° to the west as the result of many minor low-angle normal faults downthrowing to the east. This postulated fault style is a small-scale version of the major fault style affecting the whole sedimentary basin beneath the lavas, as is shown below. Although direct evidence for such fault behaviour is scant, due to the mapping problems discussed above, there is one very good example at Oisgill Bay. Figure 4.6 is an

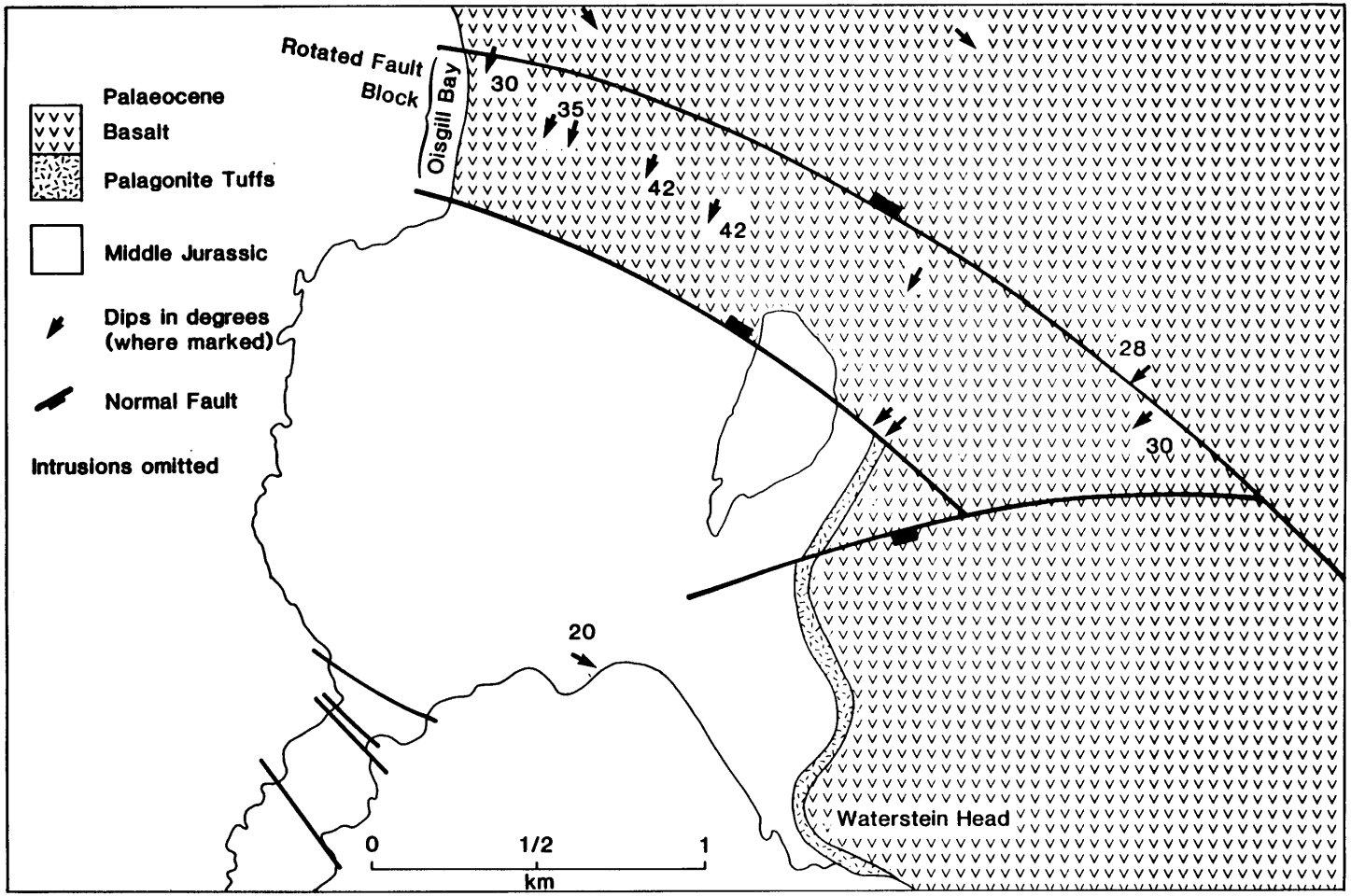

Fig. 4.6 Detail from 6" to 1 mile scale deposited reference map of the Waterstein locality, NW Skye, showing tilted and rotated fault block of basalts. Dips and dip arrows are as recorded on the reference map.

annotated part of the 6" interpreted reference sheet, showing a WNW trending block of basalt clearly downthrown and rotated against the Jurassic of Waterstein to the south. Dips within the block are 30-40° to the SSW.

4.1.3 SHALLOW STRUCTURE INFERRED FROM ONSHORE REFRACTION DATA

Figures 3.2 to 3.13 show 6 pairs of time-distance graphs of the first arrivals, or first breaks, picked from the reflection records at sites SK-1 to SK-6. These are interpreted primarily for applying static time corrections to the reflection data, but some shallow geological structure can be interpreted from them as well. A summary of this interpretation is shown in Figure 4.7.

Only one site - Staffin, SK-3 - has a data set which is simple and consistent enough to warrant a 2-dimensional model interpretation. Shooting up-dip (to the east) the later arrivals have an apparent P-wave velocity of 4.9 km/s, whereas down-dip the velocity is 4.3 km/s. The refractor is interpreted to be from the top of a sill dipping to the west at 1.5°. The refracted arrivals from the sill show rapid attenuation with offset (some of them are displayed in Figure 3.30), suggesting that the sill is very thin. Figure 4.7 illustrates a nominal thickness of 50 m.

The interpretation of the other sites uses a 1-dimensional, two-layer model to fit the arrivals. The sites over basalt, SK-4 and SK-6, have a V_P of about 4.5 km/s below some lower-velocity weathered rock. The Waterstein site, SK-6, affords an interesting comparison of the first break V_P = 5.5 km/s, clearly from the sill below the Middle Jurassic shales, with the ultrasonic velocities from samples WST and WSB collected at the top and bottom, respectively, of the cliff below the site. The upper sample site has a mean V_P of 4.7 km/s (Appendix 2), whereas the lower leaf of the exposed sill complex has the higher mean V_P of 5.59 km/s. In contrast to the Staffin site, there is no sign of amplitude attenuation of the arrivals from the sill, so the sill at Waterstein is presumably much thicker. The thin

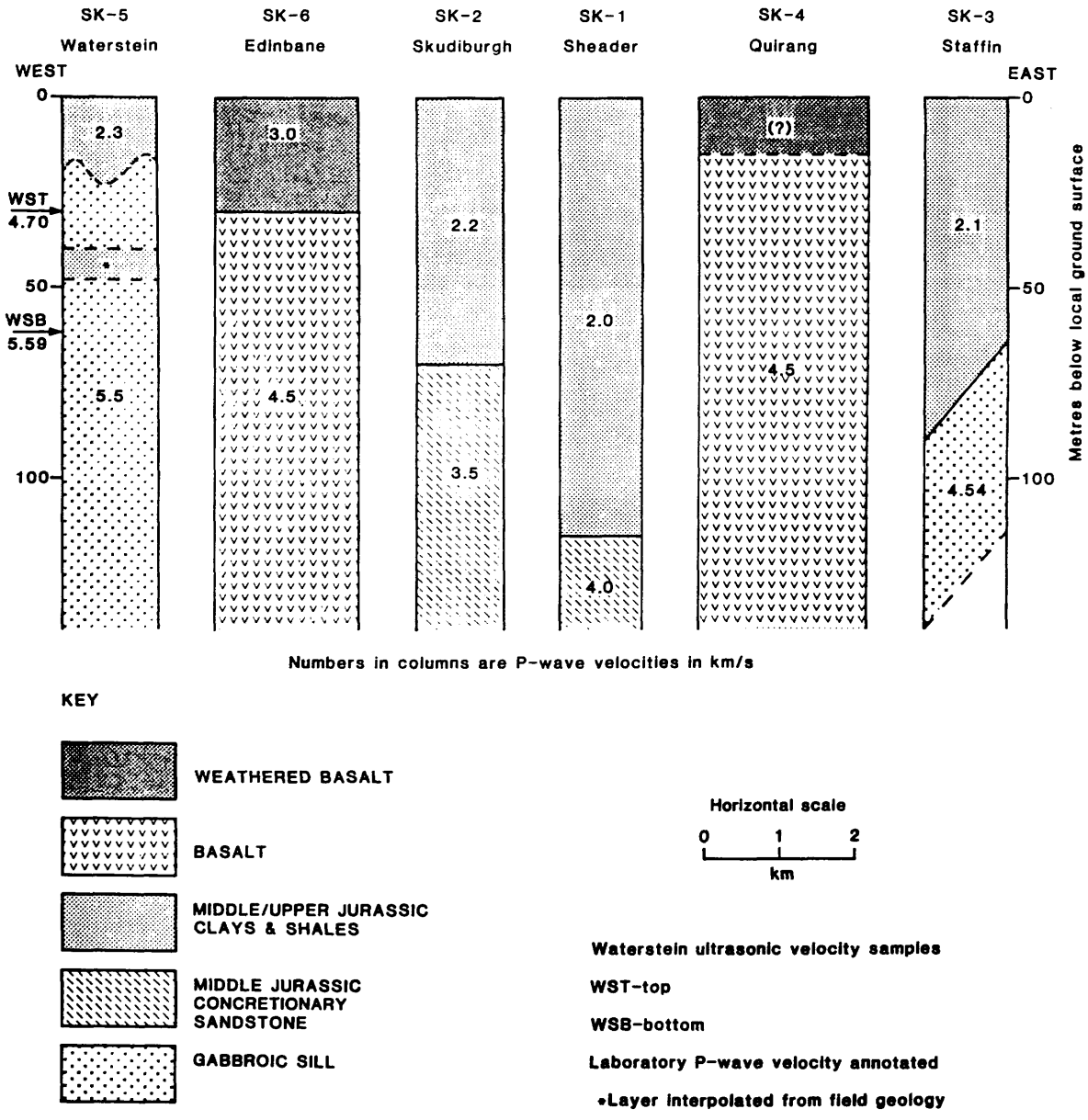

Fig. 4.7 Summary of shallow structure at the six seismic reflection sites in northern Skye, derived from interpretation of the first breaks shown in Figures 3.2 to 3.13. The interpretations are 1-dimensional, except for SK-3 (Staffin), where the top of the sill dips west at 1.5°.

layer of shales at 40-50 m shown in Figure 4.7 has been inserted on the basis of the field geology, and not from interpretation of the first breaks.

Sites SK-1 and SK-2 are both on Middle to Upper Jurassic clays, which have a low P-wave velocity of 2.0 - 2.2 km/s near the surface. The clay horizon at each outcrop is 130 m and 40 m, respectively, above the Middle Jurassic Concretionary Sandstones (see Figure 1.14), which would be expected to have a significantly higher velocity. The poorly-determined lower layer at the two sites, with V_P of about 3.5 and 4.0 km/s, respectively, occurs at the approximate depth expected from the stratigraphy for the Concretionary Sandstone.

4.1.4 THE SHALLOW GEOLOGY OF THE LITTLE MINCH

The detailed solid geology map, interpreted at 1:50,000 scale, is presented at 1:100,000 scale as Figure 4.8 (in pocket inside rear cover). The track chart of profile data upon which the interpretation rests is also enclosed in the pocket as Figure 3.70; it should be referred to for the location of the examples shown below.

4.1.4.1 Methods Of Interpretation

Gabbroic intrusives are mapped on the following criteria:

(1) They generally form bathymetric shoals, several of which have been sampled.

(2) Where they are relatively isolated, these shoals show pronounced high-amplitude magnetic edge-effect anomalies. Figure 4.9 shows a simple example, located in Figure 3.70.

(3) The outcrops tie into onshore sill outcrops, such as the Ascrib Islands and the north coast of Trotternish.

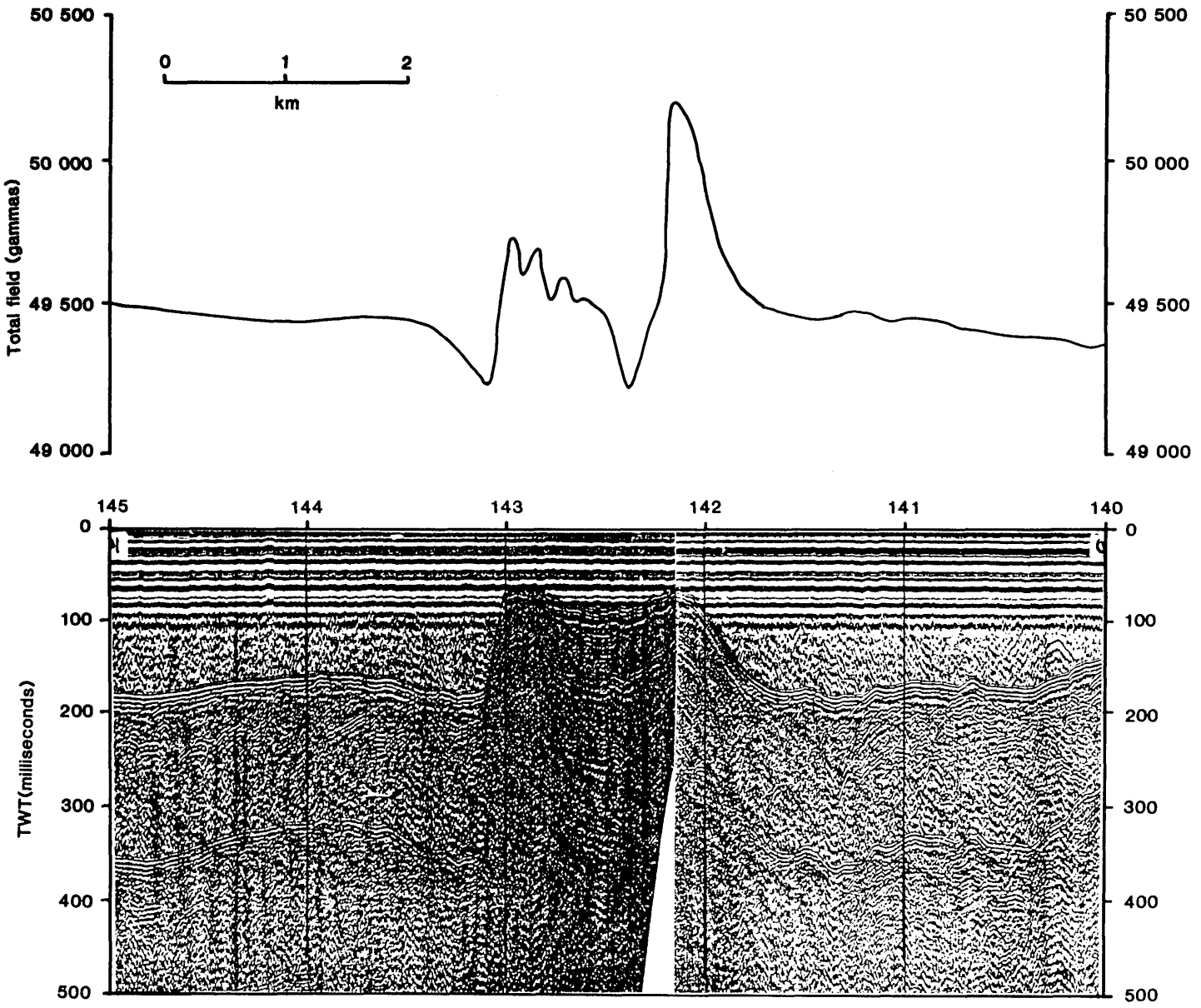

Fig. 4.9 Total field magnetic anomaly profile and sparker section between fixes 140 - 145 (located in Figure 3.70), illustrating the edge effect anomalies due to gabbroic sill, which forms the shallow feature between fixes 142 - 143.

Often, however, the sparker record of a shoal can show reflectors (due, presumably to sediments), whereas the corresponding magnetic profile shows a complicated, high-amplitude pattern indicating mafic intrusives at shallow depth. Figure 4.10 shows an example of such profiles, located in Figure 3.70. The bank between fixes 364 and 369 does not comprise 100% sill outcrop, but is made up of two or more leaves of intrusives.

Fold axes can be traced from line to line. Figure 4.11 shows a sparker section across the pronounced set of fold axes running NNW from Loch Snizort. Some fold axes clearly mark open, gentle folds, but some, such as the pair between fixes 211 and 212 on Figure 4.11, indicate tight, small-scale rucks in bedding of generally low dip; these may indicate faults, either in the section just below sea bed itself, or somewhat deeper. However, they have not been interpreted as faults on the map (with one exception), because their magnitude and sense of displacement cannot be discerned.

West of Vaternish it is possible to map the outcrop of specific horizons by correlating from record to record at intersections. By establishing the strike in this way, the true dip of the bedding can be calculated, using an assumed velocity. This has been done at several dozen locations. True dip can also be calculated from the apparent dips at the intersection of two lines; this was possible at fifteen intersections.

4.1.5 DISCUSSION OF THE SHALLOW STRUCTURE

4.1.5.1 The Minch Fault And The Tertiary Half-graben

The Minch Fault, identified as a normal fault from the preliminary interpretation of the present data (Smythe et al. 1972) has since been recognised as the reactivated Outer Isles Thrust (Smythe et al. 1982, Brewer and Smythe 1986). Such low-angle normal faults, whether they had a previous existence as thrust faults or not (Wernicke 1986) account for crustal thinning and basin extension in a way

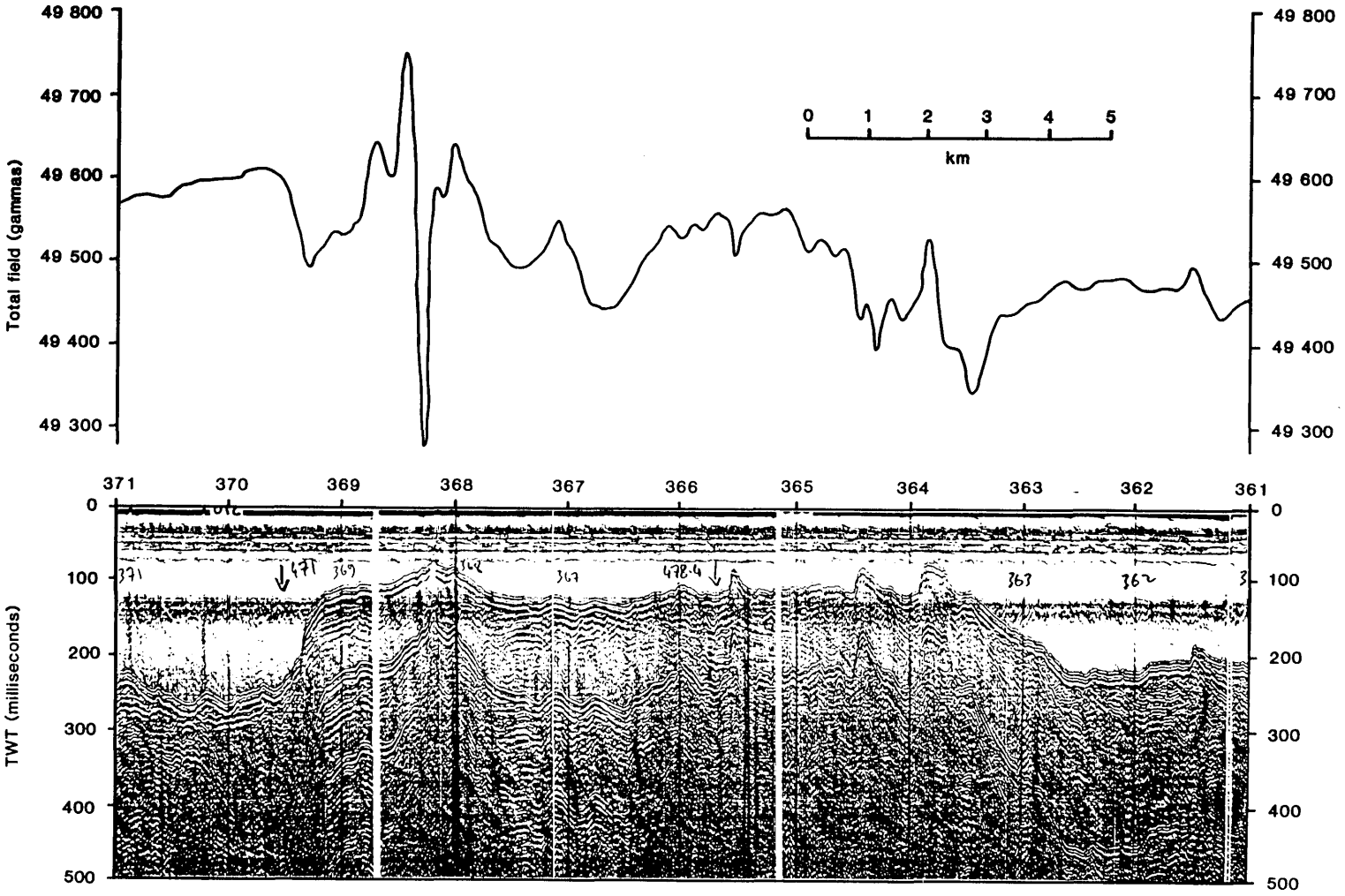

Fig. 4.10 Total field magnetic anomaly profile and sparker section between fixes 361 - 371 (located in Figure 3.70), illustrating the complex anomalies due to the leaves of a gabbroic sill intruding Jurassic, which forms the shoal feature between fixes 363 - 369. Reflectors from the sediments between the sill leaves can be seen within the shoal region.

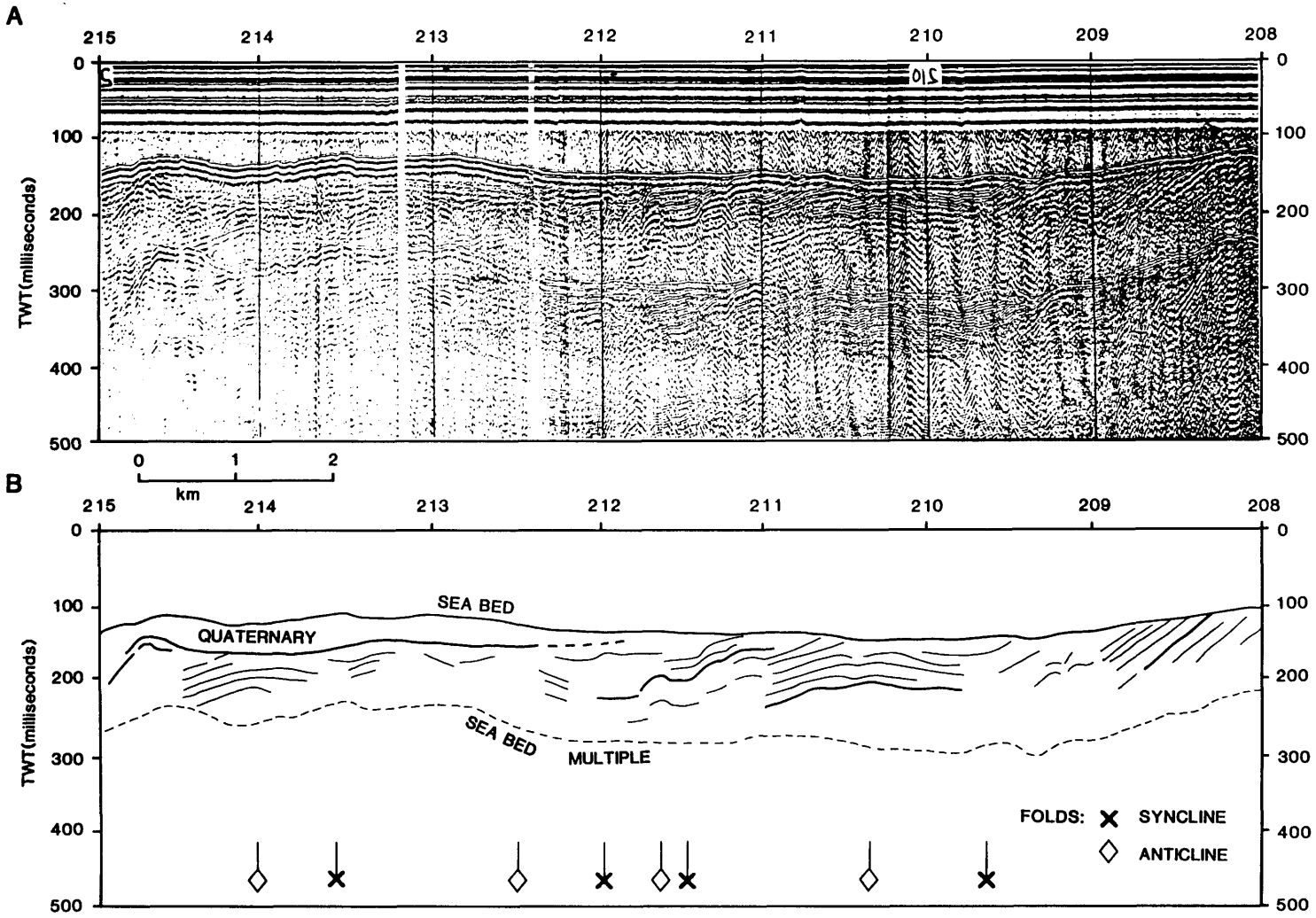

Fig. 4.11 Sparker profile and interpretation between fixes 208 - 215 (located in Figure 3.70) to illustrate the many small folds and rucks which can be mapped from line to line.

not previously understood (at least in the UK) when normal faults were nearly always presumed to have steep dips - say greater than 60°. Syndepositional bedding bounded by an extensional fault is tilted towards the fault outcrop by the combination of extension and subsidence; we should therefore expect the phases of active extension and subsidence on the Minch Fault to be revealed by sequences tilted to the west. The strip of Oligocene clays and lignites is a clear example of this; both on the sparker profiles and in the core which proved the age and lithology (IGS borehole 80/14; see Chesher et al. 1983), the bedding dips at 25-30° to the NW. Underlying the Tertiary there are more-or-less connected strips of magnetic, more resistant rock at outcrop previously interpreted as gabbroic sill (see the map enclosed as Figure 4.2). These outcrops, within 5 km of the Minch Fault, are re-interpreted here (Fig. 4.8) as basalt for two reasons:

(1) The outcrops next to the Oligocene form a very linear, characteristic double-crested ridge (first identified by Eden et al. 1973), which appears to underlie the Tertiary sediments conformably; the proven gabbroic outcrops are much more irregular in plan.

(2) The core sample from the more southerly ridge is basalt, not gabbro. There is also a sample of basalt which was cored on the presumed Lewisian footwall side of the Minch Fault, off the SE coast of Harris.

By analogy with the new model for fault-controlled eruption of the Skye basalts discussed above, it follows that the source of this strip of basalts was probably the Minch Fault itself. The fault has therefore undergone significant displacement during the Palaeocene and Oligocene.

4.1.5.2 The Harris Fault Zone

There is a strip of outcrop parallel to the Tertiary sediments and basalts described above, and lying SE of it, comprising very poor bedding (as seen on sparker data), but also dipping generally NW. It is bounded to the SE by a

feature previously identified as an "ill-defined anticline" (Chesher et al. 1983). This feature is re-interpreted here as a normal fault, downthrowing to the SE in the same manner as its neighbour, the Minch Fault. It is postulated on the following grounds:

(1) Although nowhere identifiable on the shallow profiling data as an actual fault, on some sparker profiles the acoustic bedding seems to be significantly better on the SE flank of the 'anticline' than on the NW flank.

(2) A large fault at this location accounts for the core sample of dark calcareous mudstone of Late Palaeozoic age, possibly Dinantian or Namurian, collected by a manned submersible (Eden et al. 1973, p. 21). The sample is within the NW-dipping, poorly-bedded outcrop, whereas the SE-dipping strata on the other side of the fault are of Jurassic age.

(3) The fault accounts in a similar way for the borehole sample 72/10 east of Wiay Island, Benbecula. The sheared reddish-brown mudstone with calcite veins is thought to be Permo-Triassic.

(4) The fault is required to reconcile the shallow structure with the gravity models discussed below.

(5) The 1972 refraction data in the Sound of Harris area are better explained with this new fault, as is shown below.

It is not clear whether the Harris Fault extends north of 57°45'N.

4.1.5.3 The Jurassic Basin

To the SE of the Harris Fault the sea bed outcrop is almost entirely Jurassic, intruded by many Palaeocene sills. The main structural feature of the area mapped is the change in trend from NE-SW, coming north from the Sea of the Hebrides,

into a pronounced NW-SE trend of folds (and possibly faults) in the Little Minch NW of Loch Snizort. A regional plunge to the SE is superimposed on this trend, so that the deepest part of the Jurassic basin is at the mouth of Loch Snizort.

The stratigraphic thicknesses of the Jurassic are measured in the Trotternish peninsula (see Fig. 1.14). Here the thickness from the top of the Concretionary Sandstone to the base of the Jurassic is about 400 m. However, the reflector horizon mapping west of Vaternish and Duirinish, where the structure appears to be fairly simple, suggests that the corresponding sequence of Middle to Lower Jurassic is more than twice as thick as that beneath Trotternish, viz. over 1000 m. This greater thickness of Jurassic offshore west and NW of northern Skye is also required by the gravity modelling, discussed below.

4.2 DEEP STRUCTURE OF THE NORTHERN SKYE - LITTLE MINCH BASIN

4.2.1 DEPTH MIGRATION OF SEISMIC REFLECTION STRUCTURE

Five of the six seismic reflection sites were designed to supply a 1-dimensional velocity-depth profile, whereas the exception, line SK-4, was an attempt to obtain a couple of kilometres of profile across the steepest part of Tuson's (1959) gravity gradient. However, one of the five velocity survey sites, line SK-3 (Staffin), also shows a lot of potential structural information (Fig. 3.37). It is therefore worth trying to convert both the stacked CDP record sections (Figs. 3.37 and 3.42) into a 2-dimensional depth profile.

The technique adopted to tackle this is migration by ray tracing (in the depth domain) of line drawing interpretations of the record sections. This approach has been used with considerable success for imaging deep crustal profiles, where structure is complex and signal-to-noise ratio is poor (e.g. Blundell and Raynaud 1986). The original computer program, written in FORTRAN-66 by Bernard Raynaud and kindly supplied to the author, has been

re-structured to bring it up to portable FORTRAN-77 standards. The algorithms remain, however, those designed by Raynaud (1986; in press). The innovative aspect of the program is the separation of the digitised reflector segments file from the 'ghost' structure file of constant-velocity layers, through which the zero-offset rays are traced by obeying Snell's Law at each interface.

A number of final stack displays for each of the two lines was made, and two of each are chosen for digitising (Figs. 4.12 - 4.15). Two displays of each section are digitised, as it is clear that different displays bring out different aspects of the data. The four separate digitised files are then merged onto one profile with its origin at the western end of SK-4. The velocity 'ghost' structure approximates to the velocities derived for SK-3 (Fig. 3.35), together with an interpolation between SK-3 and SK-2 to obtain velocity structure below SK-4. The resulting depth-migrated line drawing is shown in Figure 4.16A, together with an interpretation in Figure 4.16B. Although the data are very poor, they reveal steeply westward dipping layering (presumed to be bedding dipping at 30-40°) below the flatter-lying Jurassic of the uppermost 500 m. There are no significant flat layers below the Jurassic, but some of the sparse reflectors dipping east at 30-40° could conceivably be from fault-planes. These have to be postulated to avoid the problem of an unreasonably thick sedimentary succession beneath Skye, a feature that is incompatible with the gravity modelling.

4.2.2 GEOLOGICAL INTERPRETATION OF THE SEISMIC REFLECTION RESULTS

Figure 4.17 is a summary of the four velocity-depth sites on northern Skye, together with a simplified version of the migrated depth section combined from sites SK-3 and SK-4.

There is no doubt that the interval velocity of 4.8 km/s below Edinbane (SK-6) can be assigned to 1.7 km of Tertiary basalts, as it corresponds closely to the first break (refraction) velocity of 4.5 km/s (Fig 4.7). The reflector

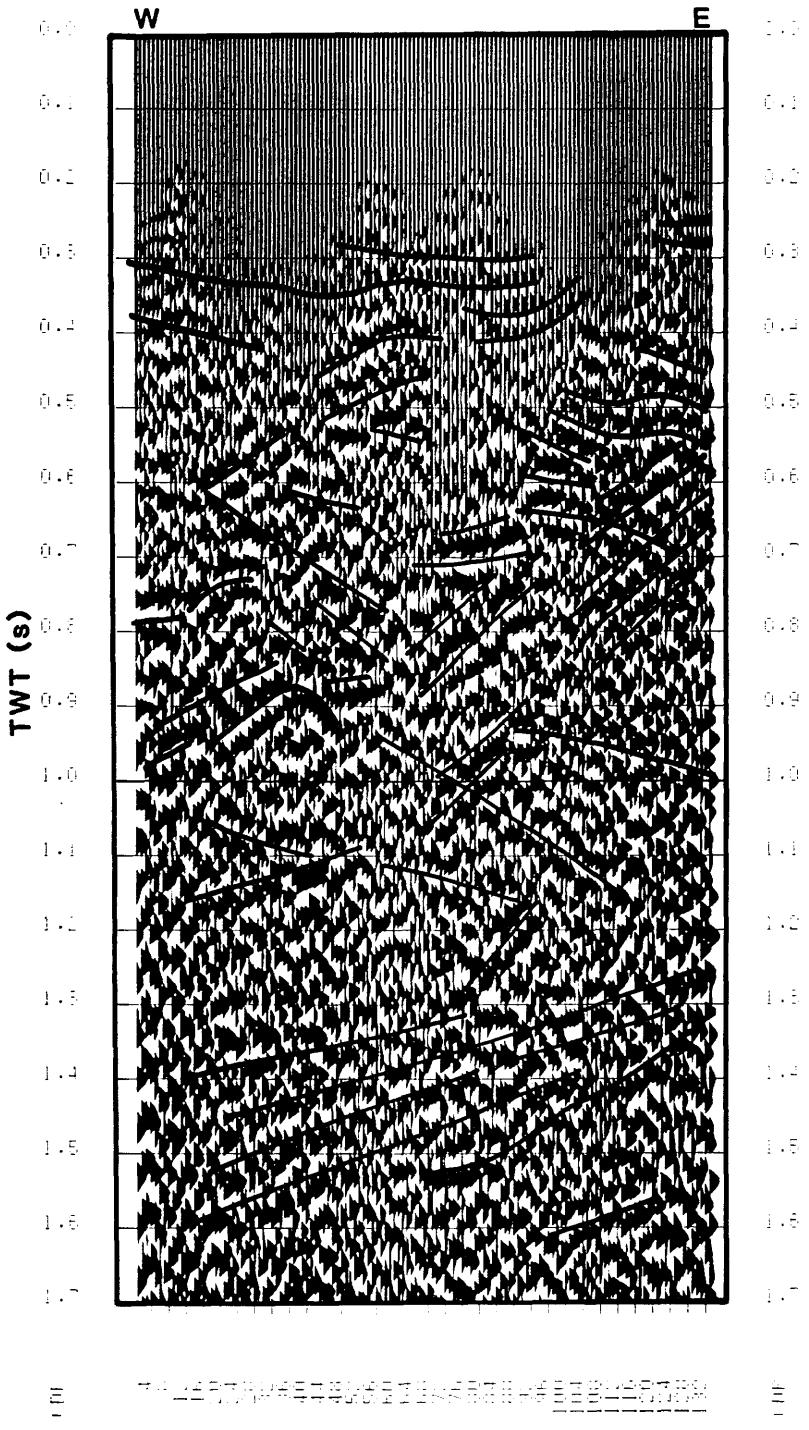

Fig. 4.12 Final stack of SK-3 (Staffin) at a horizontal scale of approximately 1:12,500, and vertical scale of 10 cm/s. Overlay shows reflectors and other events digitised for line drawing depth migration.

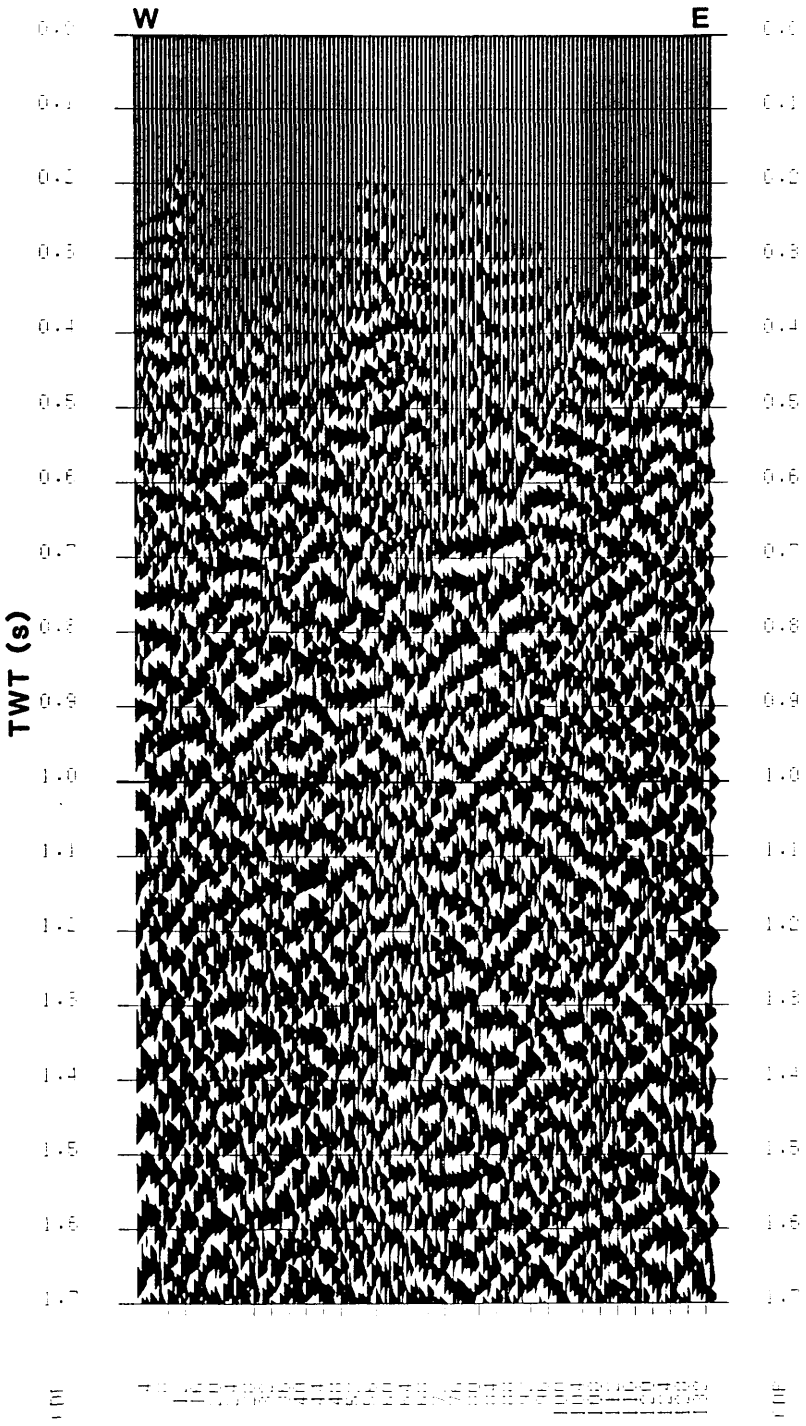

Fig. 4.12 Final stack of SK-3 (Staffin) at a horizontal scale of approximately 1:12,500, and vertical scale of 10 cm/s. Overlay shows reflectors and other events digitised for line drawing depth migration.

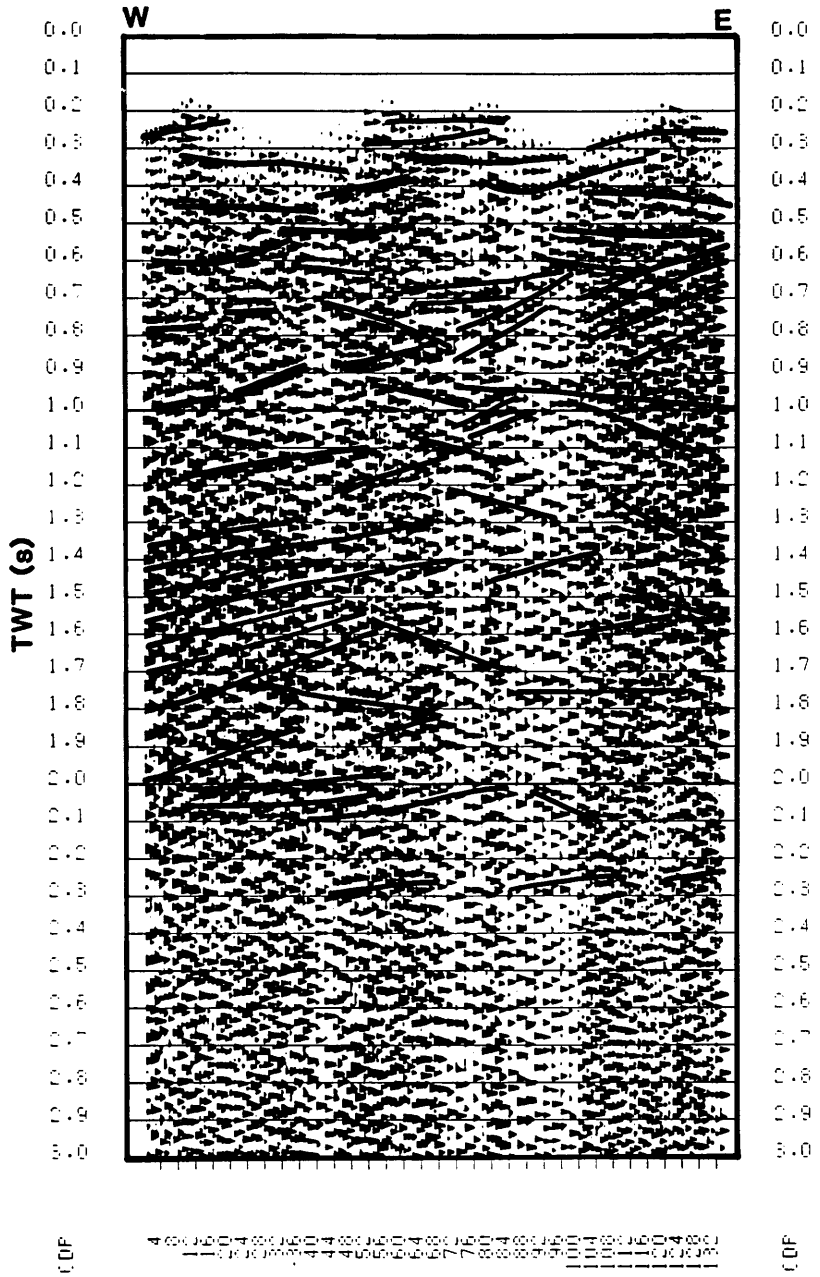

Fig. 4.13 Final stack of SK-3 (Staffin) at a horizontal scale of approximately 1:12,500, and vertical scale of 5 cm/s (same display as Figure 3.37). Overlay shows reflectors and other events digitised for line drawing depth migration.

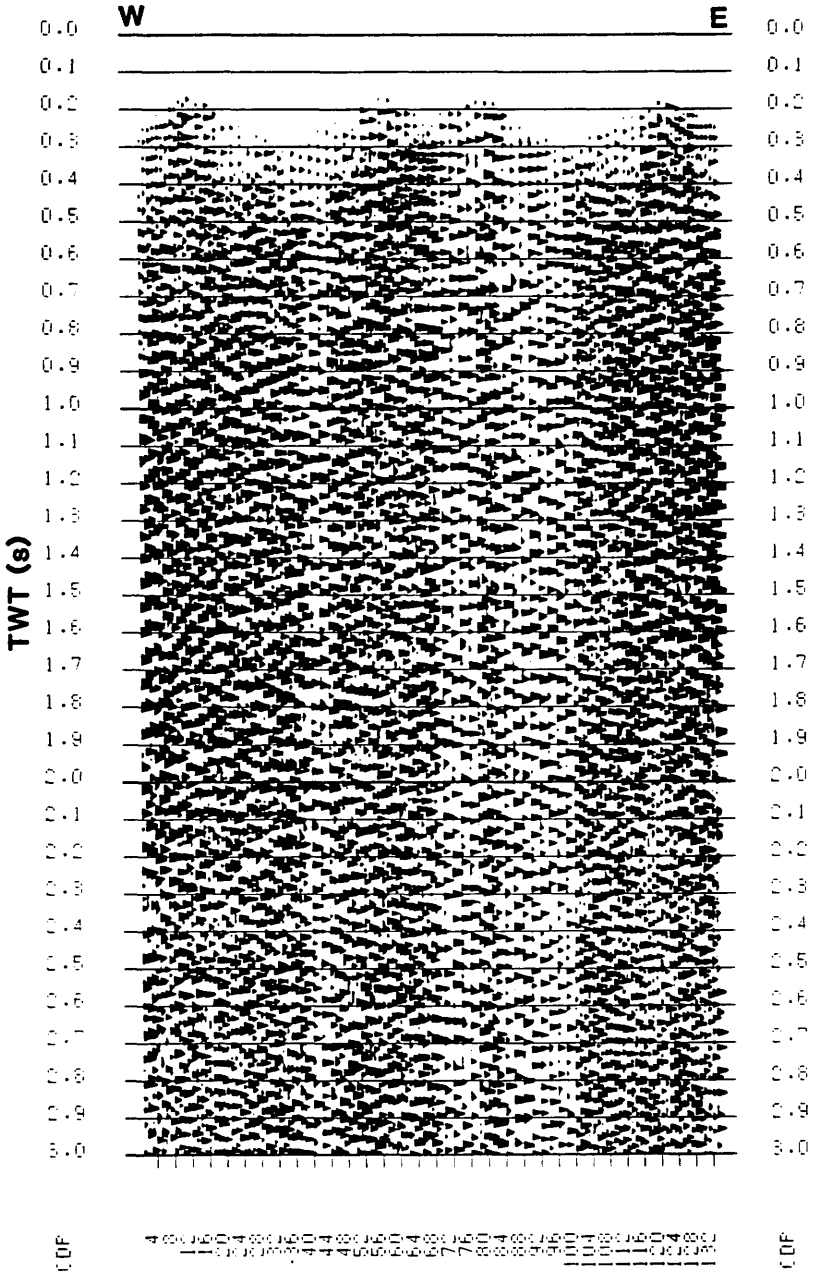

Fig. 4.13 Final stack of SK-3 (Staffin) at a horizontal scale of approximately 1:12,500, and vertical scale of 5 cm/s (same display as Figure 3.37). Overlay shows reflectors and other events digitised for line drawing depth migration.

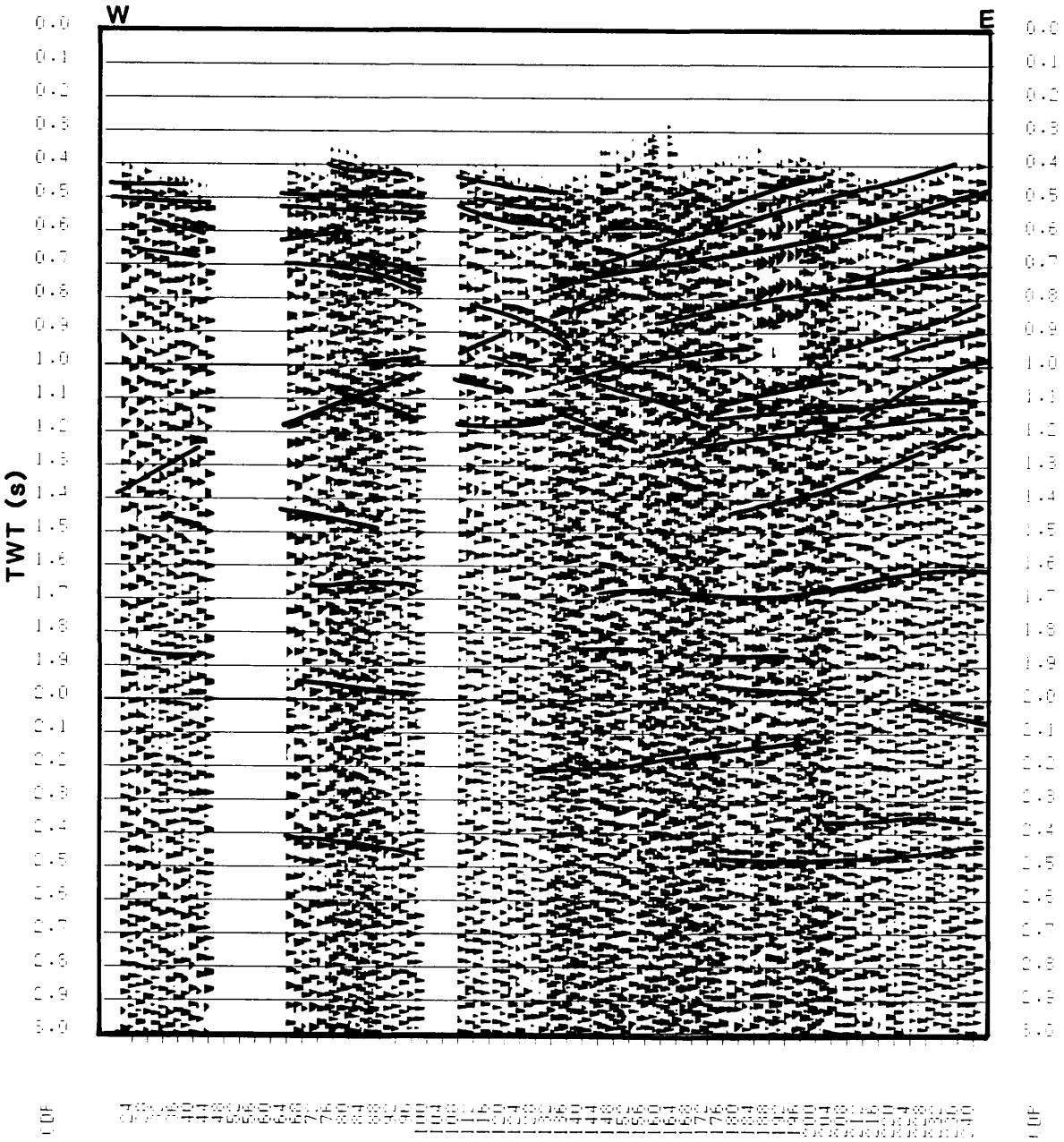

Fig. 4.14 Final stack of SK-4 (Quirang) at a horizontal scale of about 1:12,500 and vertical scale of 5 cm/s. Overlay shows reflectors and other events digitised for line drawing depth migration.

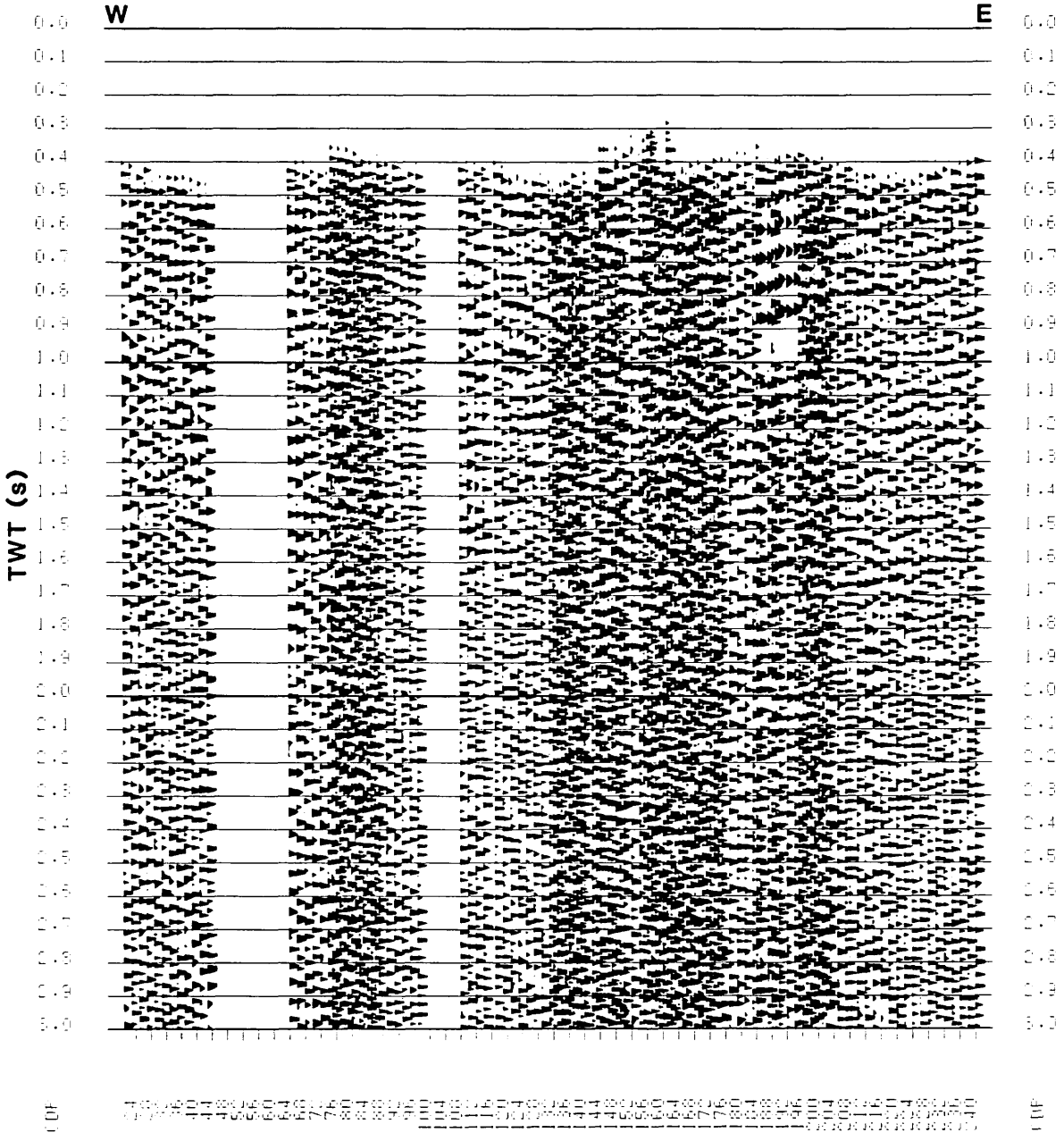

Fig. 4.14 Final stack of SK-4 (Quirang) at a horizontal scale of about 1:12,500 and vertical scale of 5 cm/s. Overlay shows reflectors and other events digitised for line drawing depth migration.

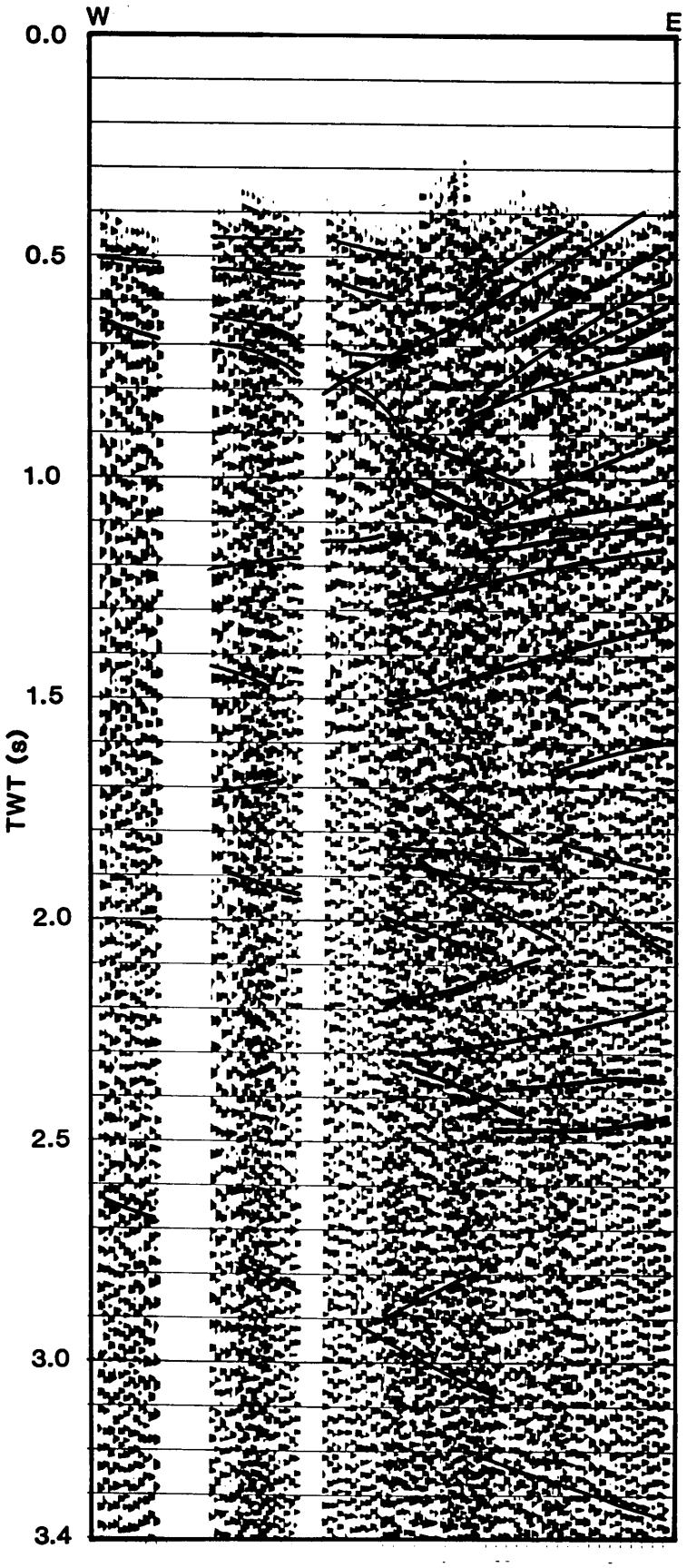

Fig. 4.15 Final stack of SK-4 (Quirang) at a horizontal scale of 1:19,500 and vertical scale of 6.5 cm/s. Overlay shows reflectors and other events digitised for line drawing depth migration.

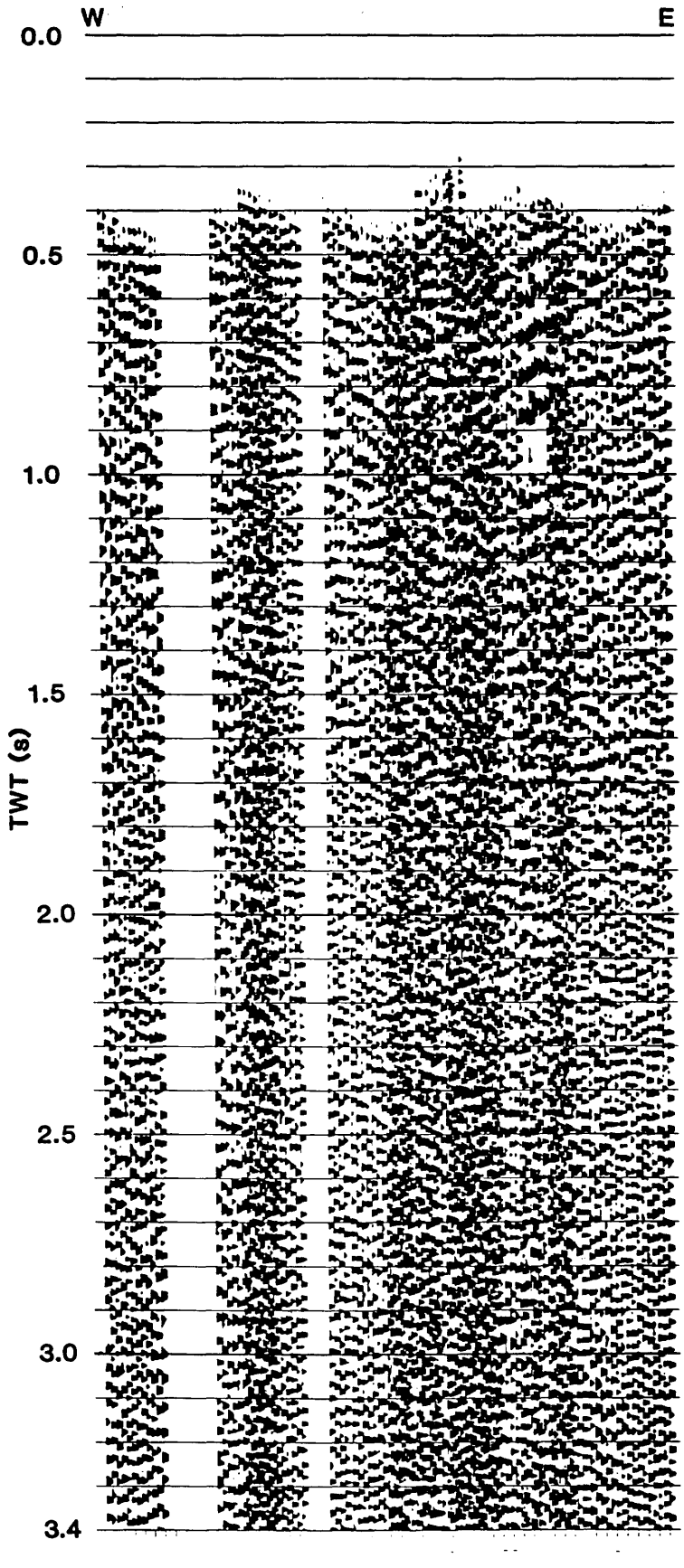

Fig. 4.15 Final stack of SK-4 (Quirang) at a horizontal scale of 1:19,500 and vertical scale of 6.5 cm/s. Overlay shows reflectors and other events digitised for line drawing depth migration.

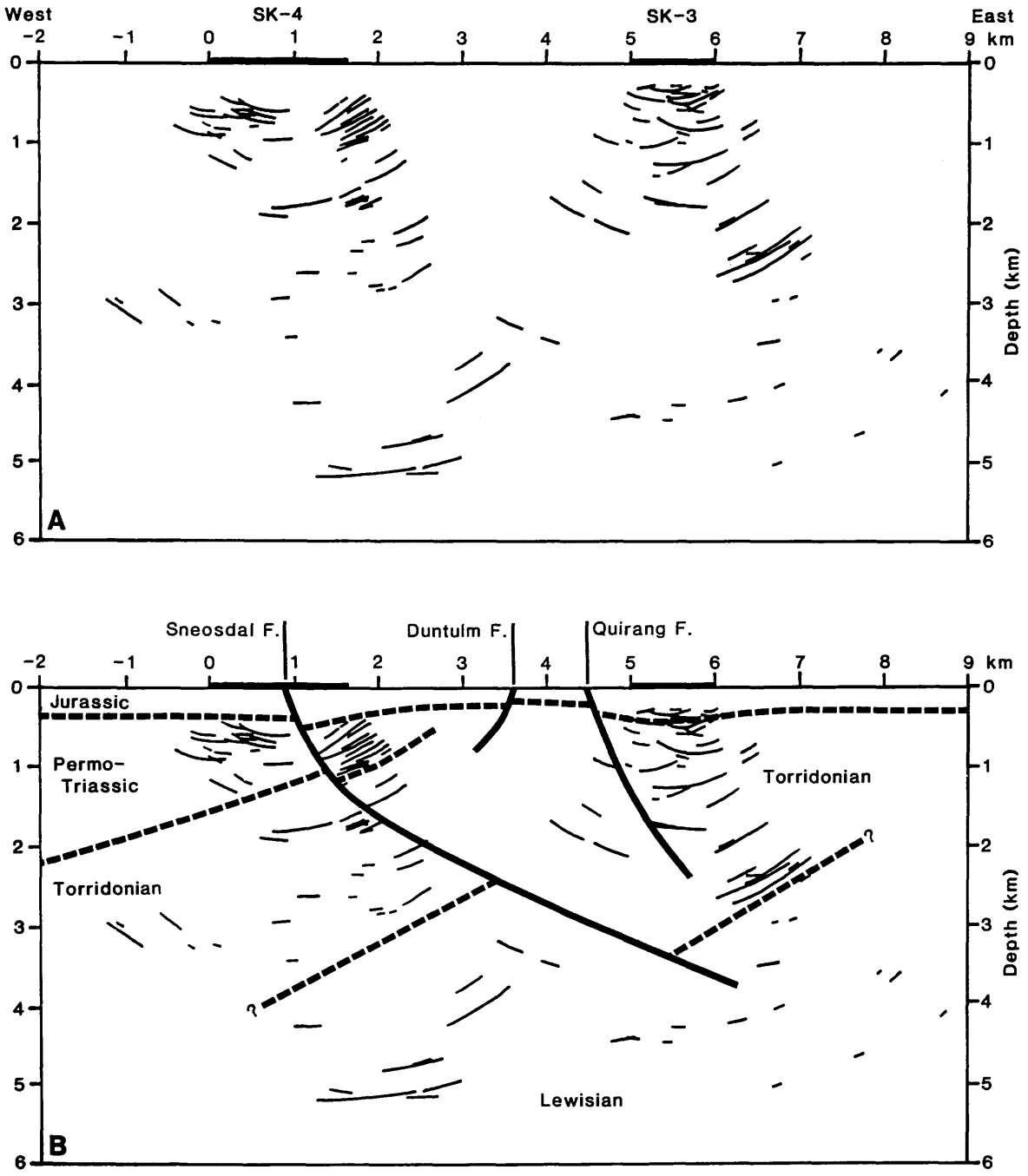

Fig. 4.16
A. Depth-migrated line drawing made by combining the four overlay interpretations of SK-3 and SK-4 (Figures 3.12 - 3.15) for input to Raynaud's (1986) ray tracing program. Origin of the X-scale is at the west end of SK-4. The velocity structure used for the ray tracing corresponds approximately to that derived from the velocity analyses carried out on SK-3 (Staffin) and SK-2 (Skudiburgh), the latter site being at around -4 km to -5 km on the above scale.
B. Structural interpretation of the depth-migrated line drawing. The normal faults are taken from the surface geology (see Figure 2.3). The E-W section above is cut at about 2 km by the WNW-ESE gravity profile 1 (located in Figure 4.1) at 64 km along the latter. Detail of the gravity profile and model in this area are shown in Figure 4.25 below; the gravity constrains the base of the Torridonian shown above to be 2-4 km deep, rather than 4-5 km, as suggested by the reflection line drawing above.

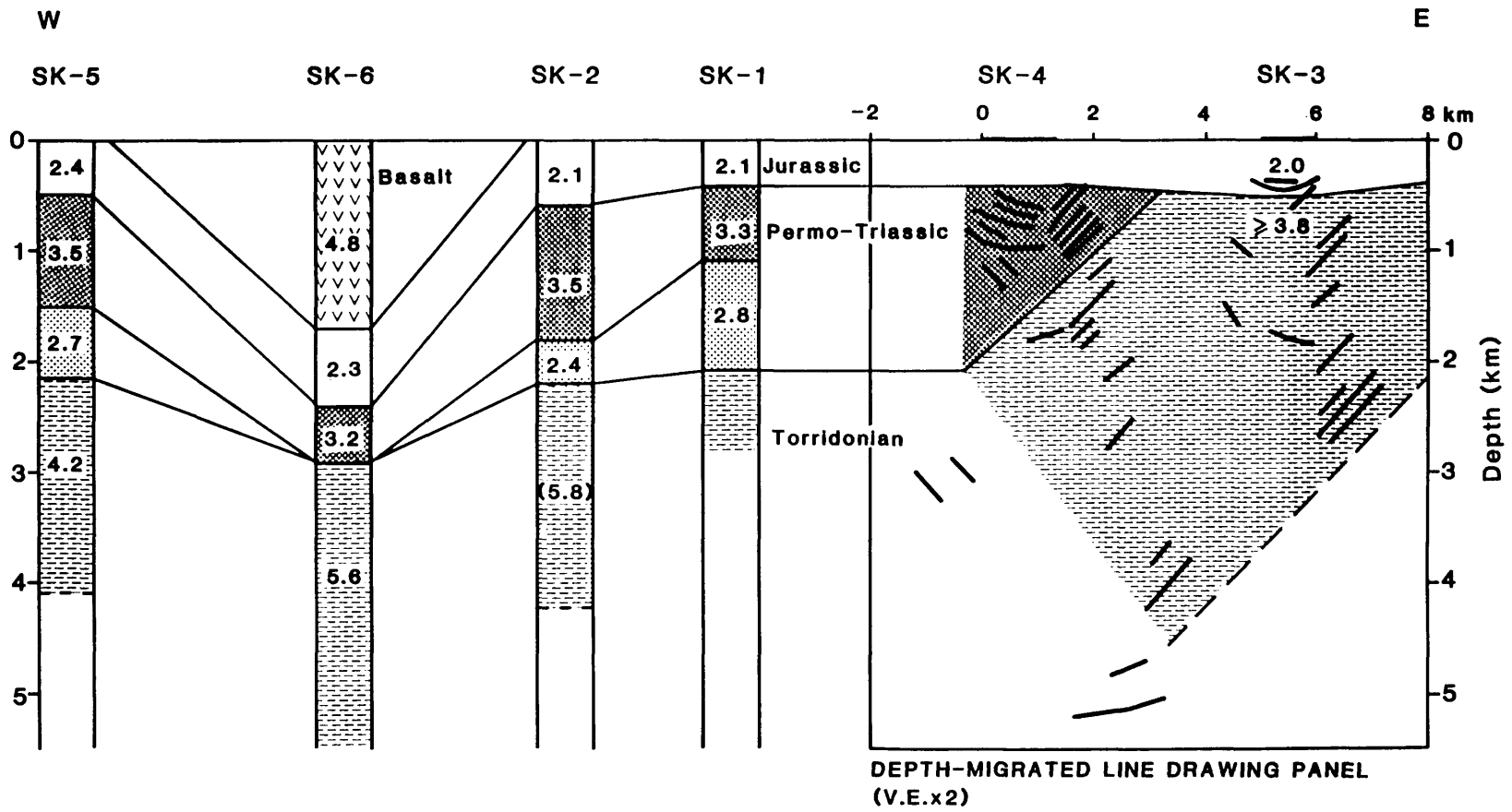

Fig. 4.17 Summary of the velocity-depth structure from the six seismic reflection sites in northern Skye. SK-3 and SK-4 are combined into a 2-dimensional section, simplified from the depth-migrated line drawings (Figs. 4.12 - 4.16). Structure at the other four sites is 1-dimensional. Note the velocity inversion within the Permo-Triassic. The unusually low velocities for the lower layer are corroborated by hammer seismic and ultrasonic velocity measurements (see text).

at 1.7 s is strong (see the semblance plot of Figure 3.57), and with the large velocity inversion beneath, can confidently be said to mark the base of the lava pile.

The half-kilometre or so thick layer at the surface of sites SK-1, SK-2, SK-3 and SK-5 with interval velocities of 2.0 - 2.4 km/s clearly belong to the Jurassic. The low velocity presumably means that the section is shale- and clay-dominated, since the higher-velocity sandstones, such as the Concretionary Sandstones identified by the first breaks at sites SK-1 and SK-2 (Section 4.1.3; Fig. 4.7), do not seem to have contributed much to an increase in the interval velocity.

The base of the Jurassic is probably soundly established below Staffin (SK-3), where the interval velocity jumps to 3.8 km/s or more at about 500 m depth, coincident with the marked angular unconformity inferred from the migrated line drawing. No intra-Jurassic reflections are seen on SK-4 due to the long offsets employed, which means that there are no reflection data before 0.4 s. The 50% increase in interval velocity at SK-1 and SK-2 at about 500-600 m depth (Fig. 4.17) corresponds well with the expected base of the Jurassic succession as measured in northern Skye (Fig. 1.7), although the lower of these two layers could perhaps include Lower Jurassic sandstones, if the succession here is somewhat thicker than expected. The same could be the case below SK-5, particularly since the Middle to Lower Jurassic section offshore, some 5-10 km further west, does seem to have doubled in thickness.

There are two groups of interval velocity assigned to the Permo-Triassic; an upper layer of P-wave velocity 3.2 - 3.5 km/s, and an inversion beneath, the lower layer being only 2.4 - 2.8 km/s in velocity. Although the inversion is by no means accurately defined at any one site (see Section 3.1.4 above, discussing the processing), the fact that it has been independently found at three sites suggests that it is genuine.

It is interesting to note that extremely low velocities were obtained using the hammer seismic method for the Stornoway Formation and for Triassic sandstone at Gruinard Bay (see

Figure 3.59 and Appendix 2). The correspondence of the ultrasonic measurements on the Gruinard Bay Triassic sandstones with the empirical curve of S-wave velocity against density (Fig. 3.58) casts doubt on the validity of both the hammer and ultrasonic measurements as having recorded P-waves. However, the full-wave recording used in the former method (cf. Fig. 3.60) demonstrates good first arrivals, followed by larger-amplitude second arrivals. The records in question are not atypical of the set of hammer records. This fact, in conjunction with the deep reflection interval velocity measurements, leads to the conclusion that there is an abnormally low interval velocity at the base of the Permo-Triassic succession.

The interval velocities beneath the Jurassic at Staffin (SK-3) are all higher than those assigned to the Permo-Triassic (Figs. 3.34, 3.35, 4.17). The hammer seismic velocity results show that 3.6 km/s is the approximate dividing line between Triassic and Torridonian. Extrapolation of the base of the Torridonian on Raasay westwards (down-dip), and along strike northwards to the latitude of Rona results in the predicted base of the sequence shown in Figure 4.17 as the dashed line. This clearly fits the interpretation of Torridonian rocks beneath Staffin. The fast intervals beneath the Permo-Triassic at the sites further west are also assigned to the Torridonian, on the basis that the figures calculated are too high for Permo-Triassic, and that there are no thick sequences of sediment known from the surface geology (Carboniferous or Devonian, for example). However, the possibility that some of this thick sequence may, in fact, be as yet unrecognised Upper Palaeozoic should not be entirely ruled out, especially if one wishes to take the oil explorationist's optimistic point of view (e.g. Kilenyi and Standley 1985).

4.2.3 GRAVITY MODELLING

4.2.3.1 Introduction

Simple interpolation of the three sedimentary sequences displayed in a fence-diagram format (Fig. 4.17) suggests that they all have a synclinal structure, which can be extrapolated further west below the Little Minch. This synclinal structure was used in a simple gravity model which accounted for the regional gravity low and the seismic reflection results (Smythe et al. 1972). However, a syncline is clearly inconsistent with the detailed structure of the basin near the Minch Fault. The aim of the revised modelling is to account for the structural style of the basin, rather than merely to determine the simplest set of polygonal density contrasts which satisfy the gravity anomaly.

The data set used for the modelling is part of the complete set of Bouguer anomalies for the UK shelf, comprising mostly BGS data. This data set (complete to early 1987) has been network-adjusted and gridded onto a uniform 2 km by 2 km grid based on extended UTM zone 30 (central meridian 3°W). Unfortunately, the data set omits the several hundred observations which were made on northern Skye during the period of the reflection field work in 1971 and 1972. These data were reduced and compiled onto a map along with the existing Durham University and IGS data in 1976 (R T Cumberland, unpublished). A preliminary contouring of these data show that the contours are similar to those obtained from the new BGS gridded data set, so that for the regional modelling required here (i.e. Outer Hebrides to mainland Scotland) the extra local detail in the Glasgow University data can safely be ignored.

The gridded BGS data set includes new marine gravity traverses in the Minches and Sea of the Hebrides. These were obtained in 1985 specifically to replace the old survey of 1968 (Table 2.4), which was known to have major problems, both with cross-coupling errors and with navigation. For this reason the otherwise excellent maps and digital data sets produced by Hipkin and Hussain (1983) are now considered to be of limited use for local Hebridean basin

modelling.

4.2.3.2 Densities

Useful formation densities for regional gravity work in Scotland have been derived by Hipkin and Hussain (1983) by regressing the Bouguer anomaly against the topography. Their results (their table 4) which are used here are as follows:

	Density (g/cm^3)
Tertiary extrusives (Skye)	2.694 ± 0.081
Torridonian	2.722 ± 0.057
Lewisian	2.879 ± 0.079

The density contrasts used are all relative to the Lewisian; they are rounded off to -0.16 g/cm^3 and -0.19 g/cm^3 for the Torridonian and Tertiary lavas, respectively (CGS units are quoted here because they are required for the modelling program, and to facilitate comparison with the laboratory density determinations).

The densities cited above are appreciably higher than those which are commonly used in gravity modelling, although the contrasts are similar. Tuson (1959), for example, found by laboratory measurements that the mean density for Lewisian granulite from Sleat is 2.76 g/cm^3, although he noted that a hornblende gneiss was as high as 2.96 g/cm^3. The density he chose for gravity modelling is weighted towards the granulite, at 2.8 g/cm^3.

Tuson also measured the densities of Lower and Middle Jurassic sandstones, shales and limestones from Skye. If most (statistical) weight is given to the shales, a mean figure of 2.55 - 2.60 g/cm^3 is suggested from his results. The modelling here therefore assumes a contrast of -0.3 g/cm^3 for the Jurassic relative to the Lewisian, i.e. an assumed density of 2.58 g/cm^3.

Tuson's assumed density for the postulated Triassic below northern Skye (Fig. 1.12) is lower than his Jurassic mean,

but is based on only two sandstone sites from Arran, and can therefore be discounted here. The densities obtained in the present study for Triassic sandstones and conglomerates are generally low, but very variable - from 2.36 to 2.66 g/cm^3 (Appendix 2). Furthermore, the sites (at Gruinard Bay and Applecross on the Scottish mainland) are not necessarily typical of the presumed thick Permo-Triassic sequence below northern Skye and the Minches. Since the P-wave velocity of the deep succession is intermediate between that for the Jurassic and that for the Torridonian, it is considered that a density which is also intermediate should be used. This is, in effect, giving weight to a presumed Nafe-Drake type of velocity-density correlation (Ludwig et al. 1970), and allowing for the possibility, mentioned above, that some of the sequence may be older than Triassic, or even older than Permian. The preliminary density contrast chosen is 0.2 g/cm^3. Since no difficulty has been encountered in modelling with this figure, there has been no need to alter it.

4.2.3.3 Removal Of Regional Field

A portion of the 2 km square gridded Bouguer anomaly values is extracted and converted to the appropriate UTM zone (central meridian 9°W) for the Little Minch region. Contouring, regional removal and cross-section display are performed using the Interactive Surface Modeling (ISM) package, which receives the data as scattered points, and re-grids it. Figure 4.18 shows the Bouguer anomaly contour map of the region. A large enough area has been chosen for a basement regional to be recognised and removed.

There is clearly a regional gradient from the linear peak following the eastern coast of the Outer Hebrides downslope to the mainland; there is also a more subtle gradient over the Lewisian platform west of the Outer Hebrides (Fig. 4.19), which is probably due to the eastward rise of the Moho towards the Outer Isles Thrust. The linear peak is explicable in terms of intra-Lewisian contrasts across the Outer Isles Thrust (McQuillin and Watson 1973), whereas the gentle westward regional gradient may be due to the footwall

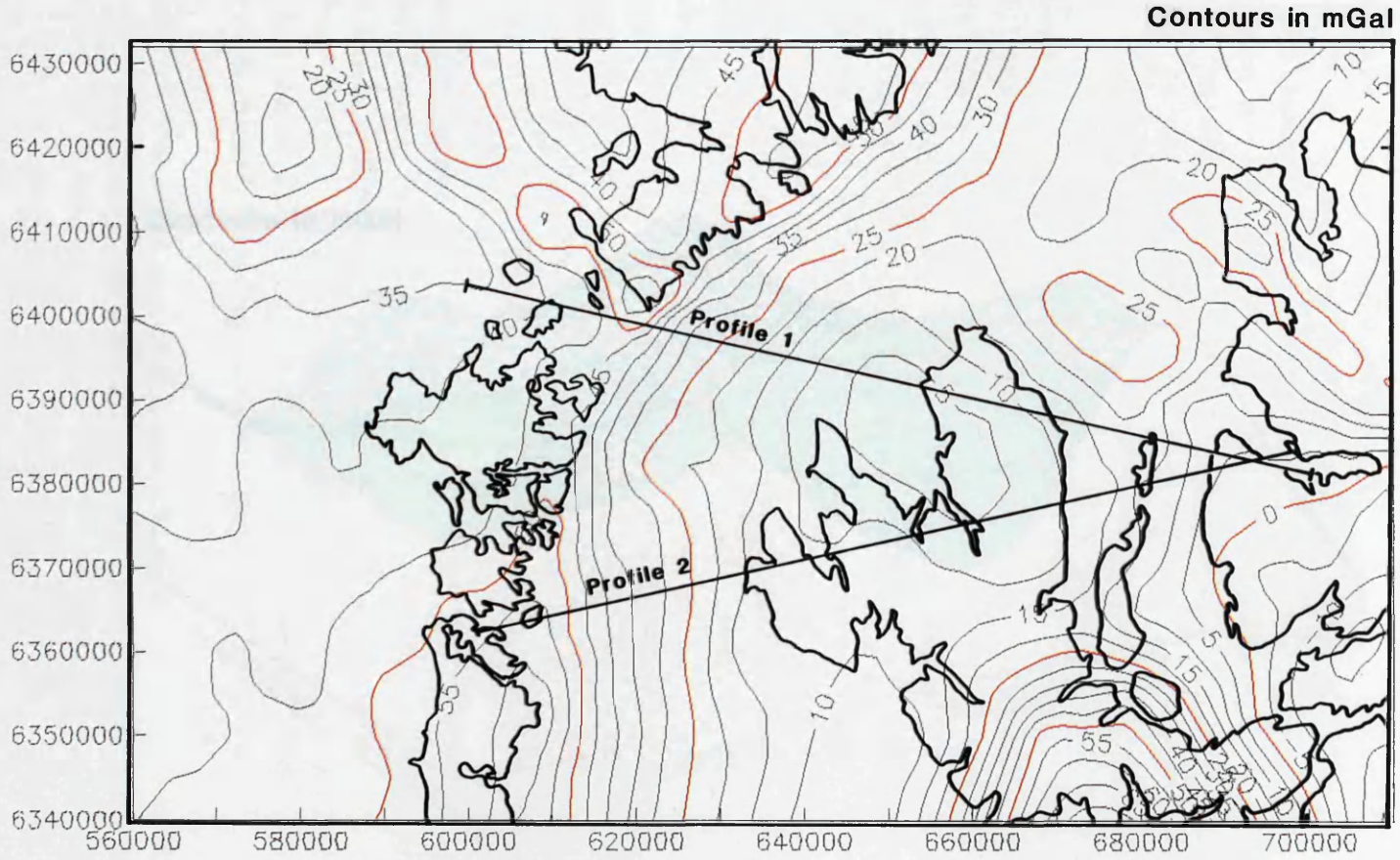

Fig. 4.18 Bouguer anomaly map of northern Skye and the Little Minch.

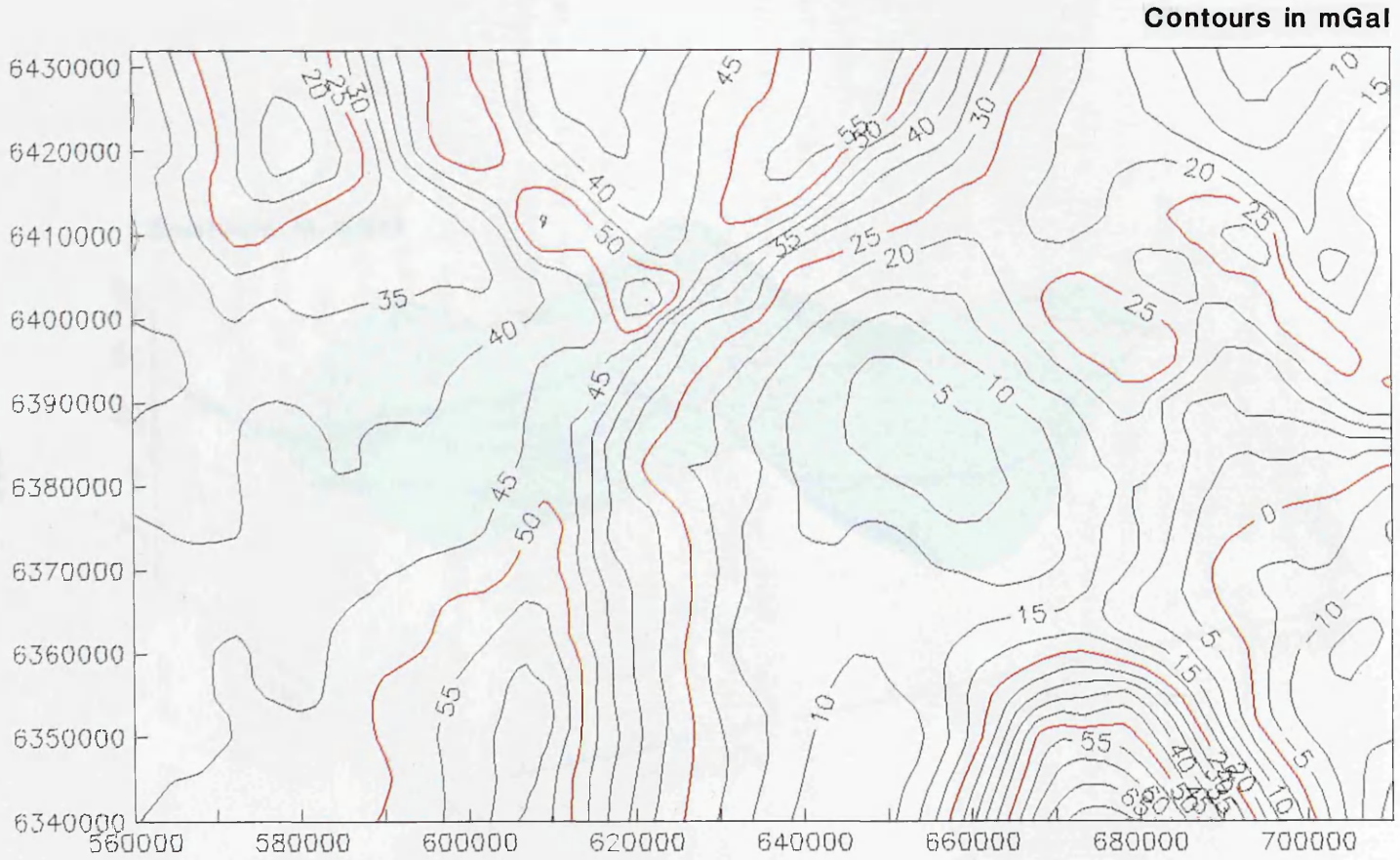

Fig. 4.18 Bouguer anomaly map of northern Skye and the Little Minch.

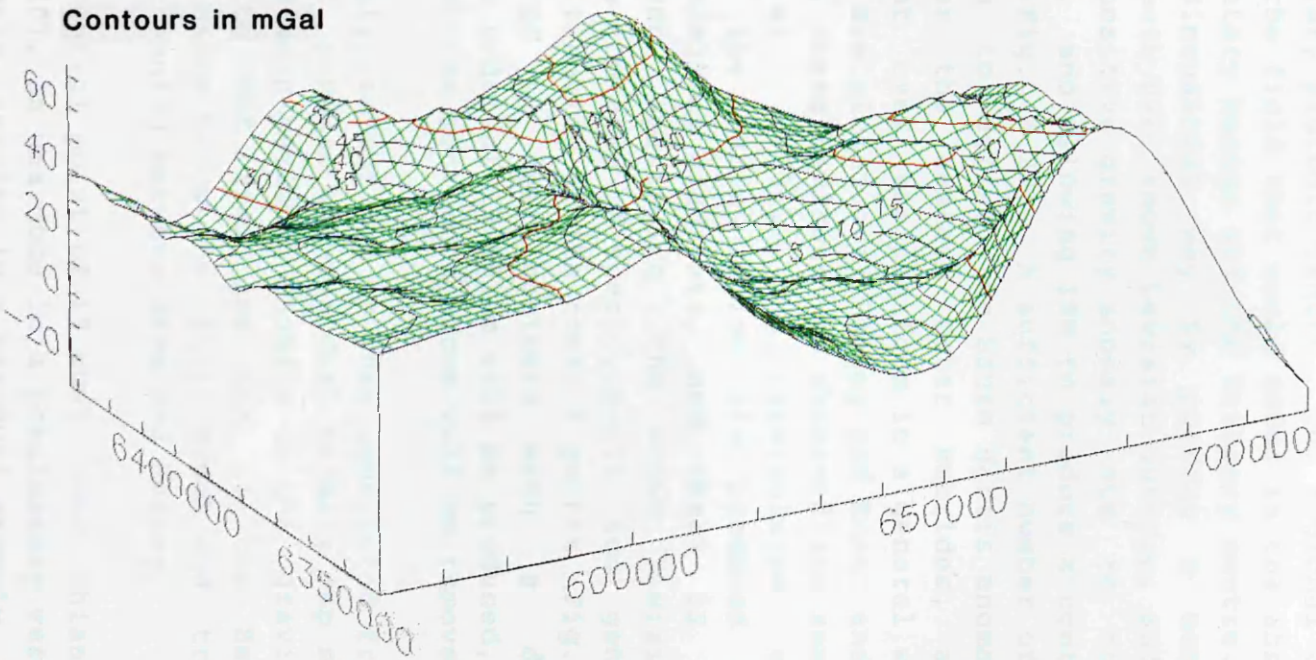

Fig. 4.19 Perspective view of Bouguer anomalies in the Little Minch, looking NE.

uplift (Jackson and Mackenzie 1983) on the Minch Fault system, caused by the removal of overburden when it acted as a normal fault (Brewer and Smythe 1986). However, the purpose of the gravity modelling is to define the geometry of the sedimentary basin; an attempt to account for the intra-basement contrasts and the structure of the whole crust is beyond the scope of the present study.

The map area includes part of the major positive anomaly due to the Skye Tertiary plutonic centre. The regional field is defined here as the field that would occur in the absence of both the sedimentary basins and the Tertiary centre. It is defined in a 3-dimensional way by picking a number of gravity points both over known Lewisian outcrop, and within the area of the positive gravity anomaly due to the Skye plutonic centre, and allowing ISM to produce a contour map from these data (Fig. 4.20). A sufficient number of points has been chosen to define the South Harris anomaly, the linear peak over the eastern Outer Hebrides, and the regional gradient over the platform in a general way. In the east, points are picked over Raasay and Rona, and one on Shiant East Bank, where Lewisian was observed and sampled in 1971 (Eden et al. 1973). The interpolated regional contours over the basin region are produced by the assumption of minimising gradients, and there is thus a trade-off between specifying the known Lewisian too precisely and the converse of specifying it too generally. The spatial distribution of the control points (Fig. 4.20) has been selected so that contours with a dominant wavelength of the order of 10-20 km will be produced, but so that the main features mentioned above will be removed.

The Bouguer anomaly contour map is then subtracted from the regional map to produce the residual anomaly map shown in Figure 4.21. The main residual anomaly is the gravity low trending north to NNE from the Sea of the Hebrides, deepening to a minimum below the Little Minch and truncated by the NNW trend running between Skye and Raasay.

Omission of the control point of 19 mGal over Shiant East Bank (Fig. 4.20), as was done in a preliminary version of the regional anomaly, results in a residual anomaly map in which the gradient over the eastern Skye - Raasay region

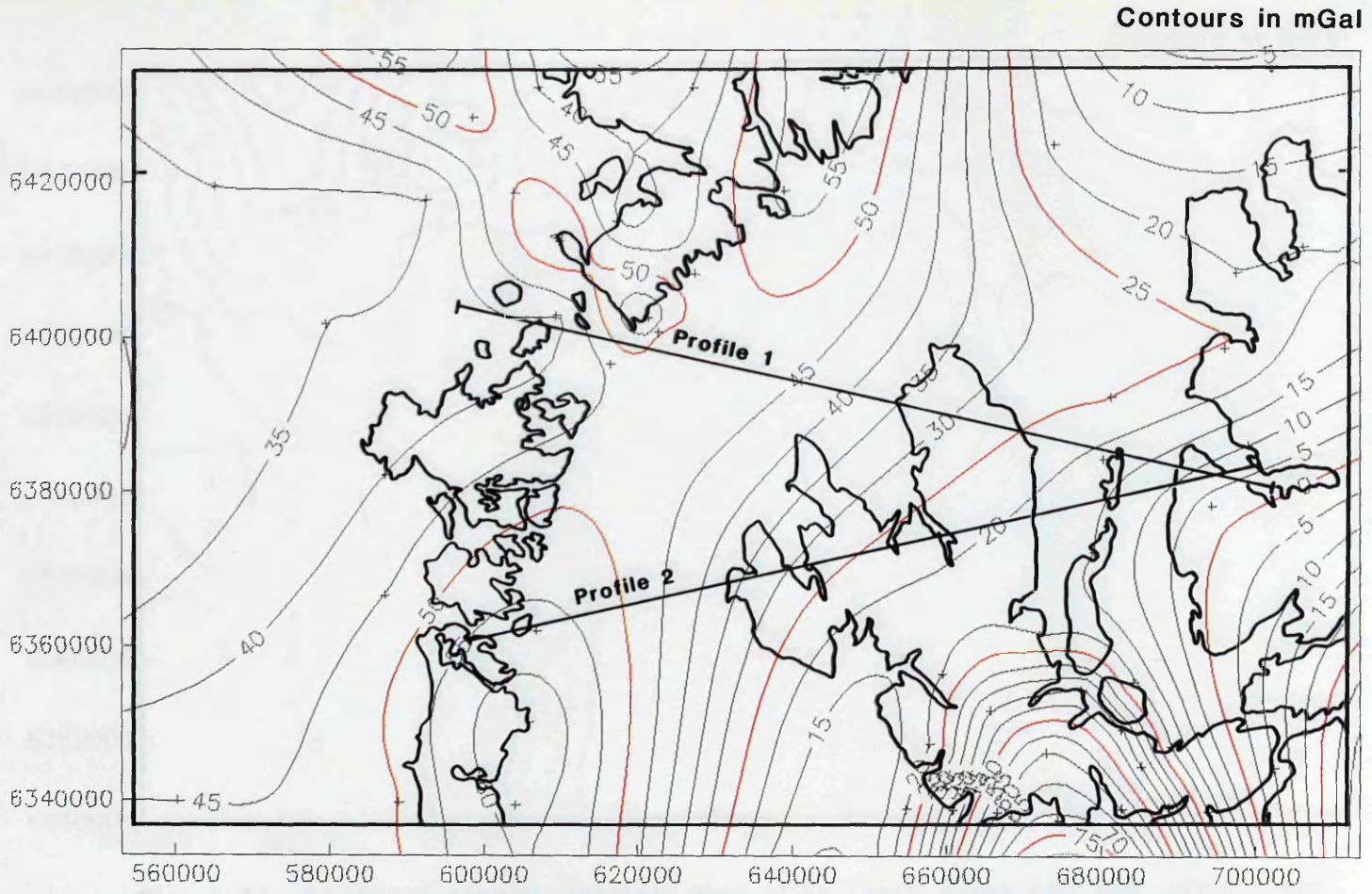

Fig. 4.20 Regional gravity field of northern Skye and the Little Minch.

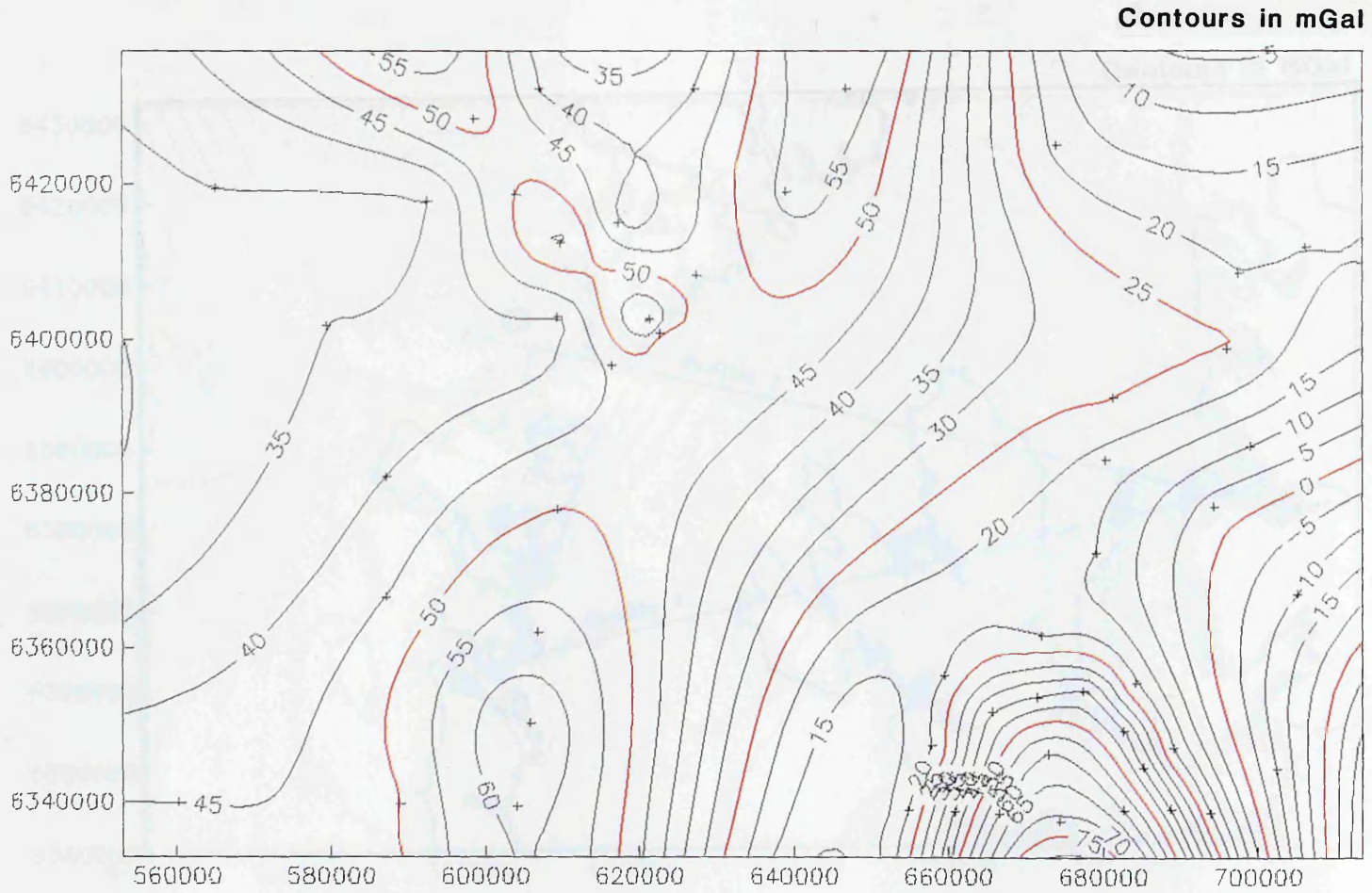

Fig. 4.20 Regional gravity field of northern Skye and the Little Minch.

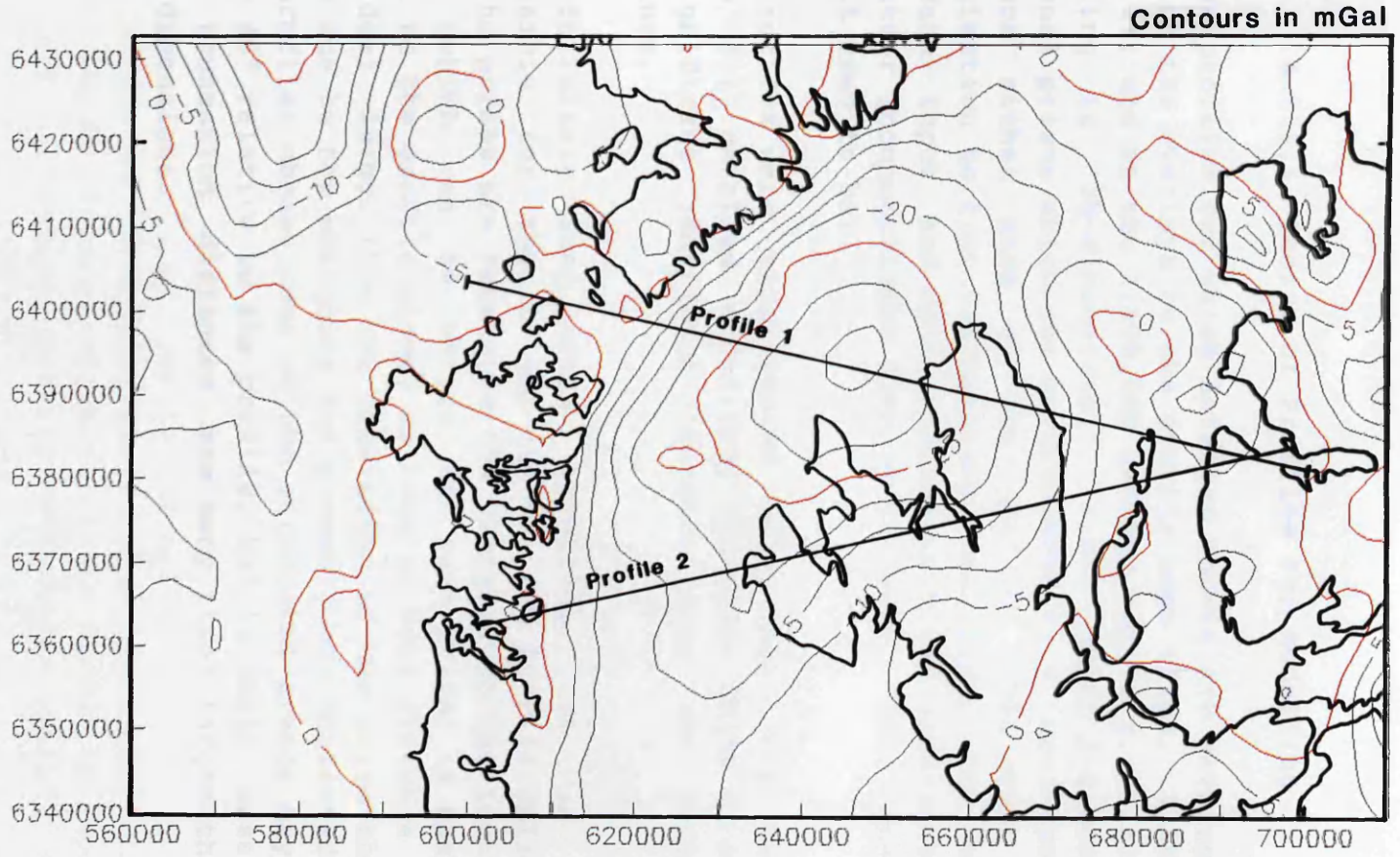

Fig. 4.21 Residual gravity anomaly map of northern Skye and the Little Minch.

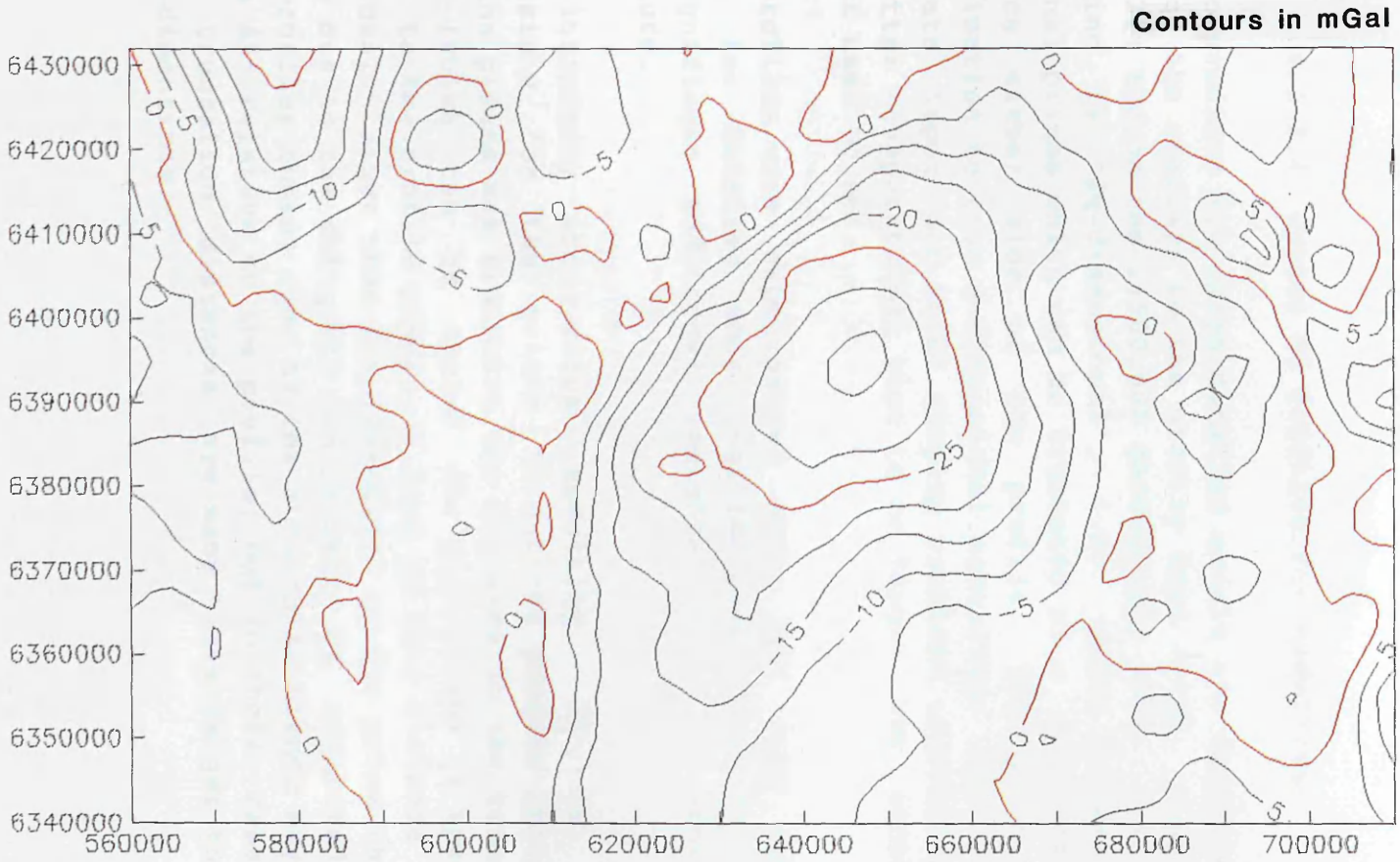

Fig. 4.21 Residual gravity anomaly map of northern Skye and the Little Minch.

trends N-S, and in which there is more continuity of the low north-eastwards into the North Minch. However, although this small outcrop of Lewisian could not, hitherto, be explained, and has been omitted from the interpretation of the published geology maps (Figs. 4.1 above, and Fig. 4.2 inside back pocket), the new interpretation of the normal faulting derived below provides a natural explanation for this geological anomaly.

4.2.3.4 Choice Of Profiles For Modelling

The two profiles for which detailed models are developed are shown on the overlays to the gravity maps (Figs. 4.18, 4.20 and 4.21) and on the 1:500,000 geology map (Fig. 4.1). The modelling is '2½-dimensional', i.e. using 2-dimensional polygonal prisms which can be truncated at a user-specified distance either side of the profile. This gives a good approximation to true 3-dimensional modelling, but without the data input and model display problems associated with the latter (computational time is no longer the constraint that it used to be).

Five profiles were experimented with, but only two are chosen for detailed modelling; the other three do not add any significant additional insights into the geological structure.

With infinitely long prism modelling, it is quite permissible for the prisms to cut the profile obliquely. When the prisms are truncated the distance to the truncation plane (which can be varied for each prism) is specified normal to the profile plane; as long as this distance is a good deal larger than the dimensions of the prism then the errors due to the obliquity can probably be neglected. In the profiles chosen some of the structural trends may be as low as 45° relative to the profile, but in these cases all prism truncation distances are many times larger than the prism dimensions.

4.2.3.5 Profile 1

Profile 1, 103 km in length, runs from west of the Sound of Harris to the mainland at Loch Torridon. Its trend is a compromise between crossing both the steep gradient of the Minch Fault and the NNW-trending gradient over northern Skye at near to perpendicular possible, while also passing through areas of maximum control, these being:

(1) The 1972 refraction line A-D in the Sound of Harris area.

(2) The Palaeocene/Oligocene half-graben between the Minch Fault and the Harris Fault.

(3) The Carboniferous sea-bed sample just west of the Harris Fault.

(4) The reflection sites SK-2, SK-4 and SK-3 on Trotternish. at about 58, 64 and 68 km distance, respectively, along the profile.

(5) The north tip of Rona, just north of the overstep of Torridonian by Mesozoic offshore to the west.

(6) Lewisian outcrop around inner Loch Torridon.

Figures 4.22 and 4.23 show the gravity model for profile 1 at vertically exaggerated and true scales, respectively. Colours for the model polygons in all the figures are:

Oligocene sediments	- yellow
Tertiary basalts	- red
Jurassic sediments	- blue
Upper Palaeozoic/Triassic	- orange
Torridonian	- green
Lewisian	- blank

Figure 4.24 shows the westernmost 20 km or so of the basin model at true scale. The Harris Fault crops out at 30 km, and accounts for NW-dipping Upper Palaeozoic, unconformably overlain by SE-dipping Jurassic. It is virtually impossible to satisfy the observed gravity without postulating such a

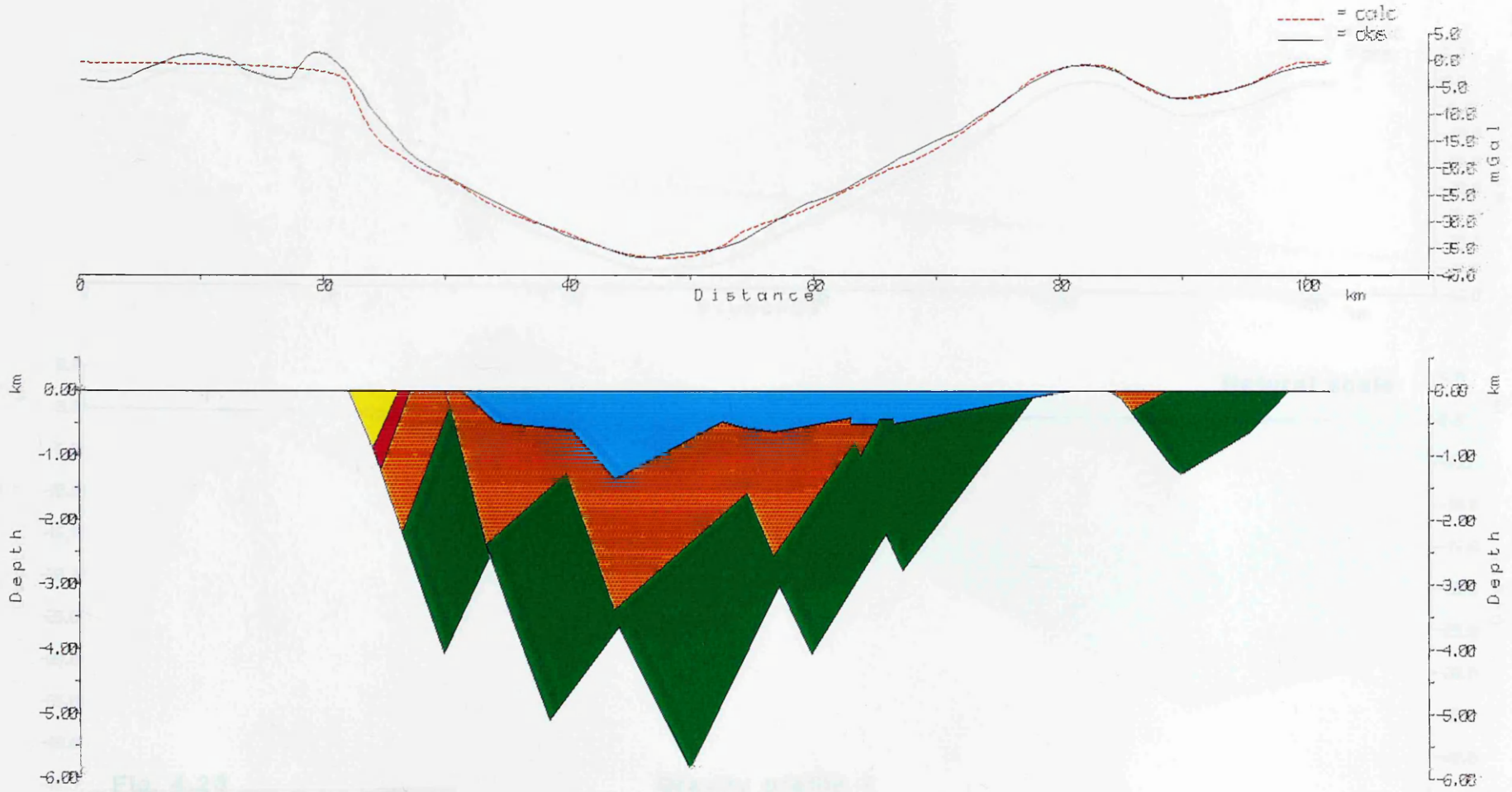

Fig. 4.22 Gravity profile 1.

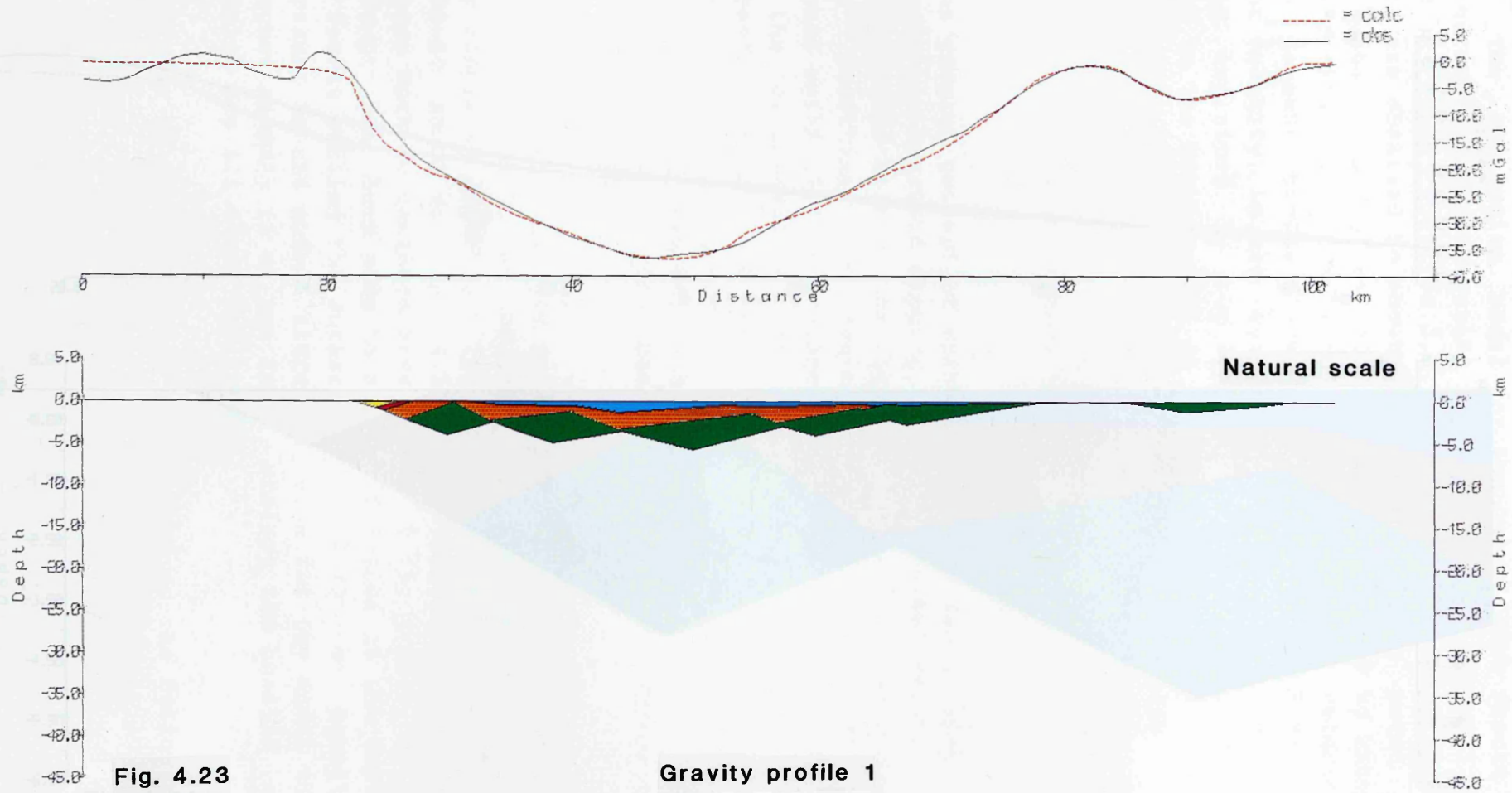

Fig. 4.23 Gravity profile 1

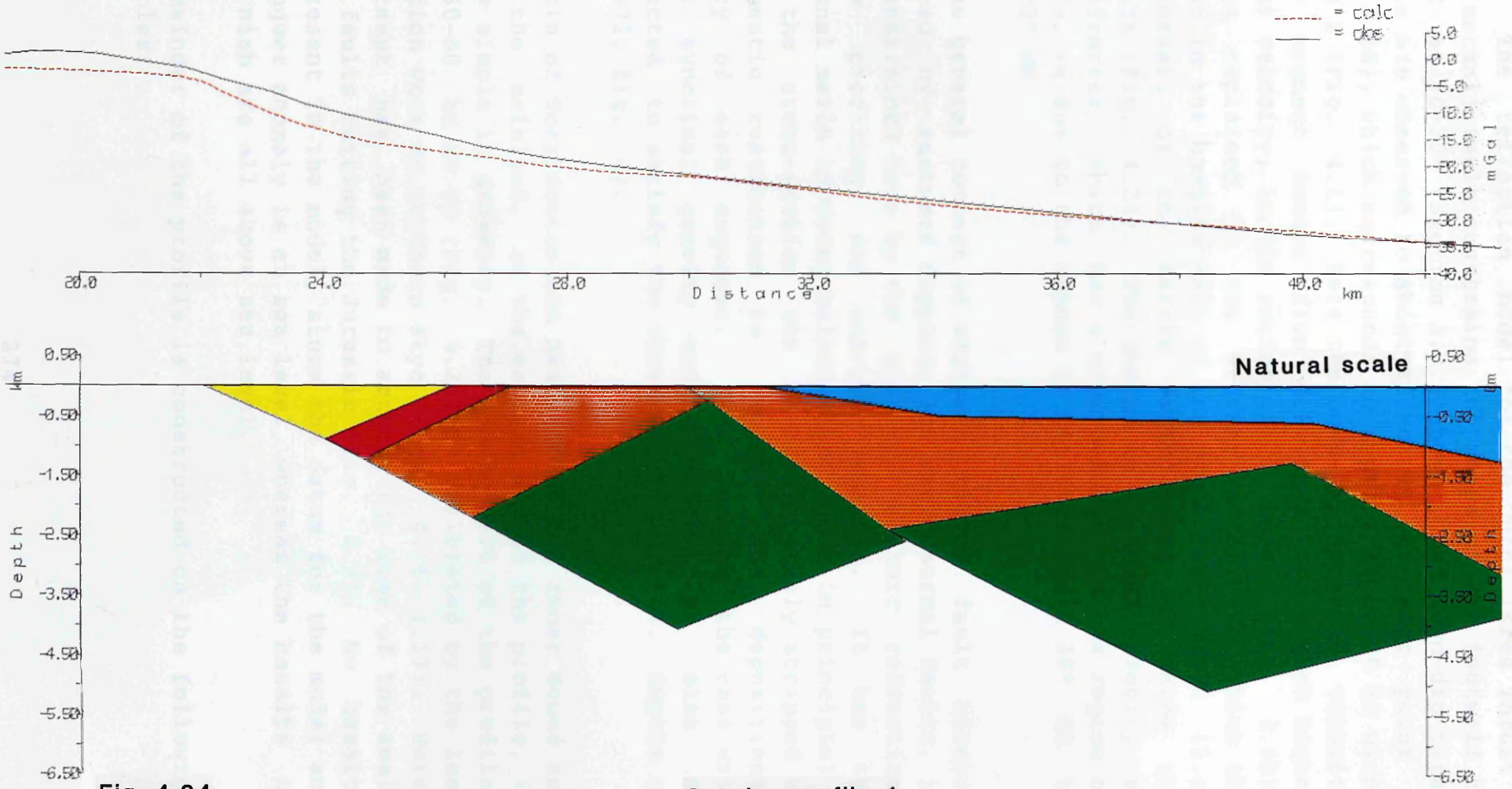

Fig. 4.24 Gravity profile 1

fault. The refraction model for the Outer Isles Thrust - Minch (normal) Fault constrains the shape of the footwall to dip SE at 20-30° (Section 3.3.2 above), and down-dip first arrivals are observed to about 12 km SE of shot point A (Fig. 3.68), which corresponds to a point about 30 km along profile 1 (Fig. 4.1). Here the down-dip apparent velocity of the segment breaks from 4.9 km/s to a much higher apparent velocity, in the region of 7 km/s (Fig. 3.68). This is explained by the gravity model, in which the Lewisian in the hanging wall of the Minch Fault block (i.e. the footwall of the Harris fault) dips NW below the sediments (Fig. 4.24). The change in apparent velocity of the refractor, which has a true velocity in the region of 6.2 km/s, is due to the change in dip from about 20° SE to about 20° NW.

Thus the general concept of westward tilted fault blocks, preserved by eastward dipping, low angle normal faults, is well constrained here by the gravity, seismic refraction, shallow profiling, and sea-bed sampling. It has the additional merit of being balanced (at least in principle) - i.e. the cross-section can be progressively stripped by palinspastic restoration to recover the depositional geometry of each sequence. This is not the case with simpler synclinal gravity models which can also be constructed to satisfy the observed gravity (cf. Smythe et al. 1972, fig. 4).

The basin of Torridonian and Mesozoic in the Inner Sound and below the mainland, at the eastern end of the profile, is clearly simple in geometry. The middle part of the profile, from 60-80 km or so (Fig. 4.25) is calibrated by the land reflection work on northern Skye (Figs. 4.16, 4.17). Here, an attempt has been made to account for some of the small normal faults cutting the Jurassic (Fig. 2.3). No basalts are present in the model, since the datum for the model and the Bouguer anomaly is at sea level, whereas the basalts of Trotternish are all above sea level.

The remainder of the profile is constructed on the following principles:

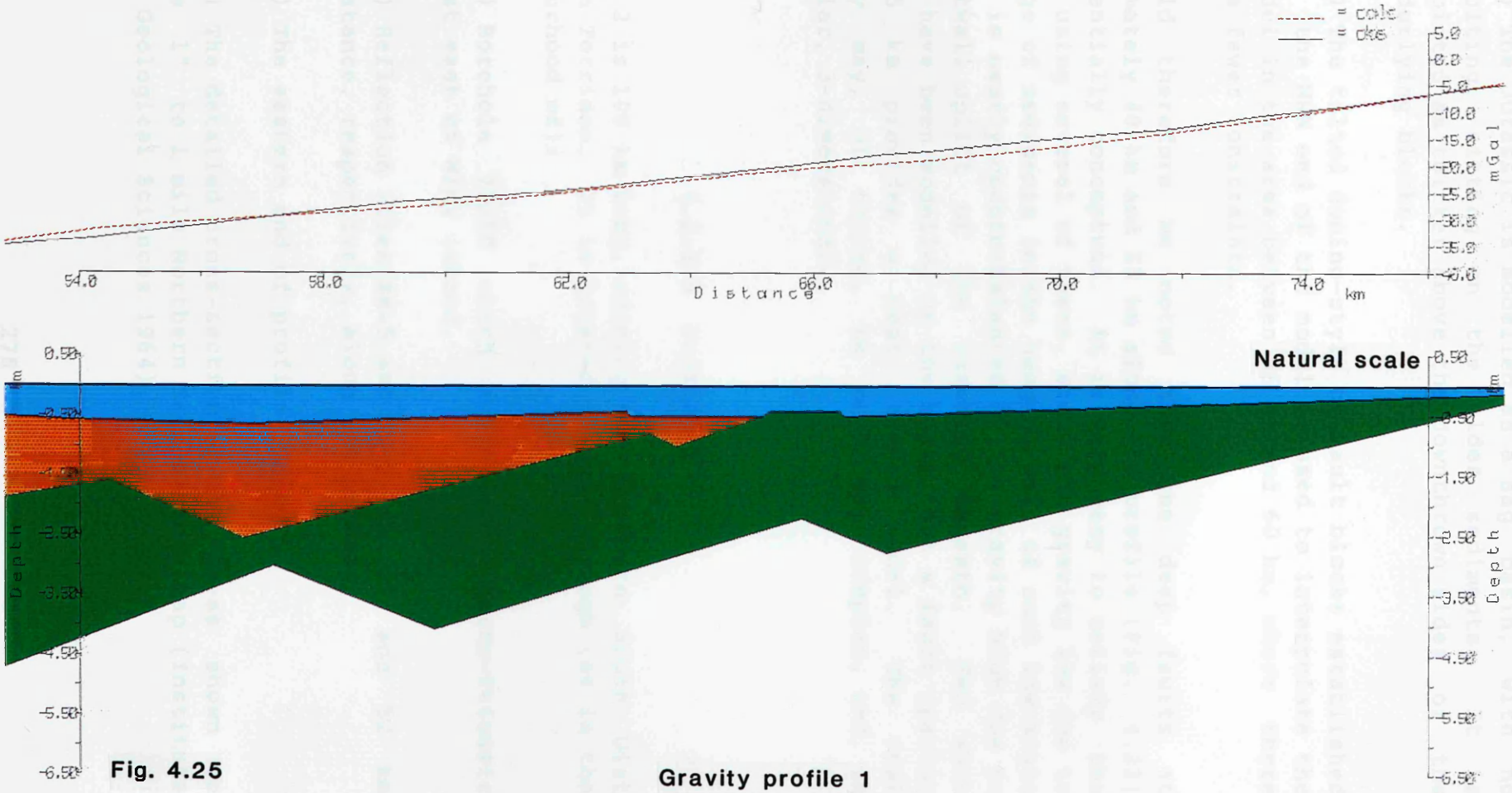

Fig. 4.25 **Gravity profile 1**

(1) The Jurassic is modelled as a sag basin, with no faulting, sitting on the older sediments. It is depicted as thicker above the downthrown sides of the underlying blocks.

(2) The tilted domino-style of fault blocks established at the WNW end of the model is used to interpolate the model in the area between 35 km and 60 km, where there are fewer constraints.

It should therefore be noted that the deep faults at approximately 40 km and 55 km along the profile (Fig. 4.22) are essentially conceptual. It is very easy to satisfy the gravity using several of these, since the gravity low due to the wedge of sediments in the hanging wall of such low-angle faults is nearly counterbalanced by the gravity high due to the footwall uplift of the basement beneath. Two such faults have been modelled on the basis that a fault spacing of 10-15 km provides a neat, simple model. The real geometry may, of course, be much more complex, and, in particular, 3-dimensional.

4.2.3.6 Profile 2

Profile 2 is 100 km long, running from northern South Uist to Loch Torridon. It is located to pass through (or in the neighbourhood of):

(1) Borehole 72/10 which encountered Permo-Triassic just east of Wiay island,

(2) Reflection sites SK-5 and SK-6, at 33 and 52 km distance, respectively, along the profile,

(3) The eastern end of profile 1, and

(4) The detailed cross-section of the lavas shown on the 1" to 1 mile Northern Skye geology map (Institute of Geological Sciences 1964).

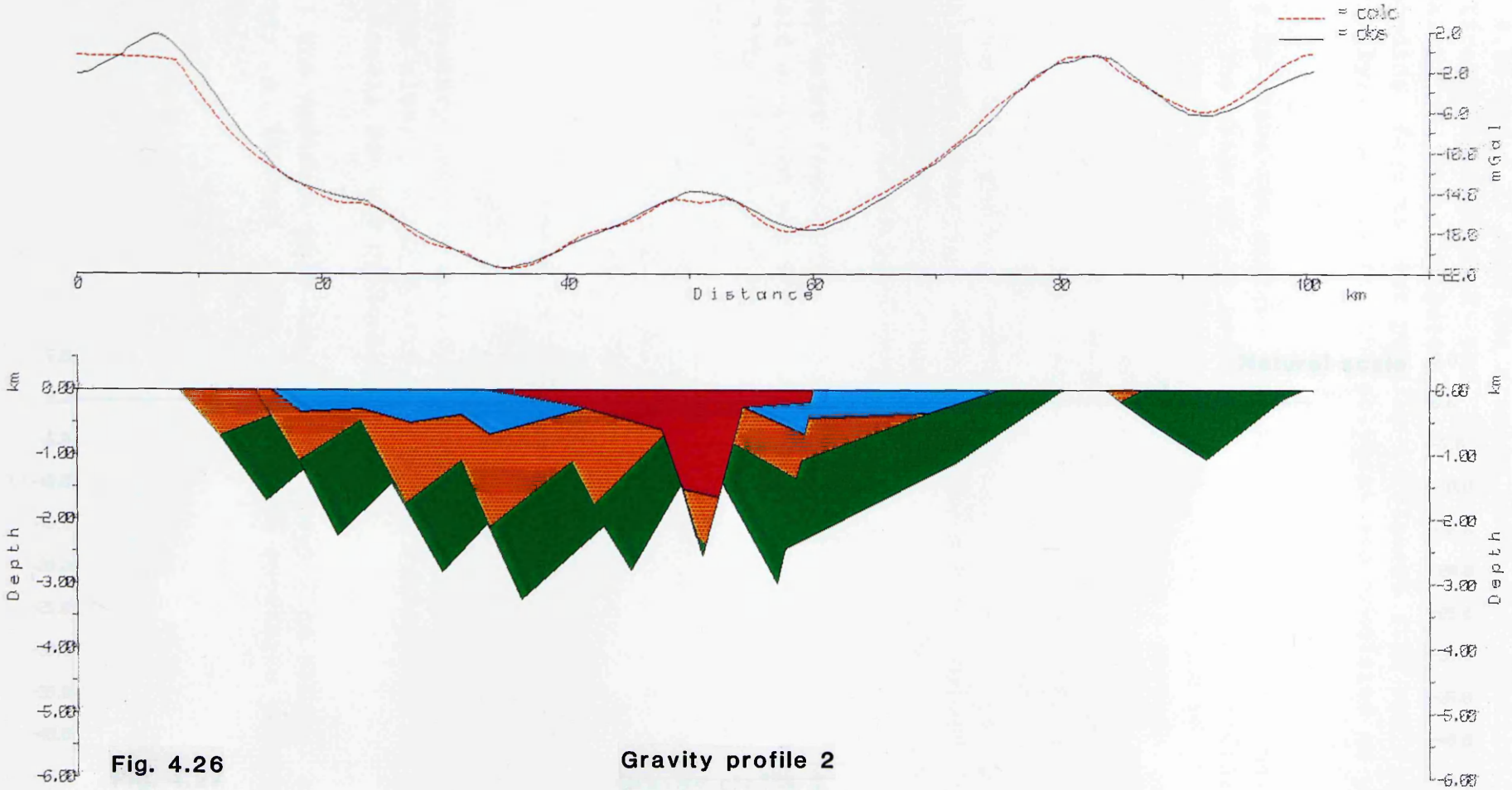

Fig. 4.26 **Gravity profile 2**

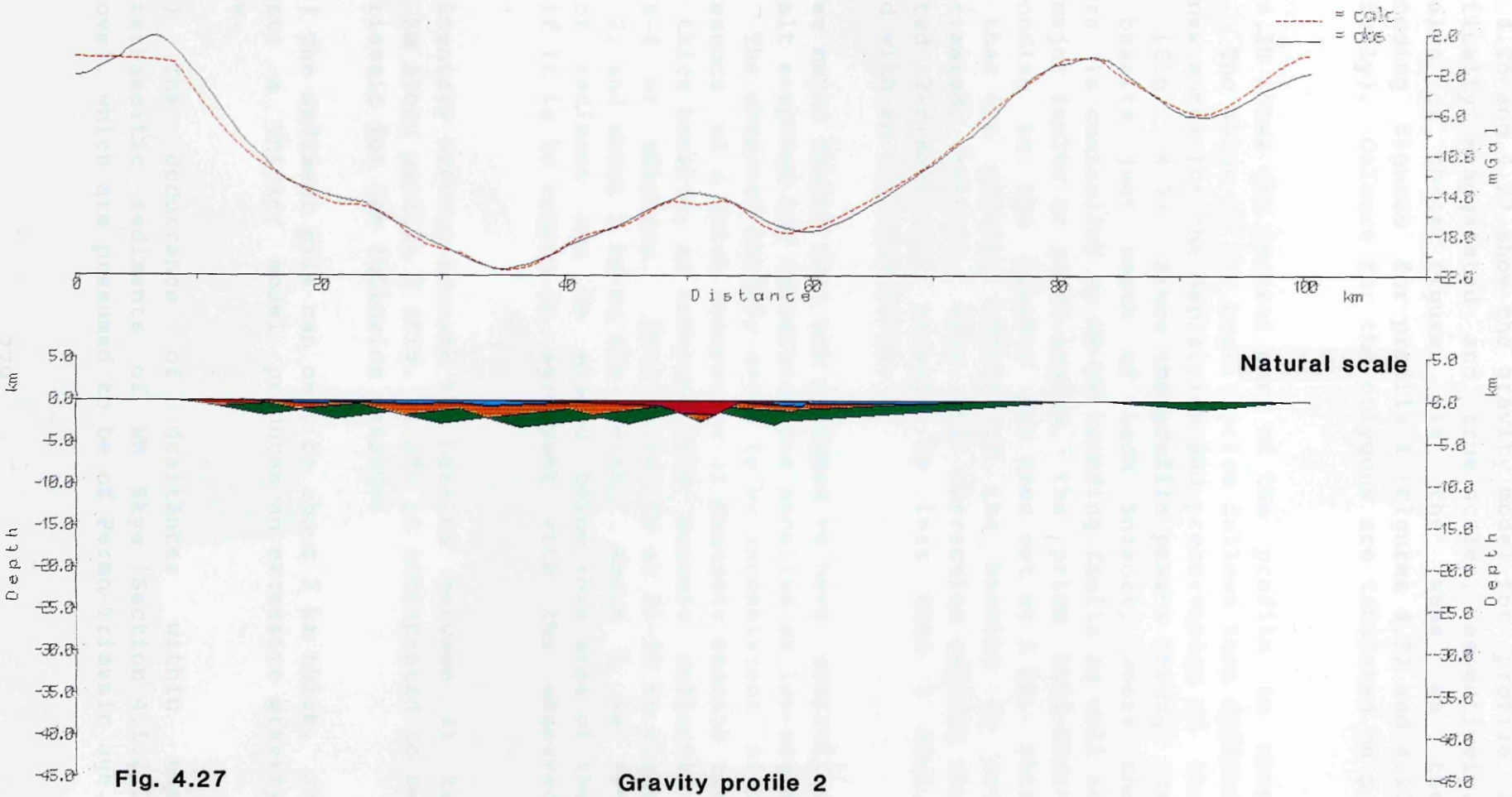

Fig. 4.27 **Gravity profile 2**

Figures 4.26 and 4.27 show the gravity model for profile 2 at vertically exaggerated and true scales, respectively. The scales of these figures are the same as the corresponding figures for profile 1 (Figures 4.22 and 4.23 respectively). Colours for the polygons are tabulated on p. 270.

Figure 4.28 shows the central part of the profile in more detail. The shape of the basalt prism follows that defined by the new model for the deposition and preservation of the basalts (Fig. 4.5). Since the profile passes through the area of basalts just south of Loch Snizort, where the structure is controlled by NE-SW trending faults as well as by the major faults at right-angles, the prism half-width corresponding to the basalts has been set at 3 km. This ensures that the gravity effect of the basalts is not over-estimated; however, this end correction reduces the calculated 2-dimensional anomaly by less than 1 mGal, compared with an infinite prism.

The three major faults that are presumed to have controlled the basalt eruption and deposition are modelled as low-angle faults. The observed anomaly seems to be inconsistent with the presence of a thick succession of Mesozoic beneath the area of thick basalts, as inferred from seismic reflection line SK-6 at Edinbane. This site is at 51-53 km along profile 2, and about 1 km to the north. About 1 km (at most) of sediment can be placed below this area of the model, if it is to remain in agreement with the observed anomaly.

The sedimentary subcrop beneath the basalts between 41 km and 54 km along profile 2 (Fig. 4.28) is interpreted to be Permo-Triassic for the following reasons:

(1) The sediment pile can only be about 2 km thick, at most; a thicker model produces an excessive gravity low.

(2) The occurrence of dreikänter within the interbasaltic sediments of NW Skye (Section 4.1.2.2 above), which are presumed to be of Permo-Triassic age.

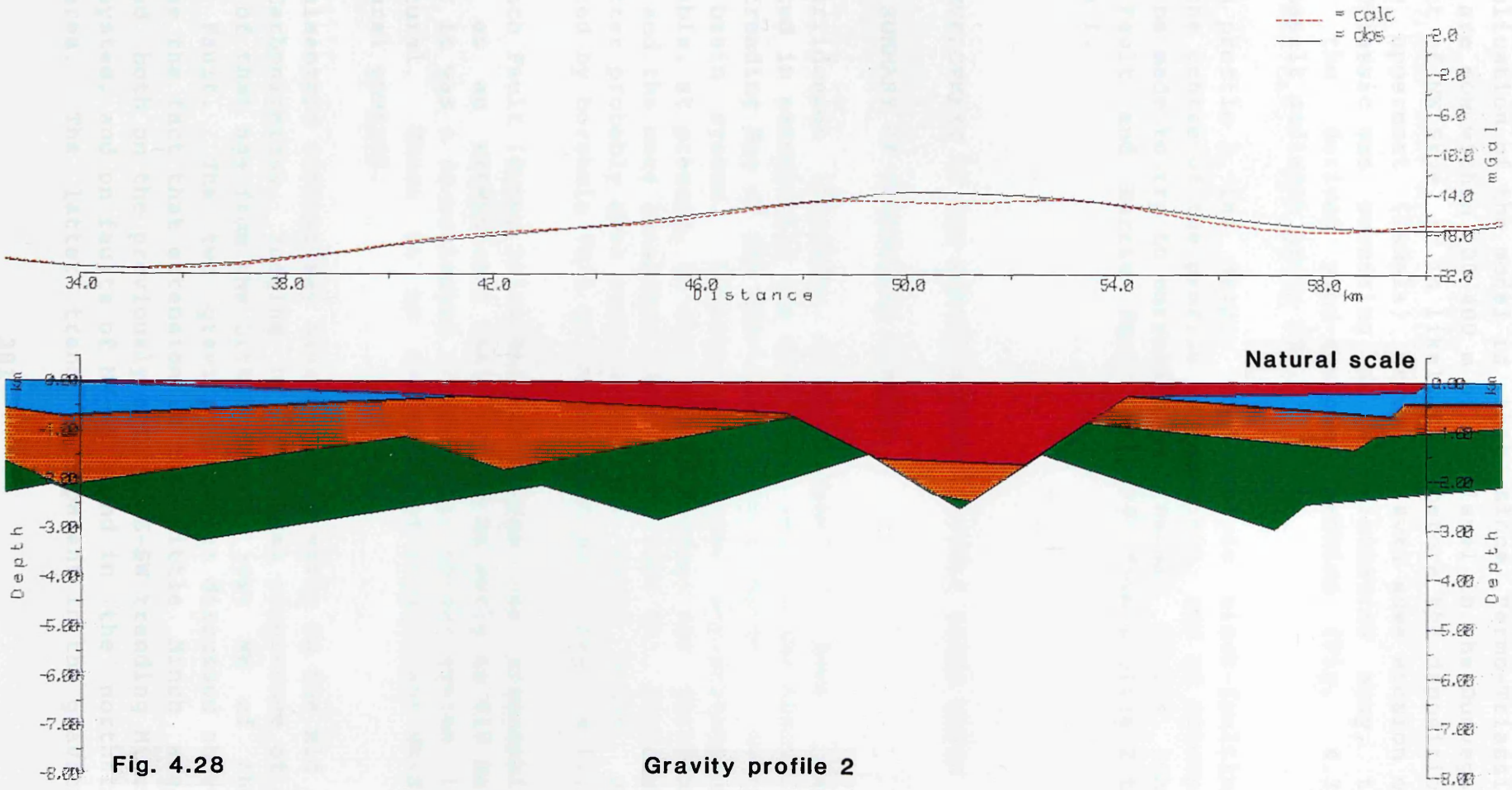

Fig. 4.28 **Gravity profile 2**

The implication of the model is that since Permo-Triassic strata are now within 300-400 m of sea level in the Dunvegan district of NW Skye, it is likely that before the deposition of the uppermost (Osdale) group of lavas some erosion of Permo-Triassic was occurring a few kilometres away, to supply the derived wind-sculpted pebbles (Fig. 4.3, intra-basalt sediment group S3).

As with profile 1, the deeper domino-style block-faulting below the centre of the profile is schematic, and no attempt should be made to try to correlate the normal faults (the Minch Fault and Harris fault excepted) from profile 2 to profile 1.

4.3 DEVELOPMENT OF THE NORTHERN SKYE - LITTLE MINCH BASIN

4.3.1 SUMMARY OF GEOLOGICAL HISTORY

The Torridonian (Torridon Group) seems to have been deposited in essentially the same basin area as the Mesozoic NE-SW trending Sea of the Hebrides - Little Minch - North Minch basin system. Regional geophysical interpretations are unable, at present, to distinguish between the Torridon Group and the more localised Stoer Group (990 Ma), although the latter probably does occur below the North Minch, as suggested by borehole 78/3 on Shiant East Bank (Fig. 4.1).

The Minch Fault (Outer Isles Thrust) system was presumably active as an extensional fault system as early as 810 Ma; whether it was a re-activated (?Grenville) thrust system is conjectural. There is no evidence of significant NW-SE structural control.

Late Palaeozoic rifting may have begun as early as the mid - late Carboniferous, judging by the local occurrence of a sample of that age from the Little Minch just NW of the Harris Fault. The two gravity profiles discussed above disguise the fact that extension in the Little Minch area occurred both on the previously active NE-SW trending Minch fault system, and on faults of NW-SE trend in the northern Skye area. The latter trend is apparent in the gravity

field, once the regional field has been removed (Fig. 4.21). A basement high of this trend continues the line of the Loch Maree Fault out into the Minches, to culminate in the Shiant East Bank, where Lewisian is exposed at the sea bed (Fig. 4.1).

Extension and subsidence within a half-graben basin-and-range environment continued through to the late Triassic.

Deposition within the Jurassic appears to fit the context of the thermal subsidence phase following lithospheric rifting and extension. The Little Minch region was a depocentre, with maximum subsidence west of Vaternish and Duirinish, above the area of thickest rift basin development. However, there is significant overstep to the SE, and corresponding non-deposition in the NW.

A minor phase of basin inversion took place in central Skye, together with folding on NE-SW trends, following a presumed episode of late Cretaceous deposition. However, there is no evidence within the northern Skye - Little Minch area either of Cretaceous sediments, or of local re-deposition (in late Cretaceous - early Palaeocene time?) of erosional products from the Cretaceous. Presumably the whole region was above sea level at that time.

Eruption of the Tertiary basalts in northern Skye was fault-controlled, the main set of faults trending NW-SE. Displacement alternated between a main synthetic fault, downthrowing to the NE, and one or other of two antithetic faults (including the Portree fault), downthrowing to the SW, which do not seem to have been previously active.

At about the same time, a separate linear zone of basalts was erupted along the downgoing side of the Minch Fault.

An Oligocene phase of subsidence on the Minch Fault in the Little Minch area resulted in the formation of NW-tilted prism of some 800 m of clays overlying the basalts. This was probably contemporaneous with the downwarping of the basalts SW of Skye to form the Canna Basin (which, in contrast, is not fault-controlled).

4.3.2 DISCUSSION

The Little Minch is the area where the NW-trending Clyde Belt of rift basins (McLean 1978) intersects the NE-trending Marginal Belt (Fig. 1.11) at a 'T-junction'. The inference from the gravity profile 1 above, that the base of the half-graben system in the Little Minch, adjacent to the Outer Hebrides, is of Namurian - Westphalian age corroborates McLean's hypothesis that the Clyde belt (initiated at that time) extends as far as the Little Minch. However, the Marginal Belt was clearly also initiated at this time, at least in the Little Minch area, since the basin belongs equally to both belts. Taking into account the regional evidence cited by Haszeldine (1984), it can be concluded that the Marginal Belt (running from the northern end of Porcupine Seabight to the West Shetland basin) came into existence in the late Carboniferous, and not in the Permian, as implied by McLean.

The New Red Sandstone rocks of NW Scotland are frequently described as being of Triassic age, rather than Permo-Triassic and older. Whereas this statement is correct for the onshore geology, it leads to the misleading impression that the rift basins did not exist until the Triassic; compare, for example, Lovell's (1983) palaeogeographic maps for the early and late Permian with those for the Triassic. The problem is that the scattered onshore outcrops around the Hebrides comprise the latest and most distal basin fill deposits, of Triassic age, whereas the earlier basin fill is deeply buried offshore, and not amenable to direct dating. Steel et al. (1975) have noted that the onshore Triassic sequence in the Skye - Raasay region seems to be diachronous, younging eastwards. Similarly, the Stornoway Formation can be viewed as the latest infill of the North Minch basin, as faulting west of the Eye peninsula (located in Figure 4.1) took control over earlier activity along the Minch Fault east of the peninsula.

It might be argued that one sample of mid Carboniferous age in the Little Minch hardly establishes the existence of a rift basin. However, the structural context in which the sample occurs clearly establishes the rift setting in the

Little Minch, both prior to the Carboniferous and, more importantly, later in the Permian and Triassic. It is precisely because the late Carboniferous comprises the basal infill of a new (or rejuvenated) rift system that samples of it are so rarely encountered. If the Carboniferous had been laid down in a different environment - say, for instance, a shallow sea following planation of the whole of northern Scotland after a phase of rifting - then isolated outcrops, preserved by local quirks of structure, would be ubiquitous.

The Shiant East Bank culmination brings Lewisian to the sea bed (Fig. 4.1). The culmination may be the intersection of the NW trending Loch Maree basement high with an inferred NE trending high. The latter is the footwall of a fault downthrowing to the SE, as shown schematically in the manual alterations to the printed map of Figure 4.1. The re-drawing shows an inlier comprising Lewisian, Stoer Group and Torridon Group surrounded by Permo-Triassic. However, in view of the half-graben style of development of the Permo-Triassic discussed above, the whole of the Shiant East Bank area deserves to be re-interpreted using the original data, rather than merely altering some outcrops, as has been done here.

The extension of the crust in the Little Minch region is considerable. In plan view it is clearly 2-dimensional, since the low-angle faults trend both NE-SW and NNW-SSE. However, the major component of extension is in a WNW-ESE direction, i.e. approximately perpendicular to the trend of the Minch Fault system, so the component of extension in this direction can be estimated by some simple measurements on profile 1 (Fig. 4.23). The extension factor ß is given by:

$$ß = \sin \Theta / \sin \Theta'$$

where Θ and Θ' are the initial and final dips of the fault planes (Jackson and Mackenzie 1983). On profile 1 these are about 45° and 25°, respectively, giving a ß-factor of about 1.7. In other words the 60 km long segment of the profile over the Minch Basin was about 35 km in length before the Torridonian and younger sediments were laid down. It is not feasible to try to estimate the extension due to the

separate episodes, since the dips of the interfaces within the sediments are poorly constrained.

CHAPTER 5
CONCLUSIONS

5.1 SUMMARY OF THE RESULTS

The principal geological results from the northern Skye and Little Minch region are as follows:

(1) The basin-bounding normal fault named the Minch Fault (Smythe et al. 1972) is the reactivated Outer Isles Thrust, as suggested by Smythe et al. (1982). This has been demonstrated by the combined interpretation of seismic refraction data, shallow seismic reflection profiles, and gravity models.

(2) The pre-Jurassic infill in the Little Minch is bounded by several eastward-dipping, low-angle normal faults.

(3) Beneath northern Skye, and northwestwards into the Little Minch, the structural trend is NNW-SSE to NW-SE, intersecting the more regional trend (represented by the Minch Fault) at nearly a right-angle.

(4) The deepest part of the basin is bounded to the NE by normal faults which mostly have a downthrow to the east, and not to the west, as might have been expected. The NW-SE gravity gradient through northern Skye is due to rapid thickening to the west of the sedimentary infill below a strong pre-Jurassic unconformity.

(5) The Minch / Outer Isles fault complex has a history of normal displacement during the late Precambrian, late Palaeozoic, and Palaeogene. There is no evidence for transcurrent displacement.

(6) The Jurassic, which occupies a simple depression, probably formed as a sag basin above the more complexly faulted sediments, though shifted relatively to the east.

(7) Offshore to the west of Skye, the Middle to Lower Jurassic succession is about twice as thick as that measured in NE Skye.

(8) The Palaeocene flood basalts and lavas of northern Skye have been extruded in a fault-controlled environment, perhaps by reactivation of the deeper NW-SE trending low-angle faults.

(9) The Minch Fault is probably also the locus of significant Palaeocene lava extrusion.

(10) Extension over the basin is 2-dimensional but probably greatest in a WNW-ESE direction. The stretching factor (ß) in this direction is about 1.7.

It is equally important to summarise the negative conclusions:

(1) The complex Tertiary sill outcrop does not form any recognisable pattern relative to the tectonic structure.

(2) The attempt to date the buried pre-Jurassic, post-Torridonian sedimentary infill by regional correlations of velocity and density has not advanced significantly since Tuson's work of nearly 30 years ago. His inference that the infill comprises rifted Triassic is still essentially correct.

5.2 WIDER RELEVANCE OF THE DETAILED RESULTS

5.2.1 THE CALEDONIAN OROGENY AND HEBRIDEAN BASIN FORMATION

Following a suggestion that the Caledonian thrusts of NW Scotland might control the deposition of the later basins (Smythe 1980), the MOIST deep reflection profile established that the Outer Isles Thrust, dipping east at 20°, was at depth reactivated as the Minch Fault (Smythe et al. 1982). In the area of the MOIST line the surface expressions of the two faults are some 30 km apart, and only converge to the

south in the more complex area of the Eye Peninsula and the Stornoway area of Lewis. A geological map (compiled by the author) has been published by Brewer and Smythe (1986, plate 2), who have summarised the arguments in favour of the Outer Isles "Thrust" (Dearnley 1962) actually having undergone reverse faulting, in response to the assertion that it may only have ever had an extensional history (Wernicke 1985, 1986).

The correlation of the thrust fault with the normal fault has previously depended on unpublished commercial seismic reflection data. None of these marine profiles actually cross the Outer Isles Thrust; a small extrapolation from the western end of one of these profiles, up-dip to the outcrop of the thrust on land, is always required. Conversely, the high resolution reflection profile obtained onshore over the exposed Outer Isles Thrust (Jones and Warner 1985, Jones 1986) does not cross the Minch Fault. However, in the Little Minch, south of 58°N, the Outer Isles Thrust and the Minch Fault are at their closest at outcrop. The results of the present study corroborate strongly the hypothesis that the two faults are one and the same at depth.

5.2.2 MECHANISMS OF CRUSTAL EXTENSION

The vertically exaggerated version of gravity profile 1 (Fig. 4.22) suggests that the Jurassic sag basin is shifted eastward with respect to the Upper Palaeozoic - Triassic rift basin by about 10 km. What does this tell us about extension in the lower crust?

The Moho is at a fairly well determined depth of 27.0 $\pm$ 0.5 km some 20 km NW of the west end of gravity profile 1 (Brewer and Smythe 1986). It presumably rises gently to the east, below the isostatically uplifted Outer Hebrides (Brewer and Smythe op. cit.), but is probably not much shallower than 26 km below the western part of the Little Minch basin.

One of the controversies of lithospheric extension is whether the upper crustal faults extend discretely right

through the crust (the simple shear model of Wernicke 1985), or whether the lithospheric extension can be approximated by pure shear (the assumption behind McKenzie's [1978] hypothesis for the formation of extensional basins).

If Wernicke's model is correct, the several faults which extend the brittle upper crust in profile 1 (Fig. 4.23) should cut the Moho some 60 to 100 km along the profile, and the thermal subsidence phase, compensating for the lithospheric thinning, should have occurred at least this far east.

On the other hand, if the brittle extension is confined to the upper crust (say 0-15 km depth), and the lower crust as well as the upper mantle has deformed by pure shear, the locus of lithospheric thinning will only be 10 to 40 km east of the outcrop of the major faults. This latter prediction seems to fit the actual location of the Jurassic basin much better, so we can conclude that the low angle faults controlling sedimentation in the Little Minch region probably pass into, and die out within, a ductile lower crust. There is no support here for the concept of upper mantle extension being displaced significantly to the east of the basin.

5.2.3 HEBRIDEAN BASIN FORMATION AND THE OPENING OF THE ROCKALL TROUGH

The conclusions concerning the review of the evidence for the age of opening of the Rockall Trough (Section 1.3.5) are summarised as follows:

(1) There is good evidence for a regional phase of rifting in the NE Atlantic region in late Palaeozoic time.

(2) The most direct evidence for the minimum age of the trough, based on regional stratigraphic correlations from the south and the north, indicates that the opening is pre-Cretaceous, and probably pre-Jurassic.

(3) The assumption of 'rift to drift' thus permits the hypothesis that the trough opened in the late Palaeozoic.

(4) A newly postulated phase of mid Cretaceous spreading in the Hatton-Rockall Basin accounts for the evidence hitherto put forward in favour of Cretaceous opening of the Rockall Trough.

The present study of northern Skye and the Little Minch clearly corroborates conclusion (1) above, but adds little of significance. McLean's (1978) synthesis of the basins of NW Britain into two belts of distinctly different late Palaeozoic age meeting in the Little Minch area is still valid and useful; however, it now appears that both the Clyde and the Marginal Belts originated at about the same time in the middle or late Carboniferous. Since intra-continental rifting is now known clearly to precede sea-floor spreading, it cannot be concluded (as did McLean) that the development of the Marginal Belt necessarily implies the prior existence of a passive margin to the west.

5.2.4 HEBRIDEAN VOLCANICITY AND VOLCANIC PASSIVE MARGIN STRUCTURE

The normal-faulted depositional setting postulated for the Palaeocene flood basalts of northern Skye is remarkably similar to the extensional environment of some dipping reflector sequences at passive margins.

The basaltic dipping reflectors west of the Rockall Plateau, for instance, appear to have been extruded onto thinned continental crust (Roberts and Ginzburg 1984, Morton and Taylor 1987). The model of Roberts and Ginzburg, however, prescribes a flat base to the seaward-dipping reflectors; but this is not supported by the seismic data. The geometry of the reflectors is not sigmoidal, as these authors suggest, but is of increasing seaward dip, with the deep (seaward) ends of the reflectors simply dying out. This geometry can be satisfied if the underlying continental crust is postulated to be cut by a number of low-angle

normal faults dipping eastwards towards the unthinned continent. The faults can be presumed, like those of northern Skye, to control the eruption of individual flows in a half-graben extensional setting. The west Rockall passive margin is therefore closely analogous to the Skye basalts in its structural setting, but progressed to the stage where intra-continental extension gave way to sea floor spreading.

5.3 TECHNICAL CONCLUSIONS AND RECOMMENDATIONS

Various geophysical and technical experiments were tried out in an attempt to improve the data quality. The results of these, together with recommendations for similar surveys in future, are as follows:

(1) The use of distributed small charges of gelignite set off in peat or clay is an effective impulsive seismic reflection source, and is clearly within the resources of small research projects.

(2) Laying the charges in a linear array helps to reduce ground roll if the array is long (c. 50 m or more).

(3) Firing two 'point' sources separated by an optimum distance and with a relative delay designed to cancel the dominant frequency of the ground roll is ineffective.

(4) When shooting over basalt (or layered intrusives), large charges (5 kg or more) generate proportionately more unwanted signal, at least within the first second or so. Large charges are only likely to reward the extra effort of preparation when the target reflectors are deeper than (say) 2 km.

(5) Remote shot detonation with a VHF radio link is too unreliable to warrant the saving in field time of not having to use a shot-firing cable.

(6) Anchoring the large Bradley sonobuoys often causes severe noise problems at the hydrophone. Even when the hydrophone/cable array is made neutrally buoyant, the array quickly gets streamed out by the tide, and water flow past the hydrophone induces noise. The system only works consistently well at times of slack water. Better alternatives involve using disposable, free-floating sonobuoys, or 'PUBS'- and 'PUMA'-type sonobuoys and arrays (Powell and Sinha 1987), which sit on the sea bed.

(7) Analogue-to-digital conversion of old land seismic data (which is costly to acquire) is worthwhile if it can be processed by modern commercial techniques.

APPENDIX 1
SEISMIC REFLECTION EQUIPMENT

Texas Instruments TI8000B 'Explorer' seismic system

The recording system comprises a 12 channel TI8000 'Explorer' seismograph, a Techno 551A recorder-reproducer, a Micro Instrument Corporation DR700 oscillograph, and power pack. Ancillary equipment includes an Electro-Tech FS-4A 50 Hz notch filter, a Shell GZ100 VAR camera, signal and power switch boxes, a Geo Space Corporation HS-200 low voltage blaster, and VHF radios for remote firing. During recording the whole system takes about 25A from one of two 12V car batteries - two are required as the VAR camera operates on 24V, as well as ensuring an adequate supply of power during a day's fieldwork.

The field gear comprises 84, 7 Hz, 70% critically-damped geophones, connected to one or two spread cables, giving a 12-channel spread of up to 330 m in length, and by using an extension cable the spread can be up to 300 m from the recording vehicle.

Fig. A1 shows the route taken by one channel of seismic data on recording and playback, together with some other control and auxiliary functions. The principal electrical characteristics of the amplifier are:-

(1) a bandwidth of 5-200 Hz (3 dB down), with zero phase shift and less than 1% distortion at 40 Hz,

(2) a dynamic range of 120 dB attenuation can be effected by the input range switch, while the AGC loop range is 90 dB, which can be attenuated by 0-80 dB in steps of 3.3 dB during linear operation by three initial attenuation switches, each ganged to four amplifiers,

(3) AGC. During linear operation the AGC is suppressed by a 10 kHz presuppression signal from the control unit. When this substitute signal is removed the gain of the amplifier becomes a function only of the seismic signal, and an 80 dB change of input level produces

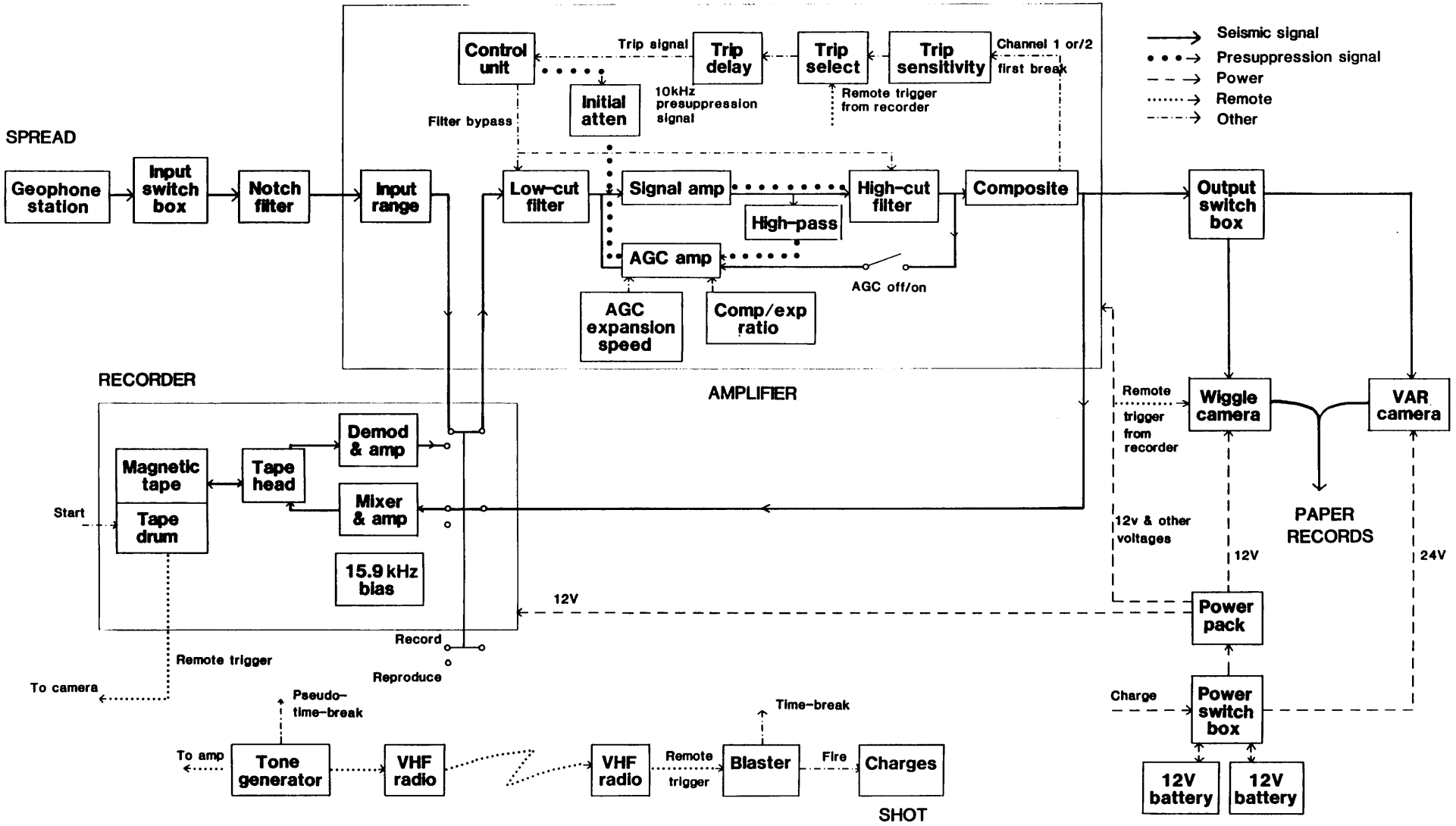

Fig. A1 Block diagram of TI 8000 seismic reflection system.

less than 6 dB (2:1) change in output. There is a choice of six AGC expansion speeds; 20, 30, 50, 80, 125, and 200 dB/s, and the compression/expansion ratio can be either 1:1 or 3:1, filters include a 50 Hz notch filter to remove power line pickup, if it occurs. It has an overall insertion loss of about 6 dB, and a further 50 dB attenuation at 50 Hz (6 dB down at 45 and 55 Hz). On both recording and play-back a wide choice of zero-loss low and high-cut filters are available, the cut-offs of the former (3 dB down) being at 14, 18, 22, 27, 33, and 40 Hz, and the latter at 40, 55, 72, 92, 125, and 160 Hz. Two types of low-cut filter can be used, with slopes of 18 and 26 dB/octave (K and M types respectively), and the high-cut is a K-type with an 18 dB/octave slope. The total number of filter settings, including both out, is thus 86.

The control unit, which supplies the presuppression signal, also enables either or both filters to be bypassed until a trip signal is received, after which the filters and AGC come into operation. This function is useful to preserve the sharpness of the first breaks. A trip select switch determines what signal is to be used - the first break of channel 1 or 12, or a remote signal from the recorder drum. A variable trip delay of 0.1 to 1.2s, in 11 steps, is then applied, for instance to ensure that the AGC and filters come into operation after the latest first break is received. The trip function can also be performed manually if necessary, if for example the first break chosen fails to do so.

The amplified and filtered output can be mixed (composited) in various ways, if desired, to enhance correlation of synchronous events (see below). However, compositing is never used on recording, only on playbacks. On recording the output is split, going simultaneously to the camera to give a monitor record of any time length desired, and to the recorder, which has a recording time of 6 s. The seismic signal amplitude-modulates a 15.9 kHz bias, which is then recorded on a 60 cm length of magnetic tape wound round a drum which rotates once. Microswitches on the drum can be used to trigger the camera paper-feed, the blaster discharge, and the amplifier trip. In addition, the

recorder supplies a head-alignment pulse to each data channel, to check on channel phase and amplitude, and a timing signal, which is recorded on a separate tape and camera channel. The time-break is recorded on its own channel (and similarly on the monitor record), but it appears on channel 4 on playbacks. The frequency response of the recorder (not given by the manufacturers) is somewhat unsatisfactory below about 20 Hz, being 6 dB down at 15 Hz (relative to 25 Hz), but in normal reflection work this is unimportant.

The camera originally supplied with the TI8000 system records the seismic data as wiggle traces on direct-writing paper 15 cm wide, which can be fed out at speeds from 12.7 to 38 cm/s. Auxiliary channels record the time break and the recorder timing signal, and timing lines 10 ms apart are produced by an independent oscillator in the camera. When several seconds of seismic data are of interest the slowest paper speed is mormally used, and monitor records are always made with this camera. The VAR camera uses the same paper, which runs at a fixed speed of 14.8 cm/s, and timing spikes 10 ms apart appear at either side of the data display.

Fig. A.2 shows a circuit diagram of the Geo Space Corp. HS-200 low voltage blaster, as modified by the author in 1971 (see Section 2.2.7 above). Output B is delayed by a calibrated variable time of 0-15 ms relative to A, so that the group of charges fired by B can be designed to cancel the ground- roll originating from the group fired by A.

Switch boxes

(1) Power switch box
This is necessary for the supply of large currents (up to 25 A) at 12 V from one of the two batteries A and B, simultaneous supply of 24 V to the VAR camera, and intermittent (but frequent) recharging of the batteries from the vehicle during fieldwork recording.

(2) Input switch box
In double-spread 12-channel recording, alternate take-outs of the two spread cables are used, whereas every take-out of one cable only is used single spread recording. The input

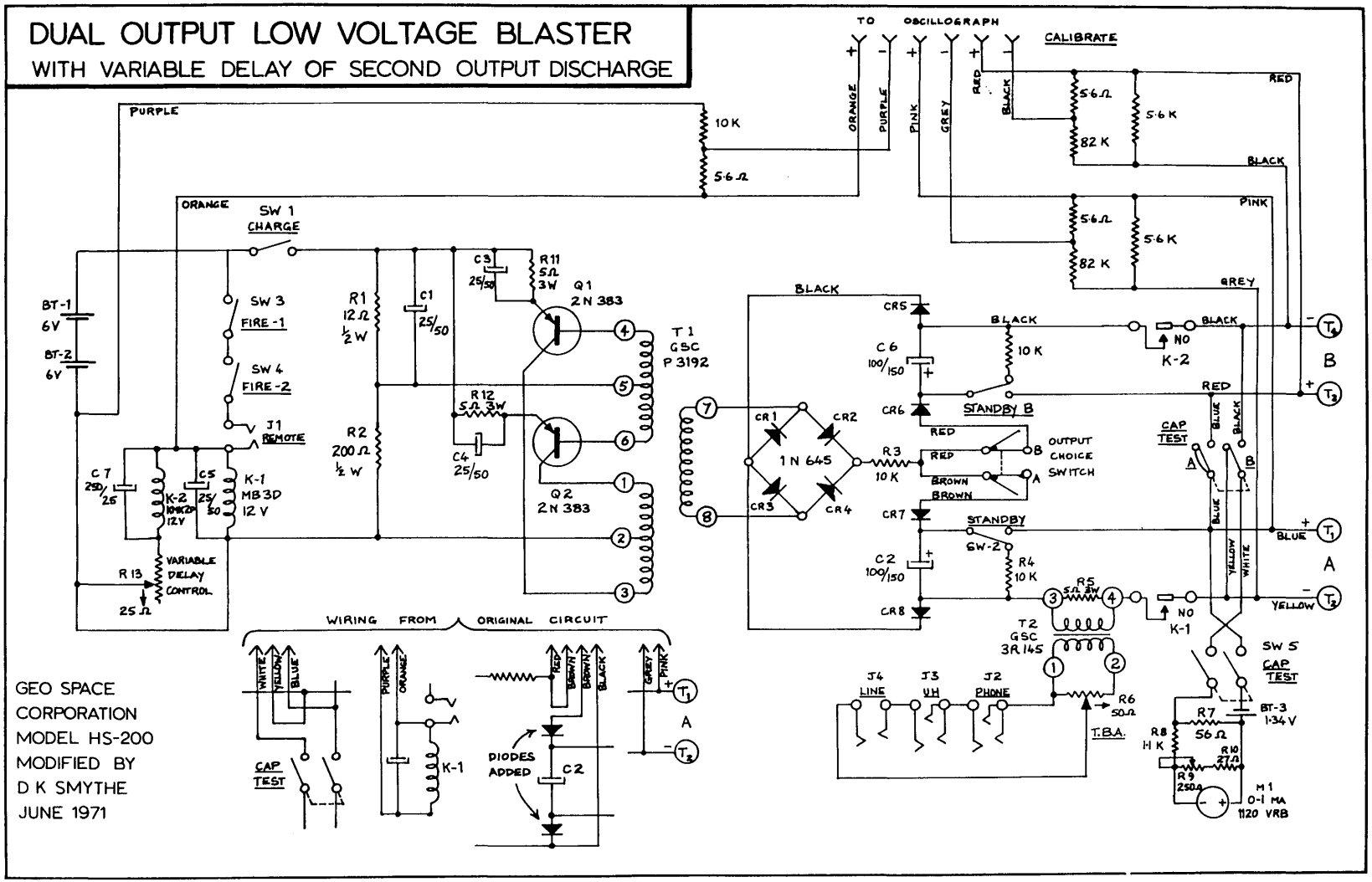

Fig. A2 Circuit diagram of dual output low voltage blaster.

switch box simply comprises male and female multi-input plugs, so that either end of the spread can be connected (to save fieldwork time), and a 24-pole 2-way wafer switch wired so that the 12 inputs go to 12 amplifiers in their correct order.

(3) Output switch box
This comprises a 12-pole 2-way wafer switch (the signal outputs have a common earth) for correcting the order of channels if a record has inadvertently been made with the input single/double switch in the wrong position. However, composite playbacks cannot be made from such recordings, as adjacent channels in the recorder and amplifier are not in their field order. A second, similar switch reverses the order of channels from 1-12 to 12-1, so that records can always be presented with the west (or north) channel at the botton, i.e. at the left-hand side with time increasing downwards. This saves field time, as otherwise the spread cables would always have to be laid out a particular way round. A third switch directs the output to either camera.

Composite patterns

The composite unit is a network of current-dividing resistors mounted on a plug-in board (Fig. A3). In conjunction with a 3-way wafer switch, it allows the 12 outputs from the amplifiers to be mixed in pre-determined ways before being applied to the 12 galvanometers in the camera. There are two units, each handling 12 channels, and they can be interchanged by opening up the amplifier case.

As originally supplied, both units provided:

(1) a straight or no-mix output, and

(2) a Comp A or Comp B, which in the 12-channel version of the TI8000 (which is built initially as a 24-channel system) are essentially the same, viz., a 50:50 mix of channels 1 and 12, 2 and 11, etc.

Composite unit no. 2 supplies:

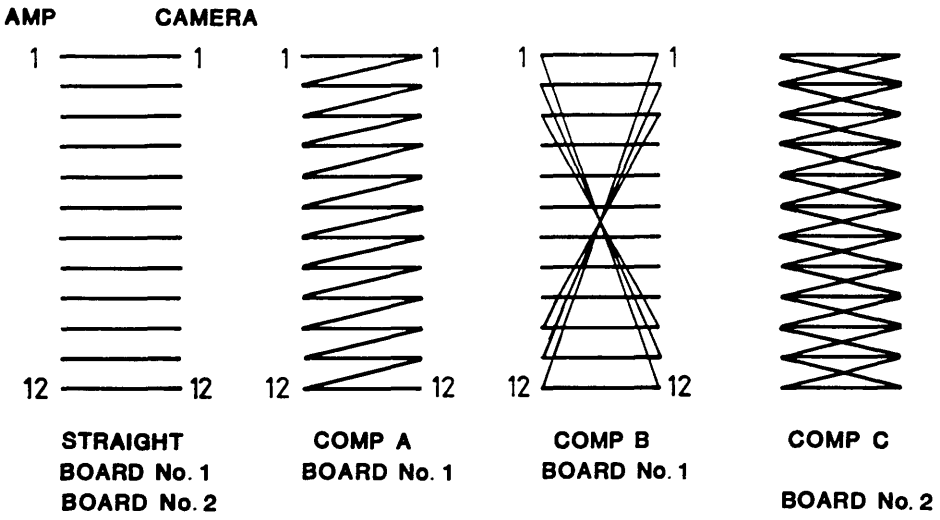

nth camera trace

n	$\frac{n+(n-1)}{2}$	$\frac{n+(13-n)}{2}$	$\frac{(n-1)}{4}+\frac{n}{2}+\frac{(n+1)}{4}$

%mix

0	50+50	50+50	50+25+25

Fig. A3 Composite unit diagrams, showing the different kinds of trace mixing possible between the amplifier output and the camera. Straight output and Comp A (a 2-trace mix) are as supplied with the TI 8000 system. Comp B and Comp C are designed to aid the interpretation of the Skye analogue data.

(1) a straight output, and

(2) Comp C, a 3-channel mix whose output takes 50% of its own amplifier output and 25% of the outputs on either side.

Straight output is always used on recording, and Straight playbacks are normally used for reflection computations. Comp patterns A and C are used for moderate and fairly severe mixing, respectively, to help in the identification of reflectors. Comp B is intended for enhancement of split spreads, since the use of the asymmetrical Comp A tends to give the record an off-centre appearance.

APPENDIX 2
VELOCITY AND DENSITY MEASUREMENTS

Ultrasonic velocity and density results

V is P-wave velocity in km/s with standard deviation s(V). D is density in g/cm^3 with standard deviation s(D)
N is the number of measurements on each specimen

FORMATION	ROCK TYPE	SITE	GRID REFERENCE	SAMPLE CODE	SPEC NO.	N	SPECIMEN MEAN V	s(V)	D	MEAN OF SITE V	s(V)	D	s(D)	MEAN OF ROCK TYPE V	s(V)	D	s(D)
Torridonian Stoer Group	Red sandstone	Gruinard Bay	NG 917913	S1	1	3	5.10	0.05	2.67								
					2	1	5.43	0.04	2.68	5.27	0.23	2.68	0.01				
		Poolewe	NG 873837	S4	1	2	5.53	0.12	2.67	5.53	0.12	2.67	-				
		Poolewe	NG 872839	S5	1	3	5.71	0.25	2.74								
					2	2	5.69	0.05	2.73	5.70	0.02	2.73	0.01	5.50	0.22	2.69	0.04
Torridonian Applecross Group	Sandstone	L Loch Broom	NG 038905	S2	1	7	5.38	0.27	2.64	5.38	0.27	2.64	-				
		L Loch Broom	NH 070890	S3	1	3	4.97	0.19	2.68								
					2	1	5.00	0.04	2.66								
					3	2	4.71	0.25	2.62								
					4	1	4.81	0.03	2.60	4.87	0.13	2.64	0.04				
		Applecross	NG 707437	SH	1	3	4.10	0.40	2.58								
					2	2	5.20	0.05	2.56	4.65	0.78	2.57	0.02	4.97	0.37	2.62	0.04
Triassic	Sandstone	Gruinard Bay	NG 902927	SD	1	1	2.35	0.01	2.46								
					2	1	2.51	0.01	2.45	2.43	0.11	2.45	-				
		Gruinard Bay NW	NG 896937	SE	1	2	2.10	0.07	2.48								
					2	2	2.05	0.01	2.44								
					3	2	2.37	0.38	2.52	2.17	0.17	2.48	0.04				
		Loch Gairloch	NG 762792	SF	1	1	2.68	0.01	2.40								
					2	1	2.21	0.01	2.36	2.44	0.34	2.38	0.03	2.35	0.15	2.44	0.05

Ultrasonic velocity and density results (continued)

FORMATION	ROCK TYPE	SITE	GRID REFERENCE	SAMPLE CODE	SPEC NO.	N	SPECIMEN MEAN V	SPECIMEN MEAN s(V)	SPECIMEN MEAN D	MEAN OF SITE V	MEAN OF SITE s(V)	MEAN OF SITE D	MEAN OF SITE s(D)	MEAN OF ROCK TYPE V	MEAN OF ROCK TYPE s(V)	MEAN OF ROCK TYPE D	MEAN OF ROCK TYPE s(D)
Triassic	Conglom. & cornstone	Applecross	NG 707438	S7	1	3	4.03	0.22	2.56								
					2	2	4.49	0.15	2.57	4.26	0.32	2.56	0.01				
		Gruinard Bay	NG 902927	SC	1	2	4.12	0.20	2.63	4.12	0.20	2.63	-				
		Gruinard Bay	NG 902927	SD3	1	2	4.31	0.37	2.58	4.31	0.37	2.58	-				
		Loch Gairloch	NG 762792	SF3	1	3	4.35	0.11	2.62	4.35	0.11	2.62	-				
		Applecross	NG 707437	SG	1	2	4.01	0.05	2.61								
					2	2	4.33	0.16	2.66	4.17	0.23	2.64	0.03	4.24	0.10	2.60	0.03
Palaeocene North Skye	Basalt	Staffin Road	NG 433674	STR	1	4	4.96	0.28	2.79								
					2	2	6.31	0.09	2.92								
					3	2	5.97	0.26	2.96	5.75	0.70	2.89	0.09	5.75	0.70	2.89	0.09
Palaeocene North Skye	Gabbro (sill)	Skudiburgh	NG 374647	SK	1	2	5.53	0.04	2.83								
					2	3	5.92	0.19	3.04								
					3	3	6.25	0.09	2.86								
					4	3	6.89	0.16	3.11								
					5	5	5.92	0.39	2.87	6.10	0.51	2.94	0.12				
		Waterstein (top)	NG 142478	WST	1	4	4.69	0.08	2.57								
					2	2	4.71	0.34	2.55	4.70	0.02	2.56	0.01				
		Waterstein (bottom)	NG 140477	WSB	1	1	5.62	0.05	2.79								
					2	1	6.32	0.11	2.94								
					3	2	5.98	0.21	2.74	5.97	0.35	2.82	0.10	5.59	0.78	2.77	0.19

Hammer seismic velocities

V is P-wave velocity in km/s with standard deviation s(V)
N is the number of measurements at each site

FORMATION	ROCK TYPE	SITE	GRID REFERENCE	ULTRASONIC SAMPLE CODE	N	SITE MEAN V	SITE MEAN s(V)	COMMENTS
Torridonian Stoer Group	Red sandstone	Gruinard Bay	NG 917913	S1	3	6.63	0.73	
		Poolewe	NG 873837	S4	3	4.84	0.06	
		Poolewe	NG 872839	S5	3	4.20	0.08	
Torridonian Applecross Group	Sandstone	L Loch Broom	NH 070890	S3	3	3.61	0.07	
		Gairloch	NG 802767	-	3	4.27	0.05	
Torridonian Kishorn Nappe SE Skye	Sandstone	Loch na Dal	NG 703152	-	3	5.58	0.30	Parallel to strike
					3	3.80	0.09	Across strike
	Sandstone	Lochain Dubha	NG 680208	-	3	4.08	0.13	Parallel to strike
Triassic	Conglom.	Breakish	NG 682232	-	3	2.84	0.05	Across strike
	Conglom.	Applecross	NG 707438	S7	3	3.21	0.05	
		Gruinard Bay	NG 902927	-	3	2.64	0.04	Sandstone - perpendicular to strike
					3	3.41	0.06	Cornstone - perpendicular to strike
					3	3.58	0.03	Conglomerate - perpendicular to strike
	Sandstone/ cornstone	Stornoway Formation	NB 492327	-	3	2.59	0.03	Parallel to strike
					3	2.52	0.03	Across strike
Jurassic Broadford Beds	Sandstone	Breakish	NG 663328	-	3	2.82	0.27	In plane of bedding

APPENDIX 3

MARINE SEISMIC REFRACTION DATA

Line A-B (1971)

Nominal ends of line: A - 57°46'N, 6°50'W
B - 57°40'N, 6°36'W

Decca hyperbolic position fixing method: H - Hifix
MC - Main Chain 6C

Buoy/Shot	Latitude (degrees, minutes)	Longitude	Fix	Time (GMT)	Buoy no.	First break (seconds)	Water break
----------First attempt: 27 June 1971----------							
Buoy 1 out	57 45.40	-6 50.95	H	1439			
Buoy 2 out	57 45.18	-6 50.46	H	1433			
Buoy 3 out	57 44.91	-6 49.95	H	1428			
Buoy 4 out	57 44.75	-6 49.35	H	1423			
Buoy 1 in	57 45.66	-6 51.46	H	1801			
Buoy 2 in	57 45.06	-6 50.79	H	1817			
Buoy 3 in	57 45.07	-6 50.28	H	1829			
Buoy 4 in	57 44.57	-6 49.35	H	1850			
Shot 8136	57 44.10	-6 48.10	H	1516	1	1.69	2.60
					2	1.66	2.21
					3	1.40	1.70
					4	1.15	1.265
Shot 8137	57 43.45	-6 46.00	H	1538	1	2.51	4.425
					2	2.27	3.70

Buoy/Shot	Latitude (degrees, minutes)	Longitude	Fix	Time (GMT)	Buoy no.	First break (seconds)	Water break
----------Second attempt: 28 June 1971----------							
Buoy 2 out	57 45.58	-6 50.50	MC	1708			
Buoy 1 out	57 45.29	-6 49.95	MC	1703			
Buoy 2 in	57 45.10	-6 51.22	MC				
Buoy 1 in	57 44.70	-6 50.38	MC				
Shot 8145	57 45.07	-6 50.30	MC	1758	1	0.24	0.27
					2	0.43	0.49
Shot 8146	57 45.00	-6 49.05	MC	1817	1	0.86	0.97
					2	1.24	1.455
----------Third attempt: 29 June 1971----------							
Buoy 4 out	57 45.00	-6 48.95	MC	0915			
Buoy 4 in	57 46.76	-6 44.35	MC				
Shot 8148	57 44.93	-6 48.05	MC	0953	4	0.34	0.385

Line A-D (1972)

Nominal ends of line: A - 57°43.7'N, 7°01.0'W
D - 57°36.5'N, 6°31.0'W
Intermediate points: B - 57°41.5'N, 6°52.5'W
C - 57°40.5'N, 6°49.0'W

Only shot-receiver pairs with useful first arrival data are given, although other pairs may have given a water break to help in line relocation. Bedrock velocity (for shot/receiver static corrections) is taken from preliminary T-X graphs; hydrophone and shot depths are both 15 m throughout.

S - shot; B - buoy; H - hydrophone

Buoy Shot	Latitude (degrees, minutes) N	Longitude W	Water depth (m)	Bedrock velocity (km/s)	Buoy no.	First break (seconds)	Water break
----------Sound of Harris (A) to SE (2 July 1972)----------							
B1 out	57 43.22	6 59.40	20	6.2			
B1 in	57 42.77	6 59.48	20	6.2			
B4 out	57 43.78	7 00.92	20	6.2			
B4 in	"	"	20	6.2			
S 2	57 42.82	6 57.78	100	4.0	1	0.39	1.06
					4	0.71	2.43
S 3	57 42.54	6 56.79	100	4.0	1	0.73	1.96
S 7	57 43.30	6 58.58	45	4.0	1	0.26	0.70

Buoy Shot	Latitude (degrees, minutes) N	Longitude W	Water depth (m)	Bedrock velocity (km/s)	Buoy no.	First break	Water break
----------Sound of Harris (A) to SE (3 July 1972)----------							
B4 out	57 43.66	7 00.58	20	6.2			
B4 in	"	"	20	6.2			
S 8	57 43.32	6 58.19	45	6.2	4	0.48	1.70
S 9	57 43.12	6 57.14	100	3.1	4	0.71	2.41
S10	57 43.02	6 56.63	110	3.1	4	0.85	2.76
S11	57 42.85	6 56.20	115	3.1	4	0.99	3.12
S12	57 42.67	6 55.71	120	3.1	4	1.22	3.54
S13	57 42.41	6 55.05	130	3.1	4	1.51	4.06
S14	57 41.95	6 53.88	115	3.1	4	1.98	5.08
-------Position C to NW (Sound of Harris) (4 July 1972)-----							
B3 out	57 40.17	6 49.75	110	3.3			
B3 in	57 41.84	6 46.40	140	3.3			
B4 out	57 39.98	6 49.30	120	3.3			
B4 in	57 43.60	6 43.92	140	3.3			
S17	57 40.69	6 51.03	115	3.3	3	0.77	1.07
					4	0.87	1.47
S18	57 40.86	6 51.44	120	3.3	3	0.92	1.50
					4	1.02	1.81
S19	57 41.07	6 51.95	115	3.3	3	1.12	1.94
					4	1.21	2.26
S20	57 41.36	6 52.66	125	3.3	3	1.30	2.34
					4	1.40	2.67
S21	57 41.68	6 53.46	115	3.0	4	1.69	3.24
S22	57 41.94	6 54.10	115	3.0	4	2.00	3.85
S23	57 42.30	6 54.96	125	2.4	4	2.35	4.44
S24	57 42.43	6 55.31	125	2.4	4	2.62	4.83

Buoy Shot	Latitude (degrees, minutes) N	Longitude W	Water depth (m)	Bedrock velocity (km/s)	Buoy no.	First break (seconds)	Water break
--------Position C to SE (Loch Snizort) (4 July 1972)-------							
B4 out	57 40.46	6 50.50	130	3.3			
B4 in	57 43.65	6 42.42	130	3.3			
S28	57 40.09	6 48.42	125	3.3	4	0.83	1.32
S29	57 39.75	6 46.70	145	3.3	4	1.19	2.23
S30	57 39.62	6 45.93	150	3.3	4	1.41	2.70
S31	57 39.52	6 45.42	155	3.3	4	1.53	3.01
S32	57 39.40	6 44.80	162	3.3	4	1.66	3.39
S33	57 39.32	6 44.35	162	3.3	4	1.79	3.65
S35	57 39.13	6 43.35	153	3.3	4	2.14	4.25
S36	57 39.02	6 42.75	147	3.3	4	2.28	4.60
---------- Sound of Harris (A) to SE (5 July 1972)----------							
B4 out	57 43.87	7 00.65	20	6.0			
B4 in	57 43.60	7 00.06	20	6.0			
S39	57 43.47	6 58.80	20	5.4	4	0.38	1.30
S40	57 43.19	6 58.05	50	5.4	4	0.58	1.98
S41	57 43.00	6 57.45	90	5.4	4	0.73	2.41
S42	57 41.98	6 53.70	115	5.4	4	1.72	5.16
S43	57 41.74	6 52.94	115	5.4	4	1.88	5.74
S44	57 41.53	6 52.13	122	5.4	4	2.11	6.37
S45	57 41.28	6 51.25	115	5.4	4	2.31	7.05
S46	57 41.01	6 50.31	115	5.4	4	2.48	7.71
S47	57 40.78	6 49.44	122	5.4	4	2.70	8.32
S48	57 40.64	6 48.92	125	5.4	4	2.80	8.74
S49	57 40.42	6 48.12	130	5.4	4	2.95	9.33
S50	57 40.21	6 47.40	135	5.4	4	3.07	9.89
S53	57 43.43	6 59.48	20	5.4	4	0.19	0.46

Buoy Shot	Latitude (degrees, minutes) N	Longitude W	Water depth (m)	Bedrock velocity (km/s)	Buoy no.	First break (seconds)	Water break
-------Position C to NW (Sound of Harris) (5 July 1972)-----							
B4 out	57 40.20	6 50.45	90	4.8			
B4 in	57 40.03	6 50.55	90	4.8			
S54	57 40.58	6 51.38	115	3.2	4	0.48	0.80
S55	57 41.71	6 54.10	118	3.2	4	1.51	3.13
S56	57 41.90	6 54.56	118	3.2	4	1.72	3.51
-------Position B to NW (Sound of Harris) (6 July 1972)-----							
B4 out	57 41.38	6 52.60	120	3.0			
B4 in	57 42.50	6 51.13	120	3.0			
S62	57 41.63	6 53.29	120	3.0	4	0.44	0.56
S63	57 41.80	6 53.65	120	3.0	4	0.61	0.90
S64	57 42.00	6 54.15	120	3.0	4	0.82	1.32
S65	57 42.25	6 54.80	125	3.0	4	1.09	1.84
S66	57 42.51	6 55.45	125	3.0	4	1.34	2.37
S67	57 42.81	6 56.23	110	3.0	4	1.60	2.98
S68	57 43.17	6 57.10	100	6.0	4	1.59	3.71
S69	57 43.33	6 57.72	50	6.0	4	1.69	4.27
S70	57 43.51	6 58.46	20	6.0	4	1.76	4.72
S71	57 43.66	6 59.17	25	6.0	4	1.86	5.41
S72	57 43.84	6 59.86	20	6.0	4	2.01	5.95
S73	57 44.04	7 00.72	20	6.0	4	2.06	6.58

Calculation of dip of refractor below
Minch Fault on Line A-D (1972)

Refer to Figure 3.69. The derivation is a modification of the standard two-layer model, the layers separated by a plane dipping refractor. Definitions are:

m_D - downdip slowness
m_U - updip slowness
V_L - velocity of Lewisian part of upper layer
V_M - velocity of Mesozoic part of upper layer
V_1 - velocity below upper layer
i_L - critical angle at V_L - V_1 interface
i_M - critical angle at V_M - V_1 interface
a - dip of interface
T_{DD} - total travel time observed downdip
T_{DU} - total travel time observed updip

Part 1 - calculation of V_1 and 'unconstrained' dip a

By Snell's Law (see Fig. 3.69A):

$$\sin i_L = V_L / V_1 \qquad (1)$$

$$\sin i_M = V_M / V_1 \qquad (2)$$

The slopes (slownesses) of the updip and downdip refractor segments are given by:

$$m_U = \sin (i_L - a) / V_L \qquad (3)$$

$$m_D = \sin (i_M + a) / V_M \qquad (4)$$

Substituting (3) and (4) into (1) and (2) and re-arranging:

$$a + \sin^{-1} (V_M/V_1) = \sin^{-1} (V_M.m_D) \qquad (5)$$

$$a - \sin^{-1} (V_L/V_1) = -\sin^{-1} (V_L.m_U) \qquad (6)$$

Subtract (6) from (5):

$$\sin^{-1}(V_M/V_1) + \sin^{-1}(V_L/V_1) = \sin^{-1}(V_M.m_D) + \sin^{-1}(V_L.m_U) \qquad (7)$$

Note that although these are general formulae, we constrain the intercept of the downdip segment m_D to pass through the origin (Fig. 3.69B) since we hypothesise that the refractor crops out at the origin (Fig 3.69A). The least-squares best fit to the data for m_D is thus slightly different from the result which would be obtained if an intercept is allowed.

The right-hand side of (7) is known; what we require is V_1, appearing in the left-hand side, which is the sum, ß, of the two critical angles i_M and i_L. The known quantities V_M, V and ß, and the unknown V_1 are related geometrically by the quadilateral of Figure A4A. This is redefined in the Cartesian XY frame of Figure A4B, in which V_1 is the length of the vector (x,y). From this figure:

$$x = V_L;\ y = z - yz$$

$$z = V_M.\cos(ß-90)$$

$$u = V_M.\sin(ß-90)$$

$$ux = V_L - u = V_L - V_M.\sin(ß-90)$$

$$yz = [\ V_L - V_M.\sin(ß-90)\ ].\tan(ß-90)$$

$$\therefore\ y = z - yz$$

$$= V_M.\sin ß - [V_L - V_M.\cos ß].\tan(ß-90)$$

$$\therefore\ V_1 = (\ x^2 + y^2\ )^{½}$$

The dip a is then obtained from (5) or (6) above. This is referred to as the 'unconstrained' dip, since the total travel time T_D between either end (A-B) of the T-X graph of Figure 3.69B has not been used explicitly yet. Only the total travel time T_{DD} for the downdip segment has been used implicitly in the best-fit line through the origin, to

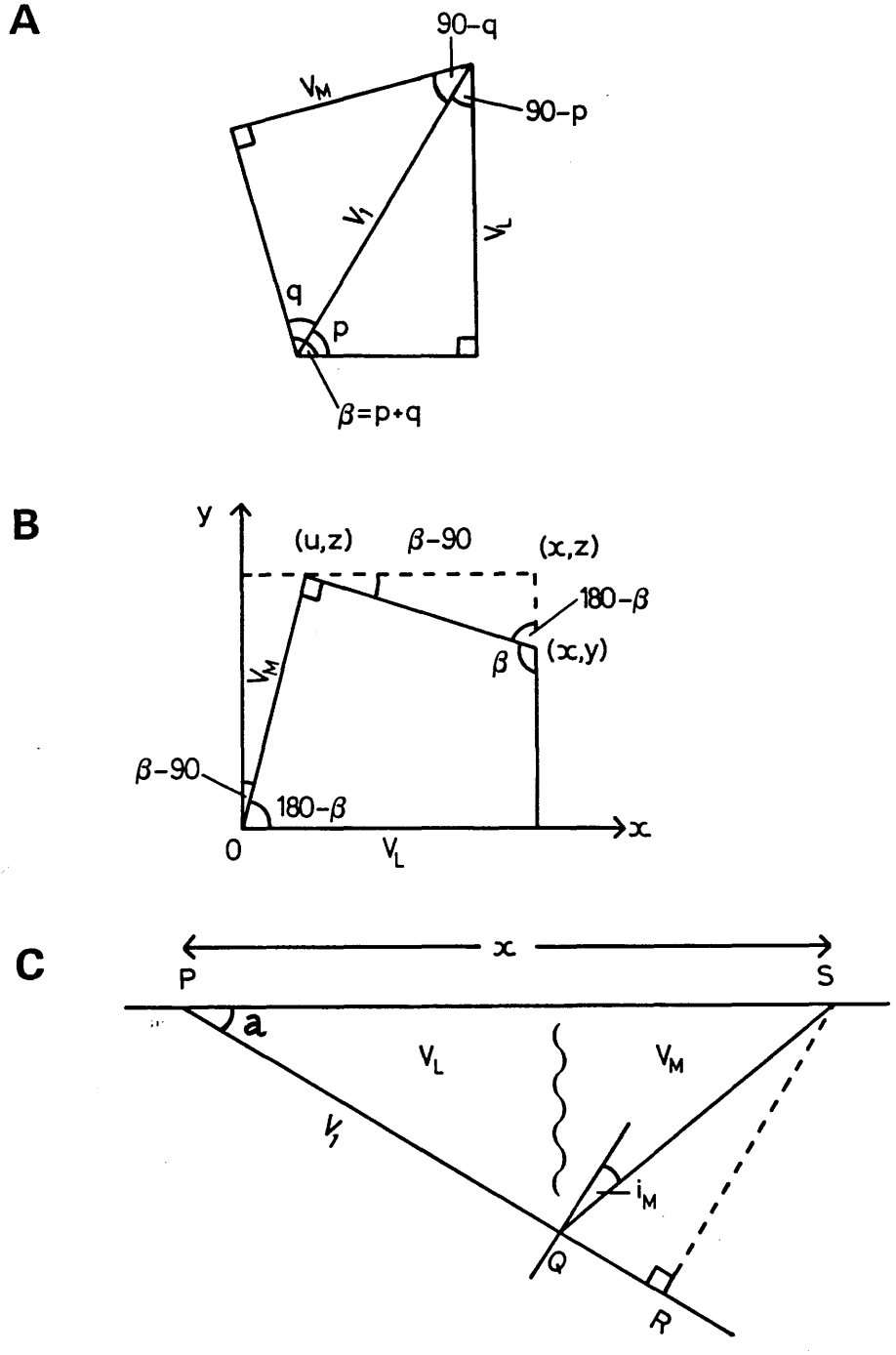

Fig. A4 Geometry of refractor below Minch Fault.

A. Geometric relationship of unknown refractor velocity V_1 to other known variables.

B. Quadilateral of Figure A4A redefined in Cartesian xy coordinates. V_1 is the length of the vector (x,y).

C. Geometry of dipping refractor (cf. Fig. 3.69).

obtain the slope m_D.

Part 2 - recalculation of dip a, constrained by T_D

We define T_D to be the mean of the total travel times for the updip and downdip segments T_{DU} and T_{DD}. The aim here is to test the hypothesis that the updip and downdip segments are actually from the same refractor, i.e. it is not just coincidence that they have similar total travel times. It also tests the hypothesis that the refractor crops out at the origin, as shown in Figure 3.69A.

We recalculate the dip a, using the value of V_1 obtained above, but with the new boundary condition of the mean total time T_D. Refer to Figure A4C:

T_D = Travel time along (PR - QR + QS)

$= (PR - QR) / V_1 + QS / V_M$

$= (x.\cos a - x.\sin a.\tan i_M) / V_1 + x.\sin a / V_M.\cos i_M$

$V_1.T_D = x.\cos a - x.\sin a.\tan i_M + x.V_1.\sin a / V_M.\cos i_M$

$= x.\cos a + x.\sin a (V_1/V_M.\cos i_M - \tan i_M)$

To solve for a, substitute $t = \tan a/2$, so that

$\cos a = (1 - t^2) / (1 + t^2)$

$\sin a = 2t / (1 + t^2)$

After some manipulation we get a quadratic of the form

$A.t^2 + B.t + C = 0$, where

$A = (V_1.T_D / x) + 1$

$B = 2 [\tan i_M - (V_1 / V_M.\cos i_M)]$

$C = (V_1.T_D / x) - 1$

The solution can produce two real roots, but one of these implies very steep dips, and would only be physically valid for very small T_D and x. It is because these two variables only enter the coefficients A and C above as a ratio that their absolute size does not constrain the solution. Therefore we can reject the steep geometric solution on grounds of scale, independently of the fact that it is geologically unrealistic.

ANDERSON, F.W., and DUNHAM, K.C. 1966. The geology of northern Skye. Mem. Geol. Surv., 216pp.

AVERY, O.E., BURTON, G.D., and HEIRTZLER, J.R. 1968. An aeromagnetic survey of the Norwegian Sea. J. Geophys. Res. 73, 4583-4600.

BALLY, A.B. 1982. Musings over sedimentary basin evolution. Phil. Trans. R. Soc. Lond. A305, 325-338.

BARRY, K.M., CAVERS, D.A. and KNEALE, C.W. 1975. Recommended standards for digital tape formats. Geophysics 40, 344-352.

BENTLEY, P.A.D. 1986. Geophysical studies in southern and central Rockall Trough, northeast Atlantic. Unpublished PhD thesis, Edinburgh University.

BLUNDELL, D.J and RAYNAUD, B. 1986. Modeling lower crust reflections observed on BIRPS profiles. In Reflection seismology: a global perspective (eds Barazangi, M. and Brown, L.), Am. Geophys. Union Geodynamics Ser. Vol. 13, 287-295.

BØEN, F., EGGEN, S. and VOLLSET, J. Structures and basins of the margin from 62° to 69°N and their development. In: Spencer, A.M. (ed.), Petroleum Geology of the North European Margin, 253-270, Norwegian Petroleum Society, Oslo.

BOTT, M.H.P., 1975. Structure and evolution of the Atlantic floor between Northern Scotland and Iceland. Nor. Geol. Unders. 316, 195-199.

BOTT, M.H.P. 1979. Subsidence mechanisms at passive continental margins. in Watkins, J.S., Montadert, L. and Dickinson, P.W. (eds). Geological and geophysical investigations of continental margins. Am. Assoc. Pet. Geol. Mem. 29, 3-9.

BOTT, M.H.P. and WATTS, A.B. 1971. Deep structure of the continental margin adjacent to the British Isles. In:

Delaney, F.M. (ed.). The geology of the East Atlantic continental margin. 2. Europe. Inst. Geol. Sci. Rep. No. 70/14, 89-109.

BOWES, D.R. 1969. The Lewisian of the north-west highlands of Scotland. In Kay, M. (Ed). North Atlantic - geology and continental drift. Am. Ass. Pet. Geol. Mem. 12, 575-594.

BREWER, J.A. and SMYTHE. D.K. 1986. Deep structure of the foreland to the Caledonian Orogen, NW Scotland: Results of the BIRPS WINCH profile. Tectonics 5, 171-194.

BRITISH GEOLOGICAL SURVEY 1987. Little Minch Sheet 57°N - 08°W. 1:250,000 Series Solid Geology.

BROWNE, E.B.C. and COOPER, R.I.B. 1949. The British submarine gravity surveys of 1939 and 1946. Phil. Trans. R. Soc. Lond. A242, 243-310.

BUKOVICS, C., CARTIER, E.G., SHAW, N.D. and ZIEGLER, P.A. 1984. Structure and development of the mid-Norway continental margin. In Spencer, A.M. (ed.), Petroleum Geology of the North European Margin, 407-423, Norwegian Petroleum Society, Oslo.

BULLARD, E.C., EVERETT, J.E. and SMITH, A.G. 1965. The fit of the continents around the Atlantic. Phil. Trans. R. Soc. Lond. A258, 41-51.

BULLARD, E.C., and JOLLY., H.L.P. 1936. Gravity measurements in Great Britain. Mon. Not. R. Astron. Soc. Geophys. Suppl. 3, 443-477.

BULLERWELL, W. 1968. Aeromagnetic map of part of Great Britain and Northern Ireland. Inst. Geol. Sci.

CALLOMON, J.H. 1975. Jurassic ammonites from the northern North Sea. Nor. Geol. Tidsskr. 55, 373-386.

CALLOMON, J.H., DONOVAN, D.T. and TRUMPY, R. 1972. An annotated map of the Permian and Mesozoic formations of East Greenland. Meddr. Grland 168, 3, 35 pp.

CASEY., R. and RAWSON, P.F. (eds) 1973. The Boreal Lower Cretaceous. Seel House Press, Liverpool, 448 pp.

CHESHER, J.A., SMYTHE, D.K. and BISHOP, P. 1983. The geology of the Minches, Inner Sound and Sound of Raasay. Rep. Inst. Geol. Sci. No. 83/6, 29 pp.

CRAIG, G.Y. (ed.) 1983. Geology of Scotland (Second Edition). Scottish Academic, Edinburgh, 472 pp.

CREER, K.M., MITCHELL, J.G. and VALENCIO, D.A. 1971. Evidence for a normal geomagnetic field polarity event at 263±5 m.y. BP within the Late Palaeozoic reversed interval. Nature 233, 87-89.

CURRAY, J.R. 1980. The IPOD programme on passive continental margins. Phil. Trans. R. Soc. Lond. A294, 17-33.

DEARNLEY, R. 1962. An outline of the Lewisian complex of the Outer Hebrides in relation to that of the Scottish mainland. Q. J. Geol. Soc. London 112, 143-176.

DE GRACIANSKI, P.C. and POAG, C.W. Leg 80 - Goban Spur. JOIDES J. 7, 12-20.

DIX, C.H. 1955. Seismic velocities from surface measurements. Geophysics 20, 68-86.

DOBRIN, M.B. 1960. Introduction to geophysical prospecting. 2nd. edition. McGraw Hill, New York. 466 pp.

EDEN, R.A., DEEGAN, C.E., RHYS, G.H., WRIGHT, J.E. and DOBSON, M.R. 1973. Geological investigations with a manned submersible in the Irish Sea and off western Scotland. 1971. Rep. Inst. Geol. Sci. No. 73/2, 27pp.

EVANS, D., CHESHER, J.A., DEEGAN, C.E. and FANNIN, N.G.T. 1981. The offshore geology of Scotland in relation to the IGS shallow drilling programme, 1970-78. Rep.Inst. Geol. Sci. No. 81/12, 36 pp.

EVANS, S., WILKINSON, G.C., and CRAIG, D.C. 1979. The Tertiary sediments of the Canna Basin, Sea of the Hebrides. Scott. J. Geol. 15, 329-332.

FRANCIS, E.H. 1978. The Midland Valley as a rift, seen in connection with the late Palaeozoic European Rift system. In Ramberg, I.B. and Neumann, E.-R. (eds), Tectonics and geophysics of continental rifts, 133-147, Reidel, Dordrecht.

FRANCIS, E.H. 1982. Magma and sediment - I. Emplacement mechanism of late Carboniferous tholeiite in northern Britain. J. Geol. Soc. 139, 1-20.

GATLIFF, R.W., HITCHEN K., RITCHIE, J.D. and SMYTHE, D.K. 1984. Internal structure of the Erlend Tertiary volcanic complex, north of Shetland, revealed by seismic reflection. J. Geol. Soc. 141, 555-562.

GEORGE, T.N. (1966) Geomorphic evolution in Hebridean Scotland. Scott. J. Geol. 2, 1-34.

GRANT, F.S., and WEST, G.F. 1965. Interpretation theory in applied geophysics. McGraw Hill, New York, 583pp.

HAGEDOORN, J.R. 1959. The plus-minus method of interpreting seismic refraction sections. Geophys. Prospect. 7, 158-182.

HALL, J. 1970a. Seismic refraction survey in the Firth of Clyde. Proc. Geol. Soc. Lond., 1662, 74-75.

HALL, J. 1970b. The correlation of seismic velocities with formations in the south-west of Scotland. Geophys. Prospect., 18, 134-148.

HALL, J. 1971. Seismic studies in the region of the Firth of Clyde. Unpublished PhD thesis, Univ. Glasgow.

HALL, J. 1974. A seismic reflection survey of the Clyde Plateau Lavas in North Ayrshire and Renfrewshire. Scott. J. Geol., 9, 253-279.

HALL, J. and SMYTHE, D.K. 1973. Discussion of the relation of the Palaeogene Ridge and basin structures of Britain to the North Atlantic. Earth Planet. Sci. Lett. 19, 54-60.

HALLAM, A. 1971. Mesozoic geology and the opening of the north Atlantic. J. Geol. 79, 129-157.

HALLAM, A. 1983. Jurassic, Cretaceous and Tertiary sediments. In: Geology of Scotland (Second Edition; ed. Craig, G.Y.), Scottish Academic, Edinburgh, 343-356.

HAMAR, G.P. and HJELLE, K. 1984. Tectonic framework of the Møre Basin and the northern North Sea. In Spencer, A.M. (ed.), Petroleum Geology of the North European Margin, 349-358, Norwegian Petroleum Society, Oslo.

HANISCH, J. 1984. The Cretaceous opening of the northeast Atlantic. Tectonophysics 101, 1-23.

HARKER, A. 1904. The Tertiary igneous rocks of Skye. Mem. Geol. Surv. U.K., 481 pp.

HASZELDINE, R.S. 1984. Carboniferous North Atlantic palaeogeography: stratigraphic evidence for rifting, not megashear or subduction. Geol. Mag. 121, 443-463.

HEIRTZLER, J.R. and HAYES, D.E. 1967. Magnetic boundaries in the North Atlantic Ocean. Science 180, 950-952.

HIMSWORTH, E.M. 1973. Marine geophysical studies between northwest Scotland and the Faeroe Plateau. Unpublished PhD thesis, Durham University.

HINZ, K., DOSTMAN, H. and HANISCH, J. 1982. Structural framework of the Norwegian Sea. In: The geologic framework and hydrocarbon potential of basins in northern seas, E4, 1-22, Norwegian Petroleum Society, Oslo.

HIPKIN, R.G. and HUSSAIN, A. 1983. Regional gravity anaomalies. 1 Northern Britain. Rep. Inst. Geol. Sci. No. 82/10, 45 pp.

HUDSON, J.D. 1962. The stratigraphy of the Great Estuarine Series (Middle Jurassic) of the Inner Hebrides. Trans. Edinb. Geol. Soc. 19, 139-165.

HUDSON, J.D. 1963. The recognition of salinity-controlled mollusc assemblages in the Great Estuarine Series (Middle Jurassic) of the Inner Hebrides. Palaeontology 6, 318-326.

HUDSON, J.D. 1964. The petrology of the sandstones of the Great Estuarine Series, and the Jurassic palaeogeography of Scotland. Proc. Geol. Ass. 75, 499-528.

INSTITUTE OF GEOLOGICAL SCIENCES 1964. North Skye (solid edition) (scale 1 inch to 1 mile).

JACKSON, J. and McKENZIE, D. 1983. The geometrical evolution of normal fault systems. J. Struct. Geol. 5, 471-482.

JEHU, T.J. and CRAIG, R.M. 1934. Geology of the Outer Hebrides. Part 5. North Harris and Lewis. Trans. R. Soc. Edinburgh, Vol. 57, 839-874.

JONES, E.J.W. 1981. Seismic refraction shooting on the continental margin west of the Outer Hebrides, northwest Scotland. J. Geophys. Res. 86, 11553-11574.

JONES, E.J.W., PERRY, R.G. and WILD, J.L. 1986. Geology of the Hebridean margin of the Rockall Trough. Proc. R. Soc. Edinb. 88B, 27-51.

JONES, R.C. 1945. On the theory of directional patterns of continuous source distributions on a plane surface. J. Acoust. Soc. Am., 16, 147-171.

JONES, R.H. Seismic reflections from major faults. Unpublished PhD thesis, Cambridge Univ.

JONES, R.H. and WARNER, M.R. 1985. Why is the Outer Isles Thrust reflective? Geophys. J. R. Astr. Soc. 81, 338.

KAY, M. (Ed), 1969. North Atlantic - Geology and continental drift. Am. Assoc. Pet. Geol. Mem. 12,

Tulsa, 1082pp.

KILENYI, T. and STANDLEY, R. 1985. Petroleum prospects in the northwest seaboard of Scotland. Oil Gas J. 7 October 1985, 101-108.

KRISTOFFERSEN, Y. 1978. Sea-floor spreading and the early opening of the North Atlantic. Earth Planet. Sci. Lett. 38, 273-290.

KURSTEN, M. 1957. The metamorphic and tectonic history of parts of the Outer Hebrides. Trans. Edinb. Geol. Soc. 17, 1-31.

LE PICHON, X. 1968. Sea-floor spreading and continental drift. J. Geophys. Res. 73, 3661-3697.

LE PICHON, X., SIBUET, J-C. and FRANCHETEAU, J. 1977. The fit of the continents around the North Atlantic ocean. Tectonophysics 38, 169-209.

LOMBARDI, L.V. 1955. Notes on the use of multiple geophones. Geophysics 20, 215-226.

LOVELL, J.P.B. 1983. Permian and Triassic. In: Geology of Scotland (Second Edition; ed. Craig, G.Y.), Scottish Academic, Edinburgh, 325-342.

LUDWIG, W.J., NAFE, J.E. and DRAKE, C.L. 1970. Seismic refraction. In: The Sea, Vol. 4. New concepts of sea floor evolution. Part I. (ed. A.E. Maxwell), Wiley, New York, 53-84.

MacCALLUM, J.A.A. 1971. Sedimentation of the Middle Liassic rocks in the Inner Hebrides of Scotland. Unpublished PhD thesis, University of Glasgow.

MacCULLOCH, J. 1819. A description of the western islands of Scotland, including the Isle of Man. 3 vols, London, Constable.

MACINTYRE, R.M., McMENAMIN, T. and PRESTON, J. 1975. K-Ar results from Western Ireland and their bearing on the timing

and siting of Thulean magmatism. Scott. J. Geol. 11, 227-249.

MacKINDER, H.J. 1907. Britain and the British Seas. 2nd edn. (Oxford: Clarendon Press.)

McELHINNEY, M.W. 1973. Palaeomagnetism and plate tectonics. University Press, Cambridge, 358 pp.

McKAY, A.E. 1954. Review of pattern shooting. Geophysics 19, 420-437.

McKENZIE, D. 1978. Some remarks on the development of sedimentary basins. Earth Planet. Sci. Lett. 40, 25-32.

McLEAN, A. 1978. Evolution of fault-controlled ensialic basins in north western Britain. In: Bowes, D.R. and Leake, B.E. (eds), Crustal evolution in northwestern Britain and adjacent areas. Geol. J. Spec. Issue. No. 10. 325-46.

McQUILLIN, R. and BINNS, P.E. 1973. Geological structure in the Sea of Hebrides. Nature Phys. Sci. 241, 2-4.

McQUILLIN, R. and WATSON, J. 1973. Large-scale basement structures of the Outer Hebrides in the light of geophysical evidence. Nature Phys. Sci. 245, 1-3.

MASSON, D.G. and MILES, P.R. 1984. Mesozoic seafloor spreading between Iberia, Europe and North America. Mar. Geol. 56, 279-287.

MILES, P.R. and ROBERTS, D.G. 1981. The magnetisation of Rosemary Bank Seamount, Rockall Trough, northeast Atlantic. Earth Planet. Sci. Lett. 54, 442-448.

MOONEY, J.M. and KAASA, R.A. 1958. New reflection seismograph. Rev. Scient. Instr. 29, 290-294.

MORTON, A.C. and TAYLOR, P.N. 1987. Lead isotope evidence for the structure of the Rockall dipping-reflector margin. Nature 326, 381-383.

MORTON, A.C., DIXON, J.E., FITTON, J.G., MACINTYRE, R.M., SMYTHE, D.K. and TAYLOR, P.N. in press. Early Tertiary volcanic rocks in well 163/6-1A, Rockall Trough. In: Early Tertiary volcanism and the opening of the NE Atlantic (eds Morton, A.C. and Parson. L.), Geol. Soc. Spec. Publ.

MORTON, N. 1965. The Bearreraig Sandstone series (Middle Jurassic) of Skye and Raasay. Scott. J. Geol. 1, 189-216.

MUTTER, J. 1984. Cenozoic and late Mesozoic stratigraphy and subsidence history of the Norwegian margin. Bull. Geol. Soc. Am. 95, 1135-1149.

NETTLETON, L.L. 1939. Determination of density for reduction of gravimeter observations. Geophysics 4, 176-183.

NUNNS, A.G. 1983. Plate tectonic evolution of the Greenland-Scotland Ridge and surrounding regions. In Bott, M.H.P., Saxov, S., Talwani, M. and Thiede, J. (eds), Structure and development of the Greenland-Scotland Ridge: new methods and concepts, Plenum, New York, 11-30.

O'BRIEN, P.N.S. 1967. The efficient use of large charges. In Musgrave, A.W. (Ed) Seismic refraction prospecting. Soc. Expl. Geophys., Tulsa, Oklahoma, 152-170.

PARR, J.O. and MAYNE, W.H. 1955. A new method of pattern shooting. Geophysics 20, 539-564.

PATTISON, J., SMITH, D.B. and WARRINGTON, G. 1973. A review of Late Permian and Early Triassic biostratigraphy in the British Isles. In Logan, A.V. and Mills, L.V. (eds), The Permian and Triassic systems and their mutual boundary. Mem. Can. Soc. Pet. Geol. 2, 220-260.

PECHERSKY, D.M. and KHRAMOV, A.N. 1973. Mesozoic palaeomagnetic scale of the USSR. Nature 244, 499-501.

PEACH, B.N. and HORNE, J. 1930. Chapters on the geology of Scotland. London, Oxford University Press, 232 pp.

PITMAN, W. and TALWANI, M. 1972. Sea-floor spreading in the North Atlantic. Bull. Geol. Soc. Am. 83, 619-646.

POWELL, C.M.R. and SINHA, M.C. 1987. The PUMA experiment west of Lewis, U.K. Geophys. J. R. Astron. Soc. 89, 259-264.

POWELL, D.W. 1970. Magnetised rocks within the Lewisian of Western Scotland and under the Southern Uplands. Scott. J. Geol. 6, 353-369.

PRICE, I. and RATTEY, R.P. 1984. Cretaceous tectonics off mid-Norway: implications for the Rockall and Faeroe-Shetland Trough. J. Geol. Soc. 141, 985-992.

RAYNAUD, B. 1986. Seismic studies of the lower crust. Unpublished PhD thesis, Cambridge University.

RAYNAUD, B. in press. A two-dimensional ray-based depth migration method for deep seismic reflections. Geophys. J. R. Astr. Soc.

RICHEY, J.E. 1961. Scotland: the Tertiary volcanic districts (3rd edition). Mem. Geol. Surv. U.K. 120 pp.

RIDD, M.F. 1981. Petroleum geology west of the Shetlands. In Illing, L.V. (Ed) Petroleum geology of the Continental Shelf of north-west Europe. London, Heyden and Son, pp. 414-425.

RIDD, M.F. 1983. Aspects of the Tertiary geology of the Faeroe-Shetland Channel. In Bott, M.H.P., Saxov, S., Talwani, M. and Thiede, J. (eds), Structure and development of the Greenland-Scotland Ridge: new methods and concepts, Plenum, New York, 91-108.

ROBERTS, D.G. 1970. Recent geophysical studies in the Rockall plateau and adjacent areas. Proc. Geol. Soc. Lond. 1662, 87-92.

ROBERTS, D.G. 1974. Structural development of the British Isles, the continental margin, and the Rockall Plateau. In Burk, C.A. and Drake, C.L. (eds), The geology of

continental margins 343-359, Springer-Verlag, New York.

ROBERTS, D.G. 1975a. Marine geology of the Rockall Plateau and Trough. Phil. Trans. R. Soc. Lond. A278, 447-509.

ROBERTS, D.G. 1975b. Tectonic and stratigraphic evolution of the Rockall Plateau and Trough. In Woodland, A.W. (ed.), Petroleum and the continental shelf of North-west Europe. Volume 1. Geology, Applied Science, Barking, 77-91.

ROBERTS, D.G., ARDUS, D.A. and DEARNLEY, R. 1973. Precambrian rocks drilled on the Rockall Bank. Nature Phys. Sci. 244, 21-23.

ROBERTS, D.G., BOTT, M.H.P. and URUSKI, C. 1983. Structure and origin of the Wyville-Thomson Ridge. In Bott, M.H.P., Saxov, S., Talwani, M. and Thiede, J. (eds), Structure and development of the Greenland-Scotland Ridge: new methods and concepts, Plenum, New York, 133-158.

ROBERTS, D.G. and GINZBURG, A. Deep crustal structure of south-west Rockall Plateau. Nature 308, 435-439.

ROBERTS, D.G. and JONES, M.T. 1979. Magnetic anomalies in the northeast Atlantic. North sheet. Reykjanes Ridge to the British Isles. Scale 1: 2 400 000. Institute of Oceanographic Sciences, Wormley.

ROBERTS, D.G., MASSON, D.G. and MILES, P.R. 1981. Age and structure of the southern Rockall Trough : new evidence. Earth Planet. Sci. Lett. 52, 115-128.

ROBINSON, J.C. 1970. An investigation of the relative accuracy of the most common normal-moveout expressions in velocity analyses. Geophys. Prospect. 18, 352-363.

RØNNEVIK, H., BERGSAGER, E.I., MOE, A., OVREBO, O., NAVRESTAD, T. and STANGENES, J. 1975. The geology of the Norwegian continental shelf. In Woodland, A.W. (ed.), Petroleum and the Continental Shelf of North-west Europe. Volume 1. Geology, Applied Science, Barking, 117-129.

RØNNEVIK, H. and NAVRESTAD, T. 1976. Geology of the Norwegian Shelf between 62°N-69°N. In Offshore Northern Seas (ONS-76), G-IV/4, 1-24, Norwegian Petroleum Society, Oslo.

RUSSELL, M.J. 1973. Base-metal mineralization in Ireland and Scotland and the formation of Rockall Trough. In Tarling, D.H. and Runcorn, S.K. (eds), Implications of continental drift to the earth sciences, Academic Press, London, 581-597.

RUSSELL, M.J. 1976. A possible Lower Permian age for the onset of ocean floor spreading in the northern North Atlantic. Scott. J. Geol. 12, 315-323.

RUSSELL, M.H., SKUCE, A.G. and SMYTHE, D.K. Late Carboniferous dyke swarm in NW Europe used to constrain finite element models of contemporaneous rifting in the North Atlantic. Unpubl. MS.

RUSSELL, M.J. and SMYTHE, D.K. 1978. Evidence for an early Permian oceanic rift in the northern North Atlantic. In Neumann, E.-R. and Ramberg, I.B. (eds), Petrology and geochemistry of continental rifts, Reidel, Dordrecht, 173-179.

RUSSELL, M.J. and SMYTHE, D.K. 1983. Origin of the Oslo Graben in relation to the Hercynian-Alleghenian orogeny and lithospheric rifting in the North Atlantic. Tectonophysics 94, 457-472.

SAVIT, C.H., BRUSTAD, J.T. and SIDER., J. 1958. The moveout filter. Geophysics. 23, 1-25.

SCRUTTON, R.A. 1970. Results of a seismic refraction experiment on Rockall Bank. Nature 227, 826-827.

SCRUTTON, R. 1971. Gravity and magnetic interpretation of Rosemary Bank, North-East Atlantic. Geophys. J. R. Astr. Soc. 24, 51-58.

SCRUTTON, R.A. 1972. The crustal structure of Rockall Plateau microcontinent. Geophys. J. R. Astr. Soc. 27,

259-275.

SCRUTTON, R.A. 1986. The geology, crustal structure and evolution of the Rockall Trough and Faeroe-Shetland Channel. Proc. R. Soc. Edinb. 88B, 7-26.

SERIFF, A.J. 1959. The response of seismometers in series and parallel connections. Geophysics 24, 49-63.

SHERIFF, R.E. and GELDART, L.P. 1982. Exploration seismology. Vol. 1. History, theory, and data acquisition. Cambridge University Press, London, 253 pp.

SMYTHE, D.K. 1980. The deep structure of the Moine and Outer Isles Thrusts north of Cape Wrath and Lewis. Geophys. J. R. Astr. Soc. 61, 199.

SMYTHE, D.K. 1983. Faeroe-Shetland Escarpment and continental margin north of the Faeroes. In Bott, M.H.P., Saxov, S., Talwani, M. and Thiede, J. (eds), Structure and development of the Greenland-Scotland Ridge: new methods and concepts, Plenum, London, 109-119.

SMYTHE, D.K. 1987. The Merlin SKS seismic reflection processing package on the Edinburgh VAX 8530 computer. Brit. Geol. Surv. Mar. Rep. No. 87/44.

SMYTHE, D.K., CHALMERS, J.A., SKUCE, A.G., DOBINSON, A. and MOULD, A.S. 1983. Early opening history of the North Atlantic - I. Structure and origin of the Faeroe-Shetland Escarpment. Geophys. J. R. Astr. Soc. 72, 373-399.

SMYTHE, D.K., DOBINSON, A., McQUILLIN, R., BREWER, J.A., MATTHEWS, D.H., BLUNDELL, D.J. and KELK, B. 1982. Deep structure of the Scottish Caledonides revealed by the MOIST reflection profile. Nature 299, 338-340.

SMYTHE, D.K. and KENOLTY, N. 1975. Tertiary sediments in the Sea of the Hebrides. J. Geol. Soc. London, 131, 227-233.

SMYTHE, D.K., SOWERBUTTS, W.T.C., BACON, M. and McQUILLIN, R. 1972. Deep sedimentary basin below northern Skye and

the Little Minch. Nature Phys. Sci. 236, 87-89.

SRIVASTAVA, S.P. 1978. Evolution of the Labrador Sea and its bearing on the early evolution of the North Atlantic. Geophys. J. R. Astr. Soc. 52, 313-357.

STEAVENSON, A.G. 1928. Some geological notes on three districts of northern Scotland. Trans. Geol. Soc. Glasgow, 18, 193-233.

STEEL, R.J. 1971. New Red Sandstone movement on the Minch Fault. Nature Phys. Sci. 234, 158-159.

STEEL, R.J. 1974. New Red Sandstone floodplain and piedmont sedimentation in the Hebridean province, Scotland. J. Sediment. Petrol. 44, 336-357.

STEEL, R.J., NICHOLSON, R. and KALANDER, L. 1975. Triassic sedimention and palaogeography in Central Skye. Scott. J. Geol. 11, 1-13.

STEEL, R.J. and WILSON, A.C. 1975. Sedimentation and tectonism (? Permo- Triassic) on the margin of the North Minch Basin, Lewis. J. Geol. Soc. Lond. 131, 183-202.

STEVENS, A. 1914. Notes on the geology of the Stornoway district of Lewis. Trans. Geol. Soc. Glasgow, 15, 51-63.

STEWART, A.D. 1969. Torridonian rocks of Scotland reviewed. In: North Atlantic - geology and continental drift (ed. Kay, M.), Am Ass. Pet. Geol. Mem. 12, 595-608.

STEWART. A.D. 1975. 'Torridonian' rocks of western Scotland. In Harris, A.L. and others (Eds.) A correlation of the Precambrian rocks in the British Isles. Spec. Rep. Geol. Soc. London, No. 6, 43-51.

STEWART, F.H. 1965. Tertiary igneous activity. In: The geology of Scotland (ed. Craig, G.Y.), Oliver and Boyd, Edinburgh, 417-465.

STOREVEDT, K.M. and STEEL, R.J. 1977. Palaeomagnetic evidence for the age of the Stornoway Formation. Scott. J. Geol. 13, 263-269.

SUMM. PROG. GEOL. SURV. G.B. 1935-1939: for 1934, pp. 70-71; for 1935, pp. 81-84; for 1936, pp. 77-79; for 1937, pp. 73-75; for 1938, pp. 74-76.

SWETT, K. 1969. Interpretation of depositional and diagenetic history of Cambrian-Ordovician succession of north-west Scotland. In Kay, M. (Ed), North Atlantic - geology and continental drift, Tulsa, Oklahoma, Am. Assoc. Pet. Geol. Mem. 12, 630-646.

TALWANI, M. (ed) 1974. Underway marine geophysical data in the North Atlantic, June 1961-January 1971, six vols + ten charts, Lamont-Doherty Geological Observatory, New York.

TALWANI, M. and ELDHOLM, O. 1972. Continental margin off Norway: a geophysical study. Bull. Geol. Soc. Am. 83, 3575-3606.

TANER, M.T. and KOEHLER, F. 1969. Velocity spectra - digital computer derivation and applications of velocity functions. Geophysics 34, 859-881.

TURNER, P. and VAUGHAN, D.J. 1977. Evidence of rapid changes in the Permian geomagnetic field during the Zechstein marine transgression. Nature 270, 593-594.

TUSON, J. 1959. A geophysical investigation of the Tertiary volcanic districts of western Scotland. Unpublished PhD thesis, Durham University.

VALENCIO, D.A. and VILAS, J.F. 1972. Palaeomagnetism of Late Palaeozoic and Early Mesozoic rocks of South America. Earth Planet. Sci. Lett. 15, 75-85.

VAN HINTE, J.E. 1976. A Cretaceous time scale. Bull. Am. Ass. Pet. Geol. 60, 498-516.

VAN MELLE, F.A. and WEATHERBURN.,K.R. 1953. Ghost reflections caused by energy initially reflected above the

level of the shot. Geophysics 18, 793-804.

VENING MEINESZ, F.A. 1950. Les grabens africains, résultats de compression ou de tension dans la croûte terrestre? Bull. Inst. Recherche Colon. Belge 21, 539-552.

WATTS, A.B. 1971. Geophysical investigations on the continental shelf and slope north of Scotland. Scott. J. Geol. 7, 189-218.

WERNICKE, B. 1985. Uniform-sense normal simple shear of the continental lithosphere. Can. J. Earth Sci. 22, 108-125.

WERNICKE, B. 1986. Whole-lithosphere normal simple shear: an interpretation of deep-reflection profiles in Great Britain. In: Reflection seismology: the continental crust (eds. Barazangi, M. and Brown, L.). Am. Geophys. Union Geodynamics Ser. Vol 14, 331-339.

WHITE., J.E. 1958. Transient behavior of patterns. Geophys., 23, 26-43.

WHITE, R.S., SPENCE, G.D., FOWLER, S.R., McKENZIE, D.P., WESTBROOK, G.K. and BOWEN, A.N. 1987. Magmatism at rifted continental margins in the North Atlantic. Nature, in press.

ZIEGLER, P.A. 1975. North Sea basin history in the tectonic framework of north-western Europe. In Woodland, A.W. (ed.), Petroleum and the continental shelf of North-west Europe. Volume 1. Geology, Applied Science, Barking, 131-149.

ZIEGLER, P.A. 1982. Geological atlas of western and central Europe. Elsevier, Amsterdam, 130 pp.

ZIOLKOWSKI, A. 1972. Science criticism (correspondence). Nature 237, 523.